Lecture Notes in Networks and Systems 1209

Sergey Kovalev · Igor Kotenko · Andrey Sukhanov · Yin Li · Yao Li *Editors*

# Proceedings of the Eighth International Scientific Conference "Intelligent Information Technologies for Industry" (IITI'24), Volume 1

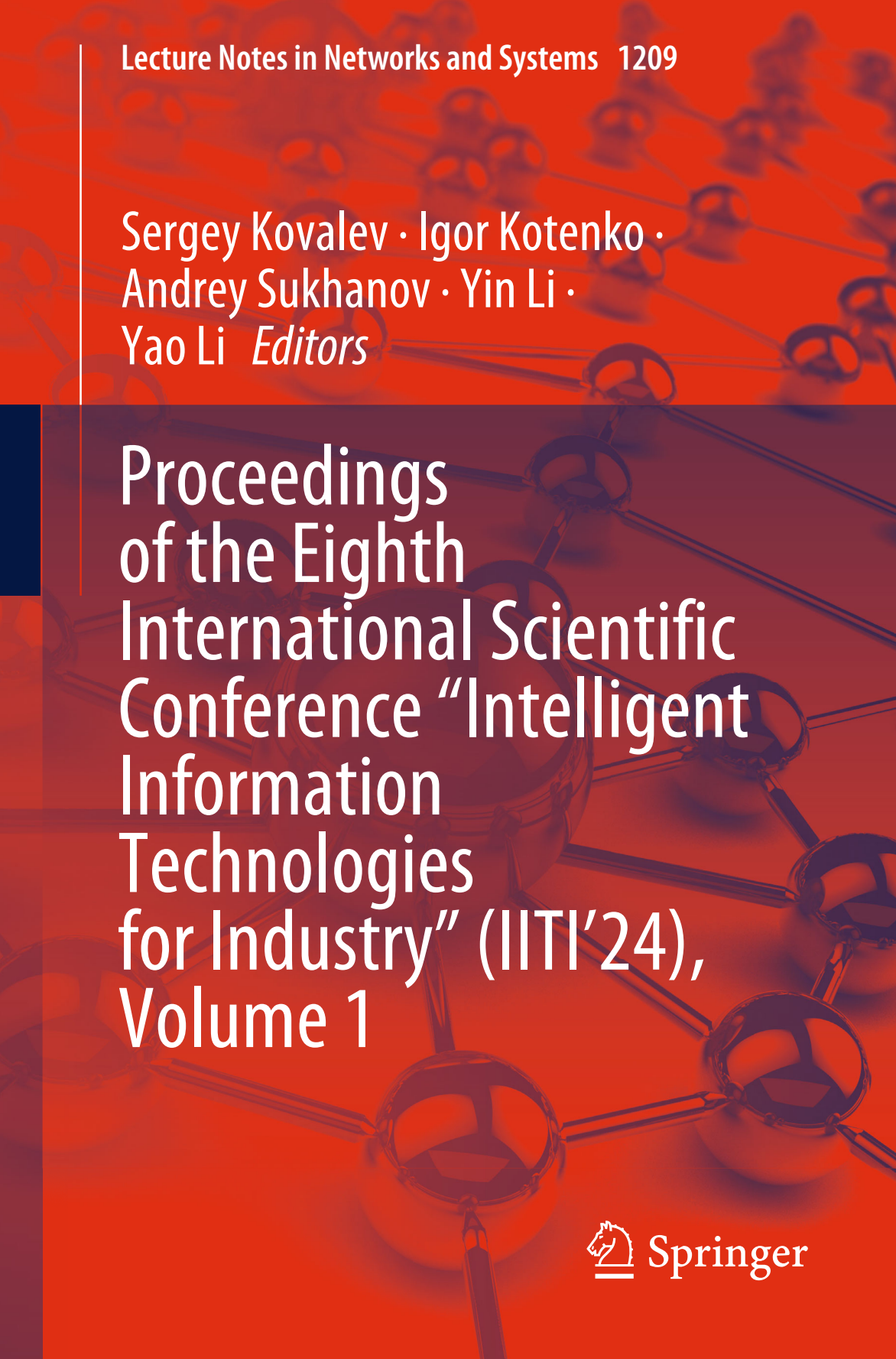

Springer

# Lecture Notes in Networks and Systems 1209

The series "Lecture Notes in Networks and Systems" publishes the latest developments in Networks and Systems—quickly, informally and with high quality. Original research reported in proceedings and post-proceedings represents the core of LNNS.

Volumes published in LNNS embrace all aspects and subfields of, as well as new challenges in, Networks and Systems.

The series contains proceedings and edited volumes in systems and networks, spanning the areas of Cyber-Physical Systems, Autonomous Systems, Sensor Networks, Control Systems, Energy Systems, Automotive Systems, Biological Systems, Vehicular Networking and Connected Vehicles, Aerospace Systems, Automation, Manufacturing, Smart Grids, Nonlinear Systems, Power Systems, Robotics, Social Systems, Economic Systems and other. Of particular value to both the contributors and the readership are the short publication timeframe and the worldwide distribution and exposure which enable both a wide and rapid dissemination of research output.

The series covers the theory, applications, and perspectives on the state of the art and future developments relevant to systems and networks, decision making, control, complex processes and related areas, as embedded in the fields of interdisciplinary and applied sciences, engineering, computer science, physics, economics, social, and life sciences, as well as the paradigms and methodologies behind them.

Indexed by SCOPUS, EI Compendex, INSPEC, WTI Frankfurt eG, zbMATH, SCImago.

All books published in the series are submitted for consideration in Web of Science.

For proposals from Asia please contact Aninda Bose (aninda.bose@springer.com).

Sergey Kovalev · Igor Kotenko ·
Andrey Sukhanov · Yin Li · Yao Li
Editors

# Proceedings of the Eighth International Scientific Conference "Intelligent Information Technologies for Industry" (IITI'24), Volume 1

Springer

*Editors*
Sergey Kovalev
Rostov State Transport University
Rostov-on-Don, Russia

Andrey Sukhanov
Rostov State Transport University
Rostov-on-Don, Russia

Yao Li
School of Mathematics
Harbin Institute of Technology
Harbin, China

Igor Kotenko
St. Petersburg Federal Research Center
of the Russian Academy of Sciences
St. Petersburg, Russia

Yin Li
School of Mathematics
Harbin Institute of Technology
Harbin, China

ISSN 2367-3370 ISSN 2367-3389 (electronic)
Lecture Notes in Networks and Systems
ISBN 978-3-031-77687-8 ISBN 978-3-031-77688-5 (eBook)
https://doi.org/10.1007/978-3-031-77688-5



This Springer imprint is published by the registered company Springer Nature Switzerland AG
The registered company address is: Gewerbestrasse 11, 6330 Cham, Switzerland

# Preface

This volume of Lecture Notes in Networks and Systems contains the papers presented in the main track of IITI'24, the Eighth International Scientific Conference on Intelligent Information Technologies for Industry held from November 1 to November 7, 2024 in Shanghai-Harbin, China. The conference was organized by Rostov State Transport University (Russia) and JSC NIIAS (Russia) with the support of the Russian Association for Artificial Intelligence. In 2024, the conference was co-organized with the Harbin Institute of Technology. The purpose of IITI is to bring together the international advanced experience in the field of development and implementation of modern techniques in automation, digitization and artificial intelligence in both fundamental and applied sciences as well as to the development of contacts in this field.

The innovative intelligent information technologies are of particular interest at the conference. Annually, IITI is held with the participation of leading international scientists. The history of the conference has included multiple international locations, such as Sirius (Russia), VSB-Technical University of Ostrava (Czech Republic), Technical University of Varna (Bulgaria), Istanbul Aydin University (Turkey). Due to IITI, more than 1000 scientists from all over the world published more than 400 scientific papers in IITI Proceedings, which are published in the Springer series.

IITI'24 was devoted to practical models and industrial applications related to intelligent information systems. It was considered as a meeting point for researchers and practitioners to enable the implementation of advanced information technologies in various industries. Nevertheless, some theoretical talks concerning the state of the art in intelligent systems were also included into proceedings. There were 125 paper submissions from five countries, especially from Russia and China. Each submission was reviewed by at least three Chairs or PC members. We accepted 78 regular papers (62%). Unfortunately, due to limitations of conference topics and edited volumes, the program committee was forced to reject some interesting papers, which did not satisfy these topics or publisher requirements. We would like to thank all authors and reviewers for their work and valuable contributions. The friendly and welcoming attitude of conference supporters and contributors made this event a success!

November 2024

Igor Kotenko
Sergey Kovalev
Andrey Sukhanov
Yin Li
Yao Li

# Contents

# Automation and Intellectualization for Industrial, Transport and Energetic Systems

# Complexity Estimate of Logical Specifications Execution for Transport Processes Prototyping

Vera V. Ilicheva(✉) and Alexander N. Guda

Rostov State Transport University, Rostov-on-Don, Russia
vilicheva@yandex.ru

**Abstract.** In this paper we examine logical specifications for rapid prototyping of complex structures and processes, including transport ones. We use a language in classical predicate logic with equality and negation, which has computable semantics. The execution of such descriptions may have exponential complexity estimates. We have obtained sufficient conditions and, accordingly, subclasses of such specifications, the complexity of constructing prototypes for which can be reduced to polynomials of low degrees. Systems were defined which solvable in time $O(n \log_2 n)$ with linear memory $O(m)$, where $n$ is the power of specified relations, $m$ is the power of relations and function values. The expressiveness of the resulting classes of specifications, as shown by practical use, is sufficient for prototyping in various subject areas.

**Keywords:** Logic language · Logic prototype · Complexity of specification execution · Rapid prototyping of transport processes

## 1 Introduction

In the context of intensive development of the digital economy, new technologies and methods of artificial intelligence in industry, robotics, and transport systems, the development of prototypes of projected objects is becoming increasingly relevant. Particular attention is paid to rapid, low-cost prototyping as a way to conveniently test decisions made. In this case, preference is often given to formal means of prototype specification to ensure the reliability of the analysis results and an accurate understanding of the project requirements [1, 2]. Formalizations are used in logics of various types – temporal, odd, modal, production systems, specially developed languages [3, 4]. The key required properties of prototype specifications are expressiveness and executability adequate to the task, and if the first is achieved by including some "convenient" operators, then the second is the ability to execute a description can present a problem. Compilation into an executable language like Prolog is not always convenient, both because of insufficient expressiveness and because of exponential estimates of execution complexity [5–8].

We develop a specification-based prototyping approach in the classical logic of first-order predicates with equality [9, 10]. The semantics of specifications allows the use of negations and equality of terms in formulas, which significantly increases the expressiveness of the logical language. The specifications are executable and can be effectively


S. Kovalev et al. (Eds.): IITI 2024, LNNS 1209, pp. 3–11, 2024.
https://doi.org/10.1007/978-3-031-77688-5_1

implemented. We used this approach in prototyping, analyzing structures and dynamic systems in various fields – system programming, space simulators, design and analysis of transport processes, anomaly analysis during information attacks, both in signature and behavioral methods of their detection [9, 10]. Now we use logical prototyping in macromodeling and analysis of transport systems to evaluate the choice of route, the logistics chain in multimodal transportation, and the evaluation of options for dividing different traffic flows into parts. The expressiveness and convenience of describing logical models are confirmed by the use in these areas. This article examines the issues of effective realizability of the selected class of formulas. The conditions under which the complexity of interpretation can be reduced to $O(n \log_2 n)$ with linear memory are determined.

## 2 Specification Logical Language

We propose an approach based on the use of predicate logic to model the current situation, evaluate it, and check for compliance with the required properties and constraints.

The essence of the approach is as follows. A formal description is constructed – a specification of the analyzed system, prototype, or process in the form of three classes of formulas (axioms) of the first-order predicate calculus language with equality. The alphabet used is the signature $\Sigma = (R,\ F,\ C)$, where $R$ are the names of predicates (relations between objects); $F$ are the names of functions (attributes of objects); $C$ are the names of constants (codes of objects in the subject area, numeric, textual values, points of time intervals), $C \neq \varnothing$, $\forall c_i, c_j \in C,\ i \neq j:\ c_i \neq c_j$. Arguments of functions, predicates, constants have a type (domain, sort). This allows us to get rid of the condition of functions totality in the entire field of interpretation and clarifies the description. For dynamics, domains are added – finite intervals of discrete time. The basis of the specification $(\Sigma,\ T)$ is the logical theory $T = T_0 \cup T_D \cup T_R$ – a set of axiom formulas, all variables of which are connected by quantifiers. Formulas $T_0$ are facts, atomic formulas with constants instead of variables, of the form $r(\overline{c})$, $\neg r(\overline{c})$, $f(\overline{c}) = c_f$, where $r \in R, f \in F, \overline{c} \in C^*, c_f \in C$. These are specific statements that initiate logical inference. The second class of $T_D$ formulas are definitions of prototype elements – relations and functions. There can be several definitions for each $r, f$ and they can be recursive. For our task of evaluating the complexity of execution, it is convenient to divide $T_D$, $T_D = T_D^P \cup T_D^N$, where $T_D^N$ are axioms that have negations. Formulas of this class:

$$T_D^P:\ \forall \overline{x}(\varphi_1(\overline{x}) \wedge \ldots \wedge \varphi_n(\overline{x}) \rightarrow \psi_1(\overline{x}) \wedge \ldots \wedge \psi_m(\overline{x})),$$

$$T_D^N:\ \forall \overline{x}(q_i(\overline{x}) \& \neg p_i(\overline{x}) \& \varphi(\overline{x}) \rightarrow \psi_1(\overline{x}) \wedge \ldots \wedge \psi_m(\overline{x}))),$$

where $\overline{x}$ is a vector of variables, conjuncts $\varphi_i(\overline{x})$ $(1 \leq i \leq n)$ are atomic formulas of the form $r_i(\overline{t})$, $t_i(\overline{x}) = t_j(\overline{x})$, conjuncts $\psi_j(\overline{x})$ $(1 \leq j \leq m)$ are formulas of the form $r(\overline{t})$, $f(\overline{x}) = t_f$, where $r_i,\ r \in R, f \in F, t_i, t_j, \overline{t}, t_f$ are terms of the signature $\Sigma$; $q_i(\overline{x})$, $p_i(\overline{x})$ are atomic formulas, $\varphi(\overline{x})$ are conjunction of pairs of the same type or atomic formulas, $V_{pi} \subseteq V_{qi}$ for sets of variable formula $p_i$ and $q_i$. Negations are included only in the left part of the implications and their scope is limited to the area when the "positive"

predicate $q_i$ is truth, so $q_i$ plays the role of a limited quantifier for every $\neg p_i(\overline{x})$. The formulas $\psi_j(\overline{x})$ define the relations $r(\overline{t})$, the functions $f(\overline{x}) = t_f$ on the values of the terms $\overline{t},\ t_f$. The third class of $T_R$ formulas are additional restrictions on the constructed model or the current state of the process, for example, the impossibility of simultaneous presence of any signals, invalid parameter values, deviations of the calculated indicators from the required values, etc. $T_R$ represents any first-order formulas with bounded quantifiers, they are tested on a model built using $T_0 \cup T_D$.

The semantics of the description is represented by inductively computable models $\mathfrak{M} = (C,\ I)$ obtained by interpretation $I:\ (\sum \to C^*)$, minimal with respect to homomorphic embeddings in the class of all $\Sigma$-generated models of the theory $T_0 \cup T_D$. It is true for them: for each atomic formula $\phi(\overline{c})$ that is true on the model, there is a fact or definition for it, with the $\varphi(\overline{x})$ true when substituting $\overline{x}/\overline{c}$. This property is necessary to constructively obtain initial models for theories with negation [10]. It provides a funded order on the model in which the terms of the definition condition can be calculated before the defined values, then the interpretation of $I$ is inductively calculated by $T_0 \cup T_D$. It is proved that such a model exists for "well-defined" specifications having the properties of $F$-completeness (each term used in $T_D$ is reduced by inference to some constant from $C$), $E$-consistency $(\forall c_i, c_j, c_i \neq c_j:\ T \nvDash c_i = c_j)$, $N$-consistency (for any atomic formula $\phi$: $T \nvDash \phi \wedge \neg\phi$).

The interpreter carries out a direct logical inference, at the input of which there is set of facts, and output – set of new facts – the logical consequences of axioms. When a fix-point of the output process is obtained, the validity of the $T_R$ constraints is checked. The interpreter implements the denotational semantics of the language, using full grids with the bottom – "uncertainty" ($\perp$), the top – "an error of redefinition" ($\top$). If a redefinition of the $f(\overline{c}) \in F$ function or a logical contradiction for $r(\overline{c}) \in R$ is obtained, the interpretation of $I(f, \overline{c})$ or $I(r, \overline{c})$ is assumed to be equal to $\top$; the asynchrony and monotony of the inference process entails setting the value of $\top$ for all relations and functions in the derivation of which these $f$ and $r$ participated. So you can see the trace of an error in the interpretation of definitions. If any function $f$ has not received a value on its domain, its value is interpreted as $\perp$, then the values of terms containing $f(\overline{c})$ will also be undefined. In these cases, the desired prototype cannot be built, the message indicates such $f(\overline{c})$ and $f(\overline{c}),\ r(\overline{c})$ with $\top$– values.

Error diagnostics is performed both during model construction (interpretation of the $T_R \cup T_D$ axioms) and during constraints verification (interpretation of the $T_R$ axioms). In the first case, contradictions, redefinitions and uncertainty of functions are diagnosed. In the second case, detected prototype errors are reported.

Although the definitions resemble production rules of expert systems, there are fundamental differences.

Firstly, the method is strictly mathematically justified. Equivalent model-theoretic, denotational, and operational semantics are defined for it. Their computability and effective implementation are proved. Secondly, in accordance with the semantics of the descriptions, uncertainty and contradictions are automatically diagnosed, which in expert systems are attributed to the mistakes of the expert (if these errors can be accidentally detected). Thirdly, there is a wider class of formulas acceptable for verification, which distinguishes this approach from logical programming in languages such as Prolog, in

which there are no equalities and negations, which significantly reduces the clarity and expressiveness of descriptions. Fourth, the method allows you to track and mark the trace of redefinition error and contradiction, which is important for non-deterministic inference, when there is a high probability of getting a «induced error». Finally, all diagnostics are carried out in a single logical formal system, without various "bindings" and "additives" in the form of program procedures with their own semantics. Note that defining any function $f$ in the form of $f(\overline{c}) = \Pr og(\overline{c})$, , through a program in a programming language, as it happens in production systems, means going beyond the logical formalism and the question of the computability of such a description (the program may loop) then falls on the developer.

## 3 Complexity Estimate

The condition that every negative occurrence of the predicate $p(\overline{x})$ implies the presence of a conjunct $q(\overline{x})$ in this formula, such that $V_p \leq V_q$ for the sets of variables $V$ of these predicates guarantees computability of their falsity domains.

The construction of the $\mathfrak{M}$ model for a theory with negations is implemented by various non contradictory strategies $s \in S$, each of which represents the chosen order of axioms interpretation with negation: the $<m, \overline{c}_m>$ element is included in $s$ if the predicate $p_m(\overline{c}_m)$ in this strategy has been interpreted as false. The construction of $\mathfrak{M}$ for $T_D^P$ does not depend on the order of interpretation, which has a single fix-point. The consistency of the strategy means that $D^+(p) \cap D^-(p) = \varnothing$ for the domains of truth $D^+$ and falsity $D^-$ of any relation $p \in R$. It is proved [10] that the desired minimal model exists if and only if all non contradictory strategies are equivalent and also give a single fix-point in direct logical inference.

Let's denote the complexity of interpreting definitions as $Com(T_D) = Com_s \cdot N_S$, where $Com_s$ is the complexity of implementing one strategy $s \in S$, $N_S$ is the power of the set $S$. If there are no negatives in $T_D$, then $Com(T)$ coincides with $Com(T_D^P)$. If there are negations, then $N_S$ grows exponentially with an increase in the set $H = \bigcup\limits_p H(p)$ for $H(p) = D^+(q) \backslash \left[D^+(p) \cap D^+(q)\right]$, i.e. with an increase in relations playing the role of bounded quantifiers in axioms with negations $T_D^N \subseteq T_D$. The way to radically reduce complexity is to find the conditions under which the $\mathfrak{M}$ model can be built using a single strategy. The nonequivalence of the strategies is due to the different possibilities of changing $H$ at step $k > 0$ for any $k$. Desired property: $H_k \subseteq H_{k+1}$ is a monotonic increase of $H$. It is proved that:

For the theory of $T_D$, where $T_D^N \subseteq T_D$ and any $s \in S$, if $H_k \subseteq H_{k+1}$ is for $\forall k \geq 0$, then all strategies in $S$ are equivalent.

It follows that if for $T$ the condition $\forall k \geq 0 : \ H_k \subseteq H_{k+1}$ is fulfilled for one strategy, then it is fulfilled for any other $s \in S$. Therefore, to build $\mathfrak{M}$, one strategy with the property of non-decreasing the set $H$ is sufficient, if this strategy will be non contradictory. This property is checked dynamically during the interpretation process.

We define sufficient statically checked conditions for the independence of order in which the clauses from the $T_D^N$ were interpreted.

Let $\alpha,\ \beta,\ \gamma \in F \cup R$. We define the transitive relation $\to^*$ of the weak inference for the theory $T_D = T_D^p \cup T_D^N :\ \alpha \to^* \beta$ if there is an axiom $\Phi$ in $T_D$ such that $\alpha$ is included in the premise, $\beta$ in the conclusion of $\Phi$, or $\exists\gamma :\ \alpha \to^* \gamma$ and $\gamma \to^* \beta$.

Let's denote $\alpha_{N,i}$ for any $\alpha \in F \cup R$ the occurrence of $\alpha$ in the formula under the negation of the axiom $\Phi_i \in T_D^N$. Note that $\alpha_{N,i} \neq \alpha_{N,j}$ at $i \neq j$, i.e. the occurrence of the same symbol in different $T_D^N$ axioms differs.

We will call the $T_D = T_D^p \cup T_D^N$ theory balanced if the condition for it is fulfilled: $\neg\exists\ \alpha_{N,i},\ \beta_{N,j}(\alpha,\ \beta \in F \cup R,\ i \neq j) :\ \alpha \to^* \beta$.

The above condition prohibits the recursive dependence of incoming relations with negation in the set of axioms $T_D^p \cup T_D^N$, but allows it within the framework of $\Phi \cup T_D^p\ \left(\Phi \in T_D^N\right)$ theory, for each $\Phi$ and $\alpha_N$ included in $\Phi$. The property of balance is obviously solvable with a complexity of no more than $O\left(l^2\right)$ (relative to the length of the theory being analyzed) and is checked statically. For such a theory, all strategies are equivalent and one is enough to build a model (prototype). If strategy is contradictory, then the desired model does not exist.

The interpretation algorithm corresponding to these constraints is the sequential execution of two stages (1–2) until the inference gives new facts. 1) – the derivation with the axioms of $T_0 \cup T_D^p$ before obtaining a fix-point. 2) – independent of each other's results ("parallel") interpretation of each axiom from $T_D^N$, new facts are temporarily stored in $D_P^+,\ D_P^-$ for each received $p(\overline{c})$, $\neg p(\overline{c})$ (the predicate $p(\overline{c})$ is assumed to be false if $p(\overline{c}) \notin D^+$, and the corresponding $q(\overline{c}) \in D^+$). Then the sets $D^+ = D^+ \cup D_P^+,\ D^- = D^- \cup D_P^-$ are replenished and, if $D^+ \cap D^- \neq \varnothing$, then the theory $T$ is contradictory. If new facts are obtained (including with the error $\top$), then the inference process is repeated from the first stage.

Now let's find the definition systems that are solvable in time $O\left(n \log_2 n\right)$ with linear memory $O(m)$, where $n$ is the total power of the defined relations, $m$ is the power of the definiteness of functions and relations. Taking into account the possibility of constructing $\mathfrak{M}$ with one strategy, we note that the complexity of interpreting $T_D^p \cup T_D^N$ and $T_D^p$ then have the same order. Therefore, let's consider the construction of $\mathfrak{M}$ according to the theory of $T_D^p$.

The time spent on interpreting $T_D^p$ is defined as $N_\phi \cdot Com_\phi$, where $N_\phi$ is the number of calls to the interpreter that resolves one axiom and $Com_\phi$ is the time complexity of its interpretation. The $N_\phi$ depends on the possible number of $\alpha(\overline{c})$ $(\alpha \in F \cup R)$ characters with a productive (giving a new value) interpretation. For theories satisfying the conditions of finite completeness, $\Delta$: $\left\{r_\varphi\right\} \neq \varnothing$ and all $r_\varphi$ conjuncts are atomic, and $V_\psi \subseteq V_{r_\varphi},\ V_{t_\varphi} \subseteq V_{r_\varphi}$ the value of $N_\phi$ is determined by the number of elements of relations from $R$ included in the left parts of the implications. Let us denote n as the total power of the relations $r \in R$ defined in $T_D^p$. Then $N_\phi$ has the order $O(n)$. The complexity of the $Com_\phi$ interpretation of one axiom, the variables of which are bound by the condition $\Delta$, is determined by the costs necessary to obtain the values of the $\overline{x}_{r_\varphi}$ variables of the $r_\varphi$ formula, on which the interpretation of $r_\varphi$ is *true* or $\top$, i.e., the complexity of selecting "effective" substitutions for the $\overline{x}_{r_\varphi}$. If $l$ is the maximum possible length of the $\overline{x}_{r_\varphi}$ set for $T_D^P$, then the upper bound for $Com_\phi$, obtained by estimating the enumeration of all vectors of length $l$ in the set of constants $C$ and the time to check the truth of the $r_\varphi$ for these arguments, has the order $O\left(|C|^l \cdot n\right)$ or $O\left(n^{l+1}\right)$, if the values of $n,\ |C|$ are

equally powerful. That is, without optimizing the process of searching for suitable $\overline{c}_{r_\varphi}$ arguments, already for clauses containing no more than two variables, the interpretation time of one definition will be of the order of $O(n^3)$.

A possible optimization consists in the selection of $\overline{c}_r$ vectors from the domain of certainty $D(r) = D^+(r) \cup D^\top(r)$ of the relation $r$ for each $r$ of $r_\varphi$ compatible with each other and the set of $\overline{c}_\alpha$ that induced the interpretation of the definition. The main role in estimating the value of $Com_\phi$ then plays the complexity of the intersection of the subformulas variables of the formula $r_\varphi$. For many applications, in particular those used by us, the following conditions are sufficient.

Let $m$ be the cardinality of the set $D^+ \cup D^\top$. Let's denote the set of arguments containing constants from $C$, of any (sub) formula $\Phi$ as $Arg(\Phi)$, and the arity of the predicate $r$ as $\mu(r)$. Replace all occurrences of constants $c \in C$ into subformula $r_\varphi$ with a single character $\beta$. Provn

*Statement.* If for each clause of $T_D^p$ there is a:

1) $\{r_\varphi\} \neq \varnothing$; $V_{t_\varphi} \subseteq V_{r_\varphi}$, $V_\psi \subseteq V_\varphi$ (finite completion condition) and
2) for the subformula $r_\varphi \equiv \underset{i=1}{\overset{k}{\&}} r_i(\overline{x})$, the following is performed: $\forall r_i (i \in [1,\ k])$ : $\mu(r_i) \leq 2$ and either

a) $V_{r_i} \cap V_{r_j} = \varnothing$ for any $r_i(\overline{x})$, $r_j(\overline{x})$ from $r_\varphi$, or b) $\underset{i=1}{\overset{k}{\cap}} V_{r_i} \neq \varnothing$, or c) $\beta \in \underset{i=1}{\overset{k}{\cap}} Arg(r_i)$, or d) If $\exists\ r_{\varphi_1},\ r_{\phi_2} :\ r_\varphi \equiv r_{\varphi_1} \& r_{\varphi_2},\ V_{r_{\varphi_1}} \cap V_{r_{\varphi_2}} = \varnothing$ and $V_{r_{\varphi_1}}$ satisfy condition a), $V_{r_{\varphi_2}}$ satisfies c), then the system of definitions $T_0 \cup T_D^P$ is solvable with complexity $O(n\ \log_2 n)$ in time and $O(m)$ in memory for any finite $T_0$.

The obtained estimates do not increase with some weakening of conditions 2): the restriction on the number of predicate arguments is not as significant as the restriction on the structure of the graph defined by the formula. It can be shown that when replacing condition 2b with a $V_{r_i} \cap V_{r_j} \subseteq \underset{l=1}{\overset{k}{\cap}} V_{r_l}$ $(i,\ j \in [1,\ k])$ constraint for any $r_i$, $r_j$ from $r_\varphi$ and condition 2c with $\{\beta\} = \underset{i=1}{\overset{k}{\cap}} Arg(r_i)$, memory costs will be on the order of $O(m)$ and time – $O(n\ \log_2 n)$ and when any multiary predicates are included in $r_\varphi$.

Each axiom $T_R$ is checked once for the domain $D = D^+ \cup D^\top \cup D^-$, so there is no multiplier $n$ in the time estimate and the memory $D$ is not growing. However, since any axioms are allowed in $T_R$, the complexity of verifying the truth of each of them can theoretically exceed $\log_2 n$. The estimate depends entirely on the way storage and access are organized in $D$ and usually ranges from constant to $n^2$.

## 4 Examples

To illustrate, we present fragments of the prototype description corresponding to the [11] model of traffic flow separation. The main parameters of the model are route time ($\tau$) and part of the flow volume ($\lambda$) (at each point, where the flow is divided into $k$ parts:

$\sum_{i=1}^{k} \lambda_i = 1$). In our example, we consider car flows; other parameters are taken into account for them, in particular, railway station capacity, the availability of infrastructure, locomotives and engine crews. Such and many other parameters are themselves functions of a large number of different quantities [12, 13]. In the description, to simplify, we take such functions as externally specified facts. There is no $T_0$ in the example, because the prototype is built for various input facts.

*Sorts:*

POINT – route point, railway station, railway junction;
TIME - finite discrete time intervals

*Relations:*

is_track (from, to): POINT × POINT – presence of a track between points;
is_route (from, to, in_time): POINT × POINT × TIME – presence of a route
is_slot (from, to, in_time): POINT × POINT × TIME – presence of free thread
overflow (from, to): POINT × POINT – too much flow
must_new_track (from, to): POINT × POINT – necessity of a new track creation;
delay (where, when): POINT × TIME – delay on station at time

*Functions:*

τ (from, to): POINT × POINT → TIME – route time
λ (from, to): POINT × POINT → INTEGER – part of the car flow between points
s_capasity (whose): POINT → INTEGER – railway station capacity
r_capasity (from, to, in_time): POINT × POINT × TIME → INTEGER – route capacity
c_capasity (from, to): POINT × POINT → INTEGER – carrier capasity
ncrews (where, when): POINT × TIME → INTEGER – free engine crews quantity
nloc (where, when): POINT × TIME → INTEGER – free locomotives quantity at time
delay_reason (where, when): POINT × TIME → TEXT

*Definitions:*

∀ x, y, z (is_track(x, y) & is_track(y, z) → is_track(x, z) & λ(x, z)= λ(x, y)·λ(y, z)&
τ(x, z)= τ(x, y) + τ(y, z));
∀ x, y (is_track(x, y) & λ(x, y) > c_capasity(x, y) → overflow(x, y);
∀ x, y (overflow(x, y) → must_new_track(x, y);
∀ x, y, t (is_track(x, y) & r_capasity(x, y, t) > 0 → is_route(x, y, t) &
r_capasity(x, y, t+1) = r_capasity(x, y, t) - 1);
∀ x, y, t (is_slot(x, y, t) & r_capasity(x, y, t) > 0 → is_route(x, y, t);
∀ x, y, t (is_route(x, y, t) & ncrews(x, t) = 0 → delay(x, t) & delay_reason(x, t) = ”no engine crews”);
∀ x, y, t (is_route(x, y, t) & nloc(x, t) = 0 → delay(x, t) & delay_reason(x, t) = ”no locomotives”);

*Restrictions:*

$\neg \exists$ x, y, t (delay(x, t)& (is_route(x, y, t) $\vee$ is_slot(x, y, t)));

$\neg \exists$ x, y, t (is_route(x, y, t) & (r_capasity(x, y, t) < 0 $\vee$ s_capasity(x) < 0));

$\neg \exists$ x, y (is_track(x, y) & $\lambda$(x, y) > 0 & c_capasity(x, y) $\leq$ 0);

$\neg \exists$ x, y, t (is_route(x, y, t) & (delay_reason(x, t) = "no locomotives");

Note that if multimodal transportation is prototyped, as in [11], then the parameter transportation_type is added to the relations is_track, is_route, in the functions $\lambda$ and $\tau$.

## 5 Conclusion

The executability of the prototype specification – the automatic construction of a logical model of an object – a project, a process – plays a major role in automating decision analysis and diagnosing unforeseen situations. However, the execution of high-level specifications, including logical ones, can have exponential complexity estimates.

We use specifications in a first-order predicate calculus language that include equalities and negations and have computable semantics. A prototype consists of a set of domain objects, connections between them (relations) and their attributes (functions). The specification defines the rules (axioms) for determining them (setting values) and verifying the correctness of the results (prototype viability). We have identified sufficient conditions and, accordingly, subclasses of such specifications, the complexity of building prototypes and analyzers for which can be reduced to low-degree polynomials. The main difficulty is the interpretation of definitions. Systems were identified that are solvable in time $O(n \log_2 n)$ with linear memory $O(m)$, where $n$– is the power of the obtained relations, $m$– is the power of certainty of functions and relations.

The expressiveness of the obtained specification classes, as shown by practical use, is sufficient for prototyping in various subject areas, including transport systems and processes of the railway industry. Each axiom describes a local area, and automatic inference over their entire set gives a global picture of their mutual influence. This process can be compared with the self-organization of the system. The use of the concept of self-organization of railway traffic to determine the best management strategy is discussed in [14] as promising in artificial intelligence [15, 16].

## References

1. Sveda, M.: Executable specifications with rapid prototyping for embedded distributed systems. IFAC Proc. Vol. **36**(1), 49–54 (2003). https://doi.org/10.1016/S1474-6670(17)33714-X
2. Kanti Das, T., Adepu, S., Zhou, J.: Anomaly detection in industrial control systems using logical analysis of data. Comput. Secur. **96**, 101935 (2020). https://doi.org/10.1016/j.cose.2020.101935
3. Beneš, N., Fahrenberg, U., et al.: Logical vs. behavioural specifications. Inf. Comput. **271**, 104487 (2019). https://doi.org/10.1016/j.ic.2019.104487

4. Kovalev, S., Kolodenkova, A., Sukhanov, A.: Incremental structure-evolving intelligent systems with advanced interpretational properties. In: Kuznetsov, S.O., Panov, A.I., Yakovlev, K.S. (eds.) RCAI 2020. LNCS, vol. 12412, pp. 134–151. Springer, Cham (2020). https://doi.org/10.1007/978-3-030-59535-7_10
5. Henning, C.: Executable specifications for hypothesis-based reasoning with Prolog and constraint handling rules. J. Appl. Log. **7**(3), 341–362 (2009). https://doi.org/10.1016/j.jal.2008.10.004
6. Ghezzi, C., Mandrioli, D., Morzenti, A.: TRIO: a logic language for executable specifications of real-time systems. J. Syst. Softw. **12**(2), 107–123 (1990). https://doi.org/10.1016/0164-1212(90)90074-V
7. Chiang, C.: Automated rapid prototyping of TUG specifications using Prolog. Inf. Softw. Technol. **46**(13), 857–873 (2004). https://doi.org/10.1016/j.infsof.2004.03.001
8. Ural, H.: Specifications of distributed systems in Prolog. J. Syst. Softw. **11**(2), 143–154 (1990). https://doi.org/10.1016/0164-1212(90)90058-T
9. Guda, A.N., Ilicheva, V.V., Chislov, O.N.: Executable logic prototypes of systems engineering complexes and processes on railway transport. In: Abraham, A., Kovalev, S., Tarassov, V., Snasel, V., Vasileva, M., Sukhanov, A. (eds.) IITI 2017. AISC, vol. 680, pp. 161–170. Springer, Cham (2018). https://doi.org/10.1007/978-3-319-68324-9_18
10. Il'icheva, O., Ilicheva V.: Logic prototyping: approach and use cases. J. Phys. Conf. Ser. **2131**(3), 032002 (2021). https://doi.org/10.1088/1742-6596/2131/3/032002
11. Ilicheva, V.V., Guda, A.N.: Acyclic structures of transport processes in transportation management problems. In: Kovalev, S., Sukhanov, A., Akperov, I., Ozdemir, S. (eds.) IITI 2022. LNNS, vol. 566, pp. 303–313. Springer, Cham (2023). https://doi.org/10.1007/978-3-031-19620-1_29
12. Hidayati, L., De Jong, G., Whiteing, A.: A stochastic logistics model for Indonesia's national freight transport model: transport chain choice from the shipper perspective. Asian Transp. Stud. **10**, 100122 (2024). https://doi.org/10.1016/j.eastsj.2023.100122
13. Xie, G., Du, X., Li, S., Yang, J., Hei, X., Wen, T.: An efficient and global interactive optimization methodology for path planning with multiple routing constraints. ISA Trans. **121**, 206–216 (2022). https://doi.org/10.1016/j.isatra.2021.03.041
14. D'Amato, L., Naldini, F., et al.: Towards self-organizing railway traffic management: concept and framework. J. Rail Transp. Plan. Manag. **29**, 100427 (2024). https://doi.org/10.1016/j.jrtpm.2023.100427
15. Tsolaki, K., Vafeiadis, T., Tzovaras, D.: Utilizing machine learning on freight transportation and logistics applications: a review. ICT Express **9**(3), 284–295 (2023). https://doi.org/10.1016/j.icte.2022.02.001
16. Tang, R., De Donato, L., et al.: A literature review of Artificial Intelligence applications in railway systems. Transp. Res. Part C Emerg. Technol. **140**, 103679 (2022). https://doi.org/10.1016/j.trc.2022.103679

# Synthesis of an Extrapolator of State Parameters of Dynamic Processes in Intelligent Transport Systems Based on the Scientific and Methodological Apparatus of Reducing the Lagrange Problem to an Isoperimetric One

Andrey A. Kostoglotov, Vladimir O. Zekhtser, Anton S. Penkov(✉), and Marina O. Nakonechnaya

Rostov State Transport University, Rostov-on-Don, Russia
pencha_@mail.ru

**Abstract.** The work proposes the structure of an adaptive extrapolator based on a dynamic model of the evolution of state parameters of dynamic systems. It was obtained using the scientific and methodological apparatus of reducing the Lagrange problem to an isoperimetric one. The numerical simulation performed demonstrates the effectiveness of the proposed solution in comparison with a traditional extrapolator.

**Keywords:** extrapolator · estimation · dynamic system · boundary value problem · intellectualization · adaptation · synthesis

## 1 Introduction

Traffic management in conditions of rapid growth in freight and passenger traffic requires the creation of intelligent centralized multi-level control systems. Their task is not only to ensure the specified indicators of quality and safety of transportation, but also to save energy resources [1].

The Order of the Ministry of Transport of the Russian Federation No. AK-60-r dated March 25, 2020 contains a list of subsystems of the intelligent transport system (ITS), among which:

- subsystem of directive control of traffic flows;
- weather monitoring subsystem;
- subsystem for monitoring traffic flow parameters;
- subsystem for monitoring pedestrian traffic parameters;
- subsystem for monitoring environmental parameters;
- subsystem for providing priority travel.

The research was carried out at the expense of a grant from the Russian science foundation № 23-29-00812, https://rscf.ru/project/23-29-00812/.


S. Kovalev et al. (Eds.): IITI 2024, LNNS 1209, pp. 12–20, 2024.
https://doi.org/10.1007/978-3-031-77688-5_2

One of the most important criteria for the effectiveness of the functioning of each of these subsystems is the accuracy of forecasting the parameters of the state of the observed dynamic processes [2]. Historically, the accuracy of forecasting dynamic processes depends on the accepted model of the system, which in general is stochastic and nonlinear [3], which significantly complicates typical extrapolators based on deterministic models of constant velocity, constant acceleration and coordinated reversal [4].

Thus, the development of promising extrapolators in ITS subsystems is associated with the task of building an adaptive motion model that takes into account the physical characteristics and mode of motion of a dynamic system. As shown in [5], adaptive extrapolators are characterized by increased efficiency in predicting random processes in ITS. This effect is achieved due to the availability of adaptation parameters that determine a specific model of the process under study, providing an acceptable margin of error for the forecast [6].

In [7], an approach is used to synthesize the structure of a dynamic system model, which consists in considering unknown causal characteristics as forces that cause a dynamic system to move in phase space along an optimal trajectory in accordance with the accepted target functional. The key stage of the approach is to find non-negativity conditions for asynchronous variation of the extended functional, which is the result of convolution of the accuracy criterion and the action integral. This makes it possible to obtain the necessary conditions for the extremum of the target functional in the form of a boundary value problem [8] obtained on the basis of the reduction of the Lagrange problem to an isoperimetric one using the Hamilton action integral.

The set of trajectories, which are a quasi-optimal solution to the boundary value problem, defines the structure of the motion model in terms of differential equations and can be successfully used in the synthesis procedure of an adaptive extrapolator.

The aim of the study is to increase the accuracy of forecasting the evolution of the parameters of the state of dynamic systems in comparison with a typical extrapolator.

The scientific objective of the study is the synthesis of an adaptive extrapolator based on the scientific and methodological apparatus for reducing the Lagrange problem to an isoperimetric one and analyzing its effectiveness in predicting the evolution of the parameters of the state of dynamic systems over time.

## 2 Problem Formulation

The basis for constructing an extrapolator is a mathematical model of the dynamics of the process under study.

Using the Lagrange formalism, the equations of motion can be represented as

$$\begin{gathered}\sum_{k=1}^{n} a_{ks}\ddot{q}_k = -\sum_{k=1}^{n}\sum_{m=1}^{n}[k,m;s]\dot{q}_k\dot{q}_m \\ +\left(u_s - \frac{\partial\Phi}{\partial\dot{q}_s} - \frac{\partial\Pi}{\partial q_s}\right) = Q_s(\mathbf{q},\dot{\mathbf{q}},\mathbf{u}), \\ \overline{s=1,n},\ k=\overline{1,n},\ \mathbf{q}(t_0) = \mathbf{q}_0, \dot{\mathbf{q}}(t_0) = \dot{\mathbf{q}}_0,\end{gathered} \tag{1}$$

where $[k,m;s] = \frac{1}{2}\left(\frac{\partial a_{ks}}{\partial q_m} + \frac{\partial a_{ms}}{\partial q_k} - \frac{\partial a_{km}}{\partial q_s}\right)$ – Christoffel symbols of the first kind for the matrix of the quadratic form of kinetic energy,

$\mathbf{q}(t) = \left[q_1(t),\ q_2(t),\ \ldots, q_n(t)\right]^T$ – vector of generalized coordinates, $\mathbf{q} \in R^n$,
$Q_s(\mathbf{q}, \dot{\mathbf{q}}, \mathbf{u})$ – generalized power,
$a_{ks}$ – inertia coefficients,
$\mathbf{u}(t) = [u_1(t),\ u_2(t),\ \ldots, u_n(t)]^T$ – vector of control actions, $\mathbf{u} \in R^n$,
$\frac{\partial \Phi}{\partial \dot{q}_s}$ – dissipative generalized forces, $\Phi$ – dissipative function,
$\frac{\partial \Pi}{\partial q_s}$ – potential generalized forces, $\Pi$ – potential energy,
$n$ – number of degrees of freedom, $t_0$ – observation start time.

In addition to setting the parameters of the control laws, the quality of operation of such a fuzzy controller depends on how well the selected structure of the fuzzy output takes into account the changing operating conditions. Since the boundaries of the areas of different control modes are determined by the selected accessory functions, the quality of the controller depends on their type and parameters. In this regard, it is necessary to analyze the efficiency of the fuzzy controller with various accessory functions.

Using model (1) to construct an extrapolator, taking into account the completeness and detail of the description of the evolution of the parameters of the object under study, is a rather difficult task, and such a model has not been widely used in the practice of statistical synthesis.

A mathematical model is usually built on the principle of minimum complexity with the criterion of ensuring a given adequacy of the description of the process under study.

One of the possible approaches to solving the problems of building models of controlled systems without using linear approximation is the principle of decomposition. The essence of this principle is to eliminate the dynamic interaction between the elements, to set the system in motion in the decomposition mode, providing a given value of the functional characterizing the quality of the state estimation process. Thus, the considered nonlinear multi-connected dynamical system of high order begins to move after a finite time interval due to the simplest system [9]. This fact can be used to build a model of the system under study.

Let's consider a variant of constructing a model of object motion in the plane in the presence of two degrees of freedom with the following assumption: the formal attribution of part of the energy to the work of generalized forces allows us to introduce the simplest definitely positive quadratic form of velocities, which is interpreted as the kinetic energy of the system (1)

$$T = \frac{1}{2}\dot{\mathbf{q}}^T \mathbf{A} \dot{\mathbf{q}}, \tag{2}$$

where $\mathbf{A} = \begin{bmatrix} a_{11} & 0 \\ 0 & a_{22} \end{bmatrix}$ is a diagonal matrix of quadratic form,

$a_{ss}$ is a inertia coefficients, $\mathbf{q} = \left[q_1\ q_2\right]^T$, $^T$ – transposition sign.

This form is used later to build a model of the dynamics of the evaluated process.

Equation (1) can be written in the compact form of Lagrange equations of the second kind

$$\frac{d}{dt}\left(\frac{\partial T}{\partial \dot{q}_s}\right) + \frac{\partial T}{\partial q_s} = Q_s,\ \ s = 1, 2 \tag{3}$$

or taking into account (2)

$$a_{ss}\ddot{q}_s = Q_s, \quad s = 1, 2. \tag{4}$$

It is known that Eq. (3) is an extremal of the action functional

$$S = \int_{t_0}^{t_1} (T + A)dt \to \min,$$

where $A$ is the work of generalized forces $Q_s$, $s = 1, 2$.

If the coordinates in which observations are made are selected as generalized coordinates, then

$$\mathbf{z} = \mathbf{q} + \mathbf{v}, \quad \mathbf{z} = \left[ z_1 \; z_2 \right]^T, \tag{5}$$

where $\mathbf{z}(t)$ is the measurement vector, $\mathbf{z}(t) \in R^2$,

$\mathbf{v}(t) \in R^2$ is a random effect with local characteristics

$$M\left[\mathbf{v}(t)\right] = 0,$$

$$M\left[\mathbf{v}(t)\mathbf{v}^T(t)\right] = \mathbf{N}\delta(t - \tau),$$

$\mathbf{N} = \begin{bmatrix} N_{11} & 0 \\ 0 & N_{22} \end{bmatrix}$ is a weight matrix characterizing the intensity of interference in the observation channel.

Let's build a mathematical model of motion taking into account information about the accuracy characteristics of the observation channel:

$$J = \frac{1}{2}\int_{t_0}^{t_1} (\mathbf{z} - \hat{\mathbf{q}})^T \mathbf{N}^{-1} (\mathbf{z} - \hat{\mathbf{q}})dt = \int_{t_0}^{t_1} F(\hat{\mathbf{q}})dt = D = const, \tag{6}$$

where D is the weighted error of the measurement results of the observation channels, the sign ^ means an estimate.

This means that the trajectory of movement must satisfy the extremum of the extended functional action

$$S^* = \int_{t_0}^{t_1} [\lambda(T + A) + F]dt \to \min, \tag{7}$$

$\lambda$ is an indefinite Lagrange multiplier.

## 3 Synthesis of a Dynamic System Model

The analysis of the variation of the extended functional (7) carried out in [8] shows that the set of trajectories for which (6) is performed satisfies the following boundary value problem [7]

$$\begin{cases} \frac{d}{dt}\left(\frac{\partial T}{\partial \dot{q}_s}\right) + \frac{\partial T}{\partial q_s} = \lambda^{-1}\left[\mu_s(q_s, \dot{q}_s)\dot{q}_s + \frac{\partial F}{\partial q_s}\right], \\ \left[(A - T) + \lambda^{-1}F\right]\Big|_{t_0}^{t_1} = 0, \end{cases} \quad s = 1, 2, \tag{8}$$

where $\mu$ – synthesizing function.

The exact solution of problem (8), as the solution of any boundary value problem, presents significant difficulties, therefore, consider the option when $A = 0$ that corresponds to the approximate (forecast) movement in the decomposition mode, then

$$T = \lambda^{-1} F, \tag{9}$$

or taking into account (2)

$$\dot{\mathbf{q}}^T \mathbf{A} \dot{\mathbf{q}} = \lambda^{-1} (\mathbf{z} - \mathbf{q})^T \mathbf{N}^{-1} (\mathbf{z} - \mathbf{q}). \tag{10}$$

The ratio (10) allows you to write down the kinematic coupling equations that are performed on the trajectory of the proposed model

$$|\dot{q}_s| = \sqrt{\lambda^{-1} a_{ss}^{-1} N_{ss}^{-1}} |z_s - q_s|, \ \ s = 1, 2, \tag{11}$$

where $N_{ss}$ are the elements of the diagonal matrix.

Then the adaptive motion model can be written in the form [7]

$$\frac{d}{dt}\left(\frac{\partial T}{\partial \dot{q}_s}\right) + \frac{\partial T}{\partial q_s} = -\sqrt{\eta_s}\dot{q}_s + \eta_s (z_s - q_s), \ \ s = \overline{1, n}, \tag{12}$$

where $\eta_s = \lambda^{-1} a_{ss}^{-1} N_{ss}^{-1}$ is the adaptation parameter.

## 4 Synthesis of an Adaptive Extrapolator

The motion model (12) can be constructed on the basis of real data, taking into account criterion (6). Then, for the class of systems under consideration, the model of the evolution of the state vector $\mathbf{x}(t)$ for each degree of freedom of a dynamic system has the form [7]

$$\dot{\mathbf{x}}(t) = \mathbf{F}\mathbf{x}(t) + \mathbf{G}w(t), \ \ \mathbf{x}(t_0) = \mathbf{x}_0, \tag{13}$$

where $\mathbf{x}(t) = \begin{bmatrix} x_1(t) \\ x_2(t) \end{bmatrix} = \begin{bmatrix} q(t) \\ \dot{q}(t) \end{bmatrix}$ is the state vector,

$\mathbf{F} = \begin{bmatrix} 0 & 1 \\ 0 & -\sqrt{\eta} \end{bmatrix}$ is the transition matrix of the state,

$\mathbf{G} = \begin{bmatrix} 0 \\ \eta \end{bmatrix}$ is the perturbation vector,

$w(t)$ is the standard white Gaussian status noise.

The deterministic component of the model (13) determines the structure of the extrapolator

$$\dot{\mathbf{x}}(t) = \mathbf{F}\mathbf{x}(t), \tag{14}$$

the transition matrix of which, unlike the traditional model of rectilinear uniform motion, has an adaptation parameter that allows taking into account the physical characteristics for various modes of operation of a dynamic system.

The implementation of an extrapolator using digital information processing processors implies its operation in discrete time. This fact determines the need for a finite-dimensional approximation (14).

It is known that the solution of Eq. (14) has the form

$$\mathbf{x}(t) = \mathbf{A}(t)\mathbf{x}(0), \tag{15}$$

where $\mathbf{A}(t) = e^{\mathbf{F}t}$ is the fundamental matrix of solutions.

The fundamental matrix can be represented as a series

$$\mathbf{A}(t) = \mathbf{I} + \sum_{m=1}^{\infty} \frac{\mathbf{F}^m t^m}{m!}. \tag{16}$$

where $\mathbf{I}$ is the unit matrix.

The fundamental matrix of the system (13), up to the second order, has the form

$$\mathbf{A}(t) = e^{\mathbf{F}t} \approx \begin{bmatrix} 1 & 0 \\ 0 & 1 \end{bmatrix} + \begin{bmatrix} 0 & t \\ 0 & -\sqrt{\eta}t \end{bmatrix} + \begin{bmatrix} 0 & -0.5\sqrt{\eta}t^2 \\ 0 & 0.5\eta t^2 \end{bmatrix} = \begin{bmatrix} 1 & t - 0.5\sqrt{\eta}t^2 \\ 0 & 1 - \sqrt{\eta}t + 0.5\eta t^2 \end{bmatrix} \tag{17}$$

The structure of a discrete adaptive extrapolator for each degree of freedom of the object [10]

$$\mathbf{x}(i) = \Phi(\eta)\mathbf{x}(i-1), \tag{18}$$

$$\Phi(\eta) = \begin{bmatrix} 1 & \Delta t - 0.5\sqrt{\eta}\Delta t^2 \\ 0 & 1 - \sqrt{\eta}\Delta t + 0.5\eta\Delta t^2 \end{bmatrix}. \tag{19}$$

where $\Delta t$ is the sampling period.

The choice of a parameter $\eta$ minimizing criterion (6) makes it possible to increase the accuracy of forecasting the evolution of the parameters of a dynamic system.

## 5 Analysis of the Effectiveness of the Proposed Solution and the Prospects for Intellectualization

Let's consider a model example of forecasting using a discrete adaptive extrapolator (18). The trajectory of the aircraft during a 45-s maneuver, obtained using a broadcast-type automatic dependent observation system at various sampling periods $\Delta t$, was taken as the initial data.

Numerical simulation of the extrapolation process for each reference is performed using the proposed expression (18) and an extrapolator based on the model of rectilinear uniform motion, which is traditionally used in various forecasting systems. The results are shown in Fig. 1.

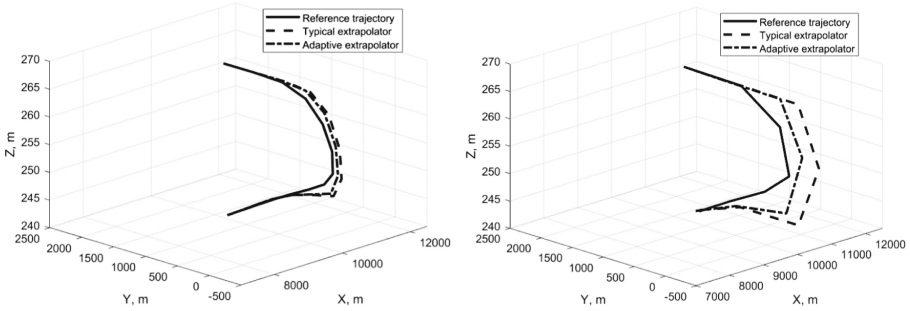


**Fig. 1.** Simulation results (a – with $\Delta t = 2\ s$, b – with $\Delta t = 6\ s$)

For small values $\Delta t$, the difference in the forecasts of the extrapolators is insignificant, however, with an increase in the sampling period, the adaptive extrapolator provides an increase in the accuracy of forecasting. The result is achieved due to the presence in the structure of the adopted model of a parameter that takes into account the dynamic characteristics and mode of motion of the aircraft.

The presence of a parameter in the structure of the accepted motion model implies carrying out a procedure for its adaptation at the stage of developing an extrapolator according to criterion (6). Due to the unpredictable characteristics of disturbances and the nonlinearity of the initial model of the dynamic system, a rational solution is to use a neural network identifier to determine the adaptation coefficient.

When building a neural network, one of the priority tasks is the formation of a representative training sample characterizing the behavior of the simulated dynamic system [11]. Such a sample can be formed by long-term registration of dynamic system parameters at certain intervals and subsequent normalization and preprocessing of data [2].

The results of the research published in [12], an adaptive extrapolator in combination with a neural network identifier (Fig. 2) can be successfully used in the structure of algorithms for estimating the parameters of dynamic systems operating under conditions of a priori unknown external influences.

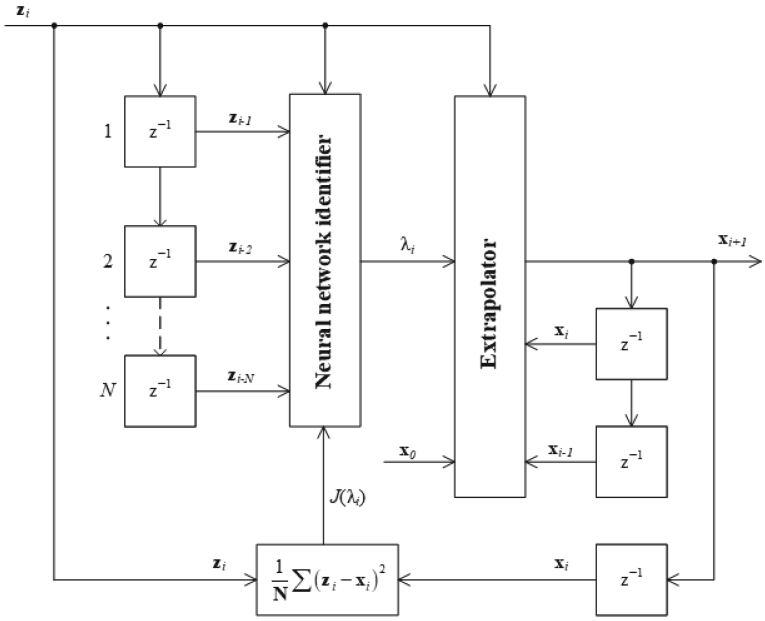


**Fig. 2.** Block diagram of a neural network extrapolator

## 6 Conclusions

The accuracy of forecasting the evolution of the parameters of dynamic systems in ITS subsystems is one of the most important criteria determining the effectiveness of ITS functioning as a whole.

The use of an adaptive extrapolator is advisable in the task of predicting the evolution of state parameters of stochastic nonlinear dynamical systems.

The motion model obtained using an approach based on the reduction of the Lagrange problem to an isoperimetric one can be used in the synthesis of the structure of an adaptive extrapolator taking into account the physical characteristics and mode of motion of a dynamic system.

The results of the numerical simulation confirm the effectiveness of the proposed solution, providing an increase in the accuracy of predicting the evolution of the parameters of the dynamic system by an average of 5–20% relative to the extrapolator based on the traditional motion model, depending on the sampling period.

## References

1. Alekseev, V.M., et al.: Building the architecture of an intelligent control system for urban rail transport system. World Transp. **19**(1(92)), 18−46 (2021)
2. Alamir, H.A., Zarganyan, E.V., Zarganyan, Yu.A.: A model for predicting traffic flow based on neural networks for predicting traffic on roads. Bull. South. Federal Univ. Tech. Sci. (6(223)), 124−132 (2021)

3. Sayed, A.S., Yasser, A.-H., Hesham, A.H.: Artificial intelligence-based traffic flow prediction: a comprehensive review. J. Electr. Syst. Inf. Technol. **10**(1), 1–42 (2023)
4. Li, X., Jilkov, V.: A survey of maneuvering target tracking - Part III: measurement models. In: Proceedings of SPIE, vol. 4473, pp. 423−446 (2001)
5. Baranov, L.A.: Adaptive extrapolator of nonstationary random processes. Electr. Eng. (9), 22−25 (2023)
6. Balakina, E.P., Baranov, L.A., Zhang, Y.: Analysis of forecast errors for intelligent control systems and predictive diagnostics. Dependability **23**(2), 12–18 (2023)
7. Andrashitov, D.S., et al.: A method for synthesizing tracking algorithms using a shaping filter and quasi-optimal laws for controlling maneuvering objects. Radio Eng. **87**(2), 93–104 (2023)
8. Kostoglotov, A.A., Lazarenko, S.V.: Method of quasi-optimal synthesis of control laws based on the reduction of the Lagrange problem to the isoperimetric problem using asynchronous variation. J. Comput. Syst. Sci. Int. **60**(6), 843–852 (2021)
9. Pyatnitskii, E.S.: Decomposition principle in mechanical control systems. Soviet Math. Doklady **33**(5), 345–346 (1988)
10. Kostoglotov, A.A., Penkov, A.S.: Quasi-optimal control laws based on the reduction of extreme tasks in dynamic algorithms for estimating the position of maneuvering objects. Bull. High. Educ. Inst. North-Cauc. Reg. Ser. Nat. Sci. (3(219)), 23−33 (2023)
11. Osovsky, S.: Neural Networks for Information Processing. Finance and Statistics, Moscow (2002)
12. Kostoglotov, A.A., et al.: Synthesis of an intelligent algorithm for estimating the orientation of mobile transport infrastructure objects based on a multiparametric identifier. Bull. Rostov State Transp. Univ. (1(89)), 144−151 (2023)

# Using State Transition Diagrams for Automated Knowledge Base Construction

Nikita O. Dorodnykh(✉) and Aleksandr Yu. Yurin

Matrosov Institute for System Dynamics and Control Theory, Siberian Branch of Russian Academy of Sciences (ISDCT SB RAS), Irkutsk, Russia
{nikidorny,iskander}@icc.ru

**Abstract.** The development of domain-specific intelligent systems is one of the key directions in modern information technologies. At the same time, automation of knowledge base engineering for these systems is one of the most relevant and promising areas in the field of artificial intelligence. Especially when it comes to using already accumulated information, presented, in particular, in the form of conceptual models. We propose an approach and software for automating the creation of knowledge bases using the analysis and transformation of conceptual models in the form of state transition diagrams. The proposed approach is based on the identification of structural elements of diagrams and their mapping into constructions of a target knowledge representation language. The main stages of the approach and implementation are described. An illustrative example of converting state transition diagrams to form a failure analysis plan is presented.

**Keywords:** knowledge engineering · knowledge acquisition · knowledge base · ontology · state transition diagram · model transformation · code generation · rules

## 1 Introduction

Intelligent system engineering is a promising direction in the field of information technology. Intelligent systems can be used to solve complex and weakly formalized tasks in the fields of medicine [1], energy [2], industry [3], natural and technogenic safety [4, 5]. As a rule, a knowledge base is the core component of such systems. It contains formalized domain knowledge presented in the form of rules, ontologies or knowledge graphs, etc. However, the creation of effective methods and tools for knowledge base engineering has not yet been fully solved so far. Therefore, research aimed at developing new methods of information processing for creating elements of knowledge-based systems when solving practical problems in various domains is relevant.

Today, various specialized editors are used to develop knowledge bases; these tools allow one to present a formalized description of domain concepts and structures of knowledge base in a specific knowledge representation language [6]. However, such systems have low integration ability with visual modeling tools and knowledge interpretation modules. As a rule, they can only support a single knowledge representation language.


S. Kovalev et al. (Eds.): IITI 2024, LNNS 1209, pp. 21–32, 2024.
https://doi.org/10.1007/978-3-031-77688-5_3

Moreover, these editors are aimed at advanced specialists (e.g., knowledge engineers, programmers) and are not focused on domain experts, who are the main source of practical knowledge and professional experience. This fact gives rise to the problem of transferring domain-specific non-formalized knowledge (competencies) from a domain expert to a knowledge base.

In this paper, we propose a new approach and software, namely the Knowledge Modeling System (KMS) [7], which supports knowledge modeling in state transition diagrams [8]. The main feature of our approach and tool is support for generating knowledge base codes based on constructed diagrams. Logical rules, decision tables [9], and ontologies are selected as target knowledge representation formalisms. In particular, we used CLIPS (C Language Integrated Production System) [10] and OWL (Web Ontology Language) [11] as the main knowledge representation languages. The proposed approach and software for knowledge base prototyping were applied to solve tasks in the field of technogenic safety provision.

The paper is organized as follows: Sect. 2 presents the state of the art of research. Section 3 describes the proposed approach and its implementation. Section 4 describes a case study for a practical task. Section 5 presents a discussion of the obtained results, while the Conclusions present concluding remarks.

## 2 The State of the Art

Currently, different conceptual models (e.g., concept or mind maps, event and failure trees, fishbone diagrams, semantic models, etc.) are actively used at the stages of knowledge extraction and structuring. These models have a system-wide orientation and are focused on knowledge systematization or decision-making support [12]. Conceptual models are a convenient and understandable way to represent knowledge for a domain expert. State transition diagrams (or statechart diagrams) [8] are an example of a conceptual model that is used to model the behavior of a system depending on its states and external influences. Each such diagram is a graph, where nodes are system states and arcs (transitions) are events or actions that lead to a change in a system state. The diagram may also indicate conditions that are met at each transition. A state transition diagram is used to design and analyze complex systems such as software, hardware devices, business processes, and others. It helps to understand the logic of a system and identify possible errors in its operation. A state transition diagram can also be used to document an already existing system or process. In general, this diagram is a very useful tool for any project or task where it is necessary to clearly define the sequence of actions and system states.

Various software tools, in the form of visual editors, are used to build state transition diagrams. Such editors are usually presented both as desktop applications and web services, in particular, Flexberry Designer [13], Visual Paradigm Online [14], Enterprise Architect [15], and EASE: State diagram editor [16]. These tools facilitate the development of visual diagrams of varying degrees of abstraction, corresponding to domain knowledge. However, they are not intended for knowledge base engineering and therefore cannot ensure the completeness of the development process from conceptual models to formalized code in a specific knowledge representation language. This feature makes

it difficult to practically use the constructed diagrams for the automated formation of knowledge bases in intelligent system engineering.

Thus, our motivation is to increase the efficiency of knowledge base engineering based on the automated analysis and transformation of state transition diagrams. For this purpose, we proposed an approach to support visual knowledge modeling for domain experts, including the ability to generate knowledge base codes based on constructed state transition diagrams.

## 3 The Proposed Approach

### 3.1 Problem Statement

The problem of state transition diagram analysis and conversion into a knowledge base can be reduced to the task of model transformation [17]. The model transformation is one of the major components of the Model-Driven Development [18]. In general, model transformation is the process of generating a target model from a source model, according to some set of transformation rules. In this case, a transformation rule describes how one or more constructs in a source modeling language can be mapped to one or more constructs in a target modeling language [19].

Thus, the problem statement can be formalized as follows:

$$T : CM^{STD} \rightarrow KB, \tag{1}$$

where $T$ is a transformation operator of a source conceptual model into a target knowledge base; $CM^{STD}$ is a source conceptual model in the form of a state transition diagram (STD); $KB$ is a target knowledge base; and: $KB = \langle Code^{CLIPS}, Code^{DT}, Code^{OWL} \rangle$.

We propose a specialized approach and software system (KMS) to solve this problem. Next, let's take a closer look at this approach and system.

### 3.2 State Transition Diagram Structure

State transition diagrams are one of the powerful means for system behavior modeling and documentation. They are a graphical representation of a sequence of system states (*nodes*) and transitions between them (*arcs*) under certain events (*conditions*). Each transition is described by an event that causes a change in the system state. At the same time, states and transitions may have certain properties (*characteristics*). These diagrams also show the beginning and end of state transitions, depending on the implementation specifics (e.g., in UML). An abstract example of a state transition diagram containing all the main elements is presented in Fig. 1.

The main features of state transition diagrams are:

1. They make it easy to represent the system behavior in the form of a sequence of states and transitions between them.
2. These diagrams can be used to model both simple and complex systems.
3. They help identify possible errors in the operation of existing systems at the design stage.

4. Such diagrams can be used to document the operation of existing systems to facilitate understanding of their operation and simplify the debugging process.
5. They can also be used to create test scenarios, check system functionality, or assess risk.

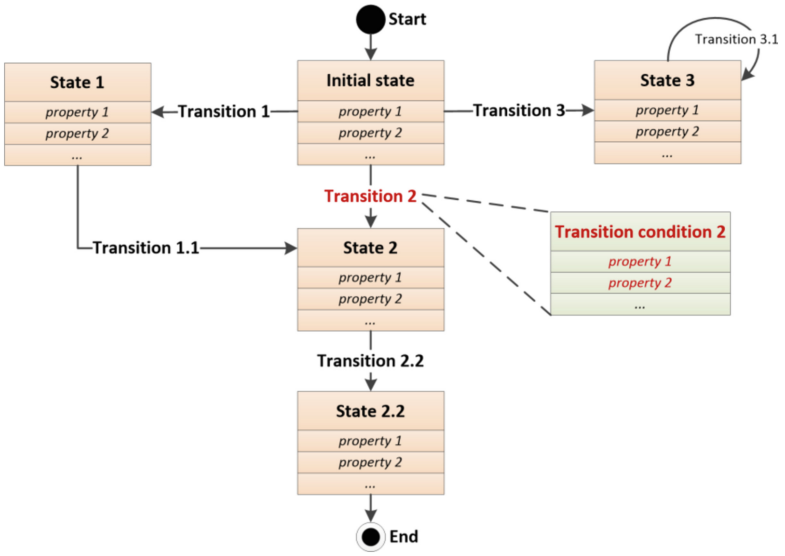


**Fig. 1.** An abstract example of a state transition diagram.

We have built a metamodel (*abstract syntax*) of a state transition diagram that defines in abstract form the main concepts of this diagram (Fig. 2). The constructed metamodel corresponds to the Ecore meta-metamodel [20], and it is further used as a source metamodel when developing transformation rules that describe the correspondence between elements of this metamodel and a target knowledge base metamodel.

Currently, there is no generally accepted unified format or standard of text notation for representing state transition diagrams. Therefore, we took into account the specifics of these diagrams and decided to develop our own specification format for the serialization of state transition diagrams using the XML language. A description of the developed XML format (*concrete syntax*) for state transition diagrams is presented in Table 1.

### 3.3 Main Stages

To solve problem (1), we specialize a generalized algorithm for the transformation of conceptual models into knowledge base code, described in [21]. Thus, our main task is to transform source state transition diagram elements, presented in XML format, into target knowledge base elements.

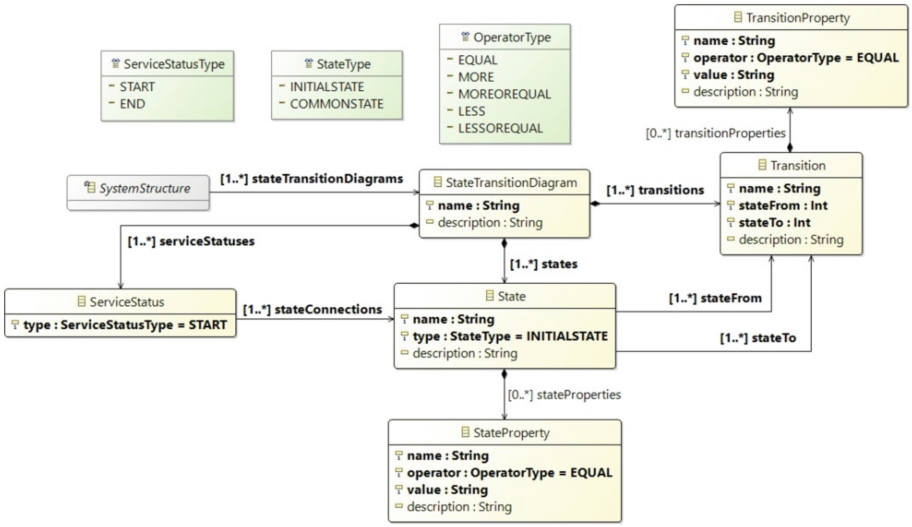


**Fig. 2.** A metamodel of a state transition diagram.

**Table 1.** Description of the XML format for representing state transition diagrams.

| Tag name | Tag attribute names | Description |
|---|---|---|
| <Diagram> | id, name, description | *A general description of a state transition diagram* |
| <State> | id, name, type, description | *Information about the system's state. It also contains a state type with two possible values: "initial state" and "common state"* |
| <StateProperty> | id, name, operator, value, description | *Information about the property of the system state. It also contains an operator ("=", ">", "<", ">=", and "<=") and a possible property value* |
| <Transition> | id, state-from, state-to, name, operator, description | *Information about the transition from one state to another* |
| <TransitionProperty> | id, name, operator, value, description | *Information about the property (condition) of the transition. It also contains an operator and a possible value for the transition condition* |

This algorithm can be presented as a sequence of actions (Fig. 3):

**Stage 1:*Visual construction of the state transition diagram.*** A non-programming user (domain expert) constructs a source state transition diagram using a specific graphical

editor called State Transition Diagram Editor (STDE), which is part of KMS. This diagram describes the sequence of state transitions in a certain system.

**Stage 2:*Representation of the state transition diagram in XML format.*** The constructed diagram is serialized in XML format using the developed specification (Table 1).

**Stage 3:*Analysis of the XML format.*** The XML structure of a source state transition diagram is analyzed. As a result, diagram elements and their relationships are extracted.

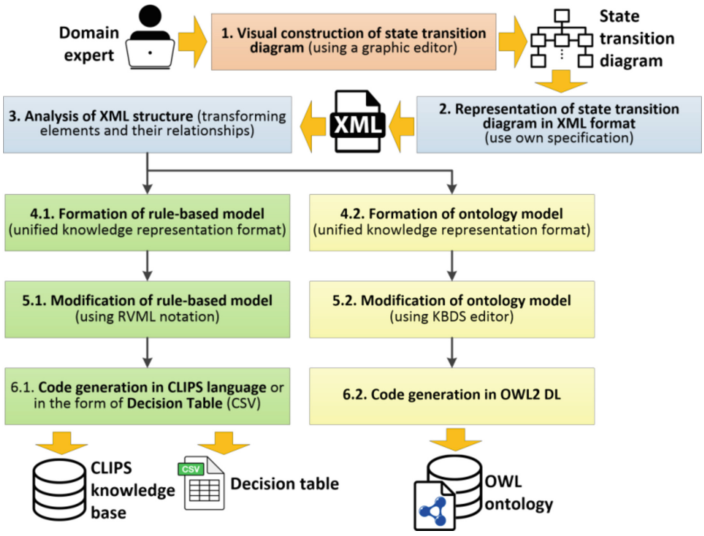


**Fig. 3.** Main stages of the proposed approach.

**Stage 4:** ***Generation of a unified knowledge representation model.*** A rule-based model or ontology model (the user selects the required one) is automatically formed based on the extracted diagram elements. These models are used as a universal abstract means for representing domain knowledge, which is independent of a target knowledge representation language (e.g., CLIPS, Jess, Drools, SWRL, OWL, and RDF) or a source of models.

**Stage5:** ***Modification of the unified knowledge representation model.*** At this stage, the user can modify the received models and also check their correctness. A rule-based model is modified using a graphical notation called Rule Visual Modeling Language (RVML) [22]. An ontology model is modified using the Knowledge Base Development System (KBDS) [23].

**Stage 6:** ***Knowledge base code generation.*** A rule-based model is generated either into a target decision table in CSV format or into a target code in CLIPS format. An ontology model is generated in OWL2 DL format.

Thus, let's clarify the transformation operator (1):

$$T = \langle T_{CM-RM}, T_{RM-RKB}, T_{CM-OM}, T_{OM-OKB} \rangle,$$
$$T_{CM-RM} : CM_{XML}^{STD} \rightarrow RM, T_{RM-RKB} : RM \rightarrow RKB, RKB = \langle Code^{CLIPS}, Code^{DT} \rangle,$$
$$T_{CM-OM} : CM_{XML}^{STD} \rightarrow OM, T_{OM-OKB} : OM \rightarrow Code^{OWL},$$

where $T_{CM-RM}$ is an operator for converting a source conceptual model in the form of a state transition diagram into an unified rule-based model; $T_{RM-RKB}$ is an operator for converting an unified rule-based model into a target knowledge base code in CLIPS format or a target decision table in CSV format; $CM_{XML}^{STD}$ is a representation of a source state transition diagram in XML format; $RM$ is an unified presentation of acquired knowledge in the form of a rule-based model; $Code^{CLIPS}$ is a target knowledge base code in CLIPS language; $Code^{DT}$ is a target decision table in CSV format; $T_{CM-OM}$ is an operator for converting a source conceptual model in the form of a state transition diagram into an unified ontology model; $T_{OM-OKB}$ is an operator for converting an unified ontology model into a target ontology code in OWL2 DL format; $OM$ is a unified presentation of acquired knowledge in the form of an ontology model; $Code^{OWL}$ is target ontology code in OWL language.

Transformation rules for all four operators are described in terms of the domain-specific language called Transformation Model Representation Language (TMRL) [24]. TMRL constructs make it possible to describe the elements of the conversion scenario in a declarative form. In particular, this scenario includes rules for describing the correspondences between elements of a source metamodel of state transition diagrams and a target metamodel of a unified model for knowledge representation or representation knowledge language. Specific examples of correspondence between the main elements of a state transition diagram, rule-based model, and CLIPS language are presented in Table 2.

**Table 2.** Specific examples of rules for the correspondences between elements.

| State Transition Diagram | Rule-based model | CLIPS |
|---|---|---|
| Diagram | Model | – |
| State | FactTemplate/Fact | Deftemplate |
| StateProperty | Slot | (slot " *<name>*") |
| Transition | RuleTemplate/Rule | defrule |
| Transition (state-from) | FactTemplate/Condition | deftemplate/defrule (*consequent*) |
| Transition (state-to) | FactTemplate/Action | deftemplate/defrule (*antecedent*) |

Specifications created on TMRL satisfy the requirements of accuracy, clarity and completeness. These specifications contain all the necessary information to solve the task, all model elements are well formalized, and the specifications are quite compact and at the same time understandable (readable). This fact provides a sufficiently high performance for the proposed conversion approach.

### 3.4 Implementation

The proposed approach is implemented in the form of web software called Knowledge Modeling System (KMS) [7]. KMS is developed in PHP 8 using the Yii2 framework and PostgreSQL 15. KMS has a client-server architecture and is aimed at non-programming users (e.g., domain experts, data analysts).

KMS includes two graphical editors:

- *Extended Event Tree Editor (EETE)* is a graphical editor for the visual modeling of semantic tree structures in the form of classic or extended event trees [25].
- *State Transition Diagram Editor (STDE)* is a graphic editor for the visual modeling of state transition diagrams.

Main functions of KMS are the following:

- CRUD API for projects that involve working with various diagrams.
- CRUD API for event tree diagrams (both classic and extended) and state transition diagrams within a specific project.
- Import and export diagrams as serialized files in XML format.
- Automatic transformation of diagrams into unified models (a rule-based model and an ontology).
- Export constructed models into files in CLIPS and OWL2 DL formats or spreadsheets in CSV format.

KMS supports two types of users:

- *Registered user* can create and manage their own diagram projects, as well as open diagram projects.
- *Administrator* can create and manage all diagram projects in the system, as well as register new users.

The implementation of these types is carried out using the incorporation of Role-Based Access Control (RBAC) into the KMS architecture. RBAC ensures data privacy and aligns KMS usage with organizational policies and compliance mandates through controlled access mechanisms. This methodical approach to managing data access significantly advances the security of KMS, providing a structured framework that supports secure and efficient operations across various levels of user engagement. Moreover, we use hashing of all user data in MD5 format when storing it in the database.

## 4 Case Study

Let's consider an example of the automated formation of a knowledge base using state transition diagrams. In [26], we developed a program in the form of a chain of steps that facilitates the computer-aided failure analysis of petrochemical technical systems. In particular, the program on CLIPS was generated from a state transition diagram (Fig. 4) accounting for a model of technical states' dynamics and a failure analysis algorithm. A rule-based model (Fig. 5) was generated based on the extracted elements from the XML structure of this state transition diagram. The resulting rule-based model was converted to knowledge base code in the CLIPS language (Fig. 6).

The developed knowledge base was filled with specific facts extracted from tables. These tables were obtained as a result of the automatic analysis of industrial safety inspection reports. We used the TabbyLD tool [27] to semantically annotate the source tables and extract facts from the annotated tabular data.

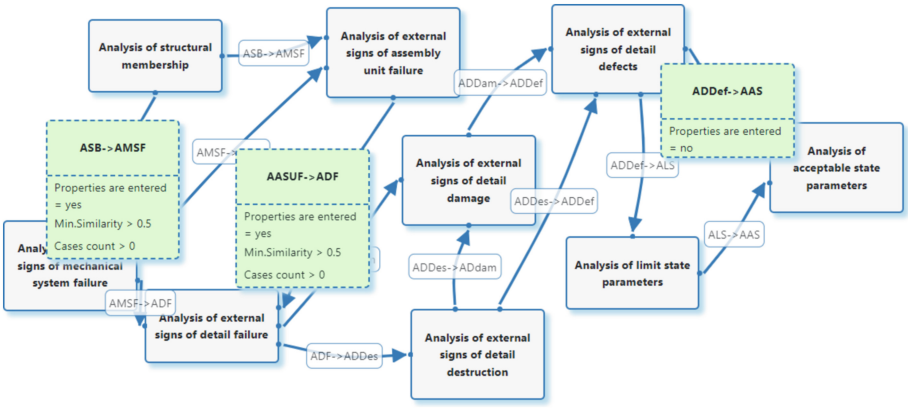


**Fig. 4.** An example of a state transition diagram fragment describing a failure analysis algorithm.

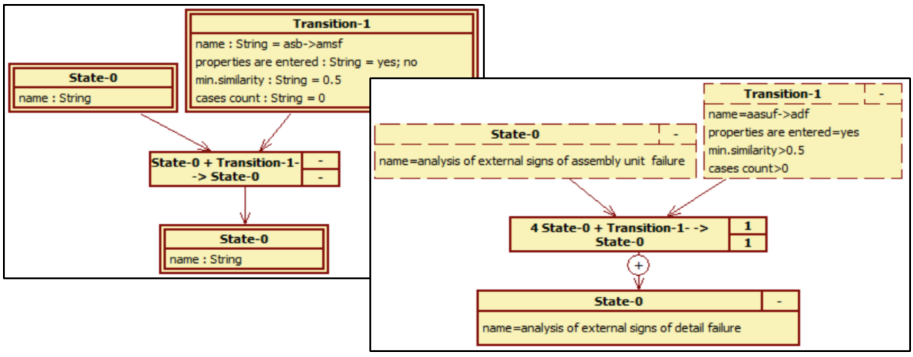


**Fig. 5.** A fragment of the resulting rule-based model in the form of RVML diagrams: a rule template and an example of a specific rule.

```
;********************* Templates ******************************
(deftemplate State-0
 (slot name)
)
(deftemplate Transition-1
 (slot name (default "ASB->AMSF"))
 (slot properties-are-entered)
 (slot minsimilarity (default "0.5"))
 (slot cases-count (default "0"))
)
;************************ Facts *******************************
(deffacts initial-settings
 (State-0 ;State-0
  (name "ANALYSIS OF STRUCTURAL MEMBERSHIP")
 )
)
```

```
(defrule 4-State-0+Transition-1->State-0
 (declare (salience 1))
  (State-0 ;State-0
   (name "ANALYSIS OF EXTERNAL SIGNS OF ASSEMBLY UNIT FAILURE")
  )
  (Transition-1 ;Transition-1
   (name "AASUF->ADF")
   (properties-are-entered "YES")
   (minsimilarity "0.5")
   (cases-count "0")
  )
=>
(assert
 (State-0 ;State-0
  (name "ANALYSIS OF EXTERNAL SIGNS OF DETAIL FAILURE")
 ))
```

**Fig. 6.** A fragment of an obtained CLIPS code.

## 5 Discussion

The development of rule-based knowledge bases and ontologies for different intelligence systems remains a complex process that requires in-depth knowledge, both in the field of software engineering and in the domain. Moreover, the use of principles of visual domain-specific modeling and accumulated information, in particular, in the form of conceptual models, is relevant. KMS shows new possibilities for knowledge base engineering. Existing approaches and software solutions (e.g., Expert System Designer [28], Exsys [29], ES-Builder [30], Protégé [31]) provide even nonprogrammers with the ability to develop knowledge bases, but they do not enable the use of conceptual models in the form of different visual diagrams. In contrast to them, KMS uses domain models, in particular state transition diagrams and extended event tree diagrams, as the main information source about domain concepts and their relationships. On the other side, there are special editors for modeling chains of states in the form of specific diagrams [13–16]. These systems do not imply further use of knowledge contained in the diagrams created by domain experts and do not provide a way to generate codes of knowledge bases in any knowledge representation language using the created diagrams. Also, it should be noted that, at the moment, there are no standards and specifications for the serialization of state transition diagrams, and each editor for their modeling uses their own storage format. We suggest using the XML format because it is the universal and most common way of integrating software systems and ensuring the exchange of information between applications today.

KMS is a sufficiently flexible and easily scalable system for the development of knowledge bases of varying complexity. This fact is confirmed by two real-life practical cases. In one case, KMS was applied to generate a code of rule-based knowledge base for predicting the degradation processes of petrochemical equipment and to support Industrial Safety Inspection (ISI) tasks. State transition diagrams made it possible to present the cause-and-effect formation and development of degradation processes in the form of logical rules and helped to solve the forecasting problem in an automated mode. In another case, it facilitated the generation of ontologies to support the process of aviation equipment troubleshooting [32]. KMS was used to design state transition diagrams for describing two types of dependencies: (1) between the external manifestations of failure and the causes; and (2) between troubleshooting operations.

Thus, we believe that KMS can be used for prototyping knowledge bases for different domain-specific intelligence systems.

## 6 Conclusions

In this paper, we propose an approach for the automated development of knowledge bases using conceptual models in the form of state transition diagrams. The proposed approach is based on the analysis of structural elements of diagrams and their transformation into constructions of a target rule-based or ontological knowledge representation language. This approach minimizes programming errors at the stage of knowledge formalization due to automatic code generation and reduces the time spent on knowledge base engineering. It also opens up the opportunity to directly involve domain experts in the development process of knowledge base prototypes, allowing them to create program code using domain-specific models that are understandable to them. The proposed approach is implemented in the form of web-based software (KMS), which can be used to model domain knowledge and generate codes of knowledge bases for various intelligent systems.

The reported study was supported by the Ministry of Education and Science of the Russian Federation (Project no. 121030500071-2 "Methods and technologies of a cloud-based service-oriented platform for collecting, storing and processing large volumes of multi-format interdisciplinary data and knowledge based upon the use of artificial intelligence, model-driven approach and machine learning") and by the Council for Grants of the President of Russia (grant No. SP-978.2022.5).

## References

1. Alam, F., Giglou, H.B., Malik, K.M.: Automated clinical knowledge graph generation framework for evidence based medicine. Expert Syst. Appl. **233**, 120964 (2023)
2. Zhang, L., Su, H., Zio, E., Jiang, L., Fan, L., Zhang, J.: A graph structure feature-based framework for the pattern recognition of the operational states of integrated energy systems. Expert Syst. Appl. **213**, 119039 (2023)
3. Zhang, J., Pu, X., Zhao, R., Li, J., Nie, Z.: Implicit contradictions identification and solution process model for complex technical systems. Comput. Ind. Eng. **177**, 108822 (2023)
4. Nicheporchuk, V., Favorskaya, M.N., Gryazin, I.: Framework for intelligent wildlife monitoring. Smart Innov. Syst. Technol. **193**, 167–177 (2020)
5. Nikolaychuk, O.A., Pestova, J.V., Yurin, A.: Wildfire susceptibility mapping in Baikal natural territory using random forest. Forests **15**(1), 170 (2024)
6. Giarratano, J.C., Riley, G.D.: Expert Systems: Principles and Programming, 4th edn. Course Technology (2004)
7. Knowledge Modeling System (KMS). http://kms.knowledge-core.ru/. Accessed 26 Apr 2024
8. Hopcroft, J.E., Motwani, R., Ullman, J.D.: Introduction to Automata Theory, Languages, and Computation, 3rd edn. Pearson (2006)
9. Eremeev, A.P.: The development of decision tables apparatus in the context of creating hybrid intelligent systems. In: Proceedings of the 3rd All-Russ. Pospelov's Conference on Hybrid and Synergistic Intelligent Systems, pp. 121–132 (2016)
10. CLIPS: A Tool for Building Expert Systems. https://www.clipsrules.net/. Accessed 26 Apr 2024

11. OWL 2 Web Ontology Language Document Overview, 2nd edn. https://www.w3.org/TR/owl2-overview. Accessed 26 Apr 2024
12. Gavrilova, T., Alkanova, O., Kuznetsova, A.: Ontology-based methodology for knowledge maps design. In: International Conference on Intelligent Information Technologies for Industry, pp. 250–259 (2023)
13. Flexberry Designer. https://flexberry.net/ru/developers-flexberry-designer.html. Accessed 26 Apr 2024
14. Visual Paradigm. https://online.visual-paradigm.com/. Accessed 26 Apr 2024
15. Enterprise Architect. https://sparxsystems.com/. Accessed 26 Apr 2024
16. EASE: State diagram editor. https://www.hdlworks.com/products/ease/state_diagram.html. Accessed 26 Apr 2024
17. Mens, T., Gorp, P.V.: A taxonomy of model transformations. Electron. Notes Theor. Comput. Sci. **152**, 125–142 (2006)
18. da Silva, A.R.: Model-driven engineering: a survey supported by the unified conceptual model. Comput. Lang. Syst. Struct. **43**, 139–155 (2015)
19. Czarnecki, K., Helsen, S.: Feature-based survey of model transformation approaches. IBM Syst. J. **45**(3), 621–645 (2006)
20. Ecore structure description (Metamodelling Language). https://download.eclipse.org/modeling/emf/emf/javadoc/2.11/org/eclipse/emf/ecore/package-summary.html. Accessed 26 Apr 2024
21. Yurin, A.Yu.: Technology for prototyping expert systems based on transformations (PESoT): a method. In: Proceedings of the 3rd Scientific-practical Workshop Information Technologies: Algorithms, Models, Systems, vol. 2677, pp. 36–50 (2020)
22. Rule Visual Modeling Language (RVML). http://knowledge-core.ru/index.php?p=rvml&lan=ru. Accessed 26 Apr 2024
23. Knowledge Base Development System (KBDS). http://www.kbds.knowledge-core.ru/. Accessed 26 Apr 2024
24. Dorodnykh, N.O., Yurin, A.Yu.: A domain-specific language for transformation models. In: CEUR Workshop Proceedings. Information Technologies: Algorithms, Models, Systems (ITAMS), vol. 2221, pp. 70–75 (2018)
25. Berman, A.F., Dorodnykh, N.O., Nikolaychuk, O.A., Yurin, A.Yu.: Event trees transformation for rule bases engineering. In: Proceedings of the 42nd International Convention on Information and Communication Technology, Electronics and Microelectronics (MIPRO), pp. 1138–1143 (2019)
26. Berman, A.F., Nikolaychuk, O.A., Yurin, A.: Intellectual data system for analyzing failures. J. Mach. Manuf. Reliab. **41**(4), 337–343 (2012)
27. Dorodnykh, N.O., Yurin, A.Y.: Using semantic annotation of tabular data for domain knowledge graph population. In: Kovalev, S., Kotenko, I., Sukhanov, A. (eds.) IITI 2023. LNNS, vol. 777, pp. 206–216. Springer, Cham (2023). https://doi.org/10.1007/978-3-031-43792-2_20
28. Expert system designer. https://www.winsite.com/Utilities/Miscellaneous/Expert-System-Designer/. Accessed 11 July 2024
29. Exsys. http://www.exsys.com/. Accessed 11 July 2024
30. ES-builder. http://www.mcgoo.com.au/esbuilder/index.php. Accessed 11 July 2024
31. Protégé. https://protege.stanford.edu/. Accessed 11 July 2024
32. Yurin, A.Yu., Dorodnykh, N.O., Kotlov, Yu.V., Kivokurtsev, A.L.: Visual designing knowledge bases for aircraft diagnostics using state transition diagrams. In: Proceedings of the 2024 IEEE Ural-Siberian Conference on Biomedical Engineering, Radioelectronics and Information Technology (USBEREIT), pp. 27–30 (2024)

# Planning Station Operations Based on Actual Station Performance Obtained "from the Wheel"

Sergey Kovalev[1,2], Andrey Sukhanov[1,2(✉)], Ivan Olgeizer[1,2], and Vladislav Ierusalimov[1,2]

[1] JSC NIIAS, Moscow, Russia
adolgy@list.ru, a.suhanov@vniias.ru
[2] RSTU, Rostov-on-Don, Russia

**Abstract.** The paper presents a new approach to station operation planning based on real data received "from the wheel". The processes at freight stations are considered and an approach to station work planning based on modeling of processes using statistical data and forecasting of key station performance indicators is proposed. The use of such a model will allow predicting critical parameters and optimizing shunting operation control. The results of the study demonstrate the effectiveness of the model in predicting abnormal scenarios and its potential as a tool for preventive decision making at freight stations.

**Keywords:** freight station · digital twin · parameter forecasting · abnormal scenarios · railway infrastructure · automation systems · operational efficiency · process optimization · statistical information

## 1 Introduction

The use of modern technologies within the framework of the Industry 4.0 concept in terms of digitalization and intellectualization [1, 2] of railway infrastructure in general and marshalling yards as the most complex components of the freight traffic service system in particular should lead to a sharp increase in labor productivity, reduction of operating costs, transition to low-traffic operation technologies with a simultaneous increase in the safety of technological processes [3].

At present, the design and implementation of digital modules, including the following, is underway at the decisive hub stations of the Russian Railways network in accordance with the approved "Updated layout and development program for marshalling yards, taking into account the development of auxiliary (technical, pre-hub) yards" and its subprogram "Digital Marshalling Complex":

- integrated post of automated reception and diagnostics of rolling stock at marshalling yards (PPSS) [4, 11];
- complex system of automated control of the sorting process (KSAU SP) [5];
- shunting automatic locomotive signaling MALS [6];


S. Kovalev et al. (Eds.): IITI 2024, LNNS 1209, pp. 33–42, 2024.
https://doi.org/10.1007/978-3-031-77688-5_4

- interactive console of the KSAU SP [7];
- automation of maneuvering movements on the slide;
- automated barricading/bolting in station parks;
- enhanced information exchange with the automated plant control system (ASU ST);
- the system of control and preparation of information on real-time movements of cars and locomotives at the station (SKPI PVL RV) [8].

A significant disadvantage of existing information systems at marshalling yards, introducing significant distortions in the formed indicators and limiting the effectiveness of automated work planning, is manual input of information on technological operations at the marshalling yard.

One of the technical solutions designed to improve the reliability of the model of rolling stock location at the station is the Universal Counting Point (STU) developed by the Institute's specialists. The universal counting point consists of rolling stock axis fixation devices (UFPO), illumination projectors to create uniform illumination of the control area and specialized cameras to identify the type of rolling stock.

The universal counting point will provide not only identification of the fact of moving and fixing the total number of axles of the repositioned group of rolling stock, but also control of the inventory number, the number of rolling units and the number of axles in each rolling unit.

Execution of STU's functions is realized by merging of data received from floor devices (axle counting sensors, rail chains), from specialized video cameras and from real-time model of location of all moving units at the station.

The data received from specialized cameras are preprocessed based on vision algorithms (Fig. 1).


**Fig. 1.** Illustration of the operation of the STU.

The use of deep learning algorithms (Fig. 2) [9] and parallel computing mechanisms [10] provides real-time data processing and their transfer to the central control module. A distinctive feature of the used toolkit is the simultaneous detection of several indicators - couplers, axles and rolling stock numbers.

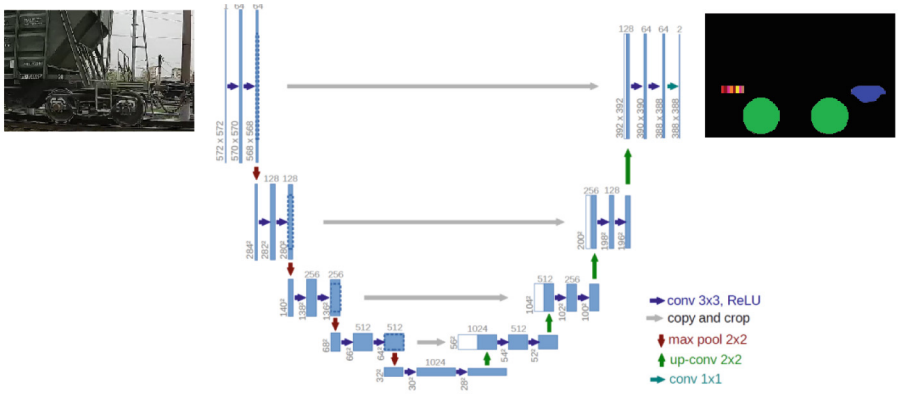


**Fig. 2.** Architecture of the used artificial neural network for extraction of coupler contours, axles and rolling stock numbers (Weng Y. et al. Nas-unet: Neural architecture search for medical image segmentation. IEEE Access. - 2019. - VOL. 7. PP. 44247–44257.).

At the same time, due to the interaction of each counting point with a common station model of rolling stock placement, very high identification accuracy is achieved with a minimum number of counting point equipment.

The study is structured as follows:

- Problem Statement: This section identifies the inefficiencies and inaccuracies of current manual input systems at marshalling yards and outlines the need for a digital twin model to enhance data accuracy and operational efficiency.
- Methods: We describe the development and implementation of the digital twin model, detailing the use of the Universal Counting Point (STU) and the integration of deep learning algorithms for real-time data processing.
- Results: The section presents the findings from our model, including statistical analyses of station performance indicators and the model's accuracy in predicting park utilization and abnormal scenarios.
- Discussion: We discuss the implications of our results, highlighting the improvements in operational efficiency and safety, and identifying areas for future research and development.
- Conclusion: This section summarizes the key contributions of our study and outlines the next steps for further enhancing the digital twin model and its integration with real-time automation systems.

By addressing these aspects, our study aims to significantly improve the operational management of marshalling yards, making them more efficient, reliable, and safer.

## 2 Problem Statement

The current system of manual data input at marshalling yards presents significant challenges to the efficiency and reliability of station operation planning. Manual data entry is prone to errors and inconsistencies, which lead to distortions in the recorded indicators.

These inaccuracies hinder the effectiveness of automated systems and decision-making processes. As a result, there is an urgent need for a more reliable and accurate method of capturing and processing operational data to enhance the overall efficiency of marshalling yards.

The inefficiency caused by these manual processes not only affects the accuracy of data but also impacts the throughput capacity of the yards. Freight cars often experience extended idle times due to delays in processing and mismanagement of resources. This inefficiency leads to higher operational costs and reduced productivity, directly affecting the profitability and operational performance of the railway infrastructure. Given the critical role of marshalling yards in the logistics and supply chain, addressing these inefficiencies is paramount for improving the overall performance of the railway system.

Moreover, the existing systems lack the capability to predict and manage abnormal scenarios effectively. The nonlinearity of processes at marshalling yards, influenced by numerous uncertain factors, complicates the optimization of shunting control. Without accurate, real-time data, it becomes challenging to anticipate and respond to potential disruptions proactively. This limitation underscores the need for an advanced solution that can provide real-time, precise data and predictive analytics to support decision-making.

This study aims to address these challenges by developing and implementing a digital twin model of the station. This model leverages real data obtained from downstream devices and integrates deep learning algorithms for real-time data processing. The goal is to enhance the accuracy and reliability of station operation indicators, optimize shunting operations, and reduce the idle time of railcars. By providing a robust tool for preventive decision-making, the proposed solution seeks to significantly improve the operational efficiency and safety of marshalling yards.

## 3 Methods

Wagon model of SKPI allows automatic unbiased recording and logging of objective indicators of the sorting station, such as the beginning and end of the technological operation, the time of car processing at the station, etc.

Currently, the SKPI is only used as a means of capturing primary data from floor equipment.

In this case, the station indicators are calculated only on the basis of rough generalized (often biased) information entered manually by the duty personnel or on the basis of planned values. This information often does not correspond to real operational data, as it is generated by a human being. Therefore, the indicators calculated on the basis of this data often do not correspond to reality. In this regard, the real duration of specific operations cannot be analyzed, which does not allow for maximum efficient use of the processing capacity of large stations, such as Chelyabinsk-Glavny station.

In 2023, we proactively started to implement additional functionality of the SKPI, which allows us to automatically calculate statistical indicators based on the database of cars that actually passed the station.

The statistical indicators calculated can be divided into 3 types: inbound, park and station-wide.

Inbound railcar flow statistics:

- the number of trains that have entered;
- number of cars in the entered trains;
- distribution of cars by direction in incoming trains.

Parks stats:

- distribution of transitions from the park;
- idle time of railcars in parks;
- number of cars in the trains to be formed in marshalling yards;
- calculation of specialization of marshalling tracks.

Station-wide statistics:

- probability of excessively overworked car (passing the slide more than 2 times);
- number of train locomotives at the station;
- the likelihood of a transit train.

Figure 3 presents the statistics of the incoming car traffic to calculate the average and maximum utilization of station entrances, where quartile values are calculated for each of the statistics: the first quartile (Q1), the second (Q2 is the median) and the third (Q3). Number of entered trains (Fig. 3.a) - median of train locomotives with cars entering through the entrance counting points for a given period of time (e.g., trains per day). Number of cars in the entered trains (Fig. 3.c) - median of the number of cars in the arriving freight trains for a given period of time. Distribution of cars by direction in incoming trains (Fig. 3.b) - the ratio of cars by direction for a given period for each fleet. The direction is selected based on information from the ASU ST or specialization of marshalling yards.

Figure 4 presents the park statistics. Distribution of transitions from park to park (Fig. 4.a) - probability of transition from park A to park B for a given period of time. Car idle time (Fig. 4.b) - median of car idle time for a given period of time. It is calculated for the station and separately by park. Probability of excessively processed railcars (Fig. 4.c) - number and percentage of railcars that passed through the marshalling yard more than twice.

Based on the real information, we calculated the relative utilization of the station's parks during the week under two systems - even and odd. Figure 5 shows the number of railcars as a percentage of total park capacity, where Park D is the receiving park, Park D is the marshalling park and Park C is the departing park.

From: 24.10.2023 to: 31.10.2023

| Start | End | Park | Q1 | Q2 | Q3 | Number of cases |
|---|---|---|---|---|---|---|
| 24.10.2023 00:00 | 01.11.2023 00:00 | Park G | 53 | 62 | 66 | 8 |
| 24.10.2023 00:00 | 01.11.2023 00:00 | Park V | 25 | 26 | 28 | 8 |
| 24.10.2023 00:00 | 01.11.2023 00:00 | Park A | 30 | 38 | 41 | 8 |
| 24.10.2023 00:00 | 01.11.2023 00:00 | All | 26 | 38 | 53 | 24 |

*a)*

From: 24.10.2023 to: 31.10.2023

| Start | End | Park | Direction | Percent |
|---|---|---|---|---|
| 24.10.2023 00:00 | 01.11.2023 00:00 | Park G | 830200:Vhodnaya | 22.84 |
| 24.10.2023 00:00 | 01.11.2023 00:00 | Park G | 780000:Ekaterinburg-Sortirovochny | 11.59 |
| 24.10.2023 00:00 | 01.11.2023 00:00 | Park G | 850000:Inskaya | 10.08 |
| 24.10.2023 00:00 | 01.11.2023 00:00 | Park G | 790400:Voynovka | 7.63 |
| 24.10.2023 00:00 | 01.11.2023 00:00 | Park G | 828500:Kurgan | 4.48 |
| 24.10.2023 00:00 | 01.11.2023 00:00 | Park G | 830000:Moskovka | 4.05 |
| 24.10.2023 00:00 | 01.11.2023 00:00 | Park G | 800008:Chelyabinsk-Glavny | 3.72 |

*b)*

From: 24.10.2023 to: 31.10.2023

| Start | End | Park | Q1 | Q2 | Q3 | Number of cases |
|---|---|---|---|---|---|---|
| 24.10.2023 00:00 | 01.11.2023 00:00 | Park G | 49 | 65 | 70 | 480 |
| 24.10.2023 00:00 | 01.11.2023 00:00 | Park V | 54 | 66 | 72 | 213 |
| 24.10.2023 00:00 | 01.11.2023 00:00 | Park A | 42 | 59 | 67 | 283 |
| 24.10.2023 00:00 | 01.11.2023 00:00 | All | 47 | 64 | 70 | 976 |

*c)*

**Fig. 3.** Inbound train statistics.

We have developed a program that, based on specified rules and statistical data, allows modeling the station operation. The program not only predicts some indicators of station operation, but also allows predicting abnormal conditions in station operation for taking preventive decisions.

Station operation is modeled by generating a hitch (train, group of cars) at the station entrance and moving the hitches between station parks.

The frequency of generation of couplings (groups of cars) is taken from the statistics "Number of entered trains". The number of wagons is a random number that is generated from the "Number of wagons in entered trains" statistic.

Each car in the train is assigned a random destination station based on the statistics "Distribution of cars by destination in incoming trains".

After entering the park, the idle time is calculated for the hitch based on the "Wagon idle time" statistic. The next park for the train is calculated based on the "Distribution of transitions from the park" statistic.

If the next park cannot accept this hitch, the hitch becomes pending.

Inbound and outbound fleets cannot accept a coupler in the event that all tracks are occupied.

A sorting yard cannot accept railcars if there are no vacant tracks or not fully occupied tracks with its destination station.

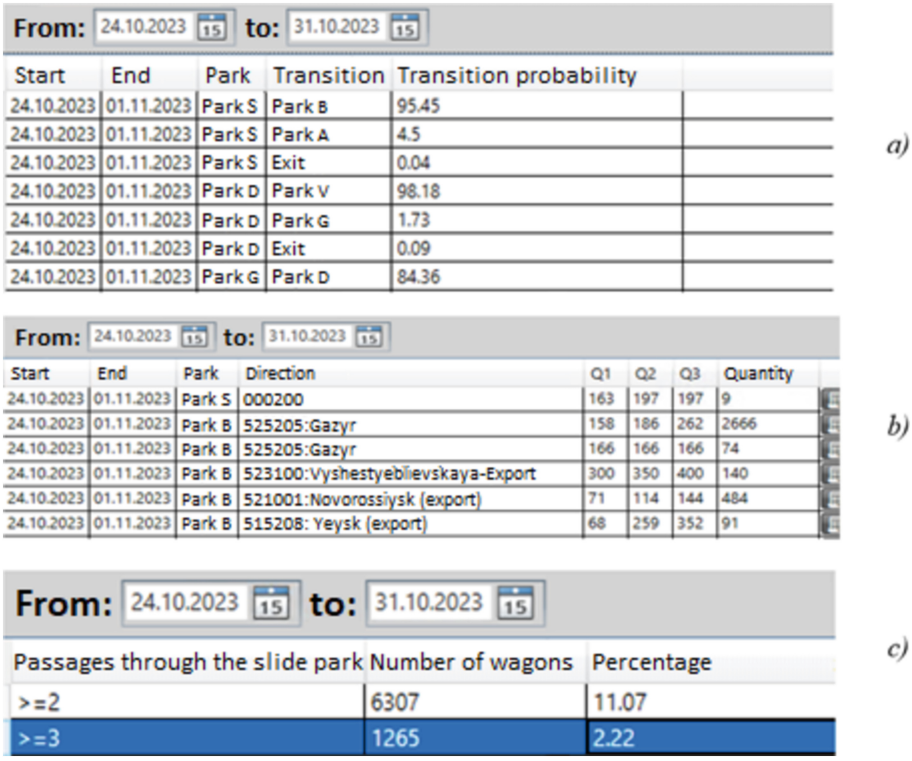

From: 24.10.2023 to: 31.10.2023

| Start | End | Park | Transition | Transition probability |
|---|---|---|---|---|
| 24.10.2023 | 01.11.2023 | Park S | Park B | 95.45 |
| 24.10.2023 | 01.11.2023 | Park S | Park A | 4.5 |
| 24.10.2023 | 01.11.2023 | Park S | Exit | 0.04 |
| 24.10.2023 | 01.11.2023 | Park D | Park V | 98.18 |
| 24.10.2023 | 01.11.2023 | Park D | Park G | 1.73 |
| 24.10.2023 | 01.11.2023 | Park D | Exit | 0.09 |
| 24.10.2023 | 01.11.2023 | Park G | Park D | 84.36 |

*a)*

From: 24.10.2023 to: 31.10.2023

| Start | End | Park | Direction | Q1 | Q2 | Q3 | Quantity |
|---|---|---|---|---|---|---|---|
| 24.10.2023 | 01.11.2023 | Park S | 000200 | 163 | 197 | 197 | 9 |
| 24.10.2023 | 01.11.2023 | Park B | 525205:Gazyr | 158 | 186 | 262 | 2666 |
| 24.10.2023 | 01.11.2023 | Park B | 525205:Gazyr | 166 | 166 | 166 | 74 |
| 24.10.2023 | 01.11.2023 | Park B | 523100:Vyshestyeblievskaya-Export | 300 | 350 | 400 | 140 |
| 24.10.2023 | 01.11.2023 | Park B | 521001:Novorossiysk (export) | 71 | 114 | 144 | 484 |
| 24.10.2023 | 01.11.2023 | Park B | 515208: Yeysk (export) | 68 | 259 | 352 | 91 |

*b)*

From: 24.10.2023 to: 31.10.2023

| Passages through the slide park | Number of wagons | Percentage |
|---|---|---|
| >=2 | 6307 | 11.07 |
| >=3 | 1265 | 2.22 |

*c)*

**Fig. 4.** Park statistics.

On the basis of the analysis of statistical information accumulated by the SKPI, generalized parameters on the operation of individual station sections (parks) were identified. Using these generalized parameters, simulation of multiple random scenarios of train situation development at the station was carried out.

## 4 Results

Our private simulation model based on statistical data allowed us to form a certain forecast of some station performance indicators, for example, such as park utilization (Fig. 6).

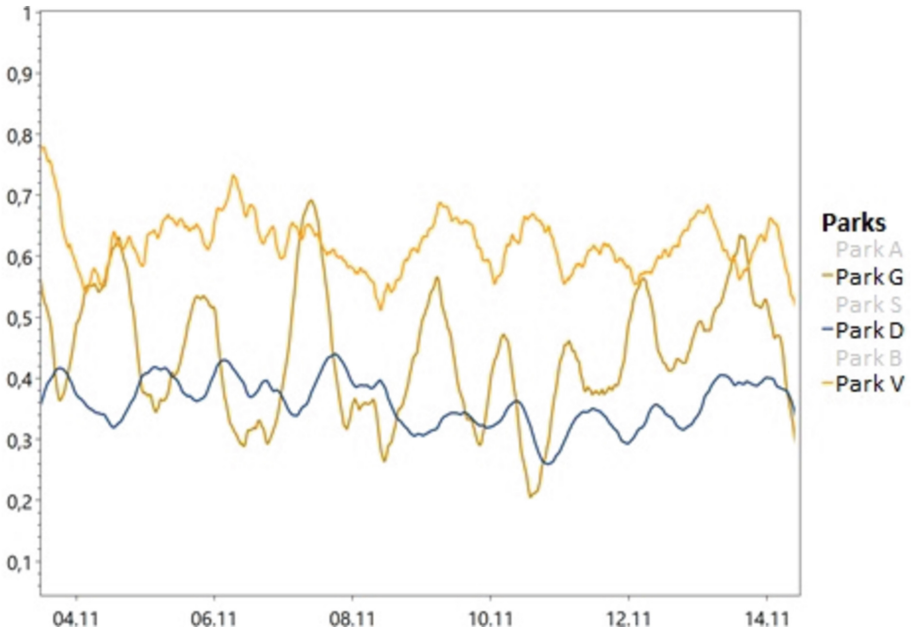


**Fig. 5.** Park congestion for November 4–13, 2023.

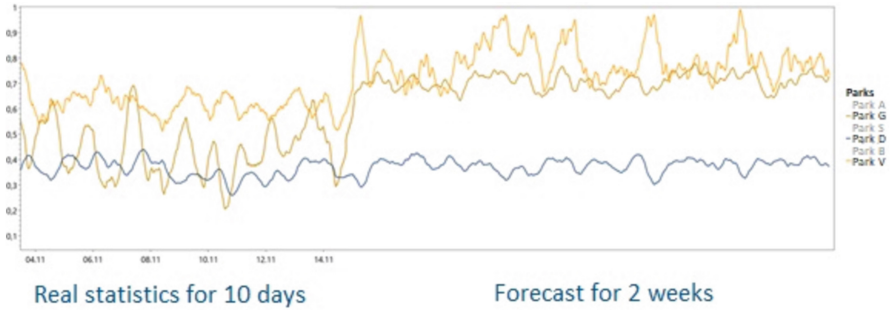


**Fig. 6.** Model of the Even sorting system based on statistical data.

One of the main goals of our private simulation model is to predict abnormal states of station operation for preventive decisions. For example, as shown in Fig. 7, the marshalling yard utilization increases when the number of marshalling tracks decreases (repair simulation). The input park loading tends to 1 after a day.

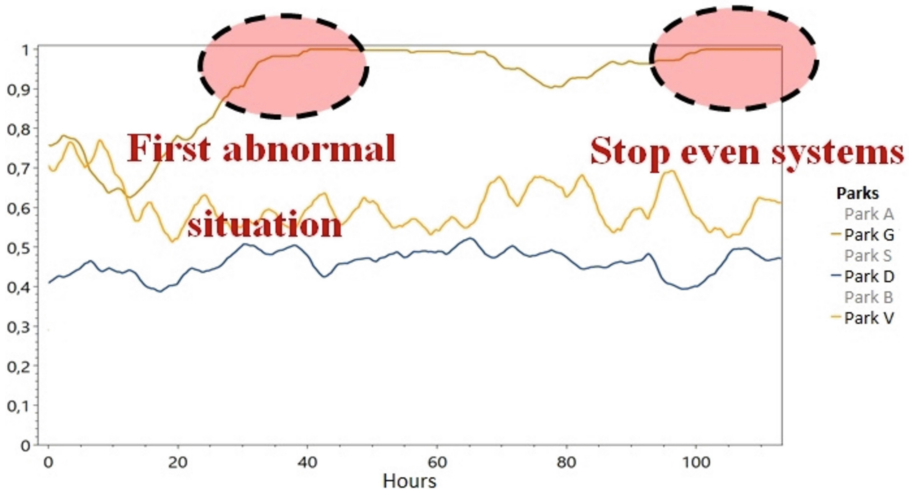


**Fig. 7.** Simulation of marshalling yard track repair (reducing the number of marshalling tracks by 2 times).

## 5 Discussion

The implementation of a digital twin model for marshalling yards represents a significant advancement in the field of railway infrastructure management. By addressing the core issue of inaccurate manual data input, this model provides a robust solution for enhancing the reliability and efficiency of station operations.

One of the primary advantages of the digital twin model is its ability to process real-time data and provide precise insights into the operational status of the yard. This capability is crucial for optimizing shunting operations and reducing idle time of railcars, which are critical factors in improving the overall efficiency and throughput capacity of marshalling yards.

Furthermore, the predictive capabilities of the digital twin model offer significant benefits for proactive management of abnormal scenarios. By analyzing historical data and real-time inputs, the model can forecast potential disruptions and allow for preventive measures to be implemented. This proactive approach not only enhances the safety and reliability of yard operations but also contributes to a reduction in operational costs by minimizing downtime and improving resource utilization.

The integration of the Universal Counting Point (STU) with the digital twin model is another key innovation that enhances the accuracy of data collection. The STU's ability to provide detailed information on rolling stock movements, including the number of axles and rolling units, significantly reduces the likelihood of errors and distortions in the recorded data. This integration ensures that the digital twin model is based on precise and reliable inputs, further enhancing its effectiveness.

Despite the significant benefits demonstrated by our study, there are still areas for future development. One of the main challenges is the synchronization of the digital twin model with existing real-time automation systems. Ensuring seamless integration and

data exchange between the digital twin and other automation tools will be critical for maximizing the model's potential. Additionally, further research is needed to refine the model's predictive algorithms and improve its ability to handle complex and nonlinear operational scenarios.

## 6 Conclusion

Our proposed simulation model based on the analysis of statistical information and generalized station operation parameters has become an effective tool for forecasting various indicators, such as park utilization. Our approach allows us not only to assess the current situation at the station, but also to predict possible abnormal scenarios, which makes the model a valuable tool for preventive decision-making. Further steps in the development of the model include the organization of synchronization with real-time automation systems, which will make it possible to promptly respond to changes and improve the efficiency of railway station management.

## References

1. Shabelnikov, A.N., Sukhanov, A.V.: Components of cyber-physical systems as a part of the KSAU SP. V. Components of cyber-physical systems as a part of the KSAU SP. Autom. Commun. Inform. **1**, 12–14 (2020). https://doi.org/10.34649/AT.2020.1.1.002
2. Shabelnikov, A.N., Olgeizer, I.A., Sukhanov, A.V.: Concept of the digital platform at the marshalling yards. World Transp. EDN OCQILC **19**(1(92)), 60–73 (2021). https://doi.org/10.30932/1992-3252-2021-19-1-60-73
3. Rosenberg, I.N., Shabelnikov, A.N.: Digital sorting station. Railr. Transp. (10), 13–17 (2018)
4. Rosenberg, E.N.N., Batraev, V.V.: Development of perspective control and safety systems for train traffic. Bulletin of the Joint Scientific Council of Russian Railways. V. Development of advanced systems of control and safety of train traffic. Bulletin of the Joint Academic Council of JSC Russian Railways, pp. 43–51 (2017)
5. Shabelnikov, A.N., Sokolov, V.N.: KSAU SP - a new direction of automation of sorting hills. Autom. Commun. Inform. (8), 2–4 (2017)
6. Zamyshlyaev, A.M., Kalinin, A.V.V., Dolganiuk, S.I.: MALS system: tasks and prospects. Autom. Commun. Inform. (10), 30–33 (2016)
7. Anoshkin, V., Shabelnikov, A.N., Shipulin, N.P.: Interactive horological console. Automation, Communications and Informatics. P. Interactive horizon console. Autom. Commun. Inform. (5), 11–12 (2020)
8. Shabelnikov, A.N., Smorodin, A.N.: Complex automation of the nodal sorting station. Automation, communication and informatics. N., Complex automation of the nodal sorting station. Autom. Commun. Inform. (4), 12–14 (2018)
9. Sergeev, A., Del Balso, M.: Horovod: fast and easy distributed deep learning in TensorFlow. arXiv preprint arXiv:1802.05799 (2018)
10. Olgeizer, I.A.: Digital twin of the sorting hill. Autom. Commun. Inform. (1), 20–22 (2020)
11. Batraev, V.V.: Unified scalable system of control and traffic safety, union of machine-builders of Russia. National Scientific and Technical Conference, no. 1, pp. 9–15 (2021)

# Method for Intellectualization of Interaction Between a Technical System and a User in the Natural Language of a Domain

Sergei Kucherov(✉), Yuri Rogozov, Yulia Lipko, Alexander Sviridov, and Artem Borisov

Institute of Computer Technologies and Information Security, Southern Federal University, 44 Nekrasovsky St., Taganrog, Russian Federation
skucherov@sfedu.ru

**Abstract.** Intellectualization is one of the main ways to improve the efficiency of interaction between the user and technical systems. The essence of modern approaches to intellectualization comes down to the concept of analyzing accumulated knowledge and synthesizing private interface solutions that take into account the parameters of the subject area. Despite all the existing achievements, the modern paradigm of intellectualization requires revision, since it excludes the logic of user perception and processing of information received from a technical system. The article discusses a method for ensuring the intellectualization of interaction between a technical system and a user, allowing the context and assessment of the state of the system to be reflected in the terminology of a specific user. The method allows the user to define in natural language the logic for forming meaningful assessments of the state of the system based on observed parameters and select for each assessment the necessary modalities used for notification.

**Keywords:** user interface · IUI · context · intellectualization · interaction · technical system

## 1 Introduction

Methods and technologies for constructing interfaces from the point of view of the interaction of technical systems with users are focused on the effective display of significant parameters associated with the context. Efficiency is understood as a combination of factors that ensure guaranteed delivery of information to the user and the necessary speed and unambiguity of its perception. Effectiveness by default is achieved through the use of adequate modalities [1], skeuomorphism [2] and other techniques. In recent years, to achieve efficiency, the use of intellectualization techniques and tools has been observed [3]. Intelligent user interfaces (IUIs) use predictive analytics for suggestions [4], natural language text communication [5], and other techniques to reimagine how information is presented to the user.


S. Kovalev et al. (Eds.): IITI 2024, LNNS 1209, pp. 43–51, 2024.
https://doi.org/10.1007/978-3-031-77688-5_5

Despite all the existing achievements, the modern paradigm of intellectualization requires revision, since it excludes the logic of user perception and processing of information received from a technical system. In reality, the user uses complex information generated by a combination of observed parameters to form inferences and meaningful conclusions about the state of a technical system. For each such combination, the user associates a certain concept that characterizes the state of the system.

To achieve a significant increase in efficiency, it is necessary that the user interface of a technical system be able to generate information signals containing a meaningful result of processing a combination of observed parameters in the same way as the user does.

Each meaningful result must be described by the user in terms of the logic of its formation. This requires the creation of methods and tools for developing user interfaces. Such interfaces should not replace, but complement the existing one. This will provide the opportunity to determine the nature of the observed state of the system if there is doubt about the conclusion made by the intelligent interface.

The article discusses a method for ensuring the intellectualization of the interaction of a technical system with the user, which makes it possible to reflect the context and assessment of the state of the system in the terminology of a specific user. The method allows the user to define in natural language the logic for forming meaningful assessments of the state of the system based on observed parameters and select for each assessment the necessary modalities used for notification.

## 2 Current State of Research

Intellectualization of user interfaces is one of the topics actively discussed by users. The analysis of publications allows us to determine the following series of trends that differ from each other in implementation features.

Trend 1. Formation of assistant interfaces that make it possible to eliminate insufficient user qualifications by generating contextual clues and offering alternatives for use. This approach is found, for example, in [6]. The authors, through the use of a frame model, provide the ability to describe complex technical systems based on a limited set of basic parameters entered by the user.

Trend 2. The use of "human-like" interfaces, which make it possible to eliminate the barrier between the user and the technical system by representing the latter in the form of a person using modalities familiar to everyday communication (text, speech messages). This approach is quite promising, but is associated with solving non-trivial problems. For example, in work [4], the problem of capturing the context of communication is solved. Work [7] discusses the problems of forming speech messages generated by the system, and work [8] discusses the interpretation of phrases spoken by the user.

Trend 3. Individualization of user interfaces based on user behavior analysis. This approach, specific solutions within which are presented in [4, 9–12], involves adjusting the interface within the framework of the built-in flexibility mechanisms in such a way as to ensure the greatest efficiency of interaction for a specific user. This trend can be considered the most ambitious among all those formulated.

Works are also highlighted, for example, research within the OSTIS project [13, 14], which are at the intersection of several trends and aimed at the comprehensive intellectualization of interaction between the user and the technical system.

The considered trends from the point of view of the problem posed are characterized by the following general features:

1. Focus on increasing the efficiency of interaction without changing the paradigm. The user and his private logic of interaction with the technical system, which is the factor determining efficiency, are beyond the scope of intelligent solutions.
2. Intellectualization through generalization. Researchers proceed from the premise that all users can be reduced to a specific number of classes, and each class can be associated with specific interface models and modalities.

## 3 Suggested Method

Existing methods of interface intellectualization are based on the premise that the problem of a person understanding the logic of the operation of technical systems lies in personalizing the interface. According to the authors, personalization is an important task, but not a priority. Providing primary signals and information to the user in a convenient form solves only part of the interaction problem. A more important aspect of the issue is the formation of meaningful conclusions about the situation or state of the technical system, which the user forms based on his own logic. This logic is developed in the course of mastering a technical system and acquiring skills to work with it. The development of such logic, in its essence, determines the need to train users when moving, for example, from one technical system to another while maintaining technological processes.

In contrast to the ideas embedded in existing approaches, an intellectualization method is proposed, aimed at formalizing the logic of interpreting a set of signals and information into specific conclusions about the state of a technical system. The idea of the method is illustrated by the following diagram (Fig. 1).

The essence of the intellectualization method is that the general channel of interaction between the user and the technical system is not replaced, as proposed in the methods discussed in the second section of the article, but is supplemented with an intellectual component. Such an intelligent component operates in a one-way mode and performs the functions of interpreting the signals and information generated by the basic interface of the technical system. Interpretation implies the formation of an assessment of the state of the system in a form determined by the end user. The intellectual part of such an interface, in contrast to well-known approaches, uses the principles of natural rather than artificial intelligence. Artificial intelligence uses retrospective principles, which can be characterized as an analysis of accumulated data and knowledge - a synthesis of a particular solution. This approach when applied to the interfaces of technical systems leads to averaging and generalization of interaction models and does not solve the problem of the effectiveness of user interaction with a technical system. In contrast, natural intelligence uses a generative principle, which can be characterized as a synthesis of a formalized description of the logic of solving a problem - an analysis of means that can be used within the current context.

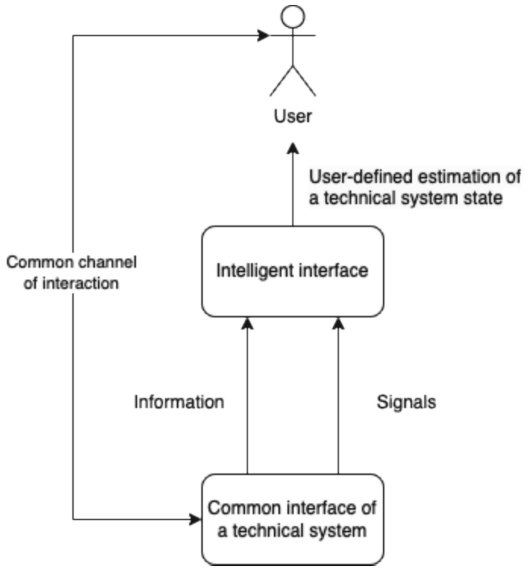


**Fig. 1.** General idea of an interaction intellectualization

Natural intelligence, in relation to the problem considered in the article, represents the user's private logic for interpreting signals and information, which can also be called context. The context is formed by the user independently in the natural language of the subject area, which is provided by previously obtained results [15].

From a structural point of view, the intelligent interface of the technical system proposed in this article can be presented as follows (Fig. 2).

To create intelligent interfaces of technical systems based on natural intelligence, the following sequence of steps is proposed.

Step 1. Determine the set of situations and system states that the user must monitor. At this step, an expert user who knows the technological process and the operating features of the technical system generates the entire possible set of system states and situations. In this case, typical cases included in the basic interface of a technical system are excluded: errors, warnings, etc. Next, the user who directly operates the system selects a subset of the states and situations he uses from those proposed by the expert.

Step 2. Description of the logic for forming meaningful conclusions (context). At this step, the user describes the individual logic for drawing conclusions about the presence of the set of states and situations selected at Step 1. For the description, natural language and a technique proposed by the authors earlier in [15] are used. An important aspect is also the choice by the user of a modality that is individually suitable for him, with the help of which an assessment of the situation will be delivered.

Step 3. The context created by the user is converted from a model represented in the language of the domain to a model represented in the language of the technology. For this purpose, a set of translation rules is used, based on dictionaries of actions in natural language and their technological implementation.

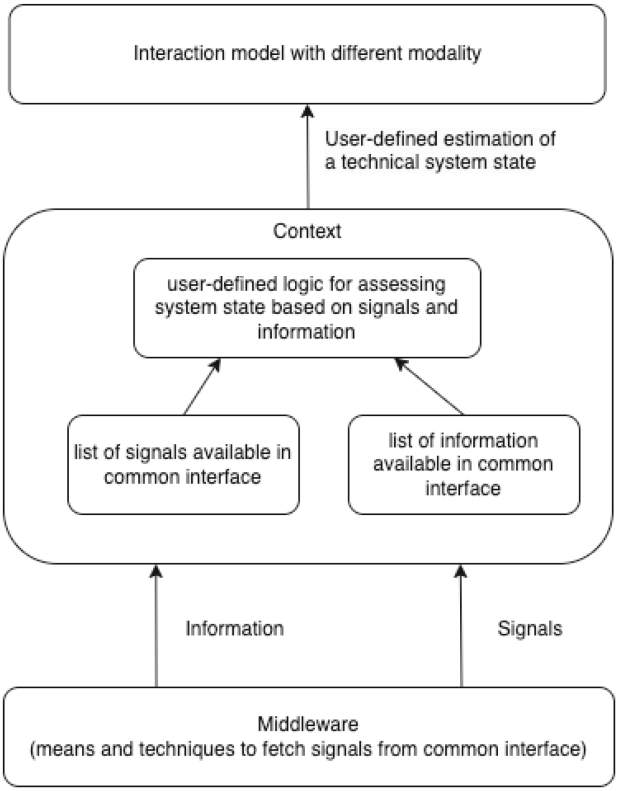


**Fig. 2.** Intelligent interface structure

Practical testing of the proposed method for intellectualizing the interaction of a technical system with a user was carried out as part of the R&D "Platform for self-design of web interfaces by the user to provide remote access to local information systems." The first step of the proposed method is implemented in the form of an editor of information objects that individual employees work with (Fig. 3).

The second step of the proposed method is implemented in the form of a graphic editor, in which the actions for processing information objects and the connections between them are described in natural language (Fig. 4).

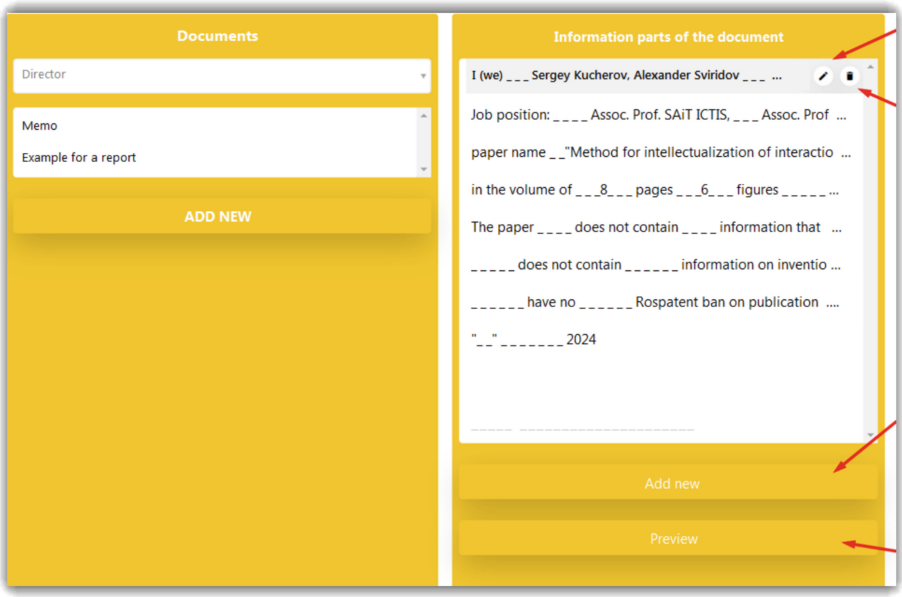


**Fig. 3.** Information Object Editor

Using translation rules, the logic described by the user is manually converted by a technical specialist in the interface designer (Fig. 5).

The interface developed in this way is an ordered combination of window forms. The order of the windows corresponds to the logic defined by the user and is also displayed on the screen (Fig. 6).

Presented software provides the opportunity to create additional interaction interfaces that isolate the user from the original system. The purpose of creating and using such an add-on is to personalize the user's interaction with the system. Personalization itself is determined by the individual logic of processing information signals, objects and data, which is formed in the natural intelligence of the user. The software package allows you to formalize and transfer this user logic into the logic of the software operation.

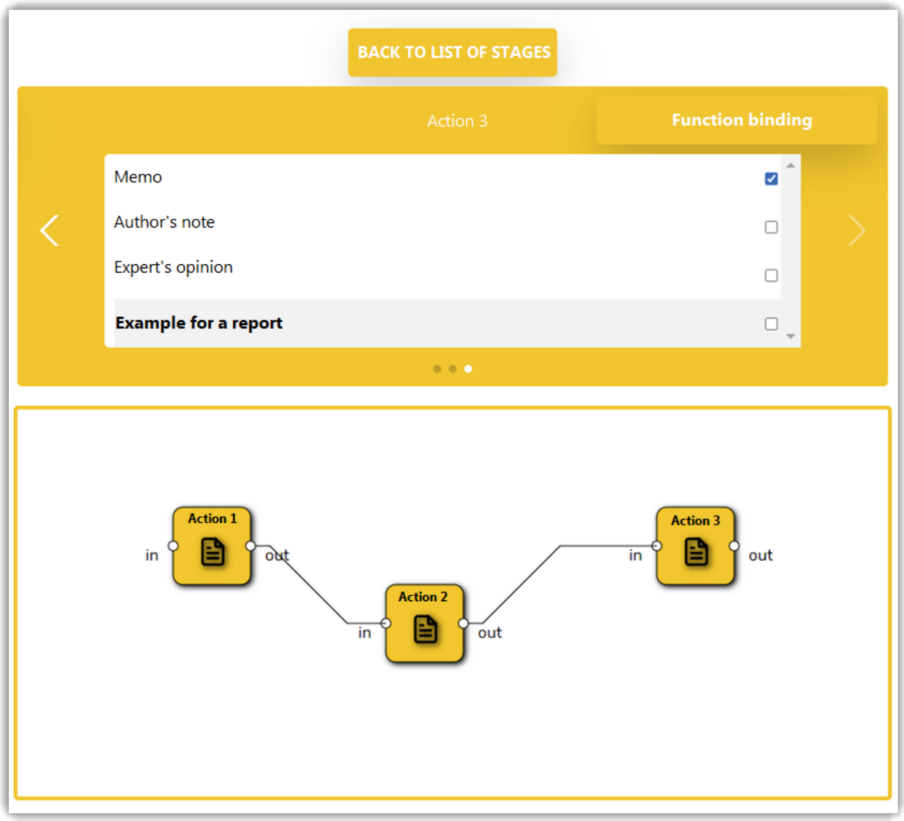


**Fig. 4.** Editor of logic for processing information objects

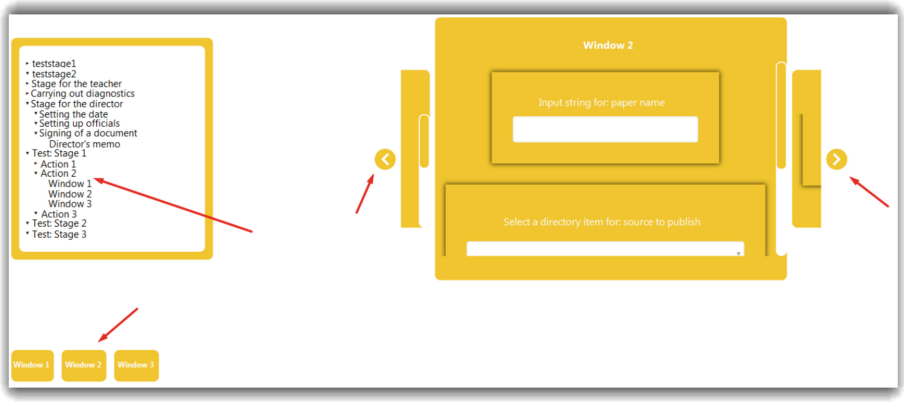


**Fig. 5.** Interface design

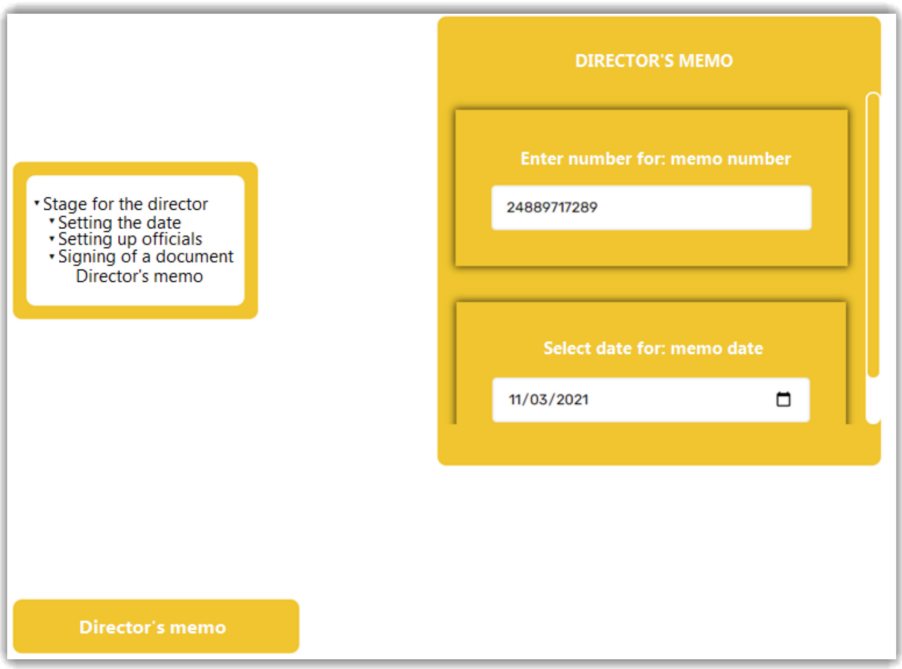


**Fig. 6.** Interface operation based on user-defined logic

## 4 Conclusions

The essence of the proposed intellectualization is the use of natural intelligence instead of artificial intelligence. Natural intelligence in the form of the user's private logic for interpreting the totality of information and signals generated by the technical system interface is transformed into an intelligent interface of the technical system. Such an intelligent interface does not replace, but complements the existing technical system. Thus, intellectualization is ensured at the level of taking into account the individual characteristics of the user, which make it possible to synthesize private interaction mechanisms that take into account the characteristics of his natural intelligence.

**Acknowledgments.** This work has been supported by the grants the Russian Science Foundation (project No. 22-19-00723).

## References

1. Karpov, A.A., Yusupov, R.M.: Mnogomodal'nye interfejsy cheloveko-mashinnogo vzaimodejstviya [Multimodal interfaces of human-machine interaction]. Vestnik Rossijskoj akademii nauk [Bull. Russ. Acad. Sci.] **88**(2), 146–155 (2018). https://doi.org/10.7868/S0869587318020056. (in Russian)

2. Backhaus, N., Trapp, A.K., Thüring, M.: Skeuomorph versus flat design: user experience and age-related preferences. In: Marcus, A., Wang, W. (eds.) DUXU 2018. LNCS, vol. 10919, pp. 527–542. Springer, Cham (2018). https://doi.org/10.1007/978-3-319-91803-7_40
3. Brdnik, S., Heričko, T., Šumak, B.: Intelligent user interfaces and their evaluation: a systematic mapping study. Sensors **22**, 5830 (2022). https://doi.org/10.3390/s22155830
4. Astahov, M.I., et al.: Integrirovannyj, predikativnyj cheloveko-sistemnyj interfejs iskusstvennogo intellekta [Integrated, predictive human-system interface of artificial intelligence]. Sovremennaya nauka: aktual'nye problemy teorii i praktiki. Seriya: Estestvennye i tekhnicheskie nauki [Mod. Sci. Curr. Probl. Theory Pract. Ser. Nat. Tech. Sci.] (6), 65–70 (2022). https://doi.org/10.37882/2223-2966.2022.06.05. (In Russian)
5. Goylo, A., Nikiforov, S.: Natural language interfaces of next-generation intelligent computer systems. Open Semant. Technol. Des. Intell. Syst. **6**, 209–216 (2022)
6. Merzlyakova, E.Y., et al.: Frejmovoe predstavlenie intellektual'nogo tekhnicheskogo agenta cheloveko-mashinnogo interfejsa dlya sozdaniya innovacionnyh proektov [Frame representation of an intelligent technical agent of a human-machine interface for creating innovative projects]. Vestnik SibGUTI [Bull. SibGUTI] (1(60)), 33–45 (2023). https://doi.org/10.55648/1998-6920-2023-17-1-33-45. (in Russian)
7. Zahariev, V., Zhaksylyk, K., Likhachov, D., et al.: Audio interface of next-generation intelligent computer systems. Open Semant. Technol. Des. Intell. Syst. (6), 239–250 (2022)
8. Abdullin, A.A., Maklakova, E.A., Ilunina, A.A., et al.: Algorithm golosovogo poiska v intellektual'nom mul'timodal'nom interfejse [Voice search algorithm in an intelligent multimodal interface ]. Modelirovanie sistem i processov [Model. Syst. Process.] **12**(1), 4–9 (2019). https://doi.org/10.12737/article_5d639c80b4a438.38023981. (in Russian)
9. Sadovskij, M.E.: Individualizaciya pol'zovatel'skih interfejsov intellektual'nyh sistem na osnove semanticheskoj modeli [Individualization of user interfaces of intelligent systems based on a semantic model]. Cifrovaya transformaciya [Digit. Transform.] **29**(3), 54–63 (2023). https://doi.org/10.35596/1729-7648-2023-29-3-54-63. (in Russian)
10. Kostenko, K.I., Belkin V.Y.: Ontologiya pol'zovatel'skih interfejsov v kiberneticheskoj modeli intellektual'nyh system [Ontology of user interfaces in the cybernetic model of intelligent systems]. Ontologiya proektirovaniya [Des. Ontol.] **11**(1(39)), 89–103 (2021). https://doi.org/10.18287/2223-9537-2021-11-1-89-103. (in Russian)
11. Gaspar, A., Gil, M., Panach, J.I., Romero, V.: Towards a general user model to develop intelligent user interfaces. Multimed. Tools Appl. (2024). https://doi.org/10.1007/s11042-024-18240-w
12. Abrahão, S., Insfran, E., Sluÿters, A., et al.: Model-based intelligent user interface adaptation: challenges and future directions. Softw. Syst. Model. **20**, 1335–1349 (2021). https://doi.org/10.1007/s10270-021-00909-7
13. Sadouski, M.: The structure of next-generation intelligent computer system interfaces. Open Semant. Technol. Des. Intell. Syst. **6**, 199–208 (2022)
14. Boriskin, A.S., Koronchik, D.N., Zhukau, I.I., et al.: Ontology-based design of intelligent systems user interface. Open Semant. Technol. Des. Intell. Syst. **7**, 95–106 (2017)
15. Lipko, Y., Sviridov, A., Belikova, S., Belikov, A.: Development of a model of user interface logic representation. In: Kovalev, S., Sukhanov, A., Akperov, I., Ozdemir, S. (eds.) IITI 2022. LNNS, vol. 566, pp. 392–400. Springer, Cham (2023). https://doi.org/10.1007/978-3-031-19620-1_37

# Modeling Pricing in the Transport Services Market: Analysis and Forecasting

Vyacheslav M. Zadorozhniy(✉), Maksim V. Bakalov, Maksim V. Kolesnikov, and Yulia A. Bakalova

Rostov State Transport University, Rostov-on-Don, Russia
zadorozniy91@mail.ru

**Abstract.** The automation and intellectualization of industrial, transport, and energy systems have become critical drivers of efficiency and innovation in the modern economy. This adoption of algorithms enables precise forecasting of demand and pricing, facilitating automated decision-making. This shift towards automated, data-driven approaches aligns with the broader trend of digital transformation in industrial and transport systems.

The theoretical foundations of pricing in the transport services market have been research. Data have been generated and indicators that affect the cost of renting a wagon have been determined. New aspects of integrating linear regression with econometric models to improve forecast accuracy are presented. This hybrid approach uses the strengths of both methods: the interpretability of linear regression and the qualitative characterization of interdependencies between real economic phenomena. A statistical assessment of models for predicting the cost of wagon rental is presented. Prospects for the development of research have been identified.

Our approach is comprehensive when applied to a dynamic pricing model in the transportation market, providing a more robust and adaptable forecasting system. The introduction of statistical criteria facilitates a precise forecasting of transport demand and cargo flow optimization, leveraging extensive econometric data.

This approach underscores the importance of innovative statistical methods in forecasting and strategizing in the transportation sector, suggesting that such adaptive models are essential for operators to remain competitive and economically stable in a dynamic market environment.

**Keywords:** modeling · regression analysis · statistical criteria · wagon · coefficient

## 1 Introduction

The automation and intellectualization of industrial, transport, and energy systems have become critical drivers of efficiency and innovation in the modern economy.

The research was supported by the Russian Science Foundation grant № 24-29-00869, https://rscf.ru/project/24-29-00869/.


S. Kovalev et al. (Eds.): IITI 2024, LNNS 1209, pp. 52–61, 2024.
https://doi.org/10.1007/978-3-031-77688-5_6

Specifically, in the railway sector, the development of automated tariff-setting mechanisms through advanced predictive models like ARIMA and LSTM is reshaping operational dynamics. This adoption of sophisticated algorithms enables precise forecasting of demand and pricing, facilitating automated decision-making that minimizes human error and accelerates adaptation to market changes.

This shift towards automated, data-driven approaches aligns with the broader trend of digital transformation in industrial and transport systems, where intelligent systems play a crucial role in optimizing resource utilization and operational efficiency.

Moreover, the integration of artificial intelligence and advanced analytics into these systems enhances strategic decision-making. For instance, rolling stock operators are now using adaptive tariff systems that harness vast datasets to foresee market movements and dynamically refine pricing strategies.

The cost of renting wagons of assets for transportation plays a central role in shaping a company's strategy and profitability. In this context, the development of statistical methods for price forecasting becomes not just an optimization tool, but also a strategic resource to anticipate and effectively respond to market fluctuations.

The purpose of the research is to develop adaptive wagon tariffs as a tool for implementing the financial strategy of rolling stock operators.

In recent decades, there has been significant interest in the development of forecasting methods in various areas of the economy, including the transport industry. This field of research focuses on the integrated use of statistical data, econometric modeling, and machine learning to analyze current trends and produce accurate future forecasts. These forecasts are crucial for planning infrastructure projects and optimizing supply chains, contributing to the broader theme of automation in industrial systems [3, 8, 9, 11, 12].

For example, the autoregressive integrated moving average (ARIMA) model is widely used for time series forecasting in various areas. Research have shown the effectiveness of ARIMA models in predicting various phenomena [5, 6, 7, 10].

In paper [1], the authors conduct a comparative analysis of the autoregressive integrated moving average (ARIMA) and the seasonal autoregressive integrated moving average (SARIMA) for forecasting prices of gasoline and diesel fuel. The coefficients of the identified models were tested for significance using the Z-test. ARIMA and SARIMA models were compared using RMSE, MAE and MAPE. In the article [2] the authors complement the comparison with the LSTM model in time series forecasting.

In the market for the services of railway rolling stock operators, pricing is determined by competitive mechanisms, which distinguishes it from the traditionally regulated sectors of railway transportation. In this market segment, prices are not subject to government regulation and are formed solely on the basis of supply and demand.

## 2 Materials and Methods

Statistical tests are mathematical tools used to analyze and interpret empirical data in the context of statistical hypotheses. They help determine whether hypothesized patterns in the data are supported or should be rejected in favor of alternative hypotheses. The main application of statistical criteria is testing hypotheses about the parameters and distributions of general populations [4].

There are many statistical methods, each used in different situations to analyze data. Here is a brief overview of some of them:

Logistic Regression:

$$ln(\frac{p}{1-p}) = \beta_0 + \beta_1 x_1 + \beta_2 x_2 + ... + \beta_k x_k \tag{1}$$

The Shapiro-Wilk test is used to check the normality of data distribution:

$$W = \frac{(\sum_{i=1}^{n} a_i x_{(i)})^2}{\sum_{i=1}^{n} (x_i - \bar{x})^2} \tag{2}$$

$x_i$ – $i$-th ordinal statistic, $a_i$– coefficients obtained from special tables, $\bar{x}$– sample mean.

Student's t test evaluates differences between the means of two groups:

$$t = \frac{\overline{X}_1 - \overline{X}_2}{S_{\overline{X}_1 - \overline{X}_2}} \tag{3}$$

$\overline{X}_1$, $\overline{X}_2$, – sample averages,
$S_{\overline{X}_1 - \overline{X}_2}$, – standard error of the difference of means.

Fisher criterion:

$$F = \frac{MS_{between}}{MS_{within}} \tag{4}$$

$MS_{between}$ – mean square of intergroup differences;
$MS_{within}$– mean square of within-group differences.

The coefficient of determination $R^2$ is a measure that is used in statistical analysis to evaluate the quality of a linear regression model. It shows how much of the variance in the dependent variable is explained by the model through the independent variables

$$R^2 = \frac{SS_{res}}{SS_{tot}} \tag{5}$$

$SS_{res}$—sum of squared residuals (difference between actual and predicted values),
$SS_{tot}$—total sum of squares (difference between actual values and their average).

The adjusted coefficient of determination $R^2_{adj}$ modifies to reflect the number of predictors in the model, providing a more precise measure of the explanatory power of the model when multiple variables are present.

$$R^2_{adj} = 1 - \frac{(1 - R^2)(n-1)}{n - p - 1} \tag{6}$$

$n$ – sample size,
$p$ – number of predictors in the model.

The initial data for the analysis are various indicators of the use of wagons, rental rates for the provision of wagons, transportation costs obtained from sources:

- Reports of the information and analytical center of the Union of Railway Operators (IAC SOZhT) [13, 14].
- Monthly monitoring Institute for Problems of Natural Monopolies (IPEM) [15].
- Daily indices of the Electronic trading platform «Freight transportation» [16].

Data time interval from 01/2020 to 12/2022. Data preprocessing stages, such as normalization using *MinMaxScaler* and specification of indicators, are presented in the next section.

The choice of regression and econometric modeling methods for forecasting time series and processing large data sets is due to the advantages of these models: the interpretability of linear regression and the qualitative characterization of interdependencies between real economic phenomena.

## 3 Result and Discussion

The current economic situation, including sanctions measures from third countries, requires from railway transport operators not only efficiency, but also flexibility in managing tariffs. Understanding the key indicators that influence wagons tariffs is critical to maintaining the competitiveness and economic sustainability of the rail industry.

The research is based on the use of an integrated approach, including statistical analysis, econometric modeling, as well as comparative and systemic analyses, and machine learning. These methods allow a comprehensive assessment of the influence of various factors on tariff components and their sensitivity to changes in the economic environment. The initial data were indicators of the use of wagons and rental rates.

At the first stage, a model was built with the found coefficients for the following characteristics:

$cena\_pv\_st_t$- selling prices for new standard wagon, million rubles, excluding VAT,
$cena\_pv\_inn_t$ – selling prices for new innovative wagon, million rubles, excluding VAT,
$cena\_vag\_kompl_t$ – price dynamics for a casting wagon set, thousand rubles,
$gen\_park_t$ – dynamics of the working wagon fleet, thousand units,
$rab\_park_t$ – dynamics of the working wagon fleet, thousand units,
$arenda\_pv_t$ – dynamics of gondola wagon rental rates, rub. per wagon per day,
$tr1_t$ – repairs in the amount of TR-1, thousand rubles,
$tr2_t$ – repairs in the amount of TR-2, thousand rubles,
$dr_t$ – repairs in the amount of depot repairs, thousand rubles,
$kr1_t$ – repairs in the amount of major repairs, thousand rubles,
$proizv_t$ – production of freight wagon in the Russian Federation, units.

The statistical significance of the model was determined using the coefficient of determination, the statistical significance of the coefficients of the model's features was determined using the Student's test.

The mathematical formula of the model can be represented as:

$$\begin{aligned} arenda\_pv_t &= b_0 + b_1 \cdot cena\_pv\_st_t + b_2 \cdot cena\_pv\_inn_t \\ &+ b_3 \cdot cena\_vag\_kompl_t + b_4 \cdot gen\_park_t + b_5 \cdot rab\_park_t \\ &+ b_6 \cdot tr1_t + b_7 \cdot tr2_t + b_8 \cdot dr_t + b_9 \cdot kr1_t + b_{10} \cdot proizv_t \\ &+ b_{11} \cdot arenda\_pv_{t-1} + \varepsilon \end{aligned} \tag{7}$$

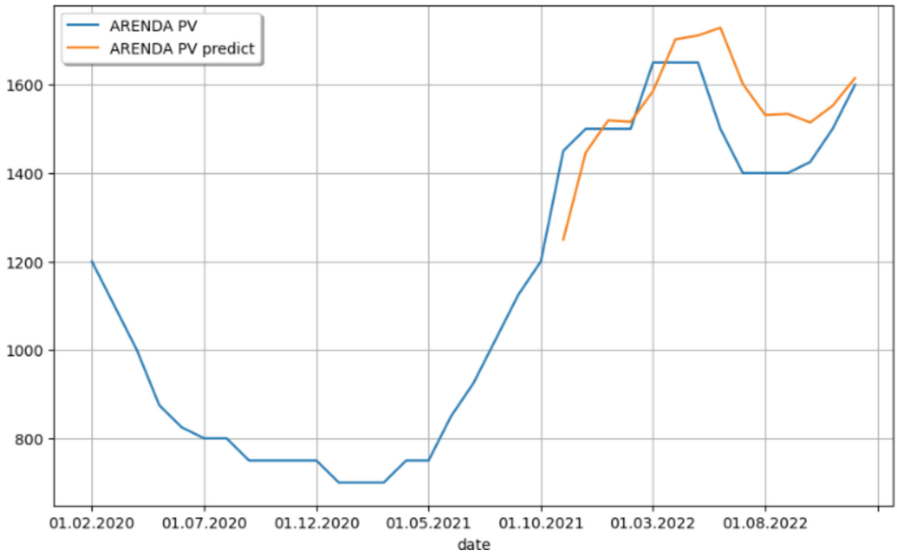


**Fig. 1.** Dynamics of wagon rental rates, rub.

When performing statistical analysis, the following results should be noted.

The model shows a high R-squared = 0.98, indicating good quality of the model and that most of the variability in the variable $y$ can be explained by the independent variables.

Not all coefficients for variables $x_1$, $x_2$, $x_3$, ..., $x_9$ are statistically significant ($p - value < 0,05$).

Adjusted R-squared equals 0.97, which is very close to the R-squared significative. This shows that adding variables to the model does not lead to overfitting, and the model adequately fits the data given the number of independent variables.

F-statistic is 62.73 with a very low probable (F-statistic) = 3.94e−07, indicating the overall statistical significance of the model. This means that the model as a whole has statistically significant predictors for predicting the dependent variable.

The coefficients for each variable ($x_1$, $x_2$, $x_3$, ..., $x_9$) show how the dependent variable changes when a given independent variable changes by one unit while holding other variables fixed. For instance, the coefficient of $x_1$ is 113.0328, which means that for each increase of one unit, it enhances by approximately 113.0328 units, assuming other variables remain unchanged.

Standard errors provide an estimate of the standard deviation of $x_1$ the coefficients. For example, for $x_1$ is 68.51, which gives an idea of the accuracy of the coefficient estimate.

$P > |t|$ indicates the statistical significance of each coefficient. Values below 0.05 indicate that the corresponding coefficient is significantly different from zero and the variable is important to the model.

The confidence intervals ([0.025 0.975]) for the coefficients indicate the range within which we expect to find the true values of the coefficients with 95% confidence. This helps assess the uncertainty around coefficient estimates.

To improve the accuracy and quality of the model, it is necessary to scale the source data using *MinMaxScaler*, which allows you to normalize the data before using it in the model, that is, bringing numerical variables to the range from 0 to 1 (Fig. 2).

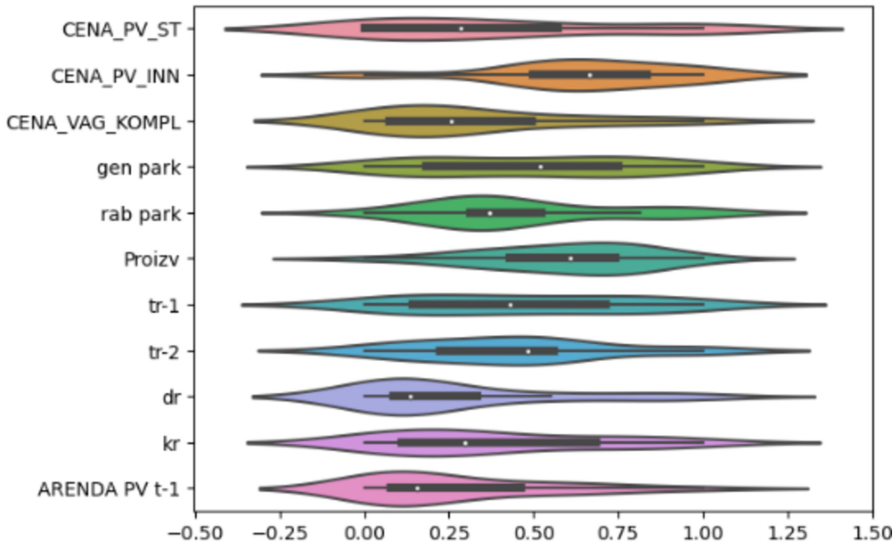


**Fig. 2.** Violin plot of features

Let us give some general explanations regarding the chart. On the graph, each "violin" represents one feature. The central black dot in each violin shows the median value of the data for the corresponding feature. The thick line inside each violin represents the interquartile range (the interval between the 25th and 75th percentiles). A thin line or violin whisker can represent the entire range of data or a specific confidence interval around the median. The width of a violin in any horizontal section is proportional to the density of values, i.e., the wider the violin, the more observations there are values in that range.

The graph helps rapidly evaluate several aspects of the data distribution:

1. form of distribution is the distribution of each characteristic symmetrical, does it have heavy tails,
2. presence of outliers is long whiskers can indicate potential outliers in the data,

3. comparison between features is although the data is scaled, differences in the width and shape of the violins may indicate differences in the distribution of values of different features.

The result of building a model on scaled data is similar to the first model (Fig. 1). Let's build a model based on top-features. The graph is shown in the Fig. 3. Let's determine the most significant features by:

$$\begin{aligned} arenda\_pv_{t-1} &= 2,153621 \\ gen\_park_t &= 0,151610 \\ cena\_pv\_st_t &= 0,062820 \\ cena\_vag\_kompl_t &= 0,040124 \end{aligned}$$

Thus, the mathematical formula for this model is:

$$\begin{aligned} arenda\_pv_t = b_0 + b_1 \cdot arenda\_pv_{t-1} + b_2 \cdot gen\_park_t \\ + b_3 \cdot cena\_pv\_st_t + b_4 \cdot cena\_vag\_kompl_t + \varepsilon \end{aligned} \tag{8}$$

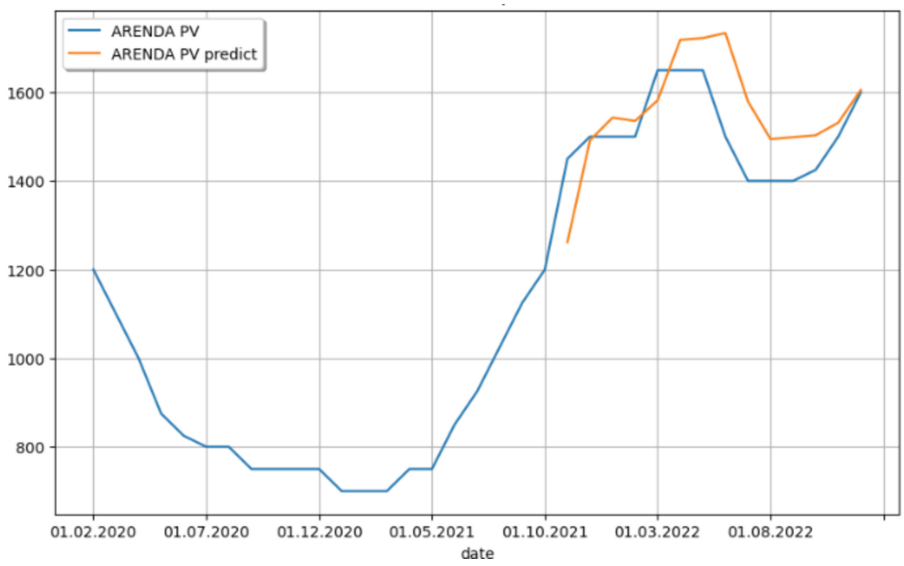


**Fig. 3.** Dynamics of rental rates for wagon

**Discussion of Model Results**

When performing statistical analysis, the following results should be noted.

The model shows a high R-squared = 0.981, indicating that the model is of good quality and that most of the variability in the variable can be explained by the independent variables.

The coefficients of the variables $x_1,\ x_2,\ x_3$ are statistically significant ($p - value\ < 0,\ 05$), which indicates the influence of these variables on the dependent variable.

The coefficient of the variable $x_4$ is $p - value$ just above the threshold of 0.05, which may indicate that it has less influence on the dependent variable in the data sample under study.

As a result, we can conclude that the presented model well describes the relationship between variables and can be used to predict values $y$ based on $x_1,\ x_2,\ x_3, x_4$ although the contribution of the variable $x_4$ may be less significant.

Adj. R-squared equals 0, which is very close to the R-squared signification. This shows that adding variables to the model does not lead to overfitting, and the model adequately fits the data given the number of independent variables.

The F-statistic is 205.5 at a very low probable (F-statistic) = 1.56e−13, indicating the overall statistical significance of the model. This means that the model as a whole has statistically significant predictors for predicting the dependent variable.

The coefficients for each variable ($x_1,\ x_2,\ x_3, x_4$ ) show how the dependent variable changes when a given independent variable changes by one unit while holding other variables fixed. For example, the coefficient of $x_1$ is 606.6701, which means that for each increase $x_1$ of one unit, $y$ increases by approximately 606.67 units, assuming that other variables remain unchanged.

Standard errors provide an estimate of the standard deviation of the coefficients. For example, for $x_1$ is 51.885, which gives an idea of the accuracy of the coefficient estimate.

$P > |t|$ indicates the statistical significance of each coefficient. Values below 0.05 indicate that the corresponding coefficient is significantly different from zero and the variable is important to the model. In this case, all variables except $x_4$, are significant, because the coefficient of the variable $x_4$ is $p - value$ just above the threshold of 0.05.

The confidence intervals ([0.025 0.975]) for the coefficients indicate the range within which we expect to find the true values of the coefficients with 95% confidence. This helps assess the uncertainty around coefficient estimates.

The Shapiro-Wilk test checks whether the residuals follow a normal distribution. Normality of residuals is one of the assumptions when using linear regression. If the p-value is less than the selected significance level (0.05), it indicates that the residuals are not normally distributed. In our case, p-value = 0.518, which means the residuals are normally distributed.

All these indicators together demonstrate that the presented linear regression model explains the variability of the dependent variable quite well and can be used for forecasting. However, when interpreting the results, it is always important to consider potential limitations of the model, such as the assumption of linear relationships, the lack of influence of other unaccounted variables, and others.

New aspects of the proposed approach, in particular the integration of linear regression with econometric models to improve the accuracy of forecasts, solve not only the current problems of transport pricing, but also contribute to the development of intelligent approaches and economic stability of transport systems.

## 4 Conclusion

The research devoted to the development of statistical methods for asset forecasting demonstrates the significant potential of an adaptive approach to tariff setting in the context of managing the financial strategy of rolling stock operators. During the work, the theoretical foundations of statistical forecasting were explored, as well as existing experience and methodologies in this area.

The paper presents the development, development and testing of models that take into account various economic and technical factors affecting the cost of using wagons. The use of statistical methods and econometric models has significantly improved the accuracy of forecasts of the economic efficiency of using wagons, which in turn contributes to more informed decision-making in the field of pricing and financial planning of transport companies.

The results of the research provide important directions for further research and development in the field of transportation and forecasting. The need to continue work to improve methodological approaches, as well as testing new models in various economic conditions, is emphasized.

## References

1. Agyare, S., Odoi, B., Wiah, E.: Predicting petrol and diesel prices in Ghana, a comparison of ARIMA and SARIMA models. Asian J. Econ. Bus. Account. **24**, 594–608 (2024). https://doi.org/10.9734/AJEBA/2024/v24i51333
2. Albeladi, K., Zafar, B., Mueen, A.: Time series forecasting using LSTM and ARIMA. Int. J. Adv. Comput. Sci. Appl. **14** (2023). https://doi.org/10.14569/IJACSA.2023.0140133
3. Chislov, O., Bogachev, V., Zadorozhniy, V., Kravets, A., Bakalov, M., Bogachev, T.: Mathematical modeling of cargo flow distribution in a regional multimodal transportation system. Transp. Probl. **16**, 153–165 (2021). https://doi.org/10.21307/tp-2021-031
4. Ivanov, A.I., Malygin, A.Yu., Polkovnikova, S.A.: New statistical high power test, obtained by differentiating random data of a small sample. University proceedings. Volga region. Technical sciences (2021). https://doi.org/10.21685/2072-3059-2021-3-7
5. Khan, S., Alghulaiakh, H.: ARIMA model for accurate time series stocks forecasting. Int. J. Adv. Comput. Sci. Appl. **11** (2020). https://doi.org/10.14569/IJACSA.2020.0110765
6. Myint, K., Hlaing, Y.: Time series data forecasting system for stock using TA and ARIMA model, pp. 72–76 (2023). https://doi.org/10.1109/ICCA51723.2023.10181415
7. Mohamad, A., et al.: Sales analytics dashboard with ARIMA and SARIMA time series model, pp. 106–112 (2023). https://doi.org/10.1109/ISCAIE57739.2023.10165270
8. Osintsev, N.: Multi-criteria decision-making in transport and logistics. Transp. Urals, 3–17 (2021). https://doi.org/10.20291/1815-9400-2021-4-3-17
9. Pokrovskaya, O.: On the requirements and principles of implementation of integrated services in railway transport. Transp. Sci. Technol. Manag., 20–27 (2020). https://doi.org/10.36535/0236-1914-2020-08-4
10. Sunki, A., SatyaKumar, C., Narayana, G., Koppera, V., Hakeem, M.: Time series forecasting of stock market using ARIMA, LSTM and FB prophet. In: MATEC Web of Conferences, vol. 392 (2024). https://doi.org/10.1051/matecconf/202439201163
11. Wardman, M.: Investigating demand models with more flexible elasticity functions: empirical insights from rail demand analysis. Transportation, 1–27 (2024). https://doi.org/10.1007/s11116-024-10462-z.

12. Zadorozhniy, V., Chislov, O., Kolesnikov, M., Bakalov, M., Khan, V.: Methodological principles of modeling and intellectualization of logistic interaction in the “railway stationport system”. Transp. Res. Procedia **63**, 1690–1699 (2022)
13. Review of the operation of freight rail transport. Analytics of the Union of Railway Operators (2022). http://www.railsovet.ru/analytics. Accessed 25 Mar 2024
14. Indicators of the market for services of railway transport operators (2022). http://www.railsovet.ru/analytics. Accessed 25 Mar 2024
15. Monitoring of key indicators and trends in the railway industry. https://ipem.ru/. Accessed 25 Mar 2024
16. Electronic trading platform «Freight transportation». https://etpgp.rzd.ru/. Accessed 25 Mar 2024

# Safety Control of the Use of Technical Vision Systems on Hump Humps

Konstantin Kornienko(✉), Pavel Borovlev, Konstantin Maksimov, Ekaterina Melnik, and Anna Kataenko

JSC NIIAS, Moscow, Russian Federation
kkonstantini@mail.ru

**Abstract.** Sorting humps are used for forming railway trains. Automation of sorting humps can increase processing capacity and operational safety. The introduction of technical vision systems has been widely used in recent years. Technical vision systems make it possible to solve tasks that were previously impossible to automate. For example, to determine the number of cars in a cut on the hump of a hump yards, a system based on the recognition of wheel pairs, automatic coupling devices and car numbers is used. The purpose of this article is to consider the issue of using technical vision systems on hump humps. An important aspect in the implementation of technical vision systems is functional safety. To solve functional safety issues, it is proposed to integrate information obtained from different sources, primarily from technical vision systems and grassroots sensors. This allows us to ensure the required level of functional safety and generally increase the speed and accuracy of the system.

**Keywords:** railway transport · Computer vision system · artificial neural networks · technical vision devices

## 1 Introduction

One of the most important areas of development of Railways is to increase the processing capacity of marshalling stations. Optimizing the railway transportation management will reduce the time spent waiting for operations and increase processing capacity. To optimize planning, reliable information about the location and progress of technological processes in real time is required. To obtain reliable information, the location of monitoring and control objects and the progress of the technological process must be obtained "from the axle" – from various sensors and control systems [1, 2]. In order to implement the task of optimizing the execution of technological processes at the station, the concept of a digital railway station was developed, which includes a number of modules, the development and implementation of which will ultimately provide an automatic station. A distinctive feature of the proposed concept is the inclusion in the network, automation and control of all processes based on objective data from sensors and control systems that ensure high accuracy of the entered data.


S. Kovalev et al. (Eds.): IITI 2024, LNNS 1209, pp. 62–69, 2024.
https://doi.org/10.1007/978-3-031-77688-5_7

Today Computer vision system (CVS) and artificial neural networks (ANN) are considered the most promising means of presenting primary information in security systems [3–14]. There are many reasons for this:

The huge bandwidth of the visual channel. Bandwidth determines the information content, detail and volume of information.

In the process of evolution, human began to use the visual as the main channel for receiving information. Through the visual channel, he receives more than 80% of all information that ensures his interaction with the external environment.

These considerations have led to the fact that in the developments of the institute, CVS has a very wide application - both in process automation systems and in diagnostic systems.

CVS make it possible to replace operations that require visual control and confirmation with machine processing of the resulting images. This led to increasing the speed and quality of processing information.

## 2 Problem Statement

Despite the increasing use of TVS in railway transport, the safety issues of these systems are the most pressing and complex.

The difficulty of proving the safety of artificial intelligence is due to the fact that artificial intelligence don't have strictly defined operating algorithms. Therefore, the connection between the input and output of the system cannot be traced.

As one of the solutions to the problem, the construction of multi-level systems is now proposed: artificial intelligence solves basic security problems, and the main security functions are solved at the level of software and hardware subsystems with hard logic.

The second possible approach is to use the approaches of adaptive immune system (AIS) of highly developed biological organisms. AIS provide safety and protection of the human body in the widest range: protection from viruses, physical damage and nervous stress.

By modeling immunological mechanisms, it is possible to integrate them into engineering applications, thereby reaching new levels of safety. Thus, the application of AI technologies based on the theory of artificial adaptive immune systems (AAIS) is proposed.

The features, and in this case, the advantages of AAIS, are:

- The mechanism of negative selection is the ability to perceive as "acceptable" known situations or a set of parameters of an object and all others as "forbidden," potentially dangerous;
- Formation of a training sample based on already known, "acceptable" states of the research object.

Thus, the entire state space of the object of control or management with the help of expert information is initially divided into two areas: the subspace X and subspace NOT_X. Subspace X is completely controlled by the AAIS. AAIS provides the required levels of operational safety in X and cannot controlled anything in NOT_X. Further, in

the learning process, subspace NOT_X is continuously narrowed through adaptation of AAIS.

In terms of the use of technical protection systems in transport, this involves, for example, the introduction of a certain number of samples of a particular system and the accumulation of data during their operation. At any point in time, the system ensures functioning with the given parameters only in situations that lie in the subspace X. If a situation occurs from subspace NOT_X, the system goes into a protective failure or offers operator intervention to correct the process. With the accumulation of the knowledge base, after additional training, the subspace X will increase, and the subspace NOT_X will correspondingly decrease.

The subspace NOT_X will be observed only when there are critical deviations of the parameters of the observed or controlled object. Next, using statistical methods aimed at analyzing the knowledge base on the operation of exploited images, it will be possible to calculate the functional safety indicators of a given system.

## 3 Materials and Methods

CVS not only replace human visual control with machine detection, but also increase the safety and predictability of technological processes. Training ANN can be implemented in much less time and with much higher quality, compared to training a human specialist. And the use of detection of the same objects over time makes it possible to determine not only their movement in space, but also its first derivative - velocity, as well as the second - acceleration, with sufficient accuracy, taking into account the inertia of large objects.

Specialized video cameras located near the object are used for technical vision in most case. Lidars or radars can also be used as technical vision devices, but it is more expensive. Specialized video cameras feed the image to the input of a neural network classifier.

To process frames received from technical vision devices (TVD) and convert them into a form suitable for comparison with signals from ground devices, a pre-trained deep neural network architecture is used [15–17]. To train a neural network classifier, a training sample is formed in the form of a set of images coming from TVD.

The disadvantage of TVS is the high probability of error, which can consist of either incorrect recognition or lack of recognition.

In this regard, an algorithm is used to merge data from TVD and data from sensors. For this purpose, an approach to merging heterogeneous data is used (Fig. 1).

In general, the operating algorithm of the TVS can be divided into three stages:

- perspective transformation
- detection
- adequacy analysis by comparing data with other sensors.

The ANN continuously analyzes data from TVD. If a rail car unit is recognized, then this rail car is added as a virtual object to the model. Next comes authentication: the process of matching virtual objects with existing rail car (RC) in the model.

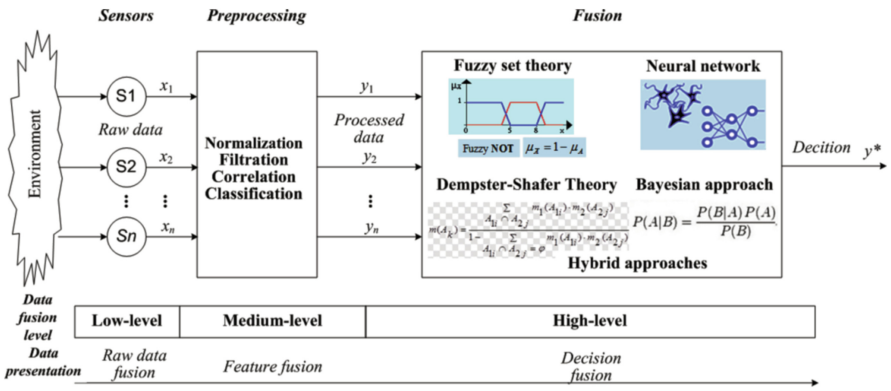


**Fig. 1.** The data fusion scheme used to combine and synchronize heterogeneous information

To do this, the virtual object is compared with existing RS obtained during previous processing. If the coordinates of the virtual object coincide with the coordinates of an existing RC in the model, then the parameters of the virtual object are transferred to the RC. Each authenticated virtual object affects the life cycle of the RC in the model. Location data is used to adjust the dynamics of the RC: calculating accelerations and speeds, determining whether it has stopped.

Virtual objects that have not passed authentication (i.e., at the previous point in time this object did not exist) are perceived by the model as potentially new RC. These objects undergo a registration process in the model. To confirm the presence of an object, sensors are used based on clear logic (for example, axle counting sensors). These sensors are installed before and after the controlled area. When a rail car enters through these sensors, RC are added in model.

If the arrival did not arrive, the model assigns the value virtual to such an object. For such objects, the maintenance time will be about 1 min, after which they are deleted from memory.

The presented algorithm allows you to filter detections and reduce the errors of the first and second types.

## 4 Results

To date, the considered algorithm is used in the following systems:

- System for monitoring and preparing information for the automated control system of the SS on the movements of cars and locomotives at the station in real time;
- Computer vision complex for monitoring the occupancy of marshalling tracks KZSP [18, 19];
- Device for counting and control of uncoupling of cars USKR [20, 21].

In 2020, specialists from JSC NIIAS developed and patented a Computer Vision Complex for monitoring the occupancy of marshalling tracks (KZSP). KZSP consists of trackside and station equipment. Trackside equipment is designed to generate data from

specialized video cameras in the format of video streams for subsequent sending to the station equipment. Video cameras locate on the lighting masts of the marshalling yard or the crossbars of rigid crossbars. The number and placement of trackside equipment depends on the size of the marshalling yard.

The station equipment consists of a video signal equipment (VSE) and workstation of railwayman (WS KZSP). VSE is intended for:

– receiving and processing data coming from the Trackside equipment,
– receiving and processing data coming from the Integrated Automation System for Marshalling Process Control (KSAU SP)
– generating and transmitting information signals about the placement of cars on the tracks of the marshalling yard in the KSAU SP and WS KZSP.

One of the important functions of the KZSP, developed and patented after the start of replication of the complex, was the function of calculating changes in the profile of sorting tracks. The function is based on calculating changes in the elevation of the longitudinal profile in given areas through calculating the speed of movement of the cars. To visualize the resulting slope, the WS KZSP is used.


**Fig. 2.** Screenshot of the longitudinal profile analysis working window at WS KZSP (Profile designation colors: red – accelerating slope, green – slope within normal limits, yellow – decelerating slope).

If the longitudinal profile deviates from the permissible values, the problem area is indicated on the WS KZSP and a decision is made to change the operating mode of the KSAU SP in automatic mode, or about the need to straighten the longitudinal profile. The function of automatic assessment of the longitudinal profile of the marshalling yard tracks allows you to display in real time the condition of sections on a mnemonic diagram, as shown in Fig. 2.

The developed method for analyzing the longitudinal profile of marshalling tracks based on the KZSP complex in real time is a relevant and effective means for the transition to infrastructure diagnostics by condition, which will have a positive impact on traffic safety. The use of objective data on the condition of the longitudinal profile will reduce the number of unsafe collisions of cars in the marshalling yard by building a more accurate model of the movement of the wagons by KSAU SP.

Since 2022, specialists from JSC NIIAS have been developing a Device for counting and control of uncoupling of cars (USCR). USKR involves equipping the measuring section of the hump with technical vision devices, as shown in Fig. 3.

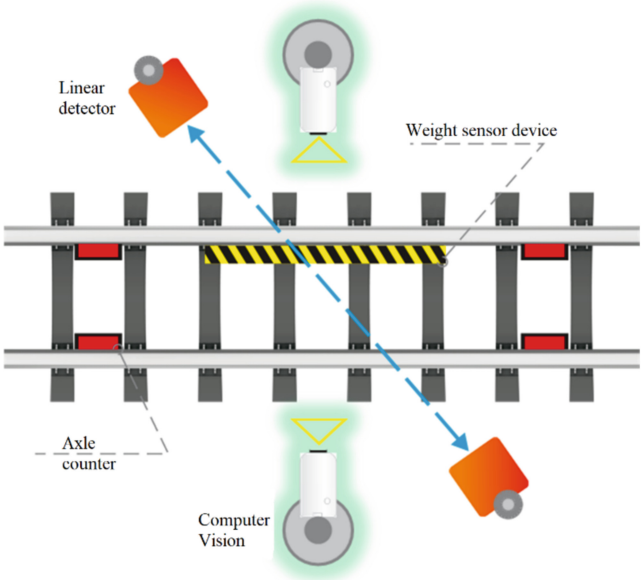


**Fig. 3.** Measuring section configuration

USKR consists of station and trackside equipment. Trackside equipment includes 4 axle counter, linear detector, 4 specialized video cameras, Weight sensor device. 4 specialized video cameras are used as technical vision devices, placed 2 each on both sides of the railway track and directed at each other perpendicular to the direction of the track.

Station equipment contains industrial computers for processing, storing, inputting and outputting information.

The advantage of the developed technical solution is the possibility of simultaneous fixation of both the axles of the wheel pairs and the automatic coupling of the cars, as well as the possibility of fixing the coupled and uncoupled state of the cars at a short distance, which makes it possible to calculate the number of cars in a moving cars.

## 5 Conclusion

The article discusses the problems of functional safety of technical vision.

Further development of the topic should focus on the application of artificial adaptive immune systems together with merging of heterogeneous data. According to experts, this will help achieve SIL4 for Computer vision system.

## References

1. Khatlamadzhiyan, A.E., Zolotarev, Yu.F., Olgeizer, I.A.: Unified station information exchange platform grassroots automation systems. Autom. Commun. Inform. (11), 34–36 (2021). https://doi.org/10.34649/AT.2021.11.11.009
2. Popov, P.A., Kudryashov, S.V.: Transition to unmanned trains. Current challenges and solutions. Autom. Commun. Inform. (11), 18–20 (2021). https://doi.org/10.34649/AT.2021.11.11.005
3. Saikin, A.M., Buznikov, S.E., Karpukhin, K.E.: The analysis of technical vision problems typical for driverless vehicles. Res. J. Pharm. Biol. Chem. Sci. **7**(4), 2053–2059 (2016)
4. Chai, J., Zeng, H., Li, A., Ngai, E.W.T.: Deep learning in computer vision: a critical review of emerging techniques and application scenarios. Mach. Learn. Appl. **6**, 100134 (2021). https://doi.org/10.1016/j.mlwa.2021.100134
5. Li, X., Zhu, M., Zhang, B., Wang, X., Liu, Z., Han, L.: A review of artificial intelligence applications in high-speed railway systems. High-Speed Railw. **2**(1), 11–16 (2024). https://doi.org/10.1016/j.hspr.2024.01.002
6. Padovano, A., Longo, F., Manca, L., Grugni, R.: Improving safety management in railway stations through a simulation-based digital twin approach. Comput. Ind. Eng. **187**, 109839 (2024). https://doi.org/10.1016/j.cie.2023.109839
7. Bouraima, M.B., Saha, A., Stević, Ž., Antucheviciene, J., Qiu, Y., Marton, P.: Assessment actions for improving railway sector performance using intuitionistic fuzzy-rough multi-criteria decision-making model. Appl. Soft Comput. **148**, 110900 (2023). https://doi.org/10.1016/j.asoc.2023.110900
8. Krishnaveni, S., Subramani, K., Sharmila, L., Sathiya, V., Maheswari, M., Priyaadarshan, B.: Enhancing human sight perceptions to optimize machine vision: untangling object recognition using deep learning techniques. Meas. Sens. **28**, 100853 (2023). https://doi.org/10.1016/j.measen.2023.100853
9. Nam, W., Jang, B.: A survey on multimodal bidirectional machine learning translation of image and natural language processing. Expert Syst. Appl. **235**, 121168 (2024). https://doi.org/10.1016/j.eswa.2023.121168
10. Abdel-Aty, M., Wang, Z., Zheng, O., Abdelraouf, A.: Advances and applications of computer vision techniques in vehicle trajectory generation and surrogate traffic safety indicators. Accid. Anal. Prev. **191**, 107191 (2023). https://doi.org/10.1016/j.aap.2023.107191
11. Dolgiy, A., Kovalyev, S., Samsonov, V., Khatlamadzhiyan, A.: Processing of fuzzy graphic images in intelligent computer vision systems on railway transport. In: 2015 9th International Conference on Application of Information and Communication Technologies (AICT), pp. 118–121. IEEE (2015)

12. Zhu, X., et al.: TPH-YOLOv5: improved YOLOv5 based on transformer prediction head for object detection on drone-captured scenarios. In: Proceedings of the IEEE/CVF International Conference on Computer Vision, pp. 2778–2788 (2021)
13. Ronneberger, O., Fischer, P., Brox, T.: U-Net: convolutional networks for biomedical image segmentation. In: Navab, N., Hornegger, J., Wells, W., Frangi, A. (eds.) MICCAI 2015. LNCS, vol. 9351, pp. 234–241. Springer, Cham (2015). https://doi.org/10.1007/978-3-319-24574-4_28
14. Brahim, A.B., Khanchel, R., Limam, M.: Solving data fusion problems using robust classifiers combination. In: 2010 International Conference of Soft Computing and Pattern Recognition, pp. 303–308. IEEE (2010)
15. Chen, Y., Bayanati, M., Ebrahimi, M., Khalijian, S.: A novel optimization approach for educational class scheduling with considering the students and teachers' preferences. Discrete Dyn. Nat. Soc. (2022). https://doi.org/10.1155/2022/5505631
16. Zhang, Q.: An optimized solution to the course scheduling problem in universities under an improved genetic algorithm. J. Intell. Syst. **31**, 1065–1073 (2022). https://doi.org/10.1515/jisys-2022-0114
17. Hossain, S.., Akhand, M.A.H., Shuvo, M., et al.: Optimization of university course scheduling problem using particle swarm optimization with selective search. Expert Syst. Appl. **127** (2019). https://doi.org/10.1016/j.eswa.2019.02.026
18. Khatlamadzhiyan A.E., Olgeizer I.A., Sukhanov A.V., Borisov V.V.: Computer vision for railway humping control. Autom. Commun. Inform. (3), 8–11 (2021). https://doi.org/10.34649/AT.2021.3.3.002
19. Dolgiy, A.I., Khatlamadzhiyan, A.E., Olgeizer, I.A., Sukhanov, A.V., Kornienko, K.I.: Innovative machine vision algorithms for diagnosing the longitudinal profile of sorting tracks. Autom. Commun. Inform. (8), 7–9 (2022). https://doi.org/10.34649/AT.2022.8.8.002
20. Dolgiy, A.I., Khatlamadzhiyan, A.E., Sokolov, V.N., Olgeizer, I.A., Sukhanov, A.V.: Counting device of railway mobile units. Autom. Commun. Inform. (6), 2–4 (2022). https://doi.org/10.34649/AT.2022.6.6.001
21. Olgeizer, I.A., Sukhanov, A.V., Kornienko, K.I., Borovlev, P.V.: Device of counting and control of uncoupling of wagons. Autom. Commun. Inform. (5), 9–11 (2024). https://doi.org/10.62994/AT.2024.5.5.001

# SMART Standards for Industry

Valeriya Gribova[1,2](✉) and Elena Shalfeeva[1,2]

[1] Institute of Automation and Control Processes FEB RAS, Vladivostok, Russia
gribova@dvo.ru
[2] Far Eastern Federal University, Vladivostok, Russia
shalf@iacp.dvo.ru

**Abstract.** An urgent task for all areas of industry is to create documents with machine-readable content (SMART-standards) that can be analyzed not only by domain specialists, but also software services for solving various professional tasks in the Industry. Such documents should be equally understandable to both experts and software systems, which is generally a contradiction. The presence of a textual, i.e. human-readable document with its subsequent translation into a machine-understandable representation is quite a difficult task due to the presence of complex semantic connections in the domain. Modern methods of natural language analysis, including Large Language Models (LLM), are not able to accurately solve this problem. Therefore, an critical task is to develop new methods and approaches to ensure human and machine comprehension while minimizing possible errors when translating from one representation to another. The purpose of this work is to describe an approach for creating and translating into a machine-understandable representation of regulatory documents of the Industry for their further use in software services and systems. The authors propose a new approach for representing normative documents as two-level graphs of knowledge. LLM models, supplemented by a specialized adapter obtained as a result of additional training, serve as the basis for ensuring the transformation of one form into another form.

**Keywords:** SMART Standards · knowledge representation · automatic extraction and transfer · normative document · knowledge graph · two-level representation · LLM

## 1 Introduction

Currently, professional activity in various sectors of the economy is impossible without the use of various types of regulatory documents (recommendations, rules, standards, instructions, technical specifications, conditions, etc.). They accumulate experience and knowledge that are necessary for work and decision-making; establish requirements for products, services, processes and systems. They help to ensure the quality of work, process efficiency, improve safety and reliability. The number of such documents is constantly growing, they are represented in various text formats (.doc, .txt, .pdf, etc.), may include tables, figures, formulas, graphs.


S. Kovalev et al. (Eds.): IITI 2024, LNNS 1209, pp. 70–82, 2024.
https://doi.org/10.1007/978-3-031-77688-5_8

Traditional methods of working with documents have limited possibilities for automating the tasks of their processing, management, and application, and, as a rule, are not compatible with modern IT technologies. Such documents are understandable to specialists in the domain area, but they do not have machine-actionable representation. That is why it is topical to develop so-called SMART-standards (Standards Machine Applicable, Readable and Transferable) [13], which are an integral part of Industry 4.0 and correspond to the fourth level of digitalization development in the field of standardization according to ISO/IEC classification. The main feature of this level of digitalization is the achievement of such a quality of standards that makes them machine–actionable, that is, along with the ability to be read by a person, it makes it possible to process and use information and cyberphysical systems, bypassing humans.

The development of digital transformation requires the creation of standards with machine - interpretable content that will allow the use of digital documents at various stages of development and production without the need for human operator participation. It is noted in [7, 14] that, despite the high relevance, research in the field of creating smart standards is insufficiently covered in scientific publications and is considered by the research community as a very specific topic. Their creation is a complex and important scientific task.

The aim of this work is to describe an approach for creating and translating into a machine-actionable representation of regulatory documents of the industry for their further use in applied software systems.

## 2 Materials and Methods

**SMART Standards.** SMART standards (as part of the use of digital technologies in standardization documents) are information models that can automatically interact with each other. Digital documents can be divided into the following types.

*Machine-Readable Format.* It is needed for processing by automated means and for presentation in a human-readable form, a specialist can read and analyze it independently. The machines can display the document, as well as design and install equipment and processes for the production of products and services in accordance with market expectations. As a rule, these are documents in DOCX, PDF, HTML format.

*A Machine-Interpreted Format.* It allows you to create human-oriented analytical services, in particular, to separate individual formulations from the document-requirements. In this case, a person still applies them, but SMART standards and SMART services created on their basis can save a lot of resources on searching, analyzing and selecting these requirements for a specific task, as well as reduce the number of errors in transmitting information and deliver certain formulations to the specialist's workplace. Such human-readable requirements and other SMART data can be exported to external application software and automated verification of their relevance. As a rule, these are documents in XML and XHTML formats. The methods of automatic interpretation are diverse: from the connection of linguistic methods to semantic graph modeling [8, 9, 15].

*A Machine-Actionable (Machine - Understandable) Format.* It allows you to transfer machine - understandable data to other information systems and directly to equipment, as

well as create machine-oriented SMART services. However, for a qualitative leap in labor productivity, it is not enough to digitalize individual enterprises – they need to interact with each other in a digital environment. And here a powerful tool of cooperation comes to the rescue: standardized documents in SMART format allow different organizations to exchange more complete data, including through communication of information systems without human participation. The purpose of SMART documents is not just to be content, but an information base and a basic component of smart human- and machine–oriented services and specialized information systems being created.

The standards normalize the activities of specialists in all fields, and they are used for various professional tasks. The range of tasks covers:

- technical and regulatory control of facilities and conditions of their existence,
- diagnosis, determination of violations (and their causes),
- determination of the criticality of the condition (threats),
- determination of the potential for elimination, correction and improvement plans,
- search for information (including filters) or answers to questions,
- criticism of the proposed solutions,
- forecast of changes in the state, monitoring,
- selection of means of influence, plans for construction, processing, cultivation and much more.

The standard should be unambiguous:

- each concept is associated with its exact definition and, possibly, a place in the hierarchy from general concepts (possibly accompanied by common synonyms);
- each formulation includes a normalizing or explanatory "bundle" of concepts, conditions, parameters, degree obligation.

Currently, various industries are only forming approaches and formats for the creation of smart standards. That is why research in this direction [4, 13] is an extremely important scientific task.

In [5], a modular approach to the formation of the content of a smart document is proposed. Considering the existing approaches to modularity, it is proposed to transfer them to the field of standardization. Based on these approaches, the concept of formula modularity is designed and developed, and in particular, the development of a formula module. The descriptive elements of the formulas are highlighted and structured. This module serves as a template for future documentation of formulas in XML standards. After that, the identified modules are integrated into the existing expert system of SMART standards to demonstrate possible options for their application.

**Graphs of Knowledge.** Knowledge graphs are actively used to formalize data and knowledge in solving various tasks; they are used to generate recommendations, analytical information, decision support, and predictive analytics. One of the key advantages of domain-specific knowledge graphs is their ability to describe complex semantic connections of the domain, and thus provide an opportunity to answer specific domain questions, identify hidden connections between elements, i.e. they provide a representation of semantic content in a machine-readable format.

Knowledge graphs can be "general", as well as focused on specific use cases or tasks, the second is considered the most relevant [4, 10, 16]. Examples of such areas of application of knowledge graphs are: financial fraud detection and prevention; financial risk assessment; regulatory compliance management; improving customer service, support and providing them with accurate and context-sensitive assistance with the integration of customer data, product information and supporting documentation; optimization of freight transportation, vehicle management; real-time traffic analysis; analysis of historical patterns about the weather; assistance in laying optimal routes for vehicles and many others.

Knowledge graphs are also actively used in medicine, and their construction is a hot spot for research in the field of artificial intelligence. The technology of building and using knowledge graphs has broad prospects for application in this field [10, 12].

The construction of knowledge graphs is steadily progressing from manual to semi-automatic and further to their automatic construction [3, 6, 12]. Various technologies and approaches of natural language processing are actively used for this purpose. It is noted that automating the creation of knowledge graphs has advantages, among which: reducing the labor required to create and maintain all stages of knowledge graph generation, improving interoperability, real-time decision support, and scalability of solutions. At the same time, it is noted that the main problem of their formation is the complexity of automating expert knowledge: to create a knowledge graph for a specific domain, it is necessary to take into account complex semantic connections of different types between objects, their insufficiently accurate and complete representation, simplification (despite the amount of data) can lead to an inefficient process of finding a solution [3].

Currently, Large Language Models (LLM) are actively used to build knowledge graphs [10, 11]. However, their known problem is "hallucinations". A language model trained on existing data may not have access to the latest results of current research. The lack of up-to-date information may hinder the model's ability to generate contextually relevant answers, which may lead to outdated or incomplete conclusions, it is impossible to encode all available knowledge in the LLM parameters for a comprehensive understanding.

Thus, knowledge graphs can be used to develop machine-readable documents or smart standards.

Their creation can be carried out manually, domain experts are involved and knowledge graph editors are used (often controlled by ontologies of this knowledge or domain).

Natural language analysis methods are used to automate the construction of knowledge graphs; currently, the use of LLM is relevant. However, despite some positive results, the problem is far from being solved and requires the creation of new models, methods and approaches to the creation of smart standards.

LLMs trained (on the "basis" of existing texts) to understand questions (simple tasks) and form answers to questions are expensive. An alternative is the method of two related domain-specific formats (related domain-specific languages). One is like a structured, ordered, placed text. The second one details the information in the texts of semantic elements-concepts and connections. This will allow you to access the necessary

fragments, manipulate them when solving or explaining some task. Semantic elements are written as nodes of knowledge graphs, and connections form named arcs (edges).

**Description of the Graph Approach to Creating SMART Standards.** The main properties of SMART standards are their comprehensibility to a person (with appropriate professional knowledge), suitability and sufficiency for standardized information, as well as "intelligibility" for software services used in solving professional problems in the domain.

Knowledge is primarily of interest in smart standards, and knowledge graphs, on the one hand, can provide an understandable and natural representation of knowledge, for example, "top-down" and with named logical arcs, unlike other knowledge representation models (for example, in the form of triplets or rules). The presence of knowledge graph editors, which make it possible, when generating new knowledge elements, to choose their meaning and the type of their "subject" connection (predetermined by the ontology of knowledge) with already generated knowledge elements, makes the process of creating and editing more rigorous and simplifies the reading of such structures. Some editors of knowledge graphs (with a top-down representation of information) supplement named arcs with specifiers and limiters (and may associate them with rules of interpretation).

But it is obvious that the professional community is not ready to move on to reading and especially creating documents represented by such graphs. The presentation of a document in such a formal form, where each node of the knowledge graphs corresponds to semantic elements (as atomic elements), and the "subject" connections are named arcs/edges of these graphs, it is not always convenient for a domain expert. Human intelligibility and "program intelligibility" are partly opposite goals: information that is as structured as possible for software processing is not convenient for human perception.

Therefore, it is proposed to provide two types of interpretation of a normative document (human-readable and machine-understandable) through two related formats (two domaint-oriented languages). One format (machine-understandable) is a network of concepts and strict formulations (part of the domain ontology), the other (human–readable) is a graph of concepts and connections, each node of which represents a text in natural language corresponding to the type of container node. A "human-readable" representation is a kind of "compromise" between rigor, unambiguity and ease of reading and creation by a person; a detailed and formal representation is put in accordance with this graph, intended for processing by software services. In other words, each node of the "human-readable" graph corresponds (in general) to a subtree of the machine-understandable knowledge graph.

The formation of graph knowledge of each of these two "levels" should be carried out according to its structure, but using a single vocabulary of the domain inherent in the current normative legal acts (limited natural language). The diagram for general approach is shown in Fig. 1.

In the traditions of the ontological approach (where any number of knowledge bases are created under the control of one ontology), an arbitrary set (class) of documents and their versions can be written in a domain-oriented language of the same and second levels.

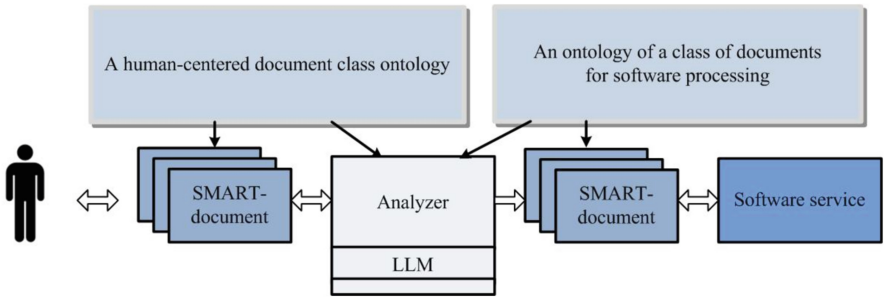


**Fig. 1.** Schematic representation of a two-level approach to SMART standards.

## 3 Results

The work proposes the minimum necessary set of tools for the production of machine-readable documents. He contains domain- and problem-independent tools, as well as domain and problem–oriented ones. Such tools include: editors of the domain terminology, editors of knowledge graphs under the control of ontology and terminology, a translator (analyzer and LLM) from human-centric smart-document to smart-document for software processing, visualizers of knowledge graphs (human- and machine-readable graph documents of the industry).

It is proposed to use the IACPaaS platform as prototype of the tool environment. The reason: there is a repeatedly tested software tool for constructing arbitrary graphs of concepts and connections of the domain. More than a hundred experiments have been conducted to test its suitability. For the formal representation of the ontological structure or structural parts (modules) of the ontology of the subject area, the information language of various levels of generality is used (IRUO, described in https://iacpaas.dvo.ru/infores) [2]. The ontological structure is constructed as an oriented graph (digraph) with special markup describing the characteristics of nodes (concepts) and relationships. Digraph nodes are divided into two types: nonterminals and terminals. Digraph arcs describe directional relationships between pairs of concepts. According to the notation of the IRUO language, relations are characterized by a set of specifiers that define the rules for generating concepts and relations in graphs (graph documents): copy (=) – “copy”; one(!) – “exactly one”; set(+) – “non-empty set”; seq(Λ) – “non-empty sequence”; copymm([=]) – “possible absence”; onemm([!]) – “zero or one”; setmm([+]) – “possibly an empty set”; seqmm([Λ]) – “possibly an empty sequence”. These constructions are sufficient to define graphs of any complexity.

Other editors implemented outside the IACPaaS platform can also act as editors/viewers of knowledge graphs, since all knowledge graphs created on the platform are exported to Json format (and imported from it to the platform).

All specialized services interpreting and processing documents, are domain-oriented. They hosted on specialized SMART standards portals (services can be located both on the IACPaaS platform and outside it).

LLM models serve as the basis for ensuring the transformation of one form of representation of a SMART standard into another. The available Lama 2 model is used

as such a model. For each domain, LLM is complemented by a specialized adapter – a problem-oriented add-on obtained as a result of further training of the LLM model using the PEFT (Parameter-Efficient Fine-Tuning) approach, which provides fine-tuning of the model to the required class of tasks based on the dataset from the examples, while reducing memory and computing power requirements.

The text analyzer, referring to the LLM with a given adapter, provides text translation from one form of the smart standard representation to another (Fig. 2).

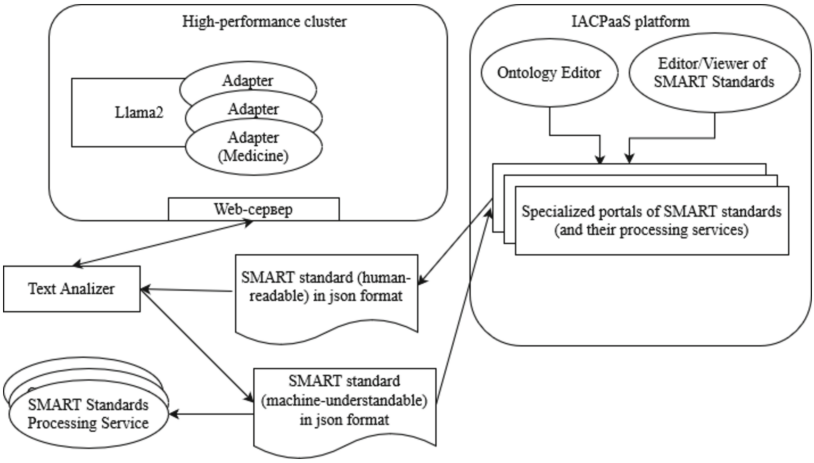


**Fig. 2.** General architecture of the software package.

A separate task is to ensure the quality of converting a human-readable smart standard into a machine-understandable one. This task is currently being investigated. As solutions, we see permanent improvement of the adapter through the expansion of datasets with examples, using various available LLM models (for example, Mistral, Mixtral, etc.) and comparing the results obtained, as well as configuring various hyperparameters of the model, for example, obtaining the same result when setting a high temperature (temperature is an LLM hyperparameter).

**Examples of Human-Readable and Machine-Understandable Smart Standards.** Many experiments have been conducted to confirm the applicability of human-readable and machine- understandable documents. So, in a machine- understandable representation, more than 50 documents with knowledge on the diagnosis of diseases were described, 11 on treatment (graphs were built using different methods, mainly manually by experts, often from several sources). In the human-readable representation - 5 different clinical guidelines of the Ministry of Health (from 65 to 95% of the text was represented, the rest was considered insignificant by experts).

Let's look at examples of a two-level representation of smart standards for the subject areas "medicine" and "construction".

The main regulatory document in medicine is the clinical recommendations, which define the rules for prevention, diagnosis, treatment, monitoring and prognosis of patient

conditions for various diseases. Each clinical recommendation is presented in a multi-page document, the table of contents of which is almost the same for all of them. In general, it is a text document, in some cases containing charts and tables. The size of these documents varies depending on the disease and reaches (for one disease) up to 250 pages of text (for example, guidelines for the treatment of covid-19, version 18). Let's consider a fragment of a clinical smart recommendation to describe the etiology and pathogenesis (Fig. 3).

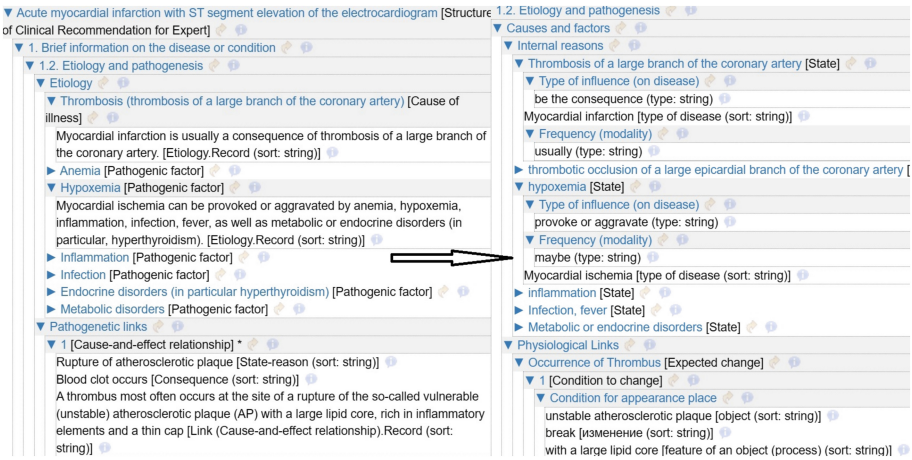


**Fig. 3.** The fragment of smart two-level clinical recommendation.

When processing the machine-readable portion of the standard (see Fig. 3) for the query "What are the most common internal causes of this disease?" the answer in terms of ontology could be constructured like this:

find in the document the section "1.2. Etiology and pathogenesis",
find in the section the subnet "Causes and factors. Internal causes",
find in the subnet all nodes of type-[state] with an internal node of type-[Type of influence (on disease)] with the internal meaning "to be a consequence", and with an internal node of type-[frequency (modality)] with the internal meaning "as a rule"
and display the values of such found nodes of type-[state].

The experiments were also conducted with documentation from the technical committee for standardization in the construction industry (Fig. 4).

The example of the request for a method for concrete structure bending calculating without reinforcement in terms of the ontology of the set of rules (see Fig. 4) can be constructed as follows: "Find in the document the node [Requirement] with the internal node [Object name] = "concrete structures" and with the node [impact type] = "bending"; find in the subnet of the found node [Requirement] the node [limit value], and in its subnet the node [formula] and show its value.

**Text Analysis Using LLM.** In general, the process of forming a knowledge graph based on text is the complex-solved problem, especially for texts that contain complex semantic

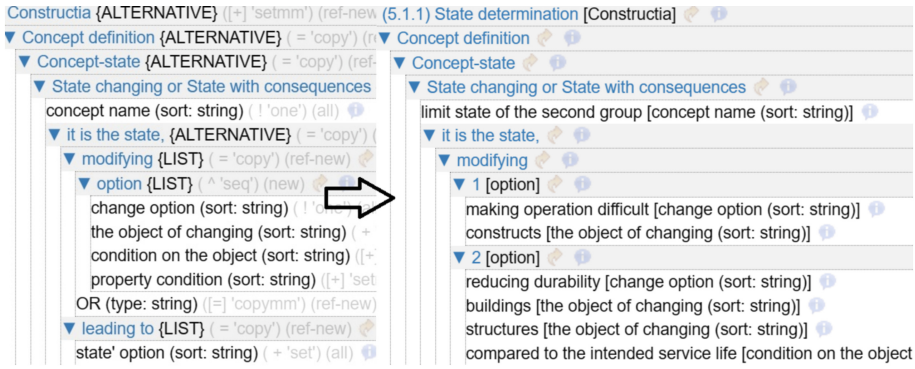


**Fig. 4.** The fragment of smart two-level set of rules.

connections. The example is medicine. At the same time, decomposition of the entire text into fragments corresponding to the elements of a human-understandable smart standard simplifies the process of its semantic analysis. Each fragment of a human-readable standard corresponds to a fragment of the ontology of a machine-readable standard.

Let us give an example of parsing medical text (from a container node in a human-oriented graph format) using a trained LLM [1]. Let's take a fragment of the treatment of COVID-19 using the drug Favipiravir. Original text:

"Treatment of COVID-19 using the drug Favipiravir.

Mechanism of action: Inhibits the RNA-dependent RNA polymerase of the SARS-CoV-2 virus. Prescription scheme. Tablets: for patients:

with body weight <75 kg: 1600 mg twice daily on the 1st day, followed by 600 mg twice daily on days 2 to 10;

with body weight ≥75 kg: 1800 mg twice daily on the 1st day, then 800 mg twice daily from the 2nd to the 10th day."

The result of processing in JSON format is given in the Application.

We used the version of LLM that has gone through fine-tuning process in order to more accurately match the specifics of medical text analysis.

In addition to fine-tuning, specialized prompts for model queries were developed and applied. These prompts were aimed at identifying and extracting key aspects of treatment, such as drug names, dosages, formulations, and evidence of effectiveness. The use of customized prompts made it possible to refine queries to the model and to obtain more relevant and accurate results.

As the result of text processing using LLM with fine-tuning and specialized prompts, we received structured data in json format. This json format can be used for processing by various services, and can be imported onto the IACPaaS platform, on which the software shell currently operates to create decision support systems for prescribing medication.

To validate graph knowledge, check quality properties of SMART standards and ensure their credibility, the reference tasks for specific situations are created. That tasks are created based on previously solved ones in the subject area. Tools are used to verify solutions generated using formalized graph knowledge bases. A sign of readiness (but not

a guarantee) is 100% concordance of the generated results or solutions to the reference ones.

## 4 Conclusion

The new two-level approach is proposed for creating and translating regulatory documents into a machine-understandable representation for their further application by intelligent systems and services.

Since domain and problem orientation are most naturally provided by the ontology of the domain, the formation of documents that help solve problems is based on ontology. Since the use of graph structures is more popular and more appropriate for modeling ontologies, the means of constructing connection graphs are required to form a document language. The requirements for these tools are universality (suitability for any fields, industries), independence from the direct consumer (person, machine) and ensuring that the documents themselves are written in a given format using a dictionary. The novelty of the work lies in the proposal of principles for building a set of tools that meet these requirements.

The principles for implementing software components preparing graph documents with knowledge for interpretation are established.

It is envisaged to construct the tool for projecting a graph of concepts and strict formulations into a detailed graph of concepts and connections and to construct a graph-interpreter as a solver of the user's professional tasks: identifying violations, searching by criteria, etc. The authors believe that the process of projection (using LLM with fine-tuning and specialized prompts) and the construction of a graphical interpreter are more effective than "training" LLM to "solve" such professional problems. The reason is: a formalized knowledge graph can be used for a wide class of solver services, while LLM needs to be trained for each class of problems and this process is quite expensive. In addition, the interpreter produces predictable result, and the trained LLM "solves" the problem with a plausible, but opaque and unstable result. So the approach proposed by the authors contributes to the confidence in the results of applying smart standards. At the same time, the problem is not "closed"; the authors continue work in this direction, primarily related to ensuring the quality of the proposed solutions.

**Acknowledgments.** The research was carried out within the state assignment of IACP FEB RAS (Theme FWFW-2021-0004 - an approach for translating models of regulatory documents into a machine-understandable representation using LLM), and the Far Eastern Federal University (Theme FZNS-2023-0010 - an approach for creating regulatory documents as two-level graphs knowledge).

**Disclosure of Interests.** We wish to confirm that there are no known conflicts of interest associated with this publication.

**Application.** The fragment of export representation of detailed graph for treatment assignment:

```
{
 "name": "COVID-19",
 "meta": "Disease",
 "successors": [
  {
   "name": "Favipiravir",
   "meta": "Recommended Drug",
   "successors": [
    {
     "name": "Mechanism of Action",
     "successors": [
      {
       "name": "Inhibits the RNA-dependent RNA polymerase of the SARS-CoV-2 virus"
                }
               ]
              },
              {
               "name": "Prescription Scheme",
               "successors": [
                {
                 "name": "1",
                 "meta": "Prescription Option",
                 "successors": [
                  {
                   "name": "Tablets",
                   "successors": [
                    {
                     "name": "Daily Dosage",
                     "successors": [
                      {
                       "name": "Condition for Dosage",
                       "successors": [
                        {
                         "name": "Condition Type",
                         "successors": [
                          {
                           "name": "Criteria Block",
```

```
"successors": [
 {
  "name": "Body Weight < 75 kg",
  "meta": "Criterion",
  "successors": [
   {
    "name": "Numerical Values",
    "successors": [
     {
      "name": "1st Day",
      "value": "1600 mg",
      "meta": "Single Dose"
     },
     {
      "name": "2nd-10th Days",
      "value": "600 mg",
      "meta": "Single Dose"
     }
    ]
   }
  ]
 },
 {
  "name": "Body Weight ≥ 75 kg",
  "meta": "Criterion",
  "successors": [
   {
    "name": "Numerical Values",
    "successors": [
     {
      "name": "1st Day",
      "value": "1800 mg",
      "meta": "Single Dose"
     },
     {
      "name": "2nd-10th Days",
      "value": "800 mg",
      "meta": "Single Dose"
} ] } ] } ] } ] } ] } ] } ] } ] } ] } ] } ] }
```

## References


1. Deng, C., Ji, X., Rainey, C., Zhang J., Lu, W.: Integrating machine learning with human knowledge. iScience **23**(11), 101656 (2020)
2. Gribova, V.V., Moskalenko, F.M., Timchenko, V.A., Shalfeeva, E.A.: The IACPaaS platform for developing systems based on ontologies: a decade of use. Sci. Tech. Inf. Process. **50**(5), 406–413 (2023)
3. Ibáñez, L.-D., Domingue, J., Kirrane, S., et al.: Trust, accountability, and autonomy in knowledge graph-based AI for self-determination. arXiv preprint arXiv:2310.19503 (2023)
4. Liu, J., Peng, G.: Designing a smart standards information service: a research framework. In: Streitz, N.A., Konomi, S. (eds.) HCII 2023. LNCS, vol. 14036, pp. 348–365. Springer, Cham (2023). https://doi.org/10.1007/978-3-031-34668-2_23
5. Luttmer, J., Ehring, D., Pluhnau, R., Kocks, C., Nagarajah, A.: SMART standards: modularization approach for engineering standards. international design engineering technical conferences and computers and information in engineering conference. Am. Soc. Mecha. Eng. **86212**, V002T02A065 (2022)
6. Melnyk, I., Dognin, P., Das, P.: Knowledge graph generation from text. arXiv preprint arXiv:2211.10511 (2022)
7. Mutule, A., Antoskova, I., Papadimitriou, C., Efthymiou, V., Morch, A.: Development of smart grid standards in view of energy system functionalities. In: 2021 6th International Conference on Smart and Sustainable Technologies (SpliTech), pp. 1–6. IEEE (2021)
8. Novais, P., Oliveira, T., Satoh, K., Neves, J.: The role of ontologies and decision frameworks in computer-interpretable guideline execution. In: Nalepa, G., Baumeister, J. (eds.) Synergies Between Knowledge Engineering and Software Engineering. AISC, vol .626, pp. 197–216. Springer, Cham (2018). https://doi.org/10.1007/978-3-319-64161-4_10
9. Peleg, M.: Computer-interpretable clinical guidelines: a methodological review. J. Biomed. Inform. **46**(4), 744–763 (2013). https://doi.org/10.1016/j.jbi.2013.06.009
10. Qu, J.: A review on the application of knowledge graph technology in the medical field. Sci. Program. **2022**, 3212370 (2022)
11. Sajid, H.: Combining Large Language Models and Knowledge Graphs. https://www.wisecube.ai/blog/combining-large-language-models-and-knowledge-graphs/. Accessed 12 Apr 2024
12. Sezgin, E., Hussain, S.A., Rust, S., Huang, Y.: Extracting medical information from free-text and unstructured patient-generated health data using natural language processing methods: feasibility study with real-world data. JMIR Form. Res. **7**, e43014 (2023)
13. SMART Standards – From a market and industry perspective. Societal and technology trend report. https://www.iec.ch/system/files/2023-10/iec_sttr_smart_standards_en_lr_0.pdf. Accessed 18 Mar 2024
14. Van de Kaa, G., Stoccuto, S., Calderón, C.V.: A battle over smart standards: compatibility, governance, and innovation in home energy management systems and smart meters in the Netherlands. Energy Res. Soc. Sci. **82**, 102302 (2021)
15. Young, O., Shahar, Y., Liel, Y., et al.: Runtime application of Hybrid-Asbru clinical guidelines. J. Biomed. Inform. **40**(5), 507–526 (2007)
16. Zhong, L., Wu, J., Li, Q., Peng, H., Wu, X.: A comprehensive survey on automatic knowledge graph construction. ACM Comput. Surv. **56**(4), 1–62 (2023)

# Intelligent Approach to Solving the Problem Control over Railway Cars in the Marshalling Yard

Andrew A. Shulzhenko[1,2(✉)], Andrey V. Sukhanov[1,2], Maria A. Butakova[1], and Vladislav S. Ierusalimov[1,2]

[1] JSC NIIAS, Rostov-on-Don, Russia
drew.shaa@gmail.com
[2] Rostov State Transport University, Rostov-on-Don, Russia

**Abstract.** This paper presents a new hybrid approach to solving the problem of wagon cuts monitoring in the classification bowl of a freight station. The approach combines vision technologies for identifying key objects in video camera images. It also involves modeling the state of the fleet based on data obtained from various sources of information about the state of the marshalling yard and classification bowl devices. The study of the problem under consideration is relevant as the solutions existing on the market do not provide accurate and comprehensive information about the movement of wagon cuts and locomotives in the classification bowl. The authors suggest combining an artificial deep learning neural network for recognizing wagon cuts to create a data-driven algorithm and a virtual model of the classification bowl based on multisensory data to build a knowledge-driven algorithm. This combination allows both to smooth out the errors of the first and second kind caused by the impossibility of obtaining all kinds of variations of wagon cuts in the frames of video cameras and to have the most complete static and dynamic picture of the marshalling yard. The paper presents the results of the algorithm and its advantages over existing solutions for the control of wagon cuts in the classification bowl.

**Keywords:** Computer Vision · Deep Learning · Hybrid System · Marshalling Yard · Railway

## 1 Introduction

Modern logistics and freight management demand highly accurate and reliable systems for controlling mobile units in sorting yards. Effective management of the movement of wagons and locomotives is critical to ensuring the seamless operation of railway stations and optimizing sorting processes. However, existing control methods often face issues related to insufficient accuracy and completeness of the provided information, leading to decreased efficiency in the sorting yard operations.


S. Kovalev et al. (Eds.): IITI 2024, LNNS 1209, pp. 83–90, 2024.
https://doi.org/10.1007/978-3-031-77688-5_9

Numerous studies [1–3] have focused on addressing these challenges with a common goal of fully automating technological processes at sorting stations through the application of intelligent technologies, machine vision, and the Internet of Things (IoT). Today, advanced automation tools such as KSAU SP [6], DDC-III [4], and others are already in use, capable of full control and management of mobile units (determining speed, positioning, and automatic rolling down sorting hills) as they move through sorting hills. However, once a mobile unit exits the sorting hill onto the sorting yard track, only the position of the last axle entering the yard can be monitored using pulse probing technology [4]. This results in reduced accuracy of mobile unit control (MU) and consequently potential collision, speed exceedance, negatively impacting the efficiency of the sorting process.

To improve the tracking process of mobile units, a computer vision system for monitoring track occupancy (KZSP) was developed [8,10].

Main problems of developed computer vision systems for mobile unit monitoring:

- Lack of unambiguous system response under incomplete data conditions when images from cameras are delayed or entirely absent for some period.
- Object overlap [9] (Fig. 1).
- Lack of trust verification for recognized objects potentially leading to monitoring errors (due to type II errors) and consequently incorrect positioning and erroneous movement dynamics calculations.


**Fig. 1.** Fragment "Recognition of Mobile Units Using YOLOv3" [9]

This article describes an algorithm that improves the reliability, accuracy, and quality of mobile unit positioning in sorting yards (classification bowl) of

sorting hills capable of avoiding the aforementioned issues. By applying computer vision technologies, high accuracy in tracking the dynamics of mobile units can be achieved. To enhance the reliability and trustworthiness of such a system, it is necessary to control both the tail and head of the wagon cut group and input data from related systems (AKU, BZU, and KSAU SP) achieved through the application of a virtual model of the yard.

A virtual model is a collection of knowledge about the state of devices, track sections, and virtual mobile units (VMU) - a reflection of real MUs in the VM at a given moment, as well as algorithms to predict the future behavior of VMUs. It reflects the objective reality of the yard's condition, devices, and VMUs at a given moment, formed based on data analysis from various information sources.

Section 2 describes the proposed hybrid algorithm for wagons cut control in a classification bowl based on data-driven and knowledge-driven approach. Section 3 demonstrates the result of approbation of the algorithm in the KZSP system and an example of the algorithms operation under poor visibility conditions. The conclusion and future work are shown in Sect. 5

## 2 Proposed Hybrid Algorithm for Wagon Cuts Control in a Classification Bowl

The proposed hybrid algorithm distinguishes itself from existing methods through its integration of both data-driven and knowledge-driven approaches. Unlike traditional methods that rely solely on video-based object detection [8], our approach combines these detections with a virtual model of the yard built from multisensory data. This integration allows for improved accuracy in scenarios where video data alone is insufficient [10]. Additionally, our method incorporates predictive algorithms to anticipate future wagon movements, a feature not present in earlier solutions [4].

### 2.1 Data-Driven Approach

The data-driven approach is based on using data from CCTV cameras and other sensors to develop algorithms for recognizing and monitoring mobile units. The main stages of this approach are:

- **Data Collection**: Surveillance cameras installed throughout the sorting yard capture images of mobile units.
- **Data Preprocessing**: Perspective transformation of images simplifies object recognition tasks and reduces scene dimensionality to 2D, enhancing the speed and accuracy of subsequent calculations.

- **Object Recognition**: YOLOv5 model is used for object detection in images from a dataset like this one https://github.com/DrewShAA/dataset-railway-car.
- **Path Segmentation**: Image segmentation is performed to determine the paths of mobile units.
- **Distance Calculation**: A function converts bounding box coordinates to meters for accurately determining the position of mobile units on the tracks.

The dataset used for our experiments consists of images captured from surveillance cameras installed throughout the sorting yard. It includes a total of 100,000 annotated images, covering various lighting and weather conditions to ensure robustness. Each image is labeled with bounding boxes around the railway cars. This comprehensive dataset allows for thorough training and evaluation of the detection algorithm. An example of this dataset can be found here https://github.com/DrewShAA/dataset-railway-car.

### 2.2 Knowledge-Driven Approach

The knowledge-driven approach involves modeling the state of the sorting yard based on prior knowledge and data from various sensors and devices. The main components of this approach are:

- **Virtual Model (VM)**: VM encompasses knowledge about the state of devices, track sections, and mobile units at a given moment, including information on track length, sensor and camera locations, and their interconnections.
- **Data Aggregation**: Data from various devices, including cameras, sensors, and other sources, are aggregated and used to update the VM's state, creating a complete picture of the yard's current condition.
- **Behavior Prediction**: Based on the VM, the future behavior of mobile units can be predicted, improving monitoring accuracy and reliability.

### 2.3 Algorithm Steps

The algorithm Integrated Neural-Sensor Fusion Algorithm for Dynamic Virtual Model Updates combining data-driven and knowledge-driven models into a single system is presented as Algorithm 1.

**Algorithm 1.** Integrated Neural-Sensor Fusion Algorithm

**Require:** Neural network (NN), Virtual model (VM), Nerual data inference (NN_data), Sensors data (sensor_data)
**Ensure:** Updated virtual model (VM)

**Step 1: Matching Neural Network Data with VMUs**
**for** each *data* in NN_data **do**
  $matching\_VMU \leftarrow$ Match(*data*, VM)
  **if** $matching\_VMU$ exists **then**
    Update $matching\_VMU$ with *data*
  **else**
    $non\_matched\_data \leftarrow data$
  **end if**
**end for**
**Step 2: Condition Update VMU**
**for** each $VMU$ in VM **do**
  $sensor\_info \leftarrow$ GetSensorData($VMU$, sensor_data)
  $NN\_info \leftarrow$ GetNNData($VMU$, NN_data)
  Update $VMU$ with $sensor\_info$ and $NN\_info$
  Evaluate and adjust $VMU$ state (location, movement)
**end for**
**Step 3: Adding New VMU**
**for** each *data* in $non\_matched\_data$ **do**
  **if** valid **then**
    $new\_VMU \leftarrow$ CreateNewVMU(*data*)
    Add $new\_VMU$ to VM
  **end if**
**end for**
**Step 4: Updating the Condition of Unmatched VMUs**
**for** each $VMU$ in VM **do**
  **if** not Updated($VMU$) **then**
    Update $VMU$ with previous static and dynamic characteristics
  **end if**
**end for**
**return** VM

- **Matching Neural Network Data with VMUs**: For each data set (*data*) from the neural network (NN_data), a corresponding VMU in the virtual model (VM) is sought. If a match is found, the VMU is updated with neural network data. If not, the data is added to the list of unmatched data ($non\_matched\_data$).
- **Updating VMU Condition**: For each VMU in the VM, information from sensors ($sensor\_data$) and neural network data ($NN\_data$) is collected to update the VMU's condition, including location and movement characteristics.
- **Adding New VMUs**: For each data set from the list of unmatched data ($non\_matched\_data$), the possibility of adding a new VME is checked. If the data meet the criteria, a new VMU is created and added to the VM.

- **Updating the Condition Of Unmatched VMUs**: For each VMU in the VM that did not match with neural network data, its conditions is updated based on previous static-dynamic characteristics.

The result is an updated state of the model as well as static and dynamic characteristics of the wagons cuts. This algorithm effectively combines data-driven and knowledge-driven approaches for monitoring mobile units in the sorting yard Fig. 2 even in the absence of new data from the neural network, ensuring high accuracy and reliability of control.

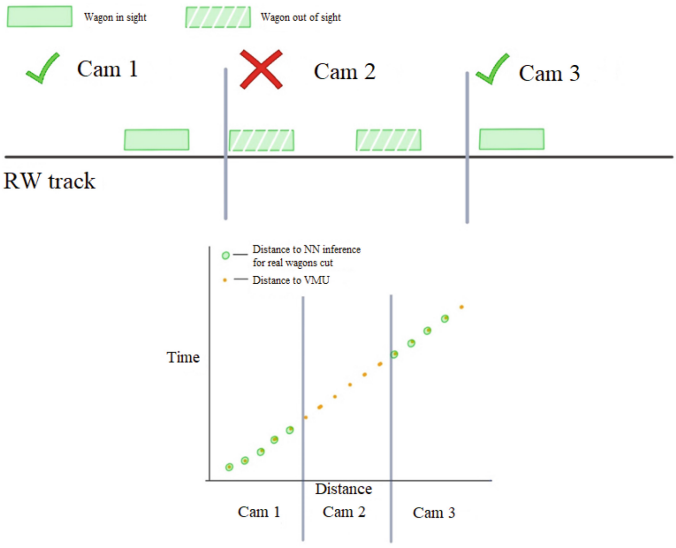


**Fig. 2.** Schematic representation of the model's output in situations with partially missing surveillance camera data

## 3 Results

The hybrid approach presented in this study, which is based on a virtual model of the yard and computer vision technologies, has improved the accuracy and quality of mobile unit monitoring in the park zone of the sorting station. Experimental results show that the proposed approach provides more accurate and reliable tracking of moving units compared to existing methods. This can significantly improve the efficiency of the sorting process, reduce the probability of errors, and improve the overall traffic control in the sorting fleet. It is also noteworthy that the KZSP system was redesigned based on the presented approach and the described algorithms. This system has been implemented and is functioning at the Kinel freight station of Russian railways sorting station. The

Fig. 3 (a) shows an area with poor visibility due to sunset (red rectangles), while the model copes remarkably well with this problem and displays the wagon cuts in the right place (green rectangle) on the KZSP schema.


**Fig. 3. A** - camera image; **B** - model output (part of KZSP user interface)

## 4 Discussion

Future developments are planned to integrate context into the neural network model used to recognize moving units, which in theory can improve the quality of monitoring changes in the dynamic characteristics of MUs. As well as optimizing the data processing algorithms and improving the accuracy of predicting the behavior of moving units. Implementation of the proposed approach to other marshalling yards and its integration with other traffic control systems will further improve the efficiency of railway transportation.

## 5 Conclusion

In this paper, a hybrid approach for the control of wagon cuts in a classification bowl is proposed, which combines data-driven and knowledge-driven methods. This approach combines the use of vision technologies and fleet condition modeling based on data obtained from different sensors and devices. Experimental results show that the proposed approach provides more accurate and reliable tracking of moving units compared to existing methods. This can significantly improve the efficiency of the sorting process, reduce the probability of errors, and improve the overall traffic control in the sorting fleet. Further research will focus on optimizing data processing algorithms and improving the accuracy of predicting the behavior of moving units. Implementation of the proposed approach at other marshalling yards and its integration with other traffic management systems will further improve the efficiency of rail transportation.

## References


1. Antognoli, M., Licciardello, R., Ricci, S., Tombesi, E.: Measuring performances of multi-mode marshalling yards. In: Lecture Notes in Intelligent Transportation and Infrastructure (2019)
2. Sun, W., Liu, Q., Li, X., Chen, M., Zhang, Y.: Research on lean operations management method of railway marshalling yard. In: IEEE 5th International Conference on Intelligent Transportation Engineering (ICITE), pp. 205–208 (2020). https://doi.org/10.1109/ICITE50838.2020.9231322.
3. Shabelnikov, A.N.: Comprehensive automated control system of the sorting process: tasks, functions, key performance indicators. (Kompleksnaya sistema avtomatizirovannogo upravleniya sortirovochnym protsessom: zadachi, funktsii, osnovnye pokazateli) Railway Transport, no. 10, pp. 34–37 (2015). (in Russian)
4. Odikadze, V.R.: Path filling control system using pulse probing method (Sistema kontrolya zapolneniya putei metodom impulsnogo zondirovaniya KZP IZ). Automation, Communication, Informatics, no. 11, pp. 14–15 (2008). (in Russian)
5. Kovalev, S.M., Kovalev, V.S., Sukhanov, A.V.: Intelligent approach to predicting emergency situations in the train separation process at sorting hills (Intellektual'nyy podkhod k prognozirovaniyu neshtatnykh situatsiy v protsesse rasformirovaniya poyezdov na sortirovochnykh gorkakh). In: Proceedings of the V Scientific and Technical Conference with International Participation "Intelligent Control Systems on Railway Transport: Computer and Mathematical Modeling", pp. 168–172 (2016). (in Russian)
6. Shabelnikov, A.N., Sokolov, V.N.: KSAU SP - a new direction in automation of sorting hills (KSAUSP - novoe napravlenie avtomatizatsii sortirovochnykh gorkok). In: Automation, Communication, Informatics, no. 8, pp. 2–4 (2017). (in Russian)
7. Zhang, C., et al.: Analysis of hump automation in China. In: Traffic and Transportation Studies, pp. 285–290 (2000)
8. Sukhanov A.V.: Railway rolling stock tracking based on computer vision algorithms. In: The International Symposium on Computer Science, Digital Economy and Intelligent Systems, pp. 56-63. Springer (2019)
9. Shabelnikov, A.N., Sukhanov, A.V., Sukhanova, M.V.: Adaptation of deep learning models for control of mobile units at the sorting station (Adaptatsiya modeley glubokogo obucheniya dlya kontrolya podvizhnykh edinits na sortirovochnoy stantsii). In: Informatics, Computing, and Engineering Education, vol. 4, no. 37, pp. 12–18. EDN UTMGHE (2019). (in Russian)
10. Khatlamadzhiyan, A.E., Olgeizer, I.A., Sukhanov, A.V., Borisov, V.V.: Computer vision for sorting processes control (Komp'yuternoe zrenie dlya kontrolya sortirovochnykh protsessov). In: Automation, Communication, Informatics, no. 3, pp. 8–11 (2021). https://doi.org/10.34649/AT.2021.3.3.002.EDN GOSIKY. (in Russian)

# Neural Network Control of the Transportation Process in Railway Transport: Problems and Future Tasks

Enver Mamaev(✉), Olesya Ignatieva, Yuri P. Bulavin, Evgeniia Chebotareva, and Dmitry Pritikin

Rostov State Transport University (RSTU), Rostov-on-Don, Russia
mamaev_enver@mail.ru

**Abstract.** For a complex organizational and technological system of transport and train management, the issues of creating a neural network control of transportation based on the resources of the operated corporate information system of JSC "Russian Railways" are considered. The high volatility of external and internal factors affecting transportation increases the dependence of the efficiency of dispatching the transportation process on the competencies of personnel. Important data from different levels of organization of a railway section operation, the state of transport infrastructure facilities and the train situation on the section, affecting the carrying capacity of the section are presented. The analysis of methodological approaches to the formalization of objects and processes of railway transport for the development and implementation of intelligent technologies for managing the transportation process is presented.

**Keywords:** Neural network control · transport process · railway transport · neural networks · machine learning

## 1 Problem Statement

Currently, intelligent systems are used in almost all areas of the economy. In railway transport, information management and intelligent systems provide support for a decision-making process at different levels of management and they are aimed at increasing the organizational and technological reliability and operating efficiency of railway transport production facilities [1–3].

The use of artificial intelligence (AI) in the tasks of managing the transportation process in railway transport can change decision-making processes, taking into account the transfer of management functions traditionally performed only by the dispatch office.

The purpose of the study is to analyze the main problems and prospects for the use of artificial intelligence in the railway transport management system, present the functionality and prospects for the use of artificial intelligence in the railway transport management system based on the analysis of advanced research. The structure of this research includes the formulation of research problems, systematization and clarification of the categorical research apparatus, analysis of the mathematical basis of the research,


S. Kovalev et al. (Eds.): IITI 2024, LNNS 1209, pp. 91–107, 2024.
https://doi.org/10.1007/978-3-031-77688-5_10

determination of the mathematical apparatus for solving the problems set in the study, identification of problems and prospects for the use of artificial intelligence in the railway transportation management system.

The research work includes:

- consideration of the state and key breakthroughs in the development of artificial intelligence, including in the company JSC "Russian Railways";
- systematization of the categorical research apparatus, research of intelligent control technology based on neural networks;
- study of the features of organizing the existing corporate information systems of JSC "Russian Railways", their general classification and characteristics by subject areas, identification of the main tasks of the digital transformation of the railway industry;
- determination of methodological approaches to the formalization of railway objects and processes, namely the railway section for the development and implementation of intelligent technologies for managing the transportation process;
- presentation of the intelligent control technology based on neural networks for improving the performance of railway transport;
- development of a formalized model for managing the transportation process for a railway section.

As a result, the main conclusions are drawn on the promising tasks and the problems of introducing artificial neural networks (ANN) into the railway transportation management system.

## 2 Intellectual Control Technologies Based on Neural Networks

At present intelligent systems are used in almost all areas of the economy. The scope of application of artificial intelligence (AI) tools continues to grow rapidly, both in Russia and in the world. According to Marketsandmarkets research, the size of the global artificial intelligence market in 2024 is estimated at $232 billion, Fig. 1.

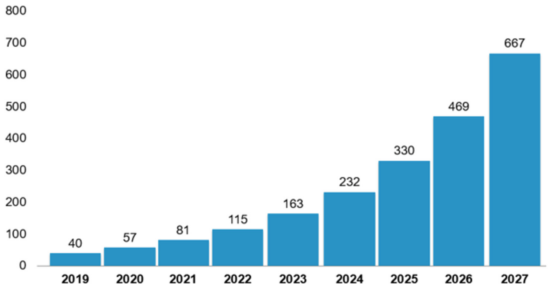


**Fig. 1.** The growth of the global AI market, billion $ (according to BCS Express)

The transport industry was no exception. In railway transport, artificial intelligence systems are designed not only to control unmanned vehicles and monitor road conditions, but also to increase the efficiency of the transportation process by optimizing resources.

At JSC "Russian Railways" the development of digital technologies is provided for by the scientific and technical project "Digital Railway" [4]. As a part of this project, a number of innovative developments are being carried out related to the most relevant areas: Internet of Things technology, big data, intelligent systems, as well as modern data transmission networks, Fig. 2.

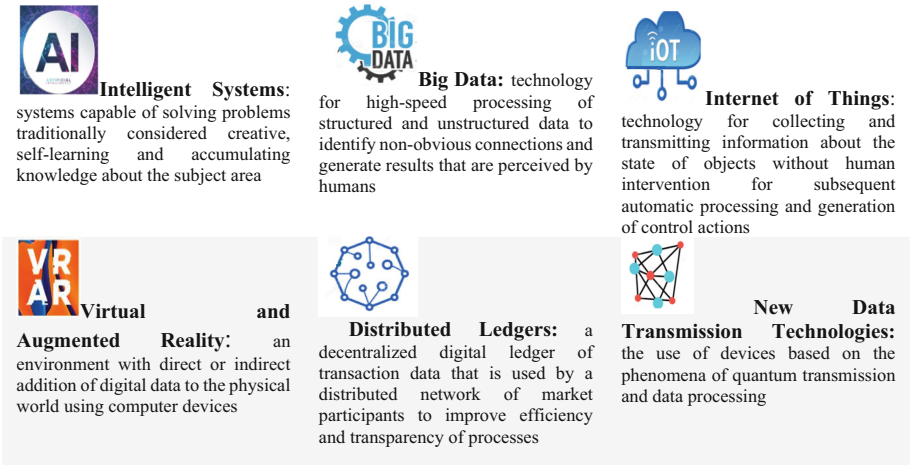


**Fig. 2.** Priority areas of digital technologies within the project "Digital Railway" by JSC "Russian Railways"

Digital transformation helps strengthening the position of JSC "Russian Railways" as an industry technology leader in the use of information systems, digital technologies and innovative solutions [4]. Digital transformation is implemented in the company's digital platforms.

Artificial intelligence technologies are being actively introduced within the "Digital Railway" program, Table 1.

**Table 1.** Application of AI technologies at JSC "Russian Railways"

| AI technology | Application direction at JSC "Russian Railways" | Implementation area |
|---|---|---|
| Natural Language Processing | Conversational AI | Reception of voice requests, speech synthesis |
| | Automation of manual processing of standard applications and requests | Robotization of processing requests for technical support |

(*continued*)

**Table 1.** (*continued*)

| AI technology | Application direction at JSC "Russian Railways" | Implementation area |
|---|---|---|
| Intelligent Decision Support | Infrastructure and rolling stock | Predictive diagnostics, maintenance and repair |
| | Railway infrastructure | Predictive diagnostics |
| | Transportation management | Recommendation service, neural network control |
| Control of unmanned vehicles | Traction rolling stock | Locomotive control using unmanned technologies |
| Software works (RPA) | Automation of routine operations | Technical support, reporting, maintaining regulatory and reference information |

Artificial neural networks (ANN) are models that are built similarly to natural neural networks of the brain. Neural networks have become a major area of research in machine learning for solving complex problems such as optimization, recognition and identification. The classical structure of an artificial neuron is shown in Fig. 3, [5].

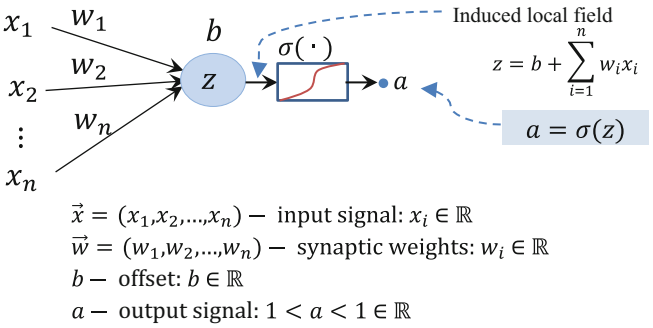


**Fig. 3.** Classic structure of an artificial neuron

To solve a specific problem, neurons are assembled into a network. There are a large number of types of ANN. The most popular are: Deep Neural Network (DNN), Convolutional Neural Networks (CNN), Recurrent Neural Networks (RNN), Generative Adversarial Networks (GAN) and others neural network architectures.

The use of a particular ANN architecture depends on the specific practical task. Neural networks are constantly being improved. At the same time, their accuracy increases. If a few years ago the results of neural networks often gave unsatisfactory results, now they sometimes exceed the results of classical algorithms. The complexity of neural networks is growing as well – the number of layers is increasing, the architecture is

becoming more complex. Neural networks require large amounts of data for training and analysis, and therefore large computing power.

## 3 TMS of JSC «Russian Railways»

It's necessary to note the complexity of managing production processes in railway transport, which is stipulated by significant number of managed objects, a variety of connections between objects and a large number of management indicators, uneven distribution of transport work, and heterogeneity of sources of information over large areas. The traditionally corporate information systems of JSC "Russian Railways" – TMS –systems, in the field of transportation process management formed the train and carriage models (in particular, the automated transportation process management system (ATPMS)).

Individual automated systems (AS) are focused on dedicated functions and control objects; in general, their purpose is related to:

- automation of calculations of basic regulatory and planning documents (train schedule, train formation plan, technical standards, etc.);
- automation of maintaining and recording the schedule of completed train movement, energy-efficient passage of trains, planning of track possessions;
- improvement of traffic control system at different levels of transportation management (range, railway, station, cargo area, container site, etc.);
- control and analysis of technological processes at linear enterprises and, above all, at stations;
- automation of individual worksites (AWS);
- ensuring control and safety of transport processes;
- automated control systems of locomotive, infrastructure and other facilities;
- collection, transmission of information and data processing;
- implementation of services in the field of freight transportation and registration of transportation documents;
- implementation of passenger services;
- statistical accounting and reporting on operational and financial indicators. So currently, the Main Computing Center generates daily, weekly, monthly, quarterly and annual reports for all levels of management of the holding in an automated mode. It should be noted that the volume of daily reports provided to the central office of Russian Railways alone is more than 12 thousand certificates.

The automated control system of Russian Railways includes more than 600 integrated automated systems and client applications, however, a much smaller number of these systems are used as a basis for scientific research and have the ability to flexibly adapt to changing operating conditions.

The digital transformation of the railway system predetermines the need to categorize existing information systems for managing the transportation process with the participation of the railway mode of transport, with the possibility of translation into synthesized transport systems of artificial intelligence. As a part of the "Digital Railway" program, artificial intelligence technologies are being actively introduced, among which the following should be highlighted:

– intelligent traffic control;
– object recognition based on neural networks;
– intelligent logistics systems;
– predictive analytics systems;
– unmanned vehicles.

At the same time, there is not enough research and development in the field of application of artificial neural network (ANN) for traffic control in railway transport. As an object of the study, we will select a section of the railway, including a number of stations, and outline methodological approaches to the formalization of objects and processes of railway transport for the development and implementation of intelligent technologies for managing the transportation process.

## 4 Technologies for Intelligent Management of Railway Transportation Based on Neural Networks

Currently, foreign and domestic experience in the field of neural network control of the transportation process is known. To manage railway transport in foreign countries an artificial intelligence (AI) mechanism is being developed to find solutions for optimal traffic schedule planning in order to increase the capacity of the railway network and minimize train delays. AI technologies are used in the European railway transport management system ERTMS [6], in the Japanese autonomous decentralized train control system ATOS [7], in the national railway network in China (China Railways) and especially in high-speed transport [8]. Overview of Conceptual Approaches of the use of ANN in railway traffic control systems are given in Table 2.

For the tasks of JSC "Russian Railways", there is also positive experience in the implementation of intelligent technologies. The leading place in the intelligent transport system is occupied by the "Unified Intelligent System for Control and Automation of Production Processes in Railway Transport" (ISCRT) [16]. JSC "NIIAS" develops unmanned technologies and technical vision systems for railway transport, automation of discharging dangerous goods at hump yards equipped with self-propelled automatic control systems [17]. In 2022, an intelligent train traffic control system (ITTCS) "Prognoz" was developed on the basis of Moscow Institute of Physics and Technology (MIPT) [18]. The next example is the use of a neural network to plan the optimal train schedule [19], which is based on the "Elbrus-M" complex, developed by VNIIZhT (All-Russian Scientific Research Institute of Railway Transport) specialists.

## 5 Parameters of the Transportation Process Management Task

The formalized representation of facilities in the transportation process management system includes entities that directly affect the transportation process by changing operational performance indicators. At the same time, a large number of factors have an indirect impact on the transportation process, creating conditions for the effective implementation of transport and technological processes that stay in the background, in fact, without affecting the operational management of the transportation process.

**Table 2.** Approaches in using ANN in control systems for the transportation process of railway transport

| | Tasks | Solutions |
|---|---|---|
| Strategy for rescheduling | | |
| 1 | Estimation of delays in the railway network [9] | Delay forecasting mainly focuses on predicting delays for each train at subsequent stations: a neural network approach on heterogeneous graphs |
| 2 | Forecasting delays using train operation and weather data based on train traffic simulation [10] | A train delay forecasting model (FCLL-Net) is developed that combines a fully connected neural network (FCNN) and two long short-term memory (LSTM) components to account for operational interactions. The performance of FCLL-Net is tested using data from two high-speed railway lines in China |
| Development of high-speed railways | | |
| 3 | Overview of artificial intelligence applications in high-speed railway systems [11] | An overview of the most advanced technologies and artificial intelligence applications in the three main application areas of the HSR system: mechanical manufacturing and electrical control, communications and signaling control, and high-speed railway control |
| 4 | Creation of hybrid models for forecasting passenger traffic on intercity high-speed railways [12] | Three hybrid models for predicting passenger flows on intercity high-speed railways based on neural networks have been developed and compared |
| Carrying capacity | | |
| 5 | Creation of a model for scheduling trains based on passenger preferences, taking into account operating costs and capacity limitations [13] | During the planning stage, passenger operators develop schedules to operate passenger services and a train plan to support those schedules. An optimization model has been developed that minimizes passenger travel costs within the limited budget available to cover operating costs |
| Digital twins | | |
| 6 | An overview of digital twin concepts (DTS) for improving product quality and optimizing production processes in railway transport: preliminary recommendations and reference architecture [14, 15] | The introduction of digital twins in the railway sector, with special attention to the role of artificial intelligence (AI) technologies as key factors contributing to the creation of value-added services and applications related to intelligent decision-making |

The key indicator of the organization of transportation by rail is the maximum use of throughput while maintaining other parameters.

The classification of indicators involved in assessing carrying capacity, Fig. 4, include infrastructure parameters and the mode of organizing train movement, which depends on the structure of train traffic on the section.

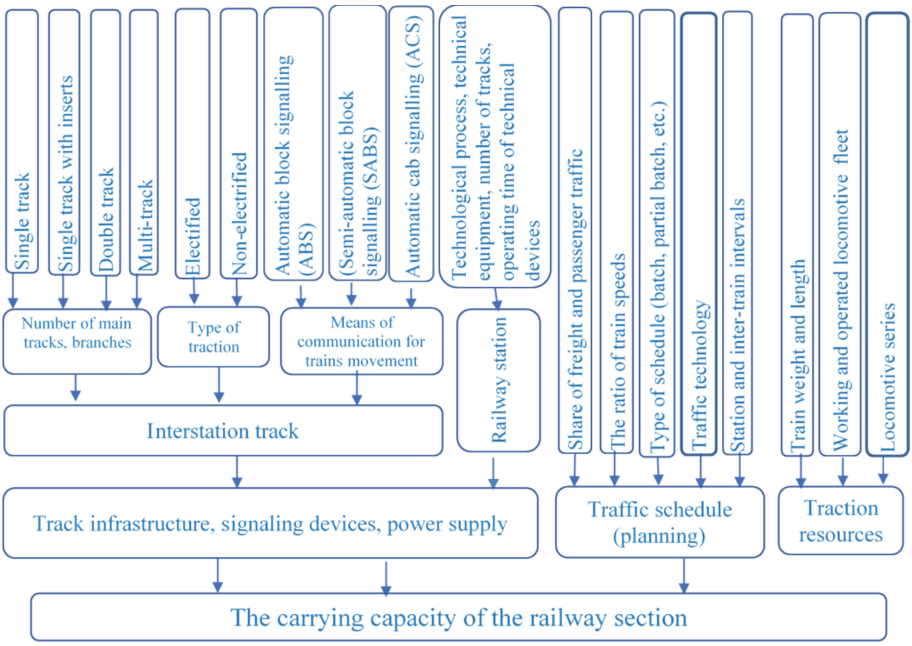


**Fig. 4.** Hierarchy of indicators for assessing the carrying capacity of a railway section

The following entities are of interest: infrastructure, train group (or "train"), regulatory actions on the part of the dispatch apparatus and means of traffic control and regulation. Thus, three parties are involved in the organization of the transportation process:

1. Railway infrastructure, which ensures the movement of a "train group" (TG).
2. The control object is a "train group" (TG), which is in a state of rest or movement;
3. A leading, regulating decision represented by a "dispatcher" who can allow/prohibit specific changes, transitions of the system from one state to another.

We denote the set of states of the elements of the section "infrastructure" by the set $\boldsymbol{S(t)} = \left\{S_l^{-1}(t), S_l^0(t), S_l^1(t)\right\}$, where

t – time point (observation, control);
$l = 1,2,\ldots,L$ – elementary sections (blocks) of infrastructure that affect the organization of the transportation process;
$S_l^{-1}(t)$ – is in the process of recovery as a result of failure of technical devices or other reasons;

$S_l^0(t)$ – is in a state of readiness for work (waiting);
$S_l^1(t)$ – is in a state of active loading (passing a "train group").

We denote the set of states of a *TG* on a section by the set $\boldsymbol{P(t)} = \left\{P^1_{l_1 l_2}(t, l), P^0_{l_1 l_2}(t, l)\right\}$, where

$l_1(l_2))$ – initial (final) station of *TG*
$P^1_{l_1 l_2}(t, l)$ – is in a state of movement (change of state) on the block $l$;
$P^0_{l_1 l_2}(t, l)$ – is in a state of waiting for a command and (or) a change in state in an adjacent section.

The model of active control of train operation on a section is specified by a set of decisions of the "dispatcher" $\boldsymbol{D(t)} = \left\{D_l(t), D_{l_1 l_2}(t), d_{l_1 l_2}(t)\right\}$, where

$D_l(t)$ – the status switch of the block section is in the on/off mode;
$D_{l_1 l_2}(t)$ – the "train group" status switch is in on/off mode;
$d_{l_1 l_2}(t)$ – the "train group" status switch "speed" of change in the state (change in the delay time of the change).

"*TG generation*" can occur according to a given train formation schedule at the boundaries of the site, namely:

– for each station (section) $a \in [1, L]$ and time point $P^1_{a,j}(t, a)$ are defined – the train departing from station (block) $a$ by destination to station (block) $j$ in accordance with the approved timetable.

The set of solutions for generating train groups is denoted by $\boldsymbol{\xi(t)}$.

A dynamic train model on a railway section is described by sets $\{\boldsymbol{S(t)}, \boldsymbol{P(t)}, \boldsymbol{D(t)}, \boldsymbol{\xi(t)}\}$. All parameters take values 0 (free, waiting) or 1 (busy, in operation) depending on the state of the object or process.

The purpose of the simulation is to evaluate (achieve) the maximum capacity of the railway section for the implementation of the formed train flows $\boldsymbol{\xi(t)}$, based on the choice of management decisions $\boldsymbol{D(t)}$ for the implementation of train flows $\boldsymbol{P(t)}$ using the capabilities (states) of infrastructure facilities $\boldsymbol{S(t)}$.

## 6 Formalized Model of Transportation Process Management

The change in the states of entities per unit of clock time $\Delta t$ determines the regulated transportation process. The moments of time at which a change of states can occur are determined by $t_i$, $i = 0, 1, 2, \ldots, I$ for the planning period [0; T], where $\mathrm{T} = \Delta t\, I$. The change of states of entities can be determined by the following relations.

*Conditions of "Infrastructure".* The section opens for work after it is "switched" by the "dispatcher", i.e.

$$S_l^{-1}(t_i) = 1 - S_l^{-1}(t_{i-1}) D_l(t_i). \tag{1}$$

The section remains in a state of waiting for work if there was no *TG* in the previous section or, while in the previous section, the "dispatcher" did not open traffic, i.e.

$$S_l^0(t_i) = (1 - P_{l_1l_2}^1(t_{i-1}, l-1))D_{l_1l_2}(t_i) + P_{l_1l_2}^0(t_{i-1}, l-1)(1 - D_{l_1l_2}(t_i)), \quad (2)$$

There is a *TG* on the previous section and the "dispatcher" did not stop the movement, or the "dispatcher" allowed the train waiting to move on the previous section to move, i.e.

$$S_l^1(t_i) = P_{l_1l_2}^1(t_{i-1}, l-1)(1 - D_{l_1l_2}(t_i)) + P_{l_1l_2}^0(t_{i-1}, l-1)D_{l_1l_2}(t_i). \quad (3)$$

*Train Group (TG) States.* *TG* is in a state of motion if the next section is free, there was no "command" from the dispatcher to stop it, and the next section is "free", i.e.

$$P_{l_1l_2}^1(t_i, l) = P_{l_1l_2}^1(t_{i-1}, l-1)(1 - D_{l_1l_2}(t_i))(1 - S_l^0(t_i)). \quad (4)$$

*TG* is in a state of waiting for movement if the next section is free, there was no "command" from the dispatcher for its movement, or following along the section *TG* was stopped by the "dispatcher", i.e.

$$P_{l_1l_2}^0(t_i, l) = P_{l_1l_2}^0(t_i, l-1)\big(1 - D_{l_1l_2}(t_i)\big) + P_{l_1l_2}^1(t_i, l-1)D_{l_1l_2}(t_i). \quad (5)$$

*States of "Infrastructure" and "Devices".* It is known that the actions of the dispatcher are associated with the analysis of the train situation, the state of infrastructure and railway devices at the corresponding "sections" and "train groups" (TG). The dispatcher will change the nature of the movement if a certain "failure" is detected, leading to a technological violation in the organization of train movement.

Let us consider a flow of failures of this kind as random parameters of external influences on movement:

$$f_l(t) = \begin{cases} 1, \text{ if there was a failure in section } l \text{ at time } t; \\ 0, \text{ otherwise} \end{cases} \quad (6)$$

$$f_{l_1l_2}(t) = \begin{cases} 1, \text{ if there was a failure in TG } (l_1l_2) \text{ at time } t; \\ 0, \text{ otherwise} \end{cases} \quad (7)$$

The process of recovery after failure of infrastructure and *TG* will be considered random. Let's define for infrastructure:

$$h_l(t) = \begin{cases} 1, \text{ if at time } t \text{ the failure is eliminated on } l; \\ 0, \text{ otherwise} \end{cases} \quad (8)$$

A similar function for TG has the form:

$$h_{l_1l_2}(t) = \begin{cases} 1, \text{ if at time } t \text{ the failure is eliminated in TG}(l_1l_2); \\ 0, \text{ otherwise} \end{cases} \quad (9)$$

Without dwelling on the probabilistic characteristics of random processes of failure occurrence and their recovery, let us move on to the decisions of the dispatcher to control traffic on the section.

*States- the dispatcher's decisions on the state of the infrastructure and the TG.*

Changing the state of the infrastructure (section) in case of failure at the command of the dispatcher, i.e.

$$D_l(t_i) = (1 - f_l(t)). \tag{10}$$

Changing the state of the *TG* in case of failure at the command of the dispatcher, i.e.

$$D_{l_1 l_2}(t_i) = (1 - f_{l_1 l_2}(t)). \tag{11}$$

Changing the state of the infrastructure (section) when restoring its operability at the command of the dispatcher

$$D_l(t_i) = h_l(t). \tag{12}$$

Changing the state of the TG when restoring its operability at the command of the dispatcher.

$$D_{l_1 l_2}(t_i) = h_{l_1 l_2}(t). \tag{13}$$

For each *TG* $k_{l_1 l_2}$ (the length of the *TG* in sections) is defined. For each *TG* there is $b_{l_1 l_2}$ such that

$$\prod_{b=b_{l_1 l_2}}^{b_{l_1 l_2}+k_{l_1 l_2}} P^1_{l_1 l_2}(t_i, b) = 1, \text{for each } t_i \in [0;\ \mathrm{T}], \tag{14}$$

and

$$P^1_{l_1 l_2}(t_i, b) = 0, \text{для } b \notin [b_{l_1 l_2};\ b_{l_1 l_2} + k_{l_1 l_2}]. \tag{15}$$

Conditions (14)–(15) determine the continuity of the TG.

Solutions to ensure the continuity of the *TG* are achieved by checking the changes at each time interval $\Delta t$. If the changes do not violate conditions (1)–(15), the corresponding changes in the state of the infrastructure and the *TG* can be implemented, i.e. the changes in the state are confirmed.

## 7 Identifying Key Tasks for Neural Network Control of Railway Transportation Processes

Modern concepts of the transition to digital control platforms provide for the creation of intelligent dispatch assistants that completely or partially replace certain functions or operations. This area includes technologies for the formation of digital twins of railway infrastructure objects and neural network algorithms for managing the transportation process. Therefore, in this study, an attempt was made to combine several tasks: the formation of a digital twin of the railway section and stations with the implementation of neural network control of the transport process. This formulation of the research problem is fundamentally different from those discussed earlier and will allow us to assess the main problems that arise during the formation of both the digital twin and the ANN architecture. In this case, neural networks will use for training not only real data from transport information systems, but also use data from digital models.

A digital twin (DT) is an accurate model of a physical object that is maintained during execution and updated with data collected from monitoring devices in real time.

From the point of view of creating a model of the operation of a railway section, a digital twin is a dynamic and self-developing virtual copy of physical objects and processes, characterized by bidirectional uninterrupted communication that allows real-time data exchange between the physical and digital worlds [14, 20]. Using DT technology, you can implement several services (for example, modeling, monitoring, forecasting).

In the study, several tasks on creating DT and selecting an element for neural network control are grouped; enlarged blocks are shown in Fig. 5.

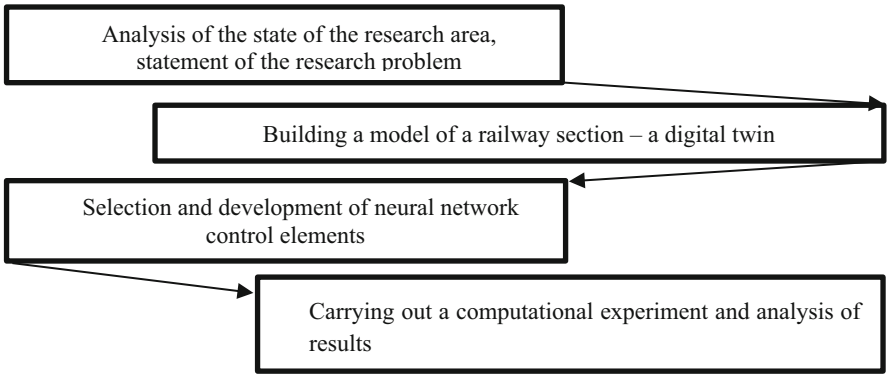


**Fig. 5.** Tasks of developing digital data and selecting elements of neural network control of train traffic

The object of the study is chosen as the real section from Vysochino station to Timashevskaya station of the North Caucasus Railway. As a basis for developing and conducting experimental research, a digital model of the railway section of the station Vysochino – station Timashevskaya, developed at the Rostov State Transport University is used within the framework of the existing educational and laboratory complex "Virtual Railway" [21–25].

To develop a control system for the process of passing trains along a railway section using ANN, it is necessary to competently formulate and solve the following subtasks:

- analysis of factors determining the operational control decision of the system. Each of these factors must be matched with an indicator suitable for entering the input layer of the neural network;
- determination of sets of ANN output data, on the basis of which a command for constructing a train route will be formed;
- choice of architecture (topology) of the neural network: the number of input signals, which determines the power (number of nodes) of the input layer; the number and type of output signals, determining the power of the output layer; determining the number of hidden layers and the number of neurons in each of them; determining the structure and initial value of the weights of connections between layers, as well as choosing the node activation function.

– choosing the method of training the ANN;
– determination of a set of training data for training the ANN;
– determination of a set of test data for verification of the ANN.

An architecture for a railway station (section) control system is proposed, the functional diagram of which is shown in Fig. 6.

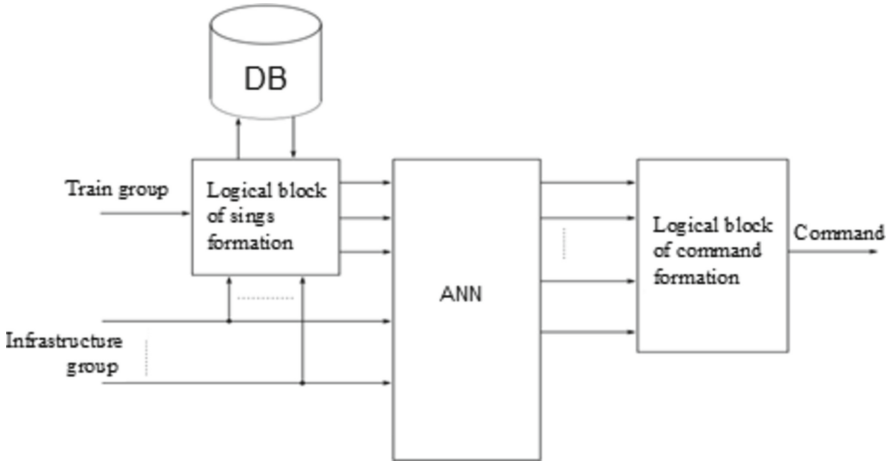


**Fig. 6.** Functional diagram of a neural network control system for a railway station/section in the mode of receiving/passing trains

The formation of a multi-parameter task of optimal control of dynamic processes for the rapid increase in carrying capacity comes down to the search for local optimal solutions to speed up the passage of train traffic through the section due to the control influence on the parameters of the passage of train traffic.

For neural network programming, the key elements are the reference states of a dynamically changing object – the train situation on the section. As a part of the presented formalization of the railway section model, it is necessary to indicate the "normative" intervals for changing the parameters of train operation. The neural network control process will include developing a sequence of actions (decisions) of the train dispatcher to "improve" the parameters of train operation.

Datasets have been formed for offline training of the neural network based on the obtained data as the result of playing scenario. The first dataset contains features which are connected with dispatcher instructions. Particularly, the following features are included:

– station - designation of a station;
– time - current time;
– cmd - command;
– cmd_state – the fact of command execution (1-done, 0-undone).

The second dataset contains features of the state of a sector:

- Time - current time;
- Block_name – the name of occupied /free track;
- State - state of block Sect. (1 – occupy the track 0 - clear the track);
- Train_num - number of a train;
- Velocity - the velocity of a train in the section.

Conducted scenarios of the train traffic allowed to make preliminary assessment of state data of block sections. The state of all sections for scenario is shown in the Fig. 7.

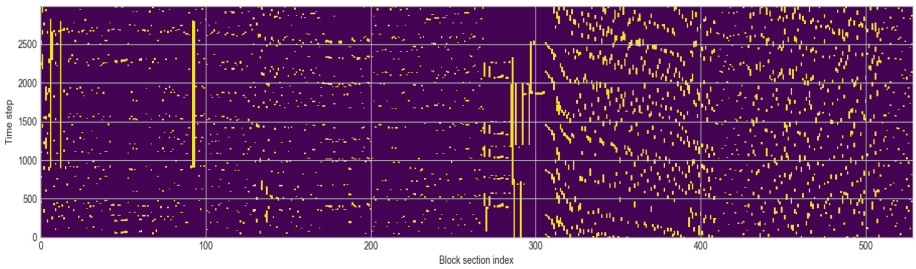


**Fig. 7.** The state of block sections of the scenario

Therefore, we receive approximately 3000 records about changes of state of over 500 block sections per single scenario which duration is around 1 h.

The total amount of commands per station scenario is not high, approximately 100. In comparison with general amount of records of state and unique commands is even smaller. Some commands, at particular stations, are carried out just once.

The analysis shows that peculiarities of issued challenge are small amount of target objects (commands for train managing) in the sample, large numbers of signs and discharged data.

In view of the above, at the first stage, within exploration data analysis, the task was to assess the possibility of dividing space of features: those which lead to the execution of command, that is the task of binary classification. For this purpose, the network architecture was used, which is shown in the Fig. 8. It might be used as a benchmark in the future.

A graph showing the performance of a classification model in the form of ROC curve is shown in the Fig. 9.

The model example itself is superficial, without specific details. It is not even clear which neural network model is being trained and on which data. I think that the work should be substantially improved for publication.

In general, the model showed decent results of classification according to area under the ROC Curve.

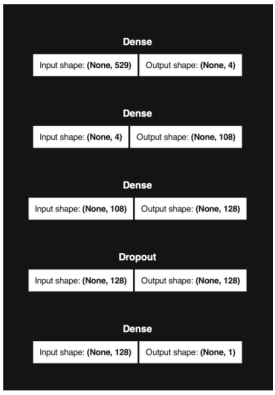


**Fig. 8.** The network architecture

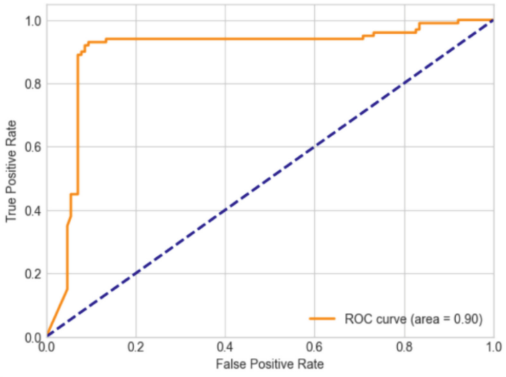


**Fig. 9.** The performance of a classification model

## 8 Conclusion

This article is devoted to the issues of neural network control of the transportation process of a railway section and stations. Since the control object (railway section) operates in a dynamically changing environment, it is proposed to use a digital twin of the real section as an object for implementing ANN. This research methodology will allow us to assess the possible risks of implementing ANN in transportation process control systems on railway lines. Since at the moment there are a huge number of them, connected:

– with data security and privacy protection when using artificial intelligence. When collecting and analyzing large amounts of sensitive data, including passenger information, operational data and maintenance records, leakage or unauthorized access to this data could result in serious privacy troubles and security risks;
– with insufficient recognition of certain types of failure modes, that may increase the risk of accidents;

– with the accuracy of the algorithm, that may lead to an incorrect assessment of certain capacity needs or priorities of train handling. Decision-making process according to AI application must consider the relationship between technological efficiency and social justice.
– with data quality and coverage. Modern rail networks are managed by a variety of tools and devices, resulting in data that is too heterogeneous and unintegrated, making collaboration and decision-making particularly difficult. Despite the widespread adoption of IoT sensors in various sectors, connectivity problems still exist, especially in real-time monitoring.

Summing up we can say that in this study we have discussed some of the challenges and opportunities associated with the implementation of artificial intelligence in the railway industry. In railway data centers, artificial intelligence is used to optimize the use of resources, reduce energy consumption and ensure high availability of services. Despite the potential benefits of AI, there are also challenges associated with its implementation, including the need for high-quality data, the reliability and interpretability of AI-based systems, and ethical and legal issues related to privacy, security, and bias. On the other hand, in the railway industry, artificial intelligence is used to optimize train schedules, reduce delays, support preventative maintenance operations and improve passenger safety by predicting and preventing accidents, so for a safer experiment, the use of ANN in digital twin systems of railway facilities is necessary.

## References

1. Lyabakh, N., Gibner, Y.: Development of an intelligent system for monitoring the technical condition of devices and objects for sorting trains and an automatic adviser for their maintenance. In: Proceedings of the V Scientific and Practical Conference with International Participation Intelligent Control Systems on Railway Transport. Computer and Mathematical Modeling, ISUZHT-2016, pp. 173–175 (2016)
2. Lyabakh, N., Saryan, A.: Automaton-adviser of the predicted technical maintenance of mobile railway transport facilities. Transp. Sci. Technol. Manag. **8**, 12–15 (2018)
3. Vereskun, V.: Organizational and Technological Reliability and Operational Efficiency of Production Facilities of Railway Transport, 256 p. Publishing house of Siberian State Transport University, Novosibirsk (2010)
4. Long-term development program of open joint-stock company "Russian Railways" until 2025 (2019)
5. Najmi, A., Emmanuel, P., Moon, T.: Modern Neural Networks. Johns Hopkins APL Technical Digest, vol. 36 (2022)
6. DB Netz and InstaDeep: Artificial intelligence for dispatch control system. Mag. Railw. World (2022)
7. Kosmin, V.: Railways of Japan: research and development. Transp. Tech. Educ. Pract. **1**, 339–344 (2020)
8. Qian, K., Zhanga, Y.: Research on automatic operation control algorithm of high speed train based on artificial neural network. IOP Conf. Ser. Mater. Sci. Eng. **677** (2019)
9. Zhongcan, L., Ping, H., Chao, W., Wei, D., Yindong, J., Filipe, R.: Railway network delay evolution: a heterogeneous graph neural network. Appl. Soft Comput. **159** (2024)
10. Huangab, P., et al.: Modeling train operation as sequences: a study of delay prediction with operation and weather data. Transp. Res. Part E Logist. Transp. Rev. **141** (2020)

11. Xuehan, L., Minghao, Z., Boyang, Z., Xiaoxuan, W., Zha, L., Liang, H.: A review of artificial intelligence applications in high-speed railway systems. High-Speed Railw. **2**(1), 11–16 (2024)
12. Su, H., Peng, S., Mo, S.: Neural network-based hybrid forecasting models for time-varying passenger flow of intercity high-speed railways. Mathematics **10** (2022)
13. Xie, J., Zhan, S., Wong, S.: A schedule-based model for passenger-oriented train planning with operating cost and capacity constraints **23**, 21314–21328 (2022)
14. Donato, L., Dirnfeld, R., Somma, A., et al.: Towards AI-assisted twins for smart railways: preliminary guideline and reference architecture Intell. Environ, 1–15 (2023)
15. Bao, L., Wang, Q., Jiang, Y.: Review of digital twin for intelligent transportation system. In: International Conference on Information Control, Electrical Engineering and Rail Transit (ICEERT) (2021)
16. Matyukhin, V., Umanskiy, V., Shabunin, A.: On the current state of the project Intelligent Control System of Railway Transport (ISUZhT) and the implementation of interval control technology on its platform. In the collection: Intelligent control systems for railway transport. In: Computer and Mathematical Modeling (ICSRT-2019). Proceedings of the Eighth Scientific and Technical Conference, pp. 3–7 (2019)
17. Bochkov, A.: On some current tasks and directions of scientific and technological development of JSC "NIIAS". Materials of the Scientific and Technical Council of JSC "NIIAS", p. 3 (2023)
18. Russian developers taught a neural network to optimize railway traffic (2022)
19. Russian Railways entrusted the management of train schedules to artificial intelligence (2023)
20. Barrichelli, B., Kaziragi, E., Fogli, D.: Overview of digital twins: definitions, characteristics, applications and design implications (2019)
21. Vereskun, V., Pritykin, D., Dagldian, B.: Development of a topological model of the power supply system of a railway section for the energy dispatcher simulator. Vestnik RGUPS **3**, 90–97 (2021)
22. Vereskun, V., Romanova, D., Pritikin, D., Musienko, N.: Features of the construction of the methodology of business games on a virtual railway, with the interaction of the staff of the directorate of traffic control and traction. Vestnik Rostovskogo Gosudarstvennogo Universiteta Putey Soobshcheniya **4**, 83–90 (2021)
23. Vereskun, V., Pritikin, D., Dagldian, B., Romanova, D.: Principles of simulation modeling of a real railway section due to the development of its topological structure and its relationship with digital models of the infrastructure objects. Vestnik Rostovskogo Gosudarstvennogo Universiteta Putey Soobshcheniya **4**, 177–183 (2022)
24. Vereskun, V., Pritikin, D., Dagldiyan, B., Balashov, E.: Development of alarm subsystem for a virtual railway. Vestnik Rostovskogo Gosudarstvennogo Universiteta Putey Soobshcheniya **1**, 152–158 (2023)
25. Vereskun, V., Pritykin, D., Dagldian, B., Balashov, E.: Development of a subsystem for simulation of train traffic in the model of performance of the normative traffic schedule at the educational and laboratory complex "Virtual Railway". Vestnik Rostovskogo Gosudarstvennogo Universiteta Putey Soobshcheniya **2**, 231–239 (2023)

# The Development of a Method for Managing Traffic Flows Based on an Agent-Based Approach

Gennady E. Veselov, Leonid A. Gladkov(✉), and Dmitriy M. Elkin

Southern Federal University, Taganrog, Russia
{gev,delkin}@sfedu.ru, leo_gladkov@mail.ru

**Abstract.** The article discusses the issue of improving traffic management efficiency. The importance of addressing this issue is justified. An analysis of existing methods' effectiveness has been conducted, identifying their advantages and drawbacks. The problem to be addressed is defined. A classification of current models and algorithms for managing traffic flow is presented. Various traffic flow management models have been analyzed. The benefits and drawbacks of existing traffic control algorithms are highlighted. A method for distributed traffic flow management utilizing the concept of proactive management is proposed. An approach to active traffic management based on agent-based technology has been developed. Additionally, a modified model for vehicle movement in a stream is proposed. The proposed method of traffic management can be applied to different types of intersections and road sections, regardless of their geometric or transportation characteristics. A model of agent interaction has been developed for various types of intersections, and it is proposed to use different types of agents to organize traffic. A general structure of agents has been developed to manage vehicle movement. Software has been implemented to implement the proposed method and obtain a list of related agents within an intersection or road section. Software in the Java and C++ programming languages has been developed. The software has been tested.

**Keywords:** intelligent transport management systems · traffic flows · adaptive distributed management · agency approach

## 1 Introduction

Modern methods of building transport flow control systems implement the principles of centralized transportation management, which limit the system's ability to respond to changes in the movement parameters of individual transport flows through intersections and handle non-standard situations that may arise during transportation [1, 2]. Systems with centralized architectures not only place heavy demands on communication channels but also geographically separate the decision-making point for management, increasing the possibility of errors and reducing the quality of the system. Additionally, such systems require human intervention (an operator), increasing the reaction time to changes in transportation conditions with a large amount of data and increasing the cost of equipment needed for these control centers.


S. Kovalev et al. (Eds.): IITI 2024, LNNS 1209, pp. 108–117, 2024.
https://doi.org/10.1007/978-3-031-77688-5_11

The analysis shows that current methods do not allow for the synthesis of a distributed control system that can effectively manage traffic (TP), taking into account the individual characteristics of traffic sub-stream movement within an intersection. This is because these methods are limited by their centralized management approach, which uses a single entity to manage each intersection [3, 4].

To improve traffic flow management efficiency on the city's road network, it is essential to develop new approaches that allow for the creation of distributed TP management systems. These systems would involve agents acting as control entities at intersections, individually determining control actions for each traffic direction based on the movement parameters of each traffic subflow and the number and location of potential conflicts [5, 6].

## 2 Models and Methods of Traffic Flow Management

A traffic flow (TF) is a complex phenomenon with several key characteristics. It is stochastic, meaning that it is influenced by a variety of factors and cannot be predicted with certainty. Additionally, the behavior of a traffic flow is constantly changing, making it difficult to accurately describe. These changes occur due to temporary fluctuations in the characteristics of the flow, such as intensity, speed, and composition. These characteristics can vary depending on time of day, day of week, and even season. Finally, the traffic flow is non-repeatable, meaning that even with the same set of control measures, the outcome will likely differ each time.

There are three main types of traffic flow, each with its own characteristics: free flow, group traffic, and saturated flow. Groups of cars moving at the same speed can form, and the density of vehicles on the road can increase. If the number of cars per unit of road reaches a certain level, a critical density can occur. This can lead to congestion and changes in the flow of traffic. Breaks in the traffic flow can also occur, causing congestion [7].

Improving the efficiency of traffic management in the city's road network can be achieved by increasing the capacity of intersections and reducing traffic delays [8].

Two approaches can be used when implementing complex traffic management models [9, 10]:

1. Multi-program hard-coded control based on simple road controllers that allow setting several control programs for one traffic light object depending on the time of day, or other approaches.
2. Adaptive traffic management with real-time information on traffic flow. To do this, traffic controllers must receive up-to-date information about the current state of traffic flow from transport detectors located at road intersections and, based on this data, calculate traffic signal cycles for each stage of operation. Transport detectors can also be used to record passing vehicles and determine their parameters.

Currently, traffic management is carried out primarily due to its cost effectiveness. However, this management model is not optimal and often leads to significant delays in vehicle movement. This model fails to take into account various factors affecting traffic, such as the randomly varying level of congestion on a particular section of the road network.

In contrast, adaptive traffic control allows addressing problems with fluctuating traffic loads, although it is a more complex and costly solution that is typically employed in traffic management systems in large cities [10].

Intersections that are more than 1 km apart are considered independent and can be managed separately. Their management algorithms are implemented in traffic controllers. These algorithms can be divided into two categories. The first category does not include adaptive control elements and is used for implementing a strict control strategy. The operation of these algorithms is based on techniques for determining control parameters and distributing periods in a cycle according to the average characteristics of traffic. The optimal duration of a traffic light cycle is determined by summing up the intensities of conflicting traffic directions, and the distribution of cycle periods is determined by adding up and dividing traffic intensities in conflicting directions.

The second group of algorithms includes elements of adaptive control and is based on the methods of switching traffic light signals in accordance with the instantaneous determination of traffic saturation. Effective use of the green signal period is possible by switching traffic lights according to the actual behavior of each vehicle at the intersection.

Local management works within the framework of a single intersection and does not take into account the intensity of traffic at neighboring intersections, making this approach ineffective for use in a city with a high density of traffic intersections.

A network-based approach to traffic management is used at intersections that are located within a distance of 1 km or less from each other and are connected by a single road system. To calculate control parameters, information about the traffic situation at all intersections in the network is needed. Managing traffic at connected intersections is a challenging process to develop and implement, as it requires taking into account numerous factors, which complicates the calculation process. In the case of an adaptive traffic management model, it is also necessary to consider the stochastic nature of traffic flow and various social factors.

Network tight control ensures the coordination of traffic lights within a certain area. Using the standard approach, we can determine and calculate the most optimal traffic light work plan, which is suitable for both urban and motorway intersections. We can also optimize traffic light signal switching programs using specialized software on the road network.

Rigid control algorithms, which are based on the repeatability of traffic situations at certain times of day or on certain days of the week, cannot handle large variations in instantaneous traffic flow intensity. In such cases, network adaptive management approaches are more suitable. At the same time, delays in each direction and the number of stops are estimated, and a performance index is calculated based on the total network bandwidth. The algorithm then gradually adjusts the traffic light operations according to this index. If the road's saturation level reaches a certain threshold, the system increases the minimum cycle time for each intersection by a small fixed amount. If the saturation level falls below this threshold, the cycle time is reduced by the same amount.

## 3 The development of a traffic flow management method based on an Agent-Based Approach

The proposed method implements the concept of active traffic management, which is based on several key principles [11]. These principles include:

1. Maintaining the capacity of the road network at its maximum level.
2. Focusing management efforts on the current situation, rather than predicting future events.
3. Recognizing that traffic conditions are constantly changing and can be unpredictable.
4. Considering drivers' needs and ensuring they can move safely and efficiently.
5. Measuring management results based on outcomes, rather than simply collecting data.
6. Prioritizing system management over system development.
7. Ensuring continuous control, even during periods of low traffic.

The method is based on a traffic flow model, which takes into account various traffic parameters such as the average speed of movement $V_j^{(l)}$, intensity $I_j^{(l)}$, density $k_j^{(l)}$, and the presence of conflict points $DP^{(l)}$. Each traffic subflow $G_j^{(l)}$ is controlled by a separate entity $\gamma_j^{(l)}$ that uses a specific algorithm to manage the flow. New algorithms for managing distributed systems, or agents, are also proposed.

The developed method can be applied to different types of intersections and road sections, regardless of their geometric or transport characteristics [12–14]. The system synthesized using this method depends on the rules for agent interaction and the algorithms used for agent operation.

The general principle of operation of the proposed method for a particular section of the road network is illustrated in Fig. 1. The exact number of agents involved in the management process depends on the specific configuration of the traffic intersection and the surrounding area. As input, we use transport and geometric data about the control object (the intersection), which is obtained through a survey of the targeted section of the road (SR) or through a comprehensive traffic management plan.

The traffic management plan includes information on the number of traffic lanes, road signs, and traffic lights on the study section of the road network. A traffic light can act as a traffic management agent at an intersection, while a road sign on the corresponding lane can be used in the SR area.

The total number of agents is determined by adding up the number of lanes in the intersection and the number of road signs in the area adjacent to the intersection, subtracting the number of lanes leading out of the intersection:

$$K_A = line + sign - line\_out,$$

where $K_A$ represents the total number of agents in the study area of the SR, *line* represents the total number of lanes at the intersection in the study road network (including incoming and outgoing), *sign* is the number of road signs in the study section of the road network (excluding information), and *line_out* is the number of outgoing lanes leading away from the intersection.

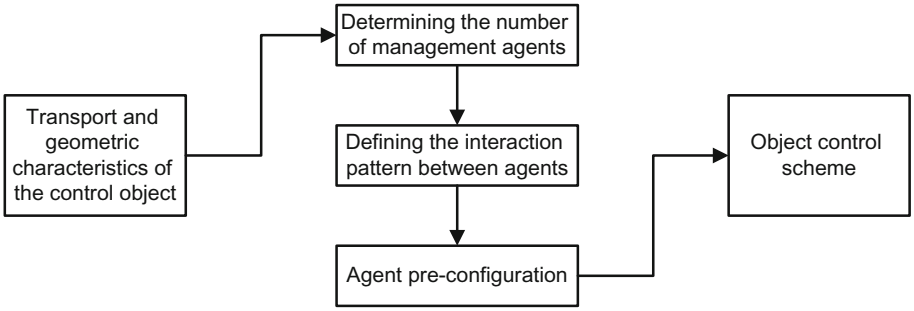


**Fig. 1.** The block diagram of the proposed method

To create an agent interaction system, it is necessary to assign each agent a unique identifier.

Agents can be divided into two categories, based on their physical location within the road network:

- Agents at intersections: These agents are physically located at transport intersections and control traffic that passes through them.
- Agents on road sections: These agents are located outside intersections and control traffic flow outside intersections. Let's take a look at an example of how agents at an intersection interact. For simplicity, we will not consider the direction of traffic for this example (see Fig. 2).

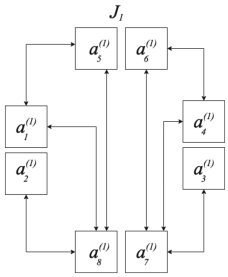


**Fig. 2.** The scheme of interaction at the intersection

Agent $a_1^{(1)}$ must exchange information with agent $a_8^{(1)}$, as the directions of vehicles moving along the lanes they control intersect.

This rule also applies to pairs of agents $a_2^{(1)}$ and $a_8^{(1)}$, $a_7^{(1)}$ and $a_4^{(1)}$, $a_6^{(1)}$ and $a_7^{(1)}$, $a_1^{(1)}$ and $a_5^{(1)}$ .

The endpoints of the movements of sub-streams controlled by agents $a_7^{(1)}$ and $a_4^{(1)}$ coincide, as do those controlled by agents $a_5^{(1)}$ and $a_8^{(1)}$. These agents interact to control traffic at an intersection.

A diagram of agent interactions for several interconnected intersections is shown in Fig. 3. In addition to agents working within a single intersection, those working within a group of intersections also interact with agents from neighboring intersections.

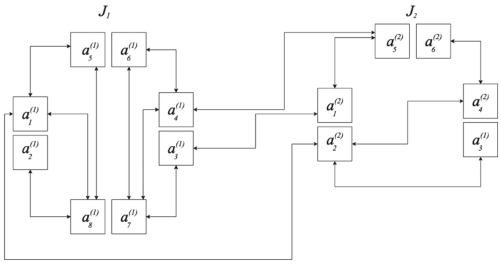


**Fig. 3.** Interaction diagram for a group of intersections

The agents $a_5^{(1)}$ at junction $J_1$ and $a_4^{(2)}$ at junction $J_2$ are on the same path of the traffic flow and need to exchange information with each other in order to effectively manage traffic. This rule also applies to agents $a_3^{(1)}$ and $a_1^{(1)}$ at junction $J_1$, as well as agents $a_1^{(2)}$ and $a_2^{(2)}$ at junction $J_2$.

Depending on the type of agent and its physical location in the road network, each agent has different functionality and needs to be configured differently. The general structure of a traffic management agent is shown in Fig. 4.

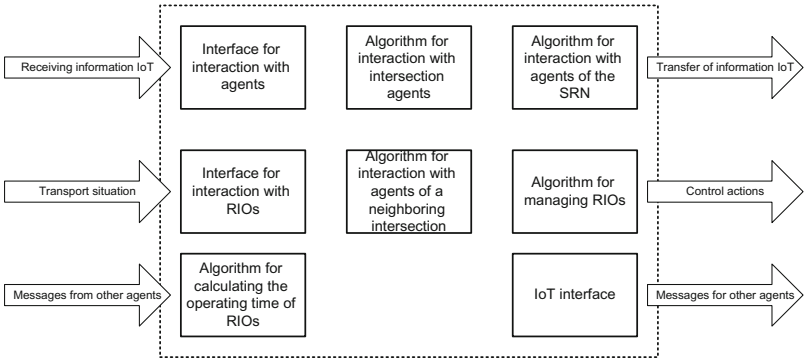


**Fig. 4.** Agent structure

The agent interaction interface is a physical interface that allows agents to communicate with each other and can be implemented using open or closed communication standards and protocols.

The interface for interacting with road infrastructure (ODI) facilities is a physical interface for receiving data or displaying information to apply control actions to the ODI.

IoT interface is a physical interface for sharing data on the transportation situation with the IoT data center.

Algorithms for agent operation are algorithms that implement various methods of interacting with other agents and generating control actions on TP. Depending on the agent type, its physical location, and the presence of nearby agents, the configuration of the agent can be changed during the initial or subsequent setup.

For agents that are located within the boundaries of a transport intersection, there are several options: a locally controlled intersection that is not connected to other transport networks; an intersection that is part of a network and is connected to other intersections; etc.

## 4 Implementation of the Proposed Method

For the effective design of distributed automation systems, it is necessary to use strict methods of description. At the same time, it is important to ensure the compatibility and interchangeability of devices included in the system, which are manufactured by different manufacturers. For these purposes, we have developed a model that uses three levels of hierarchy: the system model, the physical device model, and the functional block model. The system model describes the overall structure and behavior of the system. The physical device model represents individual components and their interactions. The functional block model describes specific functions and processes within the system. All models are presented in accordance with industry standards, in the form of functional blocks, which describe the transmission and processing of information within the system.

The model of a distributed control system in accordance with the international standard IEC 61499 “Functional blocks for industrial control systems” can be represented as a set of physical devices (for example, a PLC) interacting with each other using one or more networks (Fig. 5).

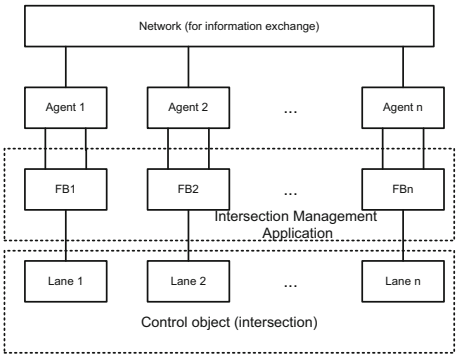


**Fig. 5.** Control scheme

Each agent for traffic control and elements of its structure (modules) can be represented as event-driven automata models. Figure 6 shows a model of an intersection controller in the form of a composite block, developed according to the IEC 61499 standard.

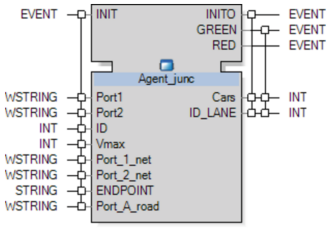


**Fig. 6.** Intersection agent in accordance with IEC 61499 standard

To implement the method proposed in the work and obtain a list of related agents within the intersection and/or section of the UDS, we developed software in Java and C++. The user provides a diagram of a road network section, for which it is necessary to create a traffic management system.

In accordance with the traffic management plan for the studied section of the road network, a traffic agent is added at each entrance to the intersection and at the locations of road signs (see Fig. 7). The directions of traffic controlled by the agent are also indicated, if necessary.

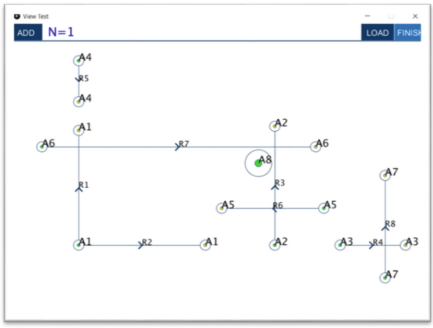


**Fig. 7.** Example of agent placement

As a result of the program, the user receives set of interconnected agents for further system design (Fig. 8). The sets of agents are categorized based on the type of intersection between traffic trajectories. “On Trajectory”: The intersection of agents in the road network whose trajectories are on the same path. “Factual Crossing”: The intersection of agents from different roads whose trajectories intersect. “Agent-Road Crossing”: Interaction between agents from the road network and those from intersections.

The results obtained from testing the performance of a distributed adaptive control system can be compared with the results demonstrated by existing motion control systems (Table 1). The efficiency of transport control for the presented systems was compared with the control existing on a section of the road network using a fixed traffic light cycle - “hard control”.

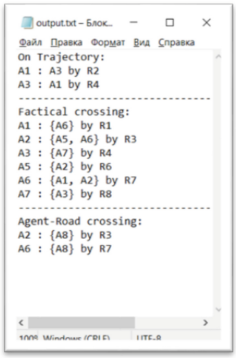


**Fig. 8.** Program output data

**Table 1.** Comparison of Traffic Management Systems

| Traffic management systems | Total delay | Bandwidth, $q$ |
|---|---|---|
| SCOOT | from +88% to −51% | from 5% to 29% |
| SCATS | from −6.3% to −12.5% | from 0% to 20% |
| OPAC | from -21.2% to -39.7 | from 10% to 26% |
| UTOPIA | ~from +23% to −2% | ~15% |
| ImFlow | ~from +37% to −8% | from 5% to 15% |
| Developed system | from −44% to −49% | from 10% to 27% |

## 5 Conclusion

The proposed method of traffic flow management, based on an agent-based approach combined with event-driven automatic models, allows for the formation of control actions on the control object as a result of the interaction between the elements of the control system. The developed algorithms for the operation of the elements of the adaptive control system enable distributed adaptive control over traffic flows on the city's road network. This is achieved through the formation of control actions based on the interaction between elements of the distributed system at intersections, groups of intersections, and sections of the street road network.

## References

1. Sakr, H., El-Afifi, M.: Intelligent traffic management systems: a review. Nile J. Commun. Comput. Sci. **5**(1), 42–56 (2023). https://doi.org/10.21608/njccs.2023.321169
2. Stevens, B.L., Lewis, F.L., Johnson, E.N.: Aircraft Control and Simulation: Dynamics, Controls Design, and Autonomous Systems. Wiley, Hoboken (2015)
3. De Souza, A.M., et al.: Traffic management systems: a classification, review, challenges, and future perspectives [Electronic resource]. Int. J. Distrib. Sens. Netw. **13**(4) (2017). https://doi.org/10.1177/1550147716683612. Accessed 15 Mar 2024

4. Gordon, R.L., Tighe, W.: Traffic Control Systems Handbook (2005 Edition). No. FHWA–HOP–06–006 (2005). 369 p.
5. Gladkov, L.A., Gladkova, N.V., Leiba, S.N., Strakhov, N.E.: Development and research of the hybrid approach to the solution of optimization design problems. In: Abraham, A., Kovalev, S., Tarassov, V., Snasel, V., Sukhanov, A. (eds.) IITI'18 2018. AISC, vol. 875, pp. 246–257. Springer, Cham (2019). https://doi.org/10.1007/978-3-030-01821-4_26
6. Gladkov, L.A., Gladkova, N.V., Gusev, D.Y., Semushina, N.S.: Integrated approach to the solution of computer-aided design problems. In: Kovalev, S., Tarassov, V., Snasel, V., Sukhanov, A. (eds.) IITI 2019. AISC, vol. 1156, pp. 465–475. Springer, Cham (2020). https://doi.org/10.1007/978-3-030-50097-9_47
7. de Souza, A.M., Villas, L.A.: A fully–distributed traffic management system to improve the overall traffic efficiency. In: Proceedings of the 19th ACM International Conference on Modeling, Analysis and Simulation of Wireless and Mobile Systems, Paris, vol. 1, pp. 19–26 (2016)
8. Ravish, R., Swamy, S.R.: Intelligent traffic management: a review of challenges, solutions, and future perspectives. Transp. Telecommun. **22**(2), 163–182 (2021). https://doi.org/10.2478/ttj-2021-0013
9. Slavin, C., et al.: Statistical study of the impact of adaptive traffic signal control on traffic and transit performance. Transp. Res. Rec. **2356**(1), 117–126 (2013)
10. Mudigonda, S., Ozbay, K., Doshi, H.: Evaluation, and selection of adaptive traffic control strategies on transportation networks: decision support tool based on geographic information system. Transp. Res. Rec. **2064**(1), 51–64 (2008)
11. Sullivan, A., et al.: Implementing active traffic management strategies in the US. University Transportation Center for Alabama (2010)
12. Haider Rizvi, S.F., Shams, R., Fattani, M.T., Siddique, A.A.: A cloud based smart parking system. In: 2022 Global Conference on Wireless and Optical Technologies, GCWOT 2022, September 2022. https://doi.org/10.1109/GCWOT53057.2022.9772885
13. Elkin, D., Vyatkin, V.: Distributed traffic control method based on interconnected agents [Electronic resource]. Inform. Cybern. Intell. Syst. **228** (2021). https://doi.org/10.1007/978-3-030-77448-6_53. Accessed 15 Jan 2022
14. El'kin, D.M., Vyatkin, V.V.: Metod razrabotki sistem dlya raspredelyonnogo upravleniya transportnymi potokami na osnove vzaimosvyazannyh agentov. Inzhenernyj vestnik Dona **1**(85), 229–249 (2022)

# Leveraging Deep Reinforcement Learning for Reducing Longitudinal Train Forces in Railway Systems

Yuri P. Bulavin(✉) and Olesya V. Ignatieva

Rostov State Transport University (RSTU), Rostov-on-Don, Russia
i@ibulavin.ru

**Abstract.** This paper explores the application of deep reinforcement learning to minimize in-train forces. A longitudinal train dynamics model incorporating differential equations is established. Track profile identification enables realistic computational experiments. Deep reinforcement learning is used to explore control strategies for braking and traction forces, aiming to minimize in-train forces and improve railway safety and efficiency.

**Keywords:** In-train forces · Deep Reinforcement Learning · Longitudinal Train Dynamics · Differential Equations · Track Profile Identification · ARX · Neural network · MPL · A2C · Ac-tor-Critic · Stable Baseline

## 1 Introduction

This research is a continuation of the works [1] on the creation of modern rolling stock including isothermal one. Its main advantages should be the cost efficiency and design modularity [2]. The rail vehicle can have different composition of modules, for example, traction drive or generator drive from the wheelset axle [3]. As an electric machine, it is reasonable to use a switched reluctance motor (SRM) capable of operating in motor and generator modes, as it is shown in [4]. Reliability and the maintenance problems of rolling stock directly affect the life cycle cost, so it seems reasonable to take into consideration the approaches [5], when designing rolling stock.

Thus, one of the wagon designs can be high-speed isothermal self-propelled rail vehicle or a platform car which are equipped with a high capacity battery and traction drive with SRM.

In the above works, the authors did not consider the problems of reducing the body unladen weight or designing its primary structure, which is an important part of designing a high-speed rail vehicle. We can identify several approaches to reducing the unladen weight of the rail vehicle: applying lighter and stronger materials, optimization of the body design, which give good results, as it is shown in [6] and [7], when designing new constructions and improving the existing ones.

In this work the problem of reducing the mass of the construction and its further optimization is considered in the light of reducing loads, affecting the rail vehicle, their


S. Kovalev et al. (Eds.): IITI 2024, LNNS 1209, pp. 118–130, 2024.
https://doi.org/10.1007/978-3-031-77688-5_12

decrease will reduce the stresses in the construction and, as a result, its mass. As it is said above, we are not limited to the existing designs, so in perspective we consider the extreme case, when motor and non-motor cars in the trainset are coupled with the coupling devices only in certain places, and the car control system keeps a given small distance between the vehicles.

It is obvious that in such a trainset configuration longitudinal forces in the rupture points will be negligible and determined by inertia forces. Designing the control system for rolling stock vehicles and the train requires solving many complex problems, including those connected with controlling tractive efforts and adhesion properties in different environmental conditions. The authors of [8] showed that the Fuzzy control system copes well with this task, but in their work the trainset is not considered as a multi-body dynamic system.

Deep reinforcement learning (DRL) is increasingly being employed to address various challenges in the railway transportation sector. Recent studies have explored the application of DRL for controlling the longitudinal, vertical, and lateral dynamics of rail vehicles [9–11]. These studies focus on a single rail vehicle and utilize differential equations of motion and cosimulation with MATLAB and Simpack. Python is employed as the programming language.

In [12], the authors investigate the application of reinforcement learning to reduce the energy consumption of freight trains. They employ a deep Q-learning algorithm and consider the operational characteristics of the railway infrastructure. The train is modeled using an ordinary differential equation that does not account forces in vehicle coupling devices.

The authors in [13] address the challenge of in-train forces monitoring under service conditions. They developed a mathematical model of train motion using the Universal Mechanism software, which was employed to train a self-attention-based causal convolutional network. The resulting neural network was then applied to predict in-train forces under automatic train operation conditions.

The development of effective braking control algorithms for heavy-haul trains is the focus of [14, 15]. The authors employ DQN-based and Q-table-based algorithms. In [14], the train model is represented by differential equations of motion and incorporates intercar connections. The authors select speed limits, total running distance, and air-braking distance as performance indexes.

In this work, we model the train as a multi-body dynamic system represented by ordinary differential equations (ODEs) in a form adapted for reinforcement learning (RL) algorithms. This approach offers advantages such as improved flexibility in algorithm design and reduced computational burden compared to traditional methods that rely on proprietary software and cosimulation. We focus on using deep RL to address the challenge of reducing longitudinal train forces for controlling the traction and braking of rail vehicles. This task has not been explicitly addressed in the existing literature on rail vehicle control.

## 2 Methods

We describe the train movement model using the system of ordinary differential equations, in which the rail vehicles are represented with the mass elements which are coupled with the coupling devices. The design (force) diagram is shown in Fig. 1.

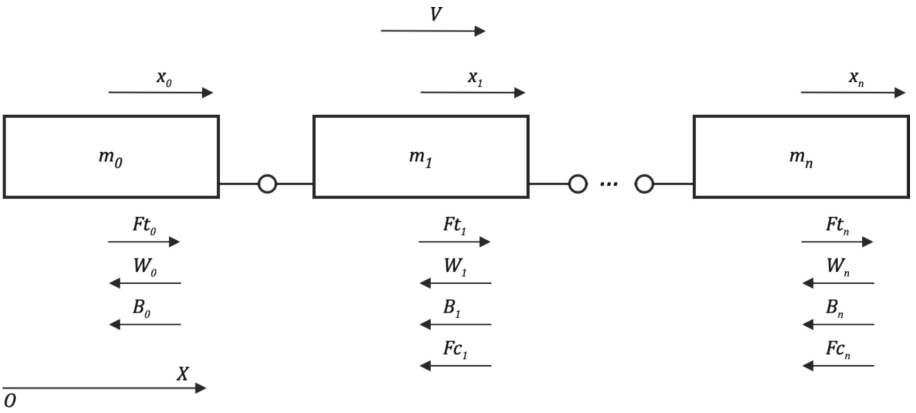


**Fig. 1.** Force diagram of the train

Forces on the diagram: $F_t$ is traction or dynamic brake force, $W$ is resistance force, $B$ is pneumatic brake force, $F_c$ is force in vehicle coupling devices (wagon connections).

In our model, each vehicle has the force $F_t$, which allows us to investigate different configurations of trainsets, the force $F_c^0$ was introduced into the equations for generality, which allows us to consider the absolute motion of the entire train at $F_c^0 = 0$ or relative motions of the arbitrary fragment.

Using the SymPy library [16] and Kane method we obtain the equations of the train motion for the case of $n + 1$ vehicles $i = 0 \ldots n, j = 0 \ldots n$:

$$M \frac{d}{dx}[x, v]^T = f(x, v).$$

The column vector of forces $f(x, v)$ is obtained as follows:

$$\begin{gathered} f(x, v) = \left[v, f^*\right]^T, \\ x = [x_0 \ldots x_n], \\ v = [v_0 \ldots v_n], \\ f_i^* = \left(\sum_{j=i}^{n} -B^i + F_t^i - W^i\right) - F_c^i, \\ f^* = \left[f_0^* \ldots f_n^*\right]. \end{gathered}$$

Mass matrix $M$

$$M = \begin{bmatrix} I_n & O_n \\ O_n & m \end{bmatrix},$$
$$m'_i = \sum_{k=i}^{n} m_k,$$
$$m_{*,0} = \left[m'_0, m'_1, m'_2 \ldots m'_n\right]^T$$
$$m_{*,1} = \left[m'_1, m'_1, m'_2 \ldots m'_n\right]^T$$
$$\ldots$$
$$m_{*,n} = \left[m'_n \ldots m'_n\right]^T.$$

$I_n$ – identity matrix $n \times n$,
$O_n$ – zero matrix $n \times n$,
$x_i$ – vehicle displacements,
$\dot{x}_i$, $v_i$ – vehicle speeds,
$m_i$ – vehicle masses.

The main specific resistance to the movement of non-motorized rail vehicle, N/t is equal to:

$$W = A + \frac{B + Cv + Dv^2}{q},$$

where $A$, $B$, $C$, $D$ – coefficients corresponding to the type of the vehicle,

$q$ – axle load.

The main specific resistance to the movement of locomotives (motorized rail vehicles), N/t is equal to

$$W = B + Cv + Dv^2.$$

Additional specific resistance to the movement due to the track gradient is calculated by the formula, N/t:

$$w_i = 9{,}81\, i,$$

where $i$ is the track gradient (slope), in per mille (‰).

Inter-car connections in the first approximation are assumed to be linear with the stiffness $c$ and damping $\beta$

$$F_c = cx + \beta v.$$

Irregularities in the plan were described on the basis of the measurement results of a real 130 km section, the fragment of which is shown in Fig. 2.

Specific resistance to the movement due to the gradient is one of the main factors, affecting the train running, thus, it is reasonable to develop the model of the track section gradients to improve the control reliability.

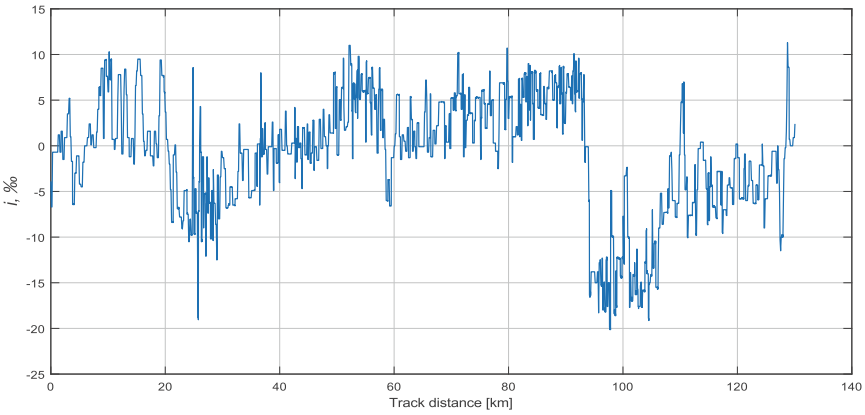


**Fig. 2.** Track gradients

Let us perform distribution Fitting and find parameters of normal distribution with mean and variance for forward and reverse directions. Figure 3 shows histogram of irregularities in the plan, the nonparametric distribution and the normal distribution with the parameters mean = 6.71269e−17 and variance = 47.4837.

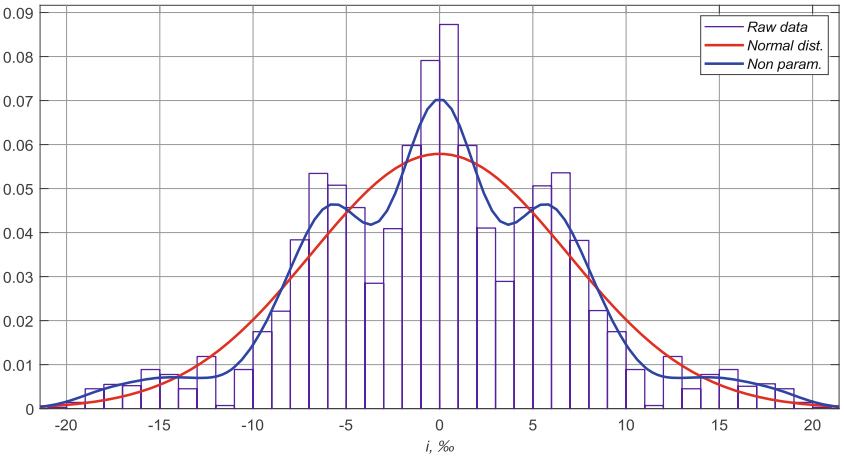


**Fig. 3.** Results of distribution Fitting

The data obtained can be used to design the track profile using the bootstrap method.

For the cases when it is not reasonable to apply the above method, we identify the parameters of the track irregularity model. The simplest variant for the forward direction

is Discrete-time ARMA model with fit to estimation data = 83.28%:

$$A(z)y(t) = C(z)\varepsilon(t),$$
$$A(z) = 1 - 0.8584 \cdot z^{-1} - 0.5442 \cdot z^{-2} - 0.02287 \cdot z^{-3} + 0.4265 \cdot z^{-4},$$
$$C(\mathrm{z}) = 1 + 0.3876 \cdot z^{-1} - 0.3214 \cdot z^{-2} - 0.6745 \cdot z^{-3} - 0.2571 \cdot z^{-4}.$$

For forward and reverse directions with fit to estimation data = 77.24%:

$$A(z) = 1 - 2.349 \cdot z^{-1} + 2.465 \cdot z^{-2} - 1.697 \cdot z^{-3} + 0.581 \cdot z^{-4},$$
$$C(\mathrm{z}) = 1 - 1.44 \cdot z^{-1} + 1.208 \cdot z^{-2} - 0.6329 \cdot z^{-3} - 0.07957 \cdot z^{-4}.$$

Deep reinforcement learning requires creating the environment for the agent to interact with it. In this work, we use Gymnasium [17]. The motion equations and the track profile model derived above were used to train the agent using algorithms, implemented in Stable Baselines 3(SB3) [18].

To identify the most rational action space $A$ and observation space $S$ for the problem under consideration, as well as and the architecture of the neural network, several environments were created. We refer to observation space as $S$ since [17] requires it to be explicitly set and passed to the agent, actually representing it as the set of all possible states the agent can be in.

We considered Model 1 for a single locomotive and Model 5 for the train with one locomotive and five cars. In the environment with Model 1 action space, observation space, reward $r$ at the step $t$ were set in several variants.

Variant 1.

$$A = [-1, 1], S \subseteq R^8, s \in S, s_t = \left(x_t, v_t, i_t, i_t^2, i_t^4, \epsilon_t, x_{t-1}, v_{t-1}\right),$$

where $x_t$ displacement, $v_t$ speed, $i_t$ gradient, $i_t^2$ gradient of 2 m forward, $i_t^4$ gradient of 4 m forward, $\epsilon_t$ difference between current and required speeds $v^*$ $x_{t-1}$ displacement at the previous step, $v_{t-1}$ speed at the previous step.

Reward with weights $\omega^d$ and $\omega^v$

$$r_t = \omega^d v_t\left[v^{*-} < v_t < v^{*+}\right] + \omega^v (v_t - v^*)^2\left(1 - \left[v^{*-} < v_t < v^{*+}\right]\right),$$
$$v^{*-} = v^* - \Theta,$$
$$v^{*+} = v^* + \Theta.$$

where $\Theta$ – speed threshold

Variant 2.

According to [19], let us discretize the action space:

$$A = \{0, 1, \ldots, n\}, S \subseteq R^8, s \in S, s_t = \left(x_t, v_t, i_t, i_t^2, i_t^4, \epsilon_t, x_{t-1}, v_{t-1}\right),$$

where $n + 1$ – number of discrete actions.

Reward with weights $\omega^d$ and $\omega^v$

$r_t = \omega^d v_t\left[v^{*-} < v_t < v^{*+}\right] + \omega^v (v_t - v^*)^2\left(1 - \left[v^{*-} < v_t < v^{*+}\right]\right).$

Variant 3.

In this case, in $S$ there is no history of the previous step $x_{t-1}, v_{t-1}$ and the displacement (the distance traveled) of the first vehicle $x_t^0$

$$A = \{0, 1, 2, 3\}, S \subseteq R^5, s \in S, s_t = \left(v_t, i_t, i_t^2, i_t^4, \epsilon_t\right),$$

The actual control values $u$ for actions $a$ with step $\delta$ were obtained as follows

$$u_t = u_{t-1} + a_t \delta[a_t < 3],$$
$$r_t = \omega^d v_t\left[v^{*-} < v_t < v^{*+}\right] + \omega^v (v_t - v^*)^2\left(1 - \left[v^{*-} < v_t < v^{*+}\right]\right).$$

Variant 4.

$$A = \{0, 1, \ldots, n\}, S \subseteq R^6, s \in S, s_t = \left(v_t, i_t, i_t^2, i_t^4, \epsilon_t, v_{t-1}\right).$$

Reward with weights $\omega^d$ and $\omega^v$

$$r_t = \omega^d v_t\left[v^{*-} < v_t < v^{*+}\right] + \omega^v \left(v_t - v^*\right)^2\left(1 - \left[v^{*-} < v_t < v^{*+}\right]\right).$$

Environment with Model 5.

Variant 1.

Due to the fact that the relative coordinates were introduced in the model, the absolute speed of the locomotive $v'$ was introduced in $S$. Reward functions were introduced according to [20].

$$A = \{0, 1, \ldots, n\}, S \subseteq R^{27}, s \in S, s_t = \left(x_t^{1\ldots5}, v_t, i_t, i_t^2, i_t^4, \epsilon_t, x_{t-1}^{1\ldots5}, v_{t-1}, v'\right),$$

$$r_t = \omega^v \exp[-0.25\left(v' - v^*\right)^2]\left(\left[1 < v_t < v^{*+}\right]\right) - [v_t < 1] - [v_t > v^{*+}],$$
$$v^{*+} = v^* + 2\Theta.$$

Variant 2.

In this case we used multi-discrete action space

$$A = \left\{\mathrm{A}^0, \mathrm{A}^1, \ldots, \mathrm{A}^n\right\}, a^i \in A^i, a^i = \{0, 1, \ldots, n\},$$
$$S \subseteq R^{27}, s \in S, s_t = s_t = \left(x_t^{1\ldots5}, v_t, i_t, i_t^2, i_t^4, \epsilon_t, x_{t-1}^{1\ldots5}, v_{t-1}, v'\right),$$
$$r_t = (\omega^v \exp[-0.1\left(v' - v^*\right)^2\Big] + \omega^d \exp[-10 \max\left(x_t^{1\ldots n} - v^*\right)^2\Big])\left(\left[1 < v'_t < v^{*+}\right]\right)$$
$$-\left[v'_t < 1\right] - [v'_t > v^{*+}],$$
$$v^{*+} = v^* + 2\Theta.$$

Training was carried out for speeds of 10, 15, 20 m/s, the control system was to keep the specified speed within the required interval $\Theta = 2$ m/s. Integration of the motion equations was performed using SciPy [21].

Our policies were trained with Actor Critic (A2C) [22] with fully-connected network (FCNN) with the same number of layers for Actor and Critic.

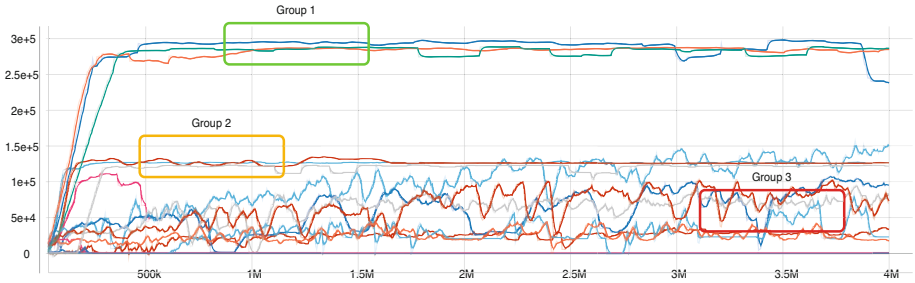


**Fig. 4.** Mean episodic training reward in Model 1 variants

## 3 Results

In order to evaluate the impact of the environment variants on training performance, mean episodic training reward values [18] have been found and shown in Fig. 4 and in the Table 1.

All results are shown on the graph, but the most important ones are summarized in the table. Models and environments are divided into three groups in descending order from best to worst.

**Table 1.** Characteristics of Model 1 variants

| Variants | Min | Max | Value | Group |
|---|---|---|---|---|
| Model 1Variant 4 10 m/s [64 64] | −3,464.4252 | 288,781.3573 | 286,219.0088 | 1 |
| Model 1Variant 4 15 m/s [64 64] | −1,122.2761 | 287,584.9127 | 284,720.2052 | 1 |
| Model 1Variant 4 15 m/s [128, 64, 32] | −3,003.1195 | 298,178.2648 | 237,709.2752 | 1 |
| Model 1Variant 2 20 m/s [64 64] | −3,744.6352 | 149,523.5488 | 148,655.8077 | 2 |
| Model 1Variant 4 20 m/s [128, 64, 32] | 120.8663 | 128,727.7447 | 126,472.7185 | 2 |
| Model 1Variant 4 10 m/s [128, 64, 32] | −211.6326 | 123,428.4299 | 121,786.2627 | 2 |
| Model 1Variant 4 20 m/s [64 64] | 4,449.3306 | 134,704.0709 | 121,429.271 | 2 |
| Model 1Variant 2 15 m/s [64 64] | −136.0347 | 107,088.4936 | 95,499.7257 | 3 |

According to the table and figure, the environment in Variant 4 seems to be the most successful.

As it follows from the obtained results in the table and the figure, the best variants are variants 4, and increasing the inner layers in FCNN to [128, 64, 32] does not give significant advantages in comparison with the configuration [64, 64].

The same approach for determining the rational network architecture was applied for the environment with model 5. The results are shown in Fig. 5 and in the Table 2.

In this case architectures with the large number of layers also do not have significant advantages.

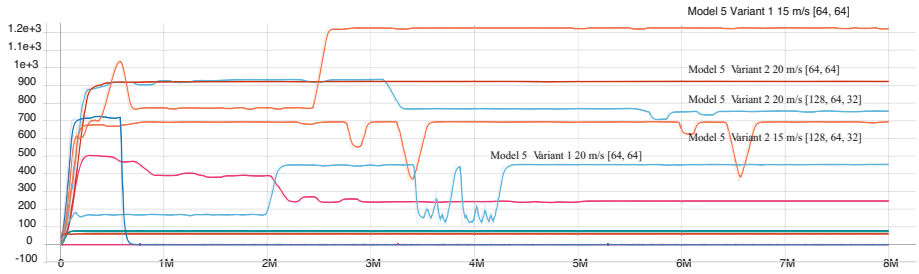


**Fig. 5.** Mean episodic training reward in Model 5 variants

**Table 2.** Characteristics of Model 5 variants

| Variants | Min | Max | Value |
|---|---|---|---|
| Model 5 Variant 1 15 m/s [64, 64] | 48.1687 | 1,226.289 | 1,172.5492 |
| Model 5 Variant 2 20 m/s [64, 64] | 2.7667 | 922.6016 | 919.4102 |
| Model 5 Variant 2 20 m/s [128, 64, 32] | 12.2292 | 933.5962 | 741.7054 |
| Model 5 Variant 2 15 m/s [128, 64, 32] | 11.0921 | 695.0649 | 682.6167 |
| Model 5 Variant 1 20 m/s [64, 64] | 29.2059 | 452.7209 | 423.1615 |

As the result of training, policy allows us to maintain the set speed constant throughout the entire section. Figure 6 shows the gradients and movement speed with upper and lower limits ± standard deviation σ of model 5 without car control.

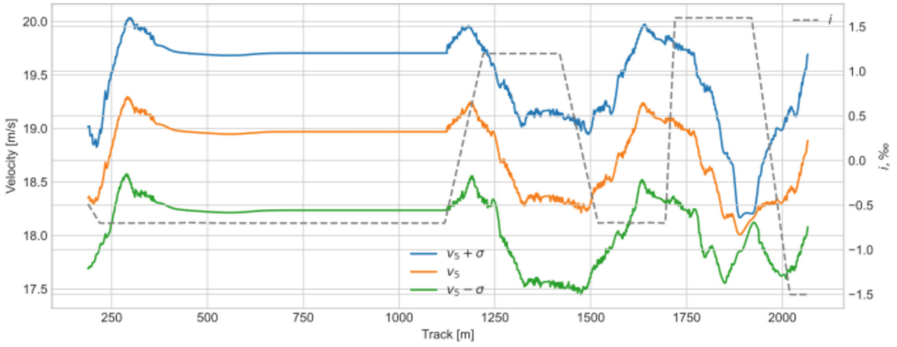


**Fig. 6.** Velocity of the trainset of 5 railway cars without car control

Similar graph in the case of control by forces *Ft* is shown in Fig. 7.

The dynamic forces in the trainset, in the case when there are no gaps in the coupling devices, are determined by the change in the distance between the railway cars. Figure 8 shows the reduced distances between cars without control.

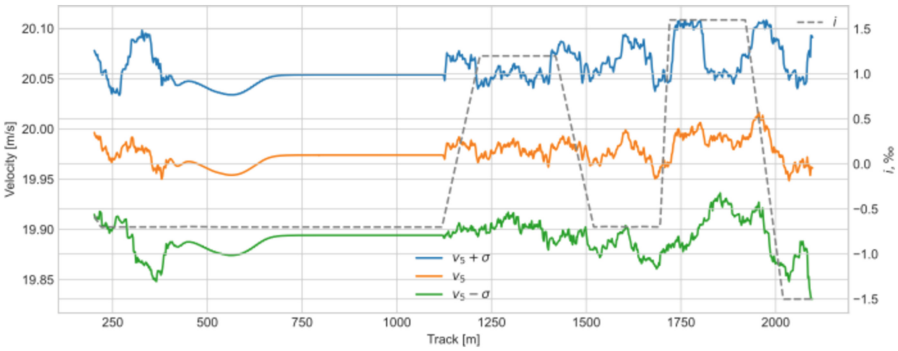


**Fig. 7.** Velocity of the trainset of 5 railway cars with car control

To bring the obtained results closer to the practical plane, Fig. 9 shows the deformations of inter-car connections $x_{1...5}$ in the cases of controlling the traction and breaking of the vehicles $\pm F_t$ and controlling only the brakes $-F_t$.

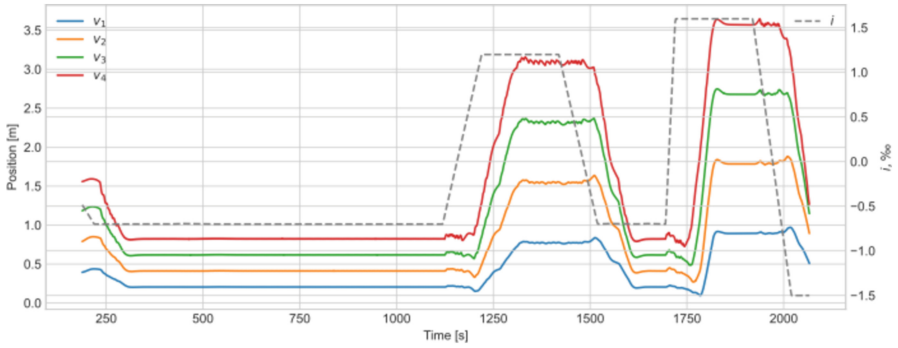


**Fig. 8.** Reduced distances between cars for the case without control

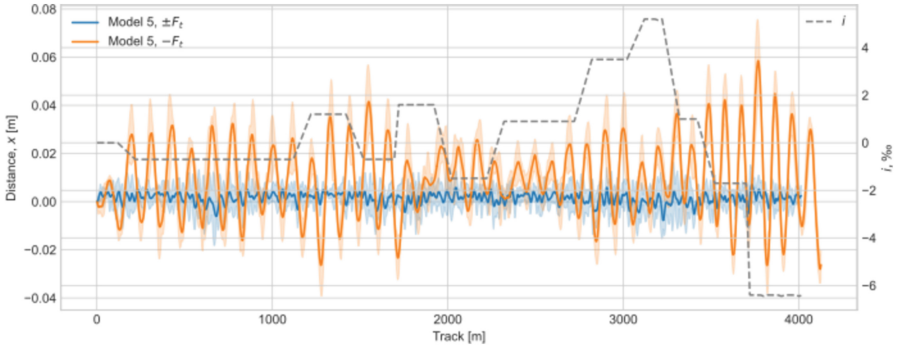


**Fig. 9.** Deformations of inter-car connections for the case with control

## 4 Discussion and Conclusions

The presented results show that using the policy found, it is possible to achieve practically predetermined distance between cars and thus to control the dynamic forces in the trainset. The strictness of fulfilling the condition $v^* = const$ and distances between the cars is determined by $\omega^v$ и $\omega^d$.

It should be noted that track characteristics affect the training performance significantly, it is reasonable to use an environment model for this kind of problems and move on to model based control.

Discretization for action space affects the training performance, the model can go into loop because of its inability to select an unintended action, besides too small discretization interval transforms the problem to continuous adjustment (control), which in this formulation of the problem required significant computational resources and was not considered further. A possible solution can be a kind of irregular grid on the continuous action space, representing the track gradients.

The following highlights the scientific novelty of this work. This work demonstrates the feasibility of controlling longitudinal train forces using reinforcement learning algorithms.

The authors have achieved several significant theoretical results. The models of track irregularities in the plan and the parameters of normal distribution have been found, which makes it possible to generate them if necessary.

The differential equations describing train movement for an arbitrary number of rolling stock units and various train configurations have been derived. The form in which these equations are presented allows for their straightforward integration into well-established machine learning environments, eliminating the need for proprietary software to model train dynamics.

This work achieves its goals by leveraging Actor Critic (A2C) with a fully-connected network (FCNN), a well-established and effective reinforcement learning algorithm. An investigation of various state spaces, actions, and reward functions revealed that incorporating the dynamic system's history into the state space is beneficial while avoiding explicit time representation. This approach avoids the need for additional time-related features, simplifying the state space and potentially improving training efficiency.

The authors consider leveraging multi-agent reinforcement learning in this kind of problems to be the most promising direction for further research. This study demonstrates the feasibility of utilizing a group of 5–6 rail vehicles as the control object.

The practical significance of this work lies in the potential to design lighter rail vehicles by reducing longitudinal train forces. For existing cars, the possibility of controlling brakes is demonstrated, which also leads to a reduction in longitudinal forces. In the case of passenger cars, this translates to improved passenger comfort.

## References

1. Voron, O.A., Mamaev, E.A.: Economic and technological basis for development of rolling stock and transport infrastructure for transportation of perishable goods. Vestnik Rostov State Univ. Econ. (RINH) **2**(74), 30–40 (2021)

2. Voron, O.A.: Methodology of research on the demand for development of transport infrastructure and rolling stock for perishable goods transportation. World Transp. Transp. **19**(3), 148–157 (2021)
3. Bulavin, Y.P., Voron, O.A., Volkov, I.V.: Modelling the dynamics of an undercar generator with a v-belt drive of an isothermal railway vehicle. In: IOP Conference Series: Materials Science and Engineering, vol. 709, no. 3, p. 033094. IOP Publishing (2020). https://doi.org/10.1088/1757-899X/709/3/033094
4. Voron, O.A., Petrushin, A.D.: Improving the energy efficiency of electric machines for specialized railway rolling stock. In: 18th International Scientific Technical Conference Alternating Current Electric Drives, ACED 2021, pp. 1–4. IEEE (2021). https://doi.org/10.1109/ACED50605.2021.9462273
5. Liabakh, N.A., Ignatieva, O.V., Shapovalov, V.V.: Intelligent maintenance and repair on railway transport. In: Kovalev, S., Kotenko, I., Sukhanov, A. (eds.) IITI 2023. LNNS, vol. 777, pp. 247–259. Springer, Cham (2023). https://doi.org/10.1007/978-3-031-43792-2_24
6. Liu, W., Zhang, Y., Liu, Q., Zhang, B., Fu, Q.: Structural optimization of the heavy haul wagon body based on MPSO-BP algorithm. Trans. Can. Soc. Mech. Eng. **45**(3), 461–472 (2020)
7. Miao, B.R., Luo, Y.X., Peng, Q.M., Qiu, Y.Z., Chen, H., Yang, Z.K.: Multidisciplinary design optimization of lightweight carbody for fatigue assessment. Mater. Des. **194**, 108910 (2020)
8. Konovalov, P., Bulavin, Y., Volkov, I.: Control of the sand feeding system operation as a reserve for improving the adhesion properties of the traction rolling stock. In: Guda, A. (ed.) NN 2022. LNNS, vol. 509, pp. 95–104. Springer, Cham (2023). https://doi.org/10.1007/978-3-031-11058-0_10
9. Wei, J., Lu, Z., Yin, Z., Jing, Z.: Multiagent reinforcement learning for active guidance control of railway vehicles with independently rotating wheels. Appl. Sci. **14**(4), 1677 (2024)
10. Hou, X., Gan, M., Zhang, J., Zhao, S., Ji, Y.: Vehicle ride comfort optimization in the post-braking phase using residual reinforcement learning. Adv. Eng. Inform. **58**, 102198 (2023). https://doi.org/10.1016/j.aei.2023.102198
11. Li, Y., Zhu, Z., Li, X.: Reinforcement learning based speed control with creep rate constraints for autonomous driving of mining electric lovomotives. Appl. Sci. **14**, 4499 (2024). https://doi.org/10.3390/app14114499
12. Lin, X., Liang, Z., Shen, L., Zhao, F., Liu, X., Sun, P., Cao, T.: Reinforcement learning method for the multi-objective speed trajectory optimization of a freight train. Control Eng. Pract. **138**, 105605 (2023). https://doi.org/10.1016/j.conengprac.2023.105605
13. Zhang, S., Huang, P., Yan, W.: A data-driven approach for railway in-train forces monitoring. Adv. Eng. Inform. **59**, 102258 (2024). https://doi.org/10.1016/j.aei.2023.102258
14. Liu, W., Su, S., Tang, T., Wang, X.: A DQN-based intelligent control method for heavy haul trains on long steep downhill section. Transp. Res. Part C Emerg. Technol. **129**, 103249 (2021). https://doi.org/10.1016/j.trc.2021.103249
15. Zhang, C., Zhou, S., He, J., Jia, L.: Cyclic air braking strategy for heavy haul trains on long downhill sections based on Q-learning algorithm. Information **15**, 271 (2024). https://doi.org/10.3390/info15050271
16. Meurer, A., et al.: SymPy: symbolic computing in Python. PeerJ Comput. Sci. **1**(3), e103 (2017). https://doi.org/10.7717/peerj-cs.103
17. Towers, M., et al.: Gymnasium. V1.0.0a1. Zenodo (2024). https://doi.org/10.5281/zenodo.10655021
18. Raffin, A.: Stable-baselines 3: reliable reinforcement learning implementations. J. Mach. Learn. Res. **22**(268), 1–8 (2021)
19. Tang, Y., Agrawal, S.: Discretizing continuous action space for on-policy optimization. In: Proceedings of the AAAI Conference on Artificial Intelligence, vol. 34, no. 04, pp. 5981–5988 (2020)

20. Peng, X.B., Abbeel, P., Levine, S., Van de Panne, M.: DeepMimic: example-guided deep reinforcement learning of physics-based character skills. ACM Trans. Graph. (TOG) **37**(4), 1–14 (2018). https://doi.org/10.1145/3197517.3201311
21. Virtanen, P., et al.: SciPy 1.0: fundamental algorithms for scientific computing in Python. Nat. Methods **17**(3), 261–272 (2020). https://doi.org/10.1038/S41592-019-0686-2
22. Mnih, V., et al.: Asynchronous methods for deep reinforcement learning. In: International Conference on Machine Learning, PMLR, vol. 48, pp. 1928–1937 (2016)

# Fuzzy Controller Using a Predictive Control Model to Optimize the Parameters of the Caustic Soda Evaporation

Elena A. Muravyova(✉), Timur M. Halmurzin, Marsel I. Sharipov, and Aleksand S. Dorofeev

Institute of Chemical Technologies and Engineering, Ufa State Petroleum Technological University, Sterlitamak, Russia
muraveva_ea@mail.ru

**Abstract.** This paper presents the development and study of a system for controlling the evaporation process of caustic soda using a model predictive control (MPC) and fuzzy logic. The main goal is to optimize temperature regimes and improve the system's adaptation to external disturbances to enhance the quality and reliability of the production process. As a result of this work, a control system for the caustic soda evaporation process was implemented, demonstrating high efficiency in maintaining stable temperature regimes and adapting to external disturbances.

**Keywords:** Model predictive control (MPC) · fuzzy logic · temperature control · caustic soda evaporation · parameter optimization · external disturbances · process automation · control system · temperature regime · control adaptation

## 1 Introduction

In modern industry, there is a growing need for the development and implementation of highly efficient and reliable systems for managing technological processes. Model predictive control (MPC) has become one of the leading tools in process automation due to its ability to analyze and optimize operational parameters in real time. This predictive capability is particularly valuable in processes that require strict adherence to temperature regimes and where parameter fluctuations can lead to reduced product quality or even emergency situations.

In the process of evaporating caustic soda, operators face a number of challenges, among which maintaining strict temperature regimes and responding to sudden disturbances in the process, such as temperature fluctuations and pressure changes, are particularly notable. In the evaporation process of caustic soda, precise adherence to temperature conditions is of paramount importance for production efficiency and the quality of the final product. In the process of caustic soda evaporation, precise adherence to temperature conditions is of paramount importance for production efficiency and the quality of the final product. Any deviation from the established temperature regime


S. Kovalev et al. (Eds.): IITI 2024, LNNS 1209, pp. 131–140, 2024.
https://doi.org/10.1007/978-3-031-77688-5_13

can lead to a chain of undesirable chemical reactions, which not only reduce the yield of valuable product but also pose a potential threat of hazardous by-product formation, representing a serious risk to production safety.

## 2 Description of the Technological Process

Figure 1 shows the FSA of caustic soda evaporation.

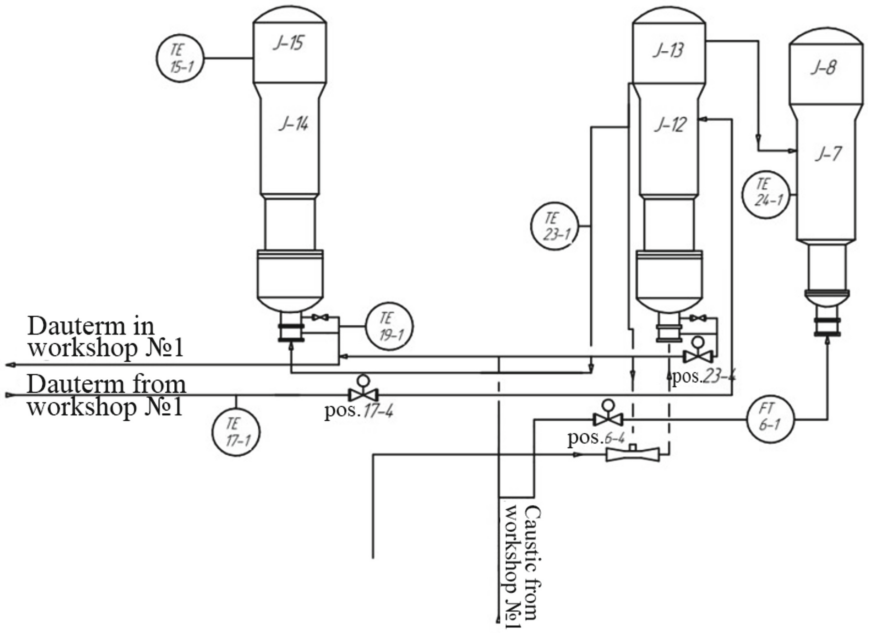


**Fig. 1.** The diagram of the evaporative unit for dehydrating caustic soda.

From workshop №1, caustic soda is pumped into degassing column J-14, where it is mixed with vapor from the separator J-15, entering the upper part of the column. The caustic soda solution exiting the degassing column is drained into a tank.

The caustic soda solution from the tank is pumped by a submerged pump into the lower part of evaporator unit J-7, where it is heated by secondary steam from separator J-12. The secondary steam from the separator is fed into the inter-tube space of evaporator unit J-7, and the steam condensate is drained into a hydroseal. The heated caustic soda solution from the evaporator unit is then transferred to separator J-8, where water vapors are separated from the caustic soda under vacuum.

In evaporator unit J-12, the caustic soda solution is heated by steam from diphenyl mixture and then enters separator J-13, where the separation of water vapors and caustic soda occurs.

To maintain the quality of the caustic soda evaporation process, it is necessary to maintain the temperature TE 15-1 of the caustic soda melt within the range of 340–365 °C

by heating the liquid with steam from diphenyl mixture (temperature sensor TE 17-1) in separator J-15, so that the melt reaches the required temperature and concentration for further application.

## 3 Conceptual Control System Model

At the core of the system lies a Model Predictive Control (MPC) model, which receives current measurements of caustic soda and steam temperatures. These parameters are inputted into the MPC, which utilizes an optimization function to determine the optimal values of three parameters: the temperature of diphenyl mixture in J-12, the flow rate of caustic soda feed, and the temperature of the caustic soda solution in J-12.

The objective function minimizes temperature deviations to achieve desired system operating conditions. Subsequently, the calculated temperature and flow rate values are inputted into a fuzzy controller.

The fuzzy controller plays a crucial role in this model as it utilizes rules and input temperature constraints to regulate three valves affecting the system's qualitative indicators.

The conceptual control system model is depicted in Fig. 2.

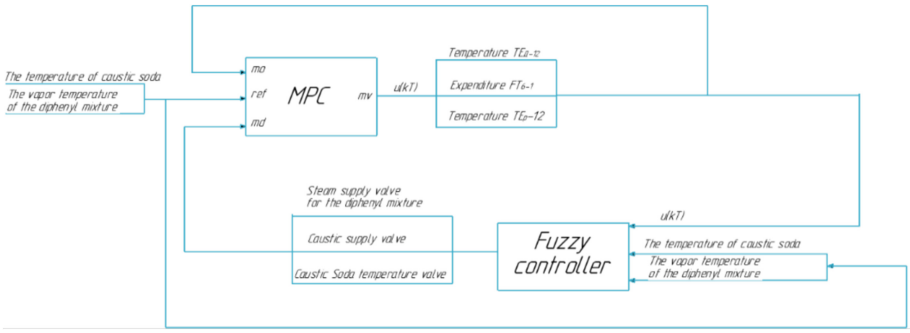


**Fig. 2.** Conceptual Control System Model.

Each block performs its function, ensuring the smooth operation of the entire control system.

## 4 Conceptual MPC Model

The MPC receives input data about the current state of the process, denoted as r(kT). Based on this input data, the MPC determines the optimal values of three temperatures: the temperature of the diphenyl mixture in J-12, the flow rate of caustic soda feed, and the temperature of the caustic soda solution in J-12 (Fig. 3). The task of these control signals is to adjust the process to meet the specified parameters while minimizing the use of resources. The mathematical model of the MPC utilizes an optimization function, allowing it to accurately obtain and process temperature values, ensuring their compliance with the specified parameters with minimal deviation.

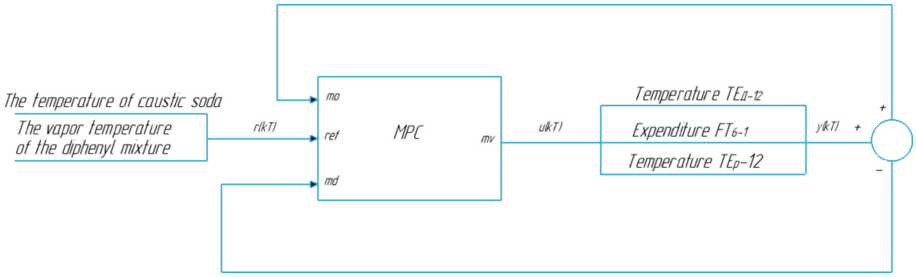


**Fig. 3.** Conceptual MPC Model.

In addition to calculating the optimal temperature values, the MPC receives feedback from the fuzzy controller in the form of adjusted valve settings (md).

## 5 Development of MPC

The optimization function in the control system of the caustic soda evaporation process plays a crucial role in ensuring the stability and efficiency of the entire system. Its main goal is to minimize deviations of critical parameters, such as temperature and flow rate, from their optimal values. The essence of the optimization function lies in finding such values of these parameters that will result in the minimum deviation from the specified conditions, thus maintaining stable and efficient process operation.

The optimization function in MPC, aiming to minimize deviations of predicted values from target values, would be as follows:

$$J = \sum_{j=0}^{Hp} [(TE_{\partial-12}(k+i) - TE_{\partial-12}targ)^2 + (TE_{p-12}(k+i) - TE_{p-12}targ)^2 + (FT_{6-1}(k+i) - FT_{6-1}targ)^2] \quad (1)$$

where $TE_{d\text{-}12}$, $TE_{p\text{-}12}$ are the temperatures of the vapor phase of diphenyl mixture and caustic soda solution, respectively; $FT_{6\text{-}1}$ is the caustic soda feed rate; Hp is the prediction horizon; $TE_{d\text{-}12}{}^{targ}$, $TE_{p\text{-}12}{}^{targ}$, $FT_{6\text{-}1}{}^{targ}$ are the target values of the process parameters.

The objective of the optimization function is to minimize the deviations of actual parameter values from these target values. Each deviation is computed as the difference between the actual parameter value and its corresponding target value. Then, each deviation is squared to account for both positive and negative deviations. This approach allows for a more sensitive response to large deviations from target values while considering their impact on the overall system performance.

The target values of process parameters in Eq. 1 are determined based on a comprehensive analysis and optimization to ensure stable and efficient operation of the caustic soda evaporation system. The primary objective of the optimization function is to minimize deviations of critical parameters, such as temperature and flow rate, from their optimal values.

The determination of target values begins with the identification of key process parameters that need to be controlled. In this case, these are the temperature of the vapor phase of the diphenyl mixture (ТЕд-12), the temperature of the caustic soda solution (TEp-12), and the caustic soda feed rate (FT6-1). These parameters are crucial for the efficiency and stability of the process.

Next, historical data on the evaporation process is collected and analyzed. At this stage, the results of previous operations are studied and experiments are conducted to determine the optimal values of temperatures and flow rates that ensure maximum efficiency. This analysis helps identify patterns and determine the ranges of values that need to be maintained to achieve optimal process conditions.

Then, process modeling is carried out using specialized software, such as Simulink. Modeling helps understand how different parameter values affect the process and identify the optimal ranges of temperatures and flow rates. At this stage, optimization algorithms, such as the least squares method, can also be used to calculate target values. The goal is to minimize deviations from specified parameters, ensuring system stability.

After determining the target values, they undergo validation. This includes conducting additional experiments and comparing the obtained values with real process data. If necessary, the target values are adjusted to achieve maximum efficiency and stability.

In addition to experimental validation, the implementation phase involves integrating the determined target values into the control system. This involves configuring the MPC controller to use these values as reference points for real-time adjustments. The effectiveness of these target values is continuously monitored, and any deviations are promptly corrected to ensure that the process remains within the desired operational parameters.

The next stage of the project after defining the evaporation optimization function is the implementation of the system in the Simulink environment (Fig. 4) and tuning of the MPC. This stage involves rigorous testing and fine-tuning of the control system to ensure that it performs optimally under various operating conditions. The integration of the MPC with the existing process control infrastructure is crucial for achieving the desired levels of stability and efficiency.

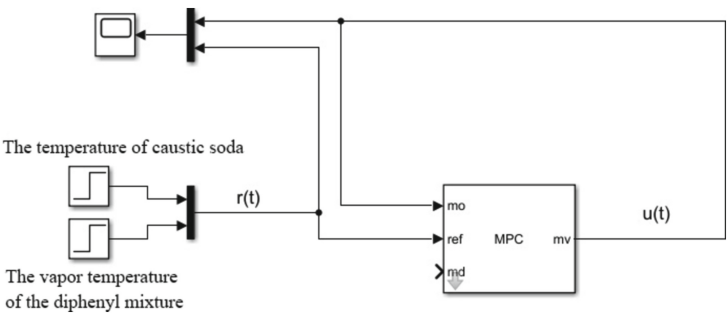


**Fig. 4.** The scheme of the MPC system in Simulink.

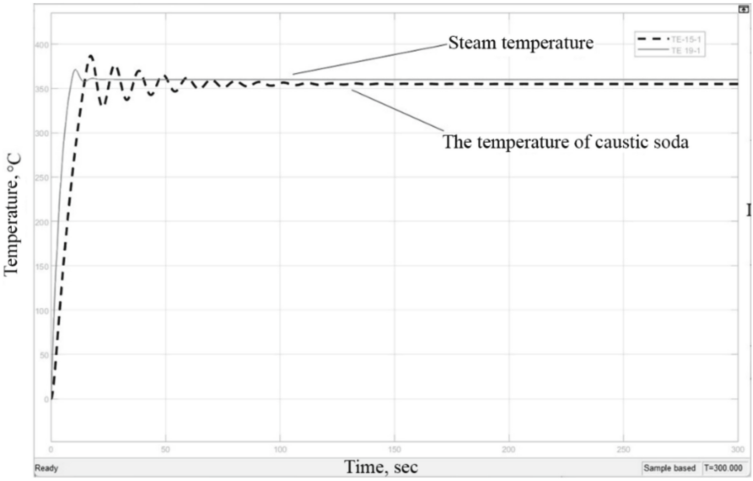


**Fig. 5.** The process of temperature maintenance using MPC.

Initially, upon system startup, fluctuations in control parameter values were observed, which is a common occurrence as the system seeks to achieve a balance between the current state of the process and the set target parameters (see Fig. 5).

The dynamics of control signals have shown that over time, the oscillations become less intense, and the frequency of their occurrence decreases, indicating a gradual approach of the system to the specified target temperature values.

## 6 Conceptual Model of Fuzzy Controller

To implement the fuzzy controller, it is necessary to establish control rules based on which the analysis will be conducted and output parameter values will be determined. Let's describe all the parameters of the caustic soda evaporation system and their ranges of variation (Tables 1 and 2).

**Table 1.** Input parameter notation.

| Position | Name | Regulation limits | Units of measurement |
|---|---|---|---|
| TE 15-1 | Temperature of caustic soda in separator at position J-15 | 340–365 | °C |
| TE 19-1 | Temperature of diphenyl mixture at the outlet of evaporator at position J-14 | 340–380 | °C |
| TE 17-1 | Temperature of the vapor phase | 350–380 | °C |
| FT 6-1 | Flow rate of caustic soda feed | 5–10 | м3/ч |
| TE 15-1 | Temperature of caustic soda solution | 80–160 | °C |

**Table 2.** Output parameter notation

| Position | Name | Regulation limits | Units of measurement |
|---|---|---|---|
| 17-4 | Control valve | 0–100 | % |
| 6-4 | Control valve | 0–100 | % |
| 23-4 | Control valve | 0–100 | % |

The application of the fuzzy controller begins with a detailed analysis of the system's operation and the determination of key parameters that will be used to control the process. In this case, the fuzzy controller will take current values of caustic soda and diphenyl vapor temperatures, as well as current values of parameters calculated by the Model Predictive Control (MPC) model. The fuzzy controller will first interpret the input data—temperature and flow rate values—using membership functions. Based on these interpretations, the controller will use a predefined rule base to issue control actions. After applying fuzzy logic rules, the results - fuzzy output signals for each variable - will be aggregated and transformed into precise numerical values through the defuzzification process.

The precise control signals obtained from the fuzzy controller (FC) will then be passed to the MPC system for further analysis. These signals represent the valve opening values, which are transformed into optimal target temperature values to maintain the initial conditions. When new valve values are passed to the MPC, they are analyzed and used to adapt new control signals for predicting temperatures and flow rates.

The precise control signals obtained from the fuzzy controller (FC) will then be passed to the MPC system for further analysis. These signals represent the opening values of the valves, which are transformed into optimal target temperature values to maintain the initial conditions. When new valve values are passed to the MPC, they are analyzed and used to adapt new control signals for predicting temperatures and flow rates.

## 7 Development of Fuzzy Controller

After the system of rules has been developed, the next step is to integrate it into the structure of the fuzzy controller. This stage involves implementing specific fuzzy logic algorithms within the Matlab software environment, utilizing the functionality provided by the fuzzy command. The Mamdani algorithm will be used, known for its reliability and versatility in modeling expert knowledge and human experience in control systems.

The developed fuzzy controller, denoted as FC, will be designed with five inputs and three outputs, reflecting the number of controlled parameters and their corresponding system responses.

For each input and output parameter, membership functions will be set up, allowing the classification and evaluation of parameter values according to predefined criteria. Membership functions are based on specified ranges and are intended to determine the degree of correspondence of current indicators to each of the possible states. Then, it is necessary to define the rules for the proper operation of the controller.

Let's consider an example rule, and the rest will be formulated similarly:

"If Steam Temperature is Low and Caustic Soda Temperature is Low and Vapor Phase Temperature is Low and Caustic Soda Solution Temperature is Low and Caustic Soda Feed Rate is Low, then Valve 17-4 is Open, Valve 6-4 is Open, Valve 23-4 is Open".

Finally, we will integrate the resulting fuzzy controller into our scheme. We will connect the fuzzy controller to regulate the variable md (Fig. 6).

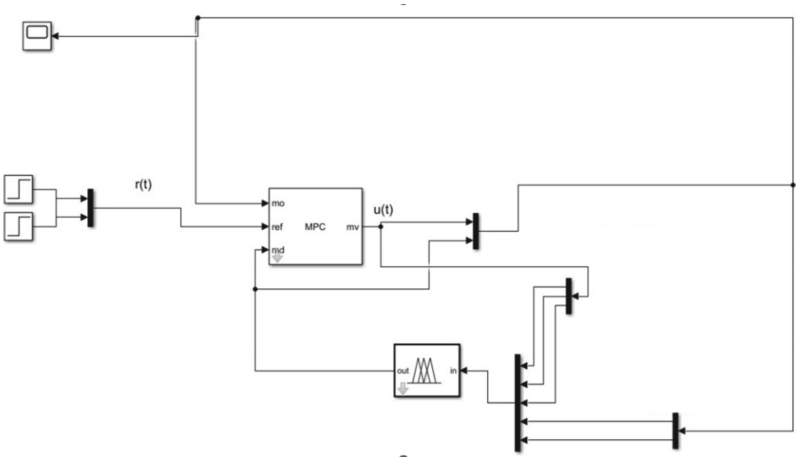


**Fig. 6.** Final MPC Scheme with Fuzzy Controller.

Further, it is necessary to test our model and compare the performance of MPC with the fuzzy controller and without the fuzzy controller. We will analyze the influence of the fuzzy controller's presence in the system.

## 8 Analysis of the Disturbance Impact

During the comparative analysis of Model Predictive Control (MPC) systems, key aspects of their operation and effectiveness were considered. The first MPC system operated without feedback from the fuzzy controller, while the second one was equipped with a valve regulation mechanism.

In the system without the fuzzy controller, the temperature maintenance process was more inertial. The response to changes in the process occurred with a noticeable delay, leading to slow return to target parameters after each deviation. It is noteworthy that in the system without considering disturbance effects, stabilization occurred at 250 s, while the system equipped with a mechanism to respond to external disturbances stabilized at 140 s (Fig. 7).

In contrast, the system with disturbance integration demonstrated more dynamic and efficient behavior. Integrating the disturbance response mechanism into the MPC algorithm allowed the system to actively adapt to the current state of the process, anticipating and compensating for potential deviations.

In addition, the inclusion of the fuzzy controller in the system provided a more robust response to disturbances by effectively adjusting control actions in real-time. This adaptive capability enabled the system to maintain stability and achieve target parameters more rapidly, ultimately enhancing the overall efficiency and performance of the process control system.

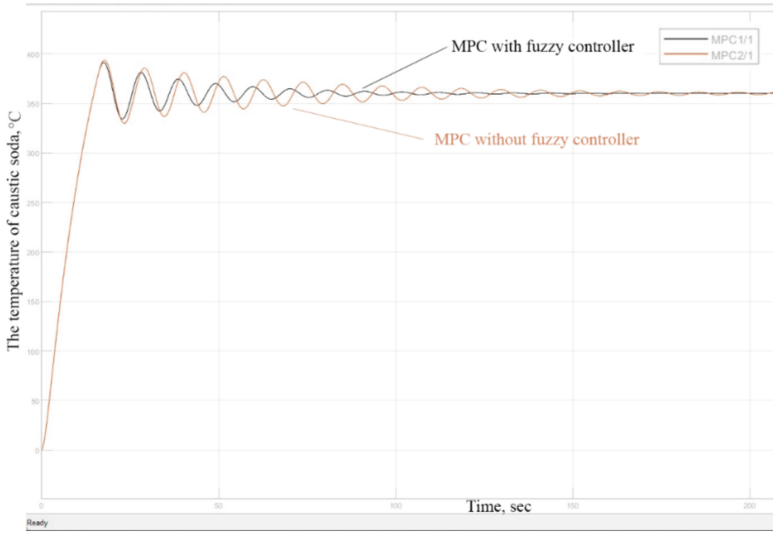


**Fig. 7.** Comparison of Caustic Soda Temperature Stabilization.

The result was a significant acceleration of the temperature stabilization process, ensuring faster achievement and maintenance of the target parameters.

## 9 Conclusion

In this work, a control system for the caustic soda evaporation process using Model Predictive Control (MPC) and fuzzy logic has been developed and investigated.

The analysis covered issues related to maintaining a stable temperature regime, including overheating, insufficient heating, thermal inertia, and temperature instability, all of which decrease product quality and increase energy costs.

A conceptual model of the control system oriented towards parameter optimization has been devised. A conceptual MPC model has been created, taking into account input and output parameters, the process of generating control signals for temperature and flow rate indicators, and an optimization function for predicting process behavior.

A fuzzy controller model has been developed to regulate key system parameters, membership functions, and control rules. The controller has been integrated into MPC to improve adaptation to external disturbances.

Input and output channels of the system, prediction and control horizons, as well as constraints for control variables and output signals have been tuned.

The fuzzy controller has been developed, forming control rules using membership functions. The controller is configured to regulate the valve closure and integrated into the control system.

The analysis revealed that the system considering disturbances demonstrates more dynamic and efficient behavior, quickly reaching and maintaining target parameters.

A fuzzy controller can predict values by dynamically adjusting rules based on the system's behavior. This allows for flexible and adaptive control, which can respond to changes in the system in real-time. The fuzzy controller uses a set of if-then rules to handle uncertainties and nonlinearities, providing a robust prediction mechanism for various operating conditions.

In our case, the process is maintained through continuous monitoring of the system's state and constant adjustment of the impact on the MPC. Instead of relying solely on predefined rules, the system uses real-time data to make precise adjustments, ensuring optimal performance. This approach allows for more accurate control and stability, as the MPC can respond immediately to any deviations or disturbances in the process.

## References

1. Ahmadi, A., Weiskopf, D., Becker, T.: Predictive maintenance enabled by machine learning: applications to fuzzy model predictive control. Expert Syst. Appl. **157**, 113464 (2020)
2. Dadios, E., Dadios, E.P.: Fuzzy Logic and Control: Advances and Applications. Springer, Cham (2019)
3. Han, J., Ahn, C., Cho, H.: A fuzzy model predictive control for HVAC systems. Energy **225**, 120923 (2021)
4. Kulakova, E., Muravyova, E.: Technical solution for monitoring climatically active gases using the turbulent pulsation method. Sensors **23**(20), 8645 (2023). EDN SUGOAM. https://doi.org/10.3390/s23208645
5. Muravyova, E.A., Sharipov, M.I., Samikov, A.A.: Development of mathematical and software parts for control system of synthesis of methyl tertiary butyl ether. In: Proceedings II International Scientific Conference on Advances in Science, Engineering and Digital Education (ASEDU-II-2021): Conference Proceedings, Krasnoyarsk, 28 октября 2021 года, vol. 2647, p. 30014. AIP Publishing, A. – Krasnoyarsk (2022). https://doi.org/10.1063/5.0104366. EDN JLTLSY
6. Muravyova, E.A., Kulakova, E.S.: Review of the instrumentation base for monitoring greenhouse gases. Nanotechnol. Constr. Sci. Online J. **14**(1), 62–69 (2022). [EDNOKWIRY]. https://doi.org/10.15828/2075-8545-2022-14-1-62-69
7. Normey-Rico, J.E., Zuluaga, L.F., Orellana, P.B.F.: Tuning of model predictive controllers based on hybrid optimization. MDPI **8**(2), 174 (2020)
8. Rawlings, J.B., Mayne, D.Q., Diehl, M.M.: Model Predictive Control: Classical, Robust and Stochastic. Springer, Cham (2020)
9. Yang, W., Zhang, W., Xu, D., Yan, W.: Fuzzy model predictive control for 2-DOF robotic arms. Assembly Autom. **38**(5), 568–575 (2018)
10. Zhang, Y., Song, J., Zhao, Y., Luo, X.: Multiple-vector model predictive control with fuzzy logic for PMSM electric drive systems. MDPI **13**(5), 1103 (2020)

# Time-Consistency in Dynamic Cooperative Games with Multiple Trajectories

Zekun Li[1], Yin Li[1,2,3(✉)], Wenwen Qiao[1(✉)], and Wantong Cheng[1]

[1] Department of Applied Mathematics and Process Control, Saint Petersburg State University, Saint Petersburg, Russia
QWW0825@outlook.com
[2] School of Mathematics, Harbin Institute of Technology, Harbin, China
Dr.liyin@hit.edu.cn
[3] School of Mathematics and Computer Science, Yanan University, Yanan, China
https://homepage.hit.edu.cn/liyin

**Abstract.** This paper considers the time consistency of multistage cooperative games in which there are multiple optimal trajectories with complete information. In dynamic cooperative games, an important condition for the distribution of players' payoffs is that individual rationality needs to be satisfied. If the players' payoffs do not satisfy individual rationality as the game progresses along the cooperative trajectory, some players will deviate from the cooperative trajectory. If there are multiple optimal trajectories in the multistage game, the situation is further complicated by the fact that the players' payoffs always satisfy individual rationality on some of the optimal trajectories, but not on others. Alternatively, players' individual rationality conditions are quite different along different optimal trajectories. Therefore, four different scenarios of multi-stage cooperative games with multiple optimal trajectories are set up in the study and analysed for each of the four different situations. Four different Payoff Distribution Procedure (PDP) formulations are proposed to modify the players' payoff distributions so that the game satisfies time-consistency on different optimal trajectories. Several theorems are given, and proofs are provided, with corresponding examples.

**Keywords:** Time consistency · Multistage cooperative games · Multiple optimal trajectories

## 1 Introduction

Game theory, founded by Von Neumann and Morgenstern [1] in 1944, is a study of strategic decision-making among individuals or groups in conflict. It involves players influencing outcomes to maximize their benefits and is applied in diverse fields like economics, management, military, AI, and more, representing an integration of natural and social sciences. It is a branch of applied mathematics and part of operations research.

The work was supported by China Scholarship Council, N:202309010291.


S. Kovalev et al. (Eds.): IITI 2024, LNNS 1209, pp. 141–150, 2024.
https://doi.org/10.1007/978-3-031-77688-5_14

Operations research emerged in the 1930 s from military, management, and economics. It's a technical science using math to study efficient resource allocation under environmental constraints, essential for effective system operation and decision-making. Known as operational research in the UK and operations research in the US, it's often called "management mathematics" [2] due to its focus on management problems and use of mathematical tools. It's rooted in management, with methods from military and economic research adapted for practical application.

In game theory, non-cooperative games are categorized into four types based on information and dynamics, each with a corresponding equilibrium concept: Nash equilibrium [3] for static games with perfect info, subgame perfect Nash for dynamic games with perfect information, Bayesian Nash [4] for static games with incomplete information, and perfect Bayesian Nash for dynamic games with incomplete information.

This paper consider how to achieve time consistency of cooperative trajectories in a multistage cooperative game with non-transferable utility if there are two and more Pareto optimal cooperative trajectories. Time consistency (Dynamic Stability) in multistage cooperative games is investigated. Yeung and Petrosyan [5] propose a new approach to study time consistency. If either player strays from the cooperative trajectory at any moment in the cooperative process, cooperation is disrupted and the players will use the same strategy as in the non-cooperative game situation. Petrosyan [6] introduced notion "PDP" (Payoff Distribution Procedure) for first time. The concept PDP and related formulas concerning multi-stage cooperative game theory were proposed by LI [7] that applies to unique optimal trajectory. With the help of a formula for PDP, the game allows no one to stray from the cooperative trajectory.

In the paper, the concept of a multistage cooperative game with complete information, and time consistency (also known as: Dynamic Stability [8]), is introduced. An Example of time inconsistency is considered.

Based on the definitions, this study constructs formulas for the distribution of four procedures in games with multiple optimal trajectories. These procedures account for whether the players' payoffs are identical and whether the games have the same number of stages in the game process. The results are presented and proved for the Payoff Distribution Procedures in multistage games. Using this formula for the payoff distribution procedure to ensure that each player satisfied the condition of individual rationality.

## 2 The Basic Definitions Of The Model

### 2.1 Multistage Games

This research involves some basic definitions of games mainly from the book of Petrosyan L [9].

**Definition 1.** *Let $Z$ be a finite set. If $\forall\ z \in Z$, $f(z) \in Z$, then $f$ is a single-valued map from $Z$ into $Z$. The set-valued map $F_z$ is the set $Z$ into $Z$, if* $\forall$

*$z \in Z$, $F_z \subset Z$. Consider the pair $G \in (Z, F)$ is a graph. $\forall x, y \in F_x$, $p = (x, y)$ is the arc form $x$ to $y$ of the graph. $p = (p_1, p_2, \ldots, p_l)$ is a sequence of arcs in the graph $G(Z, F)$, and the length is the number $l(p) = l$.*

Consider an example shown in Fig. 1 It shows the graph tree with its root at $z_{1.1}$. The vertex $z \in Z$ of the graph are represented as circles and squares.

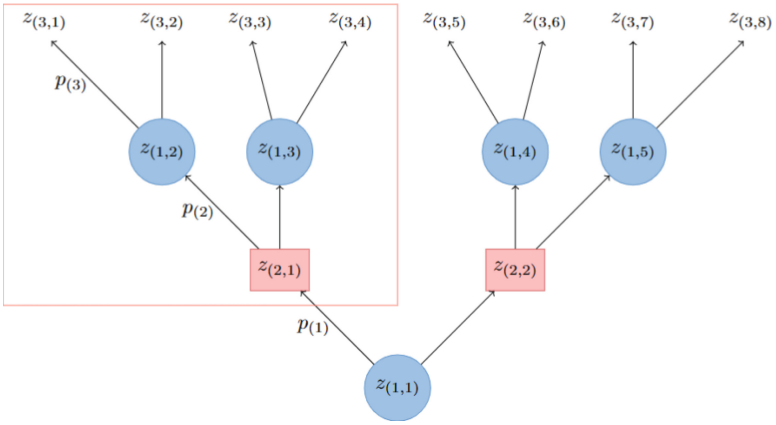


**Fig. 1.** The game tree with root $z_{(1,1)}$

**Definition 2.** *In the graph $G(Z, F)$, the subgraph is represented as $G_z(Z_z, F_z)$.*

In Fig. 1, the line encircles the subgame with as root $z_{(2,1)}$.

**Definition 3.** *Similarly, In $G(Z, F)$, the set $Z$ divided into $n + 1$ sets $Z_1$, $\ldots, Z_n$, $Z_{n+1}$, $\cup_{j=1}^{n+1} Z_j = Z, Z_k \cap Z_l = \emptyset, k \neq l$. The set $Z_j$, $j \in 1, \ldots, n$ is called the set of personal positions of the $j$th player, $Z_{n+1}$ is the terminal positions.*

**Definition 4.** *The single-valued map $u_j$ is a strategy for player $j$ in the game. The ordered set $u = (u_1, \ldots, u_j, \ldots, u_n)$, where $u_j \in U_j$, is a situation in the game, where $U = \prod_{i=1}^{n} U_i$ is the set of situations. And $u = (u_1, \ldots, u_j, \ldots, u_n)$ is uniquely determined a situation and player's payoff in the game.*

**Definition 5.** *The payoff $H_j$ along the trajectory $p = (p_1, \ldots p_i, \ldots, p_l)$, $i = 1, \ldots, l$, under the situation $u = (u_1, \ldots, u_j, \ldots, u_n)$, is*

$$K_j(u) = K_j(u_1, \ldots, u_j, \ldots, u_n) \tag{1}$$

*where $K_j$, $j = 1, \ldots, n$. $u$ are defined on the set of situations $U = \prod_{i=1}^{n} U_i$, $Z_{n+1}$ is the terminal positions of the trajectory $p = (p_1, \ldots p_i, \ldots, p_l)$, $i = 1, \ldots, l$.*

**Definition 6.** *The normal form of the game can be represented as:*

$$G = (N, \{U_j\}_{j \in N}, \{K_j\}_{j \in N}) \tag{2}$$

*where* $N = \{1, \ldots, j, \ldots, n\}$ *is the set of players,* $U_j$ *is the strategy set for each player* $j$*, and* $K_j$ *is the payoff function for player* $j$*,* $j = 1, \ldots, n$*.*

Similarly, Player $j$'s payoff $H_j^z(z)$ in the subgame $G_z(Z_z, F_z)$ can be represented as: $H_j^z(z) = H_j(z), j = 1, \ldots, n$.

The set of all possible strategies for player $j$ in the subgame is denoted by $U_j^z$ . The normal form of the subgame can be represented as:

$$G_z = \left(N, \left\{U_j^z\right\}_{j \in N}, \left\{K_j^z\right\}_{j \in N}\right) \tag{3}$$

where the payoff function $K_j^z$, $j = 1, \ldots, n$.

**Definition 7.** *Consider* $h_j(z_1) \in \mathrm{R}^+ \cup \{0\}$*,* $j = 1, \ldots, n$*, for vertices* $z_1$*,* $z_i$*,* $\ldots$*,* $z_{l+1}$ *there exist the trajectory* $p = (p_1, \ldots p_i, \ldots, p_l)$*,* $i = 1, \ldots, l$ *in the game, obtain the payoff of player* $j$ *in the game starting from vertex* $z_1$ *can be represented as:*

$$H_j(z_1) = \sum_{i=1}^{l+1} h_j(z_i) \tag{4}$$

*where* $h_j(z_1) \in \mathrm{R}^+ \cup \{0\}$.

For vertices $z_i, z_k, \ldots, z_{l+1}$ there exist the trajectory $p = (p_i, \ldots, p_k, \ldots, p_l)$, $k = 1, \ldots, l$ in the subgame, and obtain the payoff of player $j$ in the subgame starting from vertex $z_i$ can be represented as:

$$H_j(z_i) = \sum_{i=k}^{l+1} h_j(z_i) \tag{5}$$

where $h_j(z_i) \in \mathrm{R}^+ \cup \{0\}$.

And, consider an example of a multistage cooperative game with complete information shown in Fig. 1. If there are only two players in the game, it shows the graph tree with its root at $z_{(1,1)}$.

Here the circle represents player 1, i.e., the decision is made by player 1 at vertex $z_{(1,n)}$. The square is used to represent player 2, i.e., the decision is made by player 2 at vertex $z_{(2,n)}$, and the vertex $z_{(3,n)}$ represents the player's terminal payoff. And the line encircles the subgame with vertex $z_{(2,1)}$ as root.

**Definition 8.** *For vertices* $z_1, z_i, \ldots, z_{l+1}$*, if there exist the trajectory* $p = (p_1, \ldots p_i, \ldots, p_l)$*,* $i = 1, \ldots, l$*, the following conditions are satisfied:*

$$\max_{p_1, \ldots p_i, \ldots, p_l} \sum_{j=1}^{n} \sum_{i=1}^{l+1} h_j(z_i) = \sum_{j=1}^{n} \sum_{i=1}^{l+1} h_j(\overline{z}_i) \tag{6}$$

*where* $h_j(z_i) \in \mathrm{R}^+ \cup \{0\}$, *then there is a cooperative trajectory in the game.*

*In the cooperative game* $G_{z_1}$ *along the trajectory* $p = (p_1, \ldots p_i, \ldots, p_l)$, $i = 1, \ldots, l$ *the payoff of player* $j$ *in the game can be represented as:*

$$\overline{H}_j(z_1) = \sum_{i=1}^{l+1} h_j(\overline{z}_i) \tag{7}$$

*where* $h_j(z_i), h \geq 0$.

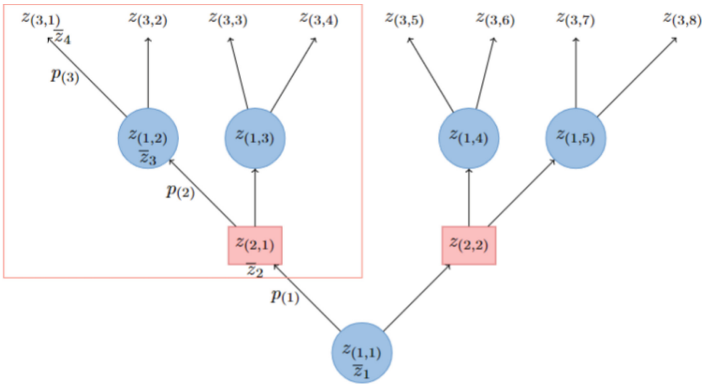


**Fig. 2.** The Subgame with root $\overline{z}_i$

As shown in the Fig.2, along the already determined cooperative trajectory $\overline{z}_1, \overline{z}_2, \overline{z}_3, \overline{z}_4$, represented the vertices in the trajectory as $\overline{z}_i$.

Subsequently, consider an example shown in Fig.3, the circle represents player 1, the square represents player 2, in the game along the trajectory $(p_{(1)}, p_{(2)}, p_{(3)})$, the payoff of players is if for vertices $z_{(1,1)}, z_{(2,1)}, z_{(3,1)}, z_{(4,1)}$, there exist the trajectory $p = (p_1, p_2, p_3)$ can obtain the maximum payoff among all possible trajectories, then along the trajectory $p = (p_1, p_2, p_3)$ is the cooperative trajectory in the game.

$$\max \sum_{j=1}^{2} \sum_{i=1}^{4} h_j(z_i) = H_1\left(z_{(1,1)}\right) + H_2\left(z_{(1,1)}\right) = 44.$$

## 2.2 Time Consistency of Cooperative Solutions

In multistage cooperative games, ensuring the stability of cooperative solutions is the key question to cooperation, and an important condition for the game is Individual Rationality. If the Individual Rationality is not satisfied along the cooperative trajectory, some players may deviate from the cooperative trajectory. Therefore, it is necessary to consider the time consistency in the multistage

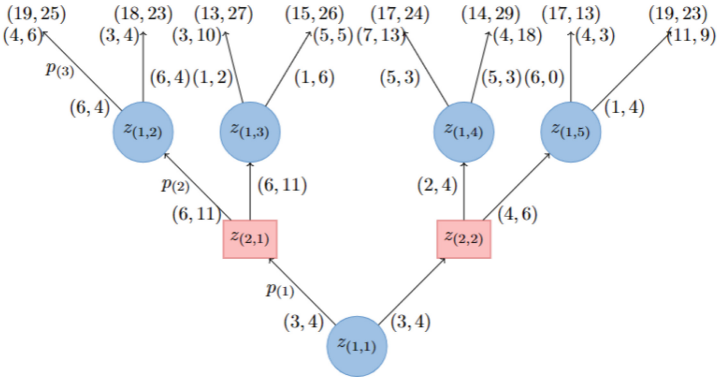


**Fig. 3.** Multistage game with 2 players

cooperative game to ensure the stability of players' cooperation, so that all players do not deviate from the cooperative trajectory[10] [11].

**Definition 9.** *Consider a noncooperative game with two players as* $\{j\}, N/\{j\}$, *the values of game* $V_j(z_1; \{j\}, N/\{j\})$ *is the payoff in the noncooperative game between* $\{j\}, N/\{j\}$. *In the game the player* $j$ *plays against the player* $N/\{j\}$, $j = 1, \ldots, n$.

And in a noncooperative subgame with $j$ players are $\{j\}, N/\{j\}$, $j = 1, \ldots, n$. The values of the subgame payoff starting from $z_i$ can be represented as $V_j(z_i)$, and is represented as $V_j(z_i; \{j\}, N/\{j\})$.

**Definition 10.** *In the game* $G_{z_i}$, *if along vertices* $z_i, z_k, \ldots, z_{l+1}$, *there exist the trajectory* $p = (p_i, \ldots p_k, \ldots, p_l)$, $k = 1, \ldots, l$, *the following conditions are satisfied:*

$$\overline{H}_j(z_1) = \sum_{i=k}^{l+1} h_j(\overline{z}_i) \geq V_j(z_i) \tag{8}$$

*Then Cooperation paths are time-consistent.*

The following is the time inconsistency of cooperative solutions:

$$\sum_{i=k}^{l+1} h_j(\overline{z}_i) < V_j(z_i) \tag{9}$$

where, the multistage cooperative game along trajectory $p = (p_i, \ldots p_k, \ldots, p_l)$, $k = 1, \ldots, l$, there exist the vertices $z_i, z_k, \ldots, z_{l+1}$.

## 3 The Formulas for Multiple Trajectories of Individual Rationality

In the multistage cooperative game, players receive different payoffs. Therefore, this paper identified four models based on the payoffs of the players in the game with different trajectories. As shown in the table below:

**Table 1.** Two models based on the payoffs of the players in the game with different trajectories

| | Number of stages of the same cooperation path(n) | Number of stages of the different cooperation path(n) |
|---|---|---|
| Pareto optimality solutions are same (H) | • $H_j^1 = H_j^2 = \ldots = H_j^n$<br>$\beta_1^{i_1} = f(H_1, V)$<br>$\beta_2^{i_2} = f(H_2, V)$<br>$\ldots$<br>$\beta_j^{i_n} = f(H_j, V)$<br>• $i_1 = i_2 = \ldots = i_n$ | • $H_j^1 = H_j^2 = \ldots = H_j^n$<br>$\beta_1^{i_1} = f(H_1, V)$<br>$\beta_2^{i_2} = f(H_2, V)$<br>$\ldots$<br>$\beta_j^{i_n} = f(H_j, V)$<br>• $i_1 \neq i_2 \neq \ldots \neq i_n$ |
| Pareto optimality solutions are different (H) | • $H_j^1 \neq H_j^2 \neq \ldots \neq H_j^n$<br>$\beta_1^{i_1} = f(H_1, V)$<br>$\beta_2^{i_2} = f(H_2, V)$<br>$\ldots$<br>$\beta_j^{i_n} = f(H_j, V)$<br>• $i_1 = i_2 = \ldots = i_n$ | • $H_j^1 \neq H_j^2 \neq \ldots \neq H_j^n$<br>$\beta_1^{i_1} = f(H_1, V)$<br>$\beta_2^{i_2} = f(H_2, V)$<br>$\ldots$<br>$\beta_j^{i_n} = f(H_j, V)$<br>• $i_1 \neq i_2 \neq \ldots \neq i_n$ |

In the Table 1, $j$ is represented as the player, $i$ is represented as the number of stages in the cooperative game, and $i_n$ is the number of stages of the cooperative game corresponding to player $j$.

Next, this paper will introduce the formula for individual rationality under the four conditions.

**Theorem 1.** *Using the following Payoff Distribution Procedure: the path to the Pareto optimal solution can be obtained when* $H_j^1 = H_j^2 = \ldots = H_j^n$ *and Pareto optimality solutions are same and Number of stages of the same cooperation path(Upper left part of Table 1) reach time consistency.*

$$V_j(\bar{z}_i) = \max\{V'(\bar{z}_i), V''(\bar{z}_i)\}, \ldots, V^n(\bar{z}_i)\}$$
$$\widehat{\beta_j^i} = \frac{\bar{H}_j(\bar{z}) - V_j(\bar{z}_1)}{l+1} - [V_j(\bar{z}_{i+1}) - V_j(\bar{z}_i)]$$

*and* $\bar{H}_j(\bar{z}) = \sum_{i=1}^{l} h_j(z_i)$, $\bar{p} = (\bar{p}_1, \ldots \bar{p}_i, \ldots, \bar{p}_l)$.

*Proof.*

$$\begin{aligned}
\widehat{\beta_j^i} &= \frac{\bar{H}_j(\bar{z}) - V_j(\bar{z}_1)}{l+1} - [V_j(\bar{z}_{i+1}) - V_j(\bar{z}_i)] \\
&= \frac{\sum_{i=1}^{1} h_j(\bar{z}_i) - V_j(\bar{z}_1)}{l+1} - [V_j(\bar{z}_{i+1}) - V_j(\bar{z}_i)] \\
\sum_{i=1}^{l} \widehat{\beta_j^i} &= \sum_{i=1}^{l} [\frac{\sum_{i=1}^{1} h_j(\bar{z}_i) - V_j(\bar{z}_1)}{l+1} - [V_j(\bar{z}_{i+1}) - V_j(\bar{z}_i)]] \\
&= \sum_{i=1}^{l} \frac{\sum_{i=1}^{1} h_j(\bar{z}_i) - V_j(\bar{z}_1)}{l+1} - \sum_{i=1}^{1} [V_j(\bar{z}_{i+1}) - V_j(\bar{z}_i)] \\
&= \sum_{i=1}^{l} \frac{\sum_{i=1}^{1} h_j(\bar{z}_i) - V_j(\bar{z}_1)}{l+1} - [\sum_{i=1}^{1} V_j(\bar{z}_{i+1}) - \sum_{i=1}^{1} V_j(\bar{z}_i)] \\
&= \sum_{i=1}^{l} \frac{\sum_{i=1}^{1} h_j(\bar{z}_i) - V_j(\bar{z}_1)}{l+1} - [V_j(\bar{z}_{i+1}) + V_j(\bar{z}_{i+2}) + \ldots + V_j(\bar{z}_l) \\
&\quad - V_j(\bar{z}_i) - V_j(\bar{z}_{i+1}) - \ldots - V_j(\bar{z}_l)] \\
&= \sum_{i=1}^{l} \frac{\sum_{i=1}^{1} h_j(\bar{z}_i) - V_j(\bar{z}_1)}{l+1} + V_j(\bar{z}_i) \geq V_j(z_i) \\
&\sum_{i=1}^{l} \frac{\sum_{i=1}^{1} h_j(\bar{z}_i) - V_j(\bar{z}_1)}{l+1} \geq 0 \\
\sum_{i=1}^{l} \widehat{\beta_j^i} &= \sum_{i=1}^{l} \frac{\sum_{i=1}^{1} h_j(\bar{z}_i) - V_j(\bar{z}_1)}{l+1} + V_j(\bar{z}_i) \geq V_j(z_i) \\
&\sum_{i=1}^{l} \widehat{\beta_j^i} \geq V_j(z_i)
\end{aligned}$$

**Theorem 2.** *Using the following Payoff Distribution Procedure: the path to the Pareto optimal solution can be obtained when* $H_j^1 \neq H_j^2 \neq \ldots \neq H_j^x; x \in \{1, \ldots, n\}$ *and Pareto optimality solutions are different and Number of stages of the same cooperation path(Lower left part of Table 1) reach time consistency.*

$$\sum_{i=1}^{l} \beta_j \geq V(z_1), \sum_{i=2}^{l} \beta_j \geq V(z_2), \ldots, \sum_{i=n}^{l} \beta_j \geq V(z_i) \tag{10}$$

$$\begin{aligned}
V_j(\bar{z}_i) &= \max\{V'(\bar{z}_i), V''(\bar{z}_i)\}, \ldots, V^n(\bar{z}_i)\}, \\
\widehat{\beta_{j_x}^i} &= \frac{\overline{H}_j^x(\bar{z}) - V_j^x(\bar{z}_1)}{l+1} - [V_j^x(\bar{z}_{i+1}) - V_j^x(\bar{z}_i)].
\end{aligned} \tag{11}$$

*and* $\bar{H}_j(\bar{z}) = \sum_{i=1}^{l} h_j(z_i)$, $\bar{p} = (\bar{p}_1, \ldots \bar{p}_i, \ldots, \bar{p}_l)$.

*In the above formula, $j$ is the players, $j_n$ is different payoff for players in different strategies, $i$ is the number of stages of the cooperative game.*

The demonstration of this theorem proceeds analogously to that of Theorem 1; however, it is omitted here due to limitations of length.

**Theorem 3.** *Using the following Payoff Distribution Procedure: the path to the Pareto optimal solution can be obtained when $H_j^1 \neq H_j^2 \neq \ldots \neq H_j^x$ and Pareto optimality solutions are different and Number of stages of the different cooperation path(Upper right part of Table 1) reach time consistency.*

$$\sum_{i=1}^{l} \beta_j \geq V(z_1), \sum_{i=2}^{l} \beta_j \geq V(z_2), \ldots, \sum_{i=n}^{l} \beta_j \geq V(z_i) \tag{12}$$

$$\begin{aligned} V_j(\overline{z}_i) &= \max\{V'(\overline{z}_i), V''(\overline{z}_i)\}, \ldots, V^n(\overline{z}_i)\}, \\ \widehat{\beta}_{j\,x}^{i} &= \frac{\overline{H}_j^x(\overline{z}) - V_j^x(\overline{z}_1)}{l+1} - [V_j^x(\overline{z}_{i+1}) - V_j^x(\overline{z}_i)]. \end{aligned} \tag{13}$$

*and $\bar{H}_j(\bar{z}) = \sum_{i=1}^{l} h_j(z_i)$, $\bar{p} = (\bar{p}_1, \ldots \bar{p}_i, \ldots, \bar{p}_l)$.*

*In the above formula, $j$ is the players, $j_n$ is different payoff for players in different strategies, $i$ is the number of stages of the cooperative game.*

The demonstration of this theorem proceeds analogously to that of Theorem 1; however, it is omitted here due to limitations of length.

**Theorem 4.** *Using the following Payoff Distribution Procedure: the path to the Pareto optimal solution can be obtained when $H_j^1 = H_j^2 = \ldots = H_j^x$. and Pareto optimality solutions are same and Number of stages of the different cooperation path(Lower right part of Table 1) reach time consistency.*

$$\sum_{i=1}^{l} \beta_j \geq V(z_1), \sum_{i=2}^{l} \beta_j \geq V(z_2), \ldots, \sum_{i=n}^{l} \beta_j \geq V(z_i) \tag{14}$$

$$\begin{aligned} V_j(\overline{z}_i) &= \max\{V'(\overline{z}_i), V''(\overline{z}_i)\}, \ldots, V^n(\overline{z}_i)\}, \\ \widehat{\beta_j^{i_x}} &= \frac{\overline{H}_j(\overline{z}) - V_j^x(\overline{z}_1)}{l+1} - [V_j^x(\overline{z}_{i+1}) - V_j^x(\overline{z}_i)], \\ & \qquad i_1 \neq i_2 \neq \ldots \neq i_x. \end{aligned} \tag{15}$$

*and $\overline{H}_j(\overline{z}) = \sum_{i=1}^{l} h_j(z_i)$,$\overline{p} = (\overline{p}_1, \ldots \overline{p}_i, \ldots, \overline{p}_l)$*

*In the above formula, $j$ is the players, $i$ is the number of stages of the cooperative game, and $i_n$ is the number of stages of the cooperative game corresponding to player $j$.*

The demonstration of this theorem proceeds analogously to that of Theorem 1; however, it is omitted here due to limitations of length.

## 4 Conclusion

This paper examines the issue of time consistency in multistage cooperative games with complete information. It proposes a method to ensure time consistency when a single optimal trajectory exists by adjusting player payoffs without changing their total sums. This maintains the cooperative trajectory's adherence to the optimality principle at all stages. Additionally, the paper addresses the complexity of payoff redistribution across multiple optimal trajectories. It categorizes four scenarios based on players' stage experiences and individual payoffs. For each, it offers and proves formulas that redistribute payoffs, maintaining the same total for each player while ensuring time consistency. This approach guarantees that players stay on the anticipated cooperative trajectory, leading to stable cooperation along optimal paths.

## References

1. Von Neumann, J., Morgenstern, O.: Theory of Games and Economic Behavior. Princeton University Press (1944)
2. Morse, P.M., Kimball, G.E.: Methods of Operations Research. MIT Press (1951)
3. Nash, John F.: Equilibrium points in N-person games. Proc. Nat. Acad. Sci. **36**(1), 48–49 (1950)
4. Yeung, D.W.K.: An irrational-behavior-proof condition in cooperative differential games. Int. Game Theory Rev.**8**(04), 739–744 (2006)
5. Harsanyi, J.C.: Games with incomplete information played by "Bayesian" players, I-III part I. The basic model. Manage. Sci. **14**(3), 159–182 (1967)
6. Petrosyan, L.A., Danilov, N.N.: Stability of Solutions in Non-zero Sum Differential Games with Transferable Payoffs. Viestnik of Leningrad Universtiy, pp. 52–59(1979)
7. Yin, L.: The dynamic shapley value in the game with spanning tree. In: 2016 International Conference Stability and Oscillations of Nonlinear Control Systems, pp. 1–4 (2016)
8. Abreu, D., Brooks, B., Sannikov, Y.: Algorithms for stochastic games with perfect monitoring. Econometrica **88**(4), 1661–1695 (2020)
9. Parilina, E., Petrosyan, L.: On a simplified method of defining characteristic function in stochastic games. Mathematics **8**(7), 1135 (2020)
10. Kuhn, H.: Extensive games and the problem of information. Contrib. Theory Games **2**, 193–216 (1953)
11. Myerson, R.: Game theory. In: Analysis of Conflict. Harvard University Press, Cambridge (1997)

# Machine Learning and Its Applications

# An Explicit Concept-Based Approach for Incorporating Expert Rules into Machine Learning Models

Andrei V. Konstantinov(✉) and Lev V. Utkin(✉)

Peter the Great St. Petersburg Polytechnic University Higher School of Artificial Intelligence Technologies, St. Petersburg, Russia
andrue.konst@gmail.com, lev.utkin@gmail.com

**Abstract.** An approach for solving a problem of incorporating the expert rules into machine learning models, in particular, into neural networks, in the framework of the concept-based learning is proposed in the paper. The first idea behind the approach is to consider the expert rules as logical functions on concepts, which restrict a joint probability distribution over all combinations of concept values, i.e. it is supposed that each combination of concepts must satisfy the expert rules, otherwise the probability of the combination is assigned to zero. The second idea is to add a neural network producing probabilities of the concept combinations by a layer which maps the probabilities of the concepts to the marginal probabilities of concepts and guarantees that the probabilities will satisfy expert rules for any input. The proposed approach can be viewed as a way for combining the inductive and deductive learning. A numerical example illustrates the approach.

**Keywords:** Concept-based learning · Neural networks · Expert rules · Deductive learning

## 1 Introduction

One of the promising approaches that focuses on using high-level concepts derived from raw features is the concept-based machine learning (CBL) [1]. It aims to combine the human-like reasoning with machine learning models in order to obtain more accurate predictions. Simultaneously, CBL can significantly improve the explainability of the model predictions by connecting the predictions with concept values which are intuitive to users [2–4]. Concepts can be annotated in different form. Often, one can meet the binary label representation of concepts meaning the presence or absence of a concept in an image. Another

The research is partially funded by the Ministry of Science and Higher Education of the Russian Federation as part of state assignments "Development and research of machine learning models for solving fundamental problems of artificial intelligence for the fuel and energy complex" (topic FSEG-2024-0027).


S. Kovalev et al. (Eds.): IITI 2024, LNNS 1209, pp. 153–162, 2024.
https://doi.org/10.1007/978-3-031-77688-5_15

form is when the concept values are represented as indices. The above forms can simply convert into each other.

Most of the CBL models are combined into the concept-based bottleneck models (CBMs). These models are based on the two-step inference procedure. They first explicitly predict the concept labels from images and then predict the final label (target) based on the concept label predictions. The prediction of the concept labels after the first step can be regarded as a lower-dimensional representation of the input features [5], which is referred to as the bottleneck. By having the bottleneck with the lower-dimensional representation, the final target can be expressed through the concept bottleneck representation [3]. This leads to the explicit explanation of the target as a function of the concept labels.

CBL can be viewed as a powerful tool for solving machine learning tasks. As a result, the CBL models, including CBMs, have been applied to image recognition, natural language processing and other applied areas [6]. However, we propose another interesting application of CBL, which significantly expands the scope of machine learning in general. We propose a new approach to combine the inductive learning tools (neural networks) with the knowledge-based expert rules of the form "IF ..., THEN ...". An example of the rule which can be constructed by using the Bird identification dataset (CUB) [7] is "IF the Head is *red*, the Back color is *black*, the Crown color is *red*, the Wing color is *white*, THEN the Bird is a *red-headed woodpecker*" It should be noted that the expert rules we incorporate into the machine learning model can have a more general representation. They can be represented as any logical functions that establish a relationship between concepts and target class labels or just concepts with each other. We use the form " IF ..., THEN ..." for simplicity. In fact, we combine inductive and deductive learning which is an important task to incorporate into a machine learning model, for example, into a neural network, the available causal relationship between concepts and class labels or between concepts. Below, we will use the expert rules in the form of logical functions.

We propose the approach for incorporating the expert rules into a neural networks, which aims to develop a model which is trained by simultaneously using concept-based data and knowledge-based rules. It is important to point out that the expert rules can be incorporated into the machine learning model by adding the corresponding regularization terms to the loss function in order to restrict a set of the output values in accordance with the expert rules. In this case, the loss function will be penalized when the rule is not satisfied. However, this does not mean that the rule is guaranteed to be implemented. Therefore, we need another way which guarantees that the expert rule is satisfied. The main idea behind the proposed approach is that expert rules change probabilities of concepts in the bottleneck of the CBM. The rules also change predictions corresponding to new instances which are classified and explained.

The paper is organized as follows. A brief review of the CBL models is given in Sect. 2. A formal problem statement of CBL and expert rules as well as a description of the proposed approach to incorporating expert rules into neural networks are considered in Sect. 3. The training procedure of the neural network

taking into account expert rules is provided in Sect. 4. Numerical experiments illustrating the proposed approach are provided in Sect. 5. Concluding remarks can be found in Sect. 6.

## 2 Related Work

Various CBL models have been proposed recently [2,4]. A comprehensive survey of the models is provided in [8]. Most CBL models study the image input data [1,9]. At the same time, a CBL model dealing with tabular data was proposed in [10]. An important question of interventions from humans in CBL was investigated in [11].

The CBL models have been applied to several areas, including medicine [12, 13], the time-series data predictions [14,15], anomaly detection [16].

CBMs as an important part of the CBL models have been also intensively developed. Various extensions of the base CBM [5] were proposed [17–21]. This is a small part of all publications devoted to CBMs.

The problem of incorporating the expert knowledge into machine learning models has been stated in literature. In particular, a review of the corresponding existing approaches was presented in [22]. A common approach to solve this problem is to add the rules as constraints to loss functions [23]. However, this approach does not guarantee that the rules will be satisfied for all training and testing examples because violation of the constraints is only penalized, but not eliminated. An interesting approach has been proposed in [24] where the authors propose an effective safe abductive learning method and show that induction and abduction are mutually beneficial. The idea behind our approach is to construct the probability distribution of concepts and to restrict it by using expert rules.

## 3 Expert Rules and Concepts

### 3.1 Problem Statement

Suppose that a training set consists of $n$ pairs $(\mathbf{x}_i, y_i)$, where $\mathbf{x}_i \in \mathcal{X} \subset \mathbb{R}^d$ is the feature vector; $y_i \in \mathcal{Y} = \{1, 2, ..., K\}$ is the target label. In addition to each pair, there is a concept vector $\mathbf{c}_i = (c_i^{(1)}, ..., c_i^{(m)}) \in \mathcal{C}$ consisting of $m$ concepts. The training set can be represented now as $(\mathbf{x}_i, y_i, \mathbf{c}_i)$, $i = 1, ..., n$. Concepts can take different values, for example, when a concept takes binary values, this means that the concept is present or not in the input $\mathbf{x}_i$. We will use another sets of the concept values. Each concept $c^{(i)}$ can take one of $n_i$ values from the $i$-th concept outcome set $\mathcal{C}^{(i)} = \{1, ..., n_i\}$, $i \in \{0, \ldots, m\}$. The concept vector is represented as $\mathbf{c} = (c^{(0)}, c^{(1)}, ..., c^{(m)}) \in \mathcal{C}^{\times}$, where $\mathcal{C}^{\times}$ is the concept domain produced by the Cartesian product $\mathcal{C}^{\times} = \mathcal{C}^{(0)} \times \cdots \times \mathcal{C}^{(m)}$. We will consider the target variable $y$ also as the concept $c^{(0)}$ with index 0.

One of the aims of CBL is to determine a function $f : \mathcal{X} \to (\mathcal{C}, \mathcal{Y})$. As we represent $y$ as a concept, then we aim to find another function $f : \mathcal{X} \to \mathcal{C}$ under condition that expert rules are incorporated into the neural network, and to

train the whole model taking into account the expert rules. Let us introduce the logical literal $h_i^{(j)}(\mathbf{c}) = [c^{(j)} = i]$ taking the value 1, if the concept $c^{(j)}$ has the value $i$, otherwise 0. A set of expert rules is represented as a logical expression $g(\mathbf{c})$ over literals $h_i^{(j)}(\mathbf{c})$ or as a mapping $g : \mathcal{C}^{\times} \mapsto \{0, 1\}$, where 0 means FALSE, and 1 means TRUE. For example, the rule "IF $c^{(1)} = 3$ THEN $c^{(2)} = 1$" means in terms of the logical function

$$g = (c^{(1)} = 3) \rightarrow (c^{(2)} = 1) = h_3^{(1)} \rightarrow h_1^{(2)} = (\neg h_3^{(1)}) \vee h_1^{(2)}, \tag{1}$$

where $\rightarrow$ and $\neg$ are the implication and negation logical operations; we omit the argument $\mathbf{c}$ for short.

Let $X$ and $C^{(0)}, \ldots, C^{(m)}$ be a random vector taking values from $\mathcal{X} \subset \mathbb{R}^d$ and discrete random variables for the concepts taking values from $\mathcal{C}^{(0)}, \ldots, \mathcal{C}^{(m)}$, respectively. The concept random vector is denoted as $C = (C^{(0)}, C^{(1)}, ..., C^{(m)})$.

Finally, we aim to estimate marginal concept probabilities $\Pr(C^{(i)} = j \mid X = \mathbf{x})$ conditioned on an input $\mathbf{x}$ for the $i$-th concept and outcome $j$ under condition of the expert rules. For brevity, we denote the marginal concept probabilities as vectors $p^{(i)}$. It should be noted that vectors $p^{(i)}$ cannot be estimated separately because the marginal probabilities are not independent due to the expert rules.

### 3.2 Joint Probability Distributions of the Concept Combinations

Let us consider the conditional joint probability distribution over concepts: $\Pr(C = \mathbf{c} \mid X = \mathbf{x})$. All concept random variables are discrete with finite outcome sets. Therefore, vectors $\mathbf{c}$ can be indexed, and the total number of distinct concept vectors is $t = n_0 \cdot n_1 \cdot \cdots \cdot n_m$. Suppose that the function $\mathcal{M} : \mathcal{C}^{\times} \mapsto \{1, \ldots, t\}$ maps a concept vector to its index. The inverse function $\mathcal{M}^{-1}$ maps the index to the corresponding concept vector. Let us define the joint probability distribution $\pi = (\pi_1, \ldots, \pi_t)$ as follows:

$$\forall \mathbf{c} \in \mathcal{C}^{\times},\ \pi_{\mathcal{M}(\mathbf{c})} = \Pr(C = \mathbf{c} \mid X = \mathbf{x}). \tag{2}$$

The joint probability distribution is constrained to satisfy the expert rules formulated as $g$, therefore:

$$\Pr(g(C) = 1) = 1. \tag{3}$$

Let us consider a binary mask of admissible states $u = (u_1, \ldots, u_t) \in \{0, 1\}^t$. Its components are equal to 1 if the rules $g(\mathbf{c})$ are satisfied for the corresponding concept vectors $\mathbf{c} \in \mathcal{C}^{\times}$, otherwise $u_k = 0$, i.e., there holds

$$u_k = g(\mathcal{M}^{-1}(k)), \quad k \in \{1, ..., t\}. \tag{4}$$

Constraints on the joint probability distribution can be reformulated as a set of the equality constraints on components of $\pi$, corresponding to invalid states that violate the rules:

$$\pi_k = 0, \quad k \in \{i \in \{1, ...t\} \mid g(\mathcal{M}^{-1}(k)) = 0\}. \tag{5}$$

Let us consider the joint probability under condition that expert rules $g(C)$ are satisfied. In this case, there holds

$$\Pr\left(C = \mathbf{c} \mid g(C) = 1\right) = \frac{\Pr(C = \mathbf{c}) \cdot \Pr(g(C) = 1 \mid C = \mathbf{c})}{\Pr\left(g(C)\right)}, \tag{6}$$

Here $\Pr(C = \mathbf{c})$ is the prior concept probability which can be computed as the output of a neural network implementing the function $f : \mathcal{X} \to \mathcal{C}$. We denote the output probability distribution of the neural network as $\widehat{\pi}_{\mathcal{M}(\mathbf{c})}$.

It should be noted that the logical function $g$ is deterministic. Hence, the posterior probability is determined as

$$\Pr(g(C) = 1 \mid C = \mathbf{c}) = g(\mathbf{c}) \tag{7}$$

The probability $\Pr\{g(C)\}$ is defined by probabilities of the concept combinations $\mathbf{k}$ from the Cartesian product $\mathcal{C}^{\times}$, which correspond to the case $g(\mathbf{k}) = 1$. Therefore, we can write

$$\Pr(g(C)) = \sum_{\mathbf{k} \in \mathcal{C}^{\times}} g(\mathbf{k}) \cdot \Pr(C = \mathbf{k}). \tag{8}$$

The above implies that there holds

$$\pi_j = \frac{\widehat{\pi}_j \cdot g(\mathcal{M}^{-1}(j))}{\sum_{\mathbf{k} \in \mathcal{C}^{\times}} \widehat{\pi}_k \cdot g(\mathcal{M}^{-1}(k))}. \tag{9}$$

For illustrative purposes, we consider a toy example with two classes of Birds: a *red-headed woodpecker* ($c^{(0)} = 1$) and an *European green woodpecker* ($c^{(0)} = 2$). The corresponding concepts describing the birds are Head ($c^{(1)}$), Bill shape ($c^{(2)}$), and Wing color ($c^{(3)}$). Concept Head takes values: *red* ($c^{(1)} = 1$), *green* ($c^{(1)} = 2$), concept Bill shape takes values: *chisel* ($c^{(2)} = 1$), *dagger* ($c^{(2)} = 2$), *all-purpose* ($c^{(2)} = 3$). Here $m = 2$, $n_0 = 2$, $n_1 = 2$, $n_2 = 3$. Suppose there is the expert rule:

$$\begin{array}{llll} \text{IF} & \text{Head} & \text{is } red & \\ \text{AND} & \text{Bill shape} & \text{is } dagger \text{OR} all-purpose, & \\ \text{THEN} & \text{Bird} & \text{is } red-headed woodpecker. & \end{array} \tag{10}$$

This rule can be represented as:

$$\begin{aligned} g(\mathbf{c}) &= \left(h_1^{(1)} \wedge \left(h_2^{(2)} \vee h_3^{(2)}\right)\right) \to h_1^{(0)} \\ &= h_1^{(0)} \vee h_2^{(1)} \vee h_1^{(2)}. \end{aligned} \tag{11}$$

Table 1 shows in bold all combinations of the concept values satisfying the above expert rule. It can be seen from Table 1 that combinations $(2, 1, 2)$ and $(2, 1, 3)$ lead to $g(\mathbf{c}) = 0$. Therefore, probabilities $\pi_8$ and $\pi_9$ are equal to zero, and $\sum_{i=1, i \neq 8,9}^{12} \pi_i = 1$.

In sum, we produce a mask $u$ for admissible probabilities $\pi_1, ..., \pi_N$, which has zero components with indices 8 and 9. It is important to note that this

**Table 1.** An example of all combinations of the concept values and the corresponding probabilities

| $c^{(0)}$ | **1** | **1** | **1** | **1** | **1** | **1** | **2** | 2 | 2 | **2** | **2** | **2** |
|---|---|---|---|---|---|---|---|---|---|---|---|---|
| $c^{(1)}$ | **1** | **1** | **1** | **2** | **2** | **2** | **1** | 1 | 1 | **2** | **2** | **2** |
| $c^{(2)}$ | **1** | **2** | **3** | **1** | **2** | **3** | **1** | 2 | 3 | **1** | **2** | **3** |
| $\pi$ | $\pi_1$ | $\pi_2$ | $\pi_3$ | $\pi_4$ | $\pi_5$ | $\pi_6$ | $\pi_7$ | $\pi_8$ | $\pi_9$ | $\pi_{10}$ | $\pi_{11}$ | $\pi_{12}$ |

approach requires to predict all components of the joint probability distribution by applying a neural network, while only admissible states will be used. So, it is quite redundant, and this motivates us not to use the approach in practice. However, it is flexible and can be useful, for example, in case when multiple conflicting expert rules are applied to different parts of one dataset, or when the choice of expert rules depends on inputs.

## 4 Neural Network and Expert Rules

Consider a partially-labeled multi-label multi-class classification problem. The training dataset $\mathcal{D}$ consists of $N$ tuples $(\mathbf{x}_j, \zeta_j^{(0)}, \ldots, \zeta_j^{(m)})$, where $\zeta_j^{(i)} \in \mathcal{C}^{(i)} \cup \{-1\}$ is a label of the $i$-th concept of the $j$-th training observation. The label $\zeta_j^{(i)}$ is assigned to $-1$ if a value of the $i$-th concept is unknown for the $j$-th observation. The target $y_j$ is denoted as the zero concept $\zeta_j^{(0)}$ and can also be partially labeled, that is $\zeta_j^{(0)}$ can also be equal to $-1$.

Let us denote the unit simplex of dimension $t$ as $\Delta_t$ and then $\widehat{\pi} \in \Delta_t$. We consider neural networks that simultaneously predict the marginal distribution for each concept. For the $i$-th concept, the prediction mapping is denoted as

$$f^{(i)} : \mathcal{X} \mapsto \Delta_{n_i}, \tag{12}$$

however, a neural network $f_\theta$ with parameters $\theta$ computes $f_\theta^{(0)}, \ldots, f_\theta^{(m)}$ simultaneously.

It should be noted that $f_\theta^{(i)}$ is nothing else but the marginal probability $p^{(i)}$ estimation. Then the training loss function is a sum of $m$ masked cross-entropy losses over each concept

$$\mathcal{L}^{(i)} = -\sum_{j=1}^{N} \mathbb{I}\left[\zeta_j^{(i)} \neq -1\right] \cdot \left(\sum_{k=1}^{n_i} \mathbb{I}[\zeta_j^{(i)} = k] \cdot \log\left(f^{(i)}(\mathbf{x})\right)_k\right). \tag{13}$$

The summation in brackets is the log-likelihood for the $i$-th concept.

The neural network can be fully-connected or convolutional depending on a solved problem, but there is one special layer at the end of the neural network. This layer maps an embedding produced by the preceding layers to the marginal class probabilities and guarantees that they will satisfy expert rules for any

input. In order to implement this scheme, the prior joint probability distribution vector $\widehat{\pi}$ is calculated by the neural network using the *softmax* operation applied to a linear layer that maps embedding to $t$ logits. To satisfy expert rules, the posterior joint probability conditioned on the rules is calculated by multiplying admissible states by the mask $u$. After multiplying, the posterior joint probability distribution has several zero values which violate the unit sum of probabilities. Therefore, the probability distribution is renormalized to get the unit sum of probabilities denoted as $\widetilde{\pi}$.

A general scheme of computing the marginal distributions $p^{(i)}$, $i = 1, ..., m$, of concepts is depicted in Fig. 1. It can be seen from Fig. 1 that the neural network produces the joint probability distribution of $\widehat{\pi}$ of the concept combinations. Expert rules form the musk which is multiplied by $\widehat{\pi}$ resulting a sparse vector having zero components corresponding to combinations of concepts which do not satisfy the rules. After normalization of the sparse vector, we again obtain a probability distribution $\widetilde{\pi}$ which produces marginal probability distributions of concepts $p^{(i)}$ after reshaping.

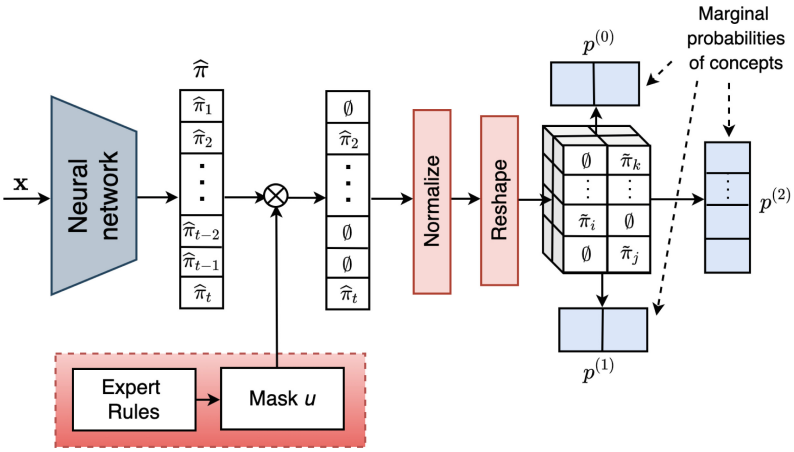


**Fig. 1.** A scheme of computing the marginal distributions: expert rules form the mask vector $u$ which is multiplied by the probability distribution $\widehat{\pi}$ (the Hadamard product); the obtained vector is normalized and reshaped to obtain a "tensor" producing marginal probability distributions of concepts

## 5 Numerical Experiments

Let us consider an artificial dataset constructed as a part of original image dataset MNIST consisting of 5000 randomly selected of $28 \times 28$ pixel handwritten digit images. Labels of digits define 10 values of the concept $c^{(1)}$. Another

concept $c^{(2)}$ is obtained by random coloring each digit in white or blue that corresponds to $c^{(2)} = 1$ or $c^{(2)} = 2$, respectively. The target label $y = c^{(0)}$ is defined as follows: odd blue digits or even white digits are labelled as $y = 1$, other digits are labelled as $y = 2$.

Three cases of CBL are compared:

- the proposed approach;
- the case of joint distribution without rules when the distribution $\widehat{\pi}$ is used for computing the marginal distributions of concepts;
- the case of independent targets when concepts are considered as independent targets (classes) and the network predicts probabilities for the targets separately.

The expert rule in this numerical experiment is the same as the rule used for constructing labels for $y$. Results of the experiment in the form of dependencies of the $F_1$ measure from the labeled data ratio for targets $y$ and for the concept $c^{(1)}$ are depicted in Fig. 2. One can see from Fig. 2 that the proposed approach provides the outperforming results when the labeled data ratio for targets is rather small. This implies that incorporation of the expert rule allows us to improve the whole model accuracy. At the same time, $F_1$ measures almost coincide when values of the labeled data ratio are large and close to 0.5. This is due to simplifying the model which leads to the similar accuracy in considered cases.

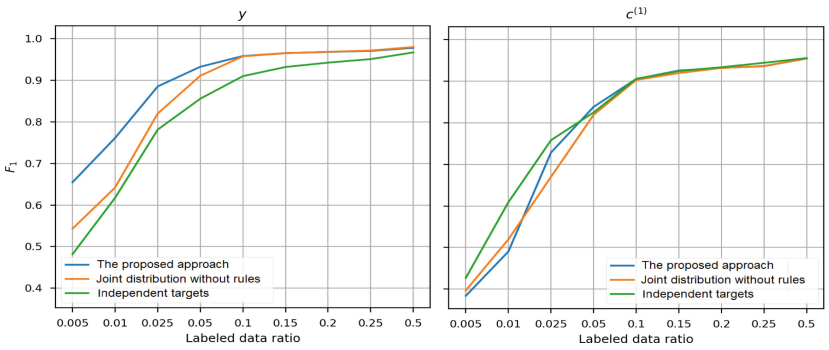


**Fig. 2.** Test performance ($F_1$) depending on labeled data ratio for concepts $c^{(0)}$ ($y$) and $c^{(1)}$

## 6 Conclusion

The problem of incorporating the expert rules into machine learning models in the framework of CBL has been stated in the paper. In fact, we have propose a way for solving the important problem of combining the deductive and inductive

learning models. The proposed approach is extremely simple from its implementation point of view. However, it is hard from the computation point of view because we need to analyze the Cartesian product of possible concept combination and to check whether each combination satisfies the expert rule. Therefore, other computationally effective approaches have to be developed. This can be regarded as a direction for further research.

We have applied the proposed approach to image data because they can be simply described by the high-level concepts, and these concepts are connected with target values. At the same time, it is interesting to study the case when the input vectors are tabular. In this case, some features can be regarded as concepts. Hence, a similar approach to incorporating the expert rules into neural networks or other machine learning models can be developed. This is also an important direction for further research. Generally, the consideration machine learning models different from neural networks in terms of CBL with expert rules is also an actual problem to be solved.

## References

1. Lage, I., Doshi-Velez, F.: Learning interpretable concept-based models with human feedback. arXiv:2012.02898 (2020)
2. Kim, B., Wattenberg, M., Gilmer, J., Cai, C., Wexler, J. Viegas, F.: Interpretability beyond feature attribution: Quantitative testing with concept activation vectors (TCAV). In: International Conference on Machine Learning, pp 2668–2677. PMLR (2018)
3. Wang, B., Li, L., Nakashima, Y., Nagahara, H.: Learning bottleneck concepts in image classification. In: Proceedings of the IEEE/CVF Conference on Computer Vision and Pattern Recognition, pp. 10962–10971 (2023)
4. Yeh, C.K., Kim, B., Arik, S., Li, C.L., Pfister, T., Ravikumar, P.: On completeness-aware concept-based explanations in deep neural networks. In: Advances in Neural Information Processing Systems, vol. 33, pp. 20554–20565 (2020)
5. Koh, P.W., et al.: Concept bottleneck models. In: International Conference on Machine Learning, pp. 5338–5348. PMLR (2020)
6. Poeta, E., Ciravegna, G., Pastor, E., Cerquitelli, T., Baralis, E.: Concept-based explainable artificial intelligence: a survey. arXiv:2312.12936 (2023)
7. Wah, C., Branson, S., Welinder, P., Perona, P., Belongie, S.: The caltech-UCSD birds-200-2011 dataset. Technical report, Technical report, California Institute of Technology (2011)
8. Lee, J.H., Lanza, S., Wermter, S.: From neural activations to concepts: a survey on explaining concepts in neural networks. arXiv:2310.11884 (2023)
9. Heidemann, L., Monnet, M., Roscher, K.: Concept correlation and its effects on concept-based models. In: Proceedings of the IEEE/CVF Winter Conference on Applications of Computer Vision, pp. 4780–4788 (2023)
10. Pendyala, V., Choi, J.: Concept-based explanations for tabular data. arXiv:2209.05690 (2022)
11. Collins, K.M., et al.: Human uncertainty in concept-based AI systems. In: Proceedings of the 2023 AAAI/ACM Conference on AI, Ethics, and Society, pp. 869–889 (2023)

12. Marcinkevičs, R., et al.: Interpretable and intervenable ultrasonography-based machine learning models for pediatric appendicitis. Med. Image Anal. **91**,103042 (2024)
13. Patrício, C., Neves, J.C., Teixeira, L.F.: Coherent concept-based explanations in medical image and its application to skin lesion diagnosis. In: Proceedings of the IEEE/CVF Conference on Computer Vision and Pattern Recognition, pp. 3798–3807 (2023)
14. Obermair, C., Fuchs, A., Pernkopf, F., Felsberger, L., Apollonio, A., Wollmann, D.: Example or prototype? learning concept-based explanations in time-series. In: Asian Conference on Machine Learning, pp. 816–831. PMLR (2023)
15. Tang, W., Liu, L., Long, G.: Interpretable time-series classification on few-shot samples. In: 2020 International Joint Conference on Neural Networks (IJCNN), pp. 1–8. IEEE (2020)
16. Choi, J., Raghuram, J., Feng, R., Chen, J., Jha, S., Prakash, A.: Concept-based explanations for out-of-distribution detectors. In: International Conference on Machine Learning, pp. 5817–5837. PMLR (2023)
17. Chauhan, K., Tiwari, R., Freyberg, J., Shenoy, P., Dvijotham, K.: Interactive concept bottleneck models. In: Proceedings of the AAAI Conference on Artificial Intelligence, vol. 37, pp. 5948–5955 (2023)
18. Zarlenga, M.E., et al.: Concept embedding models: Beyond the accuracy-explainability trade-off. In: Advances in Neural Information Processing Systems, vol. 35, pp. 21400–21413 (2022)
19. Havasi, M., Parbhoo, S., Doshi-Velez, F.: Addressing leakage in concept bottleneck models. In: Advances in Neural Information Processing Systems, vol. 35, pp. 23386–23397 (2022)
20. Ismail, A.A., Adebayo, J., Bravo, H.C., Ra, S., Cho, K.: Concept bottleneck generative models. In: Proceedings of ICML 2023. Workshop on Deployment Challenges for Generative AI, pp. 1–10 (2023). https://openreview.net/group?id=ICML.cc/2023/Workshop
21. Sawada, Y., Nakamura, K.: Concept bottleneck model with additional unsupervised concepts. IEEE Access **10**, 41758–41765 (2022)
22. Von Rueden, L., et al.: Informed machine learning-a taxonomy and survey of integrating prior knowledge into learning systems. IEEE Trans. Knowl. Data Eng. **35**(1), 614–633 (2021)
23. Diligenti, M., Gori, M., Sacca, C.: Semantic-based regularization for learning and inference. Artif. Intell. **244**, 143–165 (2017)
24. Yang, X.-W., Shao, J.-J., Wei-Wei, T., Li, Y.-F., Dai, W.-Z., Zhou, Z.-H.: Safe abductive learning in the presence of inaccurate rules. In: Proceedings of the AAAI Conference on Artificial Intelligence, vol. 38, pp. 16361–16369 (2024)

# Case-Based Decision Support System in the Field of Tourism

Olga Nikolaychuk[1](✉), Yuliya Pestova[1], Dmitriy Kosogorov[1], Alexander Pavlov[1], and Ivan Poddubnyy[2]

[1] Matrosov Institute for System Dynamics and Control Theory of Siberian Branch of Russian Academy of Sciences, Lermontova, 134, Irkutsk, Russia
nikoly@icc.ru

[2] Irkutsk State University, Karl Marx Street, 1, Irkutsk, Russia
int-office@isu.ru

**Abstract.** The paper considers the use of case-based reasoning to support decisions for choosing a vacation destination. The use case model and algorithm for their search and extraction are defined. The case model includes a description of the features of tourist attractions, accommodation facilities, public catering establishments, and services. The features of the model have quantitative, qualitative, interval, and semantic similarity values. Scales for measurement features describing cost and distance are individual and defined by a tourist. The similarity between tourists' reviews and preferences is assessed based on semantic similarity and sentiment calculated using the BERT multilingual neural network model. The similarity of cases is assessed based on the k-d tree (k-dimensional tree) method, which takes into account interval and text data types. The proposed approach is implemented on the Yandex.Cloud cloud platform and is tested in the Baikal natural territory using data collected from open sources. The proposed approach is implemented on the cloud platform Yandex.Cloud, and is being tested on the Baikal nature territory using data collected from open sources.

**Keywords:** Tourist Profile of the Territory · Collection of Data from Open Sources · Web Service · Cloud Platform · Case-Based Reasoning

## 1 Introduction

When choosing a vacation destination, a tourist faces the problem of searching for suitable information about accommodation facilities, public catering establishments, attractions, and tourist routes. Usually, information is scattered on various web-resources, is incomplete and inaccurate, and is presented in both formalized and textual unformalized forms. The search is limited to a certain number of criteria. Consequently, the tourist is forced to carry out a lengthy search, compare information from various sources, analyze numerous reviews and reviews, that creates a risk for the tourist - not finding an interesting and new vacation spot, and for the region - losing a potential tourist.

A prominent representative of web-services that aggregate the most complete information about the tourism industry is TripAdvisor - an American travel site that operates


S. Kovalev et al. (Eds.): IITI 2024, LNNS 1209, pp. 163–173, 2024.
https://doi.org/10.1007/978-3-031-77688-5_16

in 49 countries in 28 languages, that allows it to claim the title of the world's largest travel site (https://www.tripadvisor.com/).

The authors have proposed and are implementing a project to create a territorial tourism monitoring service that aggregates data on the tourist profile of a territory, and provides analysis and visualization of the collected data, and supports decisions for choosing a vacation destination or locations of tourist business facilities [1].

At present, the analysis of various web-sources is performed ("Ostrovok.ru", "101 Hotel", "Mir Tourbaz", OpenTripMap, tourist passports of the Irkutsk region and its municipalities, Russiadiscovery, the "Reserved Baikal region" website, and groups on the social networks VKontakte and OK), the ontology that provides uniform presentation and aggregation of data collected from various sources is developed, and the methods for collecting and visualizing the data that characterizes the tourist profile of Baikal territory are developed. The data about tourist objects has been processed: collective accommodation facilities: 1163 (685) (number of objects about which information has been collected; number in brackets is the number of identified objects with geolocation); services: 61 (16); public catering establishments: 2261; attractions: 395 (352); tourist routes and excursions: 94 [11].

The project is aimed at all stakeholders in the tourism sector and is intended to become the most comprehensive analytical source of information.

To improve the efficiency of the service, in addition to data visualization, decision support functions are needed.

Nowadays, various recommendation systems for tourists are being created; for example, world regions in demand by tourists have been identified based on the analysis and clustering of data from social networks [2]. In [3], the system that recommends places to visit in Barcelona on the basis of Twitter reviews analysis was described. In [4], the method that recommends attractors visit according to the tourist's position using place reviews, analysis, and ontological modeling was created. Personalized recommendations on tourism in China are formed based on a knowledge graph [5]. The recommendations on choosing a travel service are formed on the basis of multi-criteria decision support methods, contextual awareness, augmented reality, and information about the user's needs [6]. Methods used in these works belong to machine learning methods [7–9] and ontological modeling methods [4, 10].

It should be noted that the listed works solve particular problems that do not allow the tourist to get a complete picture of the territory of the planned vacation.

Among the information technologies that solve a similar problem, we can highlight recommender systems that perform content-based filtering and collaborative filtering [11]. These approaches assume the presence of some data from the user's profile or information about his past behavior.

The proposed service is not commercial and does not involve the collection of such information; users will not need to register, but will be able to share their opinion about the service and the resulting solution by liking it. However, in the initial stage, which may be quite lengthy, there will be a so-called "cold start" - a lack of data on user opinions. In this case, the most effective method is the "nearest neighbor search," which compares the user request data and the data available to the service.

It should be noted that a feature of the data set available to the authors is the presence of reviews about various objects in the tourism sector, that is an important source of data which will allow us to obtain a more accurate solution.

The availability of text data necessitates the need to complement the nearest neighbor method with a method for assessing the semantic similarity of texts (Semantic Textual Similarity, STS). This area is developing in various directions [12], but the most effective approach is the use of deep neural networks, in particular, models based on transformers (BERT, GPT-2, etc.) [13], models with self-observation mechanisms (self-attention) and positional encoding [14].

The purpose of the work is to develop a method of decision support for choosing a vacation destination based on aggregated heterogeneous information about regional tourism from open sources and case-based reasoning. The novelty of the work is the creation of a precedent model, the development of a method of case-based analysis, and the proposed visualization of the results within the framework of the Yandex.Cloud cloud platform.

## 2 Case-Based Reasoning

To support decision-making, it is proposed to use a case-based approach that allows one to get recommendations based on reasoning by analogy [15–17]. The problem statement within this approach has the form of a list of features of the domain object's and their possible values:

$$\begin{gathered} Obj = \{ob_1, ob_2, \ldots, ob_K\}, \\ ob_k = \left\{p_{k1}, p_{k2}, \ldots, p_{kM\_k}\right\}, \\ p_{km} = (v_{ml}, T), \end{gathered} \tag{1}$$

where $ob_k$ is a $k$-object of the domain, $p_{km}$ is a $m$-characteristic of the $k$-object, $v_{ml}$ is a $l$-value of the $m$-characteristic, $T$ is a characteristic type from the list: coordinates, quantitative, qualitative, or text.

The set of objects' features form a description of the "problem", that is, information that determines the initial data about some problem situation. The other part of features is the "decision" – the current part of the situation's description:

$$\begin{gathered} Case = \{c_1, \ldots, c_N\}, \\ c_i = (Problem_i, Decision_i), \\ Problem_i = \left\{(p_{km\_j}, v_{m\_jl\_j}\right\}_{k,m,l}, \\ Decision_i = \left\{\left(p_{km\_d}, v_{m\_dl\_d}\right)\right\}_{k,m,l}, \end{gathered} \tag{2}$$

where *Case* is a case base. The similarity between the feature values of the current situation $c*$ and an $i$-case $c_i$ is evaluated with a $s_i \in [0; 1]$ value:

$$s_i(c*, c_i) = \mathrm{S}_{m=1,M}\, w_m h_i(p_m*, p_{im})/M\,, \tag{3}$$

$$h_i(p_m^*, \underline{p_{im}}) = \begin{cases} \text{for coordinates values: } d,\ d = 1 - \underline{d_{KD\text{-}tree}}(v^*_{ml}, \underline{v_{iml}}) \\ \text{for quantitative values: } d,\ d = 1 - |v^*_{ml} - \underline{v_{iml}}| \\ \text{for qualitative values: } \begin{cases} 1,\ v^*_{ml} = \underline{v_{iml}} \\ 0,\ v^*_{ml} \neq \underline{v_{iml}} \end{cases} \\ \text{for text values: } \begin{cases} d,\ d(v^*_{ml}, \underline{v_{iml}}) < \delta \\ 0,\ d(v^*_{ml}, \underline{v_{iml}}) \geq \delta \end{cases} \end{cases}$$

where $w_m$ is a characteristic information weight, $v^*_{ml}$, $v_{iml}$ is a normalized values, $d$ is a proximity of different types of values.

The process of case-based reasoning consists of the following steps: retrieve, reuse (including adapt), revise, and retain [16, 17].

Case retrieval (search) is carried out by searching for the nearest analog. The methods used for search are the nearest neighbor method, the decision tree method, and others. Generally, the methods are based on summing up the similarity evaluated with various metrics: the Euclidean metric, the city block's metric, the Zhuravlev's metric, etc.

In this study, the nearest neighbors method was employed using a representation of the tree data structure k-d tree (k-dimensional tree), where precedents are described by a k-dimensional tree and the search is carried out to determine the similarity between the properties of the tourist's query and objects with similar values properties.

Conceptually, the realization and application of the approach algorithm consist of the following steps:

- building the use case model based on the created domain model,
- implementation of the use case model in the form of data structures (database, MS Excel tables, csv-files),
- filling the model with the user's case data,
- input of initial data about the current situation,
- automatic extraction of new data about the current situation by analogy,
- adaptation of the new decision,
- save the new case (self-learning).

## 3 The Case Model

The main task of the proposed approach is to define a case model that includes a description of the "problem" and "decision" for choosing a vacation destination by tourist (according to (1), (2)). Results of ontological modeling and experts' knowledge are used for creating this model [1].

Each tourist can submit an assessment, review, or comment about the objects of tourism after using such services. Those actions form a space of cases. In the initial state of a space of cases, there are no connections between tourism objects because detection of those connections is a hard task that can be performed, for example, on the basis of the formation of tourist routes as a result of the analysis of the digital footprints of tourists. However, when using such a space within our web service for search, analysis, and decision support, these connections will be formed based on user requests and assessments,

which will ensure a more effective use of case-based reasoning. Conceptually, connections have the following form: attractions – accommodation facilities – public catering establishments – services – reviews. The set of cases forms the case knowledge base, which can be separated into the case base of all tourist territory objects and the case base based on tourists‘ requests showing their individual aspects.

According to surveys of experts in the field of providing tourism services (tourism managers with 30 years of experience), choosing a vacation destination for a tourist consists of the following steps: (1) choosing attractions (natural, cultural, religious, etc.) that are attractive to visit; (2) choosing accommodation facilities; (3) choosing public catering places; (4) clarifying desired entertainments and their features (travels, excursions, etc.); (5) clarifying special wishes (viewing from the window, comfortable foot paths, unusual dishes of local cuisine, etc.).

Therefore, the case “problem” includes a features description that characterizes the classes of the domain: attractions, accommodation facilities, public catering establishments, services and entertainments, and reviews (keywords from the query with wishes), when the decision is a list of specific objects (locations) satisfying the criteria of proximity of cases (Table 1).

## 4 Algorithms and Software

The algorithm of case retrieval is carried out in two steps: (1) search among cases as the results of tourists’ requests; (2) search in the total space of cases. The second step is carried out if there are no results from the first step (“cold start”).

Most objects in the domain have qualitative values, which will be taken into account in the search method if there is a complete match. Quantitative values describe features such as cost and distance. These features are individual for a decision-maker. It is proposed to take into account the opinion of the user, who determines his own scales to select the criteria for data similarity. It is also to take into account special requests that cannot be found in the list of features but can be reflected in text comments and reviews about tourist objects. In this case, similarity is calculated based on keyword extraction, their comparison, and the assessment of semantic similarity. The space of cases for the territory at each step of the search sequence will be narrowed within the method implementation.

The approach is proposed to be implemented as a separate function of the web-service for monitoring tourism.

This function will provide sequential filtering of domain objects (in accordance with selected priorities) by using their properties as criteria, with the display of intermediate results on an information panel with geoinformation binding.

**Table 1.** The case model

| Object | Characteristic (attribute) | Characteristic description |
|---|---|---|
| *Problem* | | |
| Time duration | time duration | decade, month, season |
| Attractions | attraction category | natural, cultural, ecological, etc |
| | rating of an attraction | by the scale from 1 to 10 |
| | distance to accommodation facilities | the individual maximum distance specified by the user |
| Accommodation facilities | tourists number | the tourists number in a group |
| | children number | the children number in a group |
| | rooms number | the number of needed rooms |
| | level of improvement | the level of improvement is described by the room category |
| | rating of an accommodation facility | by the scale from 1 to 10 |
| | distance to water | the individual maximum distance |
| | cost | individual cost limits |
| | have a beach | have or have not |
| Public catering establishments | cuisine type | European, Georgian, Buryatian |
| | rating of public caretaking place | by the scale from 1 to 10 |
| | distance to accommodation facilities | the individual maximum distance |
| | distance to attractors | individual maximum distance |
| | average bill | individual cost limits |
| Services and entertainments | entertainment category | sport, excursion, SPA etc |
| | cost | individual cost limits |
| | time duration | the individual maximum time duration (hours, days) |
| | transport type | car, ship, boat, train etc |
| Keywords | positive location characteristics | Positive prompt |
| | negative location characteristics | Negative prompt |

(*continued*)

**Table 1.** (*continued*)

| Object | Characteristic (attribute) | Characteristic description |
|---|---|---|
| *Decision* | | |
| Vacation destination | accommodation facilities | name, address, geolocation |
| | public catering establishments | name, address, geolocation |
| | services and entertainments | name, address, geolocation |
| | keywords that characterize the place | words characterize natural objects, attractions, problems, representation in the form of a word cloud |
| | weather conditions | average temperature, precipitation, direction and strength of wind |
| | area workload | café workload, beach workload |

The generalized algorithm of the proposed approach is performed in stages (see Fig. 1):

1. The user specifies the coordinates or name of the attraction (recreation area) and their required characteristics.
2. Search for the nearest accommodations to the target coordinates.
3. Search for attractions, accommodations, and public catering establishments based on specified characteristics: average check, distance to the beach, comfort level considering the provided services. Distances between objects are assessed based on determining actual routes using the OSRM API (https://project-osrm.org/docs/v5.24.0/api/).
4. Search for accommodations based on the semantic similarity assessment of the tourist's text query and consumer reviews of tourism services by keywords. Such queries contain textual descriptions with positive (positive prompt) and negative (negative prompt) preferences.

The semantic similarity assessment is implemented using the Python programming language, including the SentensTransformers module (https://sbert.net/). The function uses the results of a preliminary classification of the advantages and disadvantages of vacation spots indicated in reviews of tourists. The classification was performed using the large Saiga2 language model (https://huggingface.co/IlyaGusev/saiga2_70b_lora) and prompt engineering technology, taking into account the given classes (policy\administration, transport\movement, maintenance, landscaping, tour operators\travel agencies, natural emergencies situations, ecology, food, services\entertainment). The classification accuracy is assessed by F-measure averaging metrics: Micro F1 – 0.74, Macro F1 – 0.67, Weighted F1 – 0.66. Next, using the multilingual model paraphrase-multilingual-MiniLM-L12-v2 [18], the semantic similarity of information about vacation spots and the highlighted advantages from the tourist's request is determined,

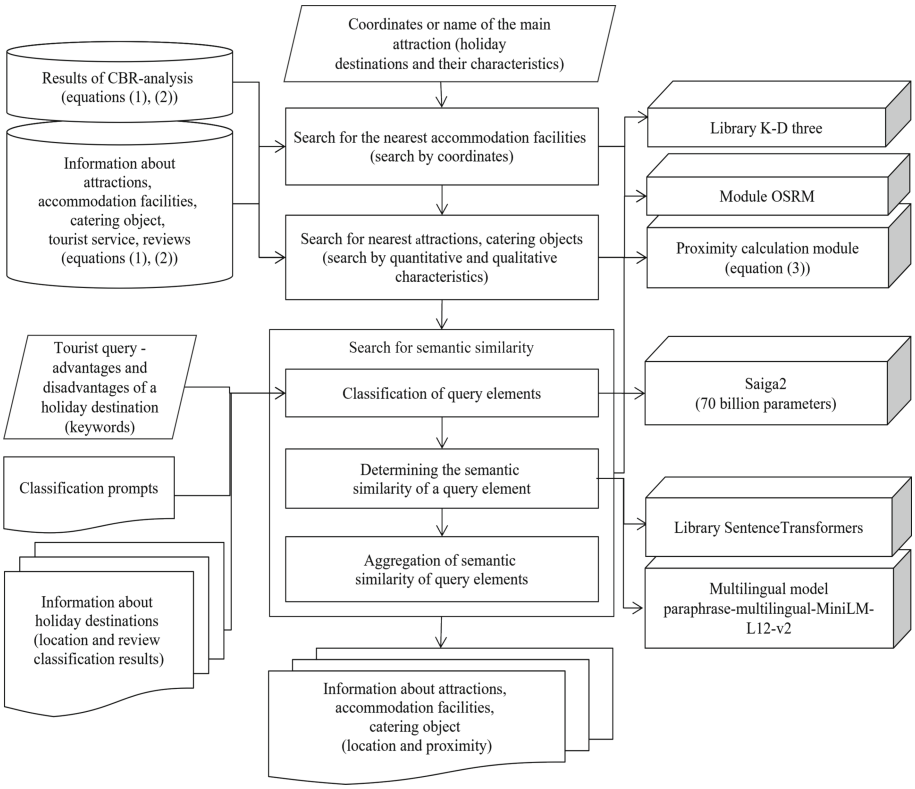


**Fig. 1.** Algorithm for assessing proximity.

which are then aggregated into a single assessment for each vacation spot. The values of semantic similarity of advantages are summed up, disadvantages are subtracted. This model has the best characteristics among publicly available multilingual models in terms of accuracy (Avg. Performance – 51.72) and time (Speed – 7500 sentences/s) of calculations.

To visualize the results, information panels (dashboards) were developed using the "Yandex DataLens" service. The proposed approach is implemented in the form of a "wizard" with a sequence of dialogs for step-by-step input of information and obtaining an intermediate result in the form of visualization information panels with geoinformation binding:

- selecting a territory and/or a category of attractions with the result displayed on the territory map,
- specifying the required properties for the accommodation facility, selecting a measurement scale for the price of accommodation, and the distance to the beach, with the results displayed on the map as point objects with additional information about prices, services, and the number of positive and negative reviews,
- selection of required properties for public catering places, selection of a measurement scale for the average bill of the public catering establishment and the distance to it,

with the results displayed on the map in the form of point objects and isolines characterizing proximity to accommodation facilities, and additional information about prices, services, and the number of positive and negative reviews,

- identification of keywords characterizing the vacation destination, with the results displayed as a cloud of words.

The efficiency of the described precedent approach at this stage is assessed based on a comparison of offers of vacation spots received by the service and experts in the field of tourism. The expert was asked to describe the requirements for 5 categories of tourists and create a list of vacation spots for each category on the island Olkhon. Next, using the service functions and the listed requirements, the initial data for case analysis is described. A comparison of the expert's and service's proposals showed that in four out of five cases, the service's results coincide with the expert's proposals, which represents an 80% rate of positive results.

## 5 The Practical Significance

The practical significance of the proposed approach is the development of algorithms and software to support decision-making by tourists when choosing vacation destinations. This support will improve the efficiency of informing and attracting tourists to the regional tourism sector. A fragment of the information panel with the request of a tourist about the need for a location on the territory of Olkhon Island is presented to demonstrate the results (see Fig. 2). The dashboard presents the characteristics set by the tourist and the result of a case-based analysis, highlighting the links between the accommodation facility and public catering establishments.

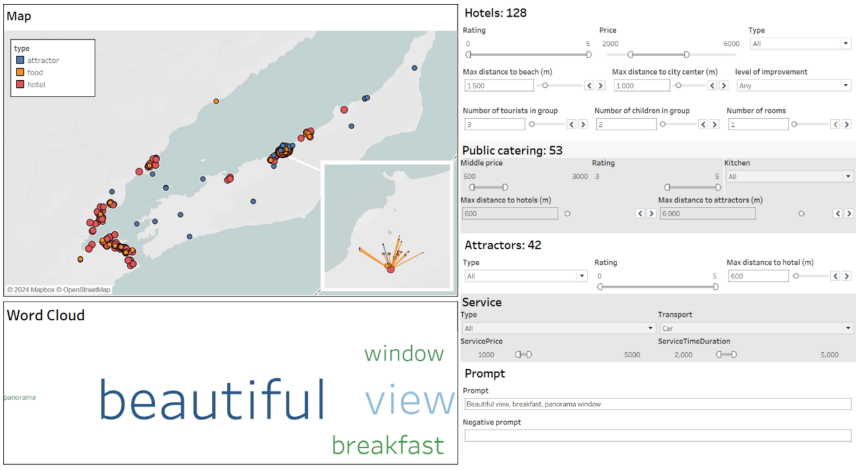


**Fig. 2.** A fragment of the dashboard with the result of a case-based analysis.

## 6 Conclusion

The method of supporting decisions on the choice of a vacation destination based on a case-based analysis of heterogeneous information from open sources was proposed in this work. When implementing the method, the authors' experience in applying this approach to solving problems of technical diagnostics and developing tools for creating knowledge processing systems was used. In the future, it is planned to develop the method, ensure the accumulation of knowledge (heuristics) of experts in the field of tourism on the choice of vacation destinations, and explore the possibility of forming a route to visit several geographically remote attractions.

**Acknowledgments.** This study was funded by Russian Science Foundation (grant number 23-28-00844).

**Disclosure of Interests.** The authors have no competing interests to declare that are relevant to the content of this article.

## References

1. Nikolaichuk, O.A., Pestova, Y., Pavlov, A.I., Kosogorov, D.E.: A concept of the tourism industry monitoring service based on the analysis of web resources. Comput. Technol. **28**(6), 118–134 (2023)
2. Dietz, L.W., Sen, A., Roy, R., Wörndl, W.: Mining trips from location-based social networks for clustering travelers and destinations. Inf. Technol. Tour. **22**(3), 131–166 (2020)
3. Orama, J.A., Borràs, J., Moreno, A.: Combining cluster-based profiling based on social media features and association rule mining for personalised recommendations of touristic activities. Appl. Sci. **11**(14), 6512 (2021)
4. Pai, M.-Y., Wang, D.-C., Hsu, T.-H., Lin, G.-Y., Chen, C.-C.: On ontology-based tourist knowledge representation and recommendation. Appl. Sci. **9**(23), 5097 (2019)
5. Su, X., He, J., Ren, J., Peng, J.: Personalized Chinese tourism recommendation algorithm based on knowledge graph. Appl. Sci. **12**(20), 10226 (2022)
6. Rokhsaritalemi, S., Sadeghi-Niaraki, A., Kang, H.-S., Lee, J.-W., Choi, S.-M.: Ubiquitous tourist system based on multicriteria decision making and augmented reality. Appl. Sci. **12**(10), 5241 (2022)
7. Li, H., Hu, M., Li, G.: Forecasting tourism demand with multisource big data. Ann. Tour. Res. **83**, 102912 (2020)
8. Soualah-Alila, F., Coustaty, M., Rempulski, Doucet, N.A.: Datatourism: designing an architecture to process tourism data. In: Inversini, A., Schegg, R. (eds.) Information and Communication Technologies in Tourism. Springer, Cham (2016). https://doi.org/10.1007/978-3-319-28231-2_54
9. Li, J., Xu, L., Tang, L., Wang, S., Li, L.: Big data in tourism research: a literature review. Tour. Manag. **68**, 301–323 (2018)
10. Mendoza-Moreno, J.F., Santamaria-Granados, L., Fraga, V.A., Ramirez-Gonzalez, G.: Ontotoutra: tourist traceability ontology based on big data analytics. Appl. Sci. **11**(22), 11061 (2021)
11. Kutyanin, A.R.: Recommender systems: overview of main statements and results" Intelligent systems. Theory and applications **21**(4), 18–30 (2017)

12. Chandrasekaran, D., Mago, V.: Evolution of semantic similarity—a survey. ACM Comput. Surv. (CSUR) **54**(2), 1–37 (2021)
13. The Illustrated Transformer–Jay Alammar–Visualizing Machine Learning One Concept at a Time. https://jalammar.github.io/illustrated-transformer/. Accessed 10 Dec 2023
14. Galli, C., Donos, N., Calciolari, E.: Performance of 4 pre-trained sentence transformer models in the semantic query of a systematic review dataset on peri-implantitis. Information **15**(2), 68 (2024)
15. Bergmann, R.: Experience Management: Foundations, Development Methodology, and Internet-Based Applications. Springer, Heidelberg (2002)
16. De Mantaras, L.R., et al.: Retrieval, reuse, revision and retention in case-based reasoning. Knowl. Eng. Rev. **20**(3), 215–240 (2006)
17. Aamodt, A., Plaza, E.: Case-based reasoning: foundational issues, methodological variations, and system approaches. AI Commun. **7**(1), 39–59 (1994)
18. Reimers, N., Gurevych, I.: Sentence-BERT: Sentence Embeddings using Siamese BERT-Networks. In: Proceedings of the 2019 Conference on Empirical Methods in Natural Language Processing. http://arxiv.org/abs/1908.10084. Accessed 20 Mar 2024

# 3d Segmentation Methods of Archaeology Sites Using Dynamic Graph CNN and Transformer Architecture

Aleksander Vokhmintcev[1(✉)], Mostafa Khater[2,3], and Mostafa Abotaleb[4]

[1] Chelyabinsk State University, Chelyabinsk, Russia
vav@csu.ru
[2] Ugra State University, Khanty-Mansiysk, Russia
[3] Xuzhou Medical University, Xuzhou, China
[4] South Ural State University, Chelyabinsk, Russia

**Abstract.** In this paper 3d segmentation methods of irregular point clouds are presents to decipher the structure of archaeological sites of the Bronze Age in the Southern Trans-Urals. The first method for 3d semantic segmentation is based on a multimodal dynamic graph, which is created by recalculating the graph's Kirchhoff matrix in each special convolutional layer of the neural network. The second method for 3d instance segmentation is based on the architecture of a deep neural network in the form of improved Mask3D transformer. The introduced modifications into the transformer architecture made it possible to significantly improve the confidence of instance segmentation and obtain a dense, complete and homogeneous point cloud for processing from various depth sensors. For computer simulation, the most promising methods for 3d semantic segmentation and 3d instance segmentation were selected. In this paper computer simulation was carried out for various methods of 3d segmentation, the results obtained were presented and discussed, and the dependence of the accuracy segmentation from 3d up-sampling and augmentation procedure of point clouds was studied.

**Keywords:** 3D semantic segmentation · 3D instance segmentation · dynamic graph convolution neural networks · transformer

## 1 Introduction

The discipline of 3d data processing is currently at a critical moment, driven by the pressing requirement to analyze and handle intricate 3d point cloud data in several domains including autonomous navigation, sophisticated robotics, architectural modeling, and geospatial analysis. In this paper, methods are proposed for studying the 3d structure of archaeological sites using machine learning, mapping and geophysics methods. The inherent intricacies of 3d point clouds, particularly their non-Euclidean and irregular characteristics, provide substantial analytical obstacles that conventional data processing approaches struggle to overcome. This requires a fundamental change

The work was supported by the Russian Science Foundation (grant no. 23-11-20007)


S. Kovalev et al. (Eds.): IITI 2024, LNNS 1209, pp. 174–184, 2024.
https://doi.org/10.1007/978-3-031-77688-5_17

in the way we approach neural network architectures and algorithms, focusing on more advanced solutions that are capable of analyzing and effectively exploiting the intricacies and complexities of 3D data. An innovative method is presented for processing point cloud data using CNN (convolutional Neural Networks) [16], this approach based on DGCNN (Dynamic Graph CNN) addresses the challenges of traditional CNNs in interpreting non-Euclidean, irregular 3D data. DGCNN utilizes dynamic construction of local graphs, significantly increasing the network's ability to discern both local and global structures in the data. This advancement is crucial for tasks such as classification and segmentation, marking a notable progression in CNN applications for complex data analysis. In the referenced study [13], a Regularized Graph Convolutional Neural Network (RGCNN) is introduced for effective point cloud segmentation. Utilizing spectral graph theory, this method dynamically updates the graph' Laplacian matrix in each layer, enhancing the model's adaptability. This approach positions RGCNN and DGCNN as a computationally efficient yet powerful tool in the realm of 3D data analysis but none computationally efficient tools for large-scale point clouds. To eliminate this disadvantage of these methods, modern algorithms for 3d semantic segmentation, for example, SPG, ConvPoint, KPConv, Superpoint Transformer have been proposed.

Firstly, let's look at the methods of 3d semantic segmentation of semantically rich large-scale point clouds according to the benchmark datasets. The study [6] proposes a deep learning framework utilizing Superpoint Graphs (SPG). This approach innovatively partitions point clouds into geometrically homogeneous elements, leveraging graph convolutions to exploit contextual relationships effectively. The study [1] discusses ConvPoint, a method is designed to handle the unstructured nature of point clouds more efficiently than traditional methods. It demonstrates significant improvements in various tasks such as classification and segmentation, particularly notable in its ability to deal with large-scale datasets. KPConv (Kernel Point Convolution) [14] is a new point convolution approach for processing point clouds. KPConv distinguishes itself by its deformable convolutional operation, which adapts to the local geometry of the data, and its efficient handling of varying point cloud densities. Superpoint Transformer [10] employs a fast algorithm for partitioning point clouds into hierarchical superpoint structures, significantly speeding up preprocessing. The model uses a self-attention tool to figure out relationships between super-points at multiple scales, achieving excellent performance on benchmark datasets with a compact model size.

Secondly, let's look at the methods of 3d instance segmentation of semantically rich large-scale point clouds according to the benchmark datasets. The advancement in 3D instance segmentation is marked by a unique methodology 3D-MPA (Multi-proposal Aggregation) [3] that emphasizes the aggregation of multiple object proposals from 3D point clouds. This technique, utilizing a graph convolutional network for processing, diverges from traditional methods that rely on pruning proposals. This innovation leads to enhanced accuracy and efficiency in 3D instance segmentation for lots of digital collections. The GICN (Learning Gaussian Instance Segmentation in Point Clouds) [8] method emphasizes the use of Gaussian heatmaps to approximate the distribution of instance centers within a given scene. Its architectural design streamlines both the training and inference processes, resulting in outstanding performance metrics on the ScanNet and S3DIS datasets. This technique's innovation is rooted in its effective management of

instance centers and sizes, offering an intuitively understandable and computationally efficient solution for 3D instance segmentation tasks. HAIS (Hierarchical Aggregation for 3D Instance Segmentation) [2] method employs hierarchical aggregation, amalgamating clustering-based frameworks with an efficient bottom-up strategy. The procedure encompasses the aggregation of points into sets, followed by the formation of complete instances, culminating in the application of a sub-network for quality enhancement. DKNet (Dynamic Kernel Network) method [17] places a primary emphasis on the precise localization of instances and comprehensive feature collection, employing 1D kernels to encode vital positional, semantic, and shape information. The novelty of this approach resides in its instance encoding methodology, which harnesses a dynamic kernel network to achieve highly effective instance segmentation. This study SSTNet (Semantic Super-point Tree Networks) [7] presents an innovative end-to-end solution for 3D instance segmentation, focusing on the creation and traversal of a semantic superpoint tree. The method has demonstrated remarkable effectiveness on benchmark datasets like ScanNet and S3DIS, showcasing its robustness and accuracy in challenging segmentation tasks. The TD3D (Top-Down 3D) [4] is a top-down, fully-convolutional approach for 3D instance segmentation, which overcomes the limitations of traditional bottom-up methods. TD3D's end-to-end, data-driven training process avoids the need for manual hyperparameter tuning. Demonstrating exceptional performance and speed on benchmarks like ScanNet v2 and S3DIS, TD3D's approach is innovative in its efficiency and effectiveness in segmenting 3D point clouds. The study presents PBNet [18], an innovative 3D instance segmentation approach for point clouds, featuring a divide-and-conquer strategy with point-wise binarization. PBNet innovatively categorizes points into high and low-density groups, aiding in effectively segmenting adjacent objects and refining instances. The approach demonstrates significant performance improvements on benchmark datasets. Mask3D [12] marks a breakthrough in 3D semantic instance segmentation, utilizing a Transformer-based model with sparse convolutional feature backbones and Transformer decoders. This innovative approach enables efficient processing of large-scale scenes, directly predicting instance masks from point clouds. With its ability to set new benchmarks on multiple datasets, Mask3D demonstrates exceptional proficiency in handling complex segmentation tasks across varied environments. One-Former3D [5] introduces a unified framework for 3D point cloud segmentation, all within a transformer-based model. This innovative approach incorporates a novel query selection mechanism and efficient matching strategy, optimizing the training process without the need for the Hungarian algorithm. One Former3D's remarkable performance on benchmark datasets, including Scan-Net, ScanNet200, and S3DIS, signifies a significant advancement in multi-task 3D segmentation, setting new state-of-the-art standards across all segmentation tasks.

In this paper original 3d semantic segmentation method based on a dynamic weighted graph, which devoids the disadvantages of the well-known CNN architectures [1, 13, 14]. Also, we have made a lot of improvements to the architectural design of instance segmentation based on transformer [12], which allowed to be effectively applied to sparse, nonhomogeneous and noisy point clouds to decipher the structure of archaeological sites of the Bronze Age of the Southern Trans-Urals. This paper is organized as follows: in the second chapter, the method for 3d segmentation was suggested, in

the third chapter method for 3d instance segmentation was proposed, the fourth chapter presents the results of computer simulation.

## 2 Semantic Segmentation Method Using Dynamic Graph

In this study the data set was compiled for archaeological sites of the Bronze Age of the Southern Trans-Urals [15]. The data sample contains: 2D data based on a collection of aerial photographs and Earth remote sensing data from the Sentinel-2, Landsat 4–9, Resurs-P, Kanopus-V satellites and 3D data in the form of tacheometric survey results, depth data from LiDAR scanners (orthophotos and point clouds), as well as electrical survey results. Let's represent an architecture system for remote research of archaeological sites using only 3d data from this dataset (see Fig. 1).

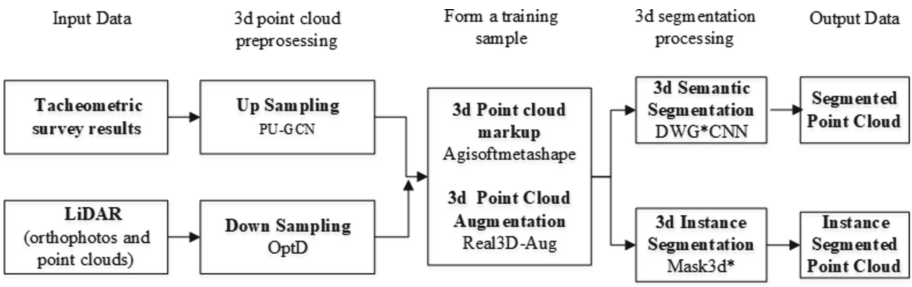


**Fig. 1.** The architecture system for remote research of archaeological sites using 3d data.

The 3d point cloud segmentation procedure can be divided into two pipe data processing: for 3d semantic segmentation based on originally method DWG*CNN (Dynamic Weight Graph Convolutional Neural Network) and for 3d instance segmentation based on improved version of Mask3d*. The adaptive point cloud up-sampling PU-GCN algorithm [9] is used for survey data from Trimble 3300 tachometer sensor (Elta R55) to obtain a dense and homogeneous point cloud; for data from LiDAR-sensors data dimensionality reduction is required using adaptive point cloud down-sampling to obtain a homogeneous, noiseless point cloud of a smaller dimension. To increase the lot of 3d models in the data set, the collection was expanded approximately 8 times using the 3d data augmentation algorithm Real3D-Aug [11]. This algorithm based on fast point cloud augmentation by placing real objects with occlusion handling for 3d detection and segmentation and allows to add new objects, such as a dwelling, mound or external/internal wall in the 3d model of an archaeological site. Geographic information system "Agisoftmetashape" was used to label the 3D data. The 3d semantic segmentation process was represented as the following iterative sequence of steps DWG*CNN (Algorithm 1): the calculating Kirchhoff matrix elements, the normalization of the elements of the Kirchhoff matrix and the convolution of a spatial weighted graph. The approximation using the Chebyshev polynomial can improve the performance of the graph filtering and convolution procedure. DWG*CNN method uses a combination of geometric and

color features points in the point cloud to get advantages in accuracy of 3d segmentation procedure.

Algorithm 1 based on DWG*CNN:

1: Input data: colored point cloud $P = \{p_1, \ldots, p_n\}$. Output data: segmented point cloud $C = \{p_1^S, \ldots, p_n^S\}$;

2: Initialization of feature vector elements $\{C_i\}$; the Chebyshev polynomial Coefficients {6,5,3}; k=1; $s_1$, $s_2$ – signals on the graph;

3: for k in 1,…, 3 do

4: Calculating Kirchhoff matrix elements $L_k$;

5: Normalization of the elements of the Kirchhoff matrix $L^{sum}$;

6: Approximation of the graph signal Chebyshev polynomial $g_\psi(k)$;

7: Convolution of a spatial weighted graph $s_2 = g_\psi(L^{sum})s_1$;

8: Initialization of feature vector elements DWG*CNN;

9: end;

10: MLP 1 (1024); MLP 2 (512);

11: Concatenation (EdgeConv 2, MLP2);

12: Determining the value of the loss function $L_{los}$.

The loss function of DWG* CNN can be represented as

$$L_{los1} = -\sum_{i=1}^{N} conv_i \log(y_i) + \lambda_{smoth1} \sum_{j=1}^{4} y_j^T DG y_j, \quad (1)$$

where $conv_i$ – the total score, $y_i$ – the probability value, $y_j$ – the feature map of the j-th EdgeConv layer, $\lambda_{smoth}$ – smoothness term (set to $10^{-9}$ in our tests), DG – the function, which form output of dynamic graph of CNN for the j-th EdgeConv layer. The loss function consists of two terms, first term presents multiclass cross-entropy and second term is responsible a graph-signal smoothing to allow significantly improves the model's resistance to noise and variations in point cloud density.

## 3 3d Instance Segmentation Method Using Mask3d Transformer

In this research for 3d instance segmentation Mask3d [12] based on generic transformer was applied which allows to directly predict instance masks from point clouds: each object instance is represented as an instance query. The model of 3d instance segmentation has the following modules architecture: Sparse Feature Backbone using convolutional U-net backbone (M1); Transformer decoder based on the Minkowski-Engine (M2); Mask module (M3). Query refinement (M4). Instance queries are trained using a transformer decoder in the form of an iterative procedure, in which functions are accessed to process a point cloud at a multiple scale. In Mask3d improvements have been introduced, the new steps are marked-up with sign * (Algorithm 2 Mask3d*): in the loss function the term was added that is responsible for smoothing signal; as a preliminary processing, a procedure for point cloud up-sampling with the option of forming a uniform distribution of points was added; feature concatenation scheme was changed,

that it improved instance segmentation; the architecture of the M1 module was changed and based on 6 sparse feature backbone; fast quantization procedure of a point cloud in voxels and procedure of adaptive detection of outliers in voxels has been added. Let's P is RGB point cloud of size N, where $P \in \mathbb{R}^{N\times 6}$ and $M_0$ is number of voxels $V \in \mathbb{R}^{M_0\times 3}$, where an initial feature for each voxel is average RGB color of the points within this voxel. Let's $F_r \in \mathbb{R}^{M_r\times D}$ is a features maps (matrixes), where D – common dimension 3d sparse, $r$ – the sparse resolution, where $r = 0$ for full-resolution feature map. If $X \in \mathbb{R}^{K\times D}$ are instance queries, where K – dataset of instance queries.

Algorithm 2 (Mask3d*) based on transformer Mask3d:
1: Input data: colored point clouds $P = \{p_1, \ldots, p_n\}$ $P \in R^{N\times 6}$. Output data: refined instance queries, semantic class predictions, instance masks B;
2:* Point Cloud Up-Sampling and 3d Augmentation of training data set;
3: Initialize the transformer' modules M1, M2, M3, M4;
4:* Fast quantize P into $M_0$ voxels $V \in R^{M0\times 3}$;
5: Determine the initial feature values;
6: Calculate feature map $F_0$ in 3d high resolution using M1;
7: for r in 0,…, R do
8: Extract features for set of $M_r$ voxels and project to dimension D: $F_r$;
9: * Adaptive outlier detection in $M_r$ voxels;
10: end;
11: Initialize $K$ dataset of queries with non-parametric queries;
12: for each $X$ do
13: Refine instance queries using M2;
14: Cross-attend to scene features and self-attend to other $X$;
15: end;
16: Apply M3 to refined $X$ and point features;
17: Predict semantic class and instance masks $B$ for each $X$;
18: Compute confidence score (F1or IoU) for each predicted;
19: Apply M4 to dominant class: select queries and calculate class confidence (CC);
20:* Calculate mask-based confidence for each voxel and fuse with CC;
21:* Form a segmented point cloud based on local and global features;
22: Post processing for segmentation result using confidence scores.

The decoder sends these instance queries $X$ and refines them to a final set of instance requests using a stack with L levels, cross-attention to the features on 3d scene allows the queries to produce data from the voxel features and a self-control mechanism. 3d data processing architecture allows to eliminate duplication of instance masks. To apply the cross-attention mechanism, a linear projection of a set of voxel objects $F_r$ to the set of keys K and dimension values V ($KV \in \mathbb{R}^{M_r\times D}$) is performed, and also a linear projection of instance queries X to the queries $Q \in \mathbb{R}^{K\times D}$ is performed. As a preprocessing before calculating cross-attention and self-attention, the positional Fourier transform of the encoding is used. Mask3d uses a masked variant cross-attention

$$X = \text{softmax}\left(\frac{QK^T}{\sqrt{D}} + B_{ij}\right)V, \tag{2}$$

where B is an instance mask, $B'_{ij} = -\infty \cdot [B_{ij} = 0]$, $[\cdot]$ are Iverson brackets.

In this paper, we use 6 the feature backbone levels instead 4 in classical version Mask3d, from bad to good resolution, an iterative procedure repeats is a 3 times, so L = 18 query refinement steps, it improved instance segmentation. To establish a correspondence between the set of instances on the scene and the set of predicted instances, this paper uses a bipartite-graphs matching based on the Hungarian algorithm. The overall loss has been improved by introducing a third term related to signal smoothing. So, the overall loss function of transformer Mask3D* for all auxiliary instance predictions after each of the L layers is defined as

$$L_{los2} = -\sum_{l=1}^{L} L_{mask}^{l} + \lambda_{cl} L_{CE_{cl}}^{l} + \lambda_{smoth2} \sum_{\mathrm{j}=1}^{6} Mask3d_j, \tag{3}$$

where $L_{mask}^{l} = \lambda_{BCE} L_{BCE} + \lambda_{Dice} L_{Dice}$, $L_{BCE}$ is the binary cross-entropy loss, $L_{Dice}$ is the Dice loss, $L_{CE_{cl}}^{l}$ is multi-class cross-entropy loss, $Mask3d_j$ is the function, which form output of Transformer decoder for the j-th sparse resolution, $\lambda_{BCE}$, $\lambda_{Dice}$, $\lambda_{cl}$ – hyperparameters of the loss function, $\lambda_{smoth2}$ – smoothness parameter. The Mask3d* transformer has a high degree of autonomy and doesn't require the involvement of an expert to select the values of hyper-parameters and geometric properties in object grouping procedures and voting procedures. The proposed loss function (3) with smoothing allow directly to optimizes an instance masks.

## 4 Computer Simulation

This section presents the results of computer simulation, it was quantitatively evaluated suggested approach (DWG*CNN + Mask3d*) and compared with state-of-the-art methods, such as OneFormer3d, Mask3d for instance segmentation and DGCNN, RGCNN for semantic segmentation. In this paper we use only 3d data from dataset: the approach based on DWG*CNN + Mask3d* was tested using geophysics data and LiDAR data at the area of archaeological sites near the settlements of Stepnoe and Levoberezhnoe. All 3d data has been preprocessed (see Fig. 2, a), consisting of the following steps: division of a 3D model into semantic blocks with step = 0.01, up-sampling of point clouds based on PU-GCN (see Fig. 2, b), calculations of normals in the point cloud.

The signs of deciphering archaeological objects characteristic of Bronze Age monuments were defined based on the Archaeological Atlas of the Chelyabinsk Region [20], created by prof. G.B. Zdanovich. In this paper the following set of classes are used to decrypt the structure of a 3d archaeological site: s1 – dwelling; s2 – moat; s3 – defensive wall; s4 – burial ground; s5 – inner wall; s6 – well; s7 – entrance to the settlement. The experiments we carried out on part of dataset which contains 116 originally 3d point cloud from 2 categories, annotated with 7 labels in total. PU-GCN algorithm allows to create the dense homogeneous point cloud, which consist of rather than 2000 points from each 3d model site. Using Real3D-Aug for point cloud augmentation, dataset size to 928 of 3d diverse point clouds was expanded (see Fig. 2, c). In our study the following hyperparameter values were used: $\lambda_{smoth1}$=$10^{-9}$ for DWG*CNN, $\lambda_{BCE} = 5.0$, $\lambda_{Dice} =$

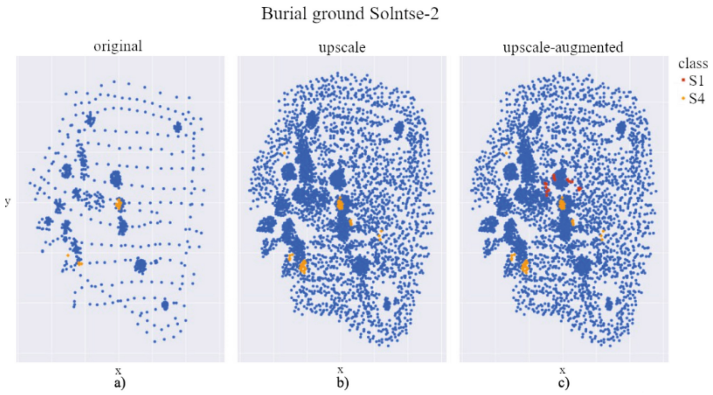


**Fig. 2.** The results of 3d preprocessing a) tacheometric survey results b) point cloud after Upsampling PU-GCN c) point cloud after 3d Augmentation Real3D-Aug*.

2.0, $\lambda_{cl}$=2.0, $\lambda_{smoth2} = 10^{-9}$ for Mask3d*. The model based on DWG*CNN is trained on a single Intel Core i7-9800X, NVIDIA GeForce RTX 2080 Ti 11264MiB with 250 epochs. The results computer simulation for RGCNN, DGCNN, DWG*CNN by Accuracy: 73.06%, 68.53%, 91.07%; IoU: 0.695, 0.530, 0.781, F1: 0.734, 0.695, 0.934. The results of instance segmentation using Mask3d* were presented on Fig. 3.

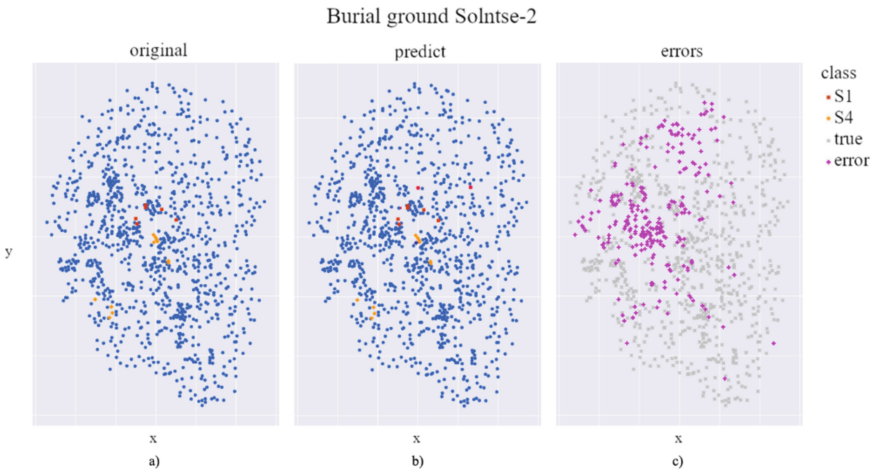


**Fig. 3.** The results of instance segmentation using Mask3d*: a) point cloud after Up-sampling b) predict of instance segmentation c) errors of instance segmentation.

Confidence score of 3d semantic segmentation by F1-score for different values of Chebyshev coefficients was evaluated (see Table 1), in this paper Chebyshev coefficients K = {6, 5, 3} are used. DWG*CNN consists of 3 convolution layers and 3 MLP layers {512, 192, 50}. Feature map has dimensions F = {128, 512, 1024}.

**Table 1.** F1-score (in $10^{-3}$) of semantic segmentation DWG*CNN.

| Chebyshev coefficients | s1 | s2 | s3 | s4 | s5 | s6 | s7 |
|---|---|---|---|---|---|---|---|
| {5,3,1} | 913 | 909 | 886 | 813 | 632 | 389 | 468 |
| {6,5,3} | 983 | 924 | 956 | 889 | 875 | 503 | 587 |
| {6,4,2} | 976 | 918 | 913 | 846 | 822 | 523 | 515 |
| {7,5,3} | 902 | 926 | 873 | 915 | 776 | 486 | 566 |

Confidence score of 3d instance segmentation by F1-score for different transformer architecture was evaluated (see Table 2). Analyzing the data in the Table 2, it can be conclude, that the proposed instance segmentation approach has significant advantages by F1-score in comparison with known segmentation methods for processing sparse, uneven and noisy point clouds. However, for classes s5, s6, s7, it's impossible to achieve acceptable quality of instance segmentation. The model based on Mask 3D* is trained on a single Nvidia GeForce GTX 1080Ti with 50 epochs.

**Table 2.** F1-score (in $10^{-3}$) of 3d instance segmentation methods.

| Name | s1 | s2 | s3 | s4 | s5 | s6 | s7 |
|---|---|---|---|---|---|---|---|
| OneFormer3d | 660 | 598 | 487 | 544 | 422 | - | - |
| Mask3d | 720 | 575 | 581 | 602 | 461 | - | - |
| Mask3d* | 899 | 914 | 813 | 815 | 673 | 440 | 364 |

The program code of segmentation methods can be found at the following link [19], archeology detailed results of computer simulation are also presented at this link.

## 5 Conclusions

In this paper, the semantic segmentation method of point clouds based on a multi-modal weighted dynamic graph CNN and the instance segmentation method were proposed, which allow to decrypt the structures of archaeological sites of the Bronze Age with higher quality by F1-score than state-of-the-art methods of point clouds segmentation. The main focus of this work was the improvement of known point cloud segmentation methods such as DGCNN, ConvPoint and Mask 3d to the processing of heterogeneous, sparse, uneven and noisy point clouds and also for 3d large-scale scenes with microrelief and non-convex objects. The paper also identifies problem related to the fact that it was not possible to obtain acceptable 3d data segmentation quality for a lot of classes. The suggested methods were tested using geophysics data in the area of archaeological sites near the settlements of Stepnoe and Levoberezhnoe. The main practical result is the discovery of two new archaeological sites in the form of fortified settlements of the

Bronze Age that existed in the Chelyabinsk region in the northern periphery of the territory inhabited by the Sintashta population in the Bronze Age: the settlements of Nizhneuspensky and Verkhneuralsky.

## References


1. Boulch, A.: Convpoint: continuous convolutions for point cloud processing. Comput. Graph. **88**, 24–34 (2020)
2. Chen, S., Fang, J., Zhang, Q., Liu, W., Wang, X.: Hierarchical aggregation for 3D instance segmentation. In: IEEE/CVF International Conference on Computer Vision, pp. 15467–15476. Montreal, Canada (2021)
3. Engelmann, F., Bokeloh, M., Fathi, A., Leibe, B., Nießner, M.: 3D-MPA: multi-proposal aggregation for 3d semantic instance segmentation. In: IEEE/CVF Conference on Computer Vision and Pattern Recognition (CVPR), pp. 9031–9040. Seattle, USA (2020)
4. Kolodiazhnyi, M., Rukhovich, D., Vorontsova, A., Konushin, A.: Top-down beats bottom-up in 3D instance segmentation. arXiv preprint arXiv:2302.02871 (2023)
5. Kolodiazhnyi, M., Vorontsova, A., Konushin, A., Rukhovich, D.: Oneformer3D: one transformer for unified point cloud segmentation. arXiv preprint arXiv:2311.14405 (2023)
6. Landrieu, L., Simonovsky, M.: Large-scale point cloud semantic segmentation with superpoint graphs. In: IEEE Conference on Computer Vision and Pattern Recognition (CVPR), pp. 4558–4567. Salt Lake City, USA (2018)
7. Liang, Z., Li, Z., Xu, S., Tan, M., Jia, K.: Instance segmentation in 3D scenes using semantic superpoint tree networks. In: IEEE/CVF International Conference on Computer Vision, pp. 2783–2792. Montreal, Canada (2021)
8. Liu, S.-H., Yu, S.-Y., Wu, S.-C., Chen, H.-T., Liu, T.-L.: Learning Gaussian instance segmentation in point clouds. arXiv preprint arXiv:2007.09860 (2020)
9. Qian, G., Abualshour, A., Li, G., Thabet, A., Ghanem B.: PU-GCN: point cloud upsampling using graph convolutional networks. In: IEEE/CVF Conference on Computer Vision and Pattern Recognition, pp. 11678–11687. Nashville, USA (2021)
10. Robert, D., Raguet, H., Landrieu, L.: Efficient 3d semantic segmentation with superpoint transformer In: IEEE/CVF International Conference on Computer Vision (ICCV), pp. 1–10. Paris, France (2023)
11. Sebek, P., Pokorný, S., Vacek, P., Svoboda, T.: Real3D-Aug: point cloud augmentation by placing real objects with occlusion handling for 3D detection and segmentation. arXiv preprint arXiv:2206.07634 (2022)
12. Schult, J., Engelmann, F., Hermans, A., Litany, O., Tang, S., Leibe, B.: Mask3D: mask transformer for 3D semantic instance segmentation. In: IEEE International Conference on Robotics and Automation, pp. 8216–8223. London, United Kingdom (2023)
13. Te, G., Hu, W., Zheng, A., Guo, Z.: RGCNN: regularized graph CNN for point cloud segmentation. In: 26th ACM International Conference on Multimedia, pp. 746–754. Seoul, Republic of Korea (2018)
14. Thomas, H., Qi, C.R., Deschaud, J.-E, Marcotegui, B., Goulette, F., Guibas, L.: KPCONV: flexible and deformable convolution for point clouds. In: IEEE/CVF International Conference on Computer Vision, pp. 6411–6420. Seoul, South Korea (2019)
15. Vokhmintcev, A.V., Khristodulo, O.I, Melnikov, A.V., Romanov, M.A.: Application of dynamic graph CNN* and FICP for detection and research archaeology sites. In: Ignatov, D., Khachay, M., Kutuzov, A., Madoyan, H., Makarov, I., et al. (eds.) AIST 2023. LNCS, vol. 14486, pp. 294–308. Springer, New York (2023). https://doi.org/10.1007/978-3-031-54534-4_21

16. Wang, Y., Sun, Y., Liu, Z., Sarma, S.E., Bronstein, M., Solomon, J.: Dynamic graph CNN for learning on point clouds. ACM Trans. Graph. **38**(5), 1–12 (2019)
17. Wu, Y., Shi, M., Du, Sh., Lu, H., Cao, Z., Zhong, W.: 3D instances as 1D kernels. In: Avidan, S., Brostow, G., Cissé, M., Farinella, G.-M., Hassner, T. (eds.) ECCV 2022. LNCS, vol. 13689, pp. 235–252. Springer, Cham (2022). https://doi.org/10.1007/978-3-031-19818-2_14
18. Zhao, W., Yan, Y., Yang, C., Ye, J., Yang, X., Huang, K.: Divide and conquer: 3D point cloud instance segmentation with point-wise binarization. In: IEEE/CVF International Conference on Computer Vision, pp. 562–571. Paris, France (2023)
19. The system for remote research of archaeological sites. https://gitlab.com/archeolog. Accessed 10 Apr 2024
20. Zdanovich, G.B., Batanina, I.M., Levit, N.V., Batanin, S.A.: Step-lesostep. Kizilskij rajon. Arheologicheskij atlas Chelyabinskoj oblasti. https://search.rsl.ru/ru/record/01002755616?ysclid=lm3sa1zfkp696194850. Accessed 10 Apr 2024

# ITLP-Campus: A Dataset for Multimodal Semantic Place Recognition

Alexander Melekhin[1(✉)], Vitaly Bezuglyj[1], Ilia Petryashin[1], Kirill Muravyev[2], Sergey Linok[1], Dmitry Yudin[1(✉)], and Aleksandr Panov[1,2]

[1] Moscow Institute of Physics and Technology, Dolgoprudny, Russia
{melekhin.aa,bezuglyj.vd,petryashin.ie,linok.sa}@phystech.edu,
{yudin.da,panov.ai}@mipt.ru
[2] Fedral Research Center "Computer Science and Control" of Russian Academy of Sciences, Moscow, Russia
muraviev@isa.ru

**Abstract.** Data is an important aspect of modern deep learning research, particularly in Place Recognition, which plays a pivotal role in various applications such as robotics, augmented reality, and autonomous navigation. In this paper, we introduce the ITLP-Campus dataset captured by a mobile robot equipped with front and back cameras and a LiDAR sensor. The dataset encompasses diverse outdoor and indoor environments within a university campus setting. Spanning different times of day, seasons, and weather conditions, ITLP-Campus offers a rich and varied set of scenes for analysis. The dataset includes unique features such as strategically placed ArUco markers along routes, automatically generated semantic masks and textual descriptions of scenes. Moreover, indoor tracks are annotated with scene text, enhancing the dataset's utility for tasks involving text recognition and understanding. We provide detailed insights into the dataset's acquisition process, annotation procedures, and potential applications. Additionally, we conduct extensive experiments by testing popular Place Recognition methods on ITLP-Campus, demonstrating its effectiveness and versatility for advancing research in multimodal semantic place recognition and related fields.

**Keywords:** place recognition · mobile robotics · deep learning · multimodal dataset

## 1 Introduction

Place Recognition is a crucial task in various domains including robotics, augmented reality, and autonomous navigation. It involves identifying a previously visited location using data from various sensors, thereby enabling systems to understand and navigate their environments effectively. Despite significant advancements, Place Recognition remains challenging due to factors such as changing lighting conditions, dynamic objects, and environmental variations.


S. Kovalev et al. (Eds.): IITI 2024, LNNS 1209, pp. 185–195, 2024.
https://doi.org/10.1007/978-3-031-77688-5_18

Data plays a crucial role in the training and evaluation of Place Recognition methods, providing the diverse environmental conditions needed to test and improve algorithmic performance. Existing datasets such as KITTI [6], Oxford RobotCar [15], Nordland [18], and NCLT [4] offer rich collections of visual data that encompass a wide range of scenarios, including urban streets, seasonal changes, and day-night cycles. These datasets are valuable resources that assist researchers in developing more robust and accurate PR systems, facilitating autonomous and reliable robot operation in real-world environments. However, many of these datasets primarily focus on either outdoor urban settings or lack sufficient indoor data, limiting their ability to test Place Recognition methods comprehensively across varied environments.

The ITLP-Campus dataset addresses this gap by providing a comprehensive collection of both indoor and outdoor data captured within a university campus. The dataset spans different times of day and seasonal variations, including winter conditions and summer days, to simulate the wide range of environmental changes that autonomous systems must handle. By incorporating these diverse conditions, the ITLP-Campus dataset enables rigorous testing and evaluation of Place Recognition methods, ensuring their robustness and adaptability to both indoor and outdoor environments under varying seasonal and weather conditions.

To capture data comprehensively, the dataset was collected using a mobile robot equipped with front and back cameras and a LiDAR sensor. ArUco markers are strategically placed along indoor routes to facilitate precise localization and ground truth annotation. The dataset includes automatically generated semantic masks and textual descriptions of scenes, which add a layer of semantic understanding, that can be used in various scenarios [11,12]. Data collection spans different times of day and various seasons, capturing changes in lighting, weather conditions, and environmental appearance. Indoor tracks are manually annotated with scene text, which can be used to improve Place Recognition methods [8] enhances the dataset's utility for tasks involving text recognition and understanding.

The ITLP-Campus dataset opens up numerous research opportunities and applications, particularly in the field of Place Recognition: benchmarking Place Recognition methods, multimodal semantic analysis, robustness to environmental variations, indoor navigation and text recognition.

The key contributions of our dataset are:

- Collection of data from both indoor and outdoor scenarios;
- Multiple modalities, including images from front and back cameras, automatically generated semantic segmentation masks and text descriptions, and LiDAR point clouds;
- Data spanning different times of day and seasonal variations, providing a diverse set of scenes;
- Inclusion of indoor ArUco markers to enable the development of more robust localization algorithms;

**Table 1.** Overview of existing datasets suitable for Place Recognition.

| Dataset | Scenario | Coverage | Data types | Diversity | | |
|---|---|---|---|---|---|---|
| | | | | Weather | Season | Day/night |
| Nordland [19] | Train ride | 748 km | RGB | + | + | – |
| HPointLoc [22] | Indoor | – | RGB, Depth | – | – | – |
| NCLT [4] | Campus | 5.5 km | LiDAR PC, RGB | + | + | – |
| Oxford RobotCar [15] | Urban + Suburban | 10 km | LiDAR PC, RGB | + | + | + |
| Mapillary [21] | Urban + Suburban | 4228 km | RGB | + | + | + |
| Ithaca365 [5] | Urban + Suburban | 15 km | LiDAR PC, RGB | + | + | + |
| Boreas [3] | Urban | 8 km | LiDAR PC, RGB, Radar | + | + | + |
| ITLP-Campus (ours) | Campus | 3.6 km | LiDAR PC, RGB, Semseg, Text desc, ArUco | +− | + | + |

Overall, the ITLP-Campus dataset aims to be a comprehensive resource for advancing research in Place Recognition and related fields. The dataset and API is publicly available: https://github.com/OPR-Project/ITLP-Campus.

## 2 Related Work

A brief overview of existing datasets that are suitable for Place Recognition are shown in Table 1.

Nordland [19] provides a long-term dataset captured from a train journey across different seasons, focusing on the challenges of visual place recognition over time. HPointLoc [22] offers a simulation dataset collected in the 50 scenes of the Habitat simulator. NCLT [4] is a comprehensive dataset that includes long-term autonomy data collected from the University of Michigan's North Campus over 15 months, featuring diverse weather conditions and sensor modalities. Oxford RobotCar [15] comprises over 1000 km of driving data through central Oxford, collected over a year, providing a rich resource for studying urban navigation and long-term localization. Mapillary [21] contains street-level sequences from various locations worldwide, offering diverse scenes for training and evaluating visual recognition algorithms. Ithaca365 [5] includes driving data from Ithaca, New York, collected under a wide range of weather conditions and seasons, designed to study driving perception in real-world scenarios. Boreas [3] captures multi-season driving data with significant environmental variations, aimed at improving the robustness of autonomous driving systems under diverse conditions. These datasets collectively contribute to the development and evaluation of Place Recognition systems by providing varied and challenging environments for testing.

The ITLP-Campus dataset offers unique data types such as semantic segmentation masks, text descriptions, and ArUco markers, making it stand out among other datasets. The only limitation compared to others is the lack of data collected outdoors during rain or snow, as our robotic platform is not designed for use in such conditions.

## 3 Data Collection

The data for the ITLP-Campus dataset was collected using a mobile robot based on the Clearpath Husky robotic platform. The robot was equipped with a Velodyne VLP-16 LiDAR, a StereoLabs ZED stereo camera at the front, and an Intel RealSense stereo camera at the back. Outdoor tracks were recorded along a repeated route on the university campus, while indoor tracks were recorded in the hallways of a building with five floors.

### 3.1 Sensors

**Velodyne VLP-16 3D LiDAR.** The Velodyne VLP-16 was mounted at the top of the robot, as illustrated in Fig. 1. This sensor provides high-resolution 3D point clouds with a 360-degree field of view. Data was collected at an average rate of 10 Hz, capturing detailed spatial information of the environment.

**StereoLabs ZED Stereo Camera.** The ZED stereo camera was used as the front-view camera. It captures high-definition stereo images from the left and right sensors, which were recorded in a compressed format with a resolution of $1280 \times 720$ pixels. The average capture rate was 10 Hz, ensuring a consistent stream of visual data for the front view.

**Intel RealSense Stereo Camera.** Positioned at the back of the robot, the Intel RealSense stereo camera provided rear-view imagery. Similar to the front-view setup, images were collected in a compressed format at a resolution of $1280 \times 720$ pixels and an average rate of 10 Hz. This setup enabled comprehensive coverage of the robot's surroundings.

### 3.2 Data Collection Process

**ITLP-Campus-Outdoor.** The outdoor route covered approximately 3.6 km around the university campus, as illustrated in Fig. 1. The route was carefully chosen to include a variety of environments, such as pathways, gardens, and open spaces, to capture diverse outdoor scenes. Data collection was performed repeatedly along this route to ensure temporal variation and to capture changes in lighting and weather conditions.

**ITLP-Campus-Indoor.** Indoor tracks were recorded within the hallways of a building with five floors. The indoor data collection aimed to simulate real-world indoor navigation scenarios, providing valuable data for Place Recognition tasks in indoor spaces.

Data was collected across different times of day and various seasons, ensuring a rich dataset with temporal and environmental diversity (see details in Table 2). The robot was manually operated along the predefined routes, and sensor data

was continuously recorded. To facilitate ground truth generation and precise localization, ArUco markers were placed along the indoor routes.

The data was recorded using Robot Operating System (ROS) in a `rosbag` format. Each `rosbag` file contains data streams from the LiDAR and stereo cameras. This format allows for efficient storage and easy retrieval of large amounts of data, enabling detailed post-processing and analysis. Additionally, the use of ROS tools facilitated real-time monitoring and verification of data quality during the collection process.

## 4 Data Processing

### 4.1 Pre-processing

**Ground Truth Poses.** We used the Cartographer open-source library [7] to build the 3D map of the route and for localization on both indoor and outdoor tracks. This process provided accurate 6DoF (Degrees of Freedom) poses. The

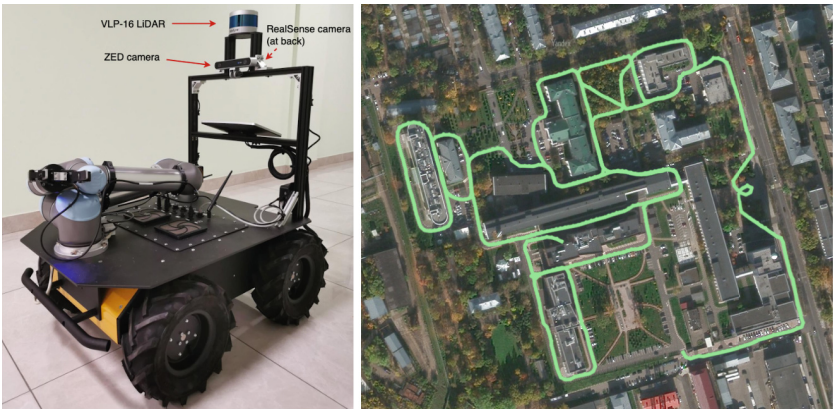


**Fig. 1.** An illustration of Husky robotic platform equipped with LiDAR and two cameras that was used to record the dataset and an outdoor route.

**Table 2.** Dataset statistics.

| | Track | Season | Time of day | Frames, pcs |
|---|---|---|---|---|
| ITLP-Campus-outdoor | 00_2023-02-21 | winter | day | 620 |
| | 01_2023-03-15 | winter | night | 626 |
| | 02_2023-02-10 | winter | twilight | 609 |
| | 03_2023-04-11 | spring | day | 638 |
| | 04_2023-04-13 | spring | night | 631 |
| ITLP-Campus-indoor | 00_2023-10-25 | – | night | 1233 |
| | 01_2023-11-09 | – | twilight | 1310 |

poses were stored in the format of position `[tx, ty, tz]` and rotation quaternion `[qx, qy, qz, qw]`.

**Subsampling.** The images from cameras and LiDAR point clouds were synchronized based on their timestamps so that the maximum difference was less than 50 milliseconds. Then the frames were subsampled based on their poses: we sample one frame for each 5 m along the route for outdoor data, and 1 frame for each 1 m along the route for indoor data. This ensures that the frames are differs from each other enough.

**Directory Structure.** Each recorded track is stored in a separate directory named `<N_date>`, where `N` is the consecutive track number. Inside each directory, there are `back_cam` and `front_cam` subdirectories containing images named `<timestamp>.png`. The `lidar` directory contains point clouds in binary format with filenames `<timestamp>.bin`. The `masks` directory contains semantic segmentation masks organized into subdirectories for each camera. The `text_descriptions` directory (only in outdoor tracks) contains `csv` files with text descriptions for front and back images. The `meta_info.yml` file in the root directory of each track contains extrinsic calibration data. The `track.csv` file contains rows with corresponding timestamps for each data type.

**Calibration.** The intrinsic camera parameters $[f_x, f_y, c_x, c_y]$ and distortion coefficients $[k_1, k_2, p_1, p_2, k_3]$ were obtained using standard OpenCV tools. The extrinsic transformations from robot's base to cameras and LiDAR were obtained using the ILCC utility [20]. The format of transforms is translation $[t_x, t_y, t_z]$ and rotation quaternion $[q_x, q_y, q_z, q_w]$. This data is provided in the repository and included in the `meta_info.yml` files within the track directories of the dataset.

### 4.2 Annotation

**Text Descriptions.** To generate text descriptions, we utilized MiniGPT-4 [23] with a Vicuna-13B-based checkpoint. The prompt "Describe this scene" was used to produce image descriptions directly, without any pre-processing of the input images or post-processing of the generated texts. Examples of the generated descriptions are shown in Fig. 2.

**Semantic Segmentation Masks.** For semantic segmentation, we employed the OneFormer model [9], which was pre-trained on the Mapillary dataset [17]. While the model supports semantic, instance, and panoptic segmentation, we concentrated solely on semantic segmentation for our dataset, using a total of 65 semantic classes. Examples of the generated masks are shown in Fig. 2.

**Indoor Text Annotations.** An indoor tracks were manually annotated with a scene text. An example of such annotation is shown in Fig. 3.


**Fig. 2.** An example of the outdoor frame with front and back cameras images semantic segmentation, text descriptions and point cloud.

**Indoor ArUco Markers.** We placed ArUco markers in the areas near the elevator that look the same on all floors, as shown in Fig. 4. This allows the robot to determine its location even if the Place Recognition methods make mistakes.

## 5 Benchmarking

To evaluate the effectiveness and generalization capabilities of the ITLP-Campus dataset, we tested several popular Place Recognition methods on our data. These methods include AnyLoc [10], MixVPR [2], MinkLoc3Dv2 [13], MinkLoc++ [14] and MSSPlace [16]. By using models pre-trained on other widely recognized


**Fig. 3.** An example of the scene text annotation.

**Fig. 4.** Three of the five images look the same despite being on different building floors.

**Table 3.** Benchmarking results.

| Model | Modality | Outdoor | | Indoor | |
|---|---|---|---|---|---|
| | | R@1 | R@1% | R@1 | R@1% |
| MixVPR [2] | I(front) | 84.89 | 92.52 | 95.67 | 99.65 |
| AnyLoc [10] | I(front) | 83.88 | 93.70 | **96.66** | **99.88** |
| MinkLoc3Dv2 [13] | L | 86.82 | 96.85 | 73.28 | 98.88 |
| MinkLoc++ [14] | L + I(front) | 88.41 | 97.24 | 80.23 | 99.37 |
| MSSPlace-LI [16] | L + I(both) | **89.81** | **97.48** | 84.32 | 99.42 |

datasets, we aimed to assess the robustness and adaptability of these methods to the diverse environments and conditions captured in ITLP-Campus.

We adopted a standard benchmarking methodology commonly used in Place Recognition research [13,14,16]. All possible pairs of tracks were constructed, with the first track as the *query* and the second as the *database*. This resulted in 20 permutations for the 5 outdoor tracks and 2 permutations for the 2 indoor tracks. For each pair, we calculated the *Recall@1* and *Recall@1%* metrics, representing the percentage of correctly recognized places from the top-1 and top-1% closest database candidates, respectively.

A place is considered correctly recognized if it falls within 25 m of the ground truth for outdoor tracks and within 10 m for indoor tracks. We then averaged these metrics across all pairs, reporting *Average Recall@1* (*AR@1*) and *Average Recall@1%* (*AR@1%*).

### 5.1 Results and Discussion

For MixVPR [2], we used the model trained on the GSV-Cities dataset [1] provided in the original repository[1]. For AnyLoc [10], we used the original code[2] and fit VLAD clusters using the database descriptors for each tested pair. For MinkLoc3Dv2 [13], MinkLoc++ [14], and MSSPlace [16], we used the code from the OpenPlaceRecognition library[3] and model weights trained on the NCLT dataset [4].

The results are reported in Table 3. These results provide insights into the generalization capabilities of each model when applied to the ITLP-Campus dataset, demonstrating their effectiveness across different environments and conditions. For the outdoor scenario, the combination of LiDAR point clouds and images from both cameras has shown the best performance, providing the most valuable descriptors. For the indoor, the methods that use LiDAR data has shown poorer performance compared to camera-only ones. This is explained by the fact that in the indoor data there are a large number of geometrically

[1] https://github.com/amaralibey/MixVPR.
[2] https://github.com/AnyLoc/AnyLoc.
[3] https://github.com/OPR-Project/OpenPlaceRecognition.

identical corridors, in which the LiDAR point clouds will be very similar, but, nevertheless, these are different locations. Thus, LiDAR data makes a negative contribution to the resulting descriptors for that scenario.

## 6 Conclusion

In this paper, we introduced the ITLP-Campus dataset, a comprehensive collection of indoor and outdoor data captured within a university campus. The data was collected using a robotic platform equipped with front and back cameras and LiDAR. Additionally, the dataset was enriched with automatically generated semantic segmentation masks and text descriptions. The indoor data also includes ArUco markers, which enable the development of robust solutions for localization in visually identical environments.

The primary purpose of our dataset is to facilitate further research into robust Place Recognition methods that can operate effectively in diverse environments across different seasons and weather conditions.

We conducted experiments on several popular Place Recognition methods, highlighting their suitability for different scenarios. The results showed that the performance of LiDAR-based methods decreases in geometrically uniform environments, which opens up research opportunities for developing more robust methods.

A limitation of our dataset is the lack of outdoor data recorded during rain or snow, as the robotic platform is not designed for operation in such conditions.

We plan to further expand the dataset by recording new tracks, which will enhance its diversity and utility.

**Acknowledgments.** This work was supported by Russian Fund for Assistance to the Development of Small Forms of Enterprises in the Scientific and Technical Sphere (Innovation Promotion Fund), agreement No. 34GUCodeAIS12-D7/81485, Application CodeAI-234388.

## References

1. Ali-bey, A., Chaib-draa, B., Giguère, P.: GSV-cities: toward appropriate supervised visual place recognition. Neurocomputing **513**, 194–203 (2022)
2. Ali-bey, A., Chaib-draa, B., Giguère, P.: MixVPR: feature mixing for visual place recognition. In: Proceedings of the IEEE/CVF Winter Conference on Applications of Computer Vision, pp. 2998–3007 (2023)
3. Burnett, K., et al.: Boreas: a multi-season autonomous driving dataset. arXiv:2203.10168 (2023)
4. Carlevaris-Bianco, N., Ushani, A.K., Eustice, R.M.: University of Michigan north campus long-term vision and lidar dataset. Int. J. Robot. Res. **35**(9), 1023–1035 (2016). https://doi.org/10.1177/0278364915614638
5. Diaz-Ruiz, C.A., et al.: Ithaca365: dataset and driving perception under repeated and challenging weather conditions. In: Proceedings of the IEEE/CVF Conference on Computer Vision and Pattern Recognition, pp. 21383–21392 (2022)

6. Geiger, A., Lenz, P., Stiller, C., Urtasun, R.: Vision meets robotics: the kitti dataset. Int. J. Robot. Res. (IJRR) (2013)
7. Hess, W., Kohler, D., Rapp, H., Andor, D.: Real-time loop closure in 2D lidar slam. In: 2016 IEEE International Conference on Robotics and Automation (ICRA), pp. 1271–1278 (2016)
8. Hong, Z., Petillot, Y., Lane, D., Miao, Y., Wang, S.: TextPlace: visual place recognition and topological localization through reading scene texts. In: Proceedings of the IEEE/CVF International Conference on Computer Vision, pp. 2861–2870 (2019)
9. Jain, J., Li, J., Chiu, M.T., Hassani, A., Orlov, N., Shi, H.: Oneformer: one transformer to rule universal image segmentation. In: Proceedings of the IEEE/CVF Conference on Computer Vision and Pattern Recognition, pp. 2989–2998 (2023)
10. Keetha, N., et al.: AnyLoc: towards universal visual place recognition. IEEE Robot. Autom. Lett. **9**(2), 1286–1293 (2024). https://doi.org/10.1109/LRA.2023.3343602
11. Kirilenko, D., Kovalev, A.K., Solomentsev, Y., Melekhin, A., Yudin, D.A., Panov, A.I.: Vector symbolic scene representation for semantic place recognition. In: 2022 International Joint Conference on Neural Networks (IJCNN), pp. 1–8 (2022). https://doi.org/10.1109/IJCNN55064.2022.9892761
12. Kolmet, M., Zhou, Q., Ošep, A., Leal-Taixé, L.: Text2Pos: text-to-point-cloud cross-modal localization. In: Proceedings of the IEEE/CVF Conference on Computer Vision and Pattern Recognition, pp. 6687–6696 (2022)
13. Komorowski, J.: Improving point cloud based place recognition with ranking-based loss and large batch training. In: 2022 26th International Conference on Pattern Recognition (ICPR), pp. 3699–3705 (2022). https://doi.org/10.1109/ICPR56361.2022.9956458
14. Komorowski, J., Wysoczańska, M., Trzcinski, T.: MinkLoc++: lidar and monocular image fusion for place recognition. In: 2021 International Joint Conference on Neural Networks (IJCNN), pp. 1–8 (2021). https://doi.org/10.1109/IJCNN52387.2021.9533373
15. Maddern, W., Pascoe, G., Linegar, C., Newman, P.: 1 year, 1000 km: the oxford robotcar dataset. Int. J. Robot. Res. **36**(1), 3–15 (2017). https://doi.org/10.1177/0278364916679498
16. Melekhin, A., Yudin, D., Petryashin, I., Bezuglyj, V.: Mssplace: multi-sensor place recognition with visual and text semantics. arXiv:2407.15663 (2024)
17. Neuhold, G., Ollmann, T., Rota Bulo, S., Kontschieder, P.: The mapillary vistas dataset for semantic understanding of street scenes. In: Proceedings of the IEEE International Conference on Computer Vision, pp. 4990–4999 (2017)
18. Olid, D., Fácil, J.M., Civera, J.: Single-view place recognition under seasonal changes. In: PPNIV Workshop at IROS 2018 (2018)
19. Sünderhauf, N., Neubert, P., Protzel, P.: Are we there yet? challenging seqslam on a 3000 km journey across all four seasons. In: Proceedings of Workshop on Long-term Autonomy, IEEE International Conference on Robotics and Automation (ICRA), p. 2013. Citeseer (2013)
20. Wang, W., Sakurada, K., Kawaguchi, N.: Reflectance intensity assisted automatic and accurate extrinsic calibration of 3D lidar and panoramic camera using a printed chessboard. Remote Sensing **9**(8) (2017). https://doi.org/10.3390/rs9080851
21. Warburg, F., Hauberg, S., Lopez-Antequera, M., Gargallo, P., Kuang, Y., Civera, J.: Mapillary street-level sequences: a dataset for lifelong place recognition. In: Proceedings of the IEEE/CVF Conference on Computer Vision and Pattern Recognition, pp. 2626–2635 (2020)

22. Yudin, D., Solomentsev, Y., Musaev, R., Staroverov, A., Panov, A.I.: Hpointloc: point-based indoor place recognition using synthetic RGB-D images. In: International Conference on Neural Information Processing, pp. 471–484. Springer (2022)
23. Zhu, D., Chen, J., Shen, X., Li, X., Elhoseiny, M.: MiniGPT-4: enhancing vision-language understanding with advanced large language models. arXiv:2304.10592 (2023)

# Generating Hypotheses Based on the Table Constraint Satisfaction Methods in JSM-Systems

Alexander Zuenko(✉) and Olga Zuenko

Kola Science Centre of the Russian Academy of Sciences, Institute for Informatics and Mathematical Modelling, Apatity, Russia
a.zuenko@ksc.ru

**Abstract.** It is known that constraint satisfaction methods are successfully used to solve many complex combinatorial search problems. As their distinctive feature, it should be noted the widespread use of logical inference procedures on constraints that implement the reduction of the search space. The article continues a series of works that deal with the development of table constraint satisfaction methods to solve data mining problems. Previously, the author's methods of inference on table constraints for clustering problems, discovering patterns of the required type, and searching for association rules were presented. In this work, using the example of solving the binary classification problem, the possibilities of applying the author's approach to modeling JSM-reasoning are considered for the first time. The article considers the case when the properties of objects are atomic and have no internal structure. Within the framework of the approach, positive and negative examples are presented using specialized table constraints, namely compressed tables of the *D*-type, and the process of generating JSM-hypotheses is performed using the rules developed for reducing the search space. The proposed method of generating JSM-hypotheses makes it possible to effectively solve high-dimensional problems.

**Keywords:** JSM method · Constraint programming · Table constraints · Binary classification · Closed pattern discovery

## 1 Introduction

The disadvantages of most existing data mining (DM) methods are primarily related to the difficulties of flexible accounting and analyzing extra knowledge: the knowledge of domain experts, user constraints. Such constraints in solving the clustering problem include prohibitions on the simultaneous presence of certain pairs of elements in certain clusters, and requirements for the size of clusters [1]. In the pattern discovery problems, such constraints are the requirements on length, pattern support, and conditions for the presence/absence of certain elements in the pattern [2]. In association rule mining problems, it is often necessary


S. Kovalev et al. (Eds.): IITI 2024, LNNS 1209, pp. 196–206, 2024.
https://doi.org/10.1007/978-3-031-77688-5_19

to find rules with additional constraints on the left and right parts of the rule, in particular, on the length of the left part or on elements that may occur in parts of the rule [3]. Usually, a rather consuming modification of the basic DM methods is required to account for each type of such constraints.

The article develops an author's approach to the implementation of DM methods based on the Constraint Programming Paradigm (CPP), which allows for sufficient flexibility to organize accounting of additional conditions of the DM problem without fundamentally changing the scheme of solving [4,5].

In the presented work, using the example of solving the binary classification problem, the possibilities of applying the author's approach to modeling reasoning that implements John Stuart Mill method (JSM method) [6] are considered for the first time. The article considers the case when the properties of objects are atomic and have no internal structure. It is proposed to reduce the problem of generating JSM-hypotheses to the frequent closed pattern discovery with the additional condition that each of the patterns should not be included as a fragment in a set of counterexamples.

The relevance of developing methods to accelerate the generating JSM–hypotheses is due to the fact that the search for these hypotheses is systematic, that is, it leads to traversing a search tree in order to identify all significant hypotheses. The early pruning unpromising branches of the search tree seems to be a necessary condition for increasing the effectiveness of JSM reasoning.

Within the framework of the approach proposed in the article, adding additional types of constraints to the DM problems not only does not reduce the performance of their solution methods, but also contributes to a deeper reduction of the search space through the use of specialized methods of logical inference (constraint propagation) for each of the constraint types.

## 2 Related Work

The article continues the series of works that deal with the topic of DM using methods of inference on table constraints. Previously, the author's methods of clustering, discovering patterns of the required type, and mining association rules were presented [4,5]. The developed methods relate to the methods of interpreted artificial intelligence. The originality of the author's approach lies in the fact that to represent the training sample, it is proposed to use a special type of table constraints – compressed tables of the $D$-type, and the DM problems are proposed to be solved as problems of table constraints satisfaction using the original method of branching the search tree and the author's rules for reducing compressed tables (rules for eliminating rows, columns, components, elements of the components of the table constraints).

There are other works that deal with application of constraint programming in DM problems, in particular, it should be noted the works describing constraint satisfaction methods for solving constrained clustering problem [7], frequent pattern discovery problem [8], as well as learning optimal decision trees problem [9].

As an article containing a review on the developing effective methods of inference on table constraints and the application of these constraints in modeling various types of relationships, the publication [10] can be recommended.

## 3 Scheme of the JSM Method

The JSM method, which is a method of DM, was developed by V. K. Finn in the mid-70 s of the last century [6]. When presenting the method, the concepts of the Itemset Mining will be used [2].

Consider the problem of binary classification in the following form: let the training sample consists of three sets of objects: 1) positive examples, that is, objects for which it is known that they have the classifying feature $c$; 2) negative examples, that is, objects for which it is known that they do not have the classifying feature $c$; 3) subdefinite examples, that is, examples about which it is unknown whether they have the classifying feature $c$. Based on the available training sample, it is required to assign subdefinite examples to one or another class. Each example is considered as a set of features it possesses.

The step of the JSM method aimed at identifying cause-effect links can be divided into two stages: 1) generation of positive and negative hypotheses regarding the causes of some classifying feature $c$; 2) verification and acceptance/unacceptance of hypotheses. In fact, in our case, the hypotheses are sets of features of objects in the training sample.

Verification and acceptance/unacceptance of hypotheses are carried out basing on so-called first kind rules (causes search rules, induction rules):

- a hypothesis is accepted as a possible cause for the presence of a feature $c$ if the hypothesis is included as a subset in $\theta_1$ and more positive examples and at the same time is included in no more than $\tau_1$ negative examples;
- a hypothesis is accepted as a possible cause for the absence of a feature $c$ if the hypothesis is included as a subset in $\theta_2$ and more negative examples and at the same time is included in no more than $\tau_2$ positive examples.

After that, a set of causes for the presence/absence of a classifying feature $c$ is formed, which is later used in classification procedures.

Also, the JSM method introduces such a concept as rules of the second kind (rules for refining initial data, rules of analogy), these rules regulate the classification procedure, on the basis of which subdefinite examples are referred to positive or negative. Here is an example of such rules (rules for a classification strategy with prohibitions on counterexamples):

1. If a subdefinite example includes at least one possible cause for the presence of the classifying feature $c$ and does not include any possible cause for the absence of feature $c$, then we refine this example as positive.
2. If a subdefinite example includes at least one possible cause for the absence of the feature $c$ and does not include any possible cause for the presence of feature $c$, then we refine this example as negative.

3. If a subdefinite example includes both causes for the presence and absence of the feature $c$, then the example remains subdefinite (classified as contradictory).

The first kind rules and the second kind rules are sequentially applied until at least one new hypothesis is generated as a result of their work. In this case, the step number is an indicator of the plausibility of the reasoning.

## 4 Constraint Programming: Table Constraints

The developed method of generating JSM-hypotheses is implemented within the framework of CPP. When using this paradigm, any problem to be solved must be represented using a network of constraints.

A network of constraints is a triple [11]: $< X, D, C >$, where $X$ is a set of variables, $D$ is a set of domains of variables, and $C$ is a set of constraints specifying acceptable combinations of variable values. A Constraint Satisfaction Problem (CSP) consists in search for such variable values that satisfy all the network constraints.

A distinctive feature of constraint satisfaction methods from other methods for solving combinatorial search problems is the implementation of certain logical inference procedures on constraints.

The presented research uses the table constraints. Table constraints, in addition to the typical tables, include: compressed tables, smart tables, etc. [10]. These types of constraints differ in what is meant by the relation tuple [4,5].

For further explanation, only compressed tables will be used. Tuples of compressed tables contain sets as components.

Compressed tables can be of the $C$- and the $D$-type [4,5]. We will be primarily interested in compressed tables of the $D$-type. In this work, they are proposed to be used to model sets of positive and negative examples.

The inference on compressed tables of the $D$-type is carried out using the following statements, which are consequences of the theorems given in [4,5]:

**Statement 1** (**S1**). If at least one row of compressed table of the $D$-type is empty (contains all empty components) then the table is empty.
**Statement 2** (**S2**). If all components of an attribute are empty then this attribute can be removed from compressed table.
**Statement 3** (**S3**). If a row of compressed table contains only one non-empty component then all domain values that are not included in this component are removed from corresponding domain.
**Statement 4** (**S4**). If a row of a compressed table of the $D$-type contains at least one full component, then it is removed.
**Statement 5** (**S5**). If a component of a compressed table of the $D$-type contains a value that does not belong to the corresponding domain, then this value is removed from the component.

The next section shows how tables of the $D$-type can be used to model positive and negative subsamples of training samples. To denote some components of the tables of the $D$-type, the symbol "$\varnothing$" will be used, which corresponds to an empty component (a component that does not contain any values from the corresponding domain).

## 5 Statement of the Binary Classification Problem Using Table Constraints

To demonstrate possibilities of the proposed approach, the paper sets the binary classification problem. Based on the available training sample, it is required to assign subdefinite examples to one of two classes.

As an example, consider the problem with "dancing men". Each object is characterized by the following features (hand position, foot position, gender): $e$ – hands down; $\overline{e}$ – hands up; $f$ – feet together; $\overline{f}$ – feet apart; $g$ – the gender is female; $\overline{g}$ – the gender is male.

Depending on the combination of features, objects are classified as positive examples or as negative ones. Based on the available training sample, an subdefinite example should be assigned to one of two classes ($h$ or $\overline{h}$).

Table 1 presents a binary matrix for the example under consideration, that is, an object-feature representation of the training sample.

**Table 1.** The binary matrix of the problem.

| | $e$ | $\overline{e}$ | $f$ | $\overline{f}$ | $g$ | $\overline{g}$ | $h$ | $\overline{h}$ |
|---|---|---|---|---|---|---|---|---|
| 1 | 1 | | 1 | | 1 | | 1 | |
| 2 | 1 | | | 1 | | 1 | 1 | |
| 3 | | 1 | 1 | | | 1 | 1 | |
| 4 | | 1 | 1 | | 1 | | | 1 |
| 5 | | 1 | | 1 | 1 | | | 1 |
| 6 | | 1 | | 1 | | 1 | | 1 |

The initial sample can be divided into two subsamples: rows 1–3 correspond to the set of positive examples relative to the classifying feature, and rows 4–6 correspond to a set of negative examples. The following compressed table of the $D$-type can be associated to positive examples:

$$K^{+}[XY] = \begin{array}{c} \begin{matrix} X & Y \end{matrix} \\ \left] \begin{matrix} \{1,2\} & \{\overline{e}, f, \overline{f}, g, \overline{g}\} \\ \{3\} & \{e, f, \overline{f}, g, \overline{g}\} \\ \{1,3\} & \{e, \overline{e}, \overline{f}, g, \overline{g}\} \\ \{2\} & \{e, \overline{e}, f, g, \overline{g}\} \\ \{1\} & \{e, \overline{e}, f, \overline{f}, \overline{g}\} \\ \{2,3\} & \{e, \overline{e}, f, \overline{f}, g\} \end{matrix} \right[ \end{array}.$$

The domain of $X$ in this case is a set of objects $\{1, 2, 3, 4, 5, 6\}$. And the domain of $Y$ is a set of attributes $\{e, \overline{e}, f, \overline{f}, g, \overline{g}, h, \overline{h}\}$.

Each row of a table of the $D$-type can be interpreted as an implication, and the entire compressed table of the $D$-type can be interpreted as a conjunction of these implications. For example, the first row of the first matrix corresponds to:

$$(Y \in \{e\}) \rightarrow (X \in \{1,2\}) = (X \in \{1,2\}) \vee (Y \in \{\overline{e}, f, \overline{f}, g, \overline{g}\}).$$

That is, if the property $e$ is considered, then the set of objects that possess it – $\{1, 2\}$. Similarly, the following table of the $D$-type can be associated to negative examples:

$$K^{-}[XY] = \begin{array}{c} \begin{matrix} X & Y \end{matrix} \\ \left] \begin{matrix} \{4\} & \{\overline{e}, \overline{f}, g, \overline{g}\} \\ \{5,6\} & \{\overline{e}, f, g, \overline{g}\} \\ \{4,5\} & \{\overline{e}, f, \overline{f}, \overline{g}\} \\ \{5\} & \{\overline{e}, f, \overline{f}, g\} \end{matrix} \right[ \end{array}.$$

The author's method of generating JSM-hypotheses is based on the described representation of positive and negative examples.

## 6 Generation of JSM-Hypotheses Based on Table Constraints

In this paper, it is proposed to reduce the problem of generating JSM-hypotheses to the problem of discovering frequent closed patterns in positive and negative subsamples. In details the frequent closed pattern discovery problem using table constraints within original author's approach is considered in [4,5].

Let there is an object-feature representation of the training sample. A *pattern* $p$ is any set of features. A *frequent pattern* is the pattern $p$ which occurs in at least $\theta$ examples. A pattern $p$ is called *closed* if all objects possessing all these features simultaneously do not have other common features [8]. Closed patterns are interesting because they represent a kind of basis in the pattern space.

In the case if the training sample is presented in the form of compressed tables of the $D$-type, then a simple way appears to enumerate all closed patterns. You

need to select exactly one component from each row of the table of the $D$-type (it does not matter from the left or right column).

In order to prune obviously unpromising branches of the search tree, it is proposed to use the above statements **S1**–**S5** [4,5]. In addition, to reduce the search space, two more statements are added to the statements formulated in Sect. 4, which allow us to take into account the requirements for the frequency of occurrence of the pattern in the training sample.

**Statement 6** (**S6**). The components of a compressed table of the $D$-type corresponding to the attribute $X$ and with cardinality below a certain threshold $\theta$ are replaced by empty components.

**Statement 7** (**S7**). If the cardinality of the domain of the attribute $X$ is below a certain threshold $\theta$, then solution to the CSP does not exist.

To prune redundant branches of the search tree, it is sufficient to analyze the column $X$, and if there is a component with a cardinality below the specified threshold, then this component is replaced with an empty one.

Let us illustrate the proposed method of generating hypotheses using the example of the problem presented in Sect. 5. Note that as positive (negative) hypotheses we are interested in fragments of objects (sets of features) that are supported by at least two objects (threshold $\theta = 2$).

First, consider a positive subsample $K^+$ (a set of positive examples). Let's simplify it, taking into account the required frequency threshold of occurrence of the desired patterns, applying the above rules. All components in column $X$ with cardinality below 2 are replaced with empty ones according to the statement **S6**:

$$K^+[XY] = \left\rceil \begin{array}{cc} X & Y \\ \{1,2\} & \{\overline{e}, f, \overline{f}, g, \overline{g}\} \\ \varnothing & \{e, f, \overline{f}, g, \overline{g}\} \\ \{1,3\} & \{e, \overline{e}, \overline{f}, g, \overline{g}\} \\ \varnothing & \{e, \overline{e}, f, g, \overline{g}\} \\ \varnothing & \{e, \overline{e}, f, \overline{f}, \overline{g}\} \\ \{2,3\} & \{e, \overline{e}, f, \overline{f}, g\} \end{array} \right\lfloor .$$

Then, according to statements **S1**–**S5**, rows with a single component are analyzed; the domain of the variable $Y$ is reduced. Rows with a single component are eliminated from the compressed table of the $D$-type, the remaining components are "tuned" on the new domain of $Y$ by excluding values not included in the new domain. We have:

$$K^+[XY] = \left\rceil \begin{array}{cc} X & Y \\ \{1,2,3\} & \{e, f, \overline{g}\} \\ \{1,2\} & \{f, \overline{g}\} \\ \{1,3\} & \{e, \overline{g}\} \\ \{2,3\} & \{e, f\} \end{array} \right\lfloor .$$

In accordance with the branching procedure described above, the search tree is being built (see Fig. 1). If only one arc comes from the node, then this means that in the node a compressed table of the $D$-type is reduced based on statements **S1**–**S7**. Leaf nodes are closed frequent patterns – in our case, positive JSM-hypotheses:

$[\{1,2\}\ \{e\}],\ [\{1,3\}\ \{f\}],\ [\{2,3\}\ \{\overline{g}\}]$.

Leaf nodes shaded in gray (see Fig. 1) correspond to hypotheses that have not passed the verification.

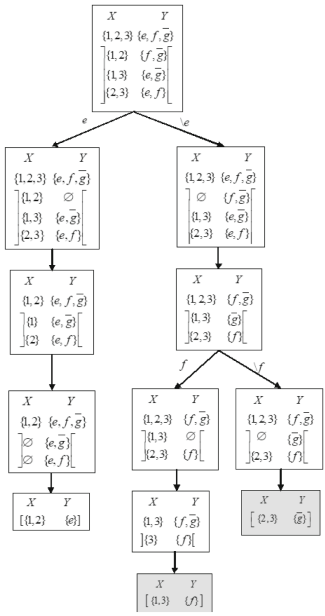

**Fig. 1.** The search tree in the case of generating positive JSM-hypotheses.

Similarly, the generation of negative JSM-hypotheses is carried out. We have 3 negative JSM-hypotheses:

$[\{5,6\}\ \{\overline{e},f\}],\ [\{4,5\}\ \{\overline{e},g\}],\ [\{4,5,6\}\ \{\overline{e}\}]$.

Basing on the rules of the first kind, the rejection of hypotheses is carried out. In this case, a positive hypothesis must satisfy at least two positive examples and not one negative. A negative hypothesis must satisfy at least two negative examples and not one positive. As a result, one positive hypothesis and two negative ones are obtained:

positive hypothesis: $[\{1,2\}\ \{e\}]$;

negative hypotheses: $[\{5,6\}\ \{\overline{e},f\}],\ [\{4,5\}\ \{\overline{e},g\}]$.

Let us classify a subdefinite example $[\{7\}\ \{g,\overline{f},e\}]$ basing on the rules of second kind. In this case, the example contains one positive hypothesis and none negative, therefore, the example refers to a set of positive examples.

The described search procedure can be improved if we analyze a set of counterexamples not only in leaf nodes but also in intermediate nodes of search tree, namely: after reaching a fixed point as a result of the reduction of table constraints, we can check whether the current domain of the variable $Y$ is not included as a fragment in at least one counterexample. If it is included, then the research on this branch should be terminated. Indeed, if a set of features is included as a fragment in some counterexamples, then any subset of it will also be included there. In other words, when generating JSM-hypotheses, it is advisable to apply the following statement at each step of the search.

**Statement 8** (**S8**). If the domain of the variable $Y$ is included as a fragment in at least one counterexample, then the CSP has no solution.

## 7 Example of Classification of Rock Cells

Here is an example from the practice of mining. There are 14 spatial cells (objects) into which a section of the rock massive is divided.

Each spatial cell is characterized by a certain set of features:

$a$ – fault 1; $b$ – fault 2; $c$ – stope boundaries; $d$ – stope boundaries of the overlying level; $e$ – ore body; $f$ – host rocks; $g$ –ore body/host rocks; $h$ –workings; $i$ – hanging wall of the ore deposit; $j$ – foot wall of the ore body; $N$ – number of seismic events in the cell. The value "0" indicates that the feature is absent, and the value "1" indicates that the feature is present.

Based on expert assessments of features, these 14 cells were classified into three clusters according to the degree of seismic activity: class $A$ – safe, class $B$ – medium activity, class $C$ – high activity [5].

As a result, three optimal partitioning were found:

*First partitioning*: class $A$ – objects 1, 2, 3, 4, 9, 10, 11, 12, 13, 14; class $B$ – objects 7, 8; class $C$ – objects 5, 6.

*Second partitioning*: class $A$ – objects 1, 2, 3, 4, 7, 9, 11, 12, 13, 14; class $B$ – objects 8, 10; class $C$ – objects 5, 6.

*Third partitioning*: class $A$ – objects 1, 2, 3, 4, 9, 11, 12, 13, 14; class $B$ – objects 7, 8, 10; class $C$ – objects 5, 6.

It can be seen that under different partitions, objects 7 and 10 are in class $A$ or in class $B$. The JSM method was used to clarify the uncertainty.

The following positive hypotheses for class $A$ were successfully verified:

$$[\{2,4,12,14\}\ \{a,\overline{c},\overline{e}\}],\ [\{1,2,3,4,9,13,14\}\ \{\overline{c},\overline{g}\}],\ [\{9,11,12,13,14\}\ \{\overline{c},\overline{i}\}].$$

The following negative hypotheses for class $A$ were successfully verified:

$$[\{6,8\}\ \{a,\overline{b},c,d,\overline{f},h,\overline{i}\}],\ [\{5,6\}\ \{\overline{b},\overline{e},\overline{f},g,h,i,\overline{j}\}].$$

Since object 7 contains two positive hypotheses and non negative ones of class $A$, it can be referred to this class. After constructing positive and negative hypotheses for class $B$, it turns out that object 10 can be referred to this class.

## 8 Conclusion

For the first time, it was proposed to solve the problem of generating JSM-hypotheses as a table constraint satisfaction problem using the author's procedures for systematic search and constraint propagation methods.

It is proposed to represent the training sample in the form of table constraints of a special type – compressed tables of the $D$-type. In this study, a problem of generating JSM-hypotheses is reduced to the frequent closed patterns discovery problem with an additional condition that each pattern should not be included as a fragment in a set of counterexamples.

The rules proposed for propagating compressed tables of the $D$-type in combination with the original methods of branching the search tree allow us to effectively solve high-dimensional DM problems.

The computational complexity of the proposed method of frequent closed pattern discovery can be estimated as:

$$O((|T||I| + |I| + |T| - min(|T|, |I|)) * 2^{min(|T|,|I|)}),$$

where: $|T|$ is the number of objects, $|I|$ is the number of attributes, which is better than the estimate for most prototype methods, which is: $O(|T||I||L|min(|T|, |I|))$, where $|L| = 2^{min(|T|,|I|)}$.

**Acknowledgments.** The work was carried out within the framework of the current research topic "Development of theoretical and organizational and technical foundations of information support for managing the viability of regional critical infrastructures of the Arctic zone of the Russian Federation" (registration number 122022800547-3).

**Disclosure of Interests.** The authors have no competing interests to declare that are relevant to the content of this article.

## References

1. Gançarski, P., Dao, T.-B.-H., Crémilleux, B., Forestier, G., Lampert, T.: Constrained clustering: current and new trends. In: Marquis, P., Papini, O., Prade, H. (eds.) A Guided Tour of Artificial Intelligence Research, pp. 447–484. Springer, Cham (2020). https://doi.org/10.1007/978-3-030-06167-8_14
2. Song, W., Ye, W., Fournier-Viger, P.: Mining sequential patterns with flexible constraints from MOOC data. Appl. Intell., 1–17 (2022). https://doi.org/10.1007/s10489-021-03122-7
3. Liu, X., Niu, X., Fournier-Viger, P.: Fast Top-K association rule mining using rule generation property pruning. Appl. Intell. **51**(4), 2077–2093 (2020). https://doi.org/10.1007/s10489-020-01994-9
4. Zuenko, A.A.: A machine learning method to reveal closed sets of common features of objects using constraint programming. Autom. Remote. Control. **83**(12), 1995–2005 (2022). https://doi.org/10.1134/S00051179220120116
5. Zuenko, A., Zuenko, O.: Frequent pattern discovery as table constraint satisfaction problem. In: Proceedings of the Sixth International Scientific Conference "Intelligent Information Technologies for Industry", pp. 1–13. Springer, Cham (2022). https://doi.org/10.1007/978-3-031-19620-1_12

6. Finn, V.K.: On empirical regularities in the JSM method of automated research support. Autom. Doc. Math. Linguist. **57**, 362–381 (2023). https://doi.org/10.3103/S0005105523060055
7. Dao, T.-B.-H., Duong, K.-C., Vrain, C.: Constrained clustering by constraint programming. Artif. Intell. **244**, 70–94 (2017). https://doi.org/10.1016/j.artint.2015.05.006
8. Hien, A., Loudni, S., Aribi, N., Lebbah, Y., Laghzaoui, M.E.A., Ouali, A., Zimmermann, A.: A relaxation-based approach for mining diverse closed patterns. In: Hutter, F., Kersting, K., Lijffijt, J., Valera, I. (eds.) ECML PKDD 2020. LNCS (LNAI), vol. 12457, pp. 36–54. Springer, Cham (2021). https://doi.org/10.1007/978-3-030-67658-2_3
9. Verhaeghe, H., Nijssen, S., Pesant, G., Quimper, C.-G., Schaus, P.: Learning optimal decision trees using constraint programming. Constraints (12), 226–250 (2020). https://doi.org/10.1007/s10601-020-09312-3
10. Mairy, J.-B., Deville, Y., Lecoutre, C.: The smart table constraint. In: Michel, L. (ed.) CPAIOR 2015. LNCS, vol. 9075, pp. 271–287. Springer, Cham (2015). https://doi.org/10.1007/978-3-319-18008-3_19
11. Björdal, G., Flener, P., Pearson, J., Stuckey, P.J., Tack, G.: Solving Satisfaction Problems Using Large-Neighbourhood Search. In: Simonis, H. (ed.) CP 2020. LNCS, vol. 12333, pp. 55–71. Springer, Cham (2020). https://doi.org/10.1007/978-3-030-58475-7_4

# Impact of Spectral and Meteorological Data Fusion on the Accuracy of Woody Plant Identification Using Deep Machine Learning Methods

Alexandr Alexandrov[1], Pavel Dmitriev[2(✉)], Anastasia Dmitrieva[2], Artem Poltavskiy[1], and Boris Kozlovsky[2]

[1] International Research Institute of Smart Materials, Southern Federal University, Rostov-on-Don 344090, Russia
alea@sfedu.ru

[2] Botanical Garden, Academy of Biology and Biotechnologies, Southern Federal University, Rostov-on-Don 344006, Russia
{pdmitriev,poltavsky}@sfedu.ru

**Abstract.** Identification of woody plant species and their states has an important role in monitoring of forest resources, as well as joint application with remote sensing. For remote monitoring there is still a problem of poor repeatability of the result. Species identification models built from spectral characteristics for a specific time interval or a specific area are often not suitable for other time intervals and areas. This paper discusses a poor repeatability study approach based on analyzing the seasonal dynamics of the annual cycle to accurately identify different maple species. The main research methods are machine learning (ML) algorithms: Random Forest and Gradient Boosting. Including a method to fuse spectral data from a hyperspectral camera with meteorological data such as temperature, precipitation and day length affecting the development of woody plants in the annual cycle. The highest accuracy rate was 58.72%. Data fusion allows the relationship between spectral characteristics and climatic conditions to be considered, resulting in a 13.21% improvement in the quality of species identification by machine learning algorithms. The results allow us to assess the variation and interrelationship of maple species over the annual cycle, as well as the differences in spectral characteristics within each annual cycle. The use of spectral and climatic data fusion made it possible to create a comprehensive model that considers spectral characteristics and their relationship with meteorological conditions, thus increasing the accuracy of species classification, and to evaluate the accuracy of machine learning algorithms in the seasonal dynamics of the annual cycle for all studied species.

**Keywords:** Data fusion · Acer · Vegetation indices · Spectral bands · Machine learning · Random Forest · Gradient Boosting

The availability of accurate information regarding the composition of tree species in a given area is a prerequisite to the development of effective strategies for the sustainable


S. Kovalev et al. (Eds.): IITI 2024, LNNS 1209, pp. 207–216, 2024.
https://doi.org/10.1007/978-3-031-77688-5_20

management of artificial and natural forests, plantations in human settlements, and fruit orchards. Over the past four decades, the field of remote sensing (RS) has witnessed significant advancements, enabling the identification of woody plant species from a distance [1]. The use of passive optical RS techniques, employing multi- and hyperspectral sensors, has yielded promising outcomes [2, 3].

Concurrently, hyperspectral images, which possess a high degree of spectral resolution, can yield more precise results in the classification of tree species, even to the extent of identifying intraspecific taxa [4, 5]. The integration of spectral characteristics with plant textural features, topographic data and the values of other features can enhance the accuracy of classification [6–8]. The analysis of time series of spectral characteristics of woody plants reflecting their phenological features offers significant advantages in classification [9–12]. A multitude of techniques have been employed to categorize woody plant species based on spectral characteristics. Among these, convolutional neural networks (CNN) have emerged as a particularly promising approach [1, 13, 14].

The study is devoted to the problem of maple species identification based on seasonal variations in the annual cycle by applying machine learning algorithms and integrating spectral and meteorological data. Heterogeneous data fusion has been employed in a variety of applications, particularly in the domains of modern medicine and healthcare. This approach involves the integration of heterogeneous medical data, such as electronic medical records, radiographic images, or other clinical data sources, through the application of machine learning techniques. This integration enables the development of more accurate diagnostic tools and methodologies [15–17]. In industrial and scientific fields, in the tasks of object detection using multiple sensors [18], increasing signal-to-noise ratio and reducing false detections [19], reducing response time by obtaining better situational awareness [20]. In RS based on multi-sensor satellite images or hyperspectral imaging data from unmanned aerial vehicles, to classify and segment images or to determine various parameters [21–23].

The integration of data from disparate sources facilitates the generation of a more comprehensive and nuanced understanding of the object of study. This approach enables the identification of intricate interrelationships between diverse phenomena, as well as the discovery of hitherto concealed patterns, thereby enhancing the accuracy of predictions. The consolidation of heterogeneous data addresses limitations that may be specific to individual sources of information. The consolidation of data from disparate sources can offset the limitations of a single data source, thereby enhancing the validity of the research findings. The advantages of utilising this strategy in modern science are related to the enhanced informativeness and accuracy of the analyses that can be achieved by combining heterogeneous data. The analysis of data from disparate sources allows for the discovery of novel trends, patterns, and relationships that may not have been identified through the analysis of data from individual sources [24].

Consequently, the integration of disparate data sets is a pivotal aspect of contemporary research, with applications across a range of scientific disciplines. The utilisation of data fusion in the construction of models enhances their accuracy and the quality of decision-making, thereby enabling the extraction of more meaningful information from disparate sources.

This study presents an approach to enhance the predictive accuracy of models for the identification of maple species, based on the integration of spectral data with meteorological data. The data from five maple species over a three-year period from 2021 to 2023 were employed in the training and testing of the models. The second section of the paper outlines the dataset and analytical techniques employed. The identification of species was achieved through the utilisation of machine learning techniques, including random forest (RF) and gradient boosting (GB). The results of the tests are presented in Sect. 3.

## 1 Materials and Methods

### 1.1 Data

The study was conducted at Southern Federal University between 2021 and 2023. The study focused on five species of maple: *Acer campestre L.*, *A. negundo L.*, *A. saccharinum L.*, *A. platanoides L.* и *A. ibericum Bieb.* Hyperspectral imaging of leaves of these maple species was performed in the laboratory using a Cubert UHD-185 hyperspectral camera, which has a spectral range of 450–950 nm and a spectral resolution of 4 nm. Leaf sampling for hyperspectral imaging was conducted throughout the growing season at 7–10 day intervals. All spectral profiles in the image were smoothed using the Savitzky-Golay filter with a step size of 15. Region of interest (ROI) extraction was performed by two-stage segmentation of the original hyperspectral images [25]. The pixels with the ROI were selected through a process of repeated random selection. Consequently, time-series of spectral band values for five maple species were obtained over a three-year period, encompassing the entirety of the growing season.

A combination of spectral and meteorological data was employed to enhance the precision of maple species identification across varying temporal intervals. The meteorological data set comprises minimum, maximum and average daily temperatures (°C), average precipitation (mm) and daylight hours. Since meteorological conditions have a delayed effect on plants, averaged values of meteorological characteristics for the last 7 days before hyperspectral imaging were taken.

However, the spectral data for 2021 contained information on only three species *A. campestre, A. negundo* and *A. saccharinum*. Therefore, spectral data augmentation was performed for the missing two species, *A. ibericum* and *A. platanoídes*. A part of the real data for 2022 and 2023 was used to augment the dataset of the two species for the year 2021, subsequently used for model training. In order to generate a new sample spectrum for the same species, the following procedure was employed:

1. Only spectra for species absent in 2021 but present in 2022 and 2023 were selected.
2. Day alignment was carried out. Each year has a different number of days, the minimum number of days from the three years was selected and the minimum total day of the start of data collection was taken as the starting point.
3. An equalisation was performed on the number of samples per species. In some cases, more than 5 leaves were taken, so we chose the minimum number in case of inconsistency in the number of spectra.
4. A small quantity of noise was introduced to each spectrum.

5. The arithmetic mean between the two spectra from 2022 and 2023 was found, the resulting spectrum was retained in 2021.

The resulting dataset has a different number of spectra for each species, this is due to the fact that each maple species has a different leaf shape and leaf area. Figure 1 shows the distribution of the number of spectra by species. To obtain a balanced data set, it was decided to use an equal number of spectra, which was equal to the minimum number of spectra of one of the species. A. ibericum has the smallest number of spectra, so the number of spectra of other species was chosen equal to it. At the same time, spectra from other species were chosen randomly so that each day contained approximately equal number of spectra.

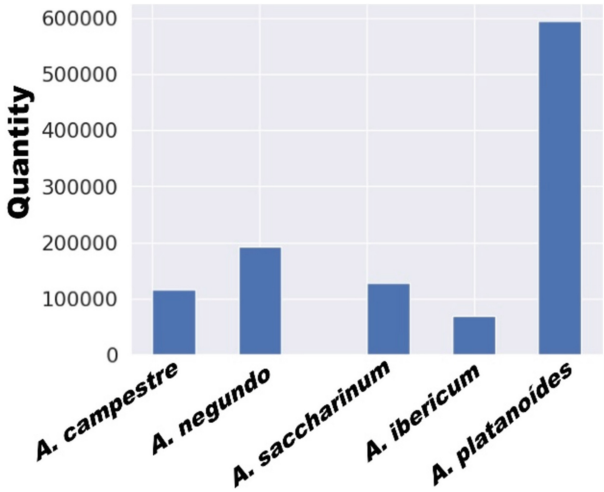


**Fig. 1.** Distribution of the number of spectra by species.

### 1.2 Deep Machine Learning Methods

The study used machine learning techniques: RF and GB. The random forest algorithm is based on the training of an ensemble of decision trees. Each tree is constructed from a subsample of the training data, and the predictions of each tree are then averaged to obtain the final prediction. This method is effective with large data sets and is less susceptible to overtraining due to the use of a random subsample and random feature subsets to construct each tree.

Gradient boosting also employs an ensemble of trees, with the objective of reducing the error of the loss function. The method works by successively adding new trees to the model, such that each new tree adjusts for the residuals left by previous trees. This method is typically associated with higher prediction accuracy, due to the more accurate correction of model errors.

Thus, both methods are based on an ensemble of trees, but they have different approaches to building these trees and combining their predictions, resulting in differences in their performance and behaviour. The RF method was employed with the following hyperparameters: the number of trees in the forest (n_estimators) was set to 150, the minimum number of samples required for splitting within a tree node (min_samples_split) was fixed at 2, and the minimum number of samples in a leaf node (min_samples_leaf) was set to 5. The maximum depth of each tree in the forest (max_depth) was left as None. A variety of hyperparameters and loss functions were employed in the training of GB models. The most accurate models were those utilising the CrossEntropy loss function and a learning rate of 0.001 at 2000 iterations.

## 2 Results

To assess the difference in spectral data for each species, Exploratory Data Analysis (EDA) was performed. In Fig. 2, the species *A. campestre* – highlighted in red, *A. negundo* – highlighted in green, *A. saccharinum* – highlighted in blue, *A. ibericum* – highlighted in pink and *A. platanoídes* highlighted in turquoise. First, the average values of spectra by day were taken for the three species *A. campestre, A. negundo* and *A. saccharinum* for the year 2022. From Fig. 2a, it can be seen that the average values of the spectra show the same shape and indices, as evidenced by their great similarity and overlap of values throughout the growing season. In Fig. 2b, the mean values of species *A. ibericum* and *A. platanoídes* are added to the three species *A. campestre, A. negundo* and *A. saccharinum*. Their values are close to each other, indicating their similarity, but their reflectance values in the infrared range are higher than those of the first three species. In the first half of the growing season, *A. ibericum* and *A. platanoídes* show differences from *A. campestre, A. negundo* and *A. saccharinum*. In the second half of the growing season, the values of all spectra overlap. Based on EDA, the presented set of spectra has close and overlapping spectra values of all maple species, which presents a difficult task of species identification.

The first step in data analysis and species identification was an experiment using spectral data without meteorological conditions. All data are numerical data included in the spectral and meteorological datasets. Data standardisation was performed, which involves centring the value at 0 and standardising the variance at 1. Data for the years 2021 and 2022 were used as the training dataset, with tests performed on the year 2023.

The RF algorithm showed the following results: Accuracy on the test sample is 0.4947. At the same time, the model training took 3 min. The GB algorithm showed the following results: Accuracy on the test sample is 0.5021. Training the model took a little more than 5 min on the GPU.

In the second step of data analysis and species identification, spectral data were combined with meteorological data. All conditions identical to the first stage, training on the dataset for the years 2021 and 2022, tests were performed on the year 2023. The RF algorithm showed the following results: Accuracy on the test sample is 0.5586. The model took just over 3 min to train. Table 1 shows the report of the classification of the main indicators for each class. The error matrix is presented in Fig. 3.

The GB algorithm showed the following results: Accuracy on the test sample is 0.5872. Training the model took a little more than 6 min on GPU.

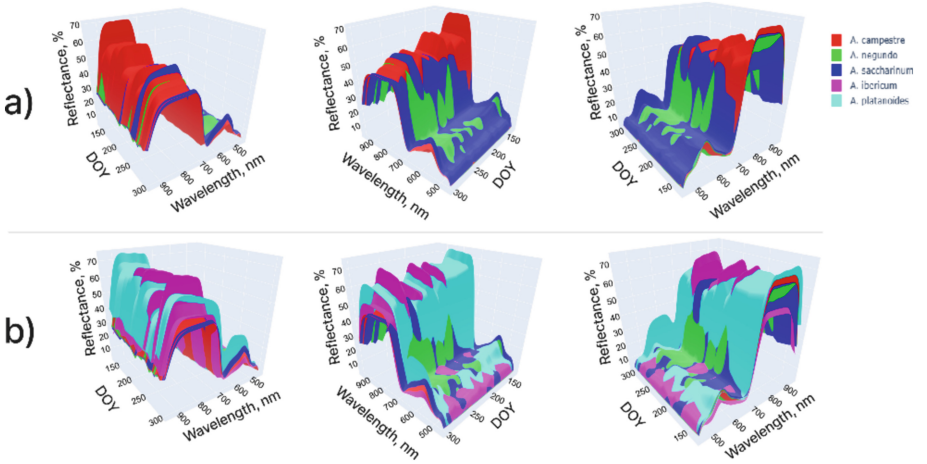


**Fig. 2.** Average of spectra by day of the year (DOY) in 2022. a – *A. campestre, A. negundo* and *A. saccharinum*, b – *A. campestre, A. negundo, A. saccharinum, A. ibericum* and *A. platanoídes.*

**Table 1.** Report on RF classification using spectral and climatic data.

| | Precision | Recall | F1-score | Support |
|---|---|---|---|---|
| *A. campestre* | 0.50 | 0.47 | 0.49 | 21436 |
| *A. negundo* | 0.63 | 0.52 | 0.57 | 21436 |
| *A. saccharinum* | 0.53 | 0.53 | 0.53 | 21436 |
| *A. ibericum* | 0.57 | 0.57 | 0.57 | 21436 |
| *A. platanoídes* | 0.56 | 0.70 | 0.62 | 21436 |
| Accuracy | | | 0.56 | 107180 |
| Macro Average | 0.56 | 0.56 | 0.56 | 107180 |
| Weighted Average | 0.56 | 0.56 | 0.56 | 107180 |

Table 2 is a matrix of the results of maple species classification by day of the year (DOY). Each row corresponds to a specific maple species and each column represents a specific day of the year. The cells of the table contain values representing the percentage of correct classification of the maple species on the corresponding day.

It is important to note that the average accuracy of 49.93% and the overall accuracy of 58.72% correct classification represent two distinct metrics. The differences between these metrics may be attributed to the uneven distribution of classes in the dataset. The overall accuracy is defined as the proportion of correctly classified objects relative to the total number of objects in the dataset. In contrast, the average accuracy considers the performance of the model in each class and then averages these values.

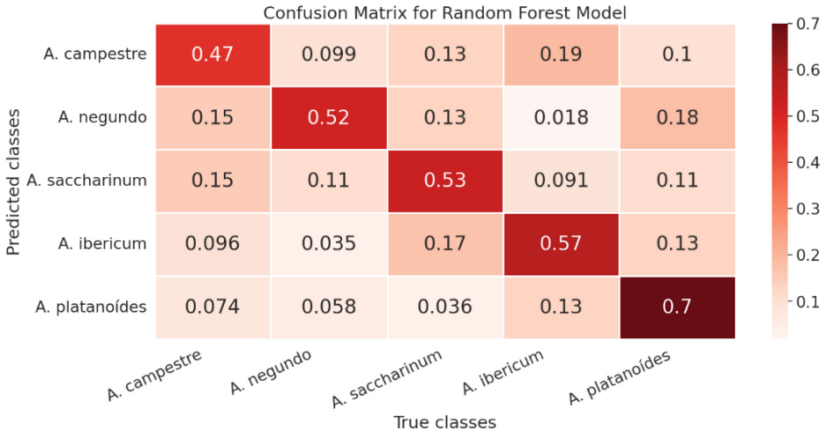


**Fig. 3.** Random Forest error matrix using spectral and climatic data.

**Table 2.** Maple species classification results by DOY.

| Species name | Day Of Year (DOY) | | | | | | Average Accuracy by species |
|---|---|---|---|---|---|---|---|
| | 137 | 173 | 205 | 240 | 269 | 290 | |
| *A. campestre* | 5.63% | 33.09% | **97.78%** | 69.55% | 59.08% | 38.30% | **50.57%** |
| *A. negundo* | 1.22% | 16.84% | 35.12% | 47.33% | 50.37% | 0.00% | **30.18%** |
| *A. saccharinum* | 75.60% | 38.14% | 28.69% | 58.72% | **83.71%** | **84.13%** | **61.50%** |
| *A. ibericum* | 5.13% | 37.62% | 3.63% | **76.13%** | 75.67% | 4.45% | **33.77%** |
| *A. platanoídes* | **91.72%** | **90.12%** | 49.45% | 75.97% | 27.53% | 87.23% | **70.34%** |
| Average accuracy by DOY | **35.86%** | **43.16%** | **42.93%** | **65.54%** | **59.27%** | **53.53%** | **49.93%** |

Thus, the differences between average accuracy and overall accuracy may be an indicator of a class imbalance problem and highlight the importance of careful analysis of multiclass classification results.

Figure 4 is a collection of classification accuracy bar charts that depict the performance of the GB model in different contexts. Each chart represents one class of maple species, where the height of the column corresponds to the classification accuracy for the corresponding class. This visualisation makes it easy to identify which maple species the model successfully identifies with high accuracy, and where there may be noticeable difficulties and improvements over the course of a year.

The results of the model accuracy tests are presented in Table 3. It can be observed that the models demonstrate an enhanced level of accuracy when combined with spectral and meteorological data.

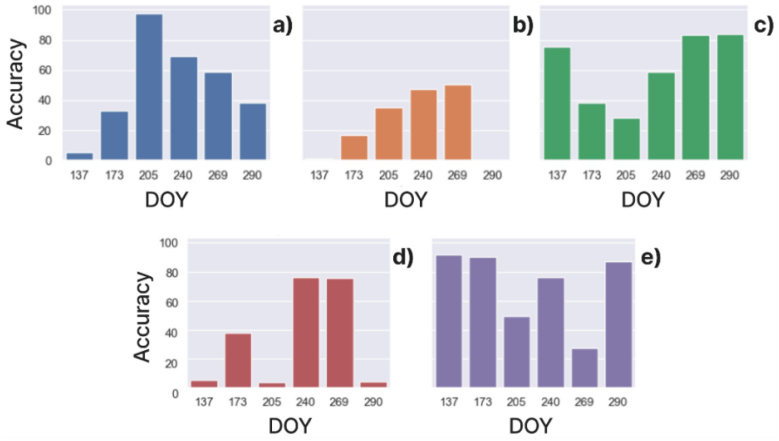


**Fig. 4.** A bar chart illustrating the classification accuracy. a – *A. campestre*, b – *A. negundo*, c – *A. saccharinum*, d – *A. ibericum*, e – *A. platanoídes.*

**Table 3.** Results of model accuracy in data analysis and species identification.

| Method | Dataset used | Accuracy |
|---|---|---|
| Random Forest | Spectral data | 49.51% |
| Gradient Boosting | Spectral data | 51.87% |
| Random Forest | Spectral and meteorological data | 55.86% |
| Gradient Boosting | Spectral and meteorological data | 58.72% |

The accuracy of the RF algorithm increased by 12.83%, while that of the GB algorithm increased by 13.21%. The GB algorithm demonstrated superior performance to the RF algorithm, with an improvement of 7.51%.

## 3 Conclusion

The identification of woody plant species and their states plays an essential role in the monitoring of forest resources and can be effectively combined with remote sensing techniques. However, there is still a problem of poor repeatability of the results when monitoring remotely. This study presents a promising approach to enhance the prediction accuracy of machine learning models for the identification of woody plant species from remotely sensed data. This is achieved through the fusion of time series of spectral bands and meteorological data. Two machine learning models, GB and RF, were employed to address the issue. The identification accuracy with GB using only spectral data was 51.87%, while with RF it was 49.51%. The fusion of spectral and meteorological data resulted in an accuracy of 58.72% for the GB model and 55.86% for the RF model. Although the accuracy of maple species identification in this study is relatively low, the proposed approach is promising as it significantly enhances the accuracy of the

models. The practical significance of this study lies in the expansion of possibilities for the monitoring of species composition in natural and artificial tree plantations, with a particular focus on the identification of invasive plant species. Further studies will additionally employ the fusion of spectral bands with vegetation indices and meteorological data, neural networks as classification algorithms, and one-versus-all as classification principles.

**Funding.** The project was supported by the Russian Science Foundation under grant No. 24-24-00405, https://rscf.ru/project/24-24-00405/ (accessed on 06.12.2024) a and performed in Southern Federal University (Rostov-on-Don, Russian Federation).

## References

1. Pu, R.: Mapping tree species using advanced remote sensing technologies: a state-of-the-art review and perspective. J. Remote Sens. **2021**, 2021/9812624 (2021). https://doi.org/10.34133/2021/9812624
2. Paz-Kagan, T., Silver, M., Panov, N., Karnieli, A.: Multispectral approach for identifying invasive plant species based on flowering phenology characteristics. Remote Sens. **11**(8), 953 (2019). https://doi.org/10.3390/rs11080953
3. Yel, S.G., Tunc Gormus, E.: Exploiting hyperspectral and multispectral images in the detection of tree species: a review. Front. Remote Sens. **4**, 1136289 (2023). https://doi.org/10.3389/frsen.2023.1136289
4. Hycza, T., Stereńczak, K., Bałazy, R.: Potential use of hyperspectral data to classify forest tree species. N. Z. J. For. Sci. **48**(1), 18 (2018). https://doi.org/10.1186/s40490-018-0123-9
5. Prakash Hati, J., et al.: Mangrove classification using airborne hyperspectral AVIRIS-NG and comparing with other spaceborne hyperspectral and multispectral data. Egypt. J. Remote Sens. Space Sci. **24**(2), 273–281 (2021). https://doi.org/10.1016/j.ejrs.2020.10.002
6. Hościło, A., Lewandowska, A.: Mapping forest type and tree species on a regional scale using multi-temporal sentinel-2 data. Remote Sens. **11**(8), 929 (2019). https://doi.org/10.3390/rs11080929
7. Pu, R., Landry, S., Yu, Q.: Assessing the potential of multi-seasonal high resolution pléiades satellite imagery for mapping urban tree species. In: 2018 Fifth International Workshop on Earth Observation and Remote Sensing Applications (EORSA), pp. 1–5. IEEE, Xi'an (2018). https://doi.org/10.1109/EORSA.2018.8598563
8. Xie, Z., Chen, Y., Lu, D., Li, G., Chen, E.: Classification of land cover, forest, and tree species classes with ZiYuan-3 multispectral and stereo data. Remote Sens. **11**(2), 164 (2019). https://doi.org/10.3390/rs11020164
9. Fang, F., et al.: Discriminating tree species at different taxonomic levels using multi-temporal WorldView-3 imagery in Washington D.C., USA. Remote Sens. Environ. **246**, 111811 (2020). https://doi.org/10.1016/j.rse.2020.111811
10. Xi, Y., Ren, C., Tian, Q., Ren, Y., Dong, X., Zhang, Z.: Exploitation of time series sentinel-2 data and different machine learning algorithms for detailed tree species classification. IEEE J. Sel. Top. Appl. Earth Obs. Remote Sens. **14**, 7589–7603 (2021). https://doi.org/10.1109/JSTARS.2021.3098817
11. Immitzer, M., Neuwirth, M., Böck, S., Brenner, H., Vuolo, F., Atzberger, C.: Optimal input features for tree species classification in central Europe based on multi-temporal sentinel-2 data. Remote Sens. **11**(22), 2599 (2019). https://doi.org/10.3390/rs11222599

12. Dmitriev, P.A., Kozlovsky, B.L., Dmitrieva, A.A., Varduni, T.V.: Maple species identification based on leaf hyperspectral imaging data. Remote Sens. Appl.: Soc. Environ. **30** (2023). https://doi.org/10.1016/j.rsase.2023.100964
13. Kattenborn, T., Leitloff, J., Schiefer, F., Hinz, S.: Review on convolutional neural networks (CNN) in vegetation remote sensing. ISPRS J. Photogramm. Remote Sens. **173**, 24–49 (2021). https://doi.org/10.1016/j.isprsjprs.2020.12.010
14. Gazzea, M., Kristensen, L.M., Pirotti, F., Ozguven, E.E., Arghandeh, R.: Tree species classification using high-resolution satellite imagery and weakly supervised learning. IEEE Trans. Geosci. Remote Sens. **60**, 1–11 (2022). https://doi.org/10.1109/TGRS.2022.3210275
15. Schilcher, J., Nilsson, A., Andlid, O., Eklund, A.: Fusion of electronic health records and radiographic images for a multimodal deep learning prediction model of atypical femur fractures. Comput. Biol. Med. **168**, 107704 (2024). https://doi.org/10.1016/j.compbiomed.2023.107704
16. Ibrahim, Sa.I., El-Tawel, Gh.S., Makhlouf, M.A.: Brain image fusion using the parameter adaptive-pulse coupled neural network (PA-PCNN) and non-subsampled contourlet transform (NSCT). Multimed. Tools Appl. **83**(9), 27379–27409 (2023). https://doi.org/10.1007/s11042-023-16515-2
17. Nikolaou, N., et al.: Quantifying the advantage of multimodal data fusion for survival prediction in cancer patients (2024). https://doi.org/10.1101/2024.01.08.574756
18. Massoud, Y., Laganiere, R.: Learnable fusion mechanisms for object detection in autonomous vehicles (2022). https://doi.org/10.36227/techrxiv.21506124
19. Frid, A., Ben-Shimol, Y., Manor, E., Greenberg, S.: Drones detection using a fusion of RF and acoustic features and deep neural networks. Sensors **24**(8), 2427 (2024). https://doi.org/10.3390/s24082427
20. Ciurapiński, W., et al.: Data fusion concept in multispectral system for perimeter protection of stationary and moving objects. In: Huckridge, D.A., Ebert, R.R. (eds.) SPIE Europe Security + Defence, Berlin, Germany, p. 748111 (2009). https://doi.org/10.1117/12.830395
21. Singh, A., Gaurav, K.: Deep learning and data fusion to estimate surface soil moisture from multi-sensor satellite images. Sci. Rep. **13**(1), 2251 (2023). https://doi.org/10.1038/s41598-023-28939-9
22. Chen, Y., Zhao, M., Bruzzone, L.: Incomplete multimodal learning for remote sensing data fusion (2023). https://doi.org/10.48550/ARXIV.2304.11381
23. Elamin, A., El-Rabbany, A.: UAV-based multi-sensor data fusion for urban land cover mapping using a deep convolutional neural network. Remote Sens. **14**(17), 4298 (2022). https://doi.org/10.3390/rs14174298
24. Pawłowski, M., Wróblewska, A., Sysko-Romańczuk, S.: Effective techniques for multimodal data fusion: a comparative analysis. Sensors **23**(5), 2381 (2023). https://doi.org/10.3390/s23052381
25. Dmitriev, P.A., Kozlovsky, B.L., Dmitrieva, A.A., Varduni, T.V.: Classification of invasive tree species based on the seasonal dynamics of the spectral characteristics of their leaves. Earth Sci. Inform. **16**(4), 3729–3743 (2023). https://doi.org/10.1007/s12145-023-01118-0


# Local Patch Active Appearance Model of the Face

Aleksandr D. Borisov(✉) and Sergey D. Makhortov

Voronezh State University, Voronezh, Russia
radiatus@yandex.ru

**Abstract.** This paper discusses the enhancement of the Active Appearance Model (AAM), a classical algorithm in machine learning traditionally applied to facial image processing tasks. The focus is on improving the accuracy and adaptability of AAM for solving complex tasks, including tracking face contours for animation creation. The model is trained on a personalized sample of facial expressions, enabling it to efficiently account for both global and local features of an individual's face images. The study highlights the limitations of traditional AAMs based on global models of shape and texture in processing local details. The use of localized texture patches and the transition to local piecewise-linear shape models significantly enhance the model's performance in tasks involving detailed processing of face images. The modified version of AAM demonstrates improved results, confirmed experimentally, and facilitates faster and more accurate tracking of facial features for use in digital animation. The algorithm is applicable for any facial landmarks, but within the scope of this article, it will be considered using the example of lips, as the most challenging region.

**Keywords:** Active Appearance Model · Computer Vision · Motion Capture

## 1 Introduction

Over the past few decades, Active Appearance Models (AAM) have established themselves as a key tool in the field of computer vision, since their introduction by Cootes and his colleagues in the mid-1990s [2]. These models, which integrate complex algorithms for analyzing shape and texture, show a high degree of adaptability to a wide range of visual tasks. They have enabled breakthroughs in accurate recognition and analysis of facial features, including detailed tracking of eye and lip movements, which has been critically important for the development of animation technologies. The results of precise tracking of eye and lip contours are an essential component of advanced approaches to facial animation capture [1, 3]. Such tracking accuracy is achieved through numerous iterations of training, testing, and re-annotation. The operator performs personalized annotation of keyframes for a specific actor, and then verifies the performance of the AAM on the remaining sequence. If the results are unsatisfactory, new keyframes are added, and the procedure is repeated.

However, despite these achievements, traditional approaches to AAM face challenges in processing the local features of the human face. Limitations related to the need for


S. Kovalev et al. (Eds.): IITI 2024, LNNS 1209, pp. 217–226, 2024.
https://doi.org/10.1007/978-3-031-77688-5_21

extensive annotation and insufficient coverage of all possible facial expressions due to the use of global models diminish the effectiveness of AAMs in tasks requiring a high level of detail and precision.

This work proposes the Local Patch Active Appearance Model (LP-AAM) to improve Active Appearance Models. By using local models for shape and texture, LP-AAM increases modeling flexibility and accuracy while reducing dependency on training data. However, replacing global models with local ones may reduce stability, potentially causing artifacts and high-frequency oscillations. The innovation lies in introducing local shape and texture subspace models, enhancing the tracking of dynamic facial expressions. Experiments show LP-AAM's superiority over traditional AAM methods, confirming its improved accuracy and efficiency.

The proposed enhancements address longstanding issues with traditional AAMs and broaden their application, making them a more powerful tool in computer vision. This approach meets the evolving demands for quality in digital animation and face recognition, offering high accuracy and flexibility in processing facial visual data.

The article is organized as follows: Sect. 2 reviews previous work on AAM, describing their key features and limitations. Section 3 is dedicated to describing traditional AAMs, which is necessary for understanding the basic principles and limitations of these models. Section 4 presents a detailed description of the proposed Local Patch Active Appearance Model. Section 5 is devoted to the experimental evaluation of the proposed approach, including a comparison with P-AAM in tasks of face tracking and face recognition with pose changes. The conclusion summarizes the findings of the research and discusses the prospects for further development of the proposed approach.

## 2 Related Work

Active appearance models are crucial in computer vision and image analysis due to their ability to adapt to various images by combining texture and shape models. This allows for accurate extraction and interpretation of visual data. They are especially valuable in animation, enabling precise tracking of facial contours like the eye and lip regions.

Since the advent of AAM, numerous alternative algorithms have been developed to address similar tasks, many of which demonstrate impressive results. Some of these algorithms are evolutions of AAM [4, 10, 12] and will be mentioned later, while others represent modern neural network approaches [1, 5, 8]. The latter require significant amounts of data and extensive training periods. In cases of poor contour tracking, the process of re-annotation and retraining is time-consuming. This makes AAM preferable, as it allows for quick re-annotation and verification using small datasets. Modern neural network approaches can utilize AAM results as training data.

The foundation of AAM work is a shape deformation model, defined through a set of specific points, which enables detailed representation of the contours of important facial regions. The texture model complements this structure, presenting possible variations in appearance based on training data, where the accuracy of the shape model is directly related to the quality and detail of the texture model.

The initiation of AAM in the scientific community is associated with the works of Tim Cootes and his colleagues [2], who first introduced the concepts of facial shape and

texture modeling. These studies have had a significant impact on the development of image analysis methods and stimulated further advancements in this area. Initial works on AAM not only shed light on the fundamental aspects of these models but also emphasized their importance for future research, including the adaptation and improvement of AAM for more complex tasks such as facial expression recognition and analysis.

Nevertheless, despite the impressive results achieved with the initial models of AAM, significant limitations of traditional approaches become evident when it comes to processing local features of the image. The use of global models for shape and texture often leads to inefficient processing of local changes, such as complex facial expressions or lighting conditions. Solving this problem requires a larger amount of additional training data, which still cannot guarantee good results. This is especially critical in tasks requiring high accuracy, for example, in medical imaging or under varying lighting conditions in face recognition. Our work proposes an approach that solves this problem by using local models.

Improvements to AAM suggested by Matthews and Baker [7], including the method of inverse composition, aim to speed up the AAM operation by reducing computations, but do not address the issue of accuracy and strong dependency on the volume of training data. Recent developments in the AAM field [4, 10, 12], especially the use of individual image patches for analyzing appearance around key shape points [10], represent a significant improvement, allowing for higher accuracy and consideration of local features. This approach makes the model more adaptable to changes in visual information, which is particularly important for tasks requiring detailed image analysis. However, even with this approach, local facial regions cannot be flexible enough as they are encoded by the same set of parameters as the rest of the face. In our research, we use this progress as a basis but propose further improvements through the application of local models for shape and texture. This innovation reduces dependence on the volume of training data and improves the efficiency of facial landmark detection, which is critically important for tasks related to animation creation and face recognition.

## 3 Overview of Active Appearance Models

Active Appearance Models (AAM) represent a comprehensive approach to modeling and interpreting facial visual data, combining statistical modeling of shape and texture. Shape refers to key points that define the contours of the face, while texture reflects visual features such as skin color, wrinkles, and other unique characteristics. The effectiveness of AAM depends on thorough training on a labeled set of images, which allows the model to adapt to new faces with a high degree of accuracy. AAM is actively used for tracking facial landmarks both on individual frames and entire sequences. This section briefly describes the traditional approach to constructing and using AAM.

### 3.1 Models of Shape and Appearance

Shape modeling in AAM is based on representing the facial shape as a set of two-dimensional points, which are defined by the vector $s = (x_1, y_1, x_2, y_2, \ldots, x_n, y_n)^T$. To formulate the shape deformation model, principal components for the training sample are

calculated in advance using PCA [11]. Before the PCA calculation, Procrustes analysis is performed to remove two-dimensional rotation and translation from the shape data. As a result of the PCA calculation, a set of basis vectors is obtained, which are used to formulate the shape model.

The linear variation of shape allows expressing a shape instance s as a linear combination of the basis vectors of shape variations:

$$s = b_0 + \sum_{i=1}^{M} w_i b_i,$$

where $b_0$ is the average shape obtained from the training data set; $b_i$ are the basis shape vectors obtained using PCA on all shapes from the training sample; $w_i$ are shape parameters that control the degree and direction of deformation relative to the average shape; $M$ is the total number of basis vectors.

To ensure the algorithm is invariant to position in the image, two-dimensional rotation and translation are used. These are accounted for in the shape model through affine transformations:

$$s = R(a)(b_0 + \sum_{i=1}^{M} w_i b_i) + t, \tag{1}$$

where $R(a)$ is the rotation matrix for angle $a$, and $t$ is the translation vector.

The texture model of AAM, on the other hand, is modeled similarly to the shape, as a linear combination of texture vectors:

$$V = T_0 + \sum_{i=1}^{N} g_i T_i,$$

where $T_0$ is the average texture; $T_i$ are the basis texture vectors obtained using PCA from all images of the training sample; $g_i$ are texture parameters. It's worth noting that not the entire input image is used, but only that part of the pixels which is directly under the shape points in the training sample [10]. The shape points form a sort of shape mask, from which pixel values are then extracted from the original images.

Very often, the parameters of shape and appearance are combined into a single set of parameters that encodes both models [9]. In the current work, this is not done as it reduces the model's flexibility, even though it simplifies computations.

### 3.2 Model Fitting

The task of fitting the AAM model involves minimizing the difference between the observed image under the synthesized shape and the synthesized image created by the model. This is achieved by optimizing the shape and texture parameters to reduce the difference between the observed image $I$ and the image generated by the model $T$:

$$\min_{w,g,a,t} \{\sum_{\boldsymbol{p} \in s} \|I(s(\boldsymbol{p}; w, a, t)) - V(\boldsymbol{p}; g)\|_2^2\},$$

where $\boldsymbol{p}$ are the pixel coordinates within the shape mask $s$.

This task is a nonlinear parameter optimization, which is solved using methods similar to the Gauss-Newton methods [6]. During the optimization process, a combination of parameters is selected. This combination best reproduces the shape of the face presented in the input image. This is achieved by reducing the differences between the image created based on the training data and the corresponding areas of the original image aligned with the synthesized shape.

## 4 Local Patch Active Appearance Model

This work proposes a local patch active appearance model (LP-AAM). The general scheme of the approach is shown in Fig. 1. This model provides increased accuracy and adaptability when working with detailed facial images, thanks to dividing the shape and appearance model into separate local sections. Such division implies the analysis and modification of each region of the deformation model separately, using individual sets of parameters. This approach allows for a more accurate reflection of local anatomical features and texture details, improving the overall accuracy and adaptability of the model. This section will detail the proposed improvements.

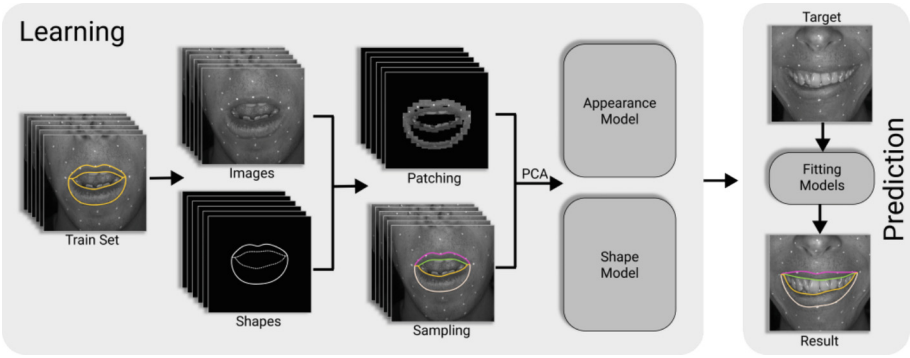


**Fig. 1.** The learning and prediction process using the local patch active appearance model (LP-AAM).

In the first stage of general scheme of the approach, training data in the form of images and shapes are used to create texture patches and region sampling. These data are used to create appearance and shape models. In the next step, the parameters of these models are adjusted to fit the input image, allowing for precise reproduction of the target facial contours.

### 4.1 Modification of Shape and Appearance Models

In LP-AAM, the principal components are determined for each local deformable shape through separate PCA analysis for each segment. This approach provides the modeling of shape with the necessary flexibility to display the unique local features of each face.

Localizing the deformation process of the shape reduces the impact of global changes on individual regions, allowing for detailed definition of each segment.

Shape modeling in LP-AAM occurs through the creation of separate local models for each region. The definition of these local regions is described in Sect. 4.3. The shape $s_j$ for each $j$ local region is defined similarly to the classical approach by formula (1):

$$s_j = R(a)(b_{j0} + \sum_{i=1}^{M} w_{ji} b_{ji}) + t.$$

It's important to note that now each local region has its own set of parameters, including its basis vectors. The exception is the parameters responsible for affine transformations, which remain common for all local regions. The final shape is formed as a union of shapes from individual local regions $s = [s_0, s_1, \ldots, s_j]$. Similarly, the shape parameters $w = [w_0, w_1, \ldots, w_j]$ are concatenated. Such shape modeling allows for defining the shape of the lower lip completely independently from the upper lip. However, this does not entirely correspond to anatomy, as both lips are connected to each other. Without considering this feature, topological discontinuities would occur at the junctions of two different local regions. To address this problem, an additional smoothness energy function for adjacent local regions is introduced, which must be considered when fitting the model:

$$E_{smooth} = \sum_{j \in J} \sum_{f \in F_j} l \left\| w_j - w_f \right\|_2^2,$$

where $J$ is the set of all local regions; $F_j$ is the set of all adjacent local regions for $j$ region; $l$ is the weight regulating the degree of similarity between adjacent regions, with its value as 1.

This additional energy function helps control the flexibility of the deformation model. With a sufficiently large weight, the solution will approach global linear blending. Therefore, the parameter l becomes a hyperparameter that needs to be adjusted depending on the situation.

The appearance model undergoes similar changes for the transition to the local version:

$$V_j = T_{j0} + \sum_{i=1}^{N} g_{ji} T_{ji}.$$

The final $V$ and $g$ are obtained by concatenating the local $V_j$ and $g_j$, respectively. Based on empirical experiments, it was found that the smoothness energy for the appearance model is redundant. For achieving smoothness, its presence is only necessary for the shape model. Therefore, to reduce computations, it is not introduced.

Another significant improvement is using patches around the shape points, as described by Tzimiropoulos and Pantic [10], which reduces computational volume and increases flexibility. This method requires only changes to the preliminary image processing.

### 4.2 Model Fitting Changes

The process of determining model parameters through solving the optimization task remains similar to that of classical AAM. However, in this paper, the mentioned smoothness energy function is added to the task:

$$\min_{w,g,a,t}\{\sum_{\boldsymbol{p}\in s}\|I(s(\boldsymbol{p};w,a,t))-V(\boldsymbol{p};g)\|_2^2+\sum_{j\in J}\sum_{f\in F_j}l\left\|w_j-w_f\right\|_2^2\}.$$

Images generated by the appearance model, constructed based on PCA, turn out too blurry, which prevents the shape model from capturing fine details. A significant improvement in the fitting process is the use of $l_1$ normalization of appearance parameters, allowing for the avoidance of PCA in calculating the appearance basis [11]. This work proposes the use of such an improvement:

$$\min_{w,g,a,t}\{\sum_{\boldsymbol{p}\in s}\|I(s(\boldsymbol{p};w,a,t))-V(\boldsymbol{p};g)\|_2^2+\sum_{j\in J}\sum_{f\in F_j}l\left\|w_j-w_f\right\|_2^2+e\|g\|_1\},$$

where $e$ is the regularization weight, which determines the importance of regularization in the optimization process, with its value as 0.1. This task is nonlinear and is solved using the Gauss-Newton algorithm with the IRLS method [13].

### 4.3 Division into Local Regions

Dividing into local areas is a fundamental stage for adjusting the model according to shape and texture. Optimal division of the shape into local segments provides the model with the necessary flexibility and adaptability; however, excessive detailing can negatively affect the quality of reproduction. Overly fine segmentation can lead to a type of overfitting, where the shape and appearance model will be able to describe views that are too different from those of the given actor. It is important to find a balance between fine division and maintaining the naturalness and integrity of the model, requiring careful analysis and experimentation.

In the context of our research, the division into local areas is performed manually, unlike automatic methods such as the Dijkstra algorithm. The choice of a manual method is driven by the desire for maximum control over the process and achieving high anatomical accuracy. This approach allows for detailed adaptation of the model to the specifics of the target object, for instance, dividing the lips into separate areas for more accurate modeling of their shape and texture.

## 5 Experiments

This section evaluates the effectiveness of the developed LP-AAM algorithm by comparing it with the approach based on using P-AAM patches, which is currently one of the most advanced models. Existing open datasets often contain insufficiently accurate annotations and data from different individuals. Therefore, a custom dataset was compiled for testing, allowing for the verification of the algorithm's accuracy for each individual actor with maximum precision. This is the most important metric for AAM in the context of facial animation for a specific actor.

Video sequences obtained from five different individuals were used to test both approaches. It is important to emphasize that this approach demonstrates the use of AAM for tracking lip contours, which is crucial for subsequent animation creation. Despite this, the algorithm is fully applicable to any facial landmarks. Moreover, it is crucial to achieve the most accurate tracking possible, hence the focus shifts towards fully personalized training for a specific actor. This means that the training data of different actors do not overlap. The data were recorded using cameras mounted on helmets designed for capturing actor performance. Each of the participating actors demonstrated the same set of emotions, also known as the "range of motion." For each participant, 30 key frames were annotated, which were then used as the training dataset. Examples of some of these frames are shown in Fig. 2.

It is important to note that the algorithm's operation is considered in the context of the overall task of facial animation capture. The algorithm is trained on keyframes of the sequence and then applied to the remaining frames. This eliminates the need for additional data augmentation, as the data for training and application are of the same nature.

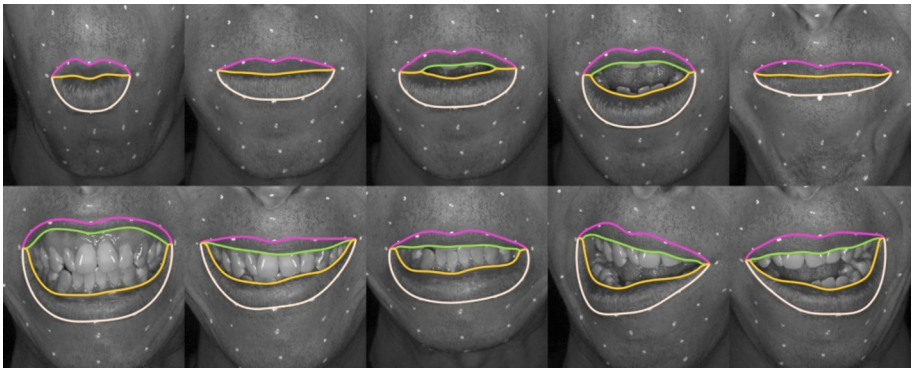

**Fig. 2.** A selection of annotated examples from the training sample.

The effectiveness of the algorithms was evaluated based on the photometric error obtained during the optimization process. This metric allowed for comparing the accuracy of P-AAM and LP-AAM. The comparison results are presented in Fig. 3. The LP-AAM algorithm demonstrated increased accuracy, which is explained by a more flexible mechanism for modeling deformations. An important advantage of the new approach is also that achieving a satisfactory level of accuracy requires fewer training examples compared to traditional models. This is confirmed by the data presented in Fig. 3: to approach the accuracy of the model using 30 frames in the training sample, only 12 frames are needed. Thus, the volume of work required for preparation and data processing is significantly reduced.

For the initialization of the starting shape model in both cases, a pre-trained facial landmark detector from the dlib library was used, providing a starting point for further optimization of the algorithms.

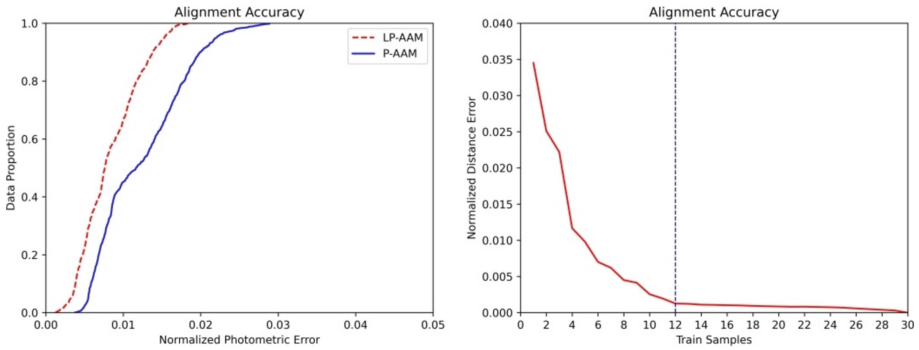


**Fig. 3.** The accuracy of the proposed LP-AAM approach. On the left - the accuracy dependency on photometric error, on the right - the impact of the number of training examples on the error.

Testing was conducted on a system with an Intel Core i7-8700K processor and 48 GB of RAM. The algorithm was implemented in C++ using a custom differentiation framework. Computation was parallelized across frames. The average processing time per frame is 1.32 s.

The experimental results confirm that the developed LP-AAM algorithm enhances accuracy and efficiency in analyzing and processing video data for actor performance capture, especially with limited training data. These qualities make it a promising tool for further research and application in computer vision and machine learning.

## 6 Conclusion

This article introduces a local patch-based active appearance model (LP-AAM) to enhance the accuracy and adaptability of active appearance models for complex image processing. By employing localized texture patches and local piecewise-linear shape models, LP-AAM overcomes the limitations of traditional AAMs, significantly improving detailed facial image processing.

Experimental results demonstrate the superiority of LP-AAM in accuracy and efficiency, expanding the applicability of AAMs for high-precision and adaptable tasks like digital animation and face recognition. The advancements in LP-AAM offer new research and practical application prospects, providing a powerful tool for generating accurate training data for neural networks.

## References

1. Chandran, P., Bradley, D., Gross, M., Beeler, T.: Attention-driven cropping for very high resolution facial landmark detection. In: 2020 IEEE/CVF Conference on Computer Vision and Pattern Recognition (CVPR), Seattle, WA, USA, pp. 5860–5869. IEEE (2020). https://doi.org/10.1109/CVPR42600.2020.00590
2. Cootes, T.F., Edwards, G.J., Taylor, C.: Active appearance models. IEEE Trans. Pattern Anal. Mach. Intell. **23**, 681–685 (2001). https://doi.org/10.1109/34.927467

3. Danecek, R., Black, M.J., Bolkart, T.: EMOCA: emotion driven monocular face capture and animation. In: 2022 IEEE Conference on Computer Vision and Pattern Recognition (CVPR), pp. 20279–20290. IEEE (2022). https://doi.org/10.1109/CVPR52688.2022.01967
4. Gonzalez-Mora, J., De la Torre, F., Murthi, R., Guil, N., Zapata, E.: Bilinear active appearance models. In: 2007 IEEE International Conference on Computer Vision, pp. 1–8. IEEE (2007). https://doi.org/10.1109/ICCV.2007.4409185
5. Huang, Y., Yang, H., Li, C., Kim, J., Wei, F.: ADNet: leveraging error-bias towards normal direction in face alignment. In: 2021 IEEE/CVF International Conference on Computer Vision (ICCV), Montreal, QC, Canada, 2021, pp. 3060–3070. IEEE (2021). https://doi.org/10.1109/ICCV48922.2021.00307
6. Kossaifi, J., Tzimiropoulos, G., Pantic, M.: Fast Newton active appearance models. In: 2014 IEEE International Conference on Image Processing (ICIP), pp. 1420–1424. IEEE (2014). https://doi.org/10.1109/ICIP.2014.7025284
7. Matthews, I., Baker, S.: Active appearance models revisited. Int. J. Comput. Vision **60**, 135–164 (2004). https://doi.org/10.1023/B:VISI.0000029666.37597.d3
8. Prados-Torreblanca, A., Buenaposada, J.M., Baumela, L.: Shape preserving facial landmarks with graph attention networks. In: 33rd British Machine Vision Conference 2022 (BMVC), London, UK, 21–24 November 2022. BMVA Press (2022). https://doi.org/10.48550/arXiv.2210.07233
9. Tzimiropoulos, G., Pantic, M.: Fast algorithms for fitting active appearance models to unconstrained images. Int. J. Comput. Vision **122** (2017). https://doi.org/10.1007/s11263-016-0950-1
10. Tzimiropoulos, G., Pantic, M.: Gauss-Newton deformable part models for face alignment in-the-wild. In: 2014 IEEE Conference on Computer Vision and Pattern Recognition (CVPR), Columbus, OH, USA, pp. 1851–1858. IEEE (2014). https://doi.org/10.1109/CVPR.2014.239
11. Watson, D., Johnston, A.: A PCA-based active appearance model for characterising modes of spatiotemporal variation in dynamic facial behaviours. Front. Psychol. **13**, 880548 (2022). https://doi.org/10.3389/fpsyg.2022.880548
12. Wilms, M., Handels, H., Ehrhardt, J.: Representative patch-based active appearance models generated from small training populations. In: Descoteaux, M., Maier-Hein, L., Franz, A., Jannin, P., Collins, D., Duchesne, S. (eds.) MICCAI 2017. LNCS, vol. 10433, pp. 152–160. Springer, Cham (2017). https://doi.org/10.1007/978-3-319-66182-7_18
13. Zhao, X., Shan, S., Chai, X., Chen, X.: Locality-constrained active appearance model. In: Lee, K.M., Matsushita, Y., Rehg, J.M., Hu, Z. (eds.) ACCV 2012. LNCS, vol. 7724, pp. 636–647. Springer, Heidelberg (2013). https://doi.org/10.1007/978-3-642-37331-2_48

# Robust Estimation of Stochastic Data in Machine Learning Systems

Agop E. Khatlamadzhiyan[1], Sergey V. Sokolov[2], Irina V. Reshetnikova[2(✉)], and Olga I. Sokolova[3]

[1] JSC NIIAS, Moscow, Russia
[2] Moscow Technical University of Communications and Informatics, Moscow, Russia
irina_reshetnikova@mail.ru
[3] Rostov State University of Railway Transport, Rostov-on-Don, Russia

**Abstract.** The instability of algorithms for filtering input data, usually stochastic, to the a priori uncertainty of their probabilistic characteristics is a serious problem of machine learning. Since such uncertainty occurs in a huge number of cases of developing and applying of artificial intelligence systems (in particular, when using streaming learning, preparing data for training, and evaluating models), the problem of ensuring accuracy and stability of algorithms for evaluation of stochastic data with unknown statistical characteristics for machine learning systems is one of the most urgent. The existing methods of nonlinear filtering in a general formulation do not allow to solve this problem. In this connection, the paper proposes a method of robust stochastic filtering, oriented to the processing of discrete data in machine learning systems. The method allows to perform dynamic estimation of a nonlinear discrete stochastic vector of state perturbed by correlated noise with an unknown probability distribution belonging to the class of distributions with limited second moments (mean squares). At the same time, the observation of this vector is also carried out in conditions of interference with unknown probabilistic characteristics. The robust estimation algorithm is synthesized by minimizing a new criterion that depends on the nonlinear measurement residual function determined by the class of the measurement noise distribution function and takes into account the correlation of state vector disturbances. In contrast to the currently developed nonlinear filtering algorithms, the proposed method does not involve knowledge of the laws of probability distributions of state vector disturbances and measurement interference, but only their belonging to a certain class of distributions At the same time, its computational implementation requires significantly less computations compared to the known nonlinear filtering methods due to the coincidence of the dimensionality of the obtained filter with the dimensionality of the estimated state vector. Such advantageous features of the developed method provide the possibility of its effective practical application in processing under uncertainty of input data of artificial intelligence systems used in various technical systems - information and control, measurement, info-communication, navigation, avionics systems and others.

**Keywords:** machine learning · stochastic discrete state vector · class of probability distributions · robust filtering


S. Kovalev et al. (Eds.): IITI 2024, LNNS 1209, pp. 227–233, 2024.
https://doi.org/10.1007/978-3-031-77688-5_22

## 1 Introduction

To date, the vast majority of recurrent machine learning methods for discrete systems (stream learning, training data preparation, model evaluation, etc.) are based on the use of various modifications of the discrete Kalman filter [1, 2]. But, as is known, the effective application of this "learning-evaluation" scheme is possible only if the probability characteristics of both perturbations of the state vector of the observed stochastic system and interference with its measurement are accurately determined a priori. At the same time, real robotic, information-measuring, and other systems operate, as a rule, under conditions of disturbances, the probability distributions of which are either a priori unknown, or, at best, known approximately (and still change randomly in the process of operation) [3–7]. Such difficulties led to the impossibility of applying the traditional Kalman scheme and determined the problem of developing new "learning-evaluation" methods that are resistant to the uncertainty of the probabilistic characteristics of model perturbations. Attempts to solve this problem have led to the creation of numerous modifications of discrete filters using various compensatory algorithms: the introduction of empirical scaling of the a posteriori covariance matrix, the use of various functional transformations of the measurement interference dispersion matrix [8–13], the expansion of the dimension of the state vector [14], etc. The obvious disadvantages of such approaches are the heuristic choice of scale coefficients or algorithms for their determination, the difficulty (or impossibility) of taking into account the correlation properties of perturbations of the estimated model, as well as a significant amount of calculations when implementing the estimation procedure. Such limitations of existing methods lead to the need to develop new discrete filtering algorithms [15–17], which provide both the possibility of stable (robust) estimation of the state vector under conditions of uncertainty in the probabilistic characteristics of object disturbances and interference from its observer, and reduce the cost of computational implementation. Below we consider one of the possible approaches to solving this problem.

## 2 Problem Statement

A dynamic discrete model, вектор состояния whose state vector $X_k$ is subject to estimation is described by a stochastic difference equation of the form:

$$X_k = f(X_{k-1}, k) + f_0(X_{k-1}, k)W_{k-1}, \tag{1}$$

where $f(X_{k-1}, k), f_0(X_{k-1}, k)$ – are the known vector and matrix functions of dimension, respectively, $N$ and $N \times M$,

$W_{k-1}$ – a vector of correlated perturbations of dimension $M$, whose components have a probability distribution density $p$, which belongs to the class of distributions with bounded second moments (mean squares: $\int_{-\infty}^{\infty} w^2 \rho(w) dw \prec \infty$) [18].

The state vector (1) is observed using the following measurements:

$$z_k = C_k X_k + V_k, \tag{2}$$

where $z_k =$ is the measurement vector of dimension $K$,

$C_k$ – the observation matrix of dimension $K \times N$,

$V_k$ – and the interference vector of dimension $K$, whose components have a probability distribution density defined in the class of distributions with bounded second moments [18].

Based on the above considerations, $\hat{X}_k$ we will further look for an estimate of the state vector $X_k$ as an estimate that guarantees the best accuracy of estimation in the minimax sense (i.e., minimizing estimation errors in the most unfavorable situation determined by a given distribution class).

## 3 Synthesis of a Robust Filtering Algorithm

Before a detailed review of the proposed method, we will briefly formulate the main stages of its development:

- at the first stage, the model estimation equation is formed in a recurrent form,
- at the second stage, a criterion for optimal estimation is formulated from the condition of ensuring a minimum of errors in model estimates for the most unfavorable class of distribution of disturbing effects (i.e., from the condition of robustness of the estimate),
- at the third stage, from the optimality condition of this criterion, a correction function is determined in a recurrent form, which provides robust properties of the model evaluation,
- at the fourth and final stage, the found correction function is substituted into the model estimation equation and after a series of matrix transformations, the desired robust discrete stochastic filter is finally formed.

Let us further consider the above stages in more detail.

Based on the form of Eq. (1), we will search for the desired estimate in the following recurrent form:

$$\hat{X}_k = f(\hat{X}_{k-1}, k) + f_0(\hat{X}_{k-1}, k)\ U_k(\hat{X}_{k-1}, z_k, k), \tag{3}$$

where $U_k(\hat{X}_{k-1}, z_k, k)$ is a vector function determined from the condition for ensuring the robustness of the estimate (3), i.e., the minimum of estimation errors for the most unfavorable class of measurement interference distribution.

Due to the assumption that the distribution density of the measurement interference vector belongs to the class of distributions with bounded second moments, we define the form of the minimized objective function as quadratic: $[z_k - C_k\hat{X}_k]^T[z_k - C_k\hat{X}_k]$ [18]. Then, taking into account the correlation of the object's noise, as well as its distribution function belonging to the class of distributions with bounded second moments, we formulate the minimax optimality criterion $J$ in the following form:

$$\begin{gathered} J_k = [z_k - C_k\hat{X}_k]^T[z_k - C_k\hat{X}_k] + \alpha U_k(\hat{X}_{k-1}, z_k, k)^T U_k(\hat{X}_{k-1}, z_k, k) \\ +\beta \cdot \Delta U_k(\hat{X}_{k-1}, z_k, k)^T \Delta U_k(\hat{X}_{k-1}, z_k, k), \\ \Delta U_k(\hat{X}_{k-1}, z_k, k) = U_k(\hat{X}_{k-1}, z_k, k) - U_{k-1}(\hat{X}_{k-2}, z_{k-1}, k-1), \end{gathered} \tag{4}$$

$\alpha = \text{const}$, $\beta = \text{const}$ - regularization parameters that ensure adaptation to specific operating conditions of the dynamic system.

To further define the desired function $U(\hat{X}_{k-1}, z_k, k)$, we differentiate $J_k$ (4) by $U_k$:

$$\begin{aligned}\frac{dJ_k}{dU_k} &= -\frac{d([z_k - C_k\hat{X}_k]^T[z_k - C_k\hat{X}_k])}{d[z_k - C_k\hat{X}_k]} C_k \frac{d\hat{X}_k}{dU_k} + 2\alpha U_k(\hat{X}_{k-1}, z_k, k)^T \\ &\quad + 2\beta[U_k(\hat{X}_{k-1}, z_k, k) - U_{k-1}(\hat{X}_{k-2}, z_{k-1}, k-1)]^T \\ &= -2[z_k - C_k\hat{X}_k]^T C_k f_0(\hat{X}_{k-1}, k) + 2(\alpha+\beta)U_k(\hat{X}_{k-1}, z_k, k)^T \\ &\quad -2\beta U_{k-1}(\hat{X}_{k-2}, z_{k-1}, k-1)^T,\end{aligned}$$

and equate the resulting expression to 0:

$$\begin{aligned}&(z_k - C_k\hat{X}_k)^T C_k f_0(\hat{X}_{k-1}, k) + \beta U_{k-1}(\hat{X}_{k-2}, z_{k-1}, k-1)^T \\ &= (\alpha+\beta)U_k(\hat{X}_{k-1}, z_k, k)^T\end{aligned}$$

From the obtained equality, we finally determine the recurrent function $U(\hat{X}_{k-1}, z_k, k)$:

$$\begin{aligned}&U_k(\hat{X}_{k-1}, z_k, k) \\ &= \tfrac{1}{\alpha+\beta} f_0(\hat{X}_{k-1}, k)^T C_k^T (z_k - C_k\hat{X}_k) + \tfrac{\beta}{\alpha+\beta} U_{k-1}(\hat{X}_{k-2}, z_{k-1}, k-1)\end{aligned}$$

Substituting the found expression $U_k$ into the estimation Eq. (3), we have:

$$\begin{aligned}&\hat{X}_k = f(\hat{X}_{k-1}, k) + \tfrac{1}{\alpha+\beta} f_0(\hat{X}_{k-1}, k) f_0(\hat{X}_{k-1}, k)^T C_k^T z_k \\ &-\tfrac{1}{\alpha+\beta} f_0(\hat{X}_{k-1}, k) f_0(\hat{X}_{k-1}, k)^T C_k^T C_k \hat{X}_k + \tfrac{\beta}{\alpha+\beta} f_0(\hat{X}_{k-1}, k) U_{k-1}(\hat{X}_{k-2}, z_{k-1}, k-1)\end{aligned} \tag{5}$$

Since the right-hand side of the resulting equation depends on the current estimate $\hat{X}_k$, for the final determination $\hat{X}_k$, we transform Eq. (5) as follows:

$$\begin{aligned}&(E + \tfrac{1}{\alpha+\beta} f_0(\hat{X}_{k-1}, k) f_0(\hat{X}_{k-1}, k)^T C_k^T C_k)\hat{X}_k \\ &= f(\hat{X}_{k-1}, k) + \tfrac{1}{\alpha+\beta} f_0(\hat{X}_{k-1}, k) f_0(\hat{X}_{k-1}, k)^T C_k^T z_k \\ &+ \tfrac{\beta}{\alpha+\beta} f_0(\hat{X}_{k-1}, k) U_{k-1}(\hat{X}_{k-2}, z_{k-1}, k-1),\end{aligned}$$

where $E$ is a unit matrix of dimension $N$,

from where we finally have the desired robust discrete stochastic filter:

$$\begin{aligned}\hat{X}_k &= (E + \tfrac{1}{\alpha+\beta} f_0(\hat{X}_{k-1}, k) f_0(\hat{X}_{k-1}, k)^T C_k^T C_k)^{-1} (f(\hat{X}_{k-1}, k) \\ &\quad + \tfrac{1}{\alpha+\beta} f_0(\hat{X}_{k-1}, k) f_0(\hat{X}_{k-1}, k)^T C_k^T z_k \\ &\quad + \tfrac{\beta}{\alpha+\beta} f_0(\hat{X}_{k-1}, k) U_{k-1}(\hat{X}_{k-2}, z_{k-1}, k-1)),\end{aligned}$$

$$\begin{aligned}&U_{k-1}(\hat{X}_{k-2}, z_{k-1}, k-1) \\ &= \tfrac{1}{\alpha+\beta} f_0(\hat{X}_{k-2}, k-1)^T C_{k-1}^T (z_{k-1} - C_{k-1}\hat{X}_{k-1}) + \tfrac{\beta}{\alpha+\beta} U_{k-2}(\hat{X}_{k-3}, z_{k-2}, k-2)\end{aligned} \tag{6}$$

It should be emphasized here that the obtained estimate (6), being optimal by criterion (4) (in contrast to the suboptimal modifications of Kalman schemes mentioned above), guarantees a minimum of errors in estimating the model with the most unfavorable class of noise distribution – i.e., the stability of the evaluation procedure in the minimax sense.

In addition to its robust properties, an important advantage of the resulting filter is its dimension, which coincides with the dimension of the estimated state vector and is minimal for this type of filtering schemes.

To evaluate the efficiency of the obtained filter, the following numerical experiment was performed.

## 4 Example

When testing a liquid heat exchanger, the temperature change of the coolant flow recorded in time by a digital temperature sensor in increments $\tau = 0.01$ s of:

$$z_k = T_k + W_k,$$

where $T_k$ is the temperature of the coolant at the $k$-th moment of time,

$Wk_k$ - measurement noise at the $k$-th time point with chi-square distribution density with mathematical expectation $m = 2$ and variance $D = 4$,

it is described by an ideal mixing model, taking into account heat transfer, which has the form:

$$T_k = T_{k-1} + \tau \frac{v}{V}(T_{in} - T_{k-1}) + \tau \frac{RF}{V\rho C}\Delta T_{k-1},$$

where $V$ - is the mixing flow volume ($m^3$); $v$ - is the volumetric flow velocity ($m^3/s$);

ρ – is the coolant density ($kg/m^3$); $C$ - is the specific heat capacity of the coolant ($J/(kg\ °C)$); $F$ - is the heat transfer surface ($m^2$); $R$ - is the heat transfer coefficient ($W/(^{m2}\ °C)$); $\Delta T_k$ - is a random correlated temperature difference between heat carriers at $k$-time point with a chi-square distribution with mathematical expectation $M_{\Delta T} = 5$ and dispersion $D_{\Delta T} = 10$; $T_{in}$ - is the inlet flow temperature (°C).

During numerical simulation, the values of the specified technical parameters were chosen equal to the following for the heat exchanger under study and the temperature sensor used:

$V = 8.5$; ρ = 1000; $C = 4200$; $v = 0.4$; $F = 32.6$; $R = 8500$; $T_{in} = 80$.

The temperature change in the coolant flow was estimated over a time interval of [0, 1000] *seconds* using a discrete Kalman filter

$$\hat{T}_i = (1 - \tau\frac{v}{V})\hat{T}_{i-1} + \tau\frac{v}{V}T_{in} + M_{\Delta T}\tau\frac{RF}{V\rho C} + \{(1 - \tau\frac{v}{V})^2 P_{i-1}$$
$$+(\tau\frac{RF}{V\rho C})^2 D_{\Delta T}\}\left((1 - \tau\frac{v}{V})^2 P_{i-1} + (\tau\frac{RF}{V\rho C})^2 D_{\Delta T} + D\right)^{-1}\left(z_i - m - (1 - \tau\frac{v}{V})\hat{T}_{i-1}\right), \quad (7)$$
$$P_i = \left(E - \{(1 - \tau\frac{v}{V})^2 P_{i-1} + (\tau\frac{RF}{V\rho C})^2 D_{\Delta T}\}\left((1 - \tau\frac{v}{V})^2 P_{i-1} + (\tau\frac{RF}{V\rho C})^2 D_{\Delta T} + D\right)^{-1}\right)$$
$$\times\{(1 - \tau\frac{v}{V})^2 P_{i-1} + (\tau\frac{RF}{V\rho C})^2 D_{\Delta T}\},$$

and the developed approach - by calculating the robust discrete filter (6) for regularization parameters $\alpha = 0.5$, $\beta = 0.01$:

$$\hat{T}_k = (1 + \frac{1}{0.51}(\tau \frac{RF}{V\rho C})^2)^{-1}(\hat{T}_{k-1} + \tau \frac{v}{V}(T_{ex} - \hat{T}_{k-1}) + \\ + \frac{z_k}{0.51}(\tau \frac{RF}{V\rho C})^2 + \frac{1}{51}\tau \frac{RF}{V\rho C} U_{k-1}(\hat{T}_{k-2}, z_{k-1}, k-1)), \quad (8)$$

$$U_{k-1}(\hat{T}_{k-2}, z_{k-1}, k-1) = \frac{1}{0.51}\tau \frac{RF}{V\rho C}(z_{k-1} - \hat{T}_{k-1}) + \frac{1}{51} U_{k-2}(\hat{T}_{k-3}, z_{k-2}, k-2)$$

A comparative analysis of the estimates obtained from the results of modeling using these methods showed that if the average temperature values practically coincide (the integral difference in the estimates over the entire time interval did not exceed 0,12 °C), the root-mean-square error of the estimate by the discrete Kalman filter turned out to be 4, 2 times higher than the root-mean-square error of the proposed approach. This excess of the root-mean-square error was due to the observed more oscillatory nature of the Kalman estimate compared to the robust one over the entire simulation time. It should also be noted that the computational cost of implementing the Kalman filter is more than twofold higher than the proposed one, which results both from the twice – larger dimension of the filter (7) compared to the filter (8), and from the significantly more complex right-hand side of the filter (7). In the more general case, with the dimension of for a model equal to $N$, the excess of the Kalman filter dimension becomes even more significant. So, taking into account the symmetry of the a posteriori covariance matrix $P$, the dimension of the Kalman filter equations is $(0.5\,N^2 + 1.5\,N)$, which is in $(0.5\,N + 1.5)$ times the dimension of the considered robust filter.

## 5 Conclusion

Thus, the advantageous features of the developed robustic discrete filter are not only the increase of filtering accuracy due to stability to uncertain measurement noise and correlated perturbations of a discrete dynamical system, but also minimal computational costs compared to the Kalman type of filtering schemes, due to its dimension coinciding with the dimension of the estimated state vector. Such advantages make it possible to effectively apply it in various machine learning systems - when using streaming learning, preparing data for training, evaluating models, etc., in the absence of any information about the statistical characteristics of disturbing influences.

## References

1. Tikhonov, V.I., Kharisov, V.N.: Statistical analysis and synthesis of radio engineering devices and systems. Moscow: Radio Commun. 608 p. (2004). (in Russian)
2. Sinitsyn, I.N.: Kalman and Pugachev filters, 640 p. Moscow: Logos Publ., (2006). (in Russian)
3. Ferrero, A., Ferrero, R., Jiang, W., Salicone, S.: The Kalman filter uncertainty concept in the possibility domain. IEEE Trans. Instrum. Meas. **68**, 4335–4347 (2019)

4. Al Bitar, N., Gavrilov, A.: A novel approach for aiding unscented Kalman filter for bridging GNSS outages in integrated navigation systems. Navig. J. Inst. Navig. **68**(3), 521–539 (2021). https://doi.org/10.1002/navi.435
5. Celentano, L., Basin, M.V.: Optimal estimator design for LTI systems with bounded noises disturbances and nonlinearities circuits systems and signal processing. Circuits Syst. Sig. Process. **40**, 3266–3285 (2021). https://doi.org/10.1007/s00034-020-01635-z
6. Jia, C., Hu, J.: Variance-constrained filtering for nonlinear systems with randomly recursive scheme and boundedness analysis occurring quantized measurements. Adv. Differ. Equations **53**, 811 (2019)
7. Dunik, J., Biswas, S.K., Dempster, A.G., Pany, T., Closas, P.: State estimation methods in navigation: overview and application. IEEE A&E Syst. Mag. **12**(35), 16–31 (2020). https://doi.org/10.1109/MAES.2020.3002001
8. Herrera, E.P., Kaufmann, H.: Adaptive methods of Kalman filtering for personal positioning systems. In: 23rd International Technical Meeting of the Satellite Division of the Institute of Navigation 2010, ION GNSS (2010)
9. Langel, S., Crespillo, O.G., Joerger, M.: Overbounding the effect of uncertain Gauss-Markov noise in Kalman filtering navigation. J. Inst. Navig. **68**(2), 259–276 (2021). https://doi.org/10.1002/navi.419
10. Lavaei, A., Soudjani, S., Zamani, M.: Approximate probabilistic relations for compositional abstractions of stochastic systems. In: Zamani, M., Zufferey, D. (eds.) NSV 2019. LNCS, vol. 11652, pp. 101–109. Springer, Cham (2019). https://doi.org/10.1007/978-3-030-28423-7_7
11. Aunsri, N.: Seismic events estimation under noisy environments using multiple model particle filter. In: 15th International Conference on Electrical Engineering. Electronics, Computer, Telecommunications and Information Technology (ECTI-CON), pp. 793–797 (2018). https://doi.org/10.1109/ECTICon.2018.8620047
12. Patent No. 1800588. Adaptive Kalman filter, USSR, N03N 21/00
13. Patent No. 2160496. Modified Kalman filter, RF, H03H 21/00
14. Wang, D., Ly, H., Wu, J.: Augmented Cubature Kalman filter for nonlinear RTK/MIMU integrated navigation with non-additive noise. Measurement. **97**, 111–125 (2017)
15. Asgari, M., Khaloozadeh, H.: Robust extended Kalman filtering for nonlinear systems with unknown input: a UBB model approach. IET Radar Sonar Navig. **14**(11), 1837–1844 (2020). https://doi.org/10.1049/iet-rsn.2020.0258
16. Izanloo, R., Fakoorian, S.A., Yazdi, H.S., Simon, D.: Kalman filtering based on the maximum correntropy criterion in the presence of non-Gaussian noise. In: Annual Conference on Information Science and Systems (CISS), Princeton, USA, vol. 14, pp.500–505 (2016)
17. Miller, B.M., Kolosov, K.S.: Robust estimation based on the least absolute deviations method and the Kalman filter. Autom. Remote Control **81**(11), 1994–2010 (2020)
18. Handbook of Automatic Control Theory / Ed. Krasovsky A. A. M.: Nauka. Chief Editor of physical and mathematical Literature, 712 p. (1987)

# Insurance Claims Fraud Detection Based on Machine Learning

Igor Kotenko[1(✉)], Ghina Özdemir[2(✉)], Mhd Wasim Raed[2(✉)], Ilham Huseyinov[2(✉)], Elena Fedorchenko[1(✉)], and Rafet Akdeniz[2(✉)]

[1] St. Petersburg Federal Research Center of the Russian Academy of Sciences (SPC RAS), St.Petersburg, Russia
{ivkote,doynikova}@comsec.spb.ru
[2] Istanbul Aydin University, Istanbul, Turkey
ghinaozdamir@stu.aydin.edu.tr,
{mhdwasimraed,ilhamhuseyinov,rafetakdeniz}@aydin.edu.tr

**Abstract.** When people or organizations purposefully mislead insurance companies in order to receive benefits or payments to which they are not legally entitled, insurance claims fraud takes place. This kind of fraud can take many different forms with respect to different insurance policies, such as life, health, vehicle, and property insurance. Healthcare insurance claims fraud poses a significant threat to the integrity of healthcare systems worldwide, resulting in substantial financial losses and compromised patient care. In this study the aim is to use machine learning to detect and prevent fraud in healthcare insurance claims. By using Medicare dataset from Kaggle which contains 4 files including inpatient, outpatient, beneficiary and target data, a dataset was created which is a combination of these datasets. The dataset is used for supervised classification problem which classifies the Healthcare Provider weather fraud or not. The model was trained using Logistic Regression, Random Forest, Decision Tree, Support Vector Machine and XGBoost, also the ensemble learning was used to create a more powerful model by combining all the models together. And the feature selection approach was used to improve models performance and to compare the results. It was determined that logistic regression shows the best performance in terms of accuracy, F1-score and AUC score. The SHapley Additive exPlanations which is a model explainability approach is used to interpret the prediction of logistic regression.

**Keywords:** Machine learning · Insurance claims · Explainable AI · SHAP

## 1 Introduction

Health insurance fraud has a long history, originating from the beginning of the industry. The complexity of insurance systems has led to various fraudulent activities, from simple claims falsification to sophisticated schemes involving


S. Kovalev et al. (Eds.): IITI 2024, LNNS 1209, pp. 234–244, 2024.
https://doi.org/10.1007/978-3-031-77688-5_23

collusion and identity theft. Health insurance fraud is a significant issue affecting insurers, healthcare providers, and patients. It increases healthcare costs, reduces eligible claims supply, delays in care, influences the denial of critical medical care coverage, and decreases trust in the healthcare system.

Identifying fraudulent activities in insurance claims necessitates a comprehensive understanding of healthcare payment practices, patient behaviors, and industry regulations. Traditional methods have shown limitations in achieving precise fraud detection [1].

The novelty of the paper lies in the utilization of Machine Learning (ML) algorithms and Explainable Artificial Intelligence (XAI) techniques specifically tailored for insurance claim fraud detection. By employing ML and XAI methodologies, this study aims to delve deeper into the intricacies of fraud detection by leveraging historical data insights and adapting to evolving fraud patterns. Additionally, the implementation of SHAP (SHapley Additive exPlanations) to enhance the interpretability and transparency of the best ML model further distinguishes this research, offering a novel approach to improving fraud detection accuracy and understanding the reasoning behind model predictions. Since the majority of fraud detection systems rely on black-box models, it is even more crucial to look at ways to make these systems' logic and outputs understandable and trustworthy to non-AI experts.

The field of artificial intelligence known as explainable AI (XAI) focuses on translating complex "black-box" AI algorithms and system outputs into easily understood representations. Alternatively, it uses so-called "white-box" AI algorithms that rely on naturally explicable and straightforward models [7]. SHapley Additive exPlanations (SHAP) is one of the most well-known methods for elucidating specific predictions made by black-box classifiers. This algorithm focuses on comprehending the logic underlying every prediction. It sheds light on the relative contributions of distinct attributes to a prediction by varying a specific data point and monitoring the impact on the classifier's output.

The aim of this study is to develop and implement ML algorithms for the detection of healthcare insurance claims fraud. By leveraging advanced analytical techniques, and using SHAP to understand the ML models in fraud detection processes, thereby mitigating financial losses and preserving the integrity of insurance systems.

The contributions of this study are as follows: (1) use ML and XAI techniques in the field of insurance claim fraud detection to get background information and understand how the model works and why the model is making certain predictions; (2) implement SHAP to the best ML method to help detect fraud; (3) use SHAP plots in insurance claims fraud detection to provide a clear understanding of the factors influencing a model's predictions by visualizing the impact of each feature on individual predictions; (4) use Ensemble Learning that combines multiple individual models to create a more powerful model that can make better predictions.

The rest of the paper is organized as follows. Section 2 provides a literature review. Section 3 shows the applied methodologies. Section 4 describes the results

and gives the discussion. Section 5 reviews the model explainability. Section 6 summarizes everything by conclusion and future work.

## 2 Literature Review

A comparative analysis of several classification algorithms, including Multi-Layer Perceptron (MLP), Naïve Bayes (NB), Linear Regression (LR), K-Nearest Neighbor (KNN), Adaboost, Decision-Tree (DT), Random-Forest (RF), and Support Vector Machine (SVM), is conducted in a paper [3] in order to identify insurance fraud. The precision, recall, and F1-score performance indicators are used to evaluate how effective the algorithms are. According to the classification algorithm comparison results, DT provides the highest accuracy of 79% when compared to the other methods. Furthermore, Adaboost displays an accuracy of 78%, which is nearer the DT.

The study [4] demonstrates an efficient method for identifying Medicare fraud using the LEIE database and random under-sampling. They found that combining RUS with existing fraud markers is effective in identifying dishonest Medicare doctors. The C4.5 model demonstrated the best learning ability, with an AUC of 0.883 and the lowest false negative rates. J. M. Johnson and T. M. Khoshgoftaar in [9] developed two new datasets for supervised learning using CMS Part B Summary by Provider datasets. They compared these datasets to a baseline dataset and found that the suggested provider summary attributes are effective in detecting healthcare fraud. When applied to existing datasets, these additional characteristics significantly improved fraud detection performance, according to a two-way analysis of variance test and 95% confidence intervals. Herland et al. use Part D, Part B, and DMEPOS CMS databases in [5] to investigate Medicare fraud detection. After merging the three datasets to produce a fourth, they examined data processing. Part B with LR at 0.805 and the Combined dataset with Logistic Regression learner at 0.816 obtained the greatest overall scores. To identify fraudulent activity when a physician submits payments across all Medicare sections, they recommend using the Combined dataset.

Yingchao Ji's study [7] aimed to evaluate XAI techniques for credit card fraud detection using a synthetic dataset. DNN and RF were selected due to their previous results. The DNN model performed marginally better than the RF model, with 96.84% accuracy. The study also assessed explainability using LIME and SHAP, with LIME outperforming SHAP slightly. Further research is recommended to improve explainability and data preprocessing. A study [2] compared supervised and unsupervised learning techniques for detecting insurance fraud. They found that unsupervised learning is effective, especially in isolated forests, while supervised learning works well. Both methods can identify new false claims, depending on the input data. The study recommends seeing supervised and unsupervised techniques as complements rather than alternatives when implementing fraud detection techniques. The SHAP analysis confirms that distinct features are prioritized by both techniques in identifying claim fraud.

In this paper, the model explainability methodology SHAP is used to offer a novel approach for enhancing the efficacy of fraud detection in insurance claims.

By leveraging SHAP, it offers a fresh perspective on the decision-making process involved in complicated machine learning models' detection of fraud.

## 3 Methodologies

In this section the selected dataset, used data preprocessing methods, and machine learning models are described.

**Dataset Overview.** The selected dataset contains [11] 4 CSV files for training and testing comprising the Medicare dataset, which is available on Kaggle. These files take into account the beneficiary information of each provider as well as their outpatient and inpatient claims. The Inpatient data includes claims information for hospitalized patients. Outpatient data claims information for patients who were merely hospital visitors. Beneficiary details include beneficiary KYC information and target data including provider numbers and the potential fraudulent status for beneficiaries.

**Data Preprocessing.** Data preprocessing is crucial for ML algorithms as it helps clean, transform, and organize raw data, ensuring it is suitable for analysis and modeling.

*EDA Findings.* The exploratory data analysis (EDA) revealed several findings, including class imbalance, which refers to an unbalanced distribution of cases. To maintain predictive accuracy for both classes, the model did not favor the majority class. The imbalance between fraud and noun fraud cases in the target variable, with over 90% being non-fraud providers and less than 10% being fraud providers, caused detection issues. The SMOTE technique was used to address this imbalance.

*Dataset Merging.* There were 4 datasets in the healthcare datasets. They were integrated to obtain the final dataset. First, the inpatient and outpatient data were combined using the same columns, and then this dataset was combined with the beneficiary data using BeneID. To obtain the final result, this dataset was combined with provider data using the provider ID.

*Convert Categorical Data to Numeric Data.* Label encoding is widely used as an encoding method for categorical values. With this technique, each tag is given a unique integer based on alphabetical order. By using this technique, the Potential Fraud target feature was converted from ['yes', 'no'] to [0, 1].

*Handle Missing Values.* The missing values for some features in the dataset were filled with zeros by using fillna(0).

*Feature Engineering.* Feature engineering is a crucial stage in machine learning, transforming raw data to improve performance. Effective feature engineering leads to higher predictive capacity. The groupby function, used in this research,

simplifies data aggregation and categorizes data, especially useful for tabular data. Its numerous permutations make it powerful.

*Data Normalization.* StandardScaler is a data preprocessing method in ML that standardizes numerical features to a range of 0 to 1, ensuring they have zero mean and unit variance. This method improves model performance by ensuring features are on a similar scale, preventing biased outputs, and allowing equal learning from each feature.

**Machine Learning Models.** In health insurance claims fraud detection, various ML models such as LR, RF, DT, SVM, and XGBoost can provide detailed insights. LR excels in vulnerability and interpretation, making it the go-to choice for basic models. RF provides robustness against overfitting and handles high-level information efficiently. DT provide intuitive decision-making processes, which allow fraud patterns to be detected. SVM excels in handling complex data classifications and is particularly useful in cases with nonlinear decision boundaries. Finally, XGBoost emerged for its exceptional predictive performance and ability to efficiently handle big data. By leveraging the strengths of these models, health insurers can develop a multi-pronged approach to detecting fraudulent providers by improving the accuracy and precision of all fraud detection.

The motivation behind utilizing classical machine learning methods such as Logistic Regression, Random Forest, Decision Tree, Support Vector Machine, and XGBoost for Insurance Claims Fraud Detection instead of more novel approaches lies in their interpretability which is the aim of this study by using XAI to understand the ML models, established track record of performance across various domains, and robustness in handling structured data. Classical methods are well-understood, making it easier to explain the reasoning behind predictions to stakeholders, regulators, and end-users in the insurance industry where interpretability and transparency are crucial. Additionally, these traditional models have been extensively studied and proven effective as in detecting fraud patterns in historical data, as well as in other applications developed by the authors [12,13] providing a reliable baseline for comparison.

Because there are 5 ML models, it was decided to use Ensemble learning which is a ML technique that combines multiple individual models to create a more powerful model that can make better predictions. Hard and soft voting are types of ensemble learning methods used in the context of combining multiple models for classification tasks.

*Feature Selection.* The feature importance approach assigns numerical values to input features in a model, determining their importance. A higher value indicates a specific feature's greater impact on the model used to predict a variable. We applied the important features for each of the 5 ML models after the feature significance approach was applied to each model. The models were retrained using these features to observe the impact of training only the crucial features present in the entire dataset. Then we compare the results when we use feature selection and when we use the whole data.

## 4 Results and Discussion

Evaluation metrics like accuracy, precision, recall, F1-score, AUC score, and ROC curve are used to evaluate how well ML models perform in this study. The results of all used ML models are shown in Table 1. According to the evaluation metrics results, LR has the highest accuracy, F1-score, and AUC score among all ML models. SVM produces the best results in recall, whereas random forest produces the best results in precision. And based on its output, we may observe that the decision tree performs the least well.

**Table 1.** Evaluation metrics of ML models.

| ML model | Accuracy | Precision | Recall | F1-score | AUC score |
|---|---|---|---|---|---|
| Logistic Regression | 91.2 | 50.9 | 75.2 | 60.7 | 92.4 |
| Random Forest | 91.1 | 51.2 | 69.8 | 59.1 | 92.1 |
| Decision Tree | 86.7 | 42.5 | 67.1 | 50.1 | 87.1 |
| SVM | 89.8 | 47.7 | 79.9 | 59.9 | 91.2 |
| XGBoost | 90.8 | 49.8 | 68.5 | 57.6 | 92.5 |

In Table 2 hard vote and soft vote which are methods to combine all ML models achieve high accuracy rates of around 90.8% to 90.9%. However, soft vote tends to have better precision and F1-score compared to hard vote, while maintaining similar recall and AUC scores.

**Table 2.** Hard and soft voting results.

| ML model | Accuracy | Precision | Recall | F1-score | AUC score |
|---|---|---|---|---|---|
| Hard Vote | 90.8 | 50.0 | 72.4 | 59.2 | 82.6 |
| Soft Vote | 90.9 | 52.2 | 72.4 | 59.3 | 82.6 |

Table 3 shows all the models, especially the decision tree model, perform noticeably better when feature selections are used. However, when it comes to feature selection, random forest, and logistic regression do not yield better results.

In the ROC curve in Fig. 1, the AUC score goes from 0 to 1, with 1 indicating perfect classification and 0.5 indicating that the model is not superior to a random one. The True Positive Rate (TPR) and the False Positive Rate (FPR) demonstrate how the classifiers behave for each threshold.

The results of the study revealed that Logistic Regression (LR) emerged as the most effective fraud detection model for health insurance claims, showcasing a good accuracy of 91.2%, an F1-score of 60.7%, and an AUC score of 92.4%. LR's

**Table 3.** Evaluation assessments of ML models with feature selection

| ML model | Accuracy | Precision | Recall | F1-score | AUC Score |
|---|---|---|---|---|---|
| Logistic Regression | 87.2 | 41.4 | 72.5 | 51.9 | 90.8 |
| Random Forest | 90.9 | 50.2 | 69.1 | 58.2 | 92.5 |
| Decision Tree | 89.8 | 46.4 | 68.5 | 53.3 | 88.8 |
| SVM | 91.2 | 46.8 | 77.1 | 67.2 | 92.3 |
| XGBoost | 90.3 | 48.0 | 72.5 | 57.8 | 92.4 |

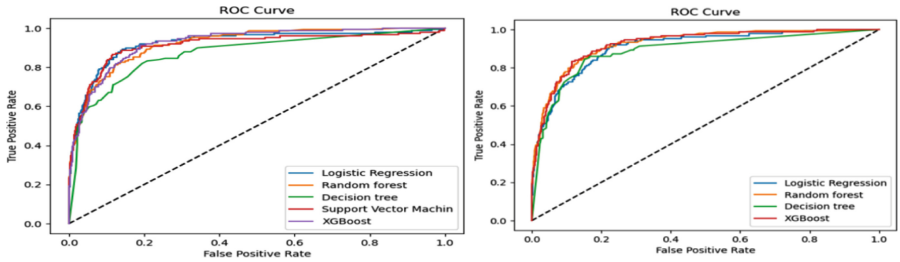


**Fig. 1.** ROC Curves for the ML models (left chart) and ML models with feature selection (right chart).

success can be attributed to its simplicity, interpretability, and consistent performance in identifying fraudulent claims and providing transparent predictions. Leveraging techniques like SHAP further enriched the predictive capabilities of LR, offering valuable insights into the model's decision-making process. The integration of SHAP not only enhanced interpretability but also set the stage for potential model refinements and synthesis. Comparative analysis demonstrated that LR consistently outperformed other models in key metrics such as accuracy, F1-score, and AUC score, reaffirming its status as the top choice for accurate fraud detection in health insurance claims.

## 5 Model Explainability

The field of explainable artificial intelligence (AI) aims to convert intricate "black-box" AI models and system outputs into comprehensible and unambiguous representations, or models that are inherently simple or explicable [10].

**SHAP** is a game-theoretic method used to interpret machine learning model output, determining the marginal advantages of records and instances. It correlates credit distribution with regional explanations using Shapley values. SHAP calculates a person's significance by calculating their contribution to the team effort, deducting income when absent, and calculating their degree of contribution. A weighted average is then computed [7].

SHAP is a tool that provides various visualization techniques to help users understand the inner workings of machine learning models. These include Beeswarm Plots, Waterfall Plots, Par Plots, Heatmaps Plots, and Force Plots. Beeswarm Plot displays the impact of each feature on model output, showcasing individual data points' SHAP values along a single axis. Waterfall Plot shows how each feature contributes to shifting the model's output. Par Plot visualizes multiple data points across different features, aiding in identifying patterns and outliers. Heatmaps provide an overview of feature interactions, and Force Plots offer detailed insights into individual predictions. These visualization tools empower users to interpret model decisions effectively and understand the factors driving predictions [6].

SHAP is essential for fraud detection because it provides information on how each feature affects a model's prediction. By identifying the primary characteristics impacting questionable claims with SHAP, insurers can improve the interpretability of their fraud detection algorithms.

Plotting the SHAP values of each feature for each sample allows one to obtain a summary of the features that are most crucial to a model. The features and their impact on fraudulent providers are explained in Fig. 2. It uses SHAP values to illustrate the distribution of the effects that each feature has on the model output and sorts the features according to the sum of the magnitudes of the SHAP values across all samples. This kind of display not only illustrates a feature's overall impact but also how particular values of this characteristic affect the prediction. In Fig. 2 if the feature value is red, its effect on the prediction is high, and blue – is low. For instance, the preoperatingphyscian-mean-ipannualreimbursement increases the likelihood of fraud providers. Conversely, for perclmdiagnosiscode-1-opannualreimbursementamt, the likelihood of being a more non-fraudulent provider increases when this feature is increased.

Figure 3 helps visualize the relative contributions of each feature to the final prediction. When used with SHAP, it displays features in a top-down manner. The average expected number of probable fraud across all 5410 records is shown as $E[f(x)] = 1622163.696$. For this specific record, the expected number of probable fraud is $f(x) = 358964.861$. All of the intermediate values are the SHAP values. The preclmdiagnosiscode-3-mean-ipannualreimbur, for instance, has increased the predicted number of potential fraud by 70316.5.

The mean absolute value of every feature across every instance will be used in the bar plot. In Fig. 4 preopertingphys-mean-ipannual had the highest mean SHAP value.

In Fig. 5 the instances are plotted on the x-axis and the model inputs are plotted on the y-axis and the SHAP values are encoded on the color scale.

Figure 6 views a condensed version of the waterfall plot. Starting from a base value of 162.200, we analyze the contribution of each attribute to the final forecast of 358964.86. Specifically, the qualities indicated by red enhance the likelihood of fraud provider, while the features indicated by blue decrease it.

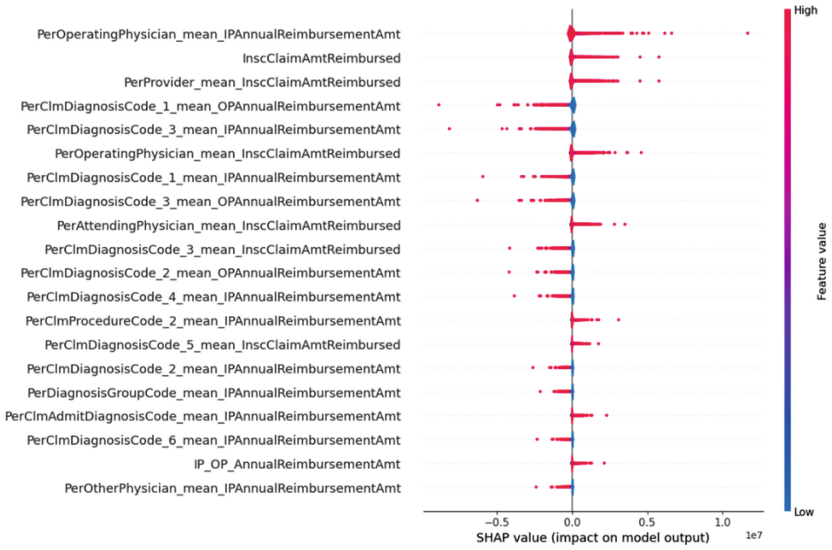


**Fig. 2.** Exploring Features Importance with SHAP Beeswarm Plot.

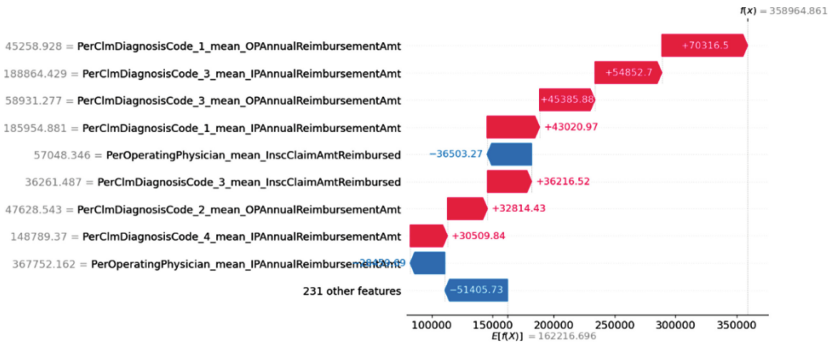


**Fig. 3.** Understanding Prediction Contributions through SHAP Waterfall Plot.

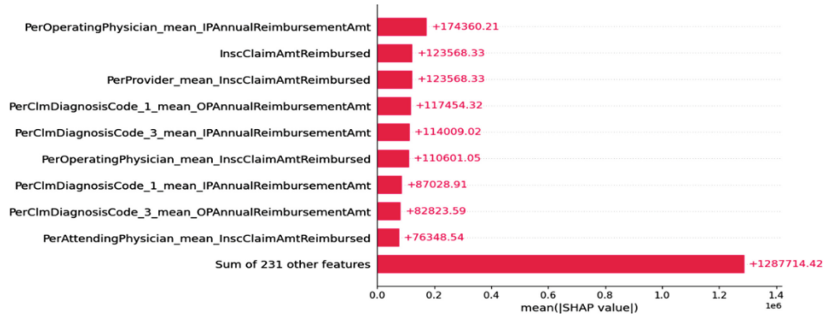


**Fig. 4.** Visualizing Features Impact with SHAP Bar Plot.

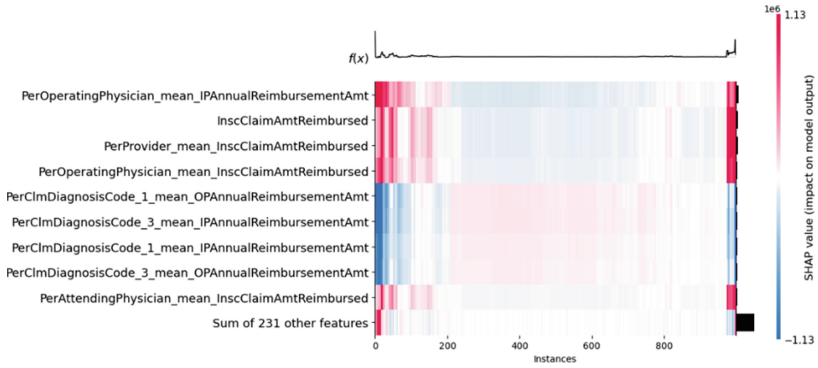


**Fig. 5.** Analyzing Relationships with SHAP Heatmap Plot.

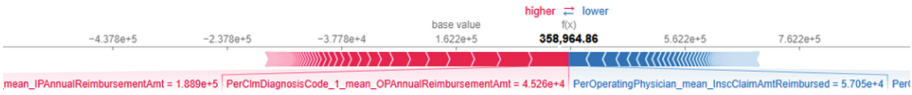


**Fig. 6.** Investigating Model Behavior with SHAP Force Plot.

## 6 Conclusion and Future Work

The study focuses on insurance claim fraud detection, aiming to improve efficiency and accuracy in identifying fraudulent activities within claims. Despite challenges like class imbalance in the Medicare dataset from Kaggle, the SMOTE Technique was successfully applied to mitigate this imbalance. The study used various machine learning algorithms, including Logistic Regression (LR), Random Forest (RF), Decision Trees (DT), Support Vector Machines (SVM), and XGBoost, along with ensemble learning techniques like hard and soft voting. The results showed that Logistic Regression (LR) performed best among the models considered with an accuracy of 91.2%, F1-score 60.7%, and AUC score of 92.4%. The SHAP study provided valuable insights into the decision-making process in the LR model, which enhanced interpretation and laid the foundation for model reconstruction and synthesis.

Future work plans include integrating XAI techniques, such as Local Interpretable Model-agnostic Explanations and G-REX, and developing a web application to detect potential healthcare provider fraud using the Flask environment.

**Disclosure of Interests.** The authors have no competing interests to declare that are relevant to the content of this article.

## References


1. Rukhsar, L., Bangyal, W., Nisar, K., Nisar, S.: Prediction of insurance fraud detection using machine learning algorithms. Mehran Univ. Res. J. Eng. Technol. **41**, 33–40 (2022)
2. Jörn, D., Heinke, V., Kriebel, J.: Detecting insurance fraud using supervised and unsupervised machine learning. J. Risk Insurance **90**(3), 743–768 (2023)
3. Rukhsar, L., Bangyal, W.H., Nisar, K., Nisar, S.: Prediction of insurance fraud detection using machine learning algorithms. Mehran Univ. Res. J. Eng. Technol. **41**(1), 33–40 (2022)
4. Sailaja, Ch., Sri Sai Kamal Teja, G., Mahesh G., Reddy Sairam Reddy, P.: Detection of fraudulent medicare providers using decision tree and logistic regression models. J. Cardiovascular Dis. Res. **12**(03), 3343–3352 (2021)
5. Herland, M., Khoshgoftaar, T.M., Bauder, R.A.: Big Data fraud detection using multiple medicare data sources. J. Big Data **5**, 29 (2018)
6. Lundberg, S., Lee, S.-I.: A unified approach to interpreting model predictions. In: Advances in Neural Information Processing Systems, vol. 30 (2017)
7. Ji, Y.: Explainable AI methods for credit card fraud detection: Evaluation of LIME and SHAP through a User Study (2021)
8. Wu, T.-Y., You-Ting, W.: Locally interpretable one-class anomaly detection for credit card fraud detection. In: 2021 International Conference on Technologies and Applications of Artificial Intelligence (TAAI). IEEE (2021)
9. Johnson, J.M., Khoshgoftaar, T.M.: Healthcare provider summary data for fraud classification. In: 2022 IEEE 23rd International Conference on Information Reuse and Integration for Data Science (IRI), pp. 236–242, San Diego, CA, USA (2022)
10. Nicodeme, C.: Build confidence and acceptance of AI-based decision support systems-Explainable and liable AI. In: 2020 13th international conference on human system interaction (HSI). IEEE (2020)
11. Gupta, R.A.: Healthcare Provider Fraud Detection Analysis. kaggle: https://www.kaggle.com/datasets/rohitrox/healthcare-provider-fraud-detection-analysis
12. Kotenko, I., Chechulin, A., Novikova, E.: Attack modelling and security evaluation for security information and event management. In: SECRYPT 2012 - Proceedings of the International Conference on Security and Cryptography, pp. 391–394 (2012)
13. Berger, I., Rieke, R., Kolomeets, M., Chechulin, A., Kotenko, I.: Comparative study of machine learning methods for in-vehicle intrusion detection. In: Lecture Notes in Computer Science, vol. 11387 LNCS, pp. 85–101 (2019)

# Classification of Mental Stress Using an Explainable Machine Learning Approach

Fatima Zohra Boulanouar[1(✉)], Mhd. Wasim Raed[1], Ilham Huseyinov[1], Rafet Akdeniz[1], Igor Kotenko[2], and Elena Fedorchenko[2]

[1] Istanbul Aydin University, Istanbul, Turkey
fatimaboulanouar@stu.aydin.edu.tr,
{ilhamhuseyinov,rafetakdeniz}@aydin.edu.tr
[2] St. Petersburg Federal Research Center of the Russian Academy of Sciences (SPC RAS), St. Petersburg, Russia
{ivkote,doynikova}@comsec.spb.ru

**Abstract.** Mental stress, characterized by feelings of strain, tension, or pressure, poses significant implications for individuals' well-being and overall health. Timely and accurate detection of mental stress is crucial to diagnose and prevent the problem. Despite successful past classifiers developed to predict mental stress, there is also a need to justify these predictions. This work aims to classify mental stress using the machine learning predictive classifiers; to interpret these classifier models using explainable machine learning methods; and to find the driving features of the developed models to assist non-technical medical personnel for early medical diagnosis and timely medical intervention. Experiments have been performed on biometric data obtained from nurses during the COVID-19 pandemic period by using a number of classifiers. The model performances were evaluated in terms of accuracy, precision, recall, and F1 metrics. According to the experiment results, the Random Forest algorithm was better than Logistic Regression, K-Nearest Neighbors, and Decision Tree. Next, explainable model techniques like SHAP and LIME are employed based on a balance between prediction strength and model interpretability to find features that best contribute to stress prediction.

**Keywords:** Mental stress prediction · Machine learning · Classifier · Explainable model

## 1 Introduction

Intense stress has become an increasingly common and unavoidable worry in modern life, resulting from both physical and mental pressures. These variables might biologically interact, possibly contributing to the beginning or aggravation of numerous diseases [1]. The healthcare sector faces a significant challenge in mental health detection, lacking an effective and proactive system. Traditional


S. Kovalev et al. (Eds.): IITI 2024, LNNS 1209, pp. 245–255, 2024.
https://doi.org/10.1007/978-3-031-77688-5_24

machine learning (ML) predictive models lack the interpretability of models posing challenges to non-technical medical personnel to correctly diagnose the problem. This research suggests that addressing stress symptoms early can prevent long-term repercussions. Early detection of stress is crucial for preventing further damage and preventing chronic conditions. Attempts have been made in predicting mental stress in the past and a number of predictive classifiers have been constructed. However, without providing a clear justification, non-technical medical personnel are not able to benefit much from classifier prediction results.

This paper proposes an explainable machine learning (XAI) approach to the problem of classification of mental stress. First, the ML predictive methods are used to classify the mental stress. Next, XAI is used to interpret the results of these classifiers. The aim is to find the driving features of the developed predictive models to produce actionable insight for early medical diagnosis and timely medical intervention. The performance of classifiers is evaluated in terms of accuracy, precision, recall, F1-score, and confusion matrix criteria. The experiment results have shown that the Random Forest (RF) classifier performs better than the other classifiers such as Decision Tree (DT), K-Nearest Neighbors (KNN), Logistic Regression (LR), Naive Bayes (NB), Light Gradient Boosted Machine (LGBM) and Gradient boosting technique (XGB) on the same dataset. Finally, model explanation and interpretability techniques like SHAP (SHapley Additive exPlanations) and LIME (Local Interpretable Model-agnostic Explanations) are employed to present a reasonable justification in terms of which features play an essential role in detecting mental stress. A balance between prediction strength and model interpretability was the major motivation to apply a XAI method.

The paper is organized as follows. Section 2 reviews the related research works. In Sect. 3, the workflow of the research is outlined. Section 4 presents the results of an experiment, an evaluation of these results, and a description of the model explanation methods. Finally, Sect. 5 is devoted to the discussion of the experiment results and conclusions.

## 2 Related Work

This section reviews research papers related to ML classifiers first, then papers related to XAI.

**Mental Stress Classification.** The problem of the mental stress classification using ML models on different datasets has been investigated in two forms: binary classification where the problem is reduced to the question if there is mental stress or not [1]; multiclass classification where the mental stress is presented by several levels [2]. The self-reported stress levels on a Likert scale as regression labels are presented in [16]. A comparison of some predictive models is presented in [3]. The gradient boost algorithm (GBM) which outperformed other ML methods is presented in [17]. However, the complexity and black-box nature of many ML algorithms make it difficult to comprehend how the model makes predictions or conclusions, as well as discover any mistakes or biases. This is a key worry in industries like healthcare, finance, and criminal justice, where model

failures can have serious implications. Another problem of black-box models is that they are typically sensitive to hyperparameter selection, making it difficult to optimize and generalize to new data. Additionally, black-box models are prone to overfitting, which can result in poor performance on unknown data.

**Mental Stress Classification using XAI.** Recently, there has been a significant shift toward XAI. This move acknowledges the importance of XAI, as demonstrated by methodologies such as SHAP and LIME, in giving transparency and interpretability to stress detection models [15]. Explanation of a model is crucial for justifying its output, gaining insight for better decision-making, improving performance, and increasing user trust [17]. Local, model-agnostic algorithms that focus on explaining individual predictions of a given black-box classifier, such as LIME [22] and SHAP [4], are among the best-known of these techniques. These strategies disrupt a specific instance in the data and measure the impact on the black-box classifier's output to quantify the contribution of individual characteristics to a prediction. In the paper [5], the SHAP method is employed to illustrate a range of behavioral patterns associated with low and high perceived stress, but the use of a simulated office environment and artificial stress restricts the applicability of their findings in the context of a real-world scenario. The work [6] introduces a new explainable AI approach for predicting stress from physiological data, enabling the identification of crucial biological features and enhancing stress prediction accuracy. However, it lacks the inclusion of explanatory features for emotional states beyond stress. In the paper [7], authors used SHAP values to measure a feature's positive or negative influence on a prediction using WESAD dataset [18] and the RF technique achieved 83% accuracy in identifying individual stress levels based on system output analysis.

Our motivation behind using XAI techniques is finding a balance between prediction strength and model interpretability.

## 3 Methodology

This section provides a comprehensive overview of the methodology employed in the study.

### 3.1 Dataset Description

The DRYAD dataset was created in a hospital setting [8]. The first 3 records of the dataset are represented in Table 1. This dataset includes biometric data of nurses during the COVID-19 epidemic. It linked biometric signals to stress-related parameters in a novel way. The collection also includes information on the relative frequency of several work-related stresses encountered throughout the epidemic. The following physiological signals were collected from the Empatica E4 wristbands for each participant: Heart rate (HR), skin temperature, Electrodermal Activity (EDA), and blood volume pulse (BVP) have varying sampling speeds. The frequency of these signals varies from 1 Hz for the heart rate to 64 Hz for the BVP. The frequency of EDA and skin temperature skin electrical

conductance changes at a rate of 4 Hz from 4 to 10 Hz. However, the authors chose a frequency of 4 Hz to reduce information loss, resulting in improved accuracy and shorter calculation time for pre-trained data used to forecast stress levels. İn reference to Table 1, X, Y, Z – numerical values indicating orientation data; TEMP (Temperature) – continuous numerical values representing temperature readings; Id – categorical data acting as identifiers for specific subjects or entities; datetime – object type encompassing a broad range of date and time entries; label – categorical data representing different states or classes; EDA (Electrodermal Activity) – contains numerical values measuring electrodermal activity; HR (Heart Rate) – continuous numerical values representing heart rate measurements.

**Table 1.** The first 3 records of the dataset.

| | X | Y | Z | EDA | HR | TEMP | id | datetime | label |
|---|---|---|---|---|---|---|---|---|---|
| 0 | –13.0 | –61.0 | 5.0 | 6.769995 | 99.43 | 31.17 | 15 | 2020-07-08 14:03:00.000000000 | 2.0 |
| 1 | –20.0 | –69.0 | –3.0 | 6.769995 | 99.43 | 31.17 | 15 | 2020-07-08 14:03:00.031249920 | 2.0 |
| 2 | –31.0 | –78.0 | –15.0 | 6.769995 | 99.43 | 31.17 | 15 | 2020-07-08 14:03:00.062500096 | 2.0 |

### 3.2 Feature Engineering and Data Augmentation

**Principal Component Analysis.** Feature Signal extraction reduces data dimensions and has the potential to enhance classification accuracy rates. Principal Component Analysis (PCA) is employed to remove superfluous variables while retaining the majority of the original variance in order to investigate the top 6 PCA components for dimensionality reduction. Features that have been chosen here include X, Y, Z, HR, EDA, and TEMP.

**Feature Importance.** Pearson's correlation matrix was used to find feature patterns. High correlations (near 1 or –1) between pairs of attributes imply comparable or duplicate information. However, characteristics with weak correlations (near to 0) have low predictive ability in ML models [9]. The top 6 features with the greatest values are selected based on Fig. 1 to determine how these features affect the outcome.

**MinMaxScaler.** The data pretreatment processes produced a dataset of 11509051 observations and 6 characteristics generated from 15 participants. To presume that the data is regularly distributed and scaled, the standard scaler was utilized – Min-Mix Normalization [19]. As a result, all the features are scaled to a range with a maximum value of 1 and a minimum value of 0 thus facilitating feature value interpretation within a consistent scale while preserving the relative connections between data points.

**Synthetic Minority Over-Sampling Technique (SMOTE).** The selected dataset is not fairly distributed among stress categories, to handle the multiclass

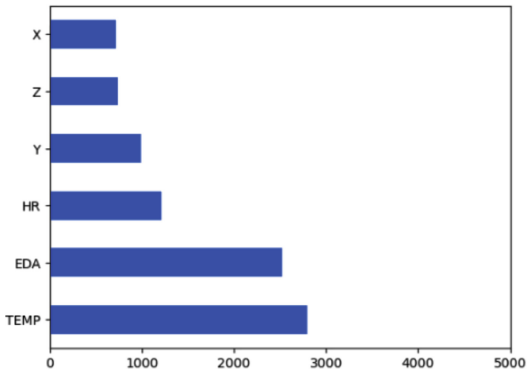


**Fig. 1.** Feature importance diagram.

imbalance we have used the SMOTE [10]. It is based on selecting data from the minority class by simply producing data points on the line segment linking a randomly picked data point to one of its KNN.

### 3.3 Classifier Training

Different classifiers were evaluated for the mental stress classification, including RF classifier which aggregates randomly generated decision trees to mitigate overfitting but may encounter slower performance with larger datasets [14]; DT classifier which comprises nodes representing data properties and tests until reaching a leaf node [11]; KNN algorithm which leverages a distance metric to locate nearest neighbors for classification, particularly resilient to outliers [23]; LR classifier which differentiates between classes [24]; XGB classifier, integrating gradient boosting decision trees (GBDT) for efficient tree-searching, albeit with longer computation times [12]; LGB, an advanced variant of GBDT like XGB, is investigated, introducing technological enhancements such as gradient-based one side sampling (GOSS) and exclusive feature bundling (EFB) to improve performance and decrease memory usage, albeit potentially prone to overfitting with small datasets [13].

The train-test split strategy was used that allocates 30% of the dataset for evaluation purposes, while the remaining 70% is dedicated to training. Following this division, all ML algorithms such as RF, LR, KNN, and DT are trained using the training data (x_train and y_train). The performance of each model is assessed using metrics like accuracy, precision, recall, and F1-score.

### 3.4 Model Explanation

This study utilized XAI techniques, such as SHAP and LIME. The study evaluated the significance of individual features in influencing prediction outcomes and analyzed the findings or choices produced by the created ML models.

**SHAP.** SHAP computes values for every observation as a local explanation technique, capturing the influence of distinct feature values on model predictions. Summary statistics or visualizations are required to comprehend the model's overall behavior. The difference between an observed feature value and the average forecast is represented by a single SHAP value. A SHAP score of 0.04 for a characteristic, for example, in classification tasks means that the likelihood of belonging to a certain class was 4% points greater than the average probability. One may determine the overall significance of each characteristic by averaging the absolute SHAP values. Understanding the impact of feature modifications on model predictions may be gained by examining the distribution of individual SHAP values in relation to feature values [20].

**LIME.** The LIME's goal is to offer comprehensible justifications for the predictions made by ML models rather than concentrating on the overall behavior of the model [21]. LIME's emphasis on locality-aiming to explain predictions on an instance-by-instance basis and its model-agnostic nature, which allows it to function with any ML model, are two of its key features. Choosing an ML model and a reference instance for clarification are steps in the LIME process. Next, new data points are created throughout the feature space, and their projected results are weighted according to how close they are to the reference instance. This weighted dataset is used to train an easily understood basic model, like a DT or Linear Model. With coefficients providing LIME explanations, the resultant model equation sheds light on the complicated ML model's decision-making process close to the reference instance. LIME provides a local, interpretable method for comprehending ML model predictions, offering insightful information about the characteristics impacting specific occurrences.

## 4 Results and Discussion

**Classification Results.** Table 2 presents the results of the experiment. The RF achieves the highest accuracy 99% compared to other models.

**Table 2.** Experiment results.

| Model | Accuracy | Precision | Recall | F1-score |
|---|---|---|---|---|
| RF | 0.99 | 0.99 | 0.99 | 0.99 |
| DT | 0.97 | 0.98 | 0.98 | 0.98 |
| KNN | 0.84 | 0.87 | 0.84 | 0.85 |
| LR | 0.49 | 0.64 | 0.49 | 0.53 |
| NB | 0.44 | 0.66 | 0.44 | 0.50 |
| LGBM | 0.81 | 0.85 | 0.81 | 0.82 |
| XGB | 0.84 | 0.88 | 0.84 | 0.85 |

We use XGB with 84.41% accuracy in XAI rather than RF, which has a greater accuracy of 99%, which is most likely due to a preference for interpretability above raw accuracy. While RF may have higher accuracy, XGB provides more transparency in model predictions, making it simpler to grasp and explain the reasons behind the decisions. Additionally, XGB's scalability, efficiency, and resistance to overfitting make it suitable for huge datasets and complicated problems. Familiarity with XGB and its interpretability characteristics, as well as the balance of accuracy and interpretability, contribute to the decision to choose XGB for XAI tasks.

**XAI Performance on Machine Learning.** XAI provides clear explanations for predictions made by ML algorithms. XAI techniques, such as SHAP and LIME, can provide clear explanations for projections that patients and clinicians without technical skills may fail to understand.

*SHAP Interpretation of XGB classifier.* The plot in Fig. 2 shows the effect of each data point on the predictions, it can be either negative or positive and indicates the significance of each aspect.

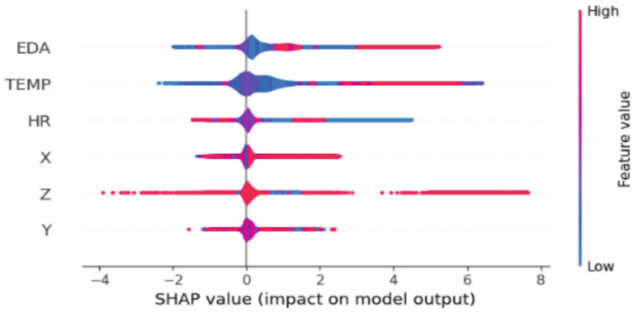


**Fig. 2.** SHAP interpretation. Beeswarm plot for XGB model.

For example, for EDA, the top left point reduced the prediction by 2. Each dot represents a Shapley value for a feature and its influence on a specific class for a given instance. Dots stack together to indicate density. Values are color-coded based on their influence on the model, with red being high and blue representing low. The color represents the actual feature value in the dataset. For example, red values for TEMP reflect high, and blue values represent a low TEMP. Overlapping dots are jittered toward the y-axis, indicating the distribution of Shapley values per feature. The SHAP Bar plot for XGB is shown in Fig. 3, it can be observed that the most important component of XGB is EDA.

In Fig. 4 EDA, HR, and TEMP have SHAP values which have a positive influence on prediction stress levels (Normal, Moderate, Severe) while they have a negative impact on the prediction of severe stress. All SHAP values added together will equal $E[f(x)] - f(x)$, where $E[f(x)]$ represents the expected value of the model's output, which is the average prediction over the entire dataset,

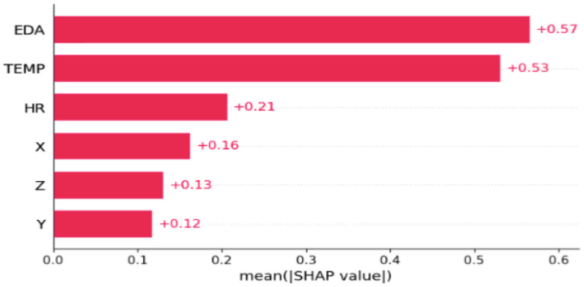


**Fig. 3.** The SHAP Bar plot for XGB.

$f(x)$ – the model's prediction for a specific instance $x$, SHAP values ($\phi$ for feature $i$) – the individual contributions of each feature to the prediction for the specific instance. The equation $\sum_{i=1}^{n} \phi_i = f(x) - E[f(x)]$ ensures that the total of all SHAP values for an instance equals the difference between the model's prediction for that instance and the average prediction. This property guarantees that the explanation provided by SHAP values is complete and additive, making them a powerful tool for interpreting machine learning model predictions.

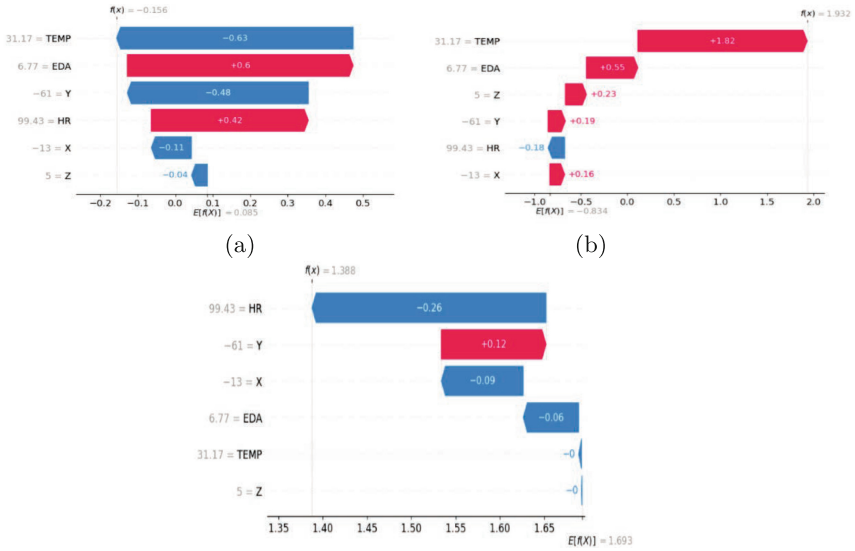


**Fig. 4.** The waterfall plot for each class Normal (a), Moderate (b), Severe (c).

*LIME Interpretation of XGB Classifier.* Fig. 5 shows two examples of the dataset's explanations. Although other classes may be anticipated, the first prediction falls into the ÃČÂćÃćâĂŽÂňÃŃÅŞsevere' class. The feature value

reveals which characteristics have a greater influence on the prediction. The XAI provides characteristics and vital information to help physicians and patients comprehend and trust computer-aided diagnoses, similar to a ÃČÂćÃćâĂŽÂňÃŃÅŞmoderate' prediction. It can be seen in Fig. 5,(a) that the classifier predicts the person's probability for severe stress is 100% and HR, EDA, and TEMP have a positive impact on predicting this result, HR had the highest value of 71.13. It can be observed from Fig. 5,(b) that the prediction probability is ÃČÂćÃćâĂŽÂňÃŃÅŞModerate' stress with a value of 54%, the 4 features EDA, TEMP, Z, and HR exhibit positive connections. Overall, all qualities influence decision-making for each class.

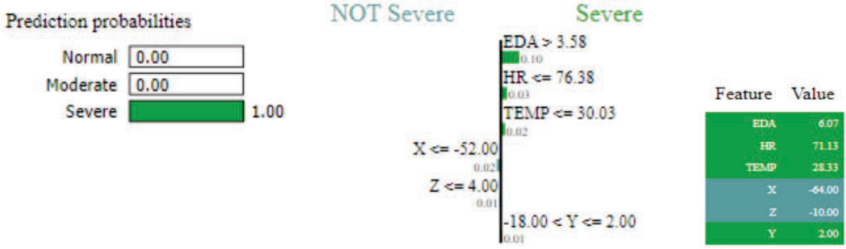


(a) Class Severe

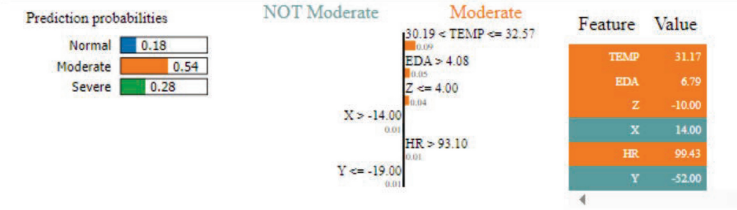


(b) Class Moderate

**Fig. 5.** LIME explanation on XGB classification for features and predicting.

Local interpretability of ML models poses substantial challenges. LIME excels at providing local interpretations by examining the model's decision-making process, though it reveals a significant push-and-pull influence on the output. In contrast, SHAP provides local interpretations that account for feature interactions, offering insights into each feature's contribution to a single instance's prediction. SHAP values are model-agnostic and adaptable to any model type without specific assumptions or design, and they can be computed individually for each class in multi-class classification, providing detailed insights into the model's behavior. Meanwhile, the Average Feature Impact measure computes the average influence of various features on the model's output over all instances in the dataset, measuring the change in output caused by changing one feature while keeping the rest constant. This measure is best suited for linear models and does not account for feature interactions. Using both SHAP and LIME together enhances interpretability by combining LIME's simplicity and intuitive explanations with SHAP's detailed interaction-aware insights. Cross-verifying explanations from both methods can increase confidence in interpretability results

and highlight areas needing further investigation. LIME provides initial, easy-to-understand local explanations, while SHAP allows for deeper analysis considering feature interactions. Both methods being model agnostic ensures consistent interpretability across different types of models. Therefore, leveraging the complementary strengths of LIME and SHAP leads to a more robust and comprehensive understanding of the model's behavior.

## 5 Conclusion and Future Work

The use of explainable machine learning improves ML systems by giving end users a better knowledge of their aims, decision-making processes, and reasoning. In this work, the multimodal Heart Rate Variability (HR) data gathered from wearable sensors was used. A range of algorithms was applied, including Logistic Regression, K-Nearest Neighbors, Decision Tree, and Random Forest, to categorize people's stress levels into three categories: normal, moderate, and severe. The results showed that the RF algorithm beat all other models examined, with a 99% accuracy rate in personalized stress detection. Furthermore, we investigated the possibility of merging HR and Electrodermal Activity (EDA) characteristics to improve stress detection accuracy, with the goal of enhancing interpretability by utilizing XAI approaches such as SHAP and LIME. These methods demonstrated promise in enhancing both the interpretability and efficacy of systems, particularly in identifying and forecasting key features associated with stress levels.

Although a good performance was obtained in all ways, there are significant limits, such as ensuring that the dataset size was enough. In addition, the dataset included a minor class imbalance. In the future, we aim to create a medical dataset for stress detection that incorporates all relevant features and intend to create a stress level prediction app using the best model.

**Disclosure of Interests.** The authors have no competing interests to declare that are relevant to the content of this article.

## References

1. Ding, C., Zhang, Y., Ding, T.: A systematic hybrid machine learning approach for stress prediction. PeerJ Comput Sci. **9**, e1154 (2023)
2. Pepa, L., Sabatelli, A., Ciabattoni, L., Monteriù, A., Lamberti, F., Morra, L.: Stress detection in computer users from keyboard and mouse dynamics. IEEE Trans. Consum. Electron. **67**(1), 12–19 (2021)
3. Smets, E., et al.: Comparison of machine learning techniques for psychophysiological stress detection. Pervasive Comput. Paradig. Ment. Health **604**, 13–22 (2015)
4. Naegelin, M., et al.: An interpretable machine learning approach to multimodal stress detection in a simulated office environment. J. Biomed. Inf. **139**, 104299 (2023)

5. Jaber, D., Hajj, H., Maalouf, F., El-Hajj, W.: Medically-oriented design for explainable AI for stress prediction from physiological measurements. BMC Med. Inform. Decis. Mak. **22**(1), 38 (2022)
6. Ng, A., et al.: Predicting the next-day perceived and physiological stress of pregnant women by using machine learning and explainability: Algorithm development and validation. JMIR MHealth UHealth **10**(8) (2022)
7. Banerjee, J. S., Mahmud, M., Brown, D.: Heart rate variability-based mental stress detection: an explainable machine learning approach. SN Comput. Sci. **4**(2), (2023)
8. Hosseini, S., et al.: A multimodal sensor dataset for continuous stress detection of nurses in a hospital. Sci. Data **9**(1), 255 (2022)
9. P. Dhal, C. Azad: A comprehensive survey on feature selection in the various fields of machine learning. Appl. Intell. 1–39 (2022)
10. Chawla, V., Bowyer, K.W., Hall, L.O., Kegelmeyer, W.P.: SMOTE: synthetic minority over-sampling technique. J. Artif. Intell. Res. **16**, 321–357 (2002)
11. Vasconcellos, E.C., et al.: Decision tree classifiers for star/galaxy separation. Astronomical J. **141**(6), 189 (2011)
12. Chen, T., He, T., Benesty, M.: Xgboost: extreme gradient boosting. R package version 0.4-2 **1**, 1–4 (2015)
13. Ke, G., et al.: Lightgbm: a highly efficient gradient boosting decision tree. Adv. Neural. Inf. Process. Syst. **30**, 3146–54 (2017)
14. Breiman, L.: Random forests. Mach. Learn. **45**, 5–32 (2001)
15. Kumar, D, Mehta, M.A.: An Overview of Explainable AI Methods, Forms and Frameworks. Springer, Cham, pp. 43–59 (2023)
16. Di Martino, F., Delmastro, F.: High-resolution physiological stress prediction models based on ensemble learning and recurrent neural networks. In: Proceedings of 2020 IEEE Symposium on Computers and Communications (ISCC), pp. 1–6 (2020)
17. Kene, A., Thakare, S.: Mental stress level prediction and classification based on machine learning. In: 2021 Smart Technologies. Communication and Robotics (STCR), pp. 1–7. Sathyamangalam, India (2021)
18. P. Schmidt, A. Reiss, R. Duerichen, C. Marberger, K. Van Laerhoven: Introducing WESAD, a multimodal dataset for wearable stress and affect detection. In: Proceedings of 20th ACM International Conference Multimodal Interaction (ICMI), pp. 400–408 (2018)
19. Panda, S.K. and Jana, P.K.: A multi-objective task scheduling algorithm for heterogeneous multi-cloud environment. In: Proceedings of International Conference on EDCAV, IEEE, Meghalaya (2015)
20. Lundberg, S. M., Lee, S.-I.: A unified approach to interpreting model predictions. In: Proceedings of the 31st International Conference on Neural Information Processing Systems (NIPS'17), pp. 4768–4777. Curran Associates Inc., Red Hook, NY (2017)
21. Ribeiro, T., Singh, S., Guestrin, C.: Why should i trust you?" explaining the predictions of any classifier. In: Proceedings of the 22nd ACM SIGKDD International Conference on Knowledge Discovery and Data Mining, pp. 1135–1144 (2016)
22. Lundberg, S.M., Allen, P.G., Lee, S.-I.: A unified approach to interpreting model predictions. https://github.com/slundberg/shap, Accessed 21 May 2024
23. k-nearest-neighbours. https://www.geeksforgeeks.org/k-nearest-neighbours/, Accessed 21 May 2024
24. Logistic Regression. https://www.ibm.com/topics/logistic-regression, Accessed 21 May 2024

# Decision-Making Intelligent Systems

# Design of Trajectory Optimization Approach for Models with Unobservable Variables in Intelligent Systems

Alexander Tselykh(✉), Vladislav Vasilev, and Larisa Tselykh

Southern Federal University, Nekrasovskii, 44, Taganrog 347922, Russia
{ant,vsvasilev,ltselykh}@sfedu.ru

**Abstract.** We present an Off-data approach to solving a finite-horizon linear quadratic (LQ) problem for a time-invariant discrete-time system with a graph dynamics matrix. Unlike the regulation problem, stability and complete controllability are not assumed. The construct of optimal control is assumed in the complete absence of data on the dynamics of the system. The design of the control trajectory is controlled by the direction of the increase in the change in the state of variables over the small number of steps, which is determined by the conditional principal eigenvector of the adjacency matrix of the graph model. An important difference from the standard discrete control problem is that the control model has been modified to estimate changes in the state of variables under the controls transmitted through the dynamics matrix. We have introduced a new interpretation of the mathematical construction of the system dynamics matrix in the standard finite-horizon discrete control problem, which can be used to design any controlled dynamic system with unobservable (by its very nature) parameters. The proposed Off-data algorithm (ODGA) using the graph dynamics matrix implements recurrent computations of dynamic equations and adjoint equations, as well as the Powell method for solving a system of linear equations (SLE).

**Keywords:** Time-invariant Discrete-time Systems · Quadratic Cost Function · Finite-horizon LQ Problem · Graph Dynamics Matrix

## 1 Introduction

Modeling dynamic systems, both for control purposes and for predicting their behavior, is quite widespread in various fields of science and engineering. Mathematical formalisms for constructing models differ in their fields of application, and the differences between them are due to the properties of the class of dynamic systems inherent in these areas.

In this paper, we are exclusively interested in the class of linear time-invariant discrete-time, finite-observation, and nonstochastic parameters dynamical systems. This class includes many problems of interest to the logic and graph models in artificial intelligence (AI) and sequential decision processes in operations research (OR).


S. Kovalev et al. (Eds.): IITI 2024, LNNS 1209, pp. 259–269, 2024.
https://doi.org/10.1007/978-3-031-77688-5_25

The problem of optimal indirect control in models of complex systems (CS) with directly unobservable parameters of variable states is considered. A complex system consists of social, economic, environmental, cultural, political, and technological elements and causal relationships among them.

It is assumed that the law of behavior of the controlled object is given by the adjacency matrix of the directed weighted signed graph, which represents the cognitive causal model (CM) of the controlled system. The system effectiveness of a node associated with the dynamics of the system is most expressed by the spectral properties of the matrix of the graph. As demonstrated in Aguiar and Bar-Yam [1], Butterworth and Dunne [2], Gadiyaram *et al.* [3], and Pei *et al.* [4], spectral properties of the graph matrices hold all the information about the dynamics of the system. As noted in [2], spectral analysis provides insight into structural, especially semantic, properties, while directed graphs provide a natural modeling formalism. Then, in the absence of observable and measurable parameters of the controlled object, the components of the principal eigenvector in the spectral decomposition of the adjacency matrix of a directed graph can serve as input and output parameters (final observations) for indirect control.

In this article, we solve a finite-horizon, LQ optimal control problem for a time-invariant discrete-time system with a graph dynamics matrix, a quadratic cost criterion, and vector input.

The construction of optimal control actions for dynamical systems is a much-studied area of control theory. There are two general methods for solving optimal control problems, the Pontryagin method and the dynamic programming method, that respectively state necessary and sufficient conditions for optimality [5]. The solution of the classic optimal control is offline and requires full knowledge of the dynamics of the system.

In the absence of complete knowledge of the dynamics of the system, solutions to optimal control problems for systems with uncertainty, including discrete-time linear systems, have generated considerable interest in recent years [6]. However, the approaches used require at least an incomplete data set. Optimal control methods in the complete absence of data on the state of the variables have not been proposed.

In this study, we attempt to fill this gap to construct optimal controls in the complete absence of data on the dynamics of the system. The main approach, when complete information about the system is not available, is the optimal control design, such that initially parameters of the system are determined, and then an algebraic equation in a dual space is solved. At the same time, the dynamics matrix expresses the law of behavior of the controlled object using an adjacency matrix, and the system parameters are determined by the direction of the principal eigenvector of the dynamics matrix.

Here we present a new interpretation of the mathematical construct of the system dynamics matrix (**A**) in the standard finite-horizon discrete control problem [7], that can be used to design any controlled dynamic system with unobservable (by its very nature) parameters. Taking into account the discrete nature of the optimization problem, the components of the principal eigenvector of the matrix **A** are interpreted as an increment in the value of the variable states.

The input values are taken as unknown inputs and are determined by the direction of the principal eigenvector of the dynamics matrix. The output values of the system are determined by the vector of optimal state changes as a reproducible trend for changes in

the states of the nodes of the controlled system using the MAEC, presented in [8]. Since only the output values of the system can be measured, an optimal feedback control is not possible, and the cost functions are expressed by quadratic control functions.

The goal of optimal control is to transfer the object to the prescribed integral change in state with the maximum value of the quality criterion. The solution to the problem is quadratic in control with an integral constraint on the state variables. The optimal solution is to distribute the quadratic energy (cost) of control actions over control steps.

Unlike the regulation problem, stability and complete controllability are not assumed. In this case, the direction of increase in the change in the state of variables over a short horizon and the optimal control that ensures this direction is of interest. The direction of the increase is determined by the conditional principal eigenvector of the dynamics matrix, the eigenvalue of which is not assumed to be within the boundaries of a unit spectral radius.

Finally, necessary and sufficient conditions for the existence and uniqueness of the optimal control problem are given. For the optimal control problem, we proved the stationarity of the Hamilton function in the state space and its extremality in the space of admissible controls, i.e., sufficient conditions for optimality in the form of the Pontryagin maximum principle (PMP).

## 2 Methods

### 2.1 Problem Statement

In this section, we present the control model, which concerns discrete-time nonstationary (or time-varying) deterministic dynamic optimization problems over a finite-horizon. Dynamic optimization problems are also known as optimal control problems.

This study examines a control model for a system with unobservable variables. A specific property of such a system is that the state variables of the system are unobservable and cannot be directly measured. Therefore, to describe the behavior of the system, we will use relative changes in the states of variables. Taking into account the specific properties of the system under consideration indicated above, we introduce the following notation.

Let the system under study be described by a model represented by a finite graph $G = \langle V, E \rangle$, where $V = \{V_1, V_2, \ldots, V_n\}$ is a finite set of vertices and $E \subset V \times V$ is a finite set of arcs. The graph is determined by the adjacency matrix $\mathbf{F}^T$, transposed of the matrix $\mathbf{F} = \left(f_{i,j}\right)_{n \times n}$, where $f_{i,j}$, $1 \leq i, j \leq n$ is the matrix weights for the arcs.

Let the change in the state of the system variables be a vector $\mathbf{z}$ and let this change in state be achieved by a sequence of change vectors $\mathbf{x}_k$, $1 \leq k \leq m$, and is written by Eq. (1):

$$\mathbf{z} = \mathbf{x}_1 + \mathbf{x}_2 + \ldots + \mathbf{x}_m, \tag{1}$$

where $\mathbf{z} \in \mathbb{R}^n$ is an $n$-dimensional and bounded vector of changes in the state of system variables over a finite horizon $m$; $\mathbb{R}^n$ is an $n$-dimensional real Euclidean space of vectors $\mathbf{x} = (x_i)_{i=1}^n$ with norm $\|\mathbf{x}\| = \sqrt{\mathbf{x}^T \mathbf{x}}$; $m$ is a natural number; in the sequel $m$ will play the role of a planning or control horizon, and will be fixed throughout. The number of

steps is assumed to be small $m \sim n$; $\mathbf{x}_1, \mathbf{x}_2, \ldots, \mathbf{x}_m$ are sequential changes in the state of the system variables.

The system's evolution is controlled by the past vector of changes in the state of the variables $\mathbf{x}_k$, $1 \leq k \leq m-1$, which transmits these changes over the system through the dynamics matrix $\mathbf{F}$, and the past vector of the control actions $\mathbf{u}_k$, $0 \leq k \leq m-1$. Future output depends on past input only through previous state. State summarizes effect of past inputs on future output – like the memory of the system.

Let us consider our control problem as a standard discrete-time optimal control [7] taking into account the introduced notation:

$$\mathbf{x}_{k+1} = \mathbf{A}_k \mathbf{x}_k + \mathbf{B}_k \mathbf{u}_k, \quad 0 \leq k \leq m-1, \tag{2}$$

where $\mathbf{x}_k$, $\mathbf{x}_{k+1} \in R^n$ is the vector of changes in the state of the system variables at step $k$, $1 \leq k \leq m-1$ and $k+1$, $0 \leq k \leq m$, respectively; $\mathbf{A}_k = \mathbf{A} = \delta\mathbf{F}$ is dynamics matrix, independent of $k$; $\mathbf{u}_k \in R^n$, $0 \leq k \leq m-1$ is an n-dimensional and bounded vector of control action on variables at step $k$ over a finite horizon $m$ that needs to be designed; $\mathbf{B}_k = \mathbf{I}$ is a constant defined as the control matrix; $\mathbf{I}$ is the identity matrix.

Let the initial change in the state of the system be determined only by the vector $\mathbf{u}_0$, and let the system's evolution be controlled over a horizon $m$ with values $k$, $1 \leq k \leq m-1$.

The trajectory of optimal control, which provides the condition (1) at the cost of minimizing the sum of the squares of the Euclidean norms of control actions, can be written as follows:

$$\|\mathbf{u}_0\|^2 + \|\mathbf{u}_1\|^2 + \ldots + \|\mathbf{u}_{m-1}\|^2 \to \min. \tag{3}$$

Then the discrete optimal control problem, taking into account the introduced notations, is defined as follows (4):

$$J(\mathbf{u}, \mathbf{x}) := \|\mathbf{u}_0\|^2 + \|\mathbf{u}_1\|^2 + \ldots + \|\mathbf{u}_{m-1}\|^2 \to \min, \tag{4}$$

subject to

$$\begin{cases} \mathbf{z} = \mathbf{x}_1 + \mathbf{x}_2 + \ldots + \mathbf{x}_m \\ \mathbf{x}_{k+1} = \delta\mathbf{F}\mathbf{x}_k + \mathbf{u}_k, \; 0 \leq k \leq m-1, \\ \mathbf{x}_0 = \mathbf{0} \end{cases} \tag{5}$$

where $J(\mathbf{u}, \mathbf{x})$ is the quadratic finite-horizon optimal control cost functional; $\mathbf{x}_0 = \mathbf{0}$ is the initial vector of changes in the state of system variables; $\mathbf{u}_0$ is the initial control vector; $\delta$, $0 < \delta \leq 1$ is the damping factor to denote the fact that we expect the variations about the nominal due to the subjectivity of assessing the elements of the adjacency matrix $\mathbf{F}^T$.

The goal of optimal control is to find a trajectory of change in state $\mathbf{z}$ under control $\mathbf{u}$ such that the functional $J(\mathbf{u}, \mathbf{x})$ is minimized over a finite horizon $m$. Stability and complete controllability are not assumed. A trajectory $\{\mathbf{x}_{k+1}, \mathbf{u}_k | 0 \leq k \leq m-1\}$ is called admissible if $\mathbf{x}_{k+1}$ and $\mathbf{u}_k$ are bounded and measurable over a finite horizon $m$ and constraints (5) of the problem (4) are satisfied. An admissible trajectory is called optimal if, among all admissible trajectories, it gives a minimum functional $J(\mathbf{u}, \mathbf{x})$.

Next, we prove a theorem that provide sufficient conditions for optimality (PMP) in problem (4)–(5). Necessary optimality conditions (PMP) for the general case were proven in [9, 10].

### 2.2 Theorem

**Theorem 1.** Suppose there is a control system

$$\mathbf{x}_{k+1} = \mathbf{u}_k + \delta\mathbf{F}\mathbf{x}_k,\ 0 \le k \le m-1,\ \mathbf{x}_0 = \mathbf{0},$$

*then there exists a unique solution* $\{\mathbf{x}_{k+1},\ \mathbf{u}_k | 0 \le k \le m-1\}$ *of the problem*

$$\|\mathbf{u}_0\|^2 + \|\mathbf{u}_1\|^2 + \ldots + \|\mathbf{u}_{m-1}\|^2 \to \min,$$

*subject to*

$$\mathbf{z} = \mathbf{x}_1 + \mathbf{x}_2 + \ldots + \mathbf{x}_m.$$

**Proof.** Let us write the standard Lagrangian function [11] for the conditional optimization problem (4)–(5):

$$L = -\tfrac{1}{2}\sum_{k=0}^{m-1}\|\mathbf{u}_k\|^2 + \mathbf{v}_1^T(\mathbf{u}_0 - \mathbf{x}_1) + \sum_{k=2}^{m}\mathbf{v}_k^T(\mathbf{u}_{k-1} + \delta\mathbf{F}\mathbf{x}_{k-1} - \mathbf{x}_k) - \mathbf{w}^T\left(\mathbf{z} - \sum_{k=1}^{m}\mathbf{x}_k\right) \to \max, \tag{6}$$

were vector $\mathbf{v}_k$, $1 \le k \le m$ and vector $\mathbf{w}$ are vectors of Lagrange multipliers.

The necessary conditions for a maximum have the following form. Derivatives of function (6) with respect to the components of vectors $\mathbf{x}_k, 1 \le k \le m$; $\mathbf{u}_k, 0 \le k \le m-1$; and $\mathbf{v}_k$, $1 \le k \le m$ represent a recurrent sequences:

$$\mathbf{w} - \mathbf{v}_1 + \delta\mathbf{F}^T\mathbf{v}_2 = \mathbf{0},\ \ldots,\ \mathbf{w} - \mathbf{v}_{m-1} + \delta\mathbf{F}^T\mathbf{v}_m = \mathbf{0},\ \mathbf{w} - \mathbf{v}_m = \mathbf{0}, \tag{7}$$

$$\mathbf{v}_1 - \mathbf{u}_0 = \mathbf{0},\ \ldots,\ \mathbf{v}_{m-1} - \mathbf{u}_{m-2} = \mathbf{0},\ \mathbf{v}_m - \mathbf{u}_{m-1} = \mathbf{0}, \tag{8}$$

$$\mathbf{u}_0 - \mathbf{x}_1 = \mathbf{0},\ \mathbf{u}_1 + \delta\mathbf{F}\mathbf{x}_1 - \mathbf{x}_2 = \mathbf{0},\ \ldots,\ \mathbf{u}_{m-1} + \delta\mathbf{F}\mathbf{x}_{m-1} - \mathbf{x}_m = \mathbf{0}. \tag{9}$$

Equations (7) and (8) express the stationarity in the state and the extremality in the control of the PMP, respectively. Substituting (9) for $\mathbf{x}$ in (1), we get:

$$\mathbf{z} = \mathbf{u}_{m-1} + (\mathbf{I} + \delta\mathbf{F})\mathbf{u}_{m-2} + \left(\mathbf{I} + \delta\mathbf{F} + (\delta\mathbf{F})^2\right)\mathbf{u}_{m-3} + \ldots + \left(\mathbf{I} + \delta\mathbf{F} + (\delta\mathbf{F})^2 + \ldots + (\delta\mathbf{F})^{m-1}\right)\mathbf{u}_0. \tag{10}$$

Substituting (8) for $\mathbf{u}$ in (11), we get:

$$\mathbf{P}_m\mathbf{w} = \mathbf{z}, \tag{11}$$

where $\mathbf{P}_m = \mathbf{I} + (\mathbf{I} + \delta\mathbf{F})(\mathbf{I} + \delta\mathbf{F})^T + \ldots + \left(\mathbf{I} + \delta\mathbf{F} + \ldots + (\delta\mathbf{F})^{m-1}\right)\left(\mathbf{I} + \delta\mathbf{F} + \ldots + (\delta\mathbf{F})^{m-1}\right)^T$.

Matrix $\mathbf{P}_m$ is positive definite since $\mathbf{w}^T\mathbf{P}_m\mathbf{w} \ge \mathbf{w}^T\mathbf{w} > \mathbf{0}$ for any non-zero vector $\mathbf{w} \ne \mathbf{0}$. Consequently, Eq. (11) is uniquely solvable of $\mathbf{w}$ for any $\mathbf{z}$. Next, vector $\mathbf{u}_k$, $m-1 \ge k \ge 0$ and vector $\mathbf{x}_k$, $1 \le k \le m$ are calculated using Eqs. (7), (8), and (9), respectively.

This completes the proof of Theorem 1.

### 2.3 Computational Algorithm

The computational algorithm for solving problems (4)–(5) uses Powell method [14] (or Conjugate directions method) to solve SLE with a symmetric positive-definite matrix **P** and reduces to three $m$-step sequential calculations of matrices **Q** and **P**, vectors $\mathbf{u}_k$ and vectors $\mathbf{x}_k$.

Let us write the recurrent sequence to calculate the matrix $\mathbf{P}_m$:

$$\mathbf{P}_1 = \mathbf{I},\ \mathbf{Q}_1 = \mathbf{I},\ \mathbf{Q}_k = \mathbf{I} + \delta\mathbf{F}\mathbf{Q}_{k-1},\ \mathbf{P}_k = \mathbf{P}_{k-1} + \mathbf{Q}_k\mathbf{Q}_k^T,\ 2 \le k \le m,$$

where $n$ is the number of model nodes, $\mathbf{Q}_k$, $1 \le k \le m$ are auxiliary matrices.

The computational complexity of the matrix $\mathbf{P}_m$ is $O(mn^3)$ operations, since computing a matrix $\mathbf{P}_m$ requires $n^3$ field operations to multiply two $n \times n$ matrices over that field and $m$ additions for computing the sum of products. The vector **z** is calculated using the MAEC algorithm presented in [8]. The MAEC is available to calculate at https://github.com/Simon1093/cognition. The output of the Algorithm 1 is the sequence of optimal controls $\mathbf{u}_k$, $0 \le k \le m-1$ and the sequence of state changes $\mathbf{x}_k$, $1 \le k \le m$. The Off-data Algorithm (ODGA) using the graph dynamics matrix to solve the LQ problem (4)–(5) is summarized in Table 1. The ODGA algorithm implements recurrent calculations of dynamic equations and adjoint equations, as well as the conjugate directions method for solving a SLE (12).

**Table 1.** Off-data algorithm using the graph dynamics matrix (ODGA).

| | |
|---|---|
| 1: | **Input:** $\mathbf{F}$, $\delta$, $\mathbf{z}$, $m$; |
| 2: | $\mathbf{P} \leftarrow \mathbf{I}$; $\mathbf{Q} \leftarrow \mathbf{I}$; |
| 3: | for $k = 2$ to $m$ do |
| 4: | $\mathbf{Q} \leftarrow \mathbf{I} + \delta\mathbf{F}\mathbf{Q}$; $\mathbf{P} \leftarrow \mathbf{P} + \mathbf{Q}\mathbf{Q}^T$; |
| 5: | endfor; |
| 6: | $\mathbf{w} \leftarrow \mathbf{P}^{-1}\mathbf{z}$; |
| 7: | $\mathbf{u}_{m-1} \leftarrow \mathbf{w}$; |
| 8: | for $k = m-2$ downto 0 do |
| 9: | $\mathbf{u}_k \leftarrow \mathbf{w} + \delta\mathbf{F}^T\mathbf{u}_{k+1}$; |
| 10: | endfor; |
| 11: | $\mathbf{x}_1 \leftarrow \mathbf{u}_0$; |
| 12: | for $k = 2$ to $m$ do |
| 13: | $\mathbf{x}_k \leftarrow \mathbf{u}_{k-1} + \delta\mathbf{F}\mathbf{x}_{k-1}$; |
| 14: | endfor; |
| 15: | **Output:** $\mathbf{u}_k$, $0 \le k \le m-1$; $\mathbf{x}_k$, $1 \le k \le m$. |

## 3 Simulation Results

In this section, to model the proposed method, the graph adjacency matrix (Eq. 12), expressing the behavioral model of the Crime and Punishment system [15], is used as the dynamics matrix $\mathbf{A}_k = \mathbf{A} = \delta\mathbf{F}$ in Eq. (2).

$$\begin{pmatrix} 0 & 0.5 & 0.5 & 0 & 0.6 & 0 \\ 0 & 0 & 0.7 & 0 & 0 & 0 \\ 0 & -0.5 & 0 & 0.5 & 0 & 0.6 \\ 0 & 0 & -0.4 & 0 & 0.4 & 0.6 \\ 0 & 0 & 0.3 & 0 & 0 & 0 \\ 0.3 & 0 & 0 & -0.8 & 0 & 0 \\ 0.5 & 0 & -0.8 & 0 & 0 & 0 \end{pmatrix}. \tag{12}$$

The following initial data are assumed to simulate optimal control:

1. Dynamics matrix $\mathbf{A}_k = \mathbf{A} = \delta\mathbf{F}$ of dimension $n = 7$.
2. The value of the damping factor is determined by accounting for the theorem from [12, 13]. The resonant boundary is $\delta_{resonance} = 1/\lambda_{\max} = 1/0.60244 = 1.6598$; then, $\delta = 1.0$.
3. $m = 10$ is a control horizon.

The output is controlled by a fixed-end state change vector $\mathbf{z}$ over a finite horizon $m = 10$. The vector $\mathbf{z}$ was calculated using the MAEC algorithm presented in [8]. The MAEC is available to calculate at https://github.com/Simon1093/cognition. The calculated components of the vector $\mathbf{z}$ are given below:

$\mathbf{z} = \left(0.610844\ 0.317196\ 0.283766\ 0.250364\ 0.367809\ 0.137910\ 0.478274\right)^T$.

The purpose of the design is to find the law for controlling the change in the states of the system variables in the direction of the principal eigenvector of the dynamics matrix of the system, represented by the adjacency matrix in Eq. (4) - (5) in such a way as to minimize the functional $J(\mathbf{u}, \mathbf{x})$.

The simulation results using the ODGA are as follows. The optimal solution is to distribute the quadratic energy (cost) of control actions at control steps. Figure 1a shows that the quadratic control energy in sequences of norms of control vectors $\mathbf{u}_1$ over different horizons $m$ sharply decreases in the last steps. As shown in Fig. 1b, the distribution of the norm values of the response variable vectors at control steps is approximated by a second-order polynomial, which characterizes the dynamics with uniform increments, positive for one branch of the parabola and negative for the other.

The resulting control sequences are evaluated using Control Efficiency by basic control vector (Eq. (15)) and Control Efficiency by response vector (Eq. (16)). The relevant Definitions are given below.

**Definition 1.** *Control Efficiency by basic control vector* ($CE_b$) – The ratio of the multi-stage to the single-stage controls:

$$CE_b = \frac{\|\mathbf{u}_0 + \mathbf{u}_1 + \cdots + \mathbf{u}_{m-1}\|}{\|\mathbf{u}_k\|},\ 0 \le k \le m-1, \tag{15}$$

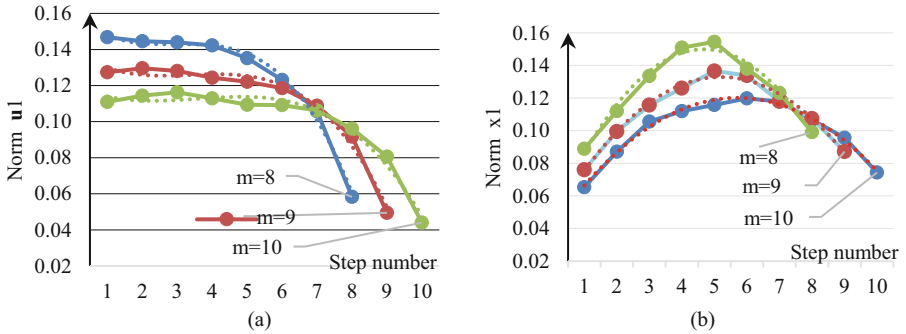


**Fig. 1.** Distribution of the norm of the control variable $\mathbf{u}_1$ (a) and the norm of the response variable $\mathbf{x}_1$ (b) at horizon $m$. *Legend*: the trend line is indicated by a dotted line; the optimal control trajectory is indicated by a solid line.

where vector $\|\mathbf{u}_k\|$ is the basic single-stage control vector, and vector $\|\mathbf{u}_0 + \mathbf{u}_1 + \cdots + \mathbf{u}_{m-1}\|$ is an evaluated multi-stage vector.

**Definition 2.** *Control Efficiency by response vector* ($CE_r$) – The control-response ratio of the multi-stage controls:

$$CE_r = \frac{\|\mathbf{u}_0 + \mathbf{u}_1 + \cdots + \mathbf{u}_{m-1}\|}{\|\mathbf{x}_0 + \mathbf{x}_1 + \cdots + \mathbf{x}_m\|}, \; 0 \le k \le m, \tag{16}$$

where vector $\|\mathbf{u}_0 + \mathbf{u}_1 + \cdots + \mathbf{u}_{m-1}\|$ is the respective response vector, and vector $\|\mathbf{x}_0 + \mathbf{x}_1 + \cdots + \mathbf{x}_m\|$ is an evaluated control vector.

As shown in Fig. 2, $CE_b$ tends to unity, which means that the sequence of multi-stage control vectors approaches the optimal single-stage control vector as the number of control stages increases. In this case, the control-reaction rate tends to $CE_r$ for single-stage controls of the model under consideration, $CE_r = 1 \Big/ \sqrt{\|\mathbf{u}_{k-1}\| \Big/ \|\mathbf{x}_k\|} \to 1 \Big/ \sqrt{5.003556} = 0,447055$.

Trajectories of changes in the states of the controlled system over different horizons according to the proposed algorithm are given in Fig. 3.

## 4 Evaluation of the Results

The ODGA was assessed according to several dimensions and evaluation criteria.

### 4.1 Runtime

On one core of an Intel Pentium 2 CPU, the 4417U 2.3 GHz, the runtime is typically in the range of a few several microseconds up to a few milliseconds for matrices of up to $n = 10^2$.

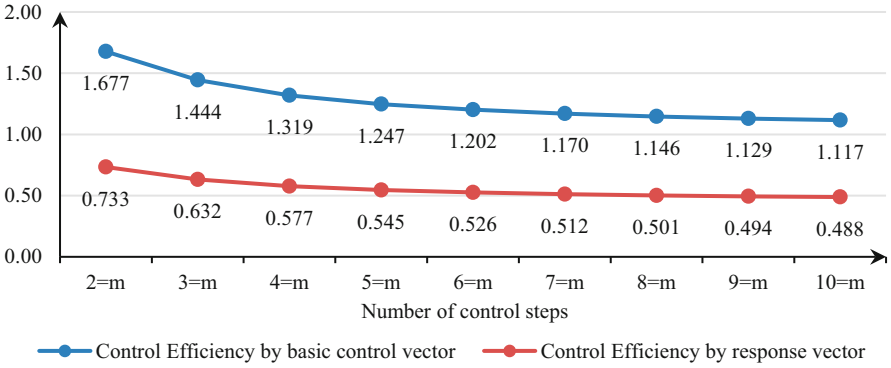


**Fig. 2.** Control Efficiency by basic control vector and response vector at control steps $m$.

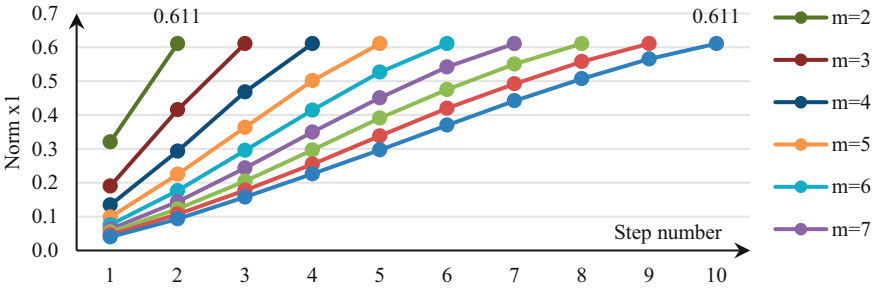


**Fig. 3.** Trajectories of changes in states $\mathbf{x}_1$ depending on the control horizon $m$.

### 4.2 Tractability

The computational process boils down to a solution a SLE with a positive definite matrix that has a unique solution. After solving the SLE, the dual and initial variables are determined as a result of one sequence of calculations. Computing a positive definite matrix requires $O(mn^3)$ computational costs. Solving the SLE using Powell method has a complexity of $O(n^3)$.

### 4.3 Robustness of Results

The robustness of results is based on the correctness of the mathematical statement of the problem, a symmetric positive-definite matrix of the SLE, and a one-off sequence of computations.

### 4.4 Limitations

Since stability and complete controllability of the control system are not required, the number of steps cannot be large. The number of steps is comparable to the number of nodes in the adjacency matrix for $n \sim 10^2$.

### 4.5 Quality of Results

The symmetric positive definite matrix of the SLE is defined by a recurrent sequence of calculations that maintains its symmetry. This ensures minimal accumulation of floating-point rounding errors. The coincidence rate of the multi-stage control trajectory with the single-stage control trajectory is in the range of 0.982863–0.999861.

## 5 Discussion and Conclusions

We have introduced an off-data approach to solve the finite-horizon LQ problem for a time-invariant discrete-time system with a graph dynamics matrix. This approach attains the control sequence that minimizes a quadratic cost function in vector input and vector output.

The input vector is generated by the algorithm from [8] in the form of the principal eigenvector components of the dynamics matrix, which is the adjacency matrix of the directed graph. This graph represents the cognitive causal model of the real-world system. The validity of the generated data was established in [8, 12].

A numerical experiment showed that the algorithm can be used to design a control trajectory to change the state of the controlled system to transfer it to a given direction of development. The direction of development is expressed by the conditional principal eigenvector of the graph CM.

An important difference from the standard discrete control problem is that the control model is interpreted in such a way that the change in the state of variables under the influence of control actions transmitted through the dynamics matrix is estimated.

An important advantage of the proposed approach is that the discrete control trajectory effectively follows the direction of the conditional principal eigenvector of the dynamics matrix with a fixed endpoint with an accuracy of 10–6 and a total deviation along the trajectory of no more than 1.714%. For the systems under consideration, sufficient conditions are obtained in the form of the maximum principle (Theorem 1).

**Acknowledgments.** This research did not receive any specific grant from funding agencies in the public, commercial, or not-for-profit sectors.

**Disclosure of Interests.** The authors have no competing interests to declare that are relevant to the content of this article.

## References

1. de Aguiar, M.A.M., Bar-Yam, Y.: Spectral analysis and the dynamic response of complex networks. Phys. Rev. E **71**, 016106 (2005). https://doi.org/10.1103/PhysRevE.71.016106
2. Butterworth, J., Dunne, P.E.: Spectral techniques in argumentation framework analysis. In: Computational Models of Argument, pp. 167–178 (2016). https://doi.org/10.3233/978-1-61499-686-6-167
3. Gadiyaram, V., Ghosh, S., Vishveshwara, S.: A graph spectral-based scoring scheme for network comparison. J. Complex Netw. cnw016 (2016). https://doi.org/10.1093/comnet/cnw016

4. Pei, S., Wang, J., Morone, F., Makse, H.A.: Influencer identification in dynamical complex systems. J. Complex Netw. (2019). https://doi.org/10.1093/comnet/cnz029
5. Razavi, S.E., Moradi, M.A., Shamaghdari, S., Menhaj, M.B.: Adaptive optimal control of unknown discrete-time linear systems with guaranteed prescribed degree of stability using reinforcement learning. Int. J. Dyn. Control. **10**, 870–878 (2022). https://doi.org/10.1007/s40435-021-00836-x
6. Moulton, R.H., Rudie, K.: Online control of discrete-event systems: a survey. Annu. Rev. Control. **54**, 24–48 (2022). https://doi.org/10.1016/j.arcontrol.2022.08.002
7. Katsuhiko, O.: Discrete-Time Control Systems. Prentice-Hall Inc., Hoboken (1995)
8. Tselykh, A., Vasilev, V., Tselykh, L.: A method for modeling the control impact strategy based on the mental frame of references of the decision-maker. (2023). https://doi.org/10.1007/978-3-031-43789-2_29
9. Pontryagin, L.S.: Mathematical Theory of Optimal Processes. Routledge, London (2018). https://doi.org/10.1201/9780203749319
10. Macki, J., Strauss, A.: Necessary Conditions for Optimal Controls—The Pontryagin Maximum Principle. (1982). https://doi.org/10.1007/978-1-4612-5671-7_5
11. Bertsekas, D.P.: Constrained Optimization and Lagrange Multiplier Methods. Athena Scientific, Belmont, MA (1996)
12. Tselykh, A., Vasilev, V., Tselykh, L., Ferreira, F.A.F.: Influence control method on directed weighted signed graphs with deterministic causality. Ann. Oper. Res. **311**, 1281–1305 (2022). https://doi.org/10.1007/s10479-020-03587-8
13. Tselykh, A., Vasilev, V., Tselykh, L.: Effect of resonance in the effective control model based on the spread of influence on directed weighted signed graphs. In: Advances in Intelligent Systems and Computing, pp. 270–280 (2020). https://doi.org/10.1007/978-3-030-50097-9_28
14. Powell, M.J.D.: An efficient method for finding the minimum of a function of several variables without calculating derivatives. Comput. J. **7**, 155–162 (1964). https://doi.org/10.1093/comjnl/7.2.155
15. Carvalho, J.P.: On the semantics and the use of fuzzy cognitive maps and dynamic cognitive maps in social sciences. Fuzzy Sets Syst. **214**, 6–19 (2013). https://doi.org/10.1016/j.fss.2011.12.009

# Development of a Program Complex for Diagnostics of Electrical Engineering Systems Under Conditions of Heterogeneous Data

Anna E. Kolodenkova[1(✉)], Svetlana S. Vereshchagina[1], Ekaterina A. Favorskaya[1], Ekaterina A. Osipova[1], and Andrey L. Okhotnikov[2]

[1] Samara State Technical University, Samara, Russia
anna82_42@mail.ru
[2] JSC NIIAS, Moscow, Russia

**Abstract.** This paper presents the structure of a program complex for diagnosing electrical systems (ES), specifically electrical equipment (EE) under conditions of heterogeneous data based on the principle of integrated modular technology. This complex is developed to prevent ES from premature failure, as well as to identify the methods and ways to solve them in real time. The principle of building such a complex is realized by implementation of the developed methods and models for decision support using methods and technologies of artificial intelligence. An important feature of realization and application of the program complex is the ability to function (training) and perform diagnostics of ES technical state in real time mode under conditions of incomplete and fuzzy information. Scientific novelty of the result is the building of a simplified complex that represents all the requirements from regulatory documentation, equipment passports, which combine interrelated cognitive, non-parmetric, fuzzy models in combination with methods for measuring the state of the equipment under conditions of uncertain initial data presented in the form of verbal descriptions, intervals of acceptable measurements and fuzzy triangular, trapezoidal numbers. When diagnosing ES, the complex will create a database and knowledge base of models for proper functioning of systems and equipment with subsequent recognition of faulty states and their classification, as well as provide recommendations to prevent their failure. The proposed program complex can be part of intelligent decision support systems for diagnostics of any ES and EE, as well as be used separately. It provides increasing informativeness of decision-making situations, reliability of conclusions about the technical state of ES and EE under conditions of incomplete and fuzzy information, as well as reducing the time to assess the ES state and make decisions about its condition.

**Keywords:** Electrical Equipment · Program Complex · Incomplete and Fuzzy · Information · Artificial Intelligence Technologies

The work was supported by the Russian Science Foundation, No. 23-29-00415.


S. Kovalev et al. (Eds.): IITI 2024, LNNS 1209, pp. 270–278, 2024.
https://doi.org/10.1007/978-3-031-77688-5_26

## 1 Introduction

The problem of providing ES fail-safety and operability at any industrial facilities is an essential condition for maintaining a high level of safety of facilities. A wide range of approaches and methods for solving this problem causes the lack of unification ("combination", "complex") [1–3]. First, obtaining diagnostic data (how and when are diagnostic data obtained?).

Data can be presented in the form of heterogeneous data and be characterized by: a variety of measurement scales; different types of data; different representation structure (statistical, fuzzy, expert data, images, etc.); different degrees of reliability, completeness and accuracy of data measured in different scales and units [4–6]. Secondly, managing the redundancy of parameters affecting the ES technical state; thirdly, choosing a relevant method for assessing the ES state. The solution of the unification problem will allow to build a unified program complex for assessing the ES technical state when diagnosing in order to solve the problem of maintaining its serviceability.

This paper proposes a program complex for ES diagnostics under conditions of heterogeneous data built on the principle of integrated modular technology.

## 2 Problem Statement and Structure of the Program Complex

Assume we have a set of different parameters ($X_i$, $i = \overline{1, h}$, $h$ – total number of parameters) affecting the technical state of ES or EE. The parameters values can be presented in the form of verbal description, statistical or fuzzy data, color images, graphs and photos. The task is to assess the technical state of ES and EE followed by providing recommendations to prevent their failure.

To solve this problem, a structure of the program complex consisting of six modules is proposed, the core of which are database (DB) and knowledge base (KB) (Fig. 1).

The database is uploaded with data coming from the equipment and duty personnel; it contains: archive of retrospective data (daily files indicating the time to which they relate), real-time measurement data, normative documentation, GOSTs [7], passport data for equipment, color images (thermograms), as well as restrictions for EE various parameter values. As a result, all the EE data obtained are located in a single location.

The values of parameters from sensors are stored in *Excel* (**.xls*) format; thermograms have extension.bmt, size 640 × 480 pixels.

The knowledge base contains experts' knowledge, as well as fuzzy and fuzzy-functional cognitive models, fuzzy and mixed production rules. The following modules are highlighted here:

1) *data/knowledge import module.* This module is built to transfer data in *Excel (*.xlsx)* format, thermograms, knowledge in the form of production rules for their further processing. Thermograms were obtained using a Testo 875-1i thermal imager, temperature sensitivity (*NETD*) < 0.05 °C at 30 °C, operating temperature from −15 to −40 °C.
2) *data/knowledge processing module.* This module allows to convert raw data ("dirty data") into a format that is suitable to assess the states of ES, EE and personnel using various mathematical methods [8]. The module also allows one to edit (add, delete)

information in the database and knowledge base, and to check the knowledge base for structural errors [9, 10].

The scientific novelty of the data/knowledge processing module is in the proposed algorithms for classifying parameters according to the nature and degree of their influence on equipment using a knowledge base containing production rules about the type of parameter (main, additional, auxiliary), a database (data on equipment failure, data from devices and sensors) based on the formalization of weights of importance of the values of term-sets of parameters.

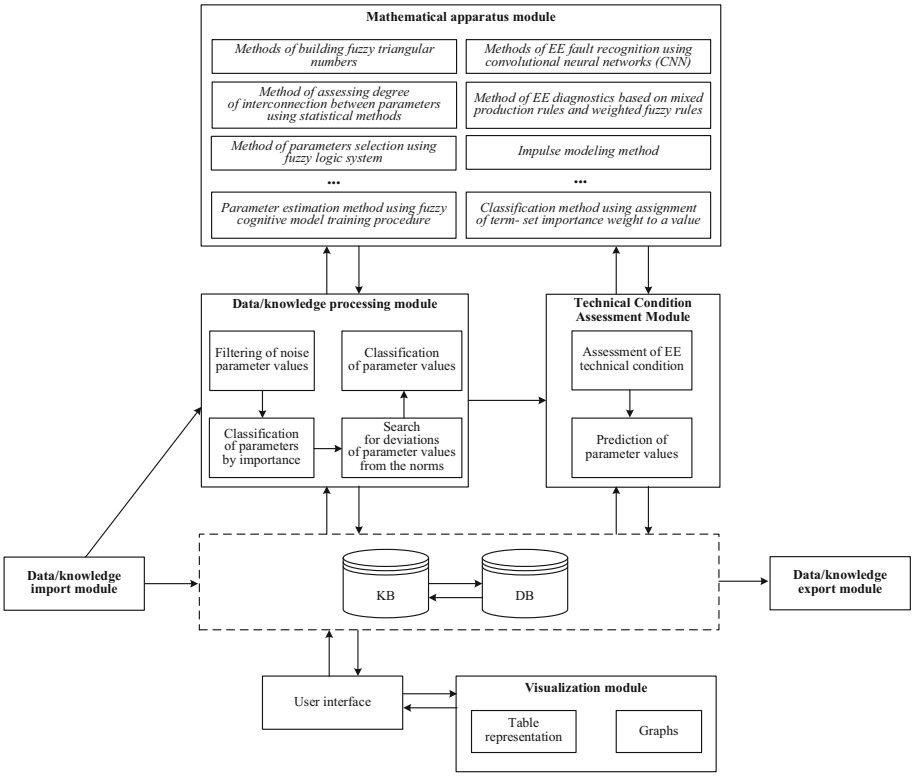


**Fig. 1.** Structure of the program complex for ES and EE diagnostics.

3) *module of the mathematical apparatus*. This module allows to solve the tasks of data/knowledge processing, as well as to assess ES and EE technical states using statistical methods, as well as artificial intelligence technologies.

For example, the concept of "Method of EE fault recognition using convolutional neural networks" (CNN) is to determine the limit or abnormal temperatures of EE by recognising thermograms obtained using a thermal imaging device; black-and-white graphs that describe changes in the values of various parameters over time based on

data from sensors; and simple color photographs. Graphs based on the values of the EE parameters are used in case thermograms/color photographs are not available or are of poor quality.

The conversion of a color photograph into a black-and-white one is done using Niblack's method [11], where the threshold value for a point with coordinates $(m, n)$ is calculated using the following formula:

$$t(m, n) = \mu(m, n) + k \cdot \sigma(m, n),$$

where $\mu(m, n)$ – mean; $\sigma$ $(m, n)$ – root-mean-square deviation in the local area of the considered image point; $k$ – value that determines which part of the object boundary is needed to be taken as the object.

The use of CNN for temperature recognition can reduce the number of non-planned failures by providing advance notification of damage and possible equipment failures. The network outputs the number of the class to which the current state of the EE refers: class 1 – operable EE; class 2 – operable EE with minor deviations. Depending on the class, a list of measures aimed at preventing EE failure is given.

For example, the concept of "Fuzzy triangular number building method" is to convert the current crisp values of EE parameters from devices into fuzzy triangular numbers using the fuzzy triangular number building algorithm [12].

The need to represent the current crisp values of parameters in fuzzy triangular numbers is due to the fact that any data coming from devices during diagnostics is inaccurate because of various errors. This is related to violations of diagnostics (human factor); to the inaccuracy of the device which must undergo regular verification; to the filtering of external "noise".

Calculation of the left boundary of the parameter $x_{mg}$, $x^*_{mg1} = x_{mg} - \delta_1$, where $\delta_1 =$ 1 – maximum allowed deviation for the left boundary, assigned by experts on experience basis and chosen from the range (1, 2, 3), assuming that 1– minimum deviation of the value from the experimental data, 3 – maximum possible deviation.

Calculation of the right boundary of the parameter $x_{mg}$, $x^*_{mg3} = x_{mg} + \delta_2$, where $\delta_2 = 2$ – maximum allowed deviation for the right boundary, assigned by experts on experience basis, chosen from the range (2, 3, 4), assuming that 2 – minimum deviation of the value from experimental data, 4 – maximum possible deviation. In addition, the condition $\delta_1 < \delta_2$, must be fulfilled, where $x_{mg}$ – current value of the parameter at a certain moment of observation ($x_{mg}$ – result of the $m$-th observation for $g$-th parameter, $l = 1, 2,\ldots, m, \ldots, t$, $t$ – number of observation; $x_i = \{x_1, x_2, x_3,\ldots,x_g,\ldots x_h\}$, $i = \overline{1, h}$, $h$ – number of parameters), each of which is defined by a value at a certain moment of observation.

As a result of calculations, the value of the parameter $x_{mg}$ is represented as a fuzzy triangular number: $x_{mg} = [x^*_{mg1}, x^*_{mg2}, x^*_{mg3}]$, where $x^*_{mg1}$, $x^*_{mg2}$, $x^*_{mg3}$ – minimum, current and maximum values of the parameter $x_{mg}$. The use of triangular fuzzy numbers will provide a sufficiently accurate formalization of boundaries for possible changes in parameter values.

4) *data/knowledge export module* is built for their conversion into *Excel* (*.*xlsx*) format or text format and their transfer.

5) *visualization module* presents the results obtained in text format, in the form of tables or graphs.
6) *user Interface is presented* in the form of main windows (input of initial data and output of results) of the program complex.

The scientific novelty of the mathematical apparatus module is in the proposed modified methods necessary for assessing the state of the electronic equipment taking into account the values of the most important parameters characterizing the technical condition of the electronic equipment.

## 3 Results of the Program Complex

The results of the study were obtained when diagnosing the asynchronous motor АИР63А4У1.

To search for deviations of parameter values from the norms, a program system (PS) written in the object-oriented programming language C# was used.

Figure 2 shows the interfaces of raw data input (the personnel chooses the type and model of equipment, as well as the type of parameter to be diagnosed based on their knowledge and experience) [13].

Note that the personnel chooses the parameter to be checked for deviations from the set of all additional parameters affecting the induction motor (harmonic oscillations are selected as an example).

Figure 3 shows the results of the search for deviations of harmonic oscillation values where the red color highlights the outputs of harmonic oscillation values beyond the limit interval which are involved in the analysis of the causes of their occurrence.

Based on the results obtained, the following measures needed to reduce the influence of harmonic oscillations can be recommended: 1) installation of soft starters/frequency converters (according to the manufacturer's agreement); 2) installation of filter compensating device; 3) installation of smoothing filter.

Next, the technical state of the engine (in general) was assessed. Figure 4 shows the screen form of input information "Adding parameters and their values".

After all variables have been added to the knowledge base, the personnel proceed with the addition of rules. This is followed by checking the knowledge base for structural errors. If contradictory rules are detected, the PS excludes the rule that has the lowest weight. In case of detection of contradictory rules with the same weight, it is up to the personnel to choose the rule to be excluded from the knowledge base.

The result of diagnostics is presented in Fig. 5. The upper box displays the rules with conditions corresponding to the input diagnosed parameters. Next, the staff selects the triggered rule, and according to this rule the fuzzy inference is performed in the lower window. All information about equipment diagnostics is recorded in the database and displayed in the Diagnostics Log tab. The default method is the maximum method (the maximum value of the membership function is accepted), since it is the simplest way to perform the defuzzification procedure.

After further diagnostics, EE faults were identified using CNN, since the personnel had thermograms (640x480 image size) for this equipment.

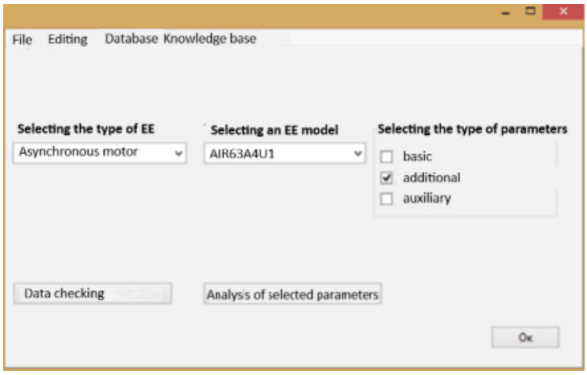


*a*)

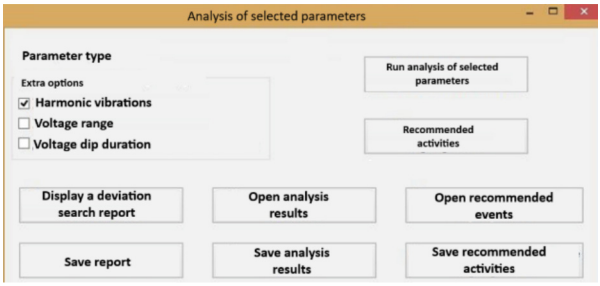


*b*)

**Fig. 2.** Interfaces of raw data input: a) System startup window; b) Window of analysis of the selected parameters.

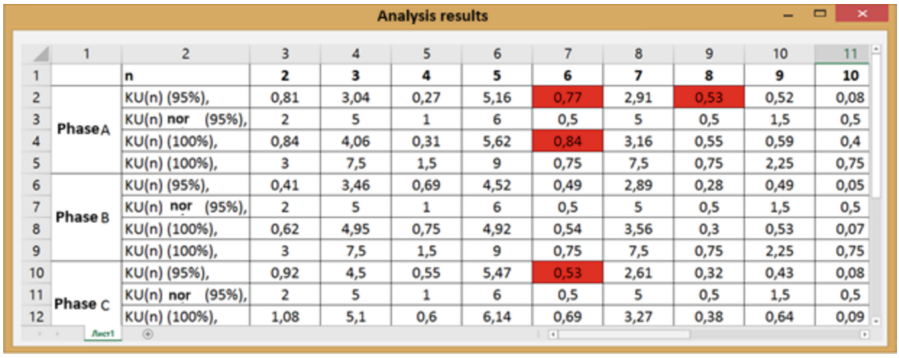


| | 1 | 2 | 3 | 4 | 5 | 6 | 7 | 8 | 9 | 10 | 11 |
|---|---|---|---|---|---|---|---|---|---|---|---|
| 1 | | n | 2 | 3 | 4 | 5 | 6 | 7 | 8 | 9 | 10 |
| 2 | Phase A | KU(n) (95%), | 0,81 | 3,04 | 0,27 | 5,16 | 0,77 | 2,91 | 0,53 | 0,52 | 0,08 |
| 3 | | KU(n) nor (95%), | 2 | 5 | 1 | 6 | 0,5 | 5 | 0,5 | 1,5 | 0,5 |
| 4 | | KU(n) (100%), | 0,84 | 4,06 | 0,31 | 5,62 | 0,84 | 3,16 | 0,55 | 0,59 | 0,4 |
| 5 | | KU(n) (100%), | 3 | 7,5 | 1,5 | 9 | 0,75 | 7,5 | 0,75 | 2,25 | 0,75 |
| 6 | Phase B | KU(n) (95%), | 0,41 | 3,46 | 0,69 | 4,52 | 0,49 | 2,89 | 0,28 | 0,49 | 0,05 |
| 7 | | KU(n) nor (95%), | 2 | 5 | 1 | 6 | 0,5 | 5 | 0,5 | 1,5 | 0,5 |
| 8 | | KU(n) (100%), | 0,62 | 4,95 | 0,75 | 4,92 | 0,54 | 3,56 | 0,3 | 0,53 | 0,07 |
| 9 | | KU(n) (100%), | 3 | 7,5 | 1,5 | 9 | 0,75 | 7,5 | 0,75 | 2,25 | 0,75 |
| 10 | Phase C | KU(n) (95%), | 0,92 | 4,5 | 0,55 | 5,47 | 0,53 | 2,61 | 0,32 | 0,43 | 0,08 |
| 11 | | KU(n) nor (95%), | 2 | 5 | 1 | 6 | 0,5 | 5 | 0,5 | 1,5 | 0,5 |
| 12 | | KU(n) (100%), | 1,08 | 5,1 | 0,6 | 6,14 | 0,69 | 3,27 | 0,38 | 0,64 | 0,09 |

**Fig. 3.** Output interface of the results of the search for deviations of harmonic oscillations values.

The TensorFlow library of the Python programming language was used for CNN development. As a quality criterion of CNN, the accuracy amounted to 96.2% was chosen which means that the EE is operable but with minor deviations.

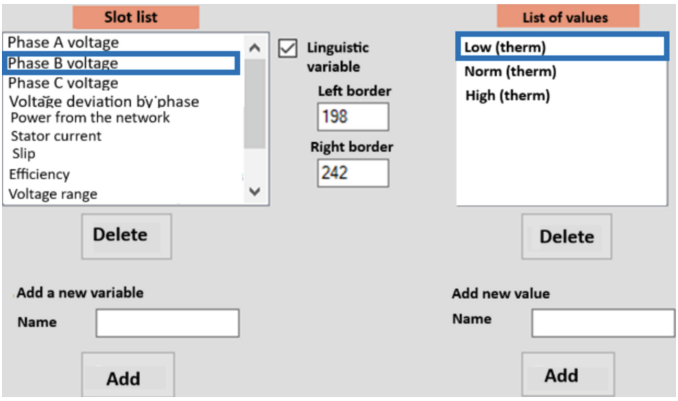


**Fig. 4.** Screen form "Adding parameters and their values".

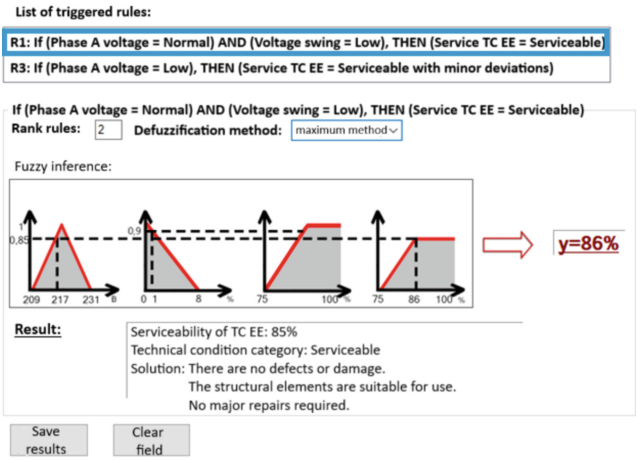


**Fig. 5.** Screen form "Diagnosis result".

The CNN accuracy graph is presented in Fig. 6 (the abscissa axis *OX* shows the number of iterations and the ordinate axis *OY* shows the accuracy).

Having analyzed the thermograms, the increased temperature on the asynchronous motor housing was observed, which is characteristic of winding overheating. In this regard, the following measures were recommended (Fig. 7):

1) analysis of the zero sequence voltage asymmetry coefficient;
2) analysis of the reverse sequence voltage asymmetry coefficient;
3) analysis of voltage asymmetry.

The "Results" button exports the measures obtained to a text document in *.doc format. The results of the studies showed that the asynchronous motor АИР63А4У1 is in serviceable condition, but with minor deviations that were identified when processing

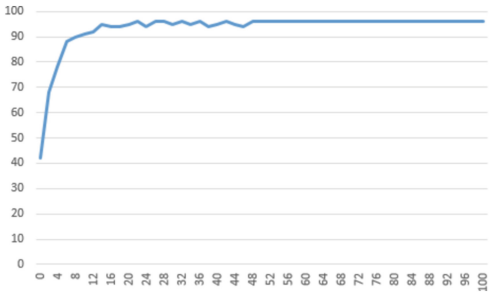


**Fig. 6.** Graph of CNN accuracy.

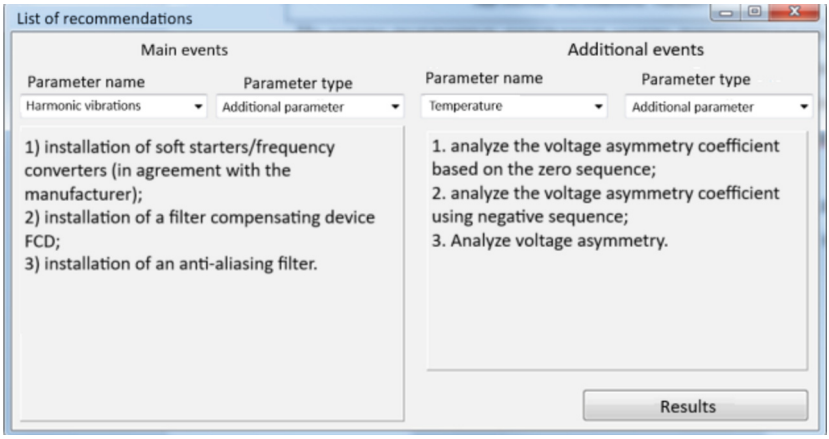


**Fig. 7.** Screen form “Recommended measures”.

data and during the very assessment of the equipment state. Therefore, recommended measures are needed to identify the causes of deviations and eliminate them.

## 4 Conclusion

This paper proposes the structure of the developed program complex for diagnosing ES and EE under conditions of heterogeneous data which is based on a certain sequence of tasks to be solved and applied models, intellectual methods, approaches. The complex is based on interrelated methods and models that are used in a certain sequence, which provides the greatest objectivity, complexity and purposefulness of the results obtained under conditions of incomplete and unclear information.

This complex provides preventing premature failure of ES and ES, increasing the informativeness of decision-making situations and reliability of conclusions about the technical state of equipment under conditions of incomplete and fuzzy information, as well as reducing the time spent on diagnostics by 2 times.

## References


1. Ghoneim, S.S.M., Farrag, T.A., Rashed, A.A., El-Kenawy, E.-S.M., Ibrahim, A.: Adaptive dynamic meta-heuristics for feature selection and classification in diagnostic accuracy of transformer faults. IEEE Access **9**, 78324–78340 (2021)
2. Bukirev, A.S., Savchenko, A.Y., Yatsechko, M.I., Malyshev, V.A.: Diagnostic system of the technical condition of the complex of aircraft on-board equipment based on intelligent information technologies. Model. Optimization Inf. Technol. **8**, 1–12 (2020). (in Russian)
3. Shao, H., Xia, M., Han, G., Zhang, Y., Wan, J.: Intelligent fault diagnosis of rotor-bearing system under varying working conditions with modified transfer convolutional neural network and thermal images. IEEE Trans. Meas. Ind. Inform. **17**, 3488–3496 (2020)
4. Jian, W., Wenbing, Z., Chao, G., Demeng, B., Kuihua, W.: The new developed health index for power transformer condition assessment. In: 2020 5th Asia Conference on Power and Electrical Engineering, pp. 1880–1884 (2020)
5. Wang, Y., Yan, J., Wang, J., Geng, Y.: A novel hybrid transfer learning approach for small-sample high-voltage circuit breaker fault diagnosis on-site. IEEE Trans. Ind. Appl. **59**, 4942–4950 (2023)
6. Ramani, U., Ambika, A., Siva, A., Suganyamahalakshmi, A., Senthilkumar, N., Ranjith, G.: Fault prediction of induction motor using machine learning algorithms. IN: International Conference on Electrical, Electronics, Communication and Computers, pp. 1–4 (2023)
7. GOST 32144-2013 INTERSTATE STANDARD Electric energy. Electromagnetic compatibility of technical means. Standards of quality of electric energy in general–purpose power supply systems. – Moscow: Standartinform 2014. (in Russian)
8. Kolodenkova, A., Vereshchagina, S.: Approach to pre-processing of diagnostic data using fuzzy logic. In: International Conference on Industrial Engineering, Applications and Manufacturing, pp. 1028–1032 (2024)
9. Cao, Q., Zanni-Merk, C., Samet, A., F.D.B de Beuvron, Reich, C.: Using rule quality measures for rule base refinement in knowledge-based predictive maintenance systems. Cybern. Syst. **2**, 161–176 (2020)
10. Kolodenkova, A.E., Vereshchagina, S.S.: Approach to the knowledge base validation of intelligent systems in industrial equipment diagnostics. Vestnik Rostovskogo Gosudarstvennogo Universiteta Putey Soobsheniya **3**, 18–27 (2023). (in Russian)
11. Saxena, L.P.: Niblack's, binarization method and its modifications to real-time applications: a review. Artif. Intell. Rev. **51**, 673–705 (2019)
12. Kolodenkova, A., Vereshchagina, S., Favorskaya, E., Osipova, E.: Approach to the assessment of the technical condition of electrical equipment using weighted fuzzy rules. Ontol. Des. **14**, 134–144 (2024)
13. Kolodenkova, A.E., Vereshchagina, S.S.: Software implementation of algorithms for electrical equipment diagnostics (by the example of harmonic oscillation analysis). Softw. Syst. **37**, 62–68 (2024). (in Russian)


# Representation and Retrieving Situation Method in Situational Knowledge Base of CBR-System Based on Neural Network and Contrastive Learning

Dmitry I. Glukhikh(✉) and Igor N. Glukhikh

Tyumen University, Tyumen, Russia
gluhihdmitry@gmail.com

**Abstract.** The case-based reasoning (CBR) method has proved to be one of the most effective in intelligent decision support systems for the operation of complex objects. CBR assumes the presence of a situational knowledge base (SKB), which stores descriptions ever existed or potentially possible problematic situations and those solutions that are recommended in these situations. When operating complex technological facilities, in order to identify situations, it is necessary to take into account large amounts of data of various types that come from various sources. This makes it difficult to use metrics to assess the similarity of situations. The article proposes to use the approach used in large language and multimodal neural network models to compare and select from SKB situations. A neural network that converts input vectors into embeddings is trained on examples of similar and dissimilar situations in such a way as to best separate the embeddings of dissimilar situations and converge similar situations. This approach can be used to store situations in vector databases (VDB) with built–in search mechanisms. This paper presents the results of a study of the architecture of a neural network, where the input module performs the task of forming embeddings, and the output module performs the task of comparing them with by calculating the similarity score for the final selection. It allows the use of a neural network both independently and in conjunction with a vector database, when the task of preliminary localization of a subset of relevant situations is assigned to the VDB tools.

**Keywords:** case-based reasoning · decision support system · contrastive learning · representation of situation · situation retrieving

## 1 Introduction

The event of potentially dangerous or other problematic situations which can lead to significant losses are possible when operating complex technological objects. The tasks of decision-making are particular relevance in those cases.

The development and implementation of intelligent decision support systems (IDSS) makes it possible to take timely measures to eliminate them, taking into account all


S. Kovalev et al. (Eds.): IITI 2024, LNNS 1209, pp. 279–287, 2024.
https://doi.org/10.1007/978-3-031-77688-5_27

existing conditions and the context of the development of the situation at a complex facility [1, 2]. One of the most effective methods for IDSS working in real time is the case-based reasoning method [3–6]. It allows to quickly proposing a solution in a difficult situation by selecting it from the previously known and stored in the situational knowledge base (SKB), which is also called the case base.

The SKB stores descriptions of practical or potentially possible problem situations and the solutions that are recommended in these situations. Thus, the SKB is a set of <Situation, Solution> pairs organized in some way. If a current problem situation arises, it is compared with those in the SKB. According to a given similarity criterion, the most similar situation is retrieved, and the solution that is paired with it is applied. If there is no situation in the SKB that meets the specified similarity conditions, one or more of the closest analogues is selected. Those analogues can serve as a basis for the operational development of a new solution. In this case, after an appropriate expert assessment, the new solution, together with its situations, can replenish the case base.

To implement CBR in the operation of complex technological facilities, a comprehensive description of the situation is necessary, which should take into account the state of the components of a complex facility, adjacent systems, the external environment and the operational environment, as well as the state of the connections between them. In this case, the solution may be a set of measures, action programs addressed to different participants (operational personnel, support services, managers, etc.). In these conditions, the tasks of developing formal representations of situations on complex objects, methods and models for their comparison and selection become particularly relevant. A common approach to representing a situation as a point in some parametric space, followed by estimating the distances between points in this space, faces difficulties caused by a large number of these parameters and their diversity. To overcome these difficulties, researchers introduce the concept of local metrics with their subsequent aggregation [7, 8].

However, this does not eliminate the difficulties of constructing models for aggregating local similarity metrics for final situation selection, which is even more complicated in conditions of variability in the relative importance of local similarity estimates in various situations.

The task of this study is to develop a method for selecting situations in the SKB based on neural network models that are trained on examples of similar and dissimilar situations. The approach of contrast learning and the use of embeddings is taken as a basis. It implies representing external objects in the internal, hidden space of a neural network, where similar objects (situations) are grouped and not similar are spread. This approach is used, in particular, in modern multimodal neural network models [9].

At the beginning of the article a description of method developed by the authors for representing the situation on an object in the form of a vector, the task of retrieving a situation from the SKB is formulated. Next, the neural network model architecture of situation retrieving is presented, the dataset used in the experiment is described, and the achieved quality metrics are given.

## 2 Methods and Materials

In work [10] proposed a model of a complex technological object (CTO) in the form of a set of Elements $O_i$, each of which is described by a vector $X_i$. Any relatively isolated component of a complex object, its operational environment or the external environment, as well as the connections between them, which must be taken into account when making decisions, can be as an element of the CTO. In the simple case, vector $X_i$ is a set of quantitative parameters that are categorized for use in a neural network. In more complex cases, vector $X_i$ is a vector in the state space. It indicated in which of the possible states (classes of status) this element is located (for example, the "Serviceable - Faulty" state). To form such vectors, state classifiers are used, which can be both rule-based classifiers and classifiers based on neural networks [10].

At the same time, the vector is a representation of the complex situation at a complex technological facility

$$\text{Sit} = \text{Concat}(X_i | i = [1 : N]),$$

where the entry [1:N] means that the index i goes through all values from 1 to N; Concat (.) is the concatenation of vectors; $\text{Sit} \in \mathbf{R}^{1xD}$, D – the total dimension of the vector obtained as a result of concatenation.

When selecting situations from the situational knowledge base, the task of choosing according to the criterion is solved

$$\text{Sim}\ (\text{Sit}, \text{Sit}_z | z = [1 : z]) \rightarrow \max, \tag{1}$$

where Sim is some indicator of similarity between situations; Z is the number of records in the SKB or in a previously allocated segment of the knowledge base.

Based on the results of this task, one Sit* or top-K situations {Sit*} are retrieved with the highest Sim value.

Due to the heterogeneity, possibly high level of autonomy and independence of CTO elements, Sim calculation becomes a problem when Sim is a vector selection criterion:

$$\text{Sim}(\text{Sit}, \text{Sit}_z) = (\text{Sim}_1, \text{Sim}_2, \ldots, \text{Sim}_k, \ldots),$$

where $\text{Sim}_k$ are local similarity metrics between CTO elements or their agglomerations, which in general can be calculated in various ways.

In practice, the choice in the presence of a vector criterion requires separate work to establish priorities between local metrics in order to eliminate multicriteriality. This task is carried out with the involvement of experts, which is time-consuming and resource-intensive. In addition, the relative importance of a local assessment of similarity may vary depending on the general context of the situation.

An alternative approach for assessing the similarity of objects is implemented in modern neural network models, in particular, multimodal networks. Here we use the idea of transferring input vectors into a hidden space and forming internal representations of these vectors in this space using embeddings. The coefficients of the matrices of transformations of the input vector into the internal embedding are selected during training so that the necessary properties and relationships between the input vectors are

most manifested in this new space. In particular, with contrast training, by introducing a loss function that takes into account the distance between vectors, such a result is achieved in order to bring similar vectors (belonging to the same class) together in a new space and separate dissimilar vectors (belonging to another class) as far as possible [11]. An illustration of the result of such a transformation is shown in Fig. 1.

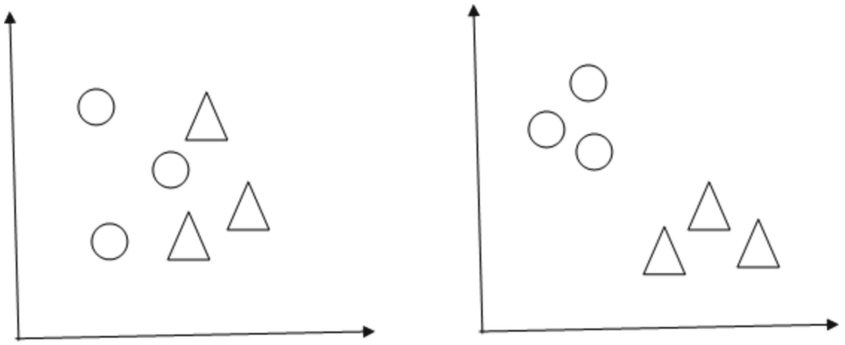

**Fig. 1.** Illustration of the transfer function operation into the hidden space of a neural network. On the left are vectors of objects of two classes in the original space. On the right are vectors of the same objects (embeddings) in the hidden space. Circles are vectors representing one class, triangles are vectors representing another class.

Taking into account this approach, the task of selection in situational knowledge bases is supplemented by another stage, at which the representation of the situation in the form of a Sit is transferred to a hidden space using a pre-trained neural network model $f_W$, which is called an embedder:

$$E = f_W(Sit, W1, L1),$$

where W1 is the set of weights of the neural network model defined during training;

$E \in \mathbf{R}^{1xd}$, d – the dimension of the embedding vector, $d < D$;

L1 – the loss function minimized during training.

The $f_W$ model is a fully connected feed-forward neural network, the number of layers, the number of neurons per layer, activation functions and loss function are hyperparameters that are selected experimentally.

At the next stage, the obtained embeddings of the current situation and the situation from the SKB are compared. For this an additional module of the neural network (retrieving module) can be used, which performs the follow transformation:

$$Sim(Sit, Sit_z) = f_W(E, E_z, W2, L2),$$

where $E_z$ – embedding of z-situation from SKB, W2 – weights of neural network into retrieving module, L2 – loss function.

## 3 Results

The approach described above is implemented in the preparation of a neural network model for comparing and retrieving situations specified by vectors (Fig. 2). The values of the hyperparameters of the model were selected during the experiments according to the quality metrics described below. The neural network model was prepared and implemented using the Keras library in Python.

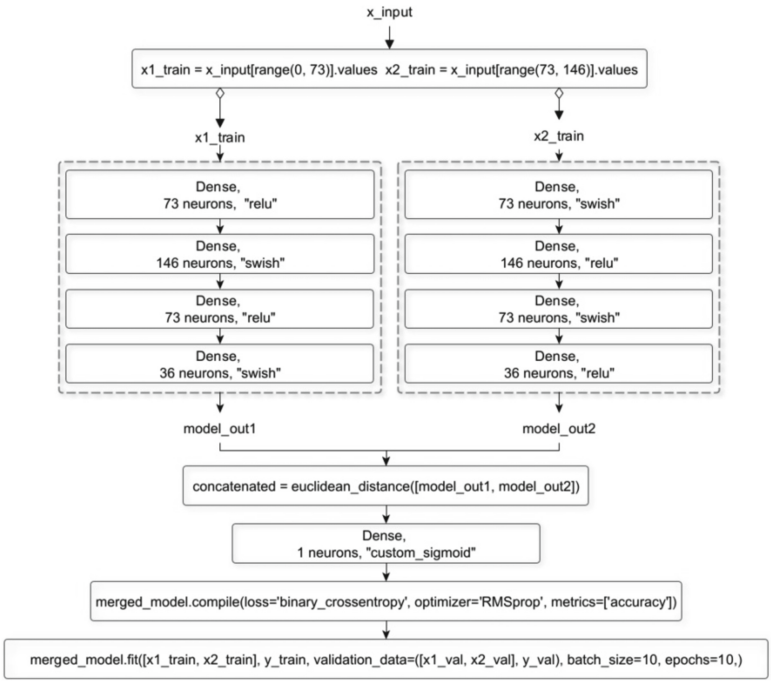


**Fig. 2.** The architecture of neural network model for comparing and retrieving situations

In this architecture, the first M layers are the embedder module, the final layer is the retrieval module. In the model shown in Fig. 2, M = 4. These are fully connected layers through which the vectors of two comparable situations pass separately. At the output, the Euclidean distance is estimated between the obtained embedding vectors of the situation with a dimension of 36 positions, the value of which is transferred to the output layer with the activation function "custom_sigmoid". The model gives similarity estimates in the range from 0 to 1, where 1 is the maximum similarity.

The input situations are represented by vectors of dimension 73 positions. In this case, this is due to the dimensionality of the representation of the situation in the training dataset. When this dimension is changed, the number of embedder layers and the number of neurons in them are defined experimentally based on the quality metrics of the model. The model of choice here is the last layer with one working neuron and the activation

function “custom_sigmoid”, the graph of which is configured for a stronger separation between the results of Sim calculation.

Contrast learning is implemented by selecting pairs of similar and dissimilar situations (positive and negative examples) and using the function of calculating the distances between the embedding vectors of situations. During training, the loss function in the form of binary cross entropy [12] and the Accuracy metric are minimized. This is due to the fact that, in the training mode, the model on the dataset with the labels “similar/dissimilar” learns to solve the binary classification problem. However, in the inference mode, we are interested in the result in the form of some quantitative assessment, which will allow us to rank and select situations. To test this possibility of the model, a separate validation (verification) dataset with labels in the form of a quantitative assessment of similarity is formed in experiments. In this case, it will not be the numbers at the output of the trained model and in the dataset that will be compared, but the ranked sequences of situations – those obtained by the model and which are based on this dataset.

The training data-set contains pairs of situation in kind of vectors combination $<Sit_i, Sit_j>$ with similarity labels $Y \in \{0,1\}$. An example of a vector combination is shown below:

0,0,0,1,0,1,0,0,1,0,0,0,1,0,0,1,0,0,0,1,0,0,0,1,0,0,1,0,0,0,1,0,0,1,0,0,0,1,0,0,1,0,0,0,
1,0,0,1,0,0,1,0,0,1,0,0,0,0,0,0,1,0,0,1,0,0,1,0,0,0,1,0,0,0,1,0,0,0,1,0,0,0,0,0,0,1,1,0,1,0,0,
0,0,0,1,0,1,0,0,0,0,1,0,0,0,1,0,1,0,0,0,1,0,0,1,0,0,0,1,0,0,1,0,0,1,0,0,1,0,0,1,0,0,0,0,0,0,1,0,0,
1,0,0,1,0,0,0,1,0,0,**1**

Here, the first 73 positions are a description of the first $Sit_i$ situation, the next 73 positions are a description of the second $Sit_j$ situation, the last position is the similarity label Y of these two situations (for the training set 0 or 1, i.e. dissimilar/similar).

The data-set contains 150 examples of situations, which appears on smart-farm, which taken as complex technological object. The smart-farm has elements which are described various data: sensors, microclimate parameter, nutrition containing, lighting parameters and condition of plants. The smart-farm and approach of forming of situation vector are considered more detail in article [13]. The training data-set include 5 subsets, each of them is imitation of knowledge base where the one situation compares with 30 other situations with various similarity (from low to high similarity).

The trained model estimated with validation data-set $\{<Sit, Sit_j, Yv_j> \mid i = [1: Nv]\}$, where label $Yv \in [0, 1]$ has obtained by expert assessment. An example of a vector combination is shown below:

0,0,1,0,0,1,0,0,1,0,0,0,1,0,0,0,0,1,0,0,1,1,0,0,0,0,0,1,0,0,1,0,0,1,0,0,0,1,0,0,1,0,0,0,
1,0,0,1,0,1,0,0,0,1,0,0,0,0,1,0,0,0,0,0,1,0,0,1,0,0,1,0,0,0,1,0,0,0,0,1,0,1,0,0,0,1,0,0,0,1,
0,0,1,0,1,0,0,0,0,0,0,1,0,0,1,0,0,1,0,0,0,1,0,0,1,0,0,0,1,0,0,1,0,1,0,0,0,1,0,0,0,0,1,0,0,0,0,
0,1,0,0,1,0,0,1,0,0,**0.884**

Here, the first 73 positions are a description of the first Sit situation, the next 73 positions are a description of the second $Sit_j$ situation, the last position is the similarity label Yv of these two situations (for the validation date set $Yv \in [0, 1]$).

The validation data-set contain 60 situation pairs. It include 4 subsets, each of them is imitation of knowledge base where the one situation compares with 15 other situations

with various similarity (from low to high similarity). Due to this it was made possible to compare for each input Sit a subset of $Sit_j$, which is ranked by down Yv on condition $Yv \geq T$ (threshold for similarity assessment).

The assessment of trained model efficiency has a next approach. The sequences ranked pairs by down similarity were made for each subset from validation data-set.

The first sequence contains pairs with calculated similarity using obtained neural network model. The second sequence contains pairs with similarity based on Yv labels. The third sequence contains pairs with similarity calculated with weighted sum model, where similarity calculated with aggregations of local similarity metrics. The weights coefficients of local similarity metrics were set by an expert and not changed.

The following metrics were used when comparing the results:

– a metric for evaluating the correctness of ranking k situations of the best in terms of magnitude [14]. A value of 98% has been achieved for the neural network model (based on nDCG@k);
– a metric for evaluating the accuracy of the definition of the Accuracy class [15]. In the case under consideration, the class of pairs of situations "similar/dissimilar" with a threshold of $Sim > 0.5$, a value of 100% has been reached for the neural network model.

The experiments have shown that in conditions of a small sample size (150 pairs of situations), the model shows high accuracy in assessing the similarity of situations to the verification data.

It is worth noting that when selecting situations from the database, it is not enough to evaluate the "similar/dissimilar" class. It is more important to evaluate the ability of the model to make the correct selection and ranking of the best options (situations and solutions), which corresponds to the practice of human-machine decision-making [16].

As a result of the mathematical model, collisions arose, i.e. 4 situations were represented by the same similarity values, while the neural network model was able to rank them, while the similarity ranks coincided with the expert's choice.

## 4 Discussion and Conclusion

The experiments have shown that in conditions of a small training sample size, the model shows high accuracy in assessing the similarity of situations from the validation data.

The relevance of ranking increases with the complexity of the object (an increase in the number of elements), when the risk of collisions increases, i.e. cases when the difference of situations in one attribute or local metrics can be compensated by their similarity in other attributes.

One of the important features of the conducted research was the use of a training and validation data-sets with different labels. In the training set, only belonging to the "similar/dissimilar" class of two situations is established, in the test set – the degree of similarity.

Unlike the earlier work of the authors [13], where a data set with labels was used to train the model - expert assessments of the similarity of situations, in this study a new modification of the model is proposed, which is trained on a data set with labels

"similar/dissimilar". At the same time, in the inference mode, the model shows high abilities to rank situations by similarity, which is confirmed by an assessment on a test dataset.

This approach allows you to significantly reduce the cost of creating training data sets. In addition, the division into embedder and output models proposed in this paper opens up additional possibilities for configuring the model taking into account the specifics of the subject area and the applied tasks being solved. It becomes possible to create a library of pre-trained embedders that will use their data sets to adjust to different aspects of the similarity of input situations. For example, it may be a similarity in individual components of situations or a similarity taking into account some additional context.

**Practical Significance**

The conducted research allows us to conclude that neural network models are applicable for selecting situations from the situational knowledge base based on an assessment of their similarity. A machine learning approach is implemented that does not require complex mathematical or logical models using expert knowledge. At the same time, at the stage of forming a training dataset, large labor costs are not required to assess the degree of similarity of each situation.

A further research plan in this direction involves the creation of a framework for CBR with the possibility of integration with modern vector databases [17]. It will allow organizing two-stage case retrieving for decision support in high volume of situational knowledge base.

## References

1. Storey, V.C., Hevner, A.R., Yoon, V.Y.: The design of human-artificial intelligence systems in decision sciences: a look back and directions forward. Decis. Support Syst. **182**, 114230 (2024). https://doi.org/10.1016/j.dss.2024.114230
2. Lin, J.-S., Chen, K.-H.: A novel decision support system based on computational intelligence and machine learning: towards zero-defect manufacturing in injection molding. J. Ind. Inf. Integr. **40**, 100621 (2024). https://doi.org/10.1016/j.jii.2024.100621
3. Kuzyakov, O.N. , Andreeva, M.A.: Applying case-based reasoning method for decision making in IIoT system. In: 2020 International Multi-conference on Industrial Engineering and Modern Technologies (FarEastCon), pp. 1–5. Vladivostok, Russia (2020). https://doi.org/10.1109/FarEastCon50210.2020.9271301
4. Zhang, W., Chen, X., Mao, J., Ke, F., Liang, H.: How to select plan in emergency decision making? A two-stage method with case-based reasoning and prospect theory. Appl. Soft Comput. **155**, 111473 (2024). https://doi.org/10.1016/j.asoc.2024.111473
5. Neykov, N., Stefanova, S.: Case-based reasoning application for parking guidance systems. IFAC-PapersOnLine **55**(11), 150–154 (2022). https://doi.org/10.1016/j.ifacol.2022.08.064
6. Sarkheyli-Hägele, A., Söffker, D.: Integration of case-based reasoning and fuzzy approaches for real-time applications in dynamic environments: current status and future directions. Artif. Intell. Rev. (2020). https://doi.org/10.1007/s10462-019-09723-6
7. Gabel, T., Godehardt, E.: Top-down induction of similarity measures using similarity clouds. In: Hüllermeier, E., Minor, M. (eds.) ICCBR 2015. LNCS, vol. 9343, pp. 149–164. Springer, Cham (2015). https://doi.org/10.1007/978-3-319-24586-7_11

8. Maltugueva, G.S., Yurin, A.Y.: Improving case-based reasoning with the aid of multi-criteria and group decision-making methods. In: 42nd International Convention on Information and Communication Technology, Electronics and Microelectronics (MIPRO), Opatija, Croatia, pp. 1031–1036 (2019). https://doi.org/10.23919/MIPRO.2019.8756874
9. Liu, P., Ren, Y., Tao, J., Ren, Z.: GIT-Mol: a multi-modal large language model for molecular science with graph, image, and text. Comput. Biol. Med. **171**, 108073 (2024). https://doi.org/10.1016/j.compbiomed.2024.108073
10. Glukhikh, I., Glukhikh, D.: Case-based reasoning with an artificial neural network for decision support in situations at complex technological objects of urban infrastructure. Appl. Syst. Innov. **4**(4), 73 (2021). https://doi.org/10.3390/asi4040073
11. Tassis, L.M., Krohling, R.A.: Few-shot learning for biotic stress classification of coffee leaves. Artif. Intell. Agric. **6**, 55–67 (2022). https://doi.org/10.1016/j.aiia.2022.04.001
12. de Boer, P.T., Kroese, D.P., Mannor, S., et al.: A tutorial on the cross-entropy method. Ann. Oper. Res. **134**, 19–67 (2005). https://doi.org/10.1007/s10479-005-5724-z
13. Glukhikh, I., Prokhoshin, A., Glukhikh, D.: Comparison and retrieval of situations in the case-based reasoning system for smart-farm. Inform. Autom. **22**(4), 853–879 (2023). https://doi.org/10.15622/ia.22.4.6
14. Wang, Y., Wang, L., Li, Y., He, D., Liu, T.Y.: A theoretical analysis of NDCG type ranking measures. Comput. Sci. (2013). arXiv:1304.6480
15. Taylor, J.R.: An Introduction to Error Analysis: The Study of Uncertainties in Physical Measurements, 2nd edn, 327 p. Paperback & Clothbound (1997)
16. Ding, R.-X., Palomares, I., Wang, X., Yang, G.-R., et al.: Large-scale decision-making: characterization, taxonomy, challenges and future directions from an artificial intelligence and applications perspective. Inf. Fusion **59**, 84–102 (2020). https://doi.org/10.1016/j.inffus.2020.01.006
17. Taipalus, T.: Vector database management systems: fundamental concepts, use-cases, and current challenges. Cogn. Syst. Res. **85**, 101216 (2024). https://doi.org/10.1016/j.cogsys.2024.101216

# Forming a Rule Base for Product Lifecycle Management Systems

Liliya Kamaletdinova, Anton Romanov(✉), Aleksey Filippov, and Nadezhda Yarushkina

Ulyanovsk State Technical University, Ulyanovsk, Russian Federation
romanov73@gmail.com
https://ulstu.ru/

**Abstract.** The production tasks often contains the integration of a product lifecycle management (PLM) systems and a third-party information systems (IS). This system may not be part of the PLM complex, but provides information support for managing production processes. An analyst is currently responsible for carrying out the integration. He must form a structural and process models of the integrated information system to make interaction rules with the system. During the operation process, besides the analyst, there is an operator involved, who performs maintaining the relevance of the integrated information system data and the entire complex, and a decision maker, who performs managing the integrated information system, namely maintaining its operational state. An approach is to reduce the load both on the analyst, who configures the interaction and display of data, and on the operator, who is involved in ensuring the relevance of data structures, and on the decision-maker, who is involved in making important decisions related to risks in production. The novelty is in using data-based management by forming a data meta-model of the integrated information system based on the analysis of its storage; mapping of the data of PLM systems and the integrated information system on the enterprise through the use of a rule base for the behavior of the integrated information system. This allow to reduce in a 67% the workload of the decision maker.

**Keywords:** Rule base · PLM systems · Data-driven management

## 1 Introduction

Many large manufacturing enterprise use PLM systems [1] to manage the product lifecycle. PLM systems are used to control data flows in production, including such tasks as storing, integrating, and maintaining data in each information subsystem within the complex. The enterprise data bus plays a key role in this [2]. Each complex of systems with a data bus has its own implementation features [3]. However, the common feature of data bus-based integration is the use of rule-based interaction. The analysts perform the following tasks to configure


S. Kovalev et al. (Eds.): IITI 2024, LNNS 1209, pp. 288–300, 2024.
https://doi.org/10.1007/978-3-031-77688-5_28

the interaction between subsystems: building a model of the information system behavior, identifying key features, forming system behavior rules.

This work considers the approach to forming interactions between systems and the approach to managing PLM subsystems. There is often a need to integrate a PLM system with an external information system (integrable IS) that is not part of the PLM complex. But these IS are involved in tasks related to supporting information for managing production processes. Integrating of the two systems perform analyst or decision-maker (DM). The analyst must create structural and process models of the integrable information systems and the create interaction rules with the system are formed. The analyst's (DM) tasks include managing the integrable IS, ensuring the data is up to date, and maintaining the system's operational state.

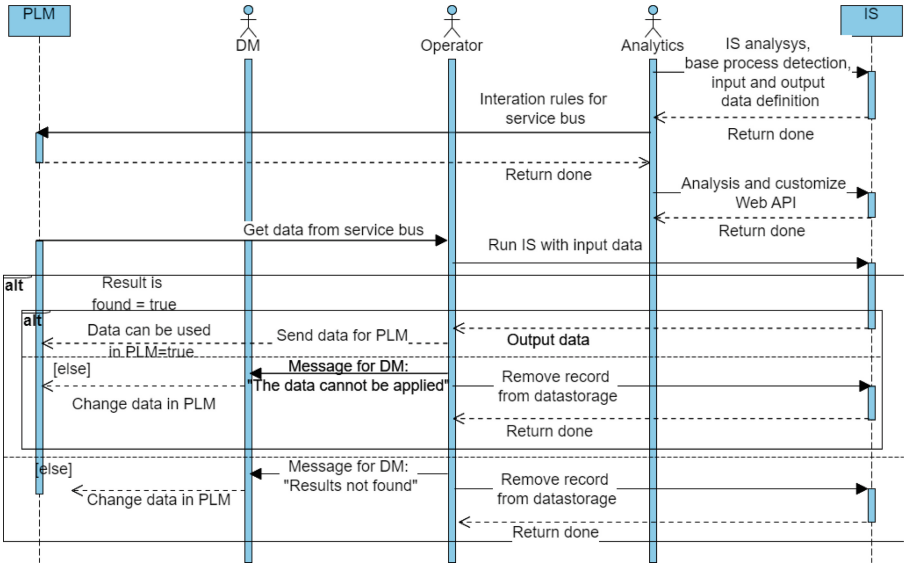


**Fig. 1.** The process of organizing interaction and maintaining a system

One of tasks the operator is the interaction configuration between the integrable IS and the entire PLM complex. The amount of work required by the operator for setting up interaction, data display, and maintaining the system's operational state is considerable. The role of the operator in this process is shown in Fig. 1.

The analyst must consider changes in the data structure of the integrable IS. The operator monitors potential risks associated with ensuring the data matches the PLM complex. The DM makes decisions regarding minimizing possible risks. An approach is proposed that helps reduce the workload on both the analyst responsible for setting up interaction and data display and the operator involved

in ensuring the data structure's timeliness, and the DM making crucial decisions related to potential risks in production.

The novelty is in using data-based management by forming a data metamodel of the integrated information system based on the analysis of its storage; mapping of the data of PLM systems and the integrated information system on the enterprise through the use of a rule base for the behavior of the integrated information system.

The primary advantage of this approach is the ability to form exchange rules not only based on the metadata of information systems, but also based on interaction logs during information exchange.

## 2 Overview of Existing Methods and Approaches to Management

Currently, approaches to managing production information systems are discussed in the following sources: [5–10]. Sources [5,6,8] suggest using an integrated IS model. These approaches directly depend on the accuracy and completeness of the model, with the model being formulated either by an analyst [5,8] or automatically [6], which does not always guarantee the adequacy and accuracy of the model. Source [5] presents classical control based on the model of processes and data in the information system, where the role of the analyst is significant. Source [6] suggests using a framework for model formation. Despite the fact that the model formation process occurs automatically, the controlling component still depends on the accuracy and completeness of the model. Source [7] proposes using a training sample and unsupervised machine learning. However, depending on the completeness and quality of the data sample, the model of the integrated IS being formed may lead to misinterpretation of the results of control mechanisms forecasting, especially if the data contains errors or is heavily noisy. In source [8], a digital twins approach is proposed. Despite the advantages of this approach overall, in the context of the set task, namely integration of information systems, data representation, and reducing the workload of analysts, operators, and managers, the digital twins approach requires additional qualitative analysis and building a model of the information system, leading to an increased workload on the analyst.

In source [9], an approach to human-in-the-loop management is described. The main idea of this approach is complete control of the control system behavior by a human and boils down to supervised machine learning. This approach is the safest in terms of preventing production-related risks, but it is more complex and requires the involvement of managers at all stages of the control system lifecycle, from forming the training sample to monitoring the control system behavior. Therefore, a data-driven control approach is proposed [10]. It is assumed to reduce the workload of the analyst and operator by integrating and partially managing the tasks of the production information system with the developed control system. The data-driven control approach implies:

1. a technique to model-based design of controllers [5];

2. data representation in the integration of PLM systems and the integrated IS of the enterprise by using the rules base of the behavior of the integrated IS;
3. reducing the risks of transitioning to a failure state and maintaining the system in a working state without the involvement of managers in this process.

## 3 Overview of Existing Approaches to Rule Base Formation

To solve the problem, it is proposed to use a production rule-based model. Classical fuzzy systems are based on the Mamdani approach [11]. In such systems, there are 2 modules for converting regular data into fuzzy data. The fuzzification module establishes a correspondence between real values of input data and fuzzy values, based on the membership function. On the other hand, the defuzzification module establishes a correspondence between fuzzy values and real values of output data of the subject area. Fuzzy rule bases (systems based on fuzzy rules) are based on the principle of converting crisp values into fuzzy values. In this case, rules represent a set of linguistic terms, and output data is associated with them; for example, a rule may have multiple input data and only a certain value of the output parameter. There are several variants of classical systems based on fuzzy rules:

1. Mamdani-type fuzzy rules system [12]. Each rule variable represents a value from a set of linguistic terms, for example. If $X_i$ is a variable represented by a set $\{l_1, l_2, l_3\}$, then in the rule variable $X_i$ can be represented as $\{l_1, l_2\}$. The variable can belong to a set of linguistic terms in the rule. This helps reduce the number of rules to avoid increasing the size of the rule base. Thus, a rule can look like: $x_1 = \{l_{11}, l_{12}\} \wedge x_2 = \{l_{23}\} \wedge ... \wedge x_n = \{l_{n1}, l_{n2}\} \rightarrow y = Y$.
2. Approximate systems based on Mamdani fuzzy rules [13]. Such systems include several elements of term sets, which can reduce the interpretability of the output. Systems can achieve greater accuracy at the cost of losing interpretability. Each rule has its own fuzzy set instead of using linguistic terms. This approach generates semantically free rules and has more expressiveness due to the use of various fuzzy sets in each rule. It can take different numbers of rules depending on the complexity of the problem. As for the drawbacks, such systems suffer from a loss of interpretability and may overfit training data, performing poorly on unseen data.
3. Classification systems based on fuzzy rules [14]. A classification system based on fuzzy rules is a system that uses fuzzy rules as a means of learning. In classical systems based on Mamdani fuzzy rules, input data is matched with a single-dimensional output, but in this case, input data is matched with one of the class labels. The rule structure looks as follows: $x_1 = l_{1i} \wedge x_2 = l_{2i} \wedge ... \wedge x_n = l_{ni} \rightarrow y = c$.

There are variants of non-classical systems based on fuzzy rules:

1. Hierarchical fuzzy systems [15] consist of several low-dimensional fuzzy systems arranged hierarchically. Rules in hierarchical fuzzy systems are grouped

into modules according to their roles in the system. Each module calculates a partial solution, which is then passed to modules of the next level. Although each module is a fuzzy system, it generates a significantly smaller number of rules than a flat fuzzy system. Despite the widespread use of hierarchical rule bases when working with big data, there are a number of drawbacks to such systems. The article [16] provides examples of generating a hierarchical fuzzy rule-based model. The article [17] provides examples of optimizing cascading hierarchical fuzzy systems using neural networks, but because the proposed method involves all input variables, the advantage of reducing the number of rules is lost.

2. Neuro-fuzzy systems [18] are a merge of systems based on fuzzy rules with artificial neural networks. The main idea of these systems is the ability to make decisions based on given rules and to learn by using neural systems. The rule base is flat (one-dimensional, unlike hierarchical fuzzy systems), which increases the size of the rule base but simplifies the process of training the neural network during system operation. Neuro-fuzzy systems consist of two modules, the first one is responsible for tuning and structuring the rule condition, and the second one is responsible for forming the consequence. Based on existing rules, the neural network adjusts the rule condition and partially calculates the membership function corresponding to the fuzzy input data. In the second stage, the consequence of the rule is calculated from the fuzzy set of consequences to precise output values.
3. Evolutionary fuzzy systems [19]. Genetic algorithms are used to form the rule base. The difference of this type of fuzzy rule bases is that they are self-learning and self-optimizing. Implementation of this approach is done in two stages:
   - in the first stage, a genetic algorithm (GA) is used to find candidates of fuzzy rules in the knowledge base;
   - in the second stage, GA is used for the knowledge base optimization procedure to exclude the worst rules that have little impact on achieving the final solution.

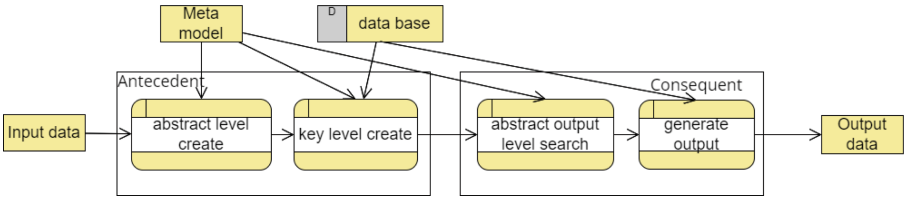


**Fig. 2.** Structure of the hybrid base with fuzzy logical inference

To solve the research problem in data organization, it was decided to combine the hierarchical fuzzy rule base and neuro-fuzzy rule base approaches with a result based on Mamdani fuzzy rules, using an evolutionary algorithm approach

for rule formation based on changes in the metamodel. Thus, the rule base will be structured as shown in Fig. 2.

According to the diagram, the knowledge base consists of several levels of conditions taking into account possible changes in the metamodel and in the database of the integrated information system, and several levels of consequences forming a clear logical inference based on the linguistic representation of rules in the rule base.

## 4 Model of the Knowledge Base of Behavior of the Integrated Information System

According to Fig. 2, the rule base will be represented as a hierarchical structure with two levels of rules. Previously, the authors obtained a structural model of the metadata $M$ of the integrated IS [20]. Thus, the first level will be represented as rules consisting of linguistic terms and will depend on changes in the metamodel. The second level of rules will be dynamically formed based on the results obtained at the first level.

Let $INP = \{INP_1, INP_2, ..., INP_z\}, z \in N$ be the set of linguistic terms representing the input data of the metadata model $M$, and $OUT = \{OUT_1, ..., OUT_w\}, w \in N$ be the set of linguistic terms representing the key processes of the metadata model $M$. Hence, the rule describing the first level will have a set-theoretic representation as follows:

$$P(INP) \rightarrow \{INP^{OUT_s}\}, OUT_s, \tag{1}$$

where $OUT_s$ is a linguistic term reflecting a specific key process of the metadata model $M$, and $\{INP^{OUT_s}\}$ is a set of linguistic terms reflecting the input data for a specific key process of the metadata model $M$.

Let's represent $\{INP^{OUT_s}\}$ as $X$ and $OUT_s$ as $Y$. Table 1 shows the input data for the second-level rule, which will be used to generate the final values of the integrated IS behavior.

**Table 1.** Tabular representation of the input data for the second level rule

| $\mathbf{X_1}$ | $\mathbf{X_2}$ | ... | $\mathbf{X_m}$ | $\mathbf{Y}$ |
|---|---|---|---|---|
| $v_1^1$ | $v_2^1$ | ... | $v_m^1$ | $y^1$ |
| $v_1^2$ | $v_2^1$ | ... | $v_m^2$ | $y^2$ |
| ... | ... | ... | ... | ... |
| $v_1^n$ | $v_2^n$ | ... | $v_m^n$ | $y^n$ |

The columns 1–4 represent the input data values for the key processes of the information system, and column 5 represents the values that are the system's reaction to the input data values.

To form second-level rules of controlling the integrated IS, let's define the following functionality:

$$p(X, V) \rightarrow Y, \tag{2}$$

where $V = \{\{v_1^1, ..., v_m^1\}, \{v_1^2, ..., v_m^2\}, ..., \{v_1^n, ..., v_m^n\}\}$ - the input values of m parameters $X = \{x_k\}, k = [1, m], m \in N, n \in N$, $Y = \{y^i\}, i = [1, n], n \in N$ - $n$ states of the integrated IS.

The system state $y^i$ is determined by the vector of input values $\{v_1^i, ..., v_m^i\}$. To form a rule for controlling the system to transition to a state (issuing control actions) $y^i$, it is necessary to include a comparison of the parameter vector $X$ with the values $\{v_1^i, ..., v_m^i\}$ in the rule's antecedent as shown in Eq. 3.

$$p^i(X, \{v_1^i, ..., v_m^i\}) \rightarrow y^i. \tag{3}$$

During the operation of the integrated IS, there may be situations where different input parameter values lead to the same state $y^i$. In this case, they should be grouped, explicitly specifying the same output state.

To account for uncertainty in input values, fuzzy membership functions of triangular form $\mu_(y^i)(x^i)$ [11] will be used. This function of input parameter values $x^i$ inherent in system state $i$ allows for logical inference even when the input value vector contains values that do not precisely match the values used in the rule antecedents.

## 5 Algorithm for Generating Output Data Based on a Hierarchical Rule Base

The generated rule base contains two levels: abstract, based on metadata of information systems, and actual, reflecting the processes of comparing the attributes of objects exchanged between information systems.

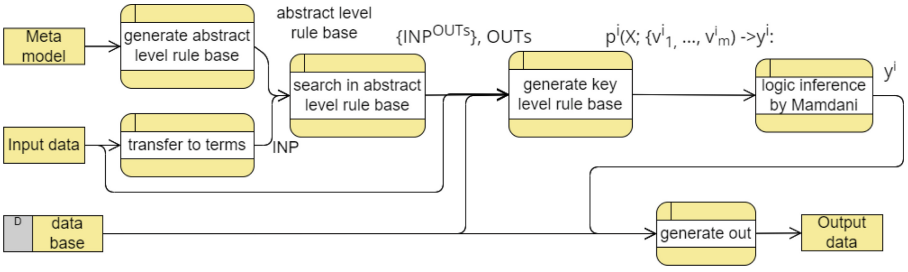


**Fig. 3.** Decision making algorithm

At the first level of the rule, antecedents and consequent contain the names of objects (entities) exchanged between information systems. The second level describes the rules for matching attributes based on the business logic of the

exchange. The fuzzy approach allows us to obtain a solution for cases where the attribute values in the antecedents do not have an exact comparison with the original data, i.e. allows you to determine the state of the system by the value of the membership function. Figure 3 shows the decision-making algorithm using a hierarchical fuzzy rule base with fuzzy logical inference based on the Mamdani approach [11].

First, on the basis of the metamodel, the first level of the rule base is formed (generate abstract level rule base), which will not change until changes occur in the metamodel of the integrated IS itself.

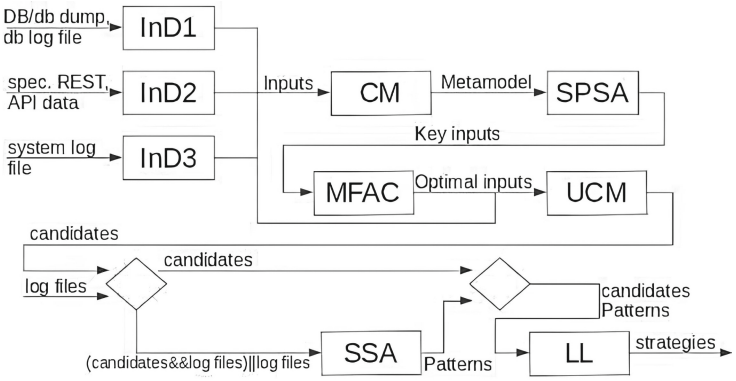


**Fig. 4.** Source data for metamodel and decision making algorithm

The algorithm presented in Fig. 3 consists of the following steps:

- Input data, represented as key-value data tuples from data storage of IS (e.g. $inp1 = 7$) of different types (integer, string, date, and boolean variables), are transformed into linguistic terms represented as $INP = \{INP_1, ..., INP_z\}$, $z \in N$, Fig. 4, for detail see [22].
- Using the first level rule base (abstract level rule base) and the transformed input data ($INP$), a logical inference is performed, represented as $\{\{INP^{OUT_s}\}, OUT_s\}, s \in N$.
- The result of the first level rule execution ($\{INP^{OUT_s}\}, OUT_s$), the original input data (key-value data tuples such as $inp1 = 7$) of different types, and the data base of the integrated IS participate in the dynamic formation of second-level rules (generate key level rule base), whose mathematical representation is given in Eq. 3.
- Through fuzzy logical inference (logic inference by Mamdani) based on the Mamdani approach, the result of rule execution ($y^i$) is obtained based on the second-level rule base.
- In the final stage (generate out), suitable output data are formed as key-value data tuples ($out1 = 7$) of different types (integer, string, date, and boolean variables). The final stage uses the data base of the integrated IS and the

result of rule execution ($y^i$) based on the second-level rule base as input data. The output contains the names of target entities (tables for insertion into integrated information systems) and identifiers for matching records in databases.

Thus, the decision-making process is based on a hierarchical fuzzy rule base with fuzzy logical inference.

## 6 Illustrative Example of a Hierarchical Rule Base

As an example, let's consider the rule base obtained based on the information system designed for processing requests, faveo service desk [21]. The data metamodel described in [22] is shown in Fig. 5.

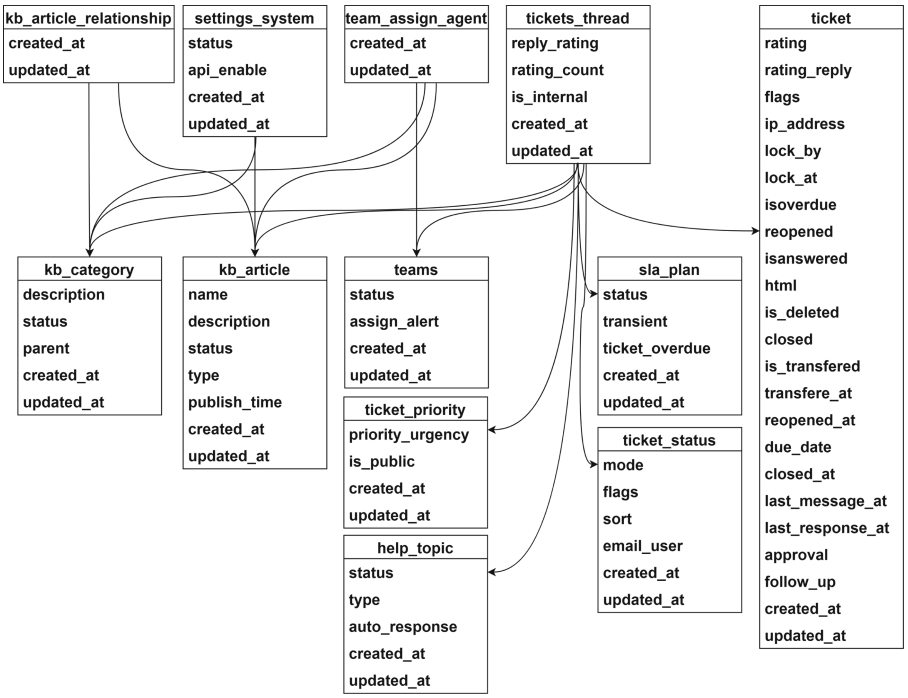


**Fig. 5.** Metamodel of the Faveo information system

Based on the metamodel, a first-level rule base is built, as shown in Fig. 6. The first level contains linguistic terms that reflect the dependency of key processes on input data. The input data has been transformed into a linguistic description beforehand. When comparing the Figs. 5 and 6, differences can be seen between the names of the input entities for the metamodel and the input

data presented as linguistic terms in the rule condition. This is because the input data is transformed before forming the first-level rule base. When following the link of one of the rules presented in Fig. 6, a second-level rule base is dynamically formed. Figure 7 shows an example of a second-level rule base for the key process ticket_thread, shown in Fig. 5. The conditions of the rules contain key parameters with integer values. In the process of fuzzy logical inference, a search for a suitable rule is carried out using the membership function, as a result of which user-friendly data corresponding to the state of the key process with the given input data are generated. An example of the output result is presented in Table 2. With the given input data, CS generated a result that reflects the state of the key process of the faveo service desk information system. This output confirms the feasibility of applying the proposed approach. The generated result reflects real data when working with the faveo service desk ticketing system. Obtaining the result does not depend on the launch of the integrated information system itself. It is an advantage when displaying data and the parallel operation of the integrated information system with the PLM complex.

```
IF
INP = {'kb_article', 'kb_category'}
THEN OUT = {'kb_article'. 'kb_category'}, 'kb_articlerelationship'
IF
INP = {'timezone', 'time_format', 'date_format', 'date_time_format'}
THEN OUT = {'timezone', 'time_format', 'date_format', 'date_time_format'}, 'settings_system'
IF
INP = {'teams', 'users'}
THEN OUT = {'teams', 'users'}, 'team_assign_agent'
IF
INP = {'tickets', 'users', ' ticket_source'}
THEN OUT = {'tickets', 'users', 'ticket_source'}, 'ticket_thread'
```

**Fig. 6.** Base of rules of the first level of the Faveo information system

```
IF
ticket_id=14 AND user_id=l AND source=NULL
THEN id=23;
IF
ticket_id=15 AND user_id=l AND source=NULL
THEN id=24;
IF
ticket_id=8 AND user_id=l AND source=NULL
THEN id=32;
```

```
IF
ticket_id=15 AND user_id=l AND source=NULL
ticket_id=14 AND user_id=l AND source=NULL
ticket_id=13 AND user_id=l AND source=NULL
ticket_id=12 AND user_id=l AND source=NULL
ticket_id=11 AND user_id=l AND source=NULL
ticket_id=10 AND user_id=l AND source=NULL
ticket_id=9 AND user_id=l AND source=NULL
THEN id=31;
```

**Fig. 7.** Base of rules of the second level of the Faveo information system for the key process ticket_thread

## 7 Control System of the Control Complex

The proposed approach involves using a control system to reduce the time and effort of the operator involved in the control process. The control system (CS)

**Table 2.** Result of rule 31

| | | | |
|---|---|---|---|
| **id** | 31 | **body** | Ticket have been deleted by Lily Kamaletdinova |
| **ticket_id** | 9 | **created_at** | 2023-11-29 14:27 |
| **user_id** | 1 | **updated_at** | 2023-11-29 14:27 |
| **format** | 0 | **reply_rating** | 0 |
| **source** | | **is_internal** | 1 |
| **title** | | **ip_address** | |
| **poster** | | **rating_count** | |

is a software tool that implements the proposed management approach based on data [20]. Control involves configuration and data exchange, in this case, through the use of the metamodel of the integrated inforamtion system (IS) and a hierarchical rule base with fuzzy logic inference. The control system acts as an adapter to facilitate the interaction of the integrated IS with the PLM software complex.

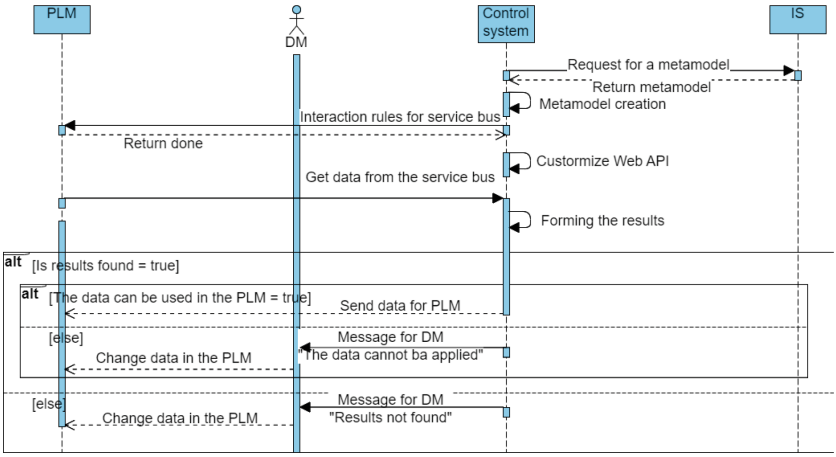


**Fig. 8.** Interaction and maintaining the system in a state of operability

Figure 8 shows the process of organizing the management of an information system with the involvement of a control system. Figures 1 and 8 demonstrate that the control process does not include the role of the analyst and the operator. The CS performs these functions. Also, there are several conditions in both cases:

1. The possible reaction of the integrated IS to input data exists;
2. The influence of the received reaction on the state of the PLM system (the possibility of adding data to the complex without errors and risks to the entire production complex).

It can be seen that the main task of the CS is to adjust the data of the overall PLM complex without interacting with the integrated information system. There were 9 scenarios where the DM was involved. After implementing the subsystem, the number of scenarios reduced to 3. The overall percentage of scenarios in which a person should be involved in working with the system without the CS is 85% 1, while the total number of scenarios when working with the CS is 18%, 8. The main task, in the case of using the CS, is to react to errors in generating results from the integrated IS. This allow to reduce in a 67% the workload of the decision maker.

## 8 Conclusion

The article presents a data-driven management approach applied to production processes. The approach involves using the data metamodel of an information system and a hierarchical rule base for the behavior of the information system with fuzzy logic inference. The described results confirming the feasibility of using this approach for data-driven control. The using its for management and interaction of information systems allow to reduce labor. The approach are relevant in many production facilities of the Russian Federation, including industrial enterprises in the Ulyanovsk region.

**Acknowledgments.** This study was supported the Ministry of Science and Higher Education of Russia in framework of project No. 075-03-2023-143 "The study of intelligent predictive analytics based on the integration of methods for constructing features of heterogeneous dynamic data for machine learn-ing and methods of predictive multimodal data analysis".

## References

1. Terzi, S., Bouras, A., Dutta, D., Garetti, M., Kiritsis, D.: Product lifecycle management - from its history to its new role. Int. J. Prod. Lifecycle Manage. **4**(4), 360–389 (2010)
2. Menge, F.: Enterprise service bus. free and open source software conference (2007). https://programm.froscon.org/2007/attachments/15-falko_menge_-_enterpise_service_bus.pdf
3. Shvedenko, V.N., Shchekochikhin, O.V.: Architecture of an integrated information system that ensures behavioral properties. Sci. Tech. Bull. Inf. Technol. Mech. Opt. **16**(6), 1078–1083 (2016). (In russian)
4. Chekal, E.G.: Reliability of information systems: textbook: in 2 parts. Part 1. In: Chekal, E.G., Chichev, A.A. (eds.) Ulyanovsk: UlGU, 118 p. (2012). (In russian)
5. Zhao, J., Gorez, R., Wertz, V.: Synthesis of fuzzy control systems based on linear Takagi-Sugeno fuzzy models. Multiple Model Approaches To Nonlinear Modelling And Control. CRC Press, pp. 307–336 (2020)
6. Sudarsan, R., Fenves, S.J., Sriram, R.D., Wang, F.: A product information modeling framework for product lifecycle management. Comput. Aided Des. **37**, 1399–1411 (2005)

7. Alahi, M.E.E., et al.: Integration of IoT-Enabled technologies and artificial intelligence (AI) for smart city scenario: recent advancements and future trends. Sensors. **23**(11), 5206 (2023). https://doi.org/10.3390/s23115206
8. Sacks, R., Brilakis, I., Pikas, E., Xie, H.S., Girolami, M.: Construction with digital twin information systems. Data-Centric Eng. **1**, e14 (2020). https://doi.org/10.1017/dce.2020.16
9. Cimini, C., Pirola, F., Pinto, R., Cavalieri, S.: A human-in-the-loop manufacturing control architecture for the next generation of production systems. J. Manuf. Syst. **54**, 258–271 (2020)
10. Hou, Z.S., Xu, J.X.: On data-driven control theory: the state of the art and perspective. Acta Automatica Sinica **35**(6), 650–667 (2009)
11. Mamdani, E.H.: Application of fuzzy algorithms for control of simple dynamic plant. In: Proceedings of the Institution of Electrical Engineers, vol. 121, pp. 1585–1588. IET (1974)
12. Gonzatlez, A., Petrez, R., Verdegay, J.L.: Learning the structure of a fuzzy rule: a genetic approach. Fuzzy Syst. Artif. Intell. **3**(1), 57–70 (1994)
13. Duckstein, L., et al.: Fuzzy Rule-Based Modeling with Applications to Geophysical, Biological, and Engineering Systems, vol. 8. CRC Press, Boca Raton (1995)
14. Chi, Z., Yan, H., Pham, T.: Fuzzy Algorithms: With Applications to Image Processing and Pattern Recognition, vol. 10. World Scientific, Singapore (1996)
15. Razak, T.R., Fauzi, S.S.M., Gining, R.A.J., Ismail, M.H., Maskat, R.: Hierarchical fuzzy systems: interpretability and complexity. Indones. J. Electr. Eng. Inform. **9**(2), 478–489 (2021)
16. Kerr-Wilson, J., Pedrycz, W.: Generating a hierarchical fuzzy rule-based model. Fuzzy Sets Syst. **381**, 124–139 (2020)
17. Duan, J.-C., Chung, F.-L.: Cascaded fuzzy neural network model based on syllogistic fuzzy reasoning. IEEE Trans. Fuzzy Syst. **9**(2), 293–306 (2001)
18. Jang, J.-S.R., et al.: Fuzzy modeling using generalized neural networks and Kalman filter algorithm. AAAI **91**, 762–767 (1991)
19. Komartsova, L.G.: Evolutionary methods for forming fuzzy rule bases (2011)
20. Kamaletdinova, L., Romanov, A.: Control system design. Syst. Anal. Math. Model. **6**, 60–77 (2024). (In russian). https://doi.org/10.17150/2713-1734.2024.6(1).60-77
21. Faveo Service Desk. https://www.faveohelpdesk.com/servicedesk/?lang=ru Accessed 1 May 2024
22. Kamaletdinova, L., Romanov, A., Yarushkina, N.: Industrial data-driven control. In: International Russian Smart Industry Conference (SmartIndustryCon). Sochi, Russian Federation, vol. 2024, pp. 62–67 (2024)

# Data Mining for the Decision Support System of the Expert Scientific Council in the Field of Higher Education

Vladimir D. Vereskun[1], Irina V. Dergacheva[1(✉)], and Sergey Y. Grishaev[2]

[1] Rostov State Transport University (RSTU), Rostov-on-Don, Russia
ira.dergacheva@gmail.com
[2] JSC NIIAS, Rostov-on-Don, Russia

**Abstract.** This study proposes using modern data mining technologies to create a decision support system for an expert scientific commission of a higher educational institution. The methodology for calculating standard values of scientometric indicators is examined. An attempt is being made to create a self-organizing system in the teaching staff, striving to avoid both excessive workload and a decrease in the quality of the educational process. Using the method of cluster data analysis, it is proposed to divide the teaching staff into "workload" groups according to the similarity of the following characteristics: position held, the amount of teaching and methodological workload, the degree of influence on the process of generating scientific ideas (co-authorship significance). It is proposed to establish its own normative intervals of scientometric indicators for each selected cluster, allowing the achievements of the majority of participants in the study group to be considered successful.

**Keywords:** scientometric indicators · scientific productivity · digital transformation · data mining · self-organization · performance-based contract · automated system for managing the educational process of the university

## 1 Introduction

The evaluation of the university teaching staff performance is a critical component of the higher education system in many countries [1–3]. In the USA, Europe, Israel, Spain and India, student ratings and teacher evaluations based on learning outcomes are most widespread. However, studies have shown contradictory results of this type of assessment and incentive methods [4, 5]. In 2021, in Beijing, the Chinese People's Political Consultative Council raised the issue of modernizing the existing system for evaluating university teachers. In the same year, the Ministry of Science and Higher Education of the Russian Federation developed new methodological recommendations within the framework of the policy of effective contracts for higher educational institutions, aimed at correcting the situation of artificially inflating the importance of publication activity over other forms of teaching activity [6]. The integration of scientific research and the


S. Kovalev et al. (Eds.): IITI 2024, LNNS 1209, pp. 301–311, 2024.
https://doi.org/10.1007/978-3-031-77688-5_29

educational process at the university level implies the existence of a direct relationship between the growth of a university's scientific achievements and the quality of its graduates' training [7]. This effect is possible only with a balanced connection between teaching and research [8]. It is necessary to avoid excessive workload for teachers caused by excessive requirements for the number of publications and an increase in classroom hours [9]. The use of the latest achievements in the field of artificial intelligence, including data mining [10], and the creation on its basis of new decision support systems in the field of higher education management [11–13] will allow us to get closer to achieving a balance between pedagogical, methodological and research work of teachers.

An analysis of the current state of research in the field of creating intelligent decision support systems in the field of education has revealed a wide range of opportunities for applying approaches and methods of data mining: from assessing the current state of educational programs and predicting possible scenarios for the digital development of educational institutions [14, 15] to determining the level of professionalism of teaching staff [16].

This study attempts to considers the teaching staff as a self-organizing system capable of regulating its standard indicators of publication activity and generating their realistically achievable values, based on the current situation for the reporting period in each individual educational institution [11, 17].

The relevance of the given research work lies in the need to develop methods that make it possible to optimally calculate the standard values of indicators of teaching work, in order to prevent excessive workload of teachers and, as a consequence, a decrease in the quality of education at the university. The methodology under consideration uses modern advances in the field of data mining and is proposed as a decision support tool in matters of monitoring and stimulating the publication activity of teachers.

## 2 Methodology for Managing the Employees' Publication Activity from the Standpoint of Self-Organization

This study is a continuation of research into the mechanisms of self-regulation of employees' publishing activity by influencing the system of two opposing forces – motivating and restraining [11, 17]. The first is aimed at meeting management requirements and is designed to stimulate performance growth. The second should prevent unnecessary tension in the system, which threatens teachers' "burnout" and a decrease in the quality of student education.

As a restraining force, a methodology for calculating standard intervals for indicators of teachers' publication activity is proposed, which will not be encouraged by additional payments, but will not be the reason for penalties from management. The values of standard intervals (valid in the next reporting period) are calculated based on the results that the main part of the staff managed to achieve over the past period. Employees who differ significantly in their performance will be considered by the system as some kind of "mutation" or outliers. The definition of such outliers and the methodology for their classification are elements of a stimulating force aimed at increasing the publication activity of teachers [11].

Monitoring of teachers' publication activity is carried out through cluster analysis of educational and scientific analytics data.

The previously proposed methodology requires a number of improvements:

- it is necessary first to divide the teaching staff into "workload" groups, according to the similarity of the following characteristics: the amount of teaching and methodological load, position held and average daily earnings for the reporting period. This will allow to take into account the workload of employees. It should be noted that the inclusion of such indicator as average daily earnings in the calculations will allow us to indirectly assess the teacher's workload with additional types of work (administrative position, supervision, carrying out assignments, etc.), for which the teacher receives additional payments;
- for each identified "workload" group, it is necessary to calculate its own specified intervals of publication activity;
- identifying teachers who fall into the "outlier" category should be conducted by repeated clustering in previously identified "workload" groups based on indicators of publication activity: the personal share of article authors and the degree of their co-authorship "significance" in the generation of scientific ideas [12];
- data on teachers falling into the "outlier" category should be sent for consideration by an expert scientific commission of the university to confirm the outlier class, by assessing the results of these employees' scientific research in accordance with the principles of DORA [18], and making a final decision on the amount of rewards or penalties.

## 3 Data Preprocessing and Clustering

**Data Preprocessing.** The initial data for the study were obtained from the educational analytics subsystem of the electronic information educational environment of one of the universities in the Rostov region. Due to the heterogeneity and varying scale of the data, their preliminary processing was required, including procedures for coding categorical variables and normalizing numerical values. In order to simplify calculations and visualize the results, a representative sample ($n = 235$) was formed from 600 teachers of the university under study, including 13 assistants, 25 senior teachers, 160 associate professors and 37 professors. A time period equal to one academic year was chosen as the calculation period.

Each row of the source data table contains a vector of characteristics ($P$) about an individual teacher: the employee's identification number ($id$), his position ($d$), average daily earnings for the reporting period ($s$), share of the rate ($ds$), the number of hours of classroom workload ($t$), as well as a number of indicators characterizing publication activity ($PS$) and methodological work ($PM$).

Let's present information about teachers in the form of a matrix $A_{n\times l}$, where $a_{id,p}$ is a personal indicator of the employee's professional activity for the reporting period $\left(id \in \overline{1,n},\ p \in P\right)$, where $P = \{d, s, ds, t, PM, PS\}$, $PM$ – types of methodological work (Table 1, column $m$), $PS = \{kSW,\ kR,\ kPt,\ SW,\ R,\ Pt,\ wSW,\ wR,\ wPt\}$.

Among the indicators of publication activity ($p \in PS$), the following ones were taken into account:

– total (for the reporting period) number of patents ($kPt$) and articles ($kSW$ and $kR$) published in reputable scientific publications, indexed in the Scopus/WoS and RSCI databases (the core of the RSCI);
– cumulative author's share in the specified scientific works ($Pt$, $SW$, $R$);
– a number of calculated indicators: co-authorship "significance" of the listed works ($wPt$, $wSW$, $wR$).

The estimated indicators of employees, reflecting the "weight" (significance) of co-authorship when publishing scientific works, are calculated as follows:

$$a_{id,wSW} = \frac{a_{id,SW}}{a_{id,kSW}}, a_{id,wPt} = \frac{a_{id,Pt}}{a_{id,kPt}}, a_{id,wR} = \frac{a_{id,R}}{a_{id,kR}},$$

where $a_{id,wPt}$, $a_{id,wSW}$, $a_{id,wR}$ – "weight" of co-authorship in obtaining patents and publishing scientific works published in reputable scientific journals indexed in the Scopus/WoS and RSCI databases (the core of the RSCI), respectively;

$a_{id,Pt}$, $a_{id,SW}$, $a_{id,R}$ – the total authorship share of the teacher in scientific works;

$a_{id,kPt}$, $a_{id,kSW}$, $a_{id,kR}$ – the number of relevant scientific works of the employee.

**Table 1.** Complexity coefficients of developing various types of methodological work

| Type of methodological work ($m$) | Development complexity factor ($k_m$) |
|---|---|
| Updating of the academic course working program, the fund of assessment tools and practice programs | 0,3 |
| Examination of working programs of disciplines, the fund of assessment tools and practice programs | 0,5 |
| Preparation of reviews for textbooks, teaching aids, methodological recommendations, etc | |
| Development of working programs of disciplines, the fund of assessment tools and practice programs | 1 |
| Publication of methodological recommendations | |
| Publishing textbooks and lecture texts | 2 |
| Publishing textbooks | 3 |
| Online course development | 5 |

The indicator of the teacher's total methodological workload is calculated using the following formula:

$$a_{id,M} = \sum_{m \in PM} \left(a_{id,m} \cdot k_m\right),$$

where $a_{id,m}$ is a cumulative authorial share in methodological developments of a certain type ($m$), expressed in the number of printed sheets or the number of presentation slides;

$k_m$ is a complexity coefficient of development, reflecting the time spent on performing a given type of methodological work (see Table 1). The value of the coefficient is established by expert means.

In order to be able to compare the vector characteristics of teachers when calculating the degree of similarity between employees when clustering a community, linear normalization of the data was performed.

**Cluster Analysis of the Degree of the Teaching Staff "Workload".** To illustrate the proposed methodology, an algorithm and a program in Python using libraries for data mining and visualization were developed. The code can be found at https://github.com/ID50/Support-system.

The t-SNE visualization method [19] was used to assess the spatial decomposition of elements in the studied set. Reducing the dimension of vectors-characteristics of $A_{n\times l}$ matrix objects from $l$-dimensional space to two-dimensional space allowed us to make a decision to divide the sample under study into three clusters ($Q^q$, $q \in \overline{0,2}$) (Fig. 1).

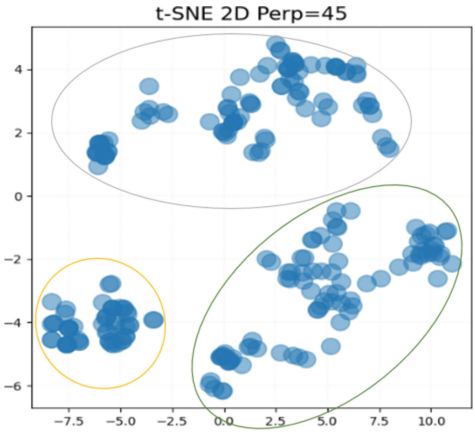


**Fig. 1.** Clustering according to the degree of "load" of the teaching staff (t-SNE)

Clustering was carried out using the K-means method according to the similarity of the following "workload" characteristics: the volume of teaching ($a_{id,t}$) and total methodological ($a_{id,M}$) load of a teacher, a position held ($a_{id,d}$) and average daily earnings for the reporting period ($a_{id,s}$) (Fig. 2).

The zero cluster ($Q^0$) included teachers with high teaching and low methodological loads. The first cluster ($Q^1$) consisted of employees who were mainly engaged not so much in teaching activities as in administrative work, who had high earnings with little auditory and methodological workload. The second cluster ($Q^2$) included teachers with a high methodological and teaching load.

**Determination of the Boundaries of Normative Intervals.** To calculate the boundaries of normative intervals for indicators of publication activity, it is proposed to use Tukey's internal boundaries method [11], which makes it possible to set the lower ($LL_p$) and upper ($UL_p$) boundaries of the interval so that it includes the values achieved during the reporting period by the majority of the studied "workload" group.

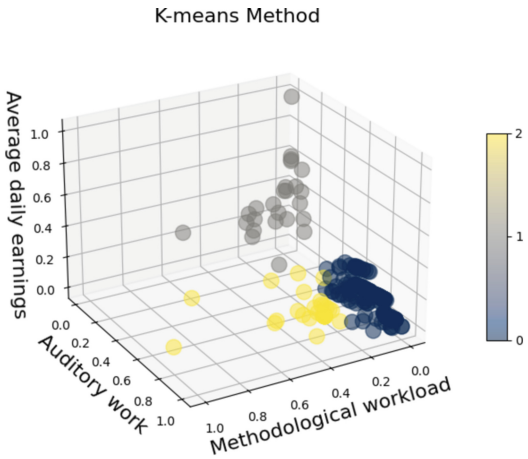


**Fig. 2.** Clustering according to the degree of "load" of the teaching staff (K-means)

Table 2 presents the calculated normative intervals of normalized indicators of publication activity for three "load" clusters, obtained during a numerical experiment carried out using the model.

**Table 2.** Normative intervals of normalized business activity indicators

| | $LL_{wSW}$ | $UL_{wSW}$ | $LL_{wR}$ | $UL_{wR}$ | $LL_{wPt}$ | $UL_{wPt}$ | $LL_{SW}$ | $UL_{SW}$ | $LL_R$ | $UL_R$ | $LL_{Pt}$ | $UL_{Pt}$ |
|---|---|---|---|---|---|---|---|---|---|---|---|---|
| $Q^0$ | –0.38 | 0.38 | –0.4 | 0.85 | 0 | 0 | –0.12 | 0.12 | 0 | 0.16 | 0 | 0 |
| $Q^1$ | 0.14 | 0.47 | 0.13 | 0.67 | 0 | 0 | –0.5 | 0.87 | –0.35 | 0.79 | 0 | 0 |
| $Q^2$ | 0 | 0 | –0.39 | 0.61 | 0 | 0 | 0 | 0 | 0 | 0.09 | 0 | 0 |

Based on the obtained values of normative intervals, the values of normalized personal indicators of publication activity were standardized:

$$x_{id,p} = \begin{cases} -1 & \text{for } a_{id,p} < LL_p, \\ 0 & \text{for } LL_p \le a_{id,p} \le UL_p, \\ a_{id,p} & \text{for } a_{id,p} > UL_p. \end{cases}$$

where, $x_{id,p}$ is a standardized personal indicator of an employee's publication activity $\left(id \in \overline{1,n},\ p \in PS\right)$, that is considered either unfulfilled $\left(x_{id,p} = -1\right)$, fulfilled $\left(x_{id,p} = 0\right)$, or exceeded $\left(x_{id,p} \in (0;1]\right)$.

## 4 Results of Cluster Analysis and Classification of Outliers

To identify teachers whose performance significantly differs from the majority of employees in the community under study, each of the "workload" groups was re-clustered according to the similarity of the monitored signs of publication activity. The DBSCAN nearest neighbors method was chosen as a clustering method, which made it possible to identify a number of employees who fell into the "outlier" category in each cluster (Fig. 3). To visualize the obtained results, the dimension of the vectors of characteristics of teachers' publication activity was reduced to three dimensions using the PCA method.

Let's introduce the concept of the final indicator of an employee's publication activity, $SumID_{id}$, the value of which will be equal to the sum of his personal standardized indicators in the specified direction for the reporting period:

$$SumID_{id} = \sum_{p \in PS} x_{id,p}, \ id \in \overline{1,n}.$$

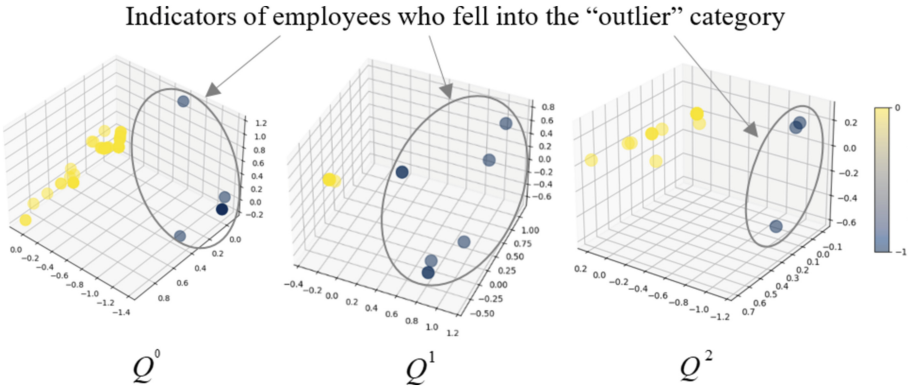


**Fig. 3.** Definition of "outliers" based on the values of publication activity indicators

To develop further recommendations, we classify "outliers" by comparing the values of the final indicators of publication activity of employees who fall into the "outlier" category with the values of the same indicators for typical representatives of their "workload" clusters.

Let us denote that an object belongs to typical representatives of the cluster by the abbreviation *tr* (typical representative), and to "outliers" by the abbreviation *er* (extreme representative).

$ID^{tr,q}$ is a set of identification numbers of employees who are typical representatives of their "workload" cluster $Q^q$, $q \in \overline{0,2}$.

$ID^{er,q}$ is a set of identification numbers of employees who fall into the "outlier" category in their "workload" cluster $Q^q$, $q \in \overline{0,2}$.

$SumID_{id}{}^{er,q}$ is the final indicator of publication activity of an employee $id$ ($id \in ID^{er,q}$) who falls into the "outlier" category in his "workload" cluster.

$F_{id}$ is a class of an employee $id\,(id \in ID^{er,q})$ who falls into the "outlier" category:

$$F_{id} = \begin{cases} 0 & \text{, a "outlier" is undescriptive} \\ 1 & \text{, a candidate for reward} \\ -1 & \text{, a candidate for penalty} \end{cases}.$$

Let's calculate the maximum and minimum values of the final publication activity of typical representatives of the cluster $q\left(q \in \overline{0,2}\right)$:

$$SumIDmax^{tr,q} = \max_{id \in ID^{tr,q}} SumID_{id}^{tr,q},\ q \in \overline{0,2},$$

$$SumIDmin^{tr,q} = \min_{id \in ID^{tr,q}} \left(SumID_{id}^{tr,q}\right),\ q \in \overline{0,2},$$

where $SumID_{id}{}^{tr,q}$ is the final indicator of the publication activity of an employee $id$ who is a typical representative of his "workload" cluster.

Below is a fragment of the outlier classification algorithm (Fig. 4).

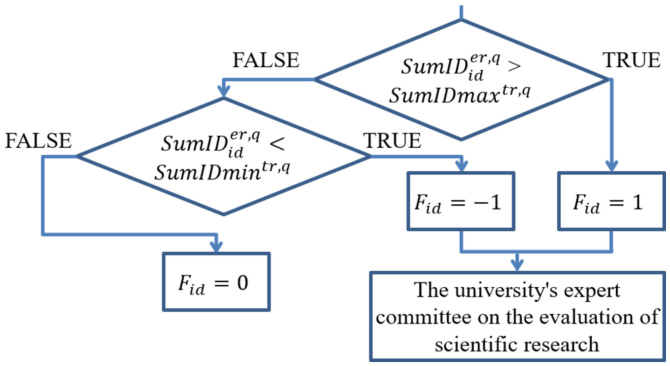


**Fig. 4.** Fragment of the "outlier" classification algorithm

Table 3 presents the values of the initial data of employees who fell into the "outlier" category. The obtained results confirmed the expected expert assessment of the publication activity of employees.

The subject of further research is the selection of the optimal amount of reward and penalties for employees who fall into the "outlier" category, the goal of which will be to achieve a balance between the pedagogical, methodological and research work of teachers.

**Table 3.** A fragment of the values table of the initial data of employees who fell into the category "outlier"

| | id | d | wSW | wR | kSW | SW | kR | R | Pt | F |
|---|---|---|---|---|---|---|---|---|---|---|
| $Q^0$ | 6 | 1 | 0 | 1 | 0 | 0 | 1 | 1 | 0 | 0 |
| | 95 | 3 | 0 | 1 | 0 | 0 | 2 | 2 | 0 | 0 |
| | 122 | 3 | 0.33 | 1 | 1 | 0.33 | 1 | 1 | 0 | 0 |
| | 131 | 3 | 0.25 | 1 | 1 | 0.25 | 1 | 1 | 0 | 0 |
| | 140 | 3 | 0.33 | 1 | 1 | 0.33 | 1 | 1 | 0 | 0 |
| | 177 | 3 | 0 | 0.5 | 0 | 0 | 13 | 6.2 | 0 | 1 |
| | 113 | 3 | 0.5 | 1 | 1 | 0.5 | 2 | 2 | 0 | 1 |
| $Q^1$ | 135 | 3 | 0.16 | 0 | 1 | 0.16 | 0 | 0 | 0 | -1 |
| | 209 | 4 | 0.29 | 0 | 6 | 1.78 | 0 | 0 | 0 | -1 |
| | 145 | 3 | 0.58 | 0.75 | 3 | 1.75 | 4 | 3 | 0 | 1 |
| | 157 | 3 | 0.25 | 1 | 1 | 0.25 | 1 | 1 | 0 | 1 |
| | 160 | 3 | 0.39 | 0.37 | 8 | 3.15 | 15 | 5.58 | 0 | 1 |
| | 207 | 4 | 0.17 | 1 | 1 | 0.17 | 3 | 3 | 0 | 1 |
| | 215 | 4 | 0.3 | 0.9 | 1 | 0.3 | 6 | 5.5 | 0 | 1 |
| | 219 | 4 | 0.5 | 0.6 | 1 | 0.5 | 11 | 6.8 | 0 | 1 |
| $Q^2$ | 58 | 3 | 0 | 0.67 | 0 | 0 | 2 | 1.33 | 0 | 0 |
| | 169 | 3 | 0 | 0.75 | 0 | 0 | 2 | 1.5 | 0 | 0 |
| | 228 | 4 | 0 | 0.58 | 0 | 0 | 6 | 3.5 | 0 | 0 |

## 5 Conclusions

The following proposals were made in the study:

- to apply clustering of data on scientific and pedagogical activities according to the degree of teachers' "workload";
- to calculate standard intervals of publication activity separately for each of the selected "workload" groups;
- to introduce an indicator reflecting the "weight" (significance) of co-authorship, taking into account the degree of personal influence on the process of generating scientific ideas;
- to determine whether an employee falls into the "outlier" category by re-clustering in previously identified "workload" groups;
- the final decision on the amount of incentives or penalties for teachers who fall into the "outlier" category should be made by the university's expert scientific commission in accordance with the principles of DORA, based on an assessment of the significance of the applicants' scientific research;
- to recommend rewarding teachers whose publication activity indicators fall into the "useful outlier" category, without canceling existing incentive payments for the publication of scientific works.

Based on Data Mining technologies, a methodology for monitoring and classifying "outliers" has been developed with the aim of integrating this methodology into the decision support system of the university's expert scientific commission in assessing the publication activity of employees.

Future research plans include:

- numerical determination of the similarity between the characteristics of the studied groups based on the measure of correspondence of the variation of the resulting characteristic from one (when studying paired dependencies) or several (multiple) factor characteristics. Since these categories are fuzzy and, as a rule, poorly formalized, to solve this problem it is assumed to determine membership functions based on statistical indicators and involve the apparatus of fuzzy logic;
- expanding the range of input parameters for assessing the activities of scientific and teaching workers and, accordingly, the application and comparative analysis of various clustering methods in the context of the task;
- analysis and improvement of methods for taking into account expert opinions to determine the "weights" (significance) of various performance indicators of the groups under study.

## References

1. Mastrokoukou, S., et al.: Rediscovering teaching in university: a scoping review of teacher effectiveness in higher education. Front. Educ. **7**, 861458 (2022). https://doi.org/10.3389/feduc.2022.861458
2. Qiaofang, L.: Personnel status and problems of teaching staff in private higher education institutions in China. Teacher XXI Century, pp. 66–75 (2020). https://doi.org/10.31862/2073-9613-2020-3-66-75
3. Isla-Díaz, R., et al.: Una mirada longitudinal: ¿Es el "Docentia" útil para la evaluación del profesorado universitario? RELIEVE - Revista Electrónica de Investigación y Evaluación Educativa **24**(2) (2018). https://doi.org/10.7203/relieve.24.2.12142
4. Springer, M.G., et al.: Team pay for performance. Educ. Eval. Policy Anal. **34**(4), 367–390 (2012). https://doi.org/10.3102/0162373712439094
5. Muralidharan, K., Sundararaman, V.: Teacher performance pay: experimental evidence from India. J. Polit. Econ. **119**(1), 39–77 (2011). https://doi.org/10.1086/659655
6. Kuznetsova, E.I., Dianov, D.V., Ovezova, U.A., Suslov, A.V., Markova, T.S.: Career and salary of a university teacher: personnel policy regulation in Russia. Revista Tempos e Espaços em Educação **14**(33), e16267 (2021). https://doi.org/10.20952/revtee.v14i33.16267
7. Unger, M., Polt, W.: The knowledge triangle between research, education and innovation – a conceptual discussion. Foresight STI Gov. **11**(2), 10–26 (2017). https://doi.org/10.17323/2500-2597.2017.2.10.26
8. Leišytė, L., Pekşen, S., Rose, A., Želvys, R.: The teaching-research nexus in the Lithuanian higher education compared to other European higher education systems. In: The Changing Academy – The Changing Academic Profession in International Comparative Perspective, pp. 137–160 (2022). https://doi.org/10.1007/978-3-031-04439-7_8
9. Rouch, D.A.: Education staff work activities and excessive workloads: where to now? Clarendon Policy & Strategy Group (9) (2019). https://www.researchgate.net/publication/344201356_Education_staff_work_activities_and_excessive_workloads_where_to_now

10. Savvas, I.K., Michos, C., Chernov, A., Butakova, M.: High performance clustering techniques: a survey. Adv. Intell. Syst. Comput. **1156**, 252–259 (2020). https://doi.org/10.1007/978-3-030-50097-9_26
11. Dergacheva, I.V.: Intelligent decision support system for improving the efficiency of higher education institutions. In: Kovalev, S., Tarassov, V., Snasel, V., Sukhanov, A. (eds.) IITI 2021, LNNS, vol. 330, pp. 331–340. Springer, Cham (2022). https://doi.org/10.1007/978-3-030-87178-9_33
12. Dergacheva, I.V.: Intelligent scoring of publication activities and personal share of Co-authorship in the decision support system for rewarding University employees. In: Kovalev, S., Sukhanov, A., Akperov, I., Ozdemir, S. (eds.) IITI 2022. LNNS, vol. 566, pp. 195–204. Springer, Cham (2023). https://doi.org/10.1007/978-3-031-19620-1_19
13. Liu, R.: Data analysis of educational evaluation using K-means clustering method. Comput. Intell. Neurosci. **2022**, 1–10 (2022). https://doi.org/10.1155/2022/3762431
14. Yağcı, M.: Educational data mining: prediction of students' academic performance using machine learning algorithms. Smart Learn. Environ. **9**(1) (2022). https://doi.org/10.1186/s40561-022-00192-z
15. Musso, M.F., Hernández, C.F., Cascallar, E.C.: Predicting key educational outcomes in academic trajectories: a machine-learning approach. High. Educ. **80**(5), 875–894 (2020). https://doi.org/10.1007/s10734-020-00520-7
16. Zyateva, O.A., Pitukhin, E.A., Astafyeva, M.P.: Clustering of scientific activity of faculty staff based on the results of publication activity. In: Silhavy, R., Silhavy, P., Prokopova, Z. (eds.) CoMeSySo 2020. AISC, vol. 1295, pp. 771–778. Springer, Cham (2020). https://doi.org/10.1007/978-3-030-63319-6_71
17. Stafford, B.: Brain of the Firm, 415 p. Wiley, Chichester (1994)
18. San Francisco declaration on research assessment: Science Editor and Publisher **5**(1), 51–53 (2020). https://doi.org/10.24069/2542-0267-2020-1-51-53
19. Kang, B., García García, D., Lijffijt, J., Santos-Rodríguez, R., De Bie, T.: Conditional t-SNE: more informative t-SNE embeddings. Mach. Learn. **110**(10), 2905–2940 (2020). https://doi.org/10.1007/s10994-020-05917-0

# Fuzzy Situational Control at the Stages of the Medical-and-Technological Process: Problems and Possible Solutions

Boris A. Kobrinskii(✉)

Intelligent Decision Support Systems, Federal Research Center "Computer Science and Control" of the Russian Academy of Sciences, Moscow, Russian Federation
bak@isa.ru

**Abstract.** Fuzzy situational control allows to identify current fuzzy situations in conditions of incomplete information about the state and operation of an object. The multi-stage diagnosis and treatment process involves a huge number of situations. Various transient states of an object (human body) represent its temporal extent. Situational control can and should be used at different stages of the medical and technological process. It involves identifying fuzzy risk situations that can affect the development of a pathology, diagnosing the developed disease, as well as analyzing data from monitoring systems to detect pre-critical conditions and providing guidelines for object (human) exposure to transform a dangerous situation into a new, more favorable one. This paper examines an approach to designing a situational management system for the medical and technical process. We present a variant of the patient's clinical pathway in a traditional setting and under conditions where a complex medical and technological process system potentially operates.

**Keywords:** situational control · medical-and-technological process · fuzzy sets · complex system · monitoring of pre-critical states

## 1 Introduction

The process of diagnosis and treatment is multi-stage. The starting points may be a polyclinic or an ambulance. The next stage may be an examination and treatment in a specialized clinical diagnostic center or hospital.

In medical systems, it is important to ensure consistent personalized control over the diagnostic and treatment process, including monitoring the occurrence of complications and other pre-critical conditions. Integrating artificial intelligence (AI) into healthcare holds great potential for improving disease diagnosis, treatment selection, and clinical laboratory testing. AI offers increased accuracy, reduced costs, and time savings while minimizing human errors. It can revolutionize personalized medicine, enhance population health management [1]. Medical-and-technological process (MTP) can be considered from the standpoint of the situational control (SP), which is a field of artificial


S. Kovalev et al. (Eds.): IITI 2024, LNNS 1209, pp. 312–323, 2024.
https://doi.org/10.1007/978-3-031-77688-5_30

intelligence. On the operational level, care delivery should consider logistic challenges, data management, and algorithmic stewardship [24].

A human body is a complex self-organizing system. In response to various internal changes (biological component) and external influences (environmental component), rapid or slow changes occur manifesting themselves either as various situations within the normal range of reaction or in the form of pathological processes. However, in decision making practice one inevitably has to deal with various difficulties caused by uncertainty, such as incomplete or unreliable information, and the presence of a factor of randomness of changes. At the same time, the safety of the planned methods for observation and treatment should be considered (taking into account side effects and comorbidity).

As a rule, decisions on how to influence a system (human body) are taken in conditions of partial uncertainty and not always considering sufficient information on the observed pathological process. This is due to the level of examination of the patient, individual characteristics of the human body, and the presence of concomitant chronic diseases. Fuzzy, uncertain, underdetermined, and ambiguous data [19] create serious problems for decision making in clinical practice.

A control system with parametric uncertainty [25] can correspond to high variability of body parameters. Subordinate control is used in multi-loop systems when there is parametric uncertainty in the object. This allows us to achieve the desired level of control, both for the system as a whole and for each individual loop [21]. This is important in terms of controlling the interconnected systems of the body. Quasi-invariant control is possible when not only the parameters of the control function are unknown, but also the parameters of the controlled object itself, in conditions of a priori parametric uncertainty and in case of external influence [10]. In medicine, this occurs in various situations, for example, with a labile form of arterial hypertension, during periods of abrupt changes in solar activity. The recognition of various pathological situations and the treatment process that ensures regression of the disease are the most important problems in medicine. An intelligent control system can play a significant role in solving this problem.

## 2 The Problem of Control in Clinical Medicine

The problem of controlling the diagnostic and treatment process cannot be solved on the basis of the traditional theory of automatic control. This obliges us to turn to non-traditional control objects characterized by such properties as uniqueness, difficulty to formalize control criteria, lack of optimality, incomplete description, and the presence of "free will" of the decision maker, since the final decision remains with the physician, who is responsible for decisions at each stage of the diagnostic and treatment process. In this regard, the theory of situational control is of particular interest [17, 18, 22]. It includes situation modeling, situation recognition, and situational reasoning. A specific feature of situational control is the ability to describe in a uniform way situations that develop at the control object, to predict the state of the object in time under the influence of controlled and uncontrollable factors, as well as to ensure the presence of the optimizing object control.

The standard control procedure cannot be applied to weakly structured objects. In medicine, outwardly similar diseases can have different etiologies and, accordingly, different mechanisms of disease development, and therefore, different treatment regimens are used. These regimens consider possible side effects of drugs. It is also necessary to consider the possibility of not only a smooth course of the disease, but sudden changes in the patient's state. In addition, it should be noted that medical-and-technological systems are especially characterized by incomplete descriptions. It is influenced by several factors, including a lack of medical history for patients in a coma and incomplete examinations, among others. The dynamism of a living system is determined by the evolution of the human body during the life of a person and during the course of pathological processes. Situational control assumes the possibility of using various methods of artificial intelligence, in particular multi-agent systems, semantic networks, self-organizing or dynamic adaptive systems, as well as sensor networks, with the simultaneous role of the human factor [11].

In the process of life activity, changes occur in the structure, parameters, and modes of functioning of the body. Ethnic and individual characteristics condition different reactions to the influence of external factors, which are stochastic or deterministic in nature. At different stages of the pathological process, unexpected situations may arise. The analogue should be a complex technical system (CTS), characterized by multi-component, many quantitative and qualitative parameters, nonlinear relations, incomplete information, various influences of internal and external factors, risks of dangerous situations, and the catastrophic nature of their consequences. Peculiarities of CTS control help to justify the feasibility of applying fuzzy situational approach that allows to consider the specifics of compositional modeling and various situational control strategies, depending on the prevailing conditions and requirements [7]. The method of fuzzy situational control over CTS based on compositional hybrid models consists in the use of a pre-built fuzzy situational control network (setting fuzzy situational features, fuzzy situations, control decisions, control transitions) to identify current situations, search and select sequences of control decisions when transferring CTS into goal situations. Neuro-fuzzy cognitive temporal models make it possible to consider the mutual influence of concepts with different time lags relative to each other [6].

Incompleteness and uncertainty of data, complexity of formalizing criteria for the effectiveness of "control" over the body (prevention and treatment) complicate the choice and implementation of appropriate strategies for achieving the goal function (maintaining health and performance), which should be reviewed and optimized in accordance with the level of health, monitoring the transition states of the body in the interval norm – pre-disease – various stages of the disease [13].

## 3 Principles of Situational Control over the Diagnostic and Treatment Process

The physician is in the human health control loop. Accordingly, we formulate the following definitions.

Definition 1. We will call the current situation at the control object (the process of diagnosing and/or treating a specific person) the totality of all available information on the control object and its functioning at a given point in time.

Definition 2. We will call a prognostic situation a set of possible trajectories of the pathological process including complications (deviations in the functioning of various body systems) that are a consequence of negative disease development or a by-product of the use of drugs.

Definition 3. We will call a complete situation a set that includes the current situation, knowledge about the state of the system (body) at a given point in time, and knowledge about control methods (theoretically possible preventive and therapeutic effects) that should be given to the user (physician) in the form of possible solutions. Thus, if a situation $Q_j$ has developed at the control object, and the state of the system and the technological control scheme determined by $S_i$ allow the use of influence $U_k$ (provided that the methods applied are safe for a particular patient, taking into account his/her condition), then it is used, and the current situation $Q_j$ is proposed to be transformed into a new situation $Q_i$ using logical transformation rules.

## 4 The Problem of Fuzziness and Uncertainty in the Control of Medical-and-Technological Process

In medicine, data received from a physician is subjective-objective or unclear. The results of auscultation depend on what and how the physician hears; descriptions of the results of instrumental studies are determined by the resolution of the equipment (potential underdetermination) and the physician's experience (subjective aspect). The fuzziness of the object of cognition in medical practice reflects the fuzziness in the world. For example, the transition from one color to another is reflected in the evaluation of a patient's complexion, which can be pale, paleish or pale pink. The assessment of overall health, including tension in regulatory systems and pre-illness is characterized by continuous changes, which are measured by doctors, who do not always use the same terms or attributes. Similarity and distance measures between membership values and between fuzzy sets are considered in many works [8, 16]. In [4, 5] the authors propose a new class of fuzzy set similarity measures, taking into account the proximity of membership values to the boundary values of 0 and 1. These similarity measures take values in [0;1] and generalize the crisp weak equality relation of fuzzy sets. The closeness of the membership values of elements of fuzzy sets to 1 or 0 can indicate the reliability with which an element of a fuzzy set "possesses" or "does not possess" the property modeled by the fuzzy set. In this case, the similarity between two membership values may depend not only on the difference between them, but also on their proximity to 1 or 0. The author presents the method of building a contrast similarity measure using a bipolar function symmetric with respect to 0.5. The method of building contrast co-symmetric dissimilarity functions using bipolar transformations [3] of membership values is based on the concept of the contrast intensification operation introduced by Zadeh [27] that makes the membership functions more contrast transforming them in the directions to the borders 0 and 1 of the interval [0;1] of membership values.

Another important but underestimated factor in the measured characteristics is conditioned by the possible deviations of the original values from the true ones. The error may be a consequence of inaccurate registration, the use of unreliable measurement techniques, or instruments with different levels of measurement accuracy (for example, medical gadgets). In medicine, this may also be due to the position of the person's body during the examination (for example, measuring blood pressure). To overcome this effect, it is proposed to use the probability distribution of feature values [15]. Numerical values have a measurement error that determines the range of values of a random variable and the corresponding probabilities of occurrence of these values, which can be represented by the distribution density function of the feature. Using information about possible deviations of feature values, we can build a distribution on a set of solutions. In this case, it will be necessary to integrate a module for preprocessing numerical characteristics into the control system. This will improve the reliability of the solutions proposed.

## 5 Control of the Medical-and-Technological Process

Control of the medical-and-technological process, including examination, diagnosis, and treatment, is complicated by the non-equilibrium state of various parameters of a patient's body. The features of control in such a situation are as follows:

- control aims to achieve the immediate goal (a subgoal of the overall goal situation) based on an analysis of monitored parameters and a subjective-objective assessment of features, taking into account safety conditions for the patient determined by the risk level of examination and treatment methods;
- overcoming uncertainty in data on the body's condition by considering and analyzing secondary parameters;
- operational aggregate intelligence analysis of changes in parameters obtained from cyber-physical systems and discrete information from other sources;
- identification of changes in health status as a quantized quasi-continuous process with fuzzy transitions;
- modification of control at each stage of the medical and technological process includes clarification of prognosis of the course of disease, selection of methods of additional examination and treatment;
- planning of actions (examinations, manipulations, methods of therapeutic and surgical treatment) based on possible trajectories of decision-making in the control system;
- selection of a sequence of control decisions to transition to a goal situation depends on the identified transition points in the body (and its individual systems) from one stage to another, and on the control strategy – the adaptation of control to changes in the structure and parameters of the object (system and external factors) during system functioning [14].

From the above, there is an interrelated task of compositional hybrid modeling and fuzzy situational control of the TS. [7] proposes a decomposition of the CTS into a set of components, in which it is necessary to: (a) determine the types of component models for analysis and modeling of system components, (b) select a set of component models to build a compositional hybrid model based on the results of comparing groups of requirements for component models in terms of the system components, (c) configure and change the types of component models in a way to ensure the required modeling accuracy both for an individual component of the system and for the system as a whole.

We will consider this in application to a complex medical-and-technological process system (MTPS). To build a compositional hybrid model of a specific system, we form a library of corresponding component models. For example, to create a compositional hybrid model of a patient's admission to a hospital, it will include a set of component models, their types and varieties, which are presented in Table 1.

**Table 1.** Component models for building the compositional hybrid model "Admission to the hospital".

| CMTPS components | Component model type |
|---|---|
| Examination of a patient in the emergency room | Fuzzy logic model |
| ECG examination | Neural network model |
| Laboratory tests | Fuzzy logic model |
| Conclusion on referral to one of the specialized departments | Fuzzy logic model |

Compositional hybrid models should be formed similarly for other levels of the MTPS. Periodically used models include: (1) examination in a specialized hospital department, including a preliminary diagnosis and the prescription of tests; (2) cumulative analysis of examination results; (3) differential diagnosis, identification of concomitant diseases, (4) choice of treatment; (5) final diagnosis. During the patient's stay in hospital, the MTP situational control system should include various models for: (a) prescribing measures, (b) controlling data from monitoring cyber-physical systems to identify pre-critical and critical conditions and providing guidelines on their elimination, (c) providing guidelines on selection and correction of therapy or surgical interventions, considering possible or developing complications.

Combining component models according to their interrelations creates a compositional hybrid model of the MTPS. The method of fuzzy situational control allows to identify the current fuzzy situation, take into account the specifics of compositional modeling and various control strategies depending on the current situation in conditions of incomplete information on the state and functioning of the object.

The experience and knowledge of experts is used in building a fuzzy intelligent control system for MTP. Fuzzy logical inference based on fuzzy rules is a generalization of traditional deductive inference (modus ponens rule). The lack of completeness of deduction can be compensated for by abductive hypothesizing [26]. The author draws attention to the fact that the peculiarity of the formalization of knowledge and logical calculus for their processing provide a flexible combination of abduction and deduction demonstrated on the tasks of searching for objects in conflict environments, technical, and medical diagnostics.

An important feature of typical situations is that the parameters of their state can be fixed in advance in the form of a set of decision options, matching them with a certain set of features or an identification vector that defines the situation at the point of the decision in a certain process. However, in medicine, one should take into account the polymorphism of features associated with the age-related dynamics of the pathological process, individual characteristics of a particular body, modification conditioned by the presence of other (concomitant) diseases and various external influences. It is necessary to consider the role of individual characteristics of the data obtained in the process of multiparameter monitoring from cyber-physical systems for controlling the body's vital functions [9, 23]. In this sense, MTPS is similar to CTS.

The method of fuzzy situational control of MTP based on compositional hybrid models should provide:

– identification of the current fuzzy situation;
– determination of the goal situation, the setting of a strategy, and the search for routes (sequences of control decisions) to achieve the desired goal situation depending on the chosen strategy.
– setting control decisions, control transitions.
– adaptation of a fuzzy situational network to changes in the compositional hybrid model.

The main role in MTPS belongs to the concept of a situation as a set of feature values that describe the state of a control object at some point in time. All possible states of the control object are described by a set of typical situations, each of them is a set of linguistic and numerical values of signs. Since a fuzzy situational network is a fuzzy oriented weighted transition graph over reference fuzzy situations, it is possible, using a limited set of situations, to analyze different states of the system and generate control strategies that can transfer it from the current state to the goal state. A set of control decisions that make it possible to transfer a system from one state to another (from one situation to another) is a control strategy in the form of a sequence of transitions between fuzzy situations within a fuzzy situational network. Considering the tree of control actions for a hierarchical system, we determine transitions from a certain top of the hierarchy, to which the typical situation turned out to be the closest, to possible reference situations of the next level of the hierarchy.

The application of control action transfers the control object to the goal situation. Fuzzy situational control of MTP is carried out under the following conditions:

– a set of fuzzy situational features that describe the states of the MTP;
– a set of fuzzy control decisions;

– a set of control transitions between fuzzy situations;
– a set of routes, including subsets of routes between various identified current and goal fuzzy situations.

The complexity of situational control in medicine is determined by the polyvariability of the dynamic pathological process, which manifests itself in the form of different scenarios. The fundamental difference between MTPS and CTS is due to significant fuzziness, underdetermination and incompleteness of data at the decision-making stages.

## 6 Fragment of the System of Situational Control over a Patient's Clinical Pathway

Healthcare pathways define the sequence of performing clinical activities as patients move through a treatment process, and they are critical for maintaining quality of care [12]. A clinical pathway was used as a tool in various clinical situations including in emergency, elective surgery, and pre-post-surgery, as well as in common clinical cases. Healthcare professionals should be engaged in active collaboration during the implementation of a clinical care pathway [2].

In continuation, we will study an example of a clinical pathway without the use of MTPS. The patient is admitted to the hospital in the emergency room with a referral diagnosis of "paroxysmal atrial fibrillation." A medical examination is carried out without functional (instrumental) studies, i.e. without the cooperation of a therapist and a functional diagnostics specialist. No preconditions for the need for emergency medical interventions are found. The patient is sent for planned treatment to a specialized cardiology department. Upon admission to the cardiology department, a severe attack of atrial fibrillation occurs. The patient is urgently transported to the intensive care unit (ICU). In this department, he/she is being treated until the end of the acute phase of atrial fibrillation. Then, he/she is transferred to the cardiology department. The basic treatment is prescribed. The tests are carried out: ECG, ultrasound (to identify heart defects that may contribute to the occurrence of atrial fibrillation), biochemical tests. Consultations with medical specialists are conducted. Selection of ongoing patient-oriented drug therapy is made.

The question arises. Could another scenario have been used in this case? What pathway could the MTPS build for this patient in the hospital?

Let us consider a decomposition based on subgoals and the corresponding requirements which can be represented by a set of features.

The main goal when a patient with atrial fibrillation is admitted to the hospital is to select adequate treatment. Subgoals at the emergency room level are to assess the patient's condition and select a specialized department for his/her treatment. In this regard, we will consider the decomposition of complete situations into components. Thus, the "State of the Cardiovascular System" component should be highlighted in the MTPS, which includes such features as external view, shortness of breath, pulse rate, ECG data. According to the characteristics of the features in this component, the MTPS should produce a local decision on the department for treatment of the patient. However, due to the intersection of classes (two or more types of different departments),

the task of choosing one or another solution from among those possible for a given situation arises. To make such a choice, it is necessary to complete special procedures to extrapolate the consequences of making a particular decision. With their help, based on knowledge about the control object and its functioning, the system should evaluate the potential results of the selected option and compare the resulting forecasts (on the one hand, efficiency, on the other, economic feasibility). If there are unclear signs of atrial fibrillation (arrhythmia on the ECG and the patient's appearance), it is necessary to implement the first subgoal, which is to assess the patient's condition (choice between a moderate and severe condition). Next, the dilemma (second subgoal) is to choose a conservative (in the cardiology department) or interventional (in the intensive care unit) medical care tactics. Those swinging scales at MTPS had to tip in favor of the ICU. The reason for this decision is one more indicator – patient's safety, i.e. minimizing the threat to the patient's life due to assessment of the condition as pre-critical in relation to an attack of atrial fibrillation.

The comparison of fuzzy situations can be carried out based on one of the following approaches [20]: (a) reducing a multi-criteria estimation problem to a single criteria one based on aggregation using various convolutions (additive, multiplicative, maximin, minimax, etc.); (b) according to one or more priority features (the other features are considered as additional). Often, the second approach in medicine is more productive due to the presence of relevant, additional, and secondary features.

In the architecture of a situational system for controlling a complex diagnostic and treatment process, it is necessary to harmonize various components corresponding to groups of business processes at different stages of clinical pathways. This is determined by the presence of a number of bifurcations and trajectories of the patient's movement in accordance with his/her current condition. Regular assessment (re-evaluation) of the condition determines the provision of the next decision and the sequence of movement along clinical pathways. Figure 1 shows a fragment of the situational control system for medical care at the emergency room stage.

Most of the information received is unclear, which leads to ambiguity in assessments of the situation. Logical inference in a system of fuzzy situations is based on a single-ball or multi-ball procedure for determining the maximum degree of similarity of the current fuzzy situation with situations accepted as reference ones, in accordance with which decisions or diagnostic conclusions are made.

The situational control system for a patient's complete clinical pathway (from admission to discharge from the hospital) includes a number of blocks that exchange the final data. The decisions made at each previous stage determine the transition to the next stage of the patient's clinical pathway.

Several levels (stages) of situational control must function as an ensemble with the transfer of control.

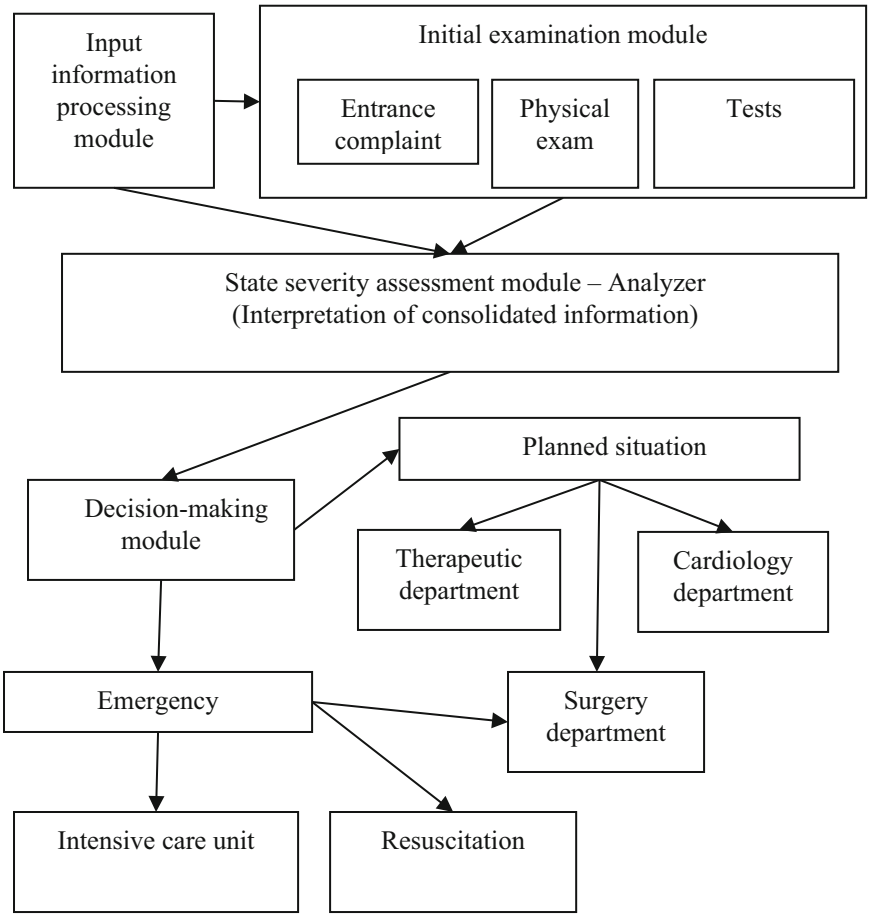


**Fig. 1.** Fragment of the system of situational control over a patient's clinical pathway (Emergency room block)

## 7 Conclusion

The method of fuzzy situational control of complex technical systems and, accordingly, of complex medical-and-technological process systems allows to use the specific features of compositional modeling and various situational control strategies depending on the prevailing conditions and requirements. It also ensures an organic combination of compositional modeling and fuzzy situational control processes. The application of fuzzy situational control to form a control action based on information about the current situation is extremely relevant in technology and medicine when critical situations and pre-critical conditions occur.

The considered approach to a complex system of medical-and-technological process in its diagnostic and therapeutic aspects from the position of situational control allows

us to largely solve the problem of fuzziness in making control decisions in clinical medicine.

The ensemble concept of building a situational control system for a medical-and-technological process will improve efficiency in a complex, branched, weakly structured medical subject area characterized by fuzziness, uncertainty and underdetermined data and situations.

**Disclosure of Interests.** The authors have no competing interests to declare that are relevant to the content of this article.

## References

1. Alowais, S.A., Alghamdi, S.S., Alsuhebany, N., et al.: Revolutionizing healthcare: the role of artificial intelligence in clinical practice. BMC Med. Educ. **23**, 689 (2023)
2. Asmirajanti, M., Hamid, A.Y., Hariyati R.T.S.: Clinical care pathway strenghens interprofessional collaboration and quality of health service: a literature review. Enfermería Clínica **27**(Suppl. P.I), 240–244 (2017)
3. Batyrshin, I., Monroy-Tenorio, F., Gelbukh, A., et al.: Bipolar rating scales: a survey and novel correlation measures based on nonlinear bipolar scoring functions. Acta Polytechnica Hungarica **14**(3), 33–57 (2017)
4. Batyrshin, I.: Towards a general theory of similarity and association measures: similarity, dissimilarity and correlation functions. J. Intell. Fuzzy Syst. **36**(4), 2977–3004 (2019)
5. Batyrshin, I., Kosheleva, O., Kreinovich, V., et al.: Contrast similarity measures of fuzzy sets. Computación y Sistemas **23**(4), 1569–1573 (2019)
6. Borisov. V., luferov, V.: Neuro-Fuzzy cognitive temporal models for predicting multi-dimensional time series with fuzzy trends. Computación y Sistemas **24**(3), 1165–1177 (2020)
7. Borisov, V.V., Avramenko, D.: Fuzzy situational control of complex systems based on composite hybrid modeling. Syst. Control Commun. Secur. **3**, 207–237 (2021). (in Russian)
8. Cross, V.: Relating fuzzy set similarity measures. Fuzzy logic in intelligent system design. In: Advances in Intelligent Systems and Computing, vol. 648, pp. 9–21. Springer, Cham (2018)
9. Davoudi, A., Malhotra, K.R., Shickel, B., et al.: Intelligent ICU for autonomous patient monitoring using pervasive sensing and deep learning. Sci. Rep. **9**, 8020 (2019)
10. Gel'fer, I.S., Kotel'nikov, I.V., Teklina, L.G.: Synthesis of a control system with a reference model under conditions of parametric indeterminate control object and external perturbations. Bull. Lobachevsky Nizhny Novgorod Univ. Ser. Math. Model. Optim. control **4**(1), 204–207 (2013). (in Russian)
11. Jakobson, G., Buford, J., Lewis, L.: Situation management: basic concepts and approaches. In: Popovich, V.V., Schrenk, M., Korolenko, K.V. (eds.) Information Fusion and Geographic Information Systems. Lecture Notes in Geoinformation and Cartography, pp.18–33. Springer, Berlin, Heidelberg (2007)
12. Kempa-Liehr, A.W., Lin, C.-C., Britten, R., et al.: Healthcare pathway discovery and probabilistic machine learning. Int. J. Med. Informatics **137**, 104087 (2020)
13. Kobrinsky, B.: Concept of the continuum of intermediate states of development: risk factors in child health. Medical Audit News **5**(2), 21–22 (1995)
14. Kobrinsky, B.A.: On simulation of transient states of the organism. Bull. Tver State Tech. Univ. Ser. Tech. Sci. **1**(17), 79–86 (2023). (in Russian)

15. Kobrinsky, B.A., Nikolaev, A.A.: Probabilistic representation of measured signs and the possibility of their reflection in artificial intelligence systems. In: XII International Scientific and Practical Conference "Integrated models and soft computing in artificial intelligence", vol. 2. pp. 86–93. Universum, Smolensk (2024). (in Russian)
16. Li, Y., Qin, K., He, X.: Some new approaches to constructing similarity measures. Fuzzy Sets Syst. **234**(1), 46–60 (2014)
17. Madarász, L., Andoga, R., Fozo, L., Lazar, T.: Situational control, modeling and diagnostics of large scale systems. In: Rudas, I.J., Fodor, J., Kacprzyk, J. (eds.) Towards Intelligent Engineering and Information Technology. Studies in Computational Intelligence, vol. 243, pp. 153–164. Springer, Berlin (2009)
18. McCarthy, J.: Actions and other events in situation calculus. In: Fensel, D. et al. (eds.) Proceedings of Proceedings of the Eighth International Conference on Principles of Knowledge Representation and Reasoning (KR-2002), pp. 615–628. Morgan Kaufmann Publishers, San Francisco (2002)
19. Narinyani, A.S.: NOT-factors: a brief introduction. Artif. Intell. News **2**, 52–63 (2004). (in Russian)
20. Ognev, I.V., Borisov, V.V., Sutula, N.A.: Associative memory, environments, systems. Hotline – Telecom, Moscow (2016) (in Russian)
21. Opeiko, OF.: Cascad control for plant with parameter uncertainty. Syst. Anal. Appl. Inf. **3**, 21–24 (2015). (in Russian)
22. Pospelov, D.A.: Situation control: an overview. In: R.J. Strohn (ed.) Proceedings of Workshop on Russian Situation Control and Cybernetic/Semiotic Modeling, pp. 7–37. Battelle, Columbus (1996)
23. Saeed, M., Villarroel, M., Reisner, A.T., et al.: Multiparameter intelligent monitoring in intensive Care II: a public-access intensive care unit database. Crit. Care Med. **39**(5), 952–960 (2011)
24. Shung, D.L., Sung, J.J.Y.: Challenges of developing artificial intelligence-assisted tools for clinical medicine. J. Gastroenterol. Hepatol. **36**(2), 295–298 (2021)
25. Sugiki, A., Furuta, K.: Posicast control design for parameter-uncertain plants. In: Proceedings of the 45th IEEE Conference on Decision and Control, pp. 3192–3197. IEEE, Diego, CA, USA (2006)
26. Vassilyev, S.N.: Abductive inference method in problems of explaining the observed. Comput. Syst. Sci. Int. **60**(1), 153–161 (2021)
27. Zadeh, L.A.: Outline of a new approach to the analysis of complex systems and decision processes. IEEE Trans. Syst. Man Cybern. Cybern. **3**(1), 28–44 (1973)

# Evaluating A* and RRT for High-DoF Path Planning

Aleksandr Onegin[1(✉)], Nuraddin Kerimov[1], and Konstantin Yakovlev[2]

[1] Moscow Institute of Physics and Technology, Moscow, Russia
onegin.as@phystech.edu
[2] Federal Research Center for Computer Science and Control of Russian Academy of Sciences, Moscow, Russia
yakovlev@isa.ru

**Abstract.** Path planning is crucial for various robots, including manipulators, that autonomously perform non-repetitive tasks in obstacle-rich environments. In this paper we focus on path planning for an n-DoF (degrees of freedom) manipulator, i.e. the one that consists of n links and n joints. We evaluate and compare head-to-head two approaches that are the most commonly used to solve this problem: search-based planning in the discretized configuration space and sampling-based planning in the continuous space. We evaluate the planners in challenging obstacle-rich scenes while varying the dimensionality of the configuration space (the number of joints/links). The memory consumption, quality of the resultant paths, runtime are tracked. Our evaluation reveals that, despite the common belief, search-based methods can outperform the sampling-based ones for 3-DoF and even 4-DoF manipulators, however for higher dimensional spaces (5-DoF and more) sampling methods are, indeed, more preferable.

**Keywords:** path planning · trajectory planning · manipulator · A* · RRT · heuristic search · sample-based planning

## 1 Introduction

Traditionally, robotic manipulators have been used in manufacturing where they typically have to perform a specific task repeatedly and there is no need to adapt when interacting with the environment. On the other hand, recently manipulators are being placed on mobile robots that are intended to autonomously perform complex tasks in obstacle-rich environments, e.g. sorting parcels, cleaning furniture, etc. Thus, path planning for manipulators becomes necessary. To this end, a variety of path finding methods have been developed and applied to manipulation planning. They can be roughly divided into the following four groups: search-based planning [1,2], sample-based planning [3,4], methods that cast a planning problem as an optimisation problem [5,6], learning-based methods [7,8].


S. Kovalev et al. (Eds.): IITI 2024, LNNS 1209, pp. 324–333, 2024.
https://doi.org/10.1007/978-3-031-77688-5_31

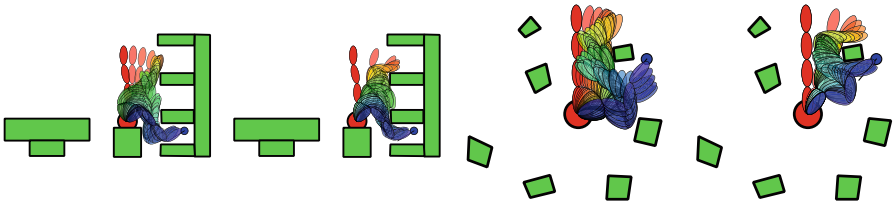

**Fig. 1.** Two examples of the path planning problem involving a 4-DoF manipulator (i.e. the one comprised of the 4 joints and 4 links). Intermediate manipulator states forming the paths are shown. Each path is shown as color gradient from red (initial state) to blue (goal state). From left to right: RRT on Scene 1, A* on Scene 1, RRT on Scene 2, A* on Scene 2.

Search-based planners systematically search the discretized configuration space to find a solution. They provide strong theoretical guarantees, e.g. they can guarantee (if certain heuristic functions are used) that the constructed solutions are optimal. On the other hand, these guarantees are only given with the respect to the imposed discretization. Moreover, as the dimensionality of the space increases, the number of possible states in the search graph grows exponentially and becomes a computational bottleneck. Sampling methods, on the other hand, do not require discretization and can operate directly in continuous space. These methods perform well in high-dimensional spaces, such as the configuration space of a manipulator, because they rely on sampling rather than systematic exploration of the search space. On the other hand, these methods can only provide probabilistic guarantees, e.g. they can guarantee to find a solution when the number of samples tends to infinity. Moreover, their solutions can vary significantly from one run to the other for the same problem instance due to their stochastic nature.

Optimization-based planning methods form desired paths by minimizing a cost function that encapsulates various factors such as distance to obstacles, torque requirements, constraint costs, and so on. These planners are fast and provide high quality solutions. On the other hand, they often require the analytical representation of the scene (i.e., the obstacles should be somehow encoded as equations) as well as the initial guess to be optimized, i.e., the initial path from start to goal. If the latter is a direct interpolation from start to goal that goes through the obstacles, the optimization process may converge slowly and may often stuck in local minima.

Recently, there has been a growing interest in learning-based, data-driven approaches to manipulation planning. Such methods can perform well when the tasks they solve are similar to those used in the training phase, but in general their ability to generalize well is not guaranteed. Similarly, they struggle to provide any kind of theoretical guarantees (even in a probabilistic sense).

Arguably, the most dominant methods nowadays when it comes to the path planning for manipulators are still search-based and sampling-based planners. However, there is almost no works (to our knowledge) dedicated to head-to-

head empirical evaluation and comparison of these methods. Our works aims at filling this gap. We compare the basic search-based and sampling-based methods, i.e. A* (A-star) and RRT (Rapidly exploring random tree), for a manipulator with an increasing number of joints (dimensionality of the configuration space) and numerically measure their strengths and weaknesses in different scenarios. Our analysis shows that in simple scenarios where the manipulator does not need to move away from the target and then avoid obstacles (which is true for many manipulation tasks), A* can compete with and even outperform RRT in planning time. However, in complex scenarios where the manipulator must first move away from the goal in order to reach it, RRT becomes more preferable.

## 2 Related Work

*Search-Based Methods.* A widely used method for robot path planning is to represent the multidimensional space of robot configurations as a weighted graph $G = (S, E, w)$, where $S$ is the set of possible robot configurations, $E$ is the set of edges representing the transitions between these configurations, and the weight $w$ of each edge represents the cost of a transition. Heuristic search-based methods can find least cost optimal paths in discrete state graphs, but one of the key characteristics of heuristic search methods is their ability to balance exploration and exploitation. Numerous modifications of A*, tailored to increase the efficiency of the algorithm, are typically used for manipulator path planning. These include Anytime A* [1,2], which weights heuristics and then improves the resulting solution, Multiheuristic A* [9], which uses multiple heuristics, A*-connect [10], which is a bidirectional search, and many other variations of the algorithm. An important aspect is the heuristic function, which is usually chosen in the end-effector workspace and can take into account the orientation of the robot arm, the distance to obstacles, or task constraints [1,2,11]. Another important aspect is the number of search successors, which can be varied at each step to improve the performance of the algorithm [12,13]. These techniques make heuristic search effective in manipulation tasks, including dynamic environments [11] and multiple robot arms [14].

*Sampling-Based Methods.* Two of the most popular sampling-based methods for path planning are the Probabilistic Roadmap (PRM) [15] and the Rapidly-exploring Random Tree (RRT) [3]. RRT has undergone a number of modifications to improve its performance: RRT-Connect [4] grows a tree of start and end points, RRT* [16] represents a significant advance in solving optimal path planning problems in high-dimensional spaces. Since then, several improvements have been made, including removing nodes that do not improve the solution [17], applying heuristics for more informative sampling [18], fixing the number of nodes for efficient memory usage [19], and using techniques like BIT* (Batch Informed Trees) with RRT* to find optimal paths in narrow passages [20].

## 3 Problem Statement

Let $\mathcal{W} \subseteq \mathbb{R}^2$ be the workspace of a manipulator consisting of $n$ joints, the first of which is fixed at the origin. The last joint of a manipulator ends with an end-effector, $EE$. The workspace contains arbitrary obstacles.

The manipulator configuration is defined as $\mathbf{q} = \{q_1, ..., q_n\}$, where $q_i$ is the rotation angle of the $i$-th joint with respect to the previous one. Let $\mathcal{C}_{free} \subseteq \mathbb{R}^n$ be the space of feasible configurations, i.e. such that the manipulator does not collide with the obstacles. The initial configuration in $\mathcal{C}_{free}$ is denoted as $\mathbf{q}_0$.

A goal position in $\mathcal{W}$ is given, $P_{\text{goal}} = (x_{\text{goal}}, y_{\text{goal}})$, to which the end-effector should be moved with a threshold of $\delta_{\text{xy}}$. Additionally, the absolute orientation of the last joint $\theta_{\text{goal}}$ and the corresponding possible error $\delta_\theta$ are also given.

*The problem now is* to find a path (see Fig. 1) of the form $Q = \{\mathbf{q}_k\}_{k=0}^{k=K}$, s.t. (a) $\|\text{EE}(\mathbf{q}_K) - P_{\text{goal}}\|_2 < \delta_{\text{xy}}$, (b) $|\theta_n(\mathbf{q}_K) - \theta_{\text{goal}}| < \delta_\theta$, (c) $\mathbf{q}_i + t(\mathbf{q}_{i+1} - \mathbf{q}_i) \in \mathcal{C}_{free}\ \forall i \in [1, K) \quad \forall t \in [0, 1]$. Here $\text{EE}(\mathbf{q}_K)$ denotes the position of the end-effector in the $K$-th configuration, $\theta_n(\mathbf{q}_K)$ denotes the absolute angle of the $n$-th joint in the $K$-th configuration. Condition (c) states that the path must be collision-free.

To evaluate the quality of the constructed path the following cost objectives can be used: the path length in the configuration space, $\sum_{i=1}^{K-1} \left|\left|\mathbf{q}_{i+1} - \mathbf{q}_i\right|\right|_2$, and the path length in the Cartesian space traveled by the end-effector, $\sum_{i=1}^{K-1} \left|\left|\text{EE}(\mathbf{q}_{i+1}) - \text{EE}(\mathbf{q}_i)\right|\right|_2$. Here $||\cdot||_2$ stands for the Euclidean norm.

## 4 Methods

*Search-based planning with A** is conducted by systematically iteratively exploring a graph of states, where each state represents a possible configuration in the search space. Search algorithms are resolution-complete and strongly depend on this resolution, which we will refer to as $\Delta$. A* maintains a search tree, namely a set of open and closed nodes. At the beginning of the search, a start state is added to the open set and then search iterations are performed. At each iteration, the algorithm selects the state from the open set with the lowest combined cost estimate (typically the sum of the cost of reaching the state from the start state and a heuristic estimate of the cost of reaching the goal from the state). This state is moved from the open list to the closed list, and its neighbours are added to the open list if they have not yet been explored or if a new path to them proves to be more efficient. The algorithm continues iterating until the final state is reached or until the open list is empty, meaning that there is no path to the goal. Once the goal is reached, the algorithm reconstructs the path by traversing from the goal to the initial state via links to parent states.

The heuristic function for the problem at hand can be constructed in several ways. The most straightforward one is to obtain a solution to the inverse kinematic problem satisfying a given point in the Cartesian space and the orientation of the last link, $\mathbf{q}_{\text{goal}}$ and introduce the heuristics and path cost as the Euclidean distance between states in configuration space: $g_{\text{conf}}(\mathbf{q}, \mathbf{q}') = ||\mathbf{q} - \mathbf{q}'||_2$,

$h_{\text{conf}}(\mathbf{q}) = ||\mathbf{q} - \mathbf{q}_{\text{goal}}||_2$. However, this approach is known to perform poorly in practice, due to the kinematic redundancy and infinite amount of the inverse kinematics solutions. Thus, the cost function and the heuristic may be defined as the Euclidean distance between the end-effector point and the start/goal states in the Cartesian space: $cost_{\text{cart}}(\mathbf{q}, \mathbf{q}') = ||EE(\mathbf{q}) - EE(\mathbf{q}')||_2$, $h_{\text{cart}}(\mathbf{q}) = ||EE(\mathbf{q}) - P_{\text{goal}}||_2$. However, in our problem formulation, this heuristic is not the best choice because it does not contain information about the orientation of the last link. Developing the ideas presented in [1], we introduce an original heuristic function of the form: $h(\mathbf{q}) = w_1 h_{\text{cart}}(\mathbf{q}) + w_2|\theta(\mathbf{q}) - \theta_{\text{goal}}|/(\beta + h_{\text{cart}(\mathbf{q})})$. Here, the first component is responsible for the manipulator arm reaching the target point, the second component is responsible for reaching the target point with a given orientation of the last joint. In our work we divide the angular part by the coordinate part, which allows to take the orientation of the last link more into account when manipulator is approaching the target. The coefficient $\beta$ prevents division by zero, the weights $(w_1, w_2)$ are determined empirically and they weight the heuristics for more efficient search. We also propose to move only one joint of manipulator per iteration during path finding. This reduces the search for variants and increases the computational efficiency of the algorithm.

*Sampling-based methods* operate in continuous configuration space and do not require discretization. At each iteration a random configuration is selected from $\mathcal{C}$. Then, from the existing state tree, the closest one to the sampled point is selected. Next, the manipulator is moved in the direction of the sample with some $\Delta$ step and if there were no collisions while moving manipulator, the resulting state is added to the tree. We also implemented the GOALBIAS [21] methodology, i.e. at each iteration with probability $p_g$ the goal configuration is used instead of a random sample, and then the tree branch continues until an obstacle is encountered or the goal is reached.

Since the target in the considered problem is given by the coordinates in the workspace and the orientation of the last link, the inverse kinematic problem is solved using the triangulation method [22] to implement GOALBIAS. There is infinite amount of inverse kinematics solutions for the redundant high-DoF manipulator. The target configuration for GOALBIAS was chosen by sampling from the obtained equally distributed set of goal configurations, that we get by solving inverse kinematics.

## 5 Experimental Setup

*Datasets and Scenes.* For the numerical experiments, four scenes of 5 by 5 m were used. The manipulator base is fixed in the centre of each scene and the obstacles are represented as convex polygons. The sum of the lengths of all joints is fixed at 2 m, with the number of joints $n$ varying during the experiment. The width of a joint is 0.2 m. The operating range of each joint is $[-170°, 170°]$. Scene 1 is a two-dimensional projection of the workspace of a manipulator standing on a platform that has to move objects from cupboard shelves to a table. Scene 2

contains a large number of small obstacles and can be represented as a top view of the manipulator lying on the table. Scene 3 presents many large obstacles and a narrow manipulator workspace, and scene 4 is semi-empty with large obstacles and wide passages. For each scene, 100 random instances were generated per each numbers of degrees of freedom, from two to eight. Totally 2800 instances were considered.

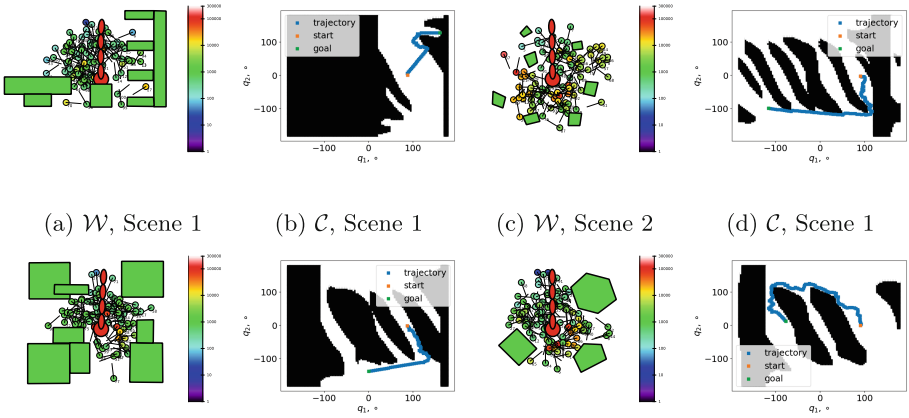


(a) $\mathcal{W}$, Scene 1 (b) $\mathcal{C}$, Scene 1 (c) $\mathcal{W}$, Scene 2 (d) $\mathcal{C}$, Scene 1

(e) $\mathcal{W}$, Scene 3 (f) $\mathcal{C}$, Scene 3 (g) $\mathcal{W}$, Scene 4 (h) $\mathcal{C}$, Scene 4

**Fig. 2.** 4 scenes used in evaluation with their workspaces, $\mathcal{W}$, and configuration spaces, $\mathcal{C}$ (the latter is presented for 2 DoF manipulator). The color bar indicates the number of nodes in the search tree of A* (the more closer the color of the target is to the red – the harder this instance is to A*).

Figure 2 shows the scenes with the distribution of tasks on them, as well as a representation of the configuration space of the two-link manipulator on these scenes. Different goal states are shown as colored circles with color encoding the hardness of the instance for search-based planner (i.e. for A*): the closer the color is to red, the more states need to be searched. As can be seen the most difficult tests for A* are those in which the manipulator has to turn largely and avoid obstacles. Noteworthy that for RRT, the most difficult tests were those with narrow passages, which is consistent with the sampling nature of the configuration space exploration.

*Technical Details.* Each test was repeated 1 time for the heuristic search algorithm (since it is deterministic) and 20 times for the sampling planner. The parameters of the heuristic algorithm have the following values: $\Delta = 6°$, $(w_1, w_2) = (10, 10)$ or $(100, 10)$, depending on whether the angle between the vector from the end-effector position in the initial configuration to the end-effector position in the final configuration and the orientation vector of the last

link in the final configuration (vector connecting the goal point with the second-to-last joint of the manipulator) is greater or less than 90°. The parameters of the RRT algorithm are $\Delta = 6°$ for maximum step size and $p_g = 0.1$ for GOAL-BIAS. The limit of the maximum number of nodes was chosen to be 3 million. Geometric collision checking was implemented via the hyperplane separation theorem, which allows us to determine whether polygons intersect or not. For this purpose we used the assumption of convexity of obstacles. Both planners were implemented in C++, using the same data structures, used one thread and were run on a four-core Intel Core i5-1135G7 @ 2.40 GHz.

**Table 1.** Results of the empirical evaluation of A* and RRT on 4 scenes (see Fig. 2) w.r.t. increasing the number of DoFs. 'sr' stands for *success rate*, 'pl' – for *path length*. The latter is measured both in the configuration space (in degrees) and in the workspace (in meters).

| | | ndof = 2 | | ndof = 3 | | ndof = 4 | | ndof = 5 | | ndof = 6 | | ndof = 7 | | ndof = 8 | |
|---|---|---|---|---|---|---|---|---|---|---|---|---|---|---|---|
| | | A* | RRT | A* | RRT | A* | RRT | A* | RRT | A* | RRT | A* | RRT | A* | RRT |
| Scene 1 | sr, % | **100** | **100** | **100** | **100** | **100** | **100** | **100** | 98 | **98** | 95 | 94 | **98** | 89 | **96** |
| | pl, ° | 150 | **103** | 285 | **136** | 414 | **182** | 489 | **187** | 524 | **197** | 552 | **201** | 634 | **225** |
| | pl, m | **0.68** | 1.33 | **0.76** | 1.34 | **1.47** | 2.25 | **1.42** | 2.57 | **1.13** | 2.53 | **0.98** | 2.63 | **1.33** | 2.47 |
| Scene 2 | sr, % | **100** | **100** | **100** | **100** | **100** | **100** | **100** | **100** | 74 | **99** | 69 | **99** | 64 | **98** |
| | pl, ° | 544 | **250** | 669 | **343** | 789 | **404** | 821 | **399** | 806 | **457** | 805 | **442** | 974 | **446** |
| | pl, m | **1.95** | 2.96 | **1.60** | 3.20 | **1.55** | 3.13 | **1.80** | 3.08 | **1.38** | 3.31 | **1.49** | 3.27 | **1.56** | 3.30 |
| Scene 3 | sr, % | **100** | **100** | **100** | **100** | **100** | **100** | **100** | **100** | **100** | 98 | 93 | **98** | 93 | **100** |
| | pl, ° | 312 | **195** | 512 | **246** | 591 | **303** | 683 | **360** | 777 | **336** | 746 | **372** | 791 | **368** |
| | pl, m | **1.38** | 1.94 | **1.81** | 2.13 | **1.29** | 2.08 | **1.26** | 2.61 | **1.71** | 2.63 | **1.40** | 2.57 | **1.22** | 2.68 |
| Scene 4 | sr, % | **100** | **100** | **100** | **100** | **100** | **100** | **100** | **100** | 98 | **100** | 95 | **100** | 90 | **99** |
| | pl, ° | 305 | **163** | 515 | **243** | 569 | **237** | 707 | **292** | 810 | **273** | 733 | **301** | 807 | **336** |
| | pl, m | **1.20** | 2.03 | **1.81** | 2.88 | **1.55** | 2.96 | **1.69** | 2.68 | **2.32** | 2.49 | **1.40** | 2.45 | **1.33** | 2.88 |

## 6 Results

Table 1 shows the amount of solved tests and the average path lengths in configuration and workspace for by A* and RRT. As the number of links increases, the configuration path length, which is defined as the Euclidean distance between the consecutive configurations in the plan, increases. For RRT planner, the configuration lengths turns out to be shorter than those of the A*. However the workspace path length turns to be shorter for A*. This is due to the fact that the heuristic and cost function is chosen in the end-effector workspace, i.e. A* minimises the path travelled by the end-effector, while the other links of the manipulator adjust to this path. It is also worth noting that in order to make A* run faster, we weighted the heuristics and thus the path is suboptimal. The percentage of completed tests for all planers is 100% when the dimensionality of a configuration space does not exceed 5. When the number of dimensions gets

larger (6, 7, 8) the success rate for both planners drops. For A* the drop is more pronounceable, especially for Scene 2, where the success rate of A* gets to 64% for 8 DoFs. RRT, which does not suffer from the curse of dimensionality, shows better success rate – more than 95% in all cases.

Figure 3 shows the boxplots of the number of states considered in the search tree and execution time for the compared algorithm. For RRT, the time also contains the time for solving the inverse kinematic problem, but it is estimated to take not more than 5% of the total time. The results of A* are marked in orange, RRT in blue. For A*, there is an exponential increase in runtime with increasing space dimensionality, so for $n = 7, 8$ the search in most complicated tests failed and exceeded the nodes in the search tree limit $3 \cdot 10^6$ (see Table 1). For this reason, the value of nodes and runtime for these DoF was underestimated because only a group of light tests were solved. Nevertheless, we have plotted them on the graph. The computational efficiency of RRT also decreases with increasing space dimensionality, but not as critically as that of A*. Note that for small $n$ (e.g., $n = 2$) A* is preferable because it is better at traversing narrow passages in configuration space. In Scenes 3 and 4, A* even overtakes RRT as these scenes are half-empty and light. However, Scene 2 is the most illustrative. It most fully reveals the essence of A* when it encounters an obstacle, when the manipulator has to make a turn in one direction, moving away from the target, and requires a huge number of nodes in the search tree that makes search infeasible in multidimensional spaces.

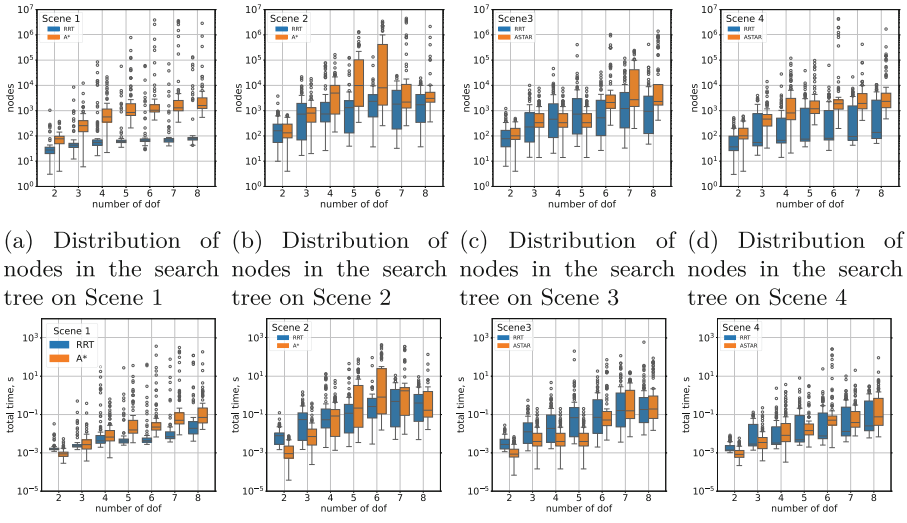


(a) Distribution of nodes in the search tree on Scene 1

(b) Distribution of nodes in the search tree on Scene 2

(c) Distribution of nodes in the search tree on Scene 3

(d) Distribution of nodes in the search tree on Scene 4

(e) Distribution of planning time on Scene 1

(f) Distribution of planning time on Scene 2

(g) Distribution of planning time on Scene 3

(h) Distribution of planning time on Scene 4

**Fig. 3.** Results of a comparative analysis of the A* and RRT algorithms.

## 7 Conclusion

Experimental findings unveiled distinct advantages and drawbacks associated with A* and RRT algorithms in the context of manipulator planning. A* demonstrates proficiency in scenarios featuring constrained passageways and exhibits enhanced speed when applied to manipulators characterized by a limited number of joints. However, its computational efficiency diminishes significantly when confronted with manipulators possessing a substantial number of degrees of freedom. Consequently, A* algorithm is deemed more suitable for manipulators with fewer joints, particularly those prone to encountering bottlenecks induced by obstacles during operation.

Conversely, Rapidly-exploring Random Trees (RRT) exhibit commendable performance in the realm of manipulators equipped with a multitude of joints, particularly with six or more degrees of freedom. Yet, the reliance on random selection hinders RRT's efficacy in addressing challenges posed by narrow passageways. RRT is most aptly applied to manipulators characterized by a high number of degrees of freedom, provided the workspace and configuration space do not impose excessively narrow constraints.

For further exploration, the source code used in our evaluation and more detailed results can be accessed in the following GitHub repository: https://github.com/kaizer-nurik/manipulator_planning_simple.

## References

1. Cohen, B.J., Chitta, S., Likhachev, M.: Search-based planning for manipulation with motion primitives. In: 2010 IEEE International Conference on Robotics and Automation, pp. 2902–2908 (2010)
2. Ferguson, D., Stentz, A.: Anytime, dynamic planning in high-dimensional search spaces. In: Proceedings 2007 IEEE International Conference on Robotics and Automation, pp. 1310–1315. IEEE (2007)
3. LaValle, S.M.: Rapidly-exploring random trees : a new tool for path planning. In: The Annual Research Report (1998)
4. Kuffner, J.J., LaValle, S.M.: Rrt-connect: an efficient approach to single-query path planning. In: Proceedings 2000 ICRA. Millennium Conference. IEEE International Conference on Robotics and Automation. Symposia Proceedings (Cat. No. 00CH37065), vol. 2, pp. 995–1001. IEEE (2000)
5. Ratliff, N., Zucker, M., Bagnell, J.A., Srinivasa, S.: Chomp: gradient optimization techniques for efficient motion planning. In: 2009 IEEE International Conference on Robotics and Automation, pp. 489–494. IEEE (2009)
6. Kalakrishnan, M., Chitta, S., Theodorou, E., Pastor, P., Schaal, S.: Stomp: stochastic trajectory optimization for motion planning. In: 2011 IEEE International Conference on Robotics and Automation, pp. 4569–4574. IEEE (2011)
7. Deisenroth, M.P., Rasmussen, C.E., Fox, D.: Learning to control a low-cost manipulator using data-efficient reinforcement learning. Robot. Sci. Syst. VII **7**, 57–64 (2011)
8. Park, J.-J., Kim, J.-H., Song, J.-B.: Path planning for a robot manipulator based on probabilistic roadmap and reinforcement learning. Int. J. Control Autom. Syst. **5**(6), 674–680 (2007)

9. Narayanan, V., Aine, S., Likhachev, M.: Improved multi-heuristic a* for searching with uncalibrated heuristics. Proc. Int. Sympos. Comb. Search **6**, 78–86 (2015)
10. Islam, F., Narayanan, V., Likhachev, M.: A-connect: bounded suboptimal bidirectional heuristic search. In: 2016 IEEE International Conference on Robotics and Automation (ICRA), pp. 2752–2758. IEEE (2016)
11. Nguyen, P.D., Hoffmann, M., Pattacini, U., Metta, G.: A fast heuristic cartesian space motion planning algorithm for many-dof robotic manipulators in dynamic environments. In: 2016 IEEE-RAS 16th International Conference on Humanoid Robots (Humanoids), pp. 884–891. IEEE (2016)
12. Cohen, B.J., Subramania, G., Chitta, S., Likhachev, M.: Planning for manipulation with adaptive motion primitives. In: 2011 IEEE International Conference on Robotics and Automation, pp. 5478–5485. IEEE (2011)
13. Saxena, D.M., Saleem, M.S., Likhachev, M.: Manipulation planning among movable obstacles using physics-based adaptive motion primitives. In: 2021 IEEE International Conference on Robotics and Automation (ICRA), pp. 6570–6576. IEEE (2021)
14. Cohen, B., Chitta, S., Likhachev, M.: Single-and dual-arm motion planning with heuristic search. Int. J. Robot. Res. **33**(2), 305–320 (2014)
15. Kavraki, L.E., Svestka, P., Latombe, J.-C., Overmars, M.H.: Probabilistic roadmaps for path planning in high-dimensional configuration spaces. IEEE Trans. Robot. Autom. **12**(4), 566–580 (1996)
16. Karaman, S., Frazzoli, E.: Sampling-based algorithms for optimal motion planning. Int. J. Robot. Res. **30**(7), 846–894 (2011)
17. Karaman, S., Walter, M.R., Perez, A., Frazzoli, E., Teller, S.: Anytime motion planning using the RRT. In: 2011 IEEE International Conference on Robotics and Automation, pp. 1478–1483. IEEE (2011)
18. Gammell, J.D., Barfoot, T.D., Srinivasa, S.S.: Informed sampling for asymptotically optimal path planning. IEEE Trans. Rob. **34**(4), 966–984 (2018)
19. Tong, B., Liu, Q., Dai, C.: A rrt* fn based path replanning algorithm. In: 2019 IEEE 4th Advanced Information Technology, Electronic and Automation Control Conference (IAEAC), pp. 1435–1445. IEEE (2019)
20. Choudhury, S., Gammell, J.D., Barfoot, T.D., Srinivasa, S.S., Scherer, S.: Regionally accelerated batch informed trees (rabit*): a framework to integrate local information into optimal path planning. In: 2016 IEEE International Conference on Robotics and Automation (ICRA), pp. 4207–4214. IEEE (2016)
21. Liu, H., Zhang, X., Wen, J., Wang, R., Chen, X.: Goal-biased bidirectional RRT based on curve-smoothing. IFAC-PapersOnLine **52**(24), 255–260 (2019)
22. Muller-Cajar, R., Mukundan, R.: Triangulation: a new algorithm for inverse kinematics. Image and Vision Computing - IVC, January 2007

# Platform Architecture for Human-AI Collaborative Decision Support

Alexander Smirnov, Andrew Ponomarev(✉), Tatiana Levashova, Nikolay Teslya, and Nikolay Shilov

St. Petersburg Federal Research Center of the Russian Academy of Sciences, Saint Petersburg, Russian Federation
{smir,ponomarev,tatiana.levashova,teslya,nick}@iias.spb.su

**Abstract.** Modern decision-maker typically uses several AI-based tools to obtain more information about the problem at hand and to evaluate possible solutions, besides, decision support in complex dynamic environment typically requires knowledge of several experts, therefore, collaboration between them. These trends naturally merge in human-AI collaborative systems, providing the means of collaboration of heterogeneous participants. However, collaborative human-AI decision support is connected with many challenges, both theoretical and technological. This paper addresses the technological side of the problem by presenting a platform for human-AI collaborative decision support systems. The platform provides a set of mechanisms and interfaces, simplifying the development of such systems: team formation and collaboration features, interfaces to define, deploy and manage AI agents, and a set of structured representations facilitating interaction between human experts and AI agents. Possible application of the platform is discussed on a use case in road safety analysis.

**Keywords:** Collaborative Decision Support Systems · Human-AI Interaction · Ontology · Neuro-Symbolic AI · Explainable AI · Service Ecosystem

## 1 Introduction

There are two prominent motives in modern decision support systems. The first one is connected with the increasing role of information processing and AI-powered tools. Modern decision-maker typically uses several such tools to obtain more information about the problem at hand and to evaluate possible solutions. The second one is related to collaborative nature of any complex activity (e.g., making important decision in dynamic environment). Typically, knowledge and expertise are scattered among several experts and to make an informed decision one has to collect this knowledge. The second motive is exacerbated with the dynamics and complexity of modern business and governmental systems – social and business environment often sets non-typical problems for which there are no established collectives, and the decision-maker has to access internal or even external expert pools (e.g., in the form of crowdsourcing).

This paper connects these two motives, addressing the problem of decision support by dynamic collectives, consisting of human experts and AI-agents. In particular, the paper


S. Kovalev et al. (Eds.): IITI 2024, LNNS 1209, pp. 334–345, 2024.
https://doi.org/10.1007/978-3-031-77688-5_32

proposes the architecture of a platform, allowing to create domain-specific collaborative decision support systems (CDSSs). The platform provides a set of mechanisms and interfaces, simplifying the development of CDSSs and making it even code-free (in some cases). In particular, the platform provides team formation and collaboration features, interfaces to define, deploy and manage AI agents, and a set of structured representations facilitating interaction between human experts and AI agents. It materializes concepts, processes and mechanisms proposed in our earlier works to enable joint decision-making in mixed collectives consisting of both human experts and AI agents. Distinguishing features of the proposed approach:

- Ontological representation of the information about the problem [1]. This radically simplifies interactions between heterogeneous team members, eliminating the necessity for AI agents to process natural language. Ontological modelling can be complex and laborious, however, many ontologies have already been developed and can be reused.
- Interaction models and interfaces supporting reliable AI, e.g. embedding explanations and provenance records to the information pieces [2].
- Collaboration support in the form of configurable team formation algorithms and interaction monitoring [3]. The latter can be used to identify non-productive situations in the collective work and recommend actions to resolve them.

The rest of the paper is structured as follows. Section 2 briefly characterize classes of applications for supporting collaboration, with an emphasis on human-AI collaboration. Section 3 presents the conceptual approach to support human-AI collaboration implemented in the platform. Main architectural decisions are described in Sect. 4 and an illustrative example in Sect. 5.

## 2 Related Work

One can identify several lines of related work. The first one is research on crowd-based computational environments, allowing to unify human and computational resources. The second is the support of collaboration. Finally, the third is human-AI interaction. In this section, we briefly characterize relevant results from these lines of research.

Computational environments leveraging the resources of loosely connected people interacting via Internet usually are discussed in the scope of crowdsourcing or crowd computing. In most crowdsourcing systems participants individually perform relatively simple tasks, playing a role of a "computing device" [4] following a predefined workflow. At the same time, it has been shown that for complex problems pre-programmed workflows are too limited (e.g., [5]), therefore, the potential of crowdsourcing for complex work is tightly connected with the mechanisms of dynamic team formation, workflow adaptation. Applying crowd computing to complex problems requires workflow flexibility and the ability of participants to influence it [6–8].

Problems closely related to the problem of collective decision-making (including human-machine teams) are also present in many publications in the area of computer-supported collaborative work (e.g., [9, 10]). The problem of supporting the collaboration processes and increasing their efficiency has received much attention both in the scope of

decision and management science in general and in the scope of group decision support systems. From the organization perspective, increasing the efficiency of the collaboration processes is usually done with a help of a dedicated person – facilitator [11]. However, the shortage of facilitation expertise is a limiting factor, especially in the case of large-scale collective intelligence systems, based on free participation (e.g., crowd-based) [12]. To overcome this limitation, two methodological and technological branches of research emerged: collaboration engineering [13] and automated facilitation [12, 14, 15]. The proposed platform supports collective action (similarly to [12]) but it does so based on the ontology-based group state representation, rather than some *ad hoc* encodings (as in [12, 14]).

There are also many papers examining scenarios of collaboration between AI agents and human experts for decision support [16–24]. As a result of the analysis of this research line, five types of interactions were identified [17, 25]: informing (initiated by the AI agent), request to the AI agent (initiated by a person), response (response of the AI agent to a person to his request without explanation), explanation (an AI agent's response to a human's request, accompanied by explanations) and human training of the AI agent.

## 3 Conceptual Approach

The core of the proposed platform and DSSs based on it is the interaction between the decision maker (DM) and a team composed of human experts and AI agents (Fig. 1). The DM formulates the problem situation, and the team consisting of both humans (experts) and AI agents (software components usually implementing some intellectual information processing functions and capable of participating in collaborative task execution) is assembled to explore possible solutions (and evaluate them). The DM may participate in the formation and coordination of the team's work. The team, in turn, dynamically forms around the problem situation. Essential characteristics of the team include the team organization model (chain of command) and methods of task distribution and responsibility allocation [26].

Working on a problem situation involves decomposing it into solving specific tasks and integrating their results. The main types of such tasks are identified, for example, in the work by [27]: recognition, prediction, decision, and action. These types can be used, in particular, in describing AI agents to facilitate automated task allocation.

A specific team to support decision-making by the Decision Maker (DM) is formed according to the selected team organization model comprising experts and AI agents, each characterized by a set of capabilities for solving various tasks. The team characteristics (organization model, task allocation, and responsibility distribution) determine its composition and rules of participant interaction. These characteristics are used both in the formation process (e.g., participant selection, role definition) and communicated to the participants as norms and rules of engagement, which can be informal or supported by functionalities of the collaborative work environment. Participation in the team is typically characterized by a role, defined as a set of duties for solving specific tasks and responsibility for the outcomes.

The key underlying processes that facilitate working on a problem include information and knowledge exchange (which reduces the overall uncertainty of the problem

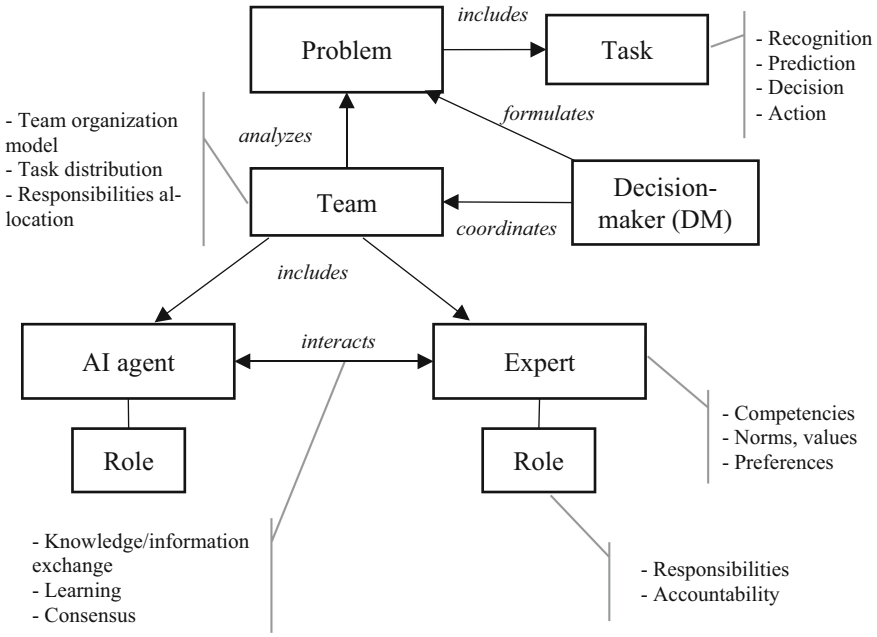


**Fig. 1.** Conceptual model of a collaborative human-AI decision support system

situation), learning, understood as the transmission of norms, teachings, and skills, as well as achieving consensus among team members. The specific mechanisms for implementing these processes determine the final design of the collaborative decision-making system.

The proposed scheme of the collaborative decision-making system is based on representing the problem situation (and other decision-relevant information) using an ontology. It is practical to use multiple ontologies that reveal various aspects of the problem: the terminology and regularities of the subject area, the structure of the decision-making task itself, argumentation logic, and so on. These aspects can be integrated into a single ontology in a problem-oriented manner using the framework of multi-aspect ontologies [1].

The information presented in this way about the problem is contained in an ontology-driven smart space [28] (storing a set of statements in ontology terms and providing convenient access and notification mechanisms), accessible to both AI agents and experts. The advantage of an ontology-driven representation is that the information becomes accessible to both humans (directly or through a specialized interface) and AI agents, which can utilize the SPARQL language capabilities to extract relevant statements from the description of the current problem state.

While the platform itself defines several service ontologies (e.g., to structure decision support of argumentation processes), it does not define any domain or application ontology – these ontologies are defined at the level of a concrete decision support system, built using the platform. Basically, selecting one or several application ontologies and linking

them to the platform's service ontologies using the apparatus of multi-aspect ontologies are the main activities performed to build a DSS based on the proposed platform.

Interaction among the members of the decision-making support team occurs indirectly through modifications to the content of the intelligent space.

In the context of the problems discussed in this paper, AI agents play the central role in the proposed platform. In terms of information processing, two categories of such agents can be distinguished. Agents in the first group transform symbolic information based on knowledge; that is, both the input and output of these agents are symbolic information (expressed as a set of statements in the domain ontology). Agents in the second group, on the other hand, convert "raw" data into symbolic information. These agents take as input images, video or audio data, or simply numerical observations, and output statements based on the domain ontology. Various technologies, including Artificial Neural Networks (ANNs), are currently used to organize such agents, enabling the mapping of this "raw" data to one of the concepts. These agents can leverage elements of neuro-symbolic intelligence, using neural network paradigm to interpret data in a symbolic (conceptual) system, which is crucial for subsequent communication.

One of the essential aspects of collaborative decision support is traceability. That is, the ability to track the source for each statement (concerning the list of alternatives or their assessments) that are formulated during joint work on a task. This capability plays a key role, for example, in the formation and use of trust mechanisms that significantly reduce verification overhead. In the proposed conceptual model, traceability is achieved through two mechanisms. Firstly, all changes in the presentation of the problem are supplied with metadata in accordance with the PROV-O ontology [29], which allows us to describe the sources of information (system participant who provided the information, reasons), secondly, agents in addition to the result of the work itself can also add an explanation as to why exactly this result was obtained (for agents that transform symbolic information, this is a chain of logical inference, and for agents that transform "raw" data into symbolic data, this is one or another type of ontology-oriented explanation).

## 4 Architecture

This section characterizes key points of the platform architecture, including typical user roles, scenarios, components and their interaction.

### 4.1 Use Case View

There are three categories of users: *End User* (decision-maker, DM), *Participant* (expert), and *Agent Developer*. The *End User* turns to the System with a certain task, the solution of which requires the joint efforts of a human-machine team. The participant takes actions that contribute to solving the problem. The agent developer publishes agents that, using the mechanisms of the environment, can also take part in solving the problem. Each of the categories in the use case view is represented by an actor of the same name.

The two roles *End User* (DM) and *Participant* (expert) share a significant number of precedents that ensure the actual interaction within the team. A use case specific to

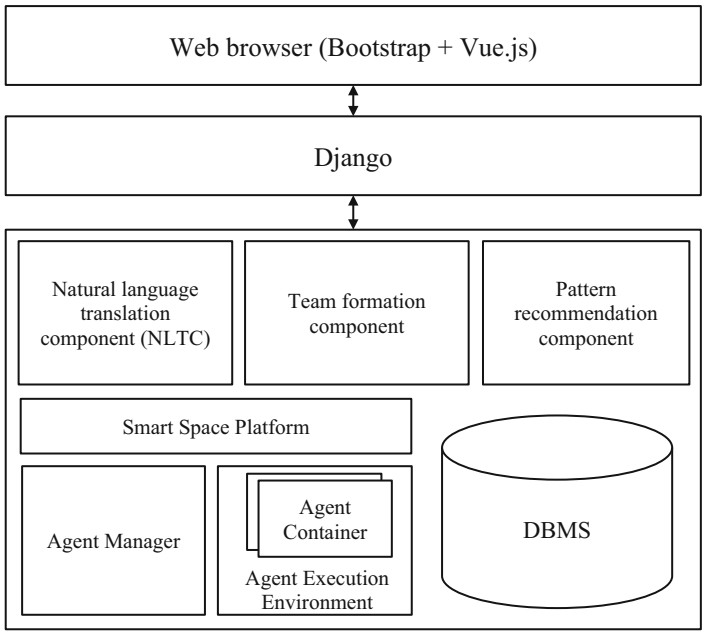


**Fig. 2.** Main platform components.

the *End User* is the creation of a problem, which includes the creation of an initial text description of the problem that requires the use of human-machine collective AI, as well as additional parameters (time constraints, compensation policy (if applicable), and others). As a result of executing this precedent, 1) a new problem is registered in the system and a workspace is created for it, 2) invitations are sent to participants whose involvement in solving the task may be promising.

A workspace is understood as a set of interface elements and related functions aimed at displaying the status of a specific problem and supplementing it with new information.

Use cases specific to the *Participant* (expert) are filling out the participant's profile and working with received invitations to join in solving problems. The participant profile combines information both reported by the user and summarizing the experience of his participation in solving problems and is used to select participants when sending out invitations. The main parameter of the profile, which the *Participant* can adjust, is the description of the existing competencies (both in natural language and in connection with the ontology of competencies).

The main use cases available to the *Agent Developer* role are creating an agent, uploading a new version, browsing information about agents, and managing agent state. Creating an agent involves specifying the characteristics of the agent created by the developer – activation conditions, conditions of use, program code. If necessary, the developer can upload a new version of the agent. At the same time, if the agent was a member of some teams, then they continue to work with the old version, and when the agent joins new teams, the new version is used. Agent state management includes activating and suspending an agent. An active agent can join teams, a suspended agent

cannot. Finally, browsing information about agents allows the developer to obtain quantitative and qualitative (ratings, reviews) information about the agent's participation in solving problems.

### 4.2 Component View

The execution of system components occurs on three computing nodes: a web server, a database server, and a user device (Fig. 2).

The web server hosts not only the component that provides the delivery of web application pages (Web Application), but also all components related to managing the smart space (Smart Space Platform), executing agents (Agent Manager, Agent Execution Environment), team formation component, pattern recommendation component, natural language translation component (NLTC), as well as infrastructure for deferred task execution.

The database server hosts the DBMS, under which the web application database itself runs.

Finally, interaction with the client occurs through a browser (Web browser), launched on the user's device and providing a computing environment for executing code associated with the design and logic of behavior of some interface elements (not requiring a reload of the entire page).

Team formation component provides a set of algorithms to build new teams and extend existing ones. It maintains a set of primitives like competency, role, historical performance, and particular DSS created on the platform can set up team formation policy using these primitives and pre-defined policies, or even implement a new policy tailored to the problem domain.

Natural language translation component (NLTC) plays an important role of parsing and transforming textual discussions to structured representation. In particular, it identifies roles of particular messages and information pieces (if it is an alternative description, evaluation, etc.) and their interdependencies (supporting statements, contradicting statements). Resulting structural representation is interactively verified and then can be used by agents, obviating the need for each agent to parse textual stream.

Pattern recommendation component analyzes current discussion situation (its structured representation) and leveraging collaboration engineering knowledge and machine learning model identifies non-productive situations and proposes ways to improve them [3].

## 5 Use Case

The scenario is devoted to the developing recommendations aimed at the prevention of accidents at sections of traffic accident concentrations. A section of traffic accident concentration is a section of highway not exceeding 1000 m outside a locality, 200 m in a locality or at a road intersection where three accidents and more of one type or five accidents and more, regardless of their type, have occurred during 12 months, as a result of which people were killed or injured.

Collaboration behind the scenario supposes that partnerships between humans and software agents are in preference to automation [18]. The decision maker initiates the collaboration providing the information necessary to start the collaboration to groups of agents and human experts. The agents start interacting to provide recommendations. If they manage to do this then the experts receive these recommendations with explanations of why the agents offer them. The experts can agree with the list of the recommendations, agree on some recommendations or decline the recommendations of the agents. If the experts reach some agreement, they deliver the agreed recommendations to the decision maker. If the agents are not able to provide any recommendations then the experts and the agents interact to develop such recommendations jointly. The experts revise the jointly developed recommendations and if they are satisfied with them then the experts deliver the recommendations to the decision maker. Based on the recommendations received from the expert group, the decision maker prepares a conclusion on the recommended measures. If the groups of agents and experts cannot propose any recommendations then the expert group informs the decision maker about this and provides explanations of the fail.

In the scenario, the collaborative team involves a human decision maker, 3 software agents, and 3 human experts.

The group of the software agents includes:

- Accident analyst – an agent that provides information about the traffic accident concentration sections occurred at the specific administrative area and analyses the accident reporting cards;
- Signs analyst – an agent that provides information about the road signs installed at the traffic accident concentration sections;
- Recommender – an AI agent that provides recommendations.

The group of the experts comprises:

- Decision maker;
- FRA – a representative of the Federal Road Agency;
- Municipal administration – a representative of the Administration;
- Police inspector – a representative of the traffic police department.

The scenario is executed as part of the regular inspection aimed at the release and prevention of accidents at the sections of traffic accident concentrations.

The input data for the scenario are as follows:

- The location of the accident concentration section;
- The accident reporting cards that fix the information about accidents occurred at the accident concentration section;
- The information about the road signs installed at the accident concentration sections.

The scenario supports the following sequence of events:

1. The decision maker sends to the agents of the agent group and to leaders of the appropriate organizations messages with the date and time of the inspection, inspection period, accident concentration to be considered and the reference to the collaborative service.

2. Interactions in the agent group. Accident analyst reports the statistics of accident types, Sign analyst provides information about relevant signs and Recommender uses the Guidelines to make recommendations.
3. Interactions in the expert group. Evaluate the recommendations. Possibly specify solutions to test with the help of agents.
4. Interactions of the agents and experts. Test and verify the proposed solutions.
5. Recommendations of the expert group.
6. The conclusion of the decision maker coincides with the recommendations received from the expert group.

The implementation of the presented scenario is carried out using the proposed platform for human-AI collaborative decision support. This platform supports the task creation, the selection of participants to solve the problem, according to the required competencies, and tracking the progress of the problem solving process. Participants can be both people and agents interacting with the platform via the REST API.

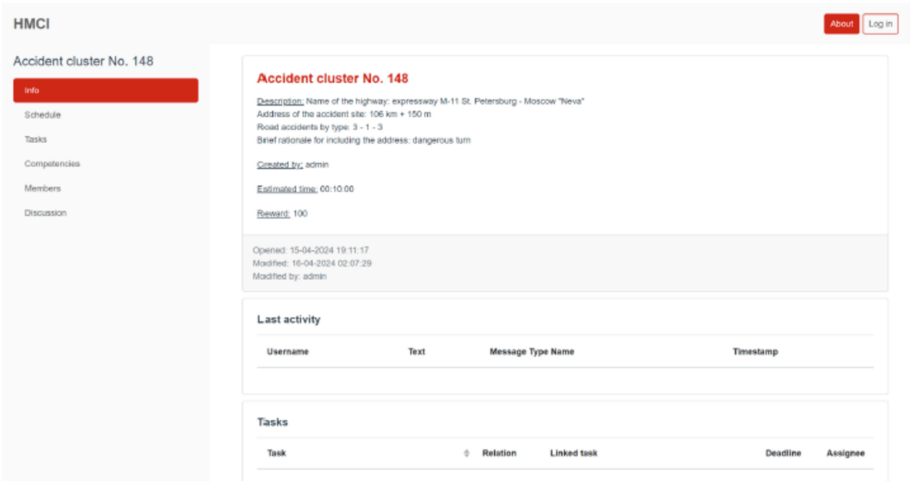


**Fig. 3.** Platform UI. Problem information page.

To work with tasks, the platform provides a web interface (Fig. 3) through which users can view the general list of tasks, track notifications about invitations to a new task or about new events in tasks for which the user is already an executor. For each task, a detailed description is available, estimated deadlines for its completion, required competencies, possible remuneration for performers and a breakdown into subtasks. If there are subtasks, their dependency graph and timeline with the deadlines for completing the subtasks are displayed. Discussion of tasks and subtasks is carried out through a built-in messenger in which users can exchange their solutions and comment on them, developing a joint solution to the problem. The discussion also involves agents selected according to the functions they perform, similar to competencies for people.

In accordance with the scenario under consideration, when a location of road accidents concentration is detected, the decision maker creates a task in which he or she

describes the coordinates of the place and the list of road accidents, and also specifies a list of competencies related to obtaining detailed information on road accidents and the corresponding section of the road network, generating recommendations and assessment the effect of the proposed recommendations. In accordance with the required competencies, software and human agents are selected to collect data and generate recommendations, as well as experts to discuss recommendations. Subtasks are formed, interaction is carried out between groups of participants and the decision maker is provided with a list of possible solutions with justification. In this case, access to agents is carried out in the general message flow through direct access to the agent in accordance with its functions with request parameters. At this point, the task is considered solved and, if there is a reward, it is paid to all participants.

## 6 Conclusion

The paper proposes a platform to mitigate the development of collaborative decision support systems based on the interaction between human experts and AI. The platform provides a set of mechanisms and interfaces, simplifying the development of CDSSs: team formation and collaboration support, interfaces to define, deploy and manage AI agents, and a set of structured representations facilitating interaction between human experts and AI agents.

Distinguishing features of the proposed approach are ontological representation of the information about the problem, interaction models and interfaces supporting reliable AI, collaboration support in the form of configurable team formation algorithms and interaction monitoring.

The paper also shows an example of a collaborative scenario that can be implemented using the proposed platform, which illustrates viability of the proposed approach and implemented set of mechanisms.

The proposed platform can be used to organize collaborative decision support in variety of domains, mostly characterized by dynamics and complexity.

It should be noted, that primary goal during the platform design and development was to satisfy some principal requirements, e.g., interoperability of the heterogeoeous collectives' members, mutual understanding, planning flexibility, etc. The resulting architecture satisfies these requirements, providing a unique combination of features for human-AI collaboration, however, not much attention was paid to temporal efficiency of the implementation. Therefore, future work is mostly related to two directions: first, using the platform for decision support in various scenarios and problem domains and collecting user feedback as well as objective success metrics, second, detecting and improving "bottlenecks" of the implementation.

**Acknowledgments.** This study was funded by the Russian Science Foundation (project 22-11-00214).

## References


1. Smirnov, A., Levashova, T., Ponomarev, A., Shilov, N.: Methodology for multi-aspect ontology development: ontology for decision support based on human-machine collective intelligence. IEEE Access. **9**, 135167–135185 (2021). https://doi.org/10.1109/ACCESS.2021.3116870
2. Smirnov, A., Ponomarev, A.: Ontology-based explanations of neural networks for collaborative human-AI decision support systems. In: Proceedings of the Seventh International Scientific Conference "Intelligent Information Technologies for Industry" (IITI'23). IITI 2023, LNNS, vol. 776. pp. 353–362 (2023). https://doi.org/10.1007/978-3-031-43789-2_33
3. Smirnov, A., Ponomarev, A.: Recommendation of collaboration patterns for human-machine collective intelligence. In: Conference of Open Innovations Association FRUCT, May 2021, pp. 330–336 (2021). https://doi.org/10.23919/FRUCT52173.2021.9435535
4. Schall, D.: Service-Oriented Crowdsourcing: Architecture, Protocols and Algorithms. Springer, New York (2012). https://doi.org/10.1007/978-1-4614-5956-9
5. Retelny, D., Bernstein, M.S., Valentine, M.A.: No workflow can ever be enough: how crowdsourcing workflows constrain complex work. In: Proceedings of ACM Human-Computer Interact. 1, Article 89 (2017). https://doi.org/10.1145/3134724
6. Valentine, M.A., Retelny, D., To, A., Rahmati, N., Doshi, T., Bernstein, M.S.: flash organizations. In: Proceedings of the 2017 CHI Conference on Human Factors in Computing Systems - CHI 2017, pp. 3523–3537. ACM Press, New York, New York, USA (2017). https://doi.org/10.1145/3025453.3025811
7. Salehi, N., McCabe, A., Valentine, M., Bernstein, M.S.: Huddler: convening stable and familiar crowd teams despite unpredictable availability. In: Proceedings of the ACM Conference on Computer Supported Cooperative Work, CSCW, pp. 1700–1713 (2017). https://doi.org/10.1145/2998181.2998300
8. Lykourentzou, I., et al.: Self-organization in online collaborative work settings. Collect. Intell. **1**, 263391372210780 (2022). https://doi.org/10.1177/26339137221078005
9. Terveen, L.G.: Overview of human-computer collaboration. Knowledge-Based Syst. **8**, 67–81 (1995)
10. Elmarzouqi, N., Garcia, E., Lapayre, J.-C.: CSCW from coordination to collaboration (2008). https://doi.org/10.1007/978-3-540-92719-8_9
11. Adla, A., Zarate, P., Soubie, J.-L.: A proposal of toolkit for GDSS facilitators. Gr. Decis. Negot. **20**, 57–77 (2011). https://doi.org/10.1007/s10726-010-9204-8
12. Gu, W., Moustafa, A., Ito, T., Zhang, M., Yang, C.: A case-based reasoning approach for automated facilitation in online discussion systems. In: Proceedings of 2018 13th International Conference on Knowledge, Information and Creativity Support Systems, KICSS 2018, pp. 1–5 (2018). https://doi.org/10.1109/KICSS45055.2018.8950535
13. Kolfschoten, G.L., de Vreede, G.J.: The collaboration engineering approach for designing collaboration processes. In: Haake, J.M., Ochoa, S.F., Cechich, A. (eds.) Groupware: Design, Implementation, and Use, CRIWG 2007, LNCS, vol. 4715. Springer, Berlin (2007). https://doi.org/10.1007/978-3-540-74812-0_8
14. Ito, T., Suzuki, S., Yamaguchi, N., Nishida, T., Hiraishi, K., Yoshino, K.: D-agree: crowd discussion support system based on automated facilitation agent. In: Proceedings of the AAAI Conference on Artificial Intelligence, vol. 34, pp. 13614–13615 (2020). https://doi.org/10.1609/aaai.v34i09.7094
15. Bittner, E., Shoury, O.: Designing automated facilitation for design thinking: a Chatbot for supporting teams in the empathy map method. In: Proceedings of the 52nd Hawaii International Conference on Systems Science, pp. 227–236 (2019). https://doi.org/10.24251/hicss.2019.029

16. Lee, M.H., Siewiorek, D.P.P., Smailagic, A., Bernardino, A., Bermúdez i Badia, S.B.: A Human-AI collaborative approach for clinical decision making on rehabilitation assessment. In: Proceedings of the 2021 CHI Conference on Human Factors in Computing Systems, pp. 1–14. ACM, New York, NY, USA (2021). https://doi.org/10.1145/3411764.3445472
17. van den Bosch, K., Bronkhorst, A.: Human-AI cooperation to benefit military decision making. In: Proceedings of Specialist Meeting Big Data & Artificial Intelligence for Military Decision Making (2018). https://doi.org/10.14339/STO-MP-IST-160
18. Pohl, J.: Collaborative decision-support and the human-machine relationship. In: A Decision-Making Tools Workshop, pp. 21–46. Collaborative Agent Design Research Center, San Luis (2019)
19. Chen, J., Lim, C.P., Tan, K.H., Govindan, K., Kumar, A.: Artificial intelligence-based human-centric decision support framework: an application to predictive maintenance in asset management under pandemic environments. Ann. Oper. Res. (2021). https://doi.org/10.1007/s10479-021-04373-w
20. Bouabdallaoui, Y., Lafhaj, Z., Yim, P., Ducoulombier, L., Bennadji, B.: Predictive maintenance in building facilities: a machine learning-based approach. Sensors. **21**, 1044 (2021). https://doi.org/10.3390/s21041044
21. Kase, S.E., Hung, C.P., Krayzman, T., Hare, J.Z., Rinderspacher, B.C., Su, S.M.: The future of collaborative human-artificial intelligence decision-making for mission planning. Front. Psychol. **13** (2022). https://doi.org/10.3389/fpsyg.2022.850628
22. Puranam, P.: Human–AI collaborative decision-making as an organization design problem. J. Organ. Des. **10**, 75–80 (2021). https://doi.org/10.1007/s41469-021-00095-2
23. Lai, V., Carton, S., Bhatnagar, R., Liao, Q.V., Zhang, Y., Tan, C.: Human-AI collaboration via conditional delegation: a case study of content moderation. In: CHI Conference on Human Factors in Computing Systems, pp. 1–18. ACM, New York, NY, USA (2022). https://doi.org/10.1145/3491102.3501999
24. Fügener, A., Grahl, J., Gupta, A., Ketter, W.: Cognitive challenges in human-artificial intelligence collaboration: investigating the path toward productive delegation. Inf. Syst. Res. **33**, 678–696 (2022). https://doi.org/10.1287/isre.2021.1079
25. Dellermann, D., Calma, A., Lipusch, N., Weber, T., Weigel, S., Ebel, P.: The future of human-AI collaboration: a taxonomy of design knowledge for hybrid intelligence systems. In: Bui, T.X. (ed.) Proceedings of the 52nd Annual Hawaii International Conference on System Sciences, pp. 274–283 (2019). https://doi.org/10.24251/HICSS.2019.034
26. Xiong, W., Fan, H., Ma, L., Wang, C.: Challenges of human—machine collaboration in risky decision-making. Front. Eng. Manag. **9**, 89–103 (2022). https://doi.org/10.1007/s42524-021-0182-0
27. Dellermann, D., Calma, A., Lipusch, N., Weber, T., Weigel, S., Ebel, P.: The future of human-AI collaboration: a taxonomy of design knowledge for hybrid intelligence systems. In: Proceedings of Annual Hawaii International Conference on System Sciences, January 2019, pp. 274–283 (2019). https://doi.org/10.24251/hicss.2019.034
28. Roffia, L., et al.: A semantic publish-subscribe architecture for the internet of things. IEEE Internet Things J. **3**, 1274–1296 (2016). https://doi.org/10.1109/JIOT.2016.2587380
29. The PROV Ontology. https://www.w3.org/TR/prov-o/, Accessed 28 Jan 2020

# An Efficient Algorithm for Calculating Optical Flow Parameters in Computer Vision Systems

Sergey V. Sokolov[1], Daniil V. Marshakov[2(✉)], Agop E. Khatlamadzhiyan[3], and Irina V. Reshetnikova[4]

[1] Rostov State University of Economics, Rostov-on-Don, Russia
[2] Rostov State Transport University, Rostov-on-Don, Russia
daniil_marshakov@mail.ru
[3] JSC "NIIAS", Moscow, Russia
[4] Moscow Technical University of Communications and Informatics, Moscow, Russia

**Abstract.** The solution to the problem of constructing the velocity field of a moving object in computer (machine) vision systems using monocular methods for determining the proper motion of a video camera is considered. The estimation of optical flow parameters is obtained on the basis of minimization of the integrand expression of the energy functional (by Horn-Schunck) with the introduction of a regularizing component by Tikhonov. Unlike the traditional procedure for minimizing the energy functional, which requires information about the optical flow values for the entire scanning area and a large amount of computational costs, the proposed method requires optical flow values determined only at a specific point in the image area. The solution is obtained in a simple analytical form, easily implemented from a computational point of view in on-board computers. A numerical experiment was carried out to illustrate the possibility of effective practical application of the proposed approach.

**Keywords:** optical flow · computer (machine) vision systems · velocity field

## 1 Introduction

One of the most important tasks solved by computer (machine) vision systems (CVS) when processing and analyzing images is constructing a velocity field of a moving object. Such a task is extremely demanded in robotics when determining the angular orientation and spatial position of autonomous robots, in space research, in electrodynamics problems, in the study of complex mechanical systems, etc. [1–9].

To date, several methods have been developed to determine the velocity field (optical flow) using CVS, among which the most effective are monocular methods for determining the self-motion of a video camera [1–18]. In turn, among these methods there are methods based on search and comparison of the so-called "special" points, and methods using algorithms for calculating dense optical flow. The methods using algorithms for

The work was carried out in accordance with State Assignment No. 1023080200012-3-2.3.4.


S. Kovalev et al. (Eds.): IITI 2024, LNNS 1209, pp. 346–354, 2024.
https://doi.org/10.1007/978-3-031-77688-5_33

calculating dense optical flow, in contrast to the methods of "special" points, have a number of important advantages, such as performance on low-textured scenes (where it is difficult to find "special" points) and the ability to obtain a detailed relief of the object without additional actions. By dense optical flow (hereinafter simply "optical flow") we understand its classical definition as an image of the apparent movement of objects, surfaces or edges of the scene, resulting from the movement of the observer (in particular, the camera) relative to the scene. Or, formalizing this definition for subsequent conclusions: if $I_0(x,y)$ is the first frame of the video (a function of intensity from the coordinate of a point on the image), and $I_1(x,y)$ is the second frame containing the same points, only shifted (intensity is preserved, the edges of the image are not considered), then the vector field $V(x,y) = (u(x,y),v(x,y))$: $I_1(x,y) = I_0(x + u,y + v)\ \forall(x,y)$ is the optical flow ("dense" means its existence at all points of the image). The main feature of the components $u(x,y)$, $v(x,y)$ of the vector field $V(x,y)$ (hereinafter referred to as "optical flow parameters") is the presence of an analytical dependence on the linear and angular velocities of the object, calculated from these parameters, in this connection, the problem of estimating them with high accuracy, and, in conditions of inevitable video recording interference, is one of the main ones in the theory and practice of technical vision.

## 2 Formulation of the Problem

The initial equation for determining the optical flow parameters $u(x,y)$, $v(x,y)$ is the so-called basic equation of optical flow [10–15]:

$$\frac{\partial I}{\partial t} + u\frac{\partial I}{\partial x} + v\frac{\partial I}{\partial y} = 0, \tag{1}$$

where $u$, $v$ are the velocity components of the brightness pattern respectively in the directions $x$ and $y$, taken at the scanning point $P$; $\frac{\partial I(x,y,t)}{\partial t}$, $\frac{\partial I(x,y,t)}{\partial x}$, $\frac{\partial I(x,y,t)}{\partial y}$ – partial derivatives of the brightness function of the observed surface, which are estimated directly from the image.

Equation (1) contains two unknown variables $u$, $v$ and, therefore, cannot be uniquely resolved. The most commonly used solution to this situation is the use of various restrictions imposed on the optical flow. For example, the use of gradient constraints from neighboring pixels, assuming that they have the same 2D-velocity, which in this case is found by minimizing constraint errors (in particular, when minimizing quadratic errors – using the least squares method); the use of phase correlation of individual image pixels, various assumptions about the dynamics of image brightness, etc. [10–16].

Thus, the method described in [12] uses the assumption of the same displacement of all points of the neighborhood under consideration and the approximation of the signal of the neighborhood of each pixel by a quadratic form, the parameters of which are found using the weighted least squares method (the weighting function is usually chosen to be Gaussian).

An alternative method is the Lucas-Kanade iterative differential method, based on two assumptions: constancy of brightness along the motion trajectories and equal displacement of neighboring pixels (as a result of which the velocity field is found only

for a certain neighborhood of the pixel by minimizing the objective functional using the least squares method). This method performs well at small displacements, but results in sparse optical flow [11]. But perhaps the most commonly used method for calculating optical flow is the Horn-Schunk algorithm [10], based on the assumption that the optical flow is smooth throughout the entire image (no sudden change in velocities) [14, 15].

The optical flow estimate is calculated based on the so-called energy functional

$$E(u, v) = \int_D (\frac{\partial I}{\partial t} + \nabla I \begin{vmatrix} u \\ v \end{vmatrix})^2 + \lambda(|\nabla u|^2 + |\nabla v|^2) dxdy, \quad (2)$$

where $D$ is the domain of existence of the variables $x$,$y$, $\nabla$ is the Hamilton operator, $\lambda$ is the regularization parameter,

minimized either using discrete approximations to the integral and derivatives, or based on the corresponding Euler-Lagrange equations under boundary conditions with reflection [10].

The advantage of this method is the formation of a dense optical flow, the disadvantage is sensitivity to noise, as well as the need to set boundary conditions.

But the main disadvantage of the above traditional methods is low computational efficiency. Even when using high-performance optimization algorithms, the computational cost are often unrealizable for on-board computers, making real-time optical flow estimation difficult. This circumstance initiated the development of a separate direction in the field of developing methods for calculating optical flow, exploring the possibility of their implementation in real time. Currently, the main results here have been obtained either on the basis of additional software and hardware processing of optical flow [3, 13, 14], or using neural networks and deep learning algorithms [4, 5, 17, 18]. Both of these approaches have obvious disadvantages - the complexity of the hardware of the information-measuring complex of a moving object and the need for preliminary training of the neural network, which, in turn, requires significant time and computational costs.

In this regard, we will further consider one of the possible approaches to determining the parameters of the optical flow, which provides, in comparison with existing methods, a significantly lower volume of computational costs while maintaining the dense structure of the optical flow.

## 3 The Solution of the Problem

Analysis of functional (2), the minimization of which in terms of the parameters of the optical flow ensures its dense structure, shows that all the integrands included in it are non-negative definite. This, in turn, allows us to move, when searching for optimal values of optical flow parameters, from minimizing integral (2), which requires information about the values of optical flow for the entire domain $D$, to minimizing the integrand $(\frac{\partial I}{\partial t} + \nabla I \begin{vmatrix} u \\ v \end{vmatrix})^2$, determined only in a specific point $(x,y)$ of domain $D$. In this case, in contrast to functional (2), we choose the regularizing addition according to Tikhonov

according to the $L^2$ norm: $\alpha \left|\begin{matrix} u \\ v \end{matrix}\right|^T \left|\begin{matrix} u \\ v \end{matrix}\right|$, where α is the regularization parameter. In this case, the optical flow estimate can be calculated from the criterion minimization condition:

$$J = (\frac{\partial I}{\partial t} + \nabla I \left|\begin{matrix} u \\ v \end{matrix}\right|)^2 + \alpha \left|\begin{matrix} u \\ v \end{matrix}\right|^T \left|\begin{matrix} u \\ v \end{matrix}\right|. \tag{3}$$

Differentiating (3) with respect to the vector $\left|\begin{matrix} u \\ v \end{matrix}\right|$ and equating it to 0, we have:

$$2\,(\frac{\partial I}{\partial t} + \left|\begin{matrix} \frac{\partial I}{\partial x} & \frac{\partial I}{\partial y} \end{matrix}\right| \left|\begin{matrix} u \\ v \end{matrix}\right|) \left|\begin{matrix} \frac{\partial I}{\partial x} & \frac{\partial I}{\partial y} \end{matrix}\right| + 2\alpha \left|\begin{matrix} u \\ v \end{matrix}\right|^T = 0.$$

Bringing the resulting vector equation to the form

$$-\left|\begin{matrix} \frac{\partial I}{\partial x} & \frac{\partial I}{\partial y} \end{matrix}\right|^T \frac{\partial I}{\partial t} - \left|\begin{matrix} \frac{\partial I}{\partial x} & \frac{\partial I}{\partial y} \end{matrix}\right|^T \left|\begin{matrix} \frac{\partial I}{\partial x} & \frac{\partial I}{\partial y} \end{matrix}\right| \left|\begin{matrix} u \\ v \end{matrix}\right| = \alpha \left|\begin{matrix} u \\ v \end{matrix}\right|,$$

we obtain a system of linear equations for the desired vector $|u\ v|^T$

$$-\left|\begin{matrix} \frac{\partial I}{\partial x} & \frac{\partial I}{\partial y} \end{matrix}\right|^T \frac{\partial I}{\partial t} = \left|\begin{matrix} \alpha + (\frac{\partial I}{\partial x})^2 & \frac{\partial I}{\partial x}\frac{\partial I}{\partial y} \\ \frac{\partial I}{\partial x}\frac{\partial I}{\partial y} & \alpha + (\frac{\partial I}{\partial y})^2 \end{matrix}\right| \left|\begin{matrix} u \\ v \end{matrix}\right|,$$

solving which, we finally have:

$$\left|\begin{matrix} u \\ v \end{matrix}\right| = -\frac{\frac{\partial I}{\partial t}}{\alpha + (\frac{\partial I}{\partial x})^2 + (\frac{\partial I}{\partial y})^2} \left|\begin{matrix} \frac{\partial I}{\partial x} \\ \frac{\partial I}{\partial y} \end{matrix}\right|. \tag{4}$$

The advantage of the obtained solution over the one proposed in [10] is the possibility of directly determining the parameters of the optical flow at a specific point on the image plane without involving the values of the optical flow at other points of the plane. Moreover, substituting the found solution (4), obtained under the assumption of noisy optical flow $I(x,y,t)$, into the original optical flow Eq. (1), leads to the appearance of a discrepancy equal to α, which makes it possible to determine the physical meaning of the regularization parameter α, as a quantity the level of general disturbance of the optical flow (more precisely, its gradients). This, in turn, allows for a more targeted and efficient determination of the value α, based on the known (or estimated) level of interference, in contrast to the choice of parameter λ in functional (2) (in known works varying from 0.5 to 100).

To evaluate the effectiveness of using the proposed approach, consider a numerical example.

## 4 Example

Spatio-temporal modeling of the optical flow $I(x,y,t)$ was carried out in the coordinate grid $\{x$:[0;5], $y$:[0;5]$\}$ with a step of 0.5 on the time interval [0;500] s with a step of 0.1 s according to the expression

$$I(x, y, t) = 0.25 \exp[-(x - 2.5)^2 - (y - 2.5)^2](\cos t + 1) \ \ (1\,\text{m}). \tag{5}$$

and using a random field measurement as noise, described as:

$$S(x, y, t) = (\cos x \cos y \sin t + 1)\, W_t, \tag{6}$$

where $W_t$ is a Gaussian sequence with zero mean and variance $D = (6{\cdot}10^{-3})^2$ $(\text{lm})^2$.

The error in determining the optical flow parameters $u,v$ was assessed at three points of the coordinate grid $\{x_i, y_i\}$: {4,2},{3,3},{2,3}, with the selected regularization parameter $\alpha = 0.0035$ with comparing the values $u,v$, obtained by substituting into Eq. (4) the true values of the optical flow, determined by expression (5), with the values $u,v$, obtained by substituting into Eq. (4) the values of the optical flow, with noisy interference (6).

Graphs of errors in estimating parameters $u,v$ for each selected point of the image plane are shown in Figs. 1, 2, 3, 4, 5 and 6.

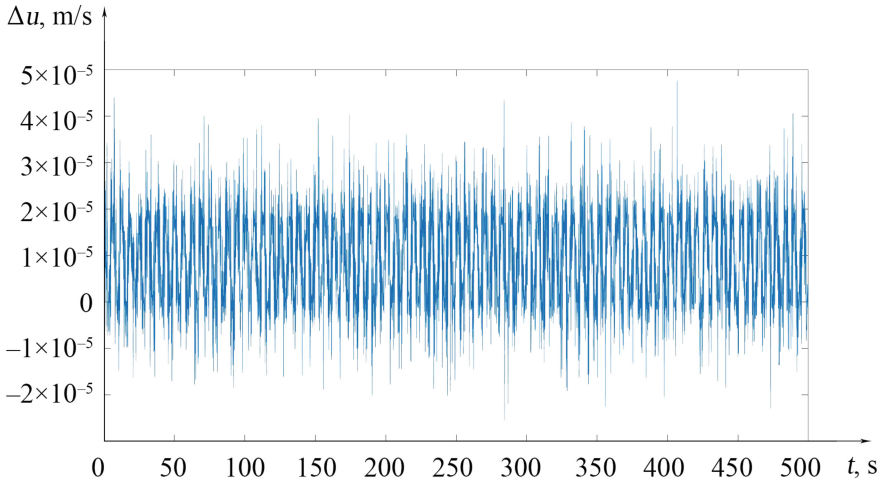


**Fig. 1.** Graph of errors in estimating parameter $u$ at coordinates {4,2}.

The mean values of the estimation errors over the entire simulation interval were in percent of the entire range of variation of the true $u,v$ values:

for coordinates {4,2} $u$ – 3%, $v$ – 4,3%,
for coordinates {3,3} $u$ – 1,8%, $v$ – 1,6%,
for coordinates {2,3} $u$ – 1,6%, $v$ – 0,4%.

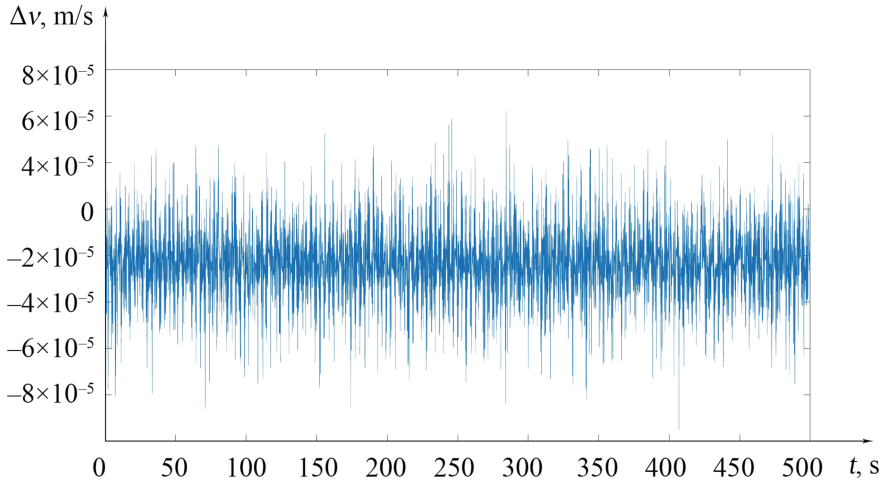


**Fig. 2.** Graph of errors in estimating parameter $v$ at coordinates {4,2}.

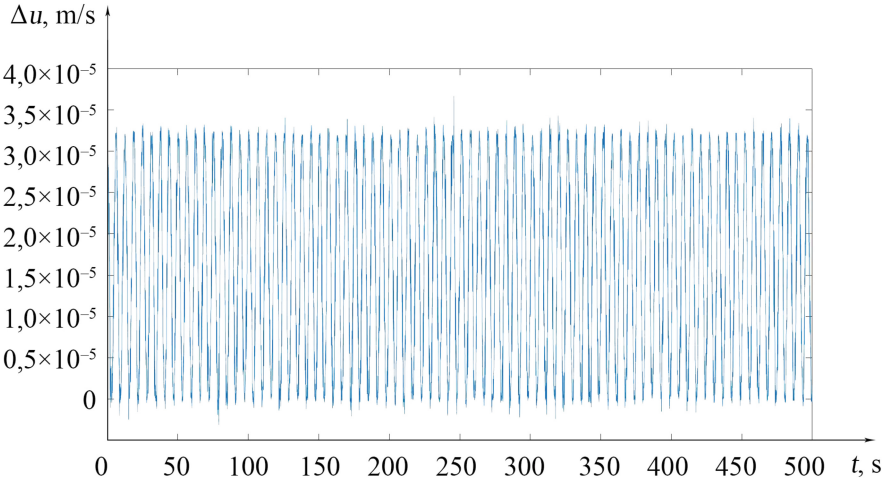


**Fig. 3.** Graph of errors in estimating parameter $u$ at coordinates {3,3}.

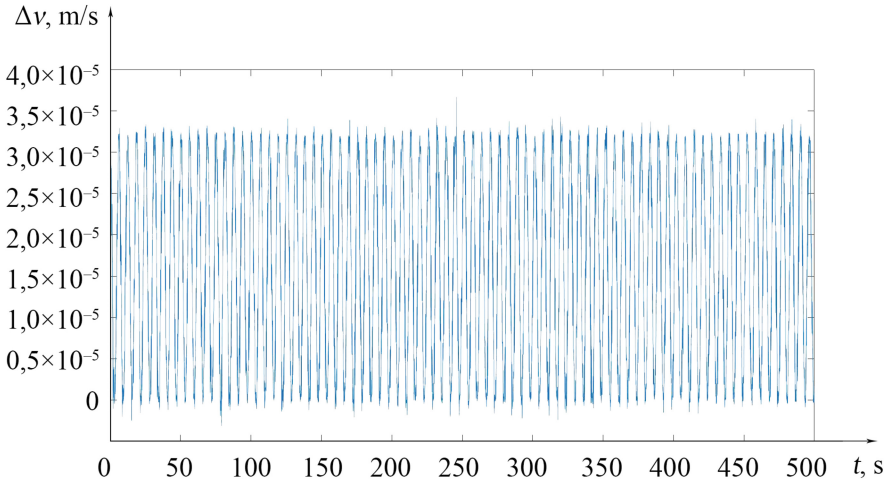


**Fig. 4.** Graph of errors in estimating parameter $v$ at coordinates {3,3}.

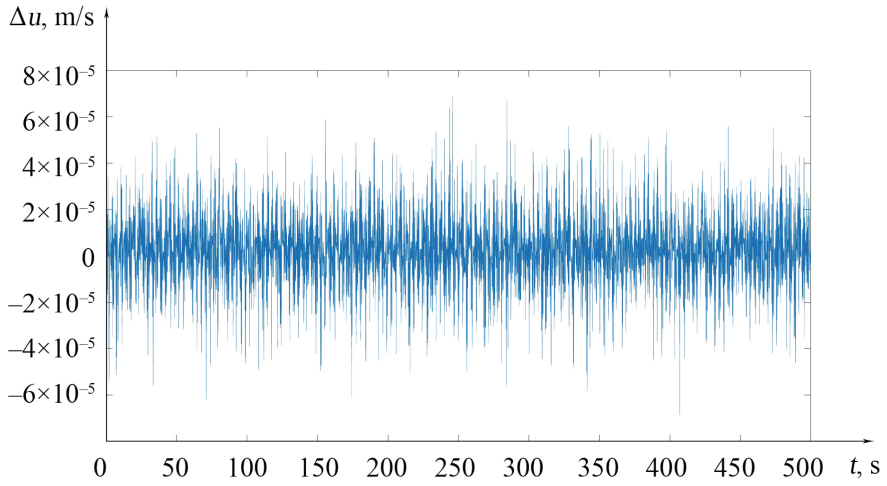


**Fig. 5.** Graph of errors in estimating parameter $u$ at coordinates {2,3}.

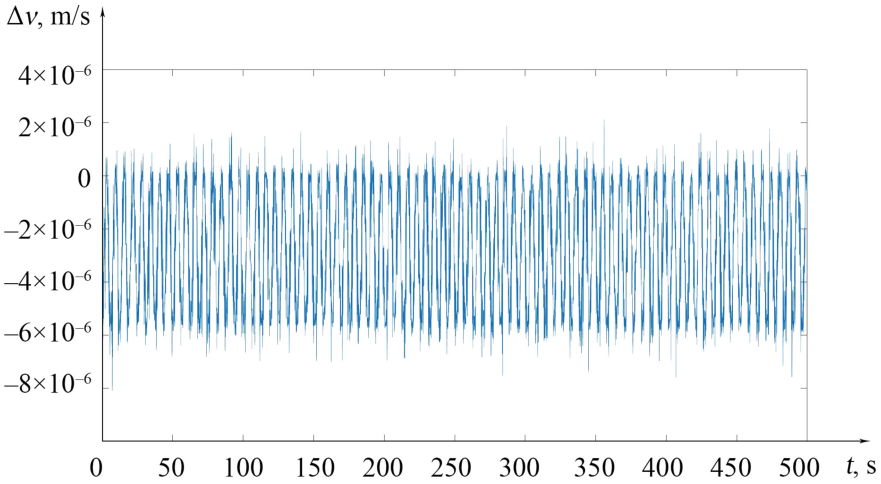


**Fig. 6.** Graph of errors in estimating parameter $v$ at coordinates {2,3}.

## 5 Conclusion

The presented results of the numerical experiment allow us to conclude, firstly, about the possibility of highly accurate determination of the parameters of the optical flow (velocity field) using the proposed algorithm, and secondly, about its computational efficiency, due to the significantly lower amount of computational costs compared to traditional methods (and while maintaining the dense structure of the optical flow), as well as the need to have information about the values of the optical flow only at a specific point in the image, and not the entire scanned image area.

Moreover, a comparative analysis of the proposed algorithm, implemented in a real-time numerical experiment, with methods for searching and comparing "special" points, requiring the implementation of complex multi-stage algorithms [19–22], also showed its advantage from a computational point of view.

Such advantage features of the approach under consideration provide the possibility of its successful practical application in CVS of robotic complexes for both general technical and special purposes.

The work was carried out in accordance with state assignment no. 1023080200012-3-2.3.4.

## References

1. Bruss, A.R., Horn, B.K.P.: Passive navigation. Comput. Vision Graph. Image Process. **21**, 3–20 (1983)
2. Kühne, J.: On-Sensor Optical Flow VIO Dataset, 1st edn. ETH Zurich, Zurich (2024)
3. Foehn, P., et al.: Agilicious: Open source and open-hardware agile quadrotor for vision-based flight. Sci. Rob. 7(67), eabl6259 (2022)
4. Bai, M., Luo, W., Kundu, K., Urtasun, R.: Exploiting semantic information and deep matching for optical flow. In: Leibe, B., Matas, J., Sebe, N., Welling, M. (eds.) Computer Vision – ECCV 2016. Lecture Notes in Computer Science, vol. 9910, pp. 154–170. Springer, Cham (2016)

5. Bailer, C., Varanasi, K., Stricker, D.: CNN-based patch matching for optical flow with thresholded hinge embedding loss. In: 2017 IEEE Conference on Computer Vision and Pattern Recognition (CVPR), Honolulu, HI, USA, pp. 2710–2719 (2017)
6. Bazhanov, P., Kotina, E., Ovsyannikov, D., Ploskikh, V.: Optimization algorithm of the velocity field determining in image processing. Cybern. Phys. **7**, 174–181 (2018)
7. Gadot, D., Wolf, L.: PatchBatch: A Batch Augmented Loss for Optical Flow. In: 2016 IEEE Conference on Computer Vision and Pattern Recognition (CVPR), pp. 4236–4245. Las Vegas, NV, USA (2016)
8. Xu, L., Jia, J., Matsushita, Y.: Motion detail preserving optical flow estimation. In: 2010 IEEE Computer Society Conference on Computer Vision and Pattern Recognition, San Francisco, CA, USA, pp. 1293–1300 (2010)
9. Mirabdollah, M.H., Mertsching, B.: On the second order statistics of essential matrix elements. In: Jiang, X., Hornegger, J., Koch, R. (eds.) Pattern Recognition. GCPR 2014. Lecture Notes in Computer Science, vol. 8753, pp. 547–557. Springer, Cham (2014)
10. Horn, B.K.P., Schunck, B.G.: Determining optical flow. Artif. Intell. **17**, 185–203 (1981)
11. Lucas, B.D., Kanade, T.: An iterative image registration technique with an application to stereo vision. In: Proceedings of Imaging Understanding Workshop, Washington, DC, USA, pp. 121–130 (1981)
12. Farnebäck, G.: Two-frame motion estimation based on polynomial expansion. In: Bigun, J., Gustavsson, T. (eds.) Image Analysis. SCIA 2003. Lecture Notes in Computer Science, vol. 2749, pp. 363–370. Springer, Heidelberg (2003)
13. Kühne, J., Magno, M., Benini, L.: Low latency visual inertial odometry with on-sensor accelerated optical flow for resource-constrained UAVs. IEEE Sensors J. (Early Access), 1–10 (2024)
14. Lele, A.S., Raychowdhury, A.: Fusing frame and event vision for high-speed optical flow for edge application. In: 2022 IEEE International Symposium on Circuits and Systems (ISCAS), Austin, TX, USA, pp. 804–808 (2022)
15. Baker, S., Scharstein, D., Lewis, J.P., Roth, S., Black, M.J., Szeliski, R.: A database and evaluation methodology for optical flow. Int. J. Comput. Vis. **92**, 1–31 (2011)
16. Ponomarev, E.S., Grigoriev, A.S.: Algorithms for calculating optical flow in the problem of determining proper motion. In: 39th Interdisciplinary School-Conference of the IITP RAS "Informacionnye tehnologii i sistemy 2015", pp. 457–470. IITP, Sochi (2015). (In Russ.)
17. Ye, C., Mitrokhin, A., Fermüller, C., Yorke, J.A., Aloimonos, Y.: Unsupervised learning of dense optical flow, depth and egomotion with event-based sensors. In: 2020 IEEE/RSJ International Conference on Intelligent Robots and Systems (IROS), Las Vegas, NV, USA, pp. 5831–5838 (2020)
18. Zeng, Q., Ou, B., Lv, C., Scherer, S., Kan, Y.: Monocular visual odometry using template matching and IMU. IEEE Sens. J. **21**(15), 17207–17218 (2021)
19. Merzlyakov, A., Macenski, S.: A comparison of modern general-purpose visual SLAM approaches. In: 2021 IEEE/RSJ International Conference on Intelligent Robots and Systems (IROS), Prague, Czech Republic, pp. 9190–9197 (2021)
20. Pu, H., Luo, J., Wang, G., Huang, T., Liu, H., Luo, J.: Visual SLAM integration with semantic segmentation and deep learning: a review. IEEE Sens. J. **23**(19), 22119–22138 (2023)
21. Kühne, J., Magno, M., Benini, L.: A fast and accurate optical flow camera for resource-constrained edge applications. In: 9th International Workshop on Advances in Sensors and Interfaces (IWASI), Monopoli (Bari), Italy, pp. 143–148 (2023)
22. Al-asadi, T.A., Obaid, A.J.: Object detection and recognition by using enhanced speeded up robust feature. Int. J. Comput. Sci. Netw. Secur. **16**(4), 66–71 (2016)

# Exponential Degradation Model Based Remaining Life Prediction for Tools of Milling Machine

Murshedul Arifeen[1(✉)], Andrei Petrovski[1], Md. Junayed Hasan[2], and Zeeshan Ahmad[1]

[1] National Subsea Centre, Robert Gordon University, Aberdeen AB21 0BH, Scotland, UK
{d.arifeen,a.petrovski,z.ahmad1}@rgu.ac.uk
[2] School of Social and Environmental Sustainability, University of Glasgow, Dumfries DG1 4ZL, Scotland, UK
j.hasan@rgu.ac.uk

**Abstract.** Cutting tools of milling machines are prone to failure, and it's essential to predict their remaining useful life to ensure cost-effective maintenance in the manufacturing industry. Recent studies have shown that deep learning techniques can effectively predict the remaining useful life. However, training a deep learning model on a small dataset can be challenging. Moreover, generating a sufficient training dataset that includes failure samples is even more complex. Therefore, this paper proposes an exponential degradation-based technique for predicting the remaining life of cutting tools due to a small dataset. The proposed method has five main steps: data processing, feature extraction, feature selection, and feature fusion to construct health indicators. Finally, using these health indicators, an exponential degradation model can estimate the remaining life. A case study of the proposed approach is demonstrated on a recently published cutting tools dataset. The experimental results show that the exponential model does not require large-size data to predict remaining life.

**Keywords:** Predictive Maintenance · Exponential Degradation Model · Remaining Useful Life (RUL) · Deep Learning Techniques

## 1 Introduction

The cutting tool is vital in manufacturing as it directly interacts with the workpiece [14]. Cutting tools must withstand mechanical, thermal, and chemical wear during regular use [12]. Unfortunately, cutting tool flank tend to wear out over time due to continuous use in machining processes. Tool flank wear is the most critical type of wear in machining-flank wear results from friction between the workpiece surface and the flank of the tool. This wear and degradation can have a significant impact on the quality and accuracy of the final product [4][14]. To


S. Kovalev et al. (Eds.): IITI 2024, LNNS 1209, pp. 355–365, 2024.
https://doi.org/10.1007/978-3-031-77688-5_34

ensure the reliability of the manufacturing system and the quality of the workpiece, it is crucial to replace cutting tools on time before they fail. Predicting the tool's remaining useful life (RUL) is essential for making informed decisions about when to replace it. Doing so not only maximizes tool life but also helps to reduce machining costs and improve quality [13].

There are two methods for predicting the RUL of tools: degradation models and data-driven models [14]. The latter employs machine learning to identify the degradation process patterns and provide highly accurate predictions. However, data-driven models necessitate sizable, consistent data samples, which can prove challenging due to cost and variability. Model-based methods use mathematical or physical models to estimate machine degradation and predict cutting tools' RUL [14]. They incorporate expert knowledge and measured information, making them more effective than data-driven methods in the case of small-sized datasets [14] [2].

The exponential model is a widely used model-based method for predicting RUL and health management. Gebraeel, who employed a Bayesian approach to update the model parameters using collected data, can be credited to its inception [5]. Over time, various adaptations and implementations of this model have been documented, including a refinement by Gebraeel, which integrates multiple historical degradation signals obtained through condition monitoring to update the model parameters.

Zhang et al., [16] proposed a hybrid RUL model by combining the exponential model and particle filter for lithium-ion batteries. The model achieved better prediction accuracy and convergence. Li et al., [9] proposed an improved exponential model to predict the RUL of bearings by overcoming two shortcomings: first, predicting time selection and random errors of a stochastic process. Similarly, Wang et al. [15] solved the first predicting time by using Kurtosis and RMS of bearing signals and utilised the exponential model to predict RUL. Kong et al., [8] also introduced an exponential degradation model for bearing RULs. Bhavsar et al., [3] used exponential degradation model for FEMTO bearings problem by extracting statistical time domain features. However, Liu et al., [10] used an exponential degradation model with a Bayesian update mechanism and expectation-maximization for power plant machinery. Therefore, data-driven models overfit and need to improve in predicting RULs. As an alternative solution, the exponential degradation model is proven effective in predicting RUL on a small-scale dataset. Apart from these, various deep learning [11] [6] models are also utilized in the literature for RUL prediction.

This paper uses an exponential degradation model to predict the RUL of the milling machine's cutting tools. The dataset used in this paper is a small-scale dataset with several sensor data representing the degradation behaviour of cutting tools. To identify the degradation pattern, we conducted feature engineering, feature extraction, feature selection, feature smoothing, feature fusion, and health indicator construction. We extracted time-domain features from each sensor data set to determine failure trajectories and performed the Man-Kendall test to select optimal features by screening monotonicity values. The exponential

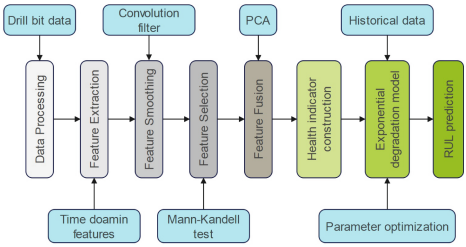


**Fig. 1.** Overview of RUL prediction model

degradation model is then fitted to the health indicators to define the parameters and predict RULs. Experimental outcomes show exponential models' effectiveness in predicting RULs on small datasets. In Sect. 2, we have discussed the steps in processing and feature engineering the dataset to establish a single health indicator for each tool. Section 3 briefly presents the description of the dataset, and Sect. 4 describes the experimental outcomes for predicting RULs. Finally, Sect. 5 concludes this paper.

**Table 1.** Time domain features and corresponding mathematical expressions

| Features | Expression | Features | Expression |
|---|---|---|---|
| Mean | $\mu = \frac{\sum_{n=1}^{N} x(t_n)}{N}$ | Standard deviation | $\sigma = \sqrt{\frac{\sum_{n=1}^{N}(x(t_n)-\mu)^2}{N-1}}$ |
| Variance | $\sigma^2 = \frac{\sum_{n=1}^{N}(x(t_n)-\mu)^2}{N-1}$ | Root mean square | $rms = \frac{\sum_{n=1}^{N}(x(t_n))^2}{N-1}$ |
| Maximum value | $Max(x(t_n))$ | Skewness | $\frac{\frac{1}{N}\sum_{n=1}^{N}(x(t_n)-\mu)^3}{\left(\sqrt{\frac{1}{N}\sum_{n=1}^{N}(x(t_n)-\mu)^2}\right)^3}$ |
| Kurtosis | $\frac{\frac{1}{N}\sum_{n=1}^{N}(x(t_n)-\mu)^4}{\left(\sqrt{\frac{1}{N}\sum_{n=1}^{N}(x(t_n)-\mu)^2}\right)^4}$ | Shape factor | $\frac{\sqrt{\frac{1}{N}\sum_{n=1}^{N}x(t_n)^2}}{\frac{1}{N}\sum_{n=1}^{N}\lvert x(t_n)\rvert}$ |
| Crest factor | $\frac{max\lvert x(t_n)\rvert}{\sqrt{\frac{1}{N}\sum_{n=1}^{N}x(t_n)^2}}$ | Margin factor | $\frac{max\lvert x(t_n)\rvert}{\left(\frac{1}{N}\sum_{n=1}^{N}\sqrt{\lvert x(t_n)\rvert}\right)^2}$ |

## 2 Methodology

A model based on exponential degradation can predict RUL with less data. It uses current historical data of equipment operation, making it suitable for drilling bits with limited failure samples. The process of RUL prediction is depicted in Fig. 1. In this section, we discussed about the RUL prediction steps for CNC machine's drilling bit.

### 2.1 Feature Extraction

The feature extraction step decomposes raw data into a feature space relevant to the system degradation condition. Features can be extracted from both the time and frequency domain. Time-domain features visually display a machine's state information by plotting the signal waveform against time, comprising both dimensional and dimensionless parameters. For cutting tool flank wear, various time-domain features can be extracted. We have extracted 10-time domain features in this work, as mentioned in Table 2 [7]. The mean and peak-to-peak values describe signal amplitude and energy over time, while the variance, skewness, and kurtosis factors serve as signal dispersion indicators.

### 2.2 Feature Selection

We used the monotonicity trend to select optimal features from extracted time domain features. A suitable condition indicator exhibits a monotonic trend as a system approaches failure. We used the Mann-Kendall test for monotonicity screening [1]. It determines consistent upward or downward monotonic trends in a variable over time, which may not be linear.The MK test assumes $H_0$ (null hypothesis) is true and requires convincing evidence to reject $H_0$ and accept $H_a$ (alternate hypothesis). $H_0$ states no monotonic trend, while $H_a$ says there is. The MK test wroks as follows:

1. Ordering the data samples sequentially over time $(x_1, x_2, ..., x_n; n = 1, 2, 3..)$
2. Calculate the sign of all $\frac{n(n-1)}{2}$ differences $x_i - x_j; i > j$.
3. Use $sgn(x_i - x_j)$ function to indicate the values 1, 0, −1 based on step 2, i.e.,

$$sgn(x_i - x_j) = \begin{cases} 1, & \text{if} x_i - x_j > 0. \\ 0, & \text{if} x_i - x_j = 0. \\ -1 & \text{if} x_i - x_j < 0 \end{cases}$$

4. Calculate the following expression:

$$S = \sum_{i-1}^{n-1} \sum_{j-i+1}^{n} sgn(x_i - x_k)$$

5. Calculate the variance of S using following expression:

$$VAR(S) = \frac{1}{18}[n(n-1)(2n+5) - \sum_{p-1}^{g} t_p(t_p-1)(2t_p+5)]$$

   where $g$ is the number of tied groups, $t_p$ is the number of observations in the $p$th group.
6. Calculate MK test statistic (decrease) with time.

$$Z_{MK} = \begin{cases} \frac{S-1}{VAR(S)} & if S > 0 \\ 0 & if S = 0 \\ \frac{S+1}{VAR(S)} & if S < 0 \end{cases}$$

We can choose the features based on the MK test z statistic where a positive (negative) value of $Z_{MK}$ indicates that the data tend to increase (decrease) time.

### 2.3 Feature Fusion and Health Indicator Construction

It isn't easy to use all the selected features from the MK test to predict the RUL of machines. Therefore, we must fuse the selected features to construct a single health indicator. Principal Component Analysis (PCA) as a dimensionality reduction technique can be a candidate for fusing the selected features. PCA uses orthogonal transformations to identify the correlated variables and convert them into uncorrelated ones. We can choose the principal component with the highest variance as the health indicator to represent the degradation behaviour of the drilling bit (Fig. 3).

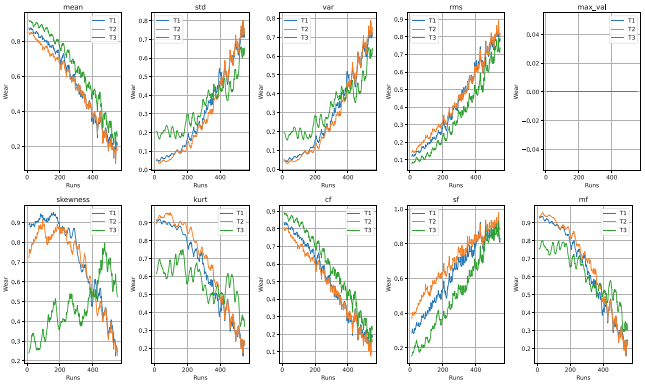


**Fig. 2.** Extracted time domain features from Tool1, Tool2 and Tool3 for the feature torque axis in y direction

### 2.4 Exponential Degradation Model

The exponential degradation model is a probabilistic model that is ideal for small scale dataset. Let H(t) denotes the health indicator fused from multiple features from previous step. It represent the continuous stochastic degradation process of the drilling bit. We can observe the degradation behaviour at some discrete points in time, such as $t1$, $t2$, $\cdot$ $tn$. Therefore, we can model the degradation health indicator at time $ti, I = 1, 2, ....$ as follows:

$$H(t_i) = \phi + \theta e^{(\beta t_i + \epsilon(t_i) - \frac{\sigma^2}{2})}$$
$$= \phi + \theta e^{\beta t_i} e^{(\epsilon(t_i) - \frac{\sigma^2}{2})}$$

where $\phi$ is a known constant, $\theta$ is log normal random variable, $\beta$ is a normal random variable and $\epsilon(t_i)$ is random error term with a normal distribution of mean 0 and variance $\sigma^2$. Assuming, $\theta$, $\beta$ and $\epsilon(t_i)$ are mutually independent,

we can show that $E[e^{\epsilon(t_i)-\frac{\sigma^2}{2}}] = 1$. Therefore, $E[H(t_i)|\theta,\beta] = \phi + \theta e^{(\beta t_i)}$. The logarithm of the exponential degradation model can be expressed as:

$$S_i{=}S(t_i){=}ln(H(t_i){-}\phi) = ln\theta + \beta t_i + \epsilon(t_i) - \frac{\sigma^2}{2}$$
$$= \theta^{'} + \beta t_i + \epsilon(t_i)$$

where $\theta^{'} = ln\theta - \frac{\sigma^2}{2}$. The posterior distribution of $\theta^{'}$ and $\beta$ is estimated using the bayesian process after logarithmic degradation features accumulated at a certain time are gathered. Lets consider that we observed $S_1, S_2, ...S_k$ at times $t_1, t_2, ..t_k$, then the conditional joint density function for estimating $\theta^{'}$ and $\beta$ can be expressed as,

$$f(S_1, S_2, ..S_k|\theta^{'}, \beta) = (\frac{1}{\sqrt{2\pi\sigma^2}})^k \times e^{-\sum_{i=1}^{k}(\frac{(L_i-\theta^{'}-\beta t_i)^2}{2\sigma^2})}$$

At each time step $t$ the distribution of $\theta^{'}$ and $\beta$ is updated based on the observations of $S_i$.

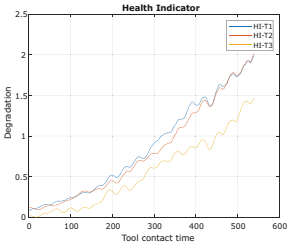


**Fig. 3.** PCA based health indicator

### 2.5 RUL Prediction

The Remaining Useful Life (RUL) of a cutting tool is the length of time from the current moment until the end of its useful lifespan. Mathematically, it is expressed as $l_k = t_{EoL} - t_k$, where $t_{EoL}$ represents the End Of Life (EOL), $t_k$ represents the current time, and $l_k$ represents the RUL at $t_k$. In this study, the RUL is defined as the time remaining before the HI of the machine crosses a failure threshold. The failure threshold can be determined based on domain knowledge. In this paper, the RUL is expressed as follows:

$$l_k = inf(l : H(l + t_k) \geq \lambda)$$

where $inf(.)$ represents the inferior limit of a variable; $H(l + t_k)$ is the HI at $l + t_k$ with $l \geq 0$ and $\lambda$ is the failure threshold.

**Table 2.** Monotonicity scores for the time domain features of MK test results

| Features | Tools | mean | std | var | rms | max | skew | kurt | sf | cf | mf | Avg |
|---|---|---|---|---|---|---|---|---|---|---|---|---|
| pcd_x | Tool1 | 9.79 | 22.11 | 22.35 | 22.11 | 22.87 | 11.88 | 16.16 | 11.25 | 16.89 | 18.05 | 17.35 |
| | Tool2 | 4.74 | 24.90 | 25.04 | 24.90 | 24.46 | 9.77 | 19.67 | 4.42 | 18.37 | 23.28 | 17.96 |
| | Tool3 | 7.56 | 26.28 | 26.58 | 26.29 | 25.38 | 8.00 | 10.37 | 13.03 | 2.80 | 24.95 | 17.12 |
| pcd_y | Tool1 | 6.52 | 20.01 | 20.01 | 19.96 | 0.00 | 21.00 | 20.81 | 6.32 | 19.96 | 20.02 | 15.46 |
| | Tool2 | 0.89 | 19.79 | 19.79 | 19.82 | 0.00 | 21.44 | 21.06 | 1.04 | 19.82 | 19.79 | 14.34 |
| | Tool3 | 7.38 | 14.13 | 14.13 | 14.24 | 0.00 | 17.14 | 16.23 | 7.24 | 14.24 | 14.13 | 11.89 |
| ta_x | Tool1 | 21.70 | 23.04 | 23.32 | 21.83 | 0.00 | 20.74 | 20.10 | 14.95 | 21.20 | 21.75 | 18.86 |
| | Tool2 | 23.19 | 24.69 | 25.01 | 23.35 | 0.00 | 22.01 | 20.57 | 15.12 | 22.29 | 23.10 | 19.93 |
| | Tool3 | 24.15 | 26.49 | 26.92 | 24.43 | 0.00 | 22.58 | 21.16 | 9.48 | 23.01 | 24.38 | 20.26 |
| ta_y | Tool1 | 25.86 | 26.28 | 26.34 | 25.88 | 0.00 | 23.45 | 26.21 | 23.68 | 25.55 | 26.04 | 22.93 |
| | Tool2 | 25.96 | 25.75 | 25.80 | 25.99 | 0.00 | 21.62 | 24.63 | 24.04 | 25.63 | 25.57 | 22.50 |
| | Tool3 | 27.44 | 24.88 | 24.89 | 27.41 | 0.00 | 16.15 | 20.09 | 25.92 | 27.08 | 24.84 | 21.87 |
| ta_z | Tool1 | 8.99 | 21.16 | 21.28 | 8.59 | 0.00 | 23.68 | 23.61 | 19.22 | 8.62 | 20.77 | 15.59 |
| | Tool2 | 16.40 | 21.88 | 22.00 | 16.24 | 0.00 | 19.59 | 19.24 | 21.99 | 16.25 | 21.42 | 17.50 |
| | Tool3 | 11.30 | 24.85 | 25.01 | 10.78 | 0.00 | 25.41 | 24.40 | 21.68 | 10.83 | 24.28 | 17.85 |
| tp_x | Tool1 | 0.07 | 0.04 | 0.39 | 0.06 | 0.07 | 0.49 | 0.38 | 0.44 | 6.45 | 1.17 | 0.96 |
| | Tool2 | 0.06 | 0.05 | 0.40 | 0.06 | 0.07 | 2.97 | 3.04 | 0.44 | 6.40 | 1.15 | 1.46 |
| | Tool3 | 0.01 | 0.01 | 0.30 | 0.01 | 0.02 | 4.07 | 4.07 | 0.19 | 6.84 | 0.85 | 1.64 |
| tp_y | Tool1 | 1.60 | 3.18 | 3.18 | 1.94 | 8.54 | 2.80 | 10.31 | 3.04 | 2.56 | 3.09 | 4.02 |
| | Tool2 | 5.51 | 13.23 | 13.23 | 3.46 | 16.40 | 0.76 | 11.50 | 13.26 | 3.11 | 12.57 | 9.30 |
| | Tool3 | 7.21 | 11.96 | 11.96 | 0.89 | 8.48 | 0.25 | 9.62 | 11.82 | 3.82 | 9.92 | 7.59 |
| tp_z | Tool1 | 7.00 | 8.78 | 8.78 | 6.99 | 0.00 | 8.56 | 8.48 | 7.28 | 7.00 | 8.76 | 7.16 |
| | Tool2 | 7.23 | 9.65 | 9.65 | 7.49 | 0.00 | 7.32 | 7.34 | 6.36 | 7.49 | 9.65 | 7.22 |
| | Tool3 | 8.74 | 9.45 | 9.46 | 8.80 | 0.00 | 9.98 | 9.96 | 8.29 | 8.80 | 9.45 | 8.29 |
| ts | Tool1 | 22.00 | 22.64 | 22.75 | 22.10 | 0.00 | 21.95 | 22.07 | 12.08 | 21.85 | 22.28 | 18.97 |
| | Tool2 | 24.37 | 23.82 | 23.97 | 24.35 | 0.00 | 22.22 | 22.65 | 23.02 | 23.91 | 23.27 | 21.16 |
| | Tool3 | 25.70 | 15.13 | 15.37 | 25.25 | 0.00 | 10.41 | 12.65 | 8.30 | 24.74 | 14.64 | 15.22 |

## 3 Dataset

The dataset comprises 6418 individual sample files in .h5 format (HDF5). These samples were taken from nine tools worn out from an unused state (VB = 0 $\mu$m) to their end of life (VB = 150 $\mu$m). The number of experimental runs (sample files) varies for each tool. Wear was quantified by the width of the flank wear or the uniform flank wear VB according to ISO 8688-2. VB was measured with a digital microscope from Keyence (model VHX600DSO, 1/1.8 CCD sensor, 1600 $\times$ 1200 pixels, 100x magnification). Additionally, the sample files themselves contain the corresponding labels (wear value). Each sample file represents a single

shoulder milling operation and includes the corresponding milling operation time series data. Two groups of time series data are recorded– machine tool controlling data and dynamo-meter data. Machine controlling data group contains position control deviation axis (x and y), tool position (x, y and z axis), torque spindle, and torque axis (x, y, and z) features. In contrast, the dynamo-meter data group contains force data on the x, y, and z-axes. In this paper, we considered the machine tool controlling data for exponential degradation model based RUL prediction problems.

## 4 Experiments and Results

The sample files for each milling operation of the dataset are in HDF5 format. Therefore, the HDF5 files first need to be converted into suitable workable files. We have used the Python h5py library to convert the HDF5 files to CSV files. In this work, we have only considered three tools (tool1, tool2, and tool3) from machine 1 to conduct this case study. Tool1 and tool2 contains 609 milling operation data files and Tool3 has 638 CSV files to represent its degradation trend. Each CSV file comprises of 2207 data samples.

The converted CSV files are unsuitable for training an exponential degradation model for RUL prediction. Features must be extracted from each CSV file to realize the degradation pattern and predict the remaining life. In this work, we extracted 10-time domain features (mentioned in Table 1) from a CSV file to learn the degradation behaviour of cutting tools. Figure 2 illustrates the extracted 10 time domain features from three tools of machine 1. From the figure, it is evident that some features (mean, kurtosis, cf, and mf) are monotonically decreasing while some (std, variance, rms, sf) are monotonically increasing. However, max_val is not showing any increasing or decreasing pattern. Therefore, the features with increasing or decreasing pattern shows the degradation patterns of the tools.

Not all the machine control deviation features equally represent the failure propagation of the machine tools. Therefore, the most significant feature needs to be selected. Also, the ten-time domain features from the most considerable machine control deviation feature are not equally important in predicting the RUL of the tools. Thus, based on the MK test, we have selected the most critical time domain features that reflect the degradation behaviour (either monotonically increasing or decreasing) of the tools and the most crucial feature of the machine control deviation feature is selected by averaging the monotonicity score of the time domain extracted features. Table 2 shows the monotonicity score for each time domain feature of all the machine control deviation features from tools 1, 2 and 3. We can see that the monotonicity score of max value is 0 for almost all the machine control deviation features, as this feature has no monotonic trend (Fig. 2). The average column shows that the feature $ta\_y$ has the highest monotonicity score for all the tools compared to other machine features. Therefore, we selected $ta\_y$ and the time domain features with monotonicity scores higher than 23 from $ta\_y$ to predict the RUL of the tools.

In the next phase of our study, we utilized PCA (Principal Component Analysis) to merge the selected features and create a singular health indicator representing our tools' failure propagation. We chose the first principal component as the health indicator, as it retains the maximum variance of the merged features. We used an exponential degradation model to fit the health indicator and forecast the tools' Remaining Useful Life (RUL). The RUL calculation begins once the degradation is detected. We match the time evolution of the HI trend using the exponential degradation model to predict the time before it reaches the threshold, indicating a failure. The parameters of this model are determined using the HI values. To do this, we used the health indicators of tools 1 and 2 as historical data to determine the exponential degradation model parameter and predict the RUL of tool 3. Similarly, we used the health indicators of tools 2 and 3 to find the model parameters and predict the RUL of tool 1. Finally, we used the health indicators of tools 1 and 3 to predict the RUL of tool 2. Table 3 shows the exponential degradation model parameters of two tools at a time to determine the model parameters and predict the RUL of the third tool.

The exponential model can identify significant slope compared to HI trend and estimate RUL based on original priors. Figure 4 shows that the proposed approach predicts new HI values after detecting the degradation threshold. Using the updated window of HI values, the model's parameters are calculated, and the slope of the model is updated to reflect the evolving changes in the HI. The process is repeated until the predicted value reaches the FT. The error between the predicted RUL and the ground truth is quantified using

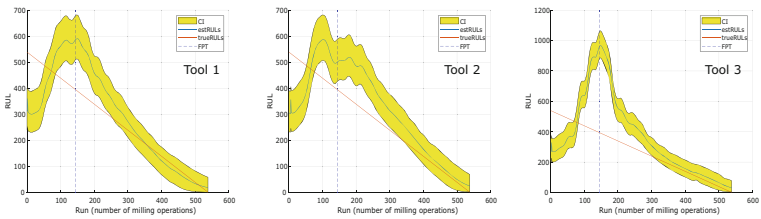


**Fig. 4.** Predicted RUL with confidence interval for tool1, 2 and 3

**Table 3.** Parameters for Exponential model of different tools

| Parameters | Tool 2 & 3 | Tool 1 & 3 | Tool 1 & 2 |
|---|---|---|---|
| Theta | 0.3037 | 0.4381 | 0.4757 |
| ThetaVariance | 0.0028 | 0.0592 | 0.0361 |
| Beta | 0.0036 | 0.0032 | 0.0032 |
| BetaVariance | 2.81E–09 | 3.52E–07 | 4.18E–07 |
| Rho | 1 | –1 | –1 |

RMSE score ($\sqrt{\frac{1}{n}\sum_{i=1}^{n} RUL_{gt} - RUL_{pr}}$). The RMSE for tool1, tool2, tool3 are 103.9395, 105.375, 216.4651 respectively.

## 5 Conclusion

In this work, we conducted a case study to predict the remaining life of milling machine drilling bits using an exponential degradation model. The exponential model is an alternate solution to deep learning-based models for RUL prediction in small-scale datasets. We extracted time-domain features from each drilling bit sensor data to identify the degradation pattern and used the MK test to select the most significant sensor. The monotonicity score of the MK test is also used to choose the time-domain extracted features from the selected sensor data. Finally, we used PCA to fuse the selected time-domain features to construct a single health indicator for training an exponential degradation model. Tools 1 and 2 are used to determine the parameters of the exponential model to predict the RUL of tool 3. Similarly, the health indicator is used to fit the degradation model to predict the RUL of Tool One and Tool Two. The experimental results show that the exponential model can capture the degradation trend and predict RULs for small-size datasets.

## References

1. Mann-Kendall Test For Monotonic Trend (2024). https://vsp.pnnl.gov/help/vsample/design_trend_mann_kendall.htm
2. Bejaoui, I., Bruneo, D., Xibilia, M.G.: A data-driven prognostics technique and rul prediction of rotating machines using an exponential degradation model. In: 2020 7th International Conference on Control, Decision and Information Technologies (CoDIT), vol. 1, pp. 703–708. IEEE (2020)
3. Bhavsar, K., Vakharia, V.: Prediction of remaining useful life (rul) of bearing using exponential degradation model. In: Recent Advancements in Mechanical Engineering: Select Proceedings of ICRAME 2021, pp. 439–447. Springer, Heidelberg (2022). https://doi.org/10.1007/978-981-19-3266-3_34
4. Denkena, B., Klemme, H., Stiehl, T.H.: Multivariate time series data of milling processes with varying tool wear and machine tools. Data Brief **50**, 109574 (2023)
5. Gebraeel, N.Z., Lawley, M.A., Li, R., Ryan, J.K.: Residual-life distributions from component degradation signals: a bayesian approach. IIE Trans. **37**(6), 543–557 (2005)
6. Habib, M.A., Hasan, M.J., Kim, J.M.: A lightweight deep learning-based approach for concrete crack characterization using acoustic emission signals. IEEE Access **9**, 104029–104050 (2021)
7. Hui, K.H., Ooi, C.S., Lim, M.H., Leong, M.S., Al-Obaidi, S.M.: An improved wrapper-based feature selection method for machinery fault diagnosis. PLoS ONE **12**(12), e0189143 (2017)
8. Kong, X., Yang, J.: Remaining useful life prediction of rolling bearings based on rms-mave and dynamic exponential regression model. IEEE Access **7**, 169705–169714 (2019)

9. Li, N., Lei, Y., Lin, J., Ding, S.X.: An improved exponential model for predicting remaining useful life of rolling element bearings. IEEE Trans. Ind. Electron. **62**(12), 7762–7773 (2015)
10. Liu, G., Fan, W., Li, F., Wang, G., You, D., et al.: Remaining useful life prediction of nuclear power machinery based on an exponential degradation model. Scie. Technol. Nucl. Install. **2022** (2022)
11. Podder, P., Alam, F.B., Mondal, M.R.H., Hasan, M.J., Rohan, A., Bharati, S.: Rethinking densely connected convolutional networks for diagnosing infectious diseases. Computers **12**(5), 95 (2023)
12. Rizzo, A., et al.: The critical raw materials in cutting tools for machining applications: a review. Materials **13**(6), 1377 (2020)
13. Shaban, Y., Yacout, S.: Predicting the remaining useful life of a cutting tool during turning titanium metal matrix composites. Proc. Inst. Mech. Engineers, Part B: J. Eng. Manuf. **232**(4), 681–689 (2018)
14. Sun, M., et al.: A novel exponential model for tool remaining useful life prediction. J. Manuf. Syst. **73**, 223–240 (2024)
15. Wang, G., Xiang, J.: Remain useful life prediction of rolling bearings based on exponential model optimized by gradient method. Measurement **176**, 109161 (2021)
16. Zhang, L., Mu, Z., Sun, C.: Remaining useful life prediction for lithium-ion batteries based on exponential model and particle filter. IEEE Access **6**, 17729–17740 (2018)

# Neural and Bayesian Networks

# Continuous Authentication with Eye Movement Biometrics

Sergei Davydenko(✉) and Evgeny Kostyuchenko

Tomsk State University of Control Systems and Radioelectronics, 634050 Tomsk, Russia
sergun_dav@mail.ru

**Abstract.** Most computer systems check user identity only at the initial login session. Continuous authentication uses data collected while using the system to check for user's identity for all session's length. This paper describes a method for authenticating user continuously using their eye movement biometrics. The new dataset was created based on data from laptop webcam, 40 features were extracted for each user. We used Siamese network to calculate the similarities of eye movement biometrics between 2 users for the task of continuous authentication. We achieved accuracy of 79.68% on video viewing task, 74.25% on slideshow task and 69.37% on reading task. Using a webcam as opposed to eye trackers allows to apply non-stop authentication without having any unique devices. Currently webcam-based eyetrackers are primarily used for behavioral analytics. However, existing Information Security studies only use this type of data for initial login (e.g., password or PIN input). Even though the achieved accuracy has some room for improvement, the suggested approach can be used as a secondary factor to help with protection against spoofing attacks.

**Keywords:** machine learning · neural networks · classification · eye movement biometrics

## 1 Introduction

User authentication is critical for computer systems. Currently, the most popular approaches to authentication are knowledge-based authentication (passwords) and possession-based authentication (e.g., smart cards). However, these factors can be easily stolen, lost, or forgotten [1]. To solve these problems, various approaches are used [2, 3], for example, biometrics [4]. Yet, the user is authenticated only at the initial login and is not authenticated again until they exit the system. To reduce the chances of an intruder performing any actions on the device, continuous authentication is used. Continuous authentication means that the user's identity is being checked during the entire work session and not only at the initial login. Eye movement biometrics is rarely used for continuous authentication. Meanwhile it is behavioral biometrics, which makes it not as discriminative as physical biometrics, but harder to be spoofed [5].


S. Kovalev et al. (Eds.): IITI 2024, LNNS 1209, pp. 369–377, 2024.
https://doi.org/10.1007/978-3-031-77688-5_35

## 2 Related Works

Continuous authentication can be divided into two types: based on behavioral biometrics and physical biometrics [6]. Eye movement biometrics is based on behavioral traits since it is not the appearance of the eye that is analyzed but the properties of its movement (e.g., speed, acceleration, etc.). Systems that use eye movement biometrics to check user's identity can be used both for daily computer work and for more sophisticated devices, such as virtual reality helmets [7–10].

In [11] Eberz S. et al. used an eye-tracking device called RED500 with a frequency of 500 Hz. 22 people (11 men and 11 women) participated in the experiment. During the data collection, the researchers obtained a timestamp, pupil coordinates and diameter. If the pupil diameter of at least one eye was not obtained, the measurement was removed. With support vector machines (SVM) the authors were able to obtain an EER ranging from 1.88% to 7.57%.

In [12] Eberz S. et al. used the device SMI RED500 with a frequency of 500 Hz. 10 people (6 men and 4 women) took part in the experiment. With SVM, the authors were able to achieve an EER of 1–10%. The quality of classification depended on the frequency of the eye tracking device; the best results were obtained at 500 Hz, while results with frequencies of 250, 100, and 50 Hz were worse.

In [13] Sluganovic I. et al. used the SMI RED 500 eye-tracking device. 30 people (23 men and 7 women) participated in the experiment. The authors were able to achieve an EER of 6.3% with SVMs with the Radial Basis Function kernel.

In [14] Kinnunen T. et al. used an eye tracking device Tobii X120, with a frequency of 120 Hz. 17 people participated in the experiment. A universal background model (UBM) was used for the classification, with an EER ranging from 28.7% to 47.1%.

In order to perform authentication, it is necessary to create a model of user behavior when working on daily tasks. Since in this paper the eye movement biometrics is used, the task must cause the person to look at different points on the screen. This requirement comes from the fact that the human eye is not focused on one point when interacting with the computer.

Concentrating one's gaze on a colored point on a monotonous background, for instance, a red point on a white background, and then shifting that point's position is an example of such task [11, 13, 15–19].

Another popular task is text reading [11, 12, 15, 19–21]. When working on a computer, users often read various documents, and continuous authentication can potentially reduce the likelihood of unauthorized access to classified data. The more complicated variant of this task would be a web-browsing simulation [11, 12, 21, 22].

Another category of tasks is photo and video viewing [20, 21]. When choosing images, the brightness of the pictures should be taken into account, as it directly affects the width of the pupil (at dim light, the pupils expand, and at bright light, they narrow). Sometimes monochrome images are used in studies to avoid the influence of colors on user behavior when collecting data. To complicate the task, in addition to a slideshow, the task of viewing a picture and subsequently performing an action can be used. For example, answering to the question (whether the molecules in the picture match [23], do you know this person [24], etc.).

When choosing a video, these parameters should also be taken into account, but a wide range of video clips, from movie trailers and documentaries [12, 14, 19] to driving records from the driver's perspective [25], are generally suitable. Since the video can have subtitles, it is also possible to add a text-reading task to the video viewing task.

It is proved that eye movement biometrics may be successfully used for continuous authentication. In most of the discussed work eye tracking devices are used. In this research paper the usage of webcam instead of eye tracker is proposed. The data obtained with web-cam may be not as precise [26] because some eye movement characteristics can't be collected without eye trackers. This will result worse accuracy but it doesn't require any special devices. This makes the proposed technology more accessible for general consumer.

## 3 Material and Methods

### 3.1 Data Collection

Eye trackers can be divided into multiple categories based on the data collection tool used, such as infrared or cameras, as well as the method used to retrieve the view data, which can be either remote or head-mounted [27]. Examples of the use of devices embedded in glasses are described in [18, 28].

However, the requirement to have such a device significantly limits the availability of continuous authentication. In this regard, there are some tools that help to obtain data about the user's gaze with a webcam.

GazePointer [29] is a program that allows users to control the cursor with their gaze. Figure 1 shows how the GazePointer works. The data was collected as follows: with GazePointer the data about user's approximate gaze point is obtained, then the cursor control is turned on, then the data about cursor position and timestamp is collected in selected CSV file. Users were asked to refrain from using the mouse in order to obtain trustworthy data, as doing so will contaminate the output. Only GazePointer will control the cursor. An independent program for data collection written in the C# programming language was created.

When the data collection starts, the column headers are added to the selected file: the user's ID, date and time, X, Y, and Unix time. Following the start of the timer, the recording is done at the assigned interval of 16 ms as follows. Data about the location of the cursor is obtained by Windows' Cursor.Position() function, date and time are obtained using the DateTime.Now.ToString() function, Unix time is obtained with ToUnixTimeMilliseconds() function.

The experiment required the participation of at least six people in order for the dataset to be sufficiently complete: three men with green, brown, and blue eyes and three women with green, brown, and blue eyes. Ultimately, four males and five females participated in the study.

In order to collect data, participants who wore glasses or contact lenses had to take them off. Due to interference from flashes and other sources, these instruments may make it more difficult to accurately determine gaze direction. Each participant who wore contacts or glasses on a daily basis attested to their ability to perform tasks without

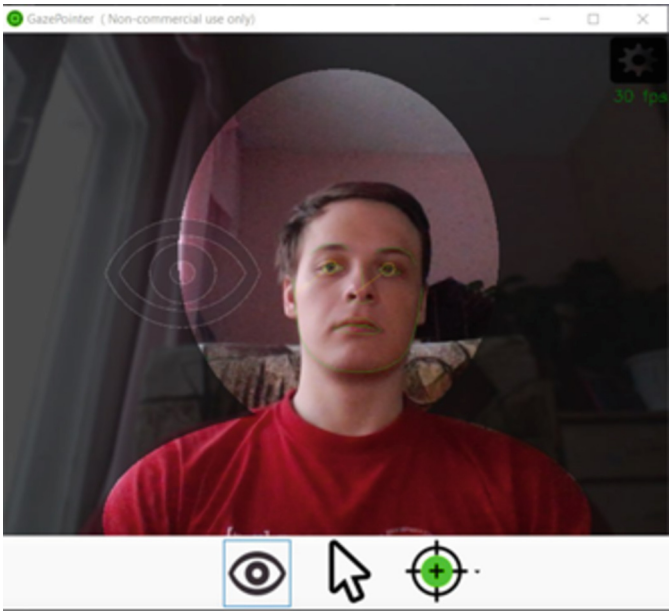


**Fig. 1.** GazePointer work process

difficulty when not wearing them. The user's image was captured using a built-in HP Wide Vision Camera with a resolution of 1 MP (720p) with 30 frames per second framerate.

As a result, after calibrating the GazePointer on the user, they were asked to perform three tasks: reading an excerpt from Lewis Carroll's poem "The Hunting of the Snark" (translated to Russian by Denis V. Gerdev) for one and a half minutes; watching the slideshow for one minute and 35 s with photo switching every 5 s (the examples of photos from slideshow are presented in Fig. 2); and watching a video on Vsause's YouTube channel for 7 min and 13 s (video resolution: 720p; it also included Russian subtitles).

The obtained data was preprocessed – some records where X and Y coordinates are the same with the previous record but are different from the next record were deleted. These records were created due to difference in the camera framerate and cursor collection data rate. This method allows us to retain data where user didn't move cursor, but delete fake records. These fake records created parts without movement, while in reality the user did change their gaze point on screen, so the data preprocessing is a necessary step before starting feature extraction.

### 3.2 Feature Extraction

Feature extraction is the process of highlighting the distinctive behavioral traits that users possess when carrying out a certain task. Since the data was collected with a cursor, it makes sense to consider the characteristics used to classify users with similar input data:

**Fig. 2.** Slideshow photos examples

a timestamp and X and Y coordinates. These include physical characteristics that can be calculated using distance and time (e.g., velocity, acceleration, jerk).

In the study [30], Fierrez-Aguilar et al. classified users by signature. Some of the features from their work could be applied to this study, as moving the pen around the graphic tablet also gathers timestamp and coordinates.

The features related to working with the graphic tablet rather than to the movement of the point in the plane (the total length of the signature, the number of pen-up events, etc.) were removed.

In Table 1, the final feature list is presented, the fh feature was calculated with the same method as any other direction change histogram, other features numbers match with [30].

Feature 36 uses the acquisition range parameter. Through experiments, it was found that the working area varies from coordinates (0;0) to (1535;863), so these numbers were used for calculations.

It should be noted that in certain cases, you might need to divide by zero in order to use the formula to get the values of certain features (like features 14, 20, 21, 23, 26, 29, and 45). This issue primarily relates to features 14, 20, 21, and 23, as events when there was no movement on one of the coordinates happen far more frequently than events when there was no movement at all on both coordinates. Since the features must be expressed numerically, it was decided to replace 0 (in case of attempted division by it) with a very small number. This method allows to obtain results that reflect the distinctive flashes of values and at the same time get rid of infinities.

**Table 1.** Selected features list

| f. | Feature Description | f. | Feature Description |
|---|---|---|---|
| 3 | Number of changes in the velocity direction of x and y axes | 45 | $a_{\text{rms}}/a_{\text{max}}$ |
| 4 | Average jerk, $\bar{j}$ | 51 | direction histogram $s_2$ |
| 5 | standard deviation of $a_y$ | 56 | direction histogram $s_5$ |
| 6 | standard deviation of $v_y$ | 57 | direction histogram $s_3$ |
| 8 | Number of local maxima in x | 58 | $T(v_x < 0)/T_w$ |
| 9 | standard deviation of $a_x$ | 59 | $T(v_y > 0)/T_w$ |
| 10 | standard deviation of $v_x$ | 60 | $T(v_y < 0)/T_w$ |
| 11 | $j_{\text{rms}}$ | 61 | direction histogram $s_8$ |
| 12 | Number of local maxima in y | 63 | direction histogram $s_6$ |
| 14 | $\bar{v}/v_x$, max | 66 | direction histogram $s_4$ |
| 20 | $(T_w\bar{v})/(y_{\text{max}} - y_{\text{min}})$ | 73 | direction histogram $s_7$ |
| 21 | $(T_w\bar{v})/(x_{\text{max}} - x_{\text{min}})$ | 76 | $j_x$, max |
| 23 | $\bar{v}/v_y$, max | 80 | $\bar{j}_x$ |
| 26 | $\bar{v}/v_{\text{max}}$ | 83 | $j_y$, max |
| 29 | $v_{rms}/v_{\text{max}}$ | 85 | $j_{max}$ |
| 33 | The number of times the speed on X axis equaled zero | 93 | direction change histogram $c_2$ |
| 34 | direction histogram $s_1$ | 95 | direction change histogram $c_4$ |
| 36 | $(x_{\text{max}} - x_{\text{min}})/x_{\text{aquisition range}}$ | 96 | $\bar{j}_y$ |
| 40 | $T(v_x > 0)/T_w$ | 97 | direction change histogram $c_3$ |
| 44 | The number of times the speed on Y axis equaled zero | fh | direction change histogram $c_1$ |

## 4 Results

The Siamese networks were trained to calculate similarities between 2 users data samples. For every sample the time windows with sizes of 1 s and 5 s were used. The gap for 1 s was 1 s, for 5 s the gap of 5 s and 2 s were used. The experiments were conducted for every task, resulting in 9 datasets for training and testing. For dataset creation the pairs of same user windows and different users windows were collected, 10000 samples each.

Every subnetwork had 2 layers, 40 neurons in each. This structure allowed to transform feature vectors for comparison by Siamese network. For an activation function ReLU was used, the distance was calculated with Euclidian distance. Automatic learning rate changing and the early stopping on plateau functions were used as well. The train and test data were splitted with 3:1 ratio.

The comparison of results is presented in table 2.

**Table 2.** Comparison results

| Task | Window size, seconds | Gap size, seconds | Accuracy |
|---|---|---|---|
| Reading | 1 | 1 | 0.68777 |
| Reading | 5 | 5 | 0.69369 |
| Reading | 5 | 2 | 0.69319 |
| Slideshow | 1 | 1 | 0.67782 |
| Slideshow | 5 | 5 | 0.69076 |
| Slideshow | 5 | 2 | 0.74251 |
| Video | 1 | 1 | 0.69050 |
| Video | 5 | 5 | 0.69127 |
| Video | 5 | 2 | 0.79681 |

These results show that the quality and size of input data matter a lot. With video viewing task (the length of which was almost 5 times longer than other tasks) the accuracy most of the time is higher (with the same widow and gap sizes). Also, the wider window and thinner gap cause better accuracy, this is proved with every task considered in this paper.

## 5 Conclusion

In this paper we used Siamese network to calculate the similarities of eye movement biometrics between 2 users for the task of continuous authentication. We achieved accuracy of 79.68% on video viewing task, 74.25% on slideshow task and 69.37% on reading task. While these results are not as good as some from related works, all data collection was conducted with web-camera instead of eye trackers, which makes the proposed system more accessible for general consumer.

In the future the results of this study may be improved by adding more users to the dataset and making the data collection time for each task longer. It's planned to add users that wear glasses and contact lenses to make the technology more applicable in real world. Also, the eye movement biometrics can be combined with some other behavioral and physical biometrics (e.g., face or mouse dynamics), which can make the system more robust. It's planned to add users that wear glasses and contact lenses to make the technology more applicable in real world.

**Acknowledgments. .** This study was funded by the Ministry of Science and Higher Education of Russia, Government Order for 2023–2025, project no. FEWM-2023–0015 (TUSUR).

**Disclosure of Interests.** The authors have no competing interests to declare that are relevant to the content of this article.

## References


1. Jain, A.K., Ross, A., Pankanti, S.: Biometrics: a tool for information security. IEEE Trans. Inf. Forensics Secur. **1**(2), 125–143 (2006)
2. Loparev, S.A., Shelupanov, A.A.: Analiz instrumental'nyh sredstv ocenki riskov utechki informacii v komp'juter-noj seti predprijatija (Analysis of tools for assessing the risk of information leakage in an enterprise computer network). Inf. Secur. Quest. **4**, 2–5 (2003)
3. Koryshev, N., Hodashinsky, I., Shelupanov, A.: Building a fuzzy classifier based on whale optimization algorithm to detect network intrusions. Symmetry **13**(7), 1211 (2021)
4. Jain, A.K., Ross, A., Prabhakar, S.: An introduction to biometric recognition. IEEE Trans. Circuits Syst. Video Technol. **14**(1), 4–20 (2004)
5. Dahia, G., Jesus, L., Pamplona Segundo, M.: Continuous authentication using biometrics: an advanced review. Wiley Interdisc. Rev. Data Mining Knowl. Disc. **10**(4), e1365 (2020)
6. Oak, R.: A literature survey on authentication using Behavioural biometric techniques. In: Intelligent Computing and Information and Communication: Proceedings of 2nd International Conference, ICICC 2017, pp. 173–181. Springer, Singapore (2018)
7. Olade, I., Fleming, C., Liang, H.N.: Biomove: biometric user identification from human kinesiological movements for virtual reality systems. Sensors **20**(10), 2944 (2020)
8. Zhu, H., Jin, W., Xiao, M., Murali, S., Li, M.: Blinkey: a two-factor user authentication method for virtual reality devices. Proc. ACM Interact. Mobile Wearable Ubiq. Technol. **4**(4), 1–29 (2020)
9. Lohr, D., Aziz, S., Friedman, L., Komogortsev, O.V.: GazeBaseVR, a large-scale, longitudinal, binocular eye-tracking dataset collected in virtual reality. Sci. Data **10**(1), 177 (2023)
10. Mustafa, T., Matovu, R., Serwadda, A., Muirhead, N.: Unsure how to authenticate on your vr headset? come on, use your head!. In: Proceedings of the Fourth ACM International Workshop on Security and Privacy Analytics, pp. 23–30 (2018)
11. Eberz, S., Lovisotto, G., Rasmussen, K.B., Lenders, V., Martinovic, I.: 28 blinks later: Tackling practical challenges of eye movement biometrics. In: Proceedings of the 2019 ACM SIGSAC Conference on Computer and Communications Security, pp. 1187–1199 (2019)
12. Eberz, S., Rasmussen, K.B., Lenders, V., Martinovic, I.: Looks like eve: exposing insider threats using eye movement biometrics. ACM Trans. Priv. Secur. (TOPS) **19**(1), 1–31 (2016)
13. Sluganovic, I., Roeschlin, M., Rasmussen, K.B., Martinovic, I.: Using reflexive eye movements for fast challenge-response authentication. In: Proceedings of the 2016 ACM SIGSAC Conference on Computer and Communications Security, pp. 1056–1067 (2016)
14. Kinnunen, T., Sedlak, F., Bednarik, R.: Towards task-independent person authentication using eye movement signals. In: Proceedings of the 2010 Symposium on Eye-Tracking Research & Applications, pp. 187–190 (2010)
15. George, A., Routray, A.: A score level fusion method for eye movement biometrics. Pattern Recogn. Lett. **82**, 207–215 (2016)
16. Rose, J., Liu, Y., Awad, A.: Biometric authentication using mouse and eye movement data. In: 2017 IEEE Security and Privacy Workshops (SPW), pp. 47–55. IEEE (2017)
17. Liu, Y., Jiang, Y., Devenere, J.: Using deep learning for fusion of eye and mouse movement based user authentication. In: 2020 IEEE International Joint Conference on Biometrics (IJCB), pp. 1–10. IEEE (2020)
18. Zhang, Y., Hu, W., Xu, W., Chou, C.T., Hu, J.: Continuous authentication using eye movement response of implicit visual stimuli. Proc. ACM Interact. Mobile Wearable Ubiq. Technol. **1**(4), 1–22 (2018)
19. Griffith, H., Lohr, D., Abdulin, E., Komogortsev, O.: GazeBase, a large-scale, multi-stimulus, longitudinal eye movement dataset. Sci. Data **8**(1), 184 (2021)

20. Lohr, D., Komogortsev, O.V.: Eye Know you too: a densenet architecture for end-to-end eye movement biometrics. arXiv preprint arXiv:2201.02110 (2022)
21. Eberz, S., Rasmussen, K.B., Lenders, V., Martinovic, I.: Evaluating behavioral biometrics for continuous authentication: challenges and metrics. In: Proceedings of the 2017 ACM on Asia Conference on Computer and Communications Security, pp. 386–399 (2017)
22. Mihajlov, M., Jerman-Blazic, B.: Eye tracking graphical passwords. In: Advances in Human Factors in Cybersecurity: Proceedings of the AHFE 2017 International Conference on Human Factors in Cybersecurity, The Westin Bonaventure Hotel, Los Angeles, California, USA, 17−21 July 2017, vol 8, pp. 37–44. Springer, Heidelberg (2018)
23. Jia, S., et al.: Biometric recognition through eye movements using a recurrent neural network. In: 2018 IEEE International Conference on Big Knowledge (ICBK), pp. 57–64. IEEE (2018)
24. Mukhopadhyay, S., Nandi, S.: LPiTrack: Eye movement pattern recognition algorithm and application to biometric identification. Mach. Learn. **107**, 313–331 (2018)
25. Seha, S.N.A., Hatzinakos, D., Zandi, A.S., Comeau, F.J.: Improving eye movement biometrics in low frame rate eye-tracking devices using periocular and eye blinking features. Image Vis. Comput. **108**, 104124 (2021)
26. Ivanko, D., et al.: Multimodal speech recognition: increasing accuracy using high speed video data. J. Multimodal User Interfaces **12**, 319–328 (2018)
27. Morimoto, C.H., Mimica, M.R.: Eye gaze tracking techniques for interactive applications. Comput. Vis. Image Underst. **98**(1), 4–24 (2005)
28. Liao, H., Zhao, W., Zhang, C., Dong, W.: Exploring eye movement biometrics in real-world activities: a case study of wayfinding. Sensors **22**(8), 2949 (2022)
29. Ghani, M.U., Chaudhry, S., Sohail, M., Geelani, M.N.: GazePointer: a real time mouse pointer control implementation based on eye gaze tracking. In: INMIC, pp. 154–159. IEEE (2013)
30. Fierrez-Aguilar, J., Nanni, L., Lopez-Penalba, J., Ortega-Garcia, J., Maltoni, D.: An on-line signature verification system based on fusion of local and global information. In: Audio-and Video-Based Biometric Person Authentication: 5th International Conference, AVBPA 2005, Hilton Rye Town, NY, USA, 20–22 July 2005. Proceedings, vol. 5, pp. 523–532. Springer, (2005)

# FedPCGA: A Federated Unlearning Method Based on Projected Conflict Gradient Ascent

Ying Liu and Jialiang Peng(✉)

School of Data Science and Technology, Heilongjiang University, Harbin, China
liuying@s.hlju.edu.cn, jialiangpeng@hlju.edu.cn

**Abstract.** As data becomes increasingly valuable, the importance of data privacy also grows. Governments and legislators worldwide have established regulations to safeguard users' "Right to Be Forgotten", which allows users to request the deletion of their data from training datasets. However, merely deleting the data is insufficient, as models may retain implicit information or knowledge about the users' data acquired during training. Therefore, it is crucial to enable models to specifically forget targeted data information. In Federated Learning, where multiple participants and incremental training are involved, existing centralized machine unlearning methods are not directly applicable. In this paper, we propose a federated unlearning method based on projected conflict gradient ascent that removes the impact of class data from the trained global model. Since the unlearning process conflicts with the gradient of the original training task, we project the conflicting unlearning gradient onto the gradient of the final training round in the target client model, thereby avoiding interference with model performance. Additionally, post-processing approach are proposed to mitigate catastrophic forgetting while maintaining overall model performance. The experimental results demonstrate that our method obtains a performance comparable to federated retraining from scratch in accomplishing the unlearning task, with significantly reduced execution time.

**Keywords:** Data Privacy · Federated Learning · Federated Unlearning · Gradient Conflict · Gradient Ascent

## 1 Introduction

In contemporary machine learning applications, high-quality training data is crucial for the accuracy and effectiveness of models. However, due to intense competition and increasingly stringent privacy and security concerns in most industries, data is often stored in a distributed manner. Therefore, federated learning (FL), an emerging and promising distributed machine learning framework. It allows multiple devices to jointly train models without directly accessing sensitive raw data, thus effectively reducing the risk of user privacy leakage.


S. Kovalev et al. (Eds.): IITI 2024, LNNS 1209, pp. 378–388, 2024.
https://doi.org/10.1007/978-3-031-77688-5_36

In FL, data distributions often change over time and usage scenarios. To ensure that the model can effectively adapt to new data distributions and environmental conditions, specific classes of data may need to be eliminated from the trained model. Furthermore, under legal frameworks such as the European Union's General Data Protection Regulation [10], users have the right to remove specific classes of data, making the implementation of class unlearning in federated learning an indispensable requirement. Effective unlearning methods can remove specific classes of data (called target classes) from a trained model without sacrificing model performance. This protects the privacy of user data [11] and ensures model performance in the face of changing data and legal requirements.

It is a complex task to remove specific classes of data from a trained fl model. Currently, the best unlearning method is to retrain the model using the remaining dataset, thus completely unlearning the contribution of target data. However, retrain can incur prohibitive storage and computation costs. Additionally, data deletion may significantly reduce model accuracy, a phenomenon known as catastrophic forgetting. Therefore, the key question is how to find an valid method to erase the effect of target data while maintaining the model's utility.

To address this problem, we propose an update algorithm based on gradient ascent, following the Projected Conflict Gradient method [14]. First, we perform reverse learning on the target data, aiming to effectively forget the effects of this data in the model. Next, we update the model parameters by projecting the gradient generated by the target client in the final round of training onto the gradient generated by gradient ascent. During this process, we add a regularization term to ensure that the knowledge of the remaining classes is maximally retained. After completing the unlearning operation, we further perform post-processing. By using the unlearned local model as initialization, the server and the remaining clients perform several rounds of federated learning to obtain an unlearned global model. The main contributions of this paper are as follows:

1. We propose a novel federated unlearning method called FedPCGA, based on the concept of Projected Conflict Gradient, which effectively forgets the effects of specified class data from the trained global model.
2. To effectively mitigate catastrophic forgetting, we introduce a regularization term in the projected gradient update process. This limits the excessive ascent of the projected gradient, avoiding drastic changes in model parameters and thus maintaining the overall performance of the model.
3. The server and the remaining clients need to perform at most two rounds of federated learning to obtain an unlearned global model. Our experiments prove that the unlearning method realizes performance comparable to the gold standard of retraining from scratch, while being highly efficient in terms of communication costs.

## 2 Related Work

Originally introduced by Cao et al. [3], the concept of machine unlearning aims to make the unlearned model no longer contain information about the data that

needs to be deleted. However, this method is only applicable to learning algorithms that can be translated into the form of summation. Bourtoule et al. [1] proposed a general SISA unlearning framework, the core idea of which is to train a sub-model for each slice. However, this approach is costly because it requires a large amount of storage space. Subsequently, there have been several studies exploring more efficient and practical approaches to machine unlearning, for example, $k$-means clustering [4], random forest [2], and variational Bayesian [9]. These machine forgetting methods are not directly applicable to federal forgetting. This is because the training process of FL is more complicated and random, making unlearning more challenging than traditional centralized training.

In a similar setting, Wang et al. [12] proposed a pruning-based class unlearning algorithm. This method calculates the TF-IDF scores of channels, allowing the federated learning model to selectively "forget" the contributions of specific classes. However, incorrect pruning choices can negatively impact model performance. Unlike these works, Liu et al. [7] and Wu et al. [13] proposed federated unlearning methods capable of unlearning the contribution of a client on the global federated learning model. However, both of these methods require the server to store client updates. Some studies [5,6,15] have similarly explored how to remove client contributions. Additionally, Liu et al. [8] proposed a Rapid Retraining method that significantly improves model update speed by utilizing a low-cost Hessian matrix approximation method, reducing computational resource consumption. Nonetheless, this method still requires a considerable time and frequent communication for retraining.

## 3 Preliminaries

### 3.1 Federated Learning

The typical architecture of FL, FedAvg, can be described as follows: there is a server and $K$ clients that jointly train a global model without disclosing their original private data. Each client $K$ holds a local training dataset $\mathcal{D}_k = \{x_i, y_i\}_{i=1}^{n_k}$, where $n_k$ is the number of samples in $D_k$. The server selects a proportion $m\,(m \leq K)$ of all clients to participate in the FL and distributes the initialized global model $w_0$ to these participating clients. Each client uses its local data to train the model and generate an optimized local model $w_t^k$. Finally, the server aggregates all uploaded local models through weighted averaging to update the global model $w_{t+1}$. Specifically, the update formula is: $w_{t+1} = \sum_{k \in K} \frac{n_k}{n} w_t^k$, where $w_t$ denotes the global model after the $t$-$th$ iteration, $w_t^k$ is the local model of client $k$, and $\frac{n_k}{n}$ is the proportion of each client's dataset size.

### 3.2 Class Unlearning

Let $U = \{u_1, \ldots, u_i\}$ be the classification space mapped from the data space, and the trained full global model $w^*$ is gotten through the learning algorithm

$\mathcal{A}$. To unlearn the $u_i$-$th$ class, we execute the unlearning algorithm $\mathcal{U}$, making its effect as if the data $\mathcal{D}_f$ for the $u_i$-$th$ class had never been seen. We measure the probability distribution of the unlearned model $\mathcal{U}\big(\mathcal{A}(\mathcal{D}), \mathcal{D}_f, w^*\big)$ to make it consistent with the probability distribution of the model $\mathcal{A}\big(\mathcal{D} \setminus \mathcal{D}_f\big)$ obtained by learning the remaining dataset:

$$\Phi[\mathcal{A}\big(\mathcal{D} \setminus \mathcal{D}_f\big)] = \Phi[\mathcal{U}\big(\mathcal{A}(\mathcal{D}), \mathcal{D}_f, w^*\big)] \tag{1}$$

where $\mathcal{D} \setminus \mathcal{D}_f$ defines the dataset without the target class $u_i$. $\Phi[\cdot]$ denotes the output probability distribution.

## 4 Method

### 4.1 Federated Unlearning Setup

In this paper, we mainly consider a scenario where most users need to forget category data from the model to protect user privacy. In the data setup for FL, the training dataset was equally divided among 100 clients, with just 10% of the clients participating in every round of training. The unlearning operation was demonstrated using 10 target clients and 1 target class as an example. The overall procedure is depicted in Fig. 1.

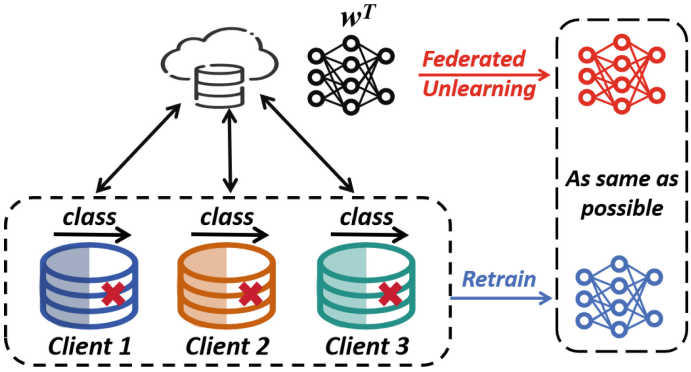


**Fig. 1.** Class-level unlearning in federated learning.

### 4.2 Projected Conflict Gradient Ascent

In this section, we propose a new federated unlearning framework, FedPCGA, to effectively address the issue of class-level unlearning in federated learning settings. First, our approach performs local unlearning operations on the clients containing the classes to be deleted, and then uploads these unlearned local models to the server. Next, several rounds of federated learning are performed by the server and the clients, thus preserving and enhancing the model's ability to classify other classes.

**Update Direction:** In the optimization process, due to the differing optimization objectives of the learning process and the forgetting process, the directions of the unlearning gradients and learning gradients may conflict. The learning gradient direction and the unlearning gradient direction might be opposite or negatively correlated, leading to gradient conflicts and subsequent model performance degradation. To address this issue, we adjust the gradient directions to mitigate such conflicts, thereby improving the fidelity of the unlearning process.

The specific steps are as follows: First, define the gradient generated by the target client during the final round of gradient updates as $g_i$. Then, perform stochastic gradient ascent on the target data at the target client to obtain the gradient $g_j$. Next, we calculate the cosine similarity to check for conflicts between $g_i$ and $g_j$. If the cosine similarity is negative, it indicates a gradient conflict. At this point, we use the projection gradient to update $g_j$, adjusting it according to the formula

$$g_j = g_j - \frac{g_j \cdot g_i}{\| g_i \|^2} g_i \tag{2}$$

This adjustment effectively decreases the negative impact of unlearning on model's performance, making the model to maintain classification accuracy for the remaining classes while unlearning the specified class.

**Update Restriction:** When the target client performs projected gradient ascent, excessive forgetting of previously learned information often occurs. This is particularly problematic in unlearning, as excessive forgetting can significantly degrade model performance on retained datasets. Therefore, in addition to adjusting conflicting gradients, we introduce a regularization term to control the distance between the unlearned model $w_u^i$ and the global model $w^t$, thereby reducing the risk of overfitting during the unlearning process. During each local training session, we test the target data. When the accuracy of the target data reaches 0, we early stop the projection gradient ascent process. By introducing the regularization term and early stopping mechanism, we ensure that the model can effectively forget specific categories without interfering with overall performance. This new loss

$$\mathcal{L}_u(w_u^i) = -\mathcal{L}_{ce}(w_u^i) + \frac{\lambda}{2}\Sigma_i \|w_u^i - w^t\|^2 \tag{3}$$

is named the unlearning loss, where $\lambda$ is the constraint strength and $\mathcal{L}_{ce}(\cdot)$ is the cross-entropy loss.

**Post Processing:** To improve the unlearned model's performance on the retained class data, the server and the clients train several rounds of federated learning on the retained class using the unlearned model $w_u^i$. Our experimental results show that the model $w_u^i$ requires at most two rounds of federated learning (far less time than training from scratch) to achieve the same accuracy as retrain.

We propose the FedPCGA algorithm, as illustrated in Algorithm 1. In Lines 1 to 9, the clients removes the contribution of the class data. Each client has a dataset $\mathcal{D}_f$ that it requests to forget and a global model. By executing projected conflict gradient ascent and applying early stopping, the clients obtain a local unlearning model that effectively forgets the specified class data. Lines 10 to 21 detail the post-processing phase, where clients and the server continue federated learning training. Specifically, in Lines 17 to 21, the clients trains on the retained class data, while in Lines 10 to 16, the server uses an aggregation rule to obtain the final unlearned model.

**Algorithm 1 : FedPCGA**

**Require:** local target dataset $\mathcal{D}_f$ of client $i$; unlearning rate $\eta_u$; learning rate $\eta$; batch size $\mathcal{B}$; number of unlearning epochs $E_u$; number of epochs $E$; number of communication rounds $T$; the gradient $g_i$; the trained global model $w^T$.

**Ensure:** the unlearned model $w_u^T$.

**Local Unlearning at Client $i$:**

1: Initialize unlearning model as $w \leftarrow w^T$
2: **for** each local $e = 1$ **to** $E_u$ epoch **do**
3: $\quad g_j \leftarrow \nabla \mathcal{L}_i(\mathrm{w}; \mathcal{D}_f)$ according to Eq. (3)
4: $\quad$ **if** $g_i \cdot g_i < 0$ **then**
5: $\quad\quad$ Set $g_j = g_j - \frac{g_j \cdot g_i}{\|g_i\|^2} g_i$
6: $\quad\quad$ $w \leftarrow w - \eta_u g_j$
7: $\quad\quad$ **if** $Acc(w; \mathcal{D}_f) = 0$ **then**
8: $\quad\quad\quad$ Set $w_i^u \leftarrow w$ and return $w_i^u$ to server
9: return $w_i^u$

**Post processing (Server executes):**

10: Initialize $w^0 \leftarrow w_i^u$
11: **for** $t = 0, ..., T-1$ **do**
12: $\quad$ Send $w^{t-1}$ to clients $i$;
13: $\quad$ **for** each client $i$ **in parallel do**
14: $\quad\quad$ $w_i^t \leftarrow \mathrm{LocalTraining}(i, w^{t-1})$
15: $\quad$ $\boldsymbol{w}^t \leftarrow \sum_i \frac{n_i}{\sum_i n} \boldsymbol{w}_i^t$
16: return $w_u^T$

LocalTraining$(i, w^{t-1})$:

17: $w \leftarrow w^{t-1}$
18: **for** each local epoch $e = 1$ **to** $E$ **do**
19: $\quad$ **for** batch $b$ **in** $\mathcal{B}$ **do**
20: $\quad\quad$ $w \leftarrow w - \eta \nabla \mathcal{L}_i(\boldsymbol{w}; b)$
21: return $w$

# 5 Experiments

## 5.1 Experimental Setup

**Datasets:** To evaluate our proposed method, we used the first class in each dataset as an example. The experiments are performed on three representative public datasets: MNIST, Fashion-MNIST, and CIFAR10.

MNIST: It is composed of 70,000 handwritten digital images in $28 \times 28$ gray scale, organized into 10 classes, 60,000 train images and 10,000 test images;

Fashion-MNIST: It contains 70,000 images, including 60,000 train images and 10,000 test images. $28 \times 28$ pixels per image, categorized into 10 classes;

CIFAR-10: It includes 50,000 train images and 10,000 test images, and each image is $32 \times 32$ in size and is categorized into 10 classes.

**Models:** We used two neural network architectures in our experiments:

CNN: This architecture has two $5 \times 5$ convolutional layers and fully connected layers with 1024, 384, and 192 neurons, respectively;

MLP: It is a fully connected neural network structure with one hidden layer, containing 64 neurons.

**Baselin:** We selected the retraining federated unlearning algorithm as our baseline. This method utilizes non-target data for retraining, which is an algorithm that precisely forgets the target data.

**Evaluation Metrics:** We first evaluated our unlearning method using three performance metrics: efficacy (measuring the impact of the data to be deleted), fidelity (measuring performance on the test dataset), and efficiency (measuring convergence and communication rounds compared to retraining from scratch). Secondly, we explicitly examined the unlearning effect through test cases. Finally, we conducted unlearning experiments and analysis on different numbers of classes.

## 5.2 Evaluation Results

**Efficient Unlearning.** Table 1 demonstrates the unlearning results of FedPCGA and the baseline Retrain on IID datasets and different model structures. $\mathcal{D}_f$ represents the data of the first class in the test dataset, used to verify if the model has forgotten that class. The results reveal that FedPCGA can effectively forget information about the target class. This can be illustrated by the fact that the classification accuracy of FedPCGA on the target dataset is close to 0%.

**Fidelity Evaluation.** We evaluate the fidelity of our unlearning method by calculating the accuracy of the unlearned model on the test dataset. It should be noted that the test dataset contains the target class, which leads to a decrease in model accuracy compared to the original accuracy, as the model is unable to recognize the target data. The accuracy on the test dataset indicates whether the unlearned model can maintain good performance on the retained data.

**Table 1.** Accuracy results after federated unlearning.

| Dataset | Models | FedAvg | | Retrain | | FedPCGA | |
|---|---|---|---|---|---|---|---|
| | | $\mathcal{D}_{test}$ | $\mathcal{D}_f$ | $\mathcal{D}_{test}$ | $\mathcal{D}_f$ | $\mathcal{D}_{test}$ | $\mathcal{D}_f$ |
| MNIST | CNN | 97.04 | 98.88 | **87.76** | 0.0 | **87.76** | 0.92 |
| | MLP | 91.35 | 97.76 | 81.40 | 0.0 | **82.61** | 0.0 |
| Fashion-MNIST | CNN | 77.21 | 81.40 | 72.02 | 0.0 | **72.52** | 0.0 |
| | MLP | 79.39 | 87.70 | **75.79** | 0.0 | 70.99 | 0.0 |
| CIFAR10 | CNN | 72.64 | 78.80 | 66.56 | 0.0 | **66.84** | 0.80 |
| | MLP | 47.45 | 53.60 | **43.74** | 0.0 | 43.32 | 0.40 |

In Table 1, we present the accuracy on the test dataset for our method and the Retrain method. We observe that FedPCGA achieves accuracy consistent with Retrain, demonstrating that our method achieves high fidelity in unlearning.

**Convergence Analysis.** To evaluate the efficiency of our method, we compared FedPCGA with Retrain on the MNIST, Fashion-MNIST, and CIFAR10 datasets. As shown in Fig. 2 and Fig. 3, the FedPCGA algorithm demonstrates faster and more stable convergence. Specifically, FedPCGA achieves high accuracy with fewer communication rounds, even surpassing the accuracy of retrain. In the first two rounds of communication, the accuracy of FedPCGA tends to stabilize and remains at a high level. However, the accuracy of the Retrain method continues to increase but has not yet reached the same level.

**Communication Rounds.** In Fig. 2 and Fig. 3, we observed that FedPCGA can maintain high accuracy even without any post-processing. In subsequent training, FedPCGA requires up to two rounds of training to achieve high-precision recovery, whereas the Retrain method requires five or more rounds of training to achieve a similar level of accuracy. This result indicates that FedPCGA can effectively forget the target class while also recovering model performance with minimal communication rounds.

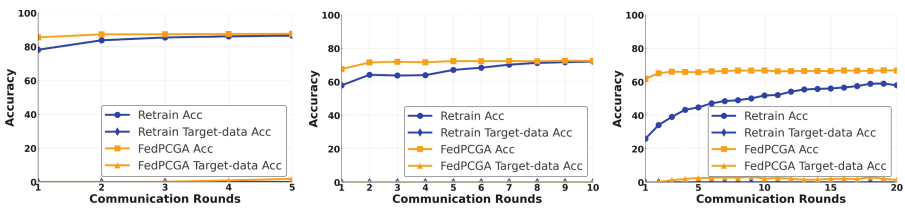


(a) MNIST (b) Fashion-MNIST (c) CIFAR10

**Fig. 2.** Convergence curves of FedPCGA and Retrain with CNN on different datasets, showing fidelity (ACC) and efficacy (Target-data ACC).

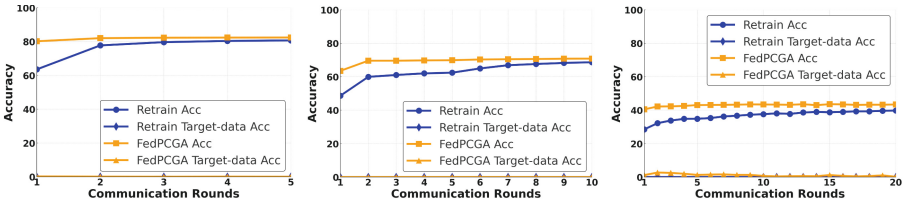


(a) MNIST (b) Fashion-MNIST (c) CIFAR10

**Fig. 3.** Convergence curves of FedPCGA and Retrain with MLP on different datasets, showing fidelity (ACC) and efficacy (Target-data ACC).

**Unlearning Test.** To visually observe the unlearning effect on class 0, we plotted histograms of the model's outputs, as shown in Fig. 4. In the figure, the output labels are marked with a star. The first column shows the original images, the second column shows the model's results before unlearning class 0, and the third column shows the results after unlearning. We randomly selected digits 0 and 3 from the MNIST dataset for testing. After the unlearning process, the model made errors in recognizing digit 0 while still correctly recognized digit 3. This result demonstrates that the model has successfully lost its ability to distinguish the target category.

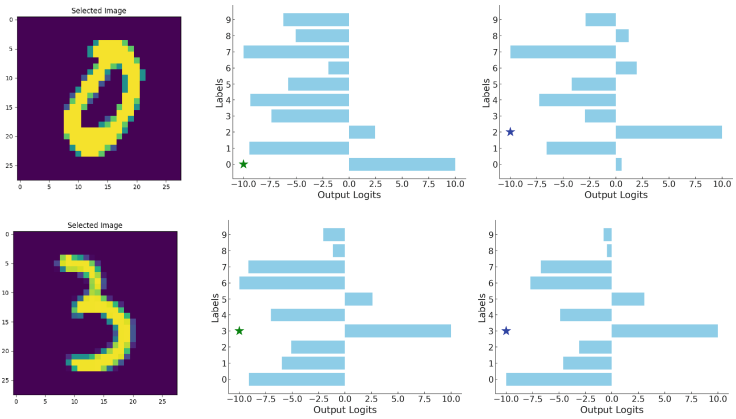


**Fig. 4.** Histograms of model outputs before and after unlearning class 0.

**Multi-class Removal.** We conducted unlearning experiments by selecting multiple classes from the dataset, attempting to forget 2, 3, and 5 classes. Figure 5 presents the accuracy results after unlearning multiple classes and compares them with the results of retrain. The left chart represents the CNN model, while

the right chart represents the MLP model. The data indicate that as the number of forgotten classes increases, the model's accuracy decreases. However, the FedPCGA unlearning method still maintains accuracy close to that of retrain. Our proposed method can simultaneously unlearn multiple classes rather than removing one class at a time, further demonstrating its effectiveness in class unlearning.

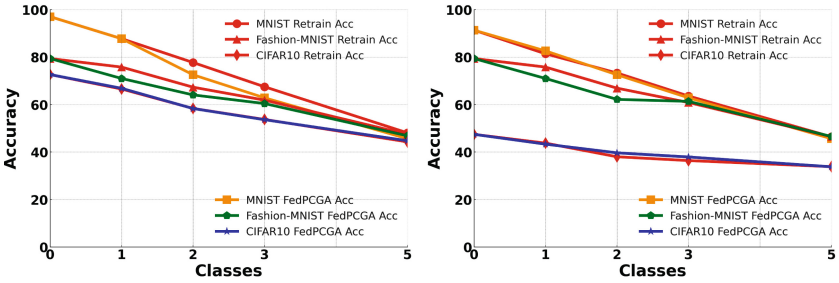


**Fig. 5.** Accuracy results after unlearning multiple classes.

## 6 Conclusion

In this paper, we propose a federated unlearning algorithm that successfully eliminates the impact of specific classes on the trained global model. Specifically, we customize an algorithm based on the gradient conflict between unlearning and learning, executing a projected conflict gradient ascent process on the target data to effectively remove the memory of this data from the model. To further enhance model utility, we incorporate regularization techniques and early stopping methods into the unlearning update strategy. These techniques help mitigate the negative effects of the unlearning process, ensuring that the model maintains high overall performance while unlearning a specific class. Additionally, our experiments demonstrate that FedPCGA not only effectively and efficiently achieves the unlearning of the target class but also avoids the high computational costs and time overhead associated with retraining.

**Acknowledgement.** This work is supported by the Fundamental Research Funds for Heilongjiang Universities, China (Grant No. 2023-KYYWF-1449).

## References

1. Bourtoule, L., et al.: Machine unlearning. In: 2021 IEEE Symposium on Security and Privacy (SP), pp. 141–159. IEEE (2021)
2. Brophy, J., Lowd, D.: Machine unlearning for random forests. In: International Conference on Machine Learning, pp. 1092–1104. PMLR (2021)

3. Cao, Y., Yang, J.: Towards making systems forget with machine unlearning. In: 2015 IEEE Symposium on Security and Privacy, pp. 463–480. IEEE (2015)
4. Ginart, A., Guan, M., Valiant, G., Zou, J.Y.: Making ai forget you: data deletion in machine learning. Adv. Neural Inf. Process. Syst. **32** (2019)
5. Halimi, A., Kadhe, S., Rawat, A., Baracaldo, N.: Federated unlearning: how to efficiently erase a client in fl? arXiv preprint arXiv:2207.05521 (2022)
6. Li, G., Shen, L., Sun, Y., Hu, Y., Hu, H., Tao, D.: Subspace based federated unlearning. arXiv preprint arXiv:2302.12448 (2023)
7. Liu, G., Ma, X., Yang, Y., Wang, C., Liu, J.: Federaser: enabling efficient client-level data removal from federated learning models. In: 2021 IEEE/ACM 29th International Symposium on Quality of Service (IWQOS), pp. 1–10. IEEE (2021)
8. Liu, Y., Xu, L., Yuan, X., Wang, C., Li, B.: The right to be forgotten in federated learning: an efficient realization with rapid retraining. In: IEEE INFOCOM 2022-IEEE Conference on Computer Communications, pp. 1749–1758. IEEE (2022)
9. Nguyen, Q.P., Low, B.K.H., Jaillet, P.: Variational bayesian unlearning. Adv. Neural. Inf. Process. Syst. **33**, 16025–16036 (2020)
10. Voigt, P., von dem Bussche, A.: The EU General Data Protection Regulation (GDPR), 1st edn. Springer, Cham (2017). https://doi.org/10.1007/978-3-319-57959-7
11. Wang, F., Li, B., Li, B.: Federated unlearning and its privacy threats. IEEE Netw. **38**(2), 294–300 (2023)
12. Wang, J., Guo, S., Xie, X., Qi, H.: Federated unlearning via class-discriminative pruning. In: Proceedings of the ACM Web Conference 2022, pp. 622–632 (2022)
13. Wu, C., Zhu, S., Mitra, P.: Federated unlearning with knowledge distillation. arXiv preprint arXiv:2201.09441 (2022)
14. Yu, T., Kumar, S., Gupta, A., Levine, S., Hausman, K., Finn, C.: Gradient surgery for multi-task learning. Adv. Neural. Inf. Process. Syst. **33**, 5824–5836 (2020)
15. Zhao, Y., Wang, P., Qi, H., Huang, J., Wei, Z., Zhang, Q.: Federated unlearning with momentum degradation. IEEE Internet Things J. (2023)

# Synthesis and Analysis of Porous Frame Structures Images Using Machine Learning Methods

Artem Poltavskiy[1](✉), Ekaterina Kolomenskaya[1], Grigory Beliavsky[2], Vera Butova[3], and Maria Butakova[1]

[1] The Smart Materials Research Institute, Southern Federal University, 178/24 Sladkova, 344090 Rostov-on-Don, Russia
poltavsky@sfedu.ru

[2] Institute of Mathematics, Mechanics and Computer Science of the Southern Federal University, 8a Milchakova, 344090 Rostov-on-Don, Russia

[3] Institute of General and Inorganic Chemistry, Bulgarian Academy of Sciences, 1113 Sofia, Bulgaria

**Abstract.** Porous frame structures are vital in various engineering applications such as scaffolding and tissue engineering. Analyzing and synthesizing images of such structures plays a crucial role in understanding their properties and optimizing their design. Through the incorporation of computer vision techniques and machine learning algorithms, we propose a modern approach to generate synthetic images of porous frame structures with high granularity. Subsequently, employing state-of-the-art image analysis techniques, we expound the intricate characteristics and properties of these structures, facilitating a comprehensive understanding of their behavior and functionality. Our findings not only contribute to the advancement of porous material design but also underscore the efficacy of machine learning in constructing complex structural patterns, thereby paving the way for novel applications in diverse domains.

**Keywords:** Image Synthesis · Image Analysis · Machine Learning · Computer Vision · Porous Frame Structure

## 1 Introduction

Porous frame structures are intricate arrangements of interconnected beams, rods, or other structural elements that leave void spaces within the framework. These structures are commonly found in various natural and synthetic materials, including foams, sponges, geological formations like rocks, and even biological tissues like bones [1, 2].

The synthesis and analysis of porous frame structures has paramount importance in various scientific and industrial applications, including materials science, medicines, filtration, and catalysis [3–5]. The ability to generate and accurately analyze images of these structures is crucial for understanding their properties and optimizing their


S. Kovalev et al. (Eds.): IITI 2024, LNNS 1209, pp. 389–401, 2024.
https://doi.org/10.1007/978-3-031-77688-5_37

performance. This work explores advanced techniques for image generation and analysis, focusing on segmentation and the subsequent calculation of key properties such as porosity, pore size distribution, specific surface area, connectivity, and tortuosity.

Porous materials are characterized by their complex and heterogeneous structures, which present significant challenges for image analysis [6]. Accurate segmentation of pores is essential to obtain reliable data for further property analysis. However, the variability in pore sizes, shapes, and connectivity patterns makes segmentation a complex task. Traditional methods often fall short in handling this complexity, necessitating the development and application of advanced machine learning techniques [7, 8].

By leveraging these methods, it becomes possible to achieve precise segmentation and comprehensive property analysis, providing valuable insights into the structural and functional characteristics of porous materials.

The progress in this field holds substantial value, as it enables the detailed characterization and optimization of porous materials for various applications. Improved segmentation and analysis techniques can lead to a better understanding and control of material properties, facilitating the design of more efficient and effective materials. This study aims to address the complexities associated with the segmentation and analysis of porous frame structures, presenting innovative machine learning approaches to overcome these challenges and advance the study of these crucial materials.

## 2 Image Generation

In the field of materials science, the ability to accurately generate and analyze images of porous frame structures is crucial for advancing understanding of materials properties and behaviors [9]. This section focuses on the use of methods to synthesize images of these structures, specifically through the implementation of a Python-based ellipse generation script based on mathematical formulas. This approach leverages the flexibility and efficiency of ellipse-based models to represent the intricate and variable porous spaces within frame structures.

We will use the following representation for image generation:

$$f = \alpha \bigcup_{i=1}^{N} El_i + \beta I. \tag{1}$$

In Eq. (1) $\alpha$ and $\beta$ – determines the contrast of the image, in the image $I(k, l) = 1$, the images of ellipses $El_i$ are defined as follows:

$$El_i(k,l) = \begin{cases} 1, & \frac{((k-a_i)c_i-(l-b_i)s_i)^2}{A_i^2} + \frac{((k-a_i)c_i-(l-b_i)s_i)^2}{B_i^2} \le 1; \\ 0, & \frac{((k-a_i)c_i+(l-b_i)s_i)^2}{A_i^2} + \frac{((k-a_i)c_i-(l-b_i)s_i)^2}{B_i^2} > 1, \end{cases}$$

$$\left(\bigcup_{i=1}^{N} El_i\right)(k,l) = \max_i El_i(k,l).$$

Equation (1) will be used as the basic one, where the natural number $N$ is the number of pores and contrasts $\alpha$ and $\beta$ satisfy constraints: $\alpha \ge 0$, $\beta \ge 0$, $\alpha + \beta \le 1$.

The expression of contrast $\alpha = \xi\eta, \beta = (1 - \xi)\eta$ is in terms of two independent random variables $\xi$ and $\eta$, which are evenly distributed over the interval [0, 1]. The center of the ellipse $(a_i, b_i)$ is evenly distributed on the points of the image grid. The orientation parameters $(c, s)$ satisfy the following constraints: $-1 \leq c \leq 1$, $c^2 + s^2 = 1$. We assume that $c$ is a uniform random variable in the interval $[-1, 1]$, $s = \delta\sqrt{1 - c^2}$, $P(\delta = 1) = P(\delta = -1) = \frac{1}{2}$.

The generator uses a standard metric: $\rho(M(i, j), R(k, l)) = \sqrt{(k - i)^2 + (l - j)^2}$. Metric includes parameters and independent random variables $A$ and $B$. Two generators were used to generate them. The first generator uses an exponential distribution law with parameters $\lambda_1$ and $\lambda_2$. Picking Parameters should be relied on the average values: $EA = \frac{1}{\lambda_1}$, $EB = \frac{1}{\lambda_2}$.

The second generator uses β- distributions: $A = \underline{A} + \xi\left(\overline{A} - \underline{A}\right), B = \underline{B} + \eta\left(\overline{B} - \underline{B}\right)$,

where $\underline{A}$, $\underline{B}$ – the smallest and $\overline{A}$, $\overline{B}$ – the largest values for parameters $A$ and $B$, random variables $\xi$ and $\eta$ are independent with β-distribution laws:

$$f_\xi(x) = \frac{1}{B(\alpha_1, \beta_1)} x^{\alpha_1 - 1}(1 - x)^{\beta_1 - 1}, x \in [0, 1], \alpha_1 > 0, \beta_1 > 0;$$

$$f_\eta(x) = \frac{1}{B(\alpha_2, \beta_2)} x^{\alpha_2 - 1}(1 - x)^{\beta_2 - 1}, x \in [0, 1], \alpha_2 > 0, \beta_2 > 0,$$

where $B(\alpha, \beta)$ – beta function. Parameters $\alpha$ and $\beta$ require additional configuration.

To generate an image, it is necessary to generate contrast, the required number of ellipsoids and calculate the image using the Eq. (1). By adjusting parameters stated in Table 1, the script can simulate a wide variety of pore structures with different sizes and spatial distributions, closely mimicking the physical characteristics observed in real-world samples.

**Table 1.** Generation script parameters with description and range/constraints.

| Parameter | Description | Range/Constraints |
|---|---|---|
| Contrast $(\alpha, \beta)$ | Determines the contrast of the generated images | $\alpha \geq 0, \beta \geq 0, \alpha + \beta \leq 1$ |
| Center $(a, b)$ | Center of each ellipse distributed across the image grid | Even distribution across image points |
| Orientation $(c, s)$ | Orientation parameters for each ellipse | $-1 \leq c \leq 1, c^2 + s^2 = 1$ |
| Random Variable $A$ | Generated using an exponential distribution | $E[A] = 1/\lambda_1$ |
| Random Variable $B$ | Generated using an exponential distribution | $E[B] = 1/\lambda_2$ |

(*continued*)

**Table 1.** (*continued*)

| Parameter | Description | Range/Constraints |
|---|---|---|
| Number of Pores ($N$) | Total number of ellipses (pores) generated in the image | Natural number |
| Ellipse Definition | Formula defining each ellipse in the image | Use of max function across ellipses |
| Random Variables ($\xi$, $\eta$) | Independent random variables for contrast and ellipse parameters | Even distribution over [0, 1] |

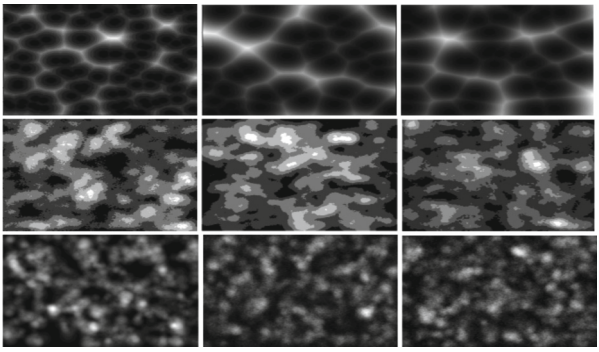

**Fig. 1.** Porous frame structure images generated by the software implementation.

Generated images using a software implementation with various parameters and morphological operations demonstrated on Fig. 1.

Synthesized dataset serves not only as a tool for visual representation but also forms the basis for further computational analysis and machine learning models training.

## 3 Image Analysis

Machine learning models are employed to analyze generated images, aiming to identify patterns and features that are critical for predicting material performance [10]. The model can learn from a set of labeled images, enhancing its ability to generalize from synthetic to real experimental data. This methodology not only improves the accuracy of material characterization but also significantly reduces the time and resources required for experimental data collection and analysis.

The use of porous frame structure image generation combined with machine learning analysis, represents a powerful toolset for deeper understanding of material properties. By training on synthetic images that accurately represent the characteristics of real porous structures, the machine learning models can effectively identify key features such as pores, sizes, shapes, and connectivity. This allows for precise predictions of material performance and optimization of material designs.

Synthetic images usage for training offers the advantage of a controlled environment where the variability of pore structures can be systematically adjusted. This helps in developing models that are not only accurate but also adaptable to variations in real-world data. The ability to automatically analyze new images and predict material properties greatly enhances efficiency and opens new possibilities for innovative applications in fields like tissue engineering, filtration, and catalysis.

### 3.1 Pores Segmentation

Pores segmentation is fundamental for the detailed analysis of porous materials. Accurate segmentation enables the precise quantification and characterization of porous frame structures, providing insights into their structural and functional properties [11].

However, pore segmentation is a complex task due to the intricate and heterogeneous nature of pore geometries. The variability in pore sizes, shapes, and connectivity patterns necessitates the use of advanced image processing techniques to achieve reliable and accurate results. Consequently, developing robust segmentation methods is a fundamental step toward advancing the study and application of porous materials.

**Outline Selection**

The selection of contours in the image refers to convolution-type operations, and to use a discrete two-dimensional Fourier transform using the fast Cooley-Tukey algorithm, the image is considered as a two-dimensional torus. The operation of convolution of an image $f$ with a filter $g$ with a pulse scattering function $g(i, j)$ can be represented as a sum:

$$(g * f)(i, j) = \sum_{-w}^{w} \sum_{-w}^{w} g(k, l) f(i - k, j - l).$$

Canny filter kernels are obtained because of discrete differentiation with respect to the corresponding Gaussian kernel variables. Differentiation by the Gaussian kernel variable $x$ leads to the kernel:

$$G_x(i, j) = C\left(\exp\left(-\frac{i^2 + j^2}{h}\right) - \exp\left(-\frac{(i-1)^2 + j^2}{h}\right)\right).$$

The kernel $G_y(i, j)$ is calculated the same way. Convolution with these kernels allows to calculate a black gradient for each point in the image and use it to determine the contour. As a result, the image is smoothed by the Gaussian kernel, which leads to interference suppression and reduces the error in calculating the blackness gradient. The larger filter size $w$ – the less interference remains on the image and the border will be smoothed even more. The search for a compromise is the subject of numerous studies.

A different approach to solving the problem is by formulating it as finding the minimum of convex functional we need to calculate: $(g * f)(0, 0) = (g, f_g)$, where $f$ is a noise-free image, an ideal image, and $f_g$ is the projection of the image onto the filter $g$. At the same time, we can use a noisy image: $\overline{f} = f + \sigma n$, where is $n$ – white noise. It

is applicable to use another core for calculating $\left(\overline{g} * \overline{f}\right)(0,0) = \left(\left(\overline{g}, f_g\right) + \sigma\left(\overline{g}, n_g\right)\right)$, where assumed that the filter $g$ and $\overline{g}$ match. The task of choosing a core $\overline{g}$ is as follows:

$$\min_{\overline{g}} \theta, P\left(\max_{f_g \leq \beta} \left|\left(\overline{g} - g, f_g\right) + \sigma\left(\overline{g}, n_g\right)\right| \leq \theta\right) \geq \alpha, \tag{2}$$

where $\theta$ is the error of calculating the derivative.

We transform the task described by (2) under the assumption that the random variable and the noise are distributed according to a normal distribution law. It follows from normality that: $\theta = \beta\overline{g} - g + \sigma\Phi^{-1}\left(\frac{1+\alpha}{2}\right)\overline{g}$, where $\Phi^{-1}(x)$ – the inverse of the Laplace function.

By dividing the functionality into $\beta > 0$ as a result we get the task:

$$\min_{\overline{g}}(\overline{g} - g + \lambda\overline{g}), \tag{3}$$

which must be solved to find the optimal kernel. It is important that this approach can be used to synthesize an optimal filter with correlated interference. To do this, we need to solve the task:

$$\min_{\overline{g}}(\overline{g} - g + \lambda(C\overline{g}, \overline{g})), \tag{4}$$

where $C$ is the covariance matrix, $\lambda = \frac{\Phi^{-1}\left(\frac{1+\alpha}{2}\right)}{\beta}$.

Results of outline selection and thresholding segmentation presented on Fig. 2.

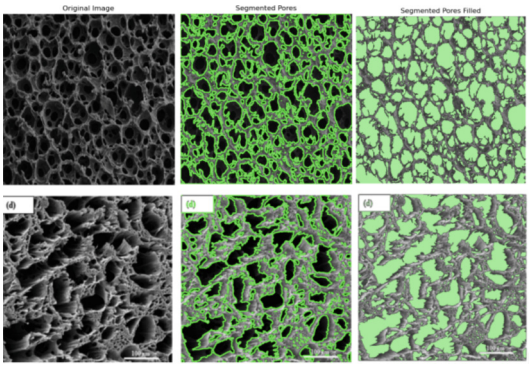


**Fig. 2.** Pores segmentation with outline selection and thresholding.

**Ellipse Fitting**

Next, we will use the following ellipse equation:

$$a(x-m)^2 + 2b(x-m)(y-n) + c(y-n)^2 = 1, \tag{5}$$

where $a,\ b,\ c,\ m,\ n$ – are the parameters satisfying the inequalities: $a > 0$, $ac - b^2 > 0$.

We have a contour at our disposal to calculate the parameters and the following characteristic property of the ellipse. For a family of parallel lines intersecting a contour, the centers of the segments connecting the points on the contour lie on a straight line. Consider two families of parallel lines intersecting an ellipse. Horizontal section points $\left(\frac{x_i^l+x_i^r}{2}, y_i\right)$ and vertical section points $\left(x_i, \frac{y_i^u+y_i^d}{2}\right)$ they are grouped around straight lines $y = k_1x + b_1$ and $y = k_2x + b_2$. The point of intersection of these lines $(m, n)$ is the center of the ellipse. For the other parameters of the ellipse, the equalities are valid:

$$a = -k_1 b,\ c = -\frac{1}{k_2} b.$$

The Hough transform was used to calculate the parameters of the lines. The least squares method was used to estimate the remaining parameter:

$$\min_b \sum_{i=1}^{N} \left(1 + b\left(k_1(x_i - m)^2 + 2(x_i - m)(y_i - n) + \frac{1}{k_2}(y_i - n)^2\right)\right)^2.$$

The family of points $(x_i, y_i)$ is localized relative to straight lines. Figure 3 illustrates the outcomes of the Ellipse fitting applied to porous frame structure images.

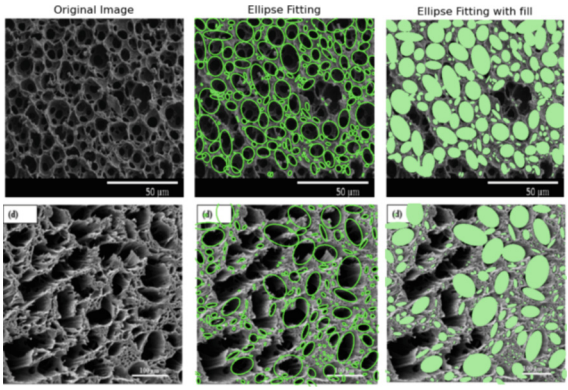


**Fig. 3.** Ellipse fitting segmentation performance across porous frame structures.

**Computer Vision Model Application**

For porous frame structure segmentation using Convolutional Neural Networks (CNNs), leveraging the U-Net [12] architecture is proposed due to its proven efficacy in capturing both low-level and high-level features crucial for precise image segmentation. The U-Net architecture consists of a contracting path and an expanding path. The contracting path includes convolutional layers and max-pooling operations that perform downsampling to capture context and reduce spatial dimensions. Conversely, the expanding path employs up-convolutions for upsampling, aiming to reconstruct the image resolution

while maintaining the learned features. This architecture is further enhanced by incorporating skip connections that are crucial as they effectively preserve spatial information, which significantly improves the accuracy of the segmentation.

The training methodology for the U-Net model involved thorough preparation of datasets, incorporating both synthetic images with predefined pore structures and real microscopy images. This comprehensive dataset preparation is critical as it allows the model to learn from a wide variety of examples, thereby enhancing its generalization capabilities. The datasets undergo meticulous preprocessing steps, including normalization to standardize the pixel values and data augmentation techniques to artificially increase the diversity of the training data. This increases the variability and robustness of the model. During training, appropriate loss functions, specifically binary cross-entropy and Dice loss functions, were utilized to optimize the model's performance. These loss functions help in measuring the accuracy of the predicted segmentations against the ground truth. The training process was closely monitored using evaluation metrics such as Intersection over Union (IoU) and Dice coefficient.

Hyperparameter tuning played a crucial role in optimizing the performance of the U-Net model. Key hyperparameters such as the learning rate, batch size, number of epochs, and the architecture of the network including the number of layers, filter sizes, and the use of dropout for regularization were fine-tuned through extensive experimentation and cross-validation to achieve the best performance. The learning rate controls how much to change the model in response to the estimated error each time the model weights are updated. Selecting an optimal learning rate is crucial for balancing between convergence speed and stability. Batch size, which determines the number of training samples used in one iteration, was carefully chosen to ensure efficient computation while maintaining the robustness of the training process. The number of epochs, which indicates the number of complete passes through the training dataset, was selected based on the point at which the model's performance on the validation set stopped improving, thereby avoiding overfitting.

Post-training, the predictions made by the model were subjected to additional post-processing steps to further refine the segmentation outcomes. This post-processing is essential to ensure that the segmentations are accurate and applicable in practical scenarios that require high precision, such as biomedical image analysis, where precise segmentation of images is crucial for tasks like disease diagnosis and treatment planning. The post-processing involved techniques such as morphological operations to clean up the segmented images, smoothing filters to reduce noise, and thresholding to ensure that the segmented areas accurately represented the porous structures.

Figure 4 illustrates the outcomes of the best fitted U-Net model applied to porous frame structure images.

### 3.2 Properties Analysis

Key properties of porous frame structures were calculated to understand their characteristics and performance. These properties included porosity, pore size distribution, specific surface area, connectivity and tortuosity, each providing valuable insights into the structural and functional aspects of the pores.

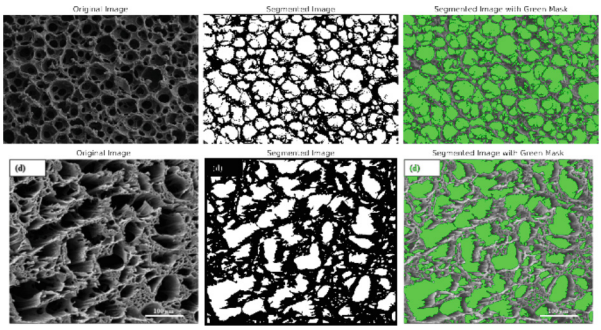


**Fig. 4.** U-Net segmentation performance across porous frame structures.

Porosity was calculated as the ratio of the pore area to the total area of the image, offering a fundamental measure of void space within the structure. Analyzing pore size distribution involved using "region props" to extract the areas of individual pores, which were then plotted to visualize their frequency and distribution. Specific surface area, calculated from the perimeters of the pores, provided an important metric for understanding the surface available for reactions or interactions, normalized by the total area of the image. Connectivity of the pore structure was assessed by determining the number of connected components within the binary image, highlighting the extent to which the pores formed a continuous network. Figure 5 demonstrates properties analysis for porous frame structures.

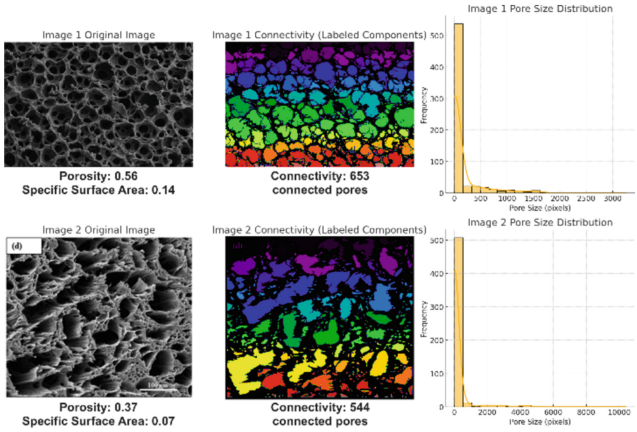


**Fig. 5.** Porous frame structures properties analysis.

These analyses provided an evaluation of the geometric and topological properties of the pore structures. By accurately quantifying these properties, the study contributed to a deeper understanding of porous frame structures. The methods and metrics used in this analysis form a robust framework for further research and practical applications in evaluating and optimizing porous materials.

## 4 Computational Comparison

For segmentation accuracy testing, Intersection over Union (IoU) and the Dice Coefficient are picked. IoU measures the overlap between the predicted segmentation and the actual segmentation by calculating the ratio of their intersection over their union. It is a critical metric for evaluating segmentation performance because it provides a clear indication of how well the predicted segmentation aligns with the true segmentation. The Dice coefficient, on the other hand, measures the similarity between the predicted and actual segmentations by doubling the area of overlap and dividing it by the total number of pixels in both segmentations. This metric is particularly useful for evaluating the accuracy of pixel-level predictions, making it ideal for tasks that require precise segmentation such as biomedical image analysis.

Together, these metrics provide a comprehensive evaluation of segmentation performance, ensuring accuracy and reliability.

Segmentation methods were compared on a test dataset of 500 synthesized images and 50 real images. The synthetic images were generated using algorithm described in image generation section, which allows for the adjustment of various parameters to represent a wide range of porous frame structures. By tuning parameters such as pore size, shape, distribution, and contrast, a diverse set of synthetic images were created that mimic the complexity and variability of real porous materials. For the real images, we sourced data from multiple origins to ensure a rich and varied dataset. This included images of scaffolds, which were acquired through extensive web crawling to collect publicly available images of porous structures used in biomedical applications. Additionally, we utilized high-resolution images obtained from transmission electron microscopy (TEM) and scanning transmission electron microscopy (STEM) analyses of metal-organic frameworks (MOFs). These techniques provide detailed visualizations of the pore structures at the microscopic level, capturing the intricate details essential for accurate segmentation.

The combination of synthetic and real datasets allows for a thorough evaluation of the segmentation methods. The synthetic dataset, with its controlled variability, helps in understanding the model's performance under different conditions, while the real dataset ensures that the model is applicable to practical scenarios. This dual approach not only tests the robustness of the segmentation methods but also validates their effectiveness in real-world applications. By comparing segmentation results on these datasets, we can comprehensively assess the accuracy and reliability of the methods. The results of these comparisons are summarized in Table 2, showcasing the performance of different segmentation methods on both synthetic and real images. This evaluation highlights the strengths and weaknesses of each method, providing insights into their suitability for various applications in material science and biomedical imaging.

While U-Net demonstrated the highest accuracy on both synthesized and real images, its performance dropped by approximately 3–4% when applied to real images. The model's sensitivity to variations in real-world data accounts for this decrease.

Outline selection with thresholding showed a more significant drop of 7–8% in accuracy for real images. The method relies on specific threshold values, which can be less robust to variations and noise present in real images.

**Table 2.** Methods computational comparison on real and generated images.

| Method | IoU gen | IoU real | Abs.Diff | Dice gen | Dice real | Abs.Diff |
|---|---|---|---|---|---|---|
| *U-Net* | 91.2% | 87.8% | 3.4% | 93.1% | 89.5% | 3.6% |
| *Outline selection with thresholding* | 81.4% | 74.2% | 7.2% | 83.2% | 75.7% | 7.5% |
| *Ellipse Fitting* | 63.7% | 58.1% | 5.6% | 65.5% | 59.6% | 5.9% |

Although Ellipse Fitting performed the least accurately overall, it experienced a moderate drop less than 6% in accuracy for real images. The technique is particularly sensitive to irregular pore shapes, which are more prevalent in real images.

Overall, segmentation methods achieved higher accuracy on generated images. In contrast, real porous images exhibited additional complexity for segmentation algorithms due to factors such as natural irregularities in pore shapes, variations in lighting, resolution and noise. That led to a drop in accuracy across all methods, where U-Net proved to be the most accurate.

## 5 Conclusion

In this study, we synthesized and analyzed porous frame structure images using machine learning methods.

For pores segmentation both synthetic and real images were used to train and evaluate different segmentation approaches, including Outline selection with thresholding, Ellipse fitting, and U-Net, ensuring a comprehensive performance assessment. To measure segmentation accuracy, Intersection over Union and the Dice Coefficient were employed. These metrics provided clear indications of the overlap and accuracy of the predicted segmentations. The synthetic images played a crucial role in training the U-Net, enabling it to learn complex patterns and enhance its segmentation performance.

The results demonstrated the strengths of each approach. Outline selection with thresholding effectively highlighted edges, while Ellipse fitting provided robust geometric approximations. However, the U-Net method showed superior performance across all image styles, achieving higher accuracy and reliability in segmenting porous frame structures.

By utilizing segmented pore images, key properties of porous frame structures, including porosity, pore size distribution, specific surface area, connectivity, and tortuosity, were calculated to understand their structural and functional characteristics. Porosity and specific surface area were fundamental measures of void space and surface availability, while connectivity and tortuosity provided insights into the network formation and complexity of pore paths. These analyses offered a comprehensive evaluation of the pore structures, essential for applications in materials science, filtration, and catalysis.

This study underscores the effectiveness of using synthetic images for training advanced machine learning models, paving the way for further research in image synthesis and analysis. By achieving high segmentation accuracy and reliability through

the U-Net model, the aim of developing robust computer vision methods for studying porous frame structures has been met. This success demonstrates the potential of our approach in reducing the time and resources required for experimental data collection and analysis, and in providing valuable insights into the properties and functionalities of porous materials. The methodologies and findings presented in this study lay a strong foundation for future advancements in the synthesis and analysis of porous structures, highlighting the practical applications and scientific contributions of integrating machine learning with materials science.

**Funding.** The project was supported by the Russian Science Foundation under grant No. 23-21-00331, https://rscf.ru/project/23-21-00331/ (accessed on 17.05.2024) and performed in Southern Federal University (Rostov-on-Don, Russian Federation).

## References

1. Gräf, J., Anspach, L., Horn, C., Winkelmann, A., Zaeh, M.F.: Design and fabrication of microporous metallic implants with tailored pore structures. J. Funct. Biomater. **14**(5), 286 (2023). https://doi.org/10.3390/jfb14050286
2. Moussa, H., Zhang, X., Benkirane, M.: 3D porous materials for biomedical applications: a review. Front. Bioeng. Biotechnol. **10**, 954699 (2022). https://doi.org/10.3389/fbioe.2022.954699
3. Mosalaganti, S., et al.: AI-based structure prediction empowers integrative structural analysis of human nuclear pores. Science **376**(6598), eabm9506 (2022). https://doi.org/10.1126/science.abm9506
4. Zhao, Y., et al.: Photocatalytic synthesis of small-molecule drugs by porous framework materials. Chin. Chem. Lett. **35**, 109065 (2023). https://doi.org/10.1016/j.cclet.2023.109065
5. Rezaee, S., Shahrokhian, S.: Facile synthesis of petal-like NiCo/NiO-CoO/nanoporous carbon composite based on mixed-metallic MOFs and their application for electrocatalytic oxidation of methanol. Appl. Catal. B **244**, 802–813 (2019). https://doi.org/10.1016/j.apcatb.2018.12.013
6. Lu, Y., Luo, X., Xu, Z., Zhang, Y.: Recent advances in the design and fabrication of porous biomaterials for bone tissue engineering. Acta Biomater. **131**, 276–293 (2021). https://doi.org/10.1016/j.actbio.2021.09.042
7. Wan, H., et al.: Importance of appropriate segmentation in pore structure analysis of coral reef limestone from CT images. Mar. Georesour. Geotechnol. **42**(4), 327–347 (2024). https://doi.org/10.1080/1064119X.2023.205022
8. Shi, X., Misch, D., Vranjes-Wessely, S.: A comprehensive assessment of image processing variability in pore structural investigations: conventional thresholding vs. machine learning approaches. Gas Sci. Eng. **115**, 205022 (2023). https://doi.org/10.1080/1064119X.2023.205022
9. Pais, A.I., Belinha, J., Alves, J.L.: Advances in computational techniques for bio-inspired cellular materials in the field of biomechanics: current trends and prospects. Materials **16**(11), 3946 (2023). https://doi.org/10.3390/ma16113946
10. Butler, K.T., Davies, D.W., Cartwright, H., Isayev, O., Walsh, A.: Machine learning approaches for the prediction of materials properties. APL Mater. **9**(3), 041801 (2021). https://doi.org/10.1063/5.0041483

11. Hong, G.Y., Mamun, A.A., Ping, E.P., Wu, Q.: Deep learning-based segmentation of 3D volumetric image and microstructural analysis. Sensors **23**(5), 2640 (2023). https://doi.org/10.3390/s23052640
12. Siddique, N., Paheding, S., Elkin, C.P., Devabhaktuni, V.: U-net and its variants for medical image segmentation: a review of theory and applications. IEEE Access **9**, 82031–82057 (2021). https://doi.org/10.1109/ACCESS.2021.3086020

# Data Mining Methods Application to Solve the Oil and Gas Flow Regimes of Oil Well Production Classification Problem

Ilya S. Mikhaylov(✉), Pavel R. Varshavskii, Marina V. Fomina, and Kirill O. Sidorov

National Research University "MPEI", Krasnokazarmennaya Street, 14, Moscow 111250, Russia
kirill.sidoroff2014@yandex.ru

**Abstract.** In the article the flow regimes types of oil well production are considered. The oil well production flow regime determining problem in real time relevance is substantiated. An overview of the neural networks for solving the problem is provided. An ensemble method based on neural networks is proposed. The application of this method in an oil field is shown. Real time data, received from multiphase flowmeter, installed on the oil well, is the basis for the considered problem solution.

**Keywords:** data mining · neural networks · support vector machine · domain constraints · oil production

## 1 Introduction

Artificial intelligence techniques are increasingly used in various fields, assisting in data management, process optimization, and solving complex computational challenges [1]. Among Data Mining methods like neural networks and decision trees, speed is a critical factor. While traditional methods offer wide applicability, they may not fully utilize data structure knowledge, limiting their effectiveness. However, incorporating domain-specific insights can enhance method efficiency or substitute complex methods with simpler, equally accurate ones [2, 3].

## 2 Neural Network Architectures

### 2.1 Perceptron (PNN)

In 1958, F. Rosenblatt invents the single-layer perceptron [4, 5], based on the McCulloch-Pitts neuron, developed in 1943 [6], and demonstrates its ability to solve classification problems. At the output, the perceptron produces a result $y$ based on several real input objects $x$ by forming a linear combination using the weights $w$, adding a bias $b$, and then passing the result through a nonlinear activation function $\varphi$:

$$y = \varphi\left(\sum_{i=1}^{n} w_i x_i + b\right) = \varphi(w^T x + b)$$

The research was supported by RSF (project No. 24–11-00285).


S. Kovalev et al. (Eds.): IITI 2024, LNNS 1209, pp. 402–409, 2024.
https://doi.org/10.1007/978-3-031-77688-5_38

The perceptron can be effective in the following cases:

- Linearly separable tasks. When data can be easily separated by a line or plane;
- Simple dependencies. If there is a clear and uncomplicated relationship between input and output data;
- Small amounts of data. For small datasets where the perceptron can learn quickly;
- Simple models. In situations where a simple model is required for rapid prototyping or preliminary data analysis.

Rosenblatt's perceptron demonstrates the highest efficiency in classification tasks characterized by linear separability of data, due to its fast adaptive potential and ability to provide high accuracy under appropriate conditions. This is especially important in our research, as we strive to apply this algorithm to solve specific classification problems where data can be divided linearly, which allows us to expect high results and confirm the theoretical foundations of the effectiveness of Rosenblatt's perceptron in real conditions.

### 2.2 Multilayer Neural Networks (MLNN)

A MLNN is a form of artificial neural network made up of at least three layers of processing elements or neurons. Typically, these layers are organized into an input layer, one or several hidden layers, and an output layer. As a crucial asset in the toolkit of machine learning professionals, multilayer neural networks enable the representation of intricate patterns and associations within datasets. An example of this type of network is one that includes just a single hidden layer (SLNN).

There are three types of layers in a neural network: an input layer that receives a vector $x$; output layer, responsible for outputting the result after processing by the network; and one or more hidden layers in between. It is important to note that the input layer $x$ is not involved in performing arithmetic operations; its task is only to transfer the vector to the next layer and provide its information connection.

In general, this architecture is quite flexible and universal for solving most problems of classical data mining.

### 2.3 Convolutional Neural Networks (CNN)

CNN, developed by Yann LeCun in 1988, are a unique type of artificial neural networks focused on highly efficient pattern detection [7]. CNNs are particularly useful for working with images and videos, using convolution techniques using kernels to extract key features, including edges and textures. These filters slide over the surface of the input image using a convolution operation, allowing the model to analyze the data at different levels of detail. After passing through the convolution stage, the data is processed through aggregation layers (pooling), which reduce the amount of information, and then through fully connected layers, where the process of classifying or identifying objects is carried out.

CNNs are mainly used for text processing and computer vision image analysis. However, the computational complexity of the convolutional layer is high relative to the linear layer.

### 2.4 Recurrent Neural Networks (RNN)

RNNs come in many different types, architectures, and components. The main problem with RNNs is the need to process each time point separately, which requires creating a new layer of neurons for each time point. This leads to significant computational costs. Multilayer structures often suffer from computational stability problems because weights can quickly increase or decrease to zero. Limiting calculations to a fixed time interval may result in models not being able to effectively capture long-term trends. Various methods explore ways to improve the model's ability to remember the past and control the processes of remembering and forgetting (LSTM [8], GRU [9], etc.).

Recurrent neural networks are a very important architecture that is used in various fields, mainly in text processing and time series analysis. However, there is a problem that they are computationally complex. This is an important limitation for this work.

### 2.5 Restricted Boltzmann Machine (RBM)

RBM was first created in 1986 by Paul Smolensky and was named Harmonium [10]. However, it only became widely known after Hinton developed high-speed learning algorithms in the mid-2000s. RBM is a model designed to analyze the probability distribution inherent in the training dataset, leveraging this understanding to predict outcomes for new data inputs. It consists of an input layer and one or more hidden layers.

One of the key advantages of RBMs is their ability to learn unsupervised, although in some contexts they can use a supervised learning approach. The deep characteristics of the data that become visible during training form the so-called hidden layer in the structure of the machine.

The Restricted Boltzmann Machine (RBM) has advantages in modeling probability distributions, learning without the need for error back propagation, and flexibility in data processing, which makes them useful in various fields, including recommendation systems and natural language processing. However, despite these advantages, RBMs face a number of disadvantages, such as the complexity of interpreting results, sensitivity to hyperparameters, and limited ability to model complex dependencies, which may make their application difficult in some scenarios.

## 3 The FSNN Method Development

The operation of neural networks involves complex computations, resulting in significant computational expenses [11, 12]. In this context, it is proposed to introduce restrictions, such as functional separability of domain classes, to create neural networks with a single hidden layer, which helps to improve classification accuracy [11].

Classes are functionally separated if for each class there is a functional relationship between its output parameters and a set of input parameters, which ensures continuity and monotony of the function over a given range of input data. This property is important for the application of the UAT, which states that any continuous function defined on a limited closed interval can be accurately approximated using a single hidden perceptron layer, thereby confirming the possibility of using neural networks to solve a wide range of problems [11].

The proposed property of functional separability allows for solving the classification problem through a neural network with one hidden layer and a sigmoid activation function, leveraging the UAT capability to approximate any continuous function in a compact domain [11]. With functional separability, several values of y1*,…, yn* can exist for one value of x* (Fig. 1).

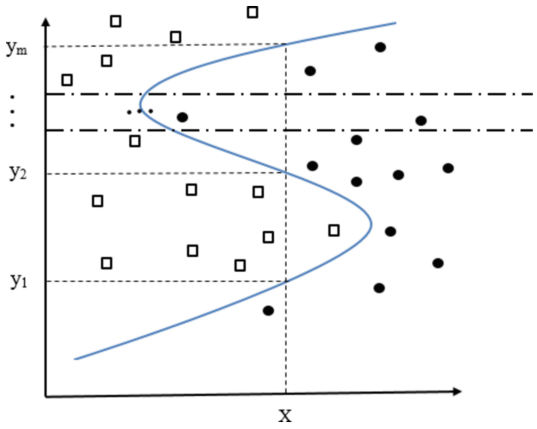


**Fig. 1.** Functionally separable classes example

In this case, the classification problem solution should be divided into n regions R1,… Rn, in each of which a section of the usual functional dependence between variables will be represented (Fig. 2). Thus, by simplifying the obtained mathematical descriptions of neural networks, we obtain a linear combination with summed weight coefficients. This is a mathematical description of a neural network with one hidden layer and a sigmoidal activation function.

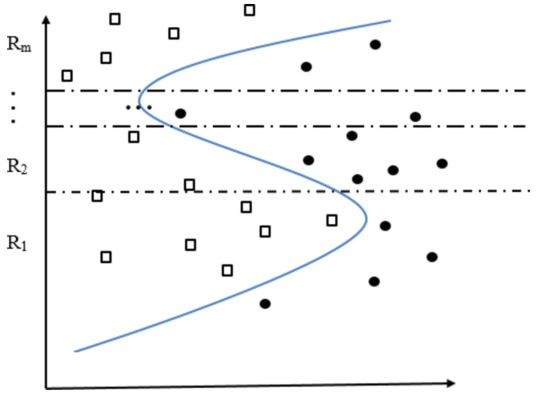


**Fig. 2.** Example of dividing into regions $R_1$, …, $R_n$, in which classes are separated by monotone functions

## 4 FSNN Approach Application. The Classification Problem of Oil and Gas Flow Regimes

Our research focuses on a specific application of physical processes—specifically, the oil extraction process. Oil production is a complex process that requires careful consideration of the use of various components during the operation of oil wells. The key point here is the need to monitor the consumption of these components in real time.

One of the main problems in this area is the significant number of wells in one group, which can reach dozens. Each well has unique characteristics, including its properties, parameters and equipment used. This highlights the importance of individualizing the management approach for each well.

In the context of the physical process of oil production, there are complex functional relationships between input (independent variables) and output (dependent variables) parameters. These connections are continuous and play a key role in optimizing the mining process. The use of mathematical models and algorithms to analyze these relationships allows us to develop effective strategies for managing resources and increasing well productivity [13].

It should be noted that the computing equipment used in oil fields should ensure stable operation of the system at temperatures from −40 to +85 °C. In this regard, its cost increases significantly with an increase in the computing power of industrial computers used. Therefore, the task of reducing computational costs and using the simplest intelligent models that ensure the resulting solution high quality becomes very urgent.

Thus, the integration of modern methods of data analysis and modeling into the oil production management process can significantly increase its efficiency and environmental safety. In our case, the mode classes satisfy the conditions of CFS and FSNN, therefore, the flow mode classes have the property of functional separability for the classification problem and, accordingly, the solution can be found using the generated neural network with one hidden layer [13].

The final neural network with all parameters is shown in Fig. 3.

After training, the neural network turned out to be not only surprisingly accurate, but also extremely effective in performing tasks, demonstrating high data processing speed without significant resource expenditure. Its simplicity of architecture made it possible to avoid retraining, while maintaining high adaptability to new data. This model highlights the importance of balancing complexity and efficiency in the development of artificial intelligence.

The solution process involves real-time monitoring and calculation of flow parameters, employing a pre-trained decision support system that utilizes both FSNN and convolutional neural networks to classify flow regimes, with results validated by a modified FS-SVM support vector machine before being presented to the user through a voting mechanism.

As part of the study, using various architectures and activation functions, a comprehensive analysis of the generated data set was carried out, where for the D0 subset the best results were achieved using SLNN, and for the D subset using CNN (see Table 1), while the results obtained turned out to be stable when changing the ratio of training and testing data sets. The application of the previously considered neural network architectures to solve this problem is given in the article [11].

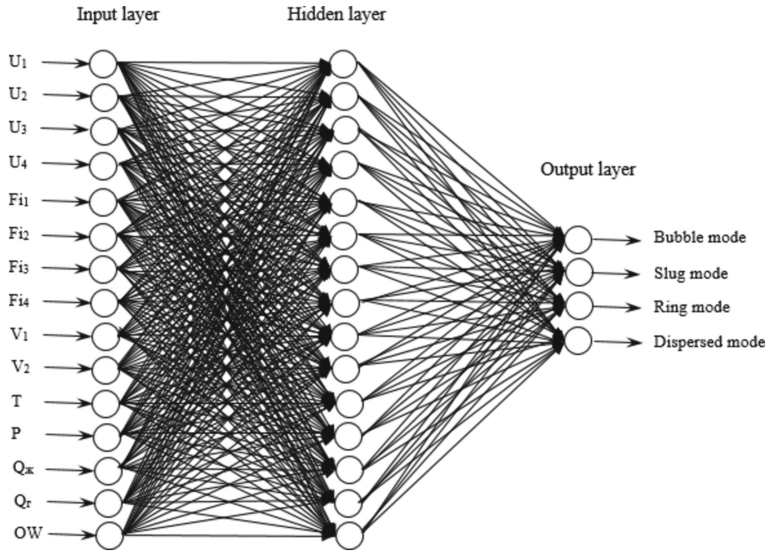


**Fig. 3.** Neural network with one hidden layer for solving the classification problem of oil and gas flow regime

In classification, neural networks have demonstrated outstanding performance due to their ability to perform deep learning and process unstructured data. They are able to automatically detect hidden patterns and patterns in data, allowing them to effectively classify objects with high accuracy. This ability to adapt and improve their predictions with increasing amounts of training data makes neural networks an ideal choice for a wide range of classification problems. The performance results of the various architectures considered are shown in Table 1.

The developed algorithms successfully cope with the assigned tasks, ensuring high accuracy and efficiency of operations.

**Table 1.** Neural networks test results.

| Neural Network Architecture | The training and test sets ratio, % / % | Testing accuracy (%) | F1 measure (%) |
|---|---|---|---|
| Single Layer NN, SLNN (dataset $D_0$) | 90/10 (37800/4200) | 99.56 | 99.30 |
| | 80/20 (33600/8400) | 99.38 | 99.05 |
| | 70/30 (29400/12600) | 99.38 | 99.05 |
| | 60/40 (25200/16800) | 99.43 | 99.12 |
| Single Layer NN, SLNN (dataset D) | 90/10(39150/4350) | 93.73 | 93.44 |
| | 80/20(3480/8700) | 93.96 | 93.68 |
| | 70/30(30450/13050) | 92.62 | 92.22 |
| | 60/40(26100/17400) | 92.95 | 92.58 |
| Convolutional NN, CNN (dataset D) | 90/10(39150/4350) | 99.97 | 99.98 |
| | 80/20(3480/8700) | 99.02 | 99.02 |
| | 70/30(30450/13050) | 99.88 | 99.88 |
| | 60/40(26100/17400) | 99.80 | 99.79 |

## 5 Conclusion

As part of this work, the following results were achieved:

- A definition of "functional separability" of classes was formulated, which was later used to limit the subject area. This made it possible to apply the developed FSNN algorithm;
- The FSNN algorithm has been developed. An ensemble FSNN algorithm is proposed using a CNN-based voting system. The research was supported by RSF (project No. 24–11-00285);
- The proposed solution fully meets the requirements of mathematical validity and limitations in the form of complexity of the neural network architecture.

**Acknowledgments.** The work was supported out with financial support from the Russian Science Foundation (project 24-11-00285), https://rscf.ru/project/24-11-00285/.

## References

1. Aggarwal, C.: Data Mining: The Textbook. Springer, Cham (2015). https://doi.org/10.1007/978-3-319-14142-8
2. Aggarwal, C.: Data Classification: Algorithms and Applications. CRC Press (2014)
3. Eremeev, A., Varshavskii, P., Kozhevnikov, A., Polyakov, S.: Integrated approach for data mining based on case-based reasoning and neural networks. In: Kovalev, S., Tarassov, V., Snasel, V., Sukhanov, A. (eds.) IITI 2021. LNNS, vol. 330, pp. 15–23. Springer, Cham (2022). https://doi.org/10.1007/978-3-030-87178-9_2

4. Haikin, Simon Neural networks: a complete course; M.: Williams - Moscow (2006). 781 p.
5. Rosenblatt, F.: The Perceptron: a probabilistic model for information storage and organization in the brain. Psychol. Rev. **65**, 386–408 (1958)
6. McCulloch W.S., Pitts W. A logical calculus of the ideas immanent in nervous activity // Bulletin of Mathematical Biophysics. 1943. Vol. 5. P. 115–133
7. LeCun, Y., et al.: Backpropagation applied to handwritten zip code recognition. Neural Comput. **1**(4), 541–551 (1989)
8. Hochreiter, S., Schmidhuber, J.: Long short-term memory. Neural Comput. **9**(8), 1735–1780 (1997)
9. Chung, J., Gulcehre, C., Cho, K., Bengio, Y.: Empirical evaluation of gated recurrent neural networks on sequence modeling. CoRR, vol. abs/1412.3555 (2014)
10. Smolensky, P.: Chapter 6: Information processing in dynamical systems: foundations of harmony theory. In: Rumelhart, D.E. McLelland, J.L. (eds.) Parallel Distributed Processing: Explorations in the Microstructure of Cognition, Volume 1: Foundations (англ.), pp. 194–281. MIT Press (1986). ISBN 0-262-68053-X
11. Ye, T.A.: Neural networks application for the classification problem solving with domain constraints. In: Ye, T.A., Mikhaylov, I.S., Myo, H.W., Zayar, A. (eds.) 2023 3rd International Conference on Technology Enhanced Learning in Higher Education (TELE). – Lipetsk, Russian Federation, pp. 220–224 (2023). https://doi.org/10.1109/TELE58910.2023.10184380
12. Guzhov, S., Varshavsky, P., Torop, D., Sesin, A., Bashlykov, M., Anokhov, D.: Development of a neural network module for forecasting demand for energy consumption by mass construction projects. In: E3S Web Conference, International Conference on Ensuring Sustainable Development: Ecology, Energy, Earth Science and Agriculture (AEES2023), volume 494, Article Number 03004, p. 9 (2024). https://doi.org/10.1051/e3sconf/202449403004
13. Ye, T.A.: Data mining methods application to solve oil wellproduction flow regimes problem classification. In: Ye, T.A., Mikhaylov, I.S., Myo, H.W., Zayar, A. (eds.) 2022 4th International Conference on Control Systems, Mathematical Modeling, Automation and Energy Efficiency (SUMMA), pp. 306–309 (2022). https://doi.org/10.1109/SUMMA57301.2022.9974010

# Signal Spreading Through a Ring of Asynchronous Threshold Elements

Oleg P. Kuznetsov(✉)

Institute of Control Sciences of RAS, Moscow, Russia
olpkuz@yandex.ru

**Abstract.** The processes of signal spreading in rings of asynchronous threshold elements are considered. An element can be in an active or passive state: if its potential exceeds a threshold, it is active. A chain is a network of elements $N_1$,…, $N_n$, in which the only output $N_i$ is connected to the only input $N_{i+1}$. The ring is obtained from the circuit by connecting the output $N_n$ to the input $N_1$. The conditions are given under which the ring, after applying an external signal, turns into a system of two-phase oscillators.

**Keywords:** threshold element · ring of elements · signal spreading · reverberation

## 1 Introduction

In works [1, 2], the propagation of signals in circuits of homogeneous (having the same parameters) threshold elements was considered. Three cases are possible: 1) the signal, passing through the circuit, maintains its duration; 2) the duration of the signal decreases, and in a sufficiently long circuit the signal fades, i.e. will not reach the last element; 3) the duration of the signal increases. This paper studies the propagation of signals in networks with a cyclic structure, i.e. having the form of a ring: a circuit in which the output of the last element is connected to the input of the first element. Since the ring case uses concepts and results for a chain, we repeat them here.

## 2 Basic Definitions. Signal Spreading Through a Chain

An asynchronous threshold element $N_i$ is an element whose state $y_i(t)$ is determined by the value of its potential $U_i(t)$, varying in the interval $U_{i0} \le U_i(t) \le U_{i\max}$, and the threshold $P_i$, lying in the same interval:

$$y_i(t) = \begin{cases} 1, \text{ if } U_i(t) \ge P_i; \\ 0 \ \ otherwise. \end{cases}$$

In the active state ($y_i(t) = 1$), element $N_i$ generates a power signal $d_i$. Other parameters of the element are the weights $w_{ij}$ of the inputs ($i$ - element number, $j$ - input


S. Kovalev et al. (Eds.): IITI 2024, LNNS 1209, pp. 410–419, 2024.
https://doi.org/10.1007/978-3-031-77688-5_39

number) and two endogenous rates of potential change ($v^0_{ien}$ for the passive state and $v^1_{ien}$ for the active state), independent of external influences. An element is called reactive if both endogenous velocities are negative. It is activated only in the presence of sufficiently strong external influences; in their absence, its potential tends to $U_{i0}$. The element is called asynchronous because the passage of the signal through it is significantly affected by switching on and off transient processes, which can create serious problems in asynchronous circuitry [3].

A homogeneous asynchronous chain of reactive elements $N_1$,…, $N_n$ is a network in which 1) the output $N_i$ is connected to a single input $N_{i+1}$, $i = 1, \ldots, n-1$; 2) input $N_1$ and output $N_n$ are external to the chain; 3) the values of the parameters $U_{i0}$, $U_{imax}$, $v^0_{ien}$, $v^1_{ien}$, $d_i$ are the same for any element; therefore the index $i$ is omitted. An example of a table specifying the chain parameters is given in Table 1. $N_0$ – external excitation source.

**Table 1.** Example of element parameters

| | $P$ | $U_{max}$ | $U_0$ | $v^0_{en}$ | $v^1_{en}$ | $D$ | $w$ |
|---|---|---|---|---|---|---|---|
| $N_0$ | | | | | | 1.3 | |
| $Ni$ | 0.4 | 0.8 | 0 | −0.8 | −0.5 | 1.3 | 1.0 |

The input action (signal) is supplied to input $N_1$. A signal passes through an element if, some time after the signal arrives, the element is activated and generates an output signal. The signal arrives at the $N_i$ if $N_{i\text{-}1}$ is active; as a result, the potential $N_i$ begins to change at a rate $v_i$, defined as follows:

$v_i(t) = s_i(t) + v^0_{en} = wdy_{i\text{-}1}(t) + v^0_{en}$, if the element is passive, and $v_i(t) = s_i(t) + v^1_{en} = wdy_{i\text{-}1}(t) + v^1_{en}$, if the element is active, where $wdy_{i\text{-}1}(t)$ is the exogenous speed determined by the power $d$ of the signal and the weight $w$ of the input $N_i$. The rate sign indicates the direction of change (increase or decrease) of the potential. Obviously, for the signal to pass through the element, the condition $s_i(t) > |v^0_{en}|$. is necessary.

Events in the chain are the moments of change in the state of any element, as well as the moments of reaching $U_0$ and $U_{max}$. They are represented by points on a continuous time scale, dividing the scale into time-steps. The boundaries of time-steps are numbered with natural numbers 0, 1,… And are called discrete moments of time. Time-step $t$ is a half-interval $[t, t + 1)$; its duration is denoted by $\tau(t)$.

In the absence of an external signal, the chain elements have potential $U_0$. When a signal of sufficient duration is applied, element $N_1$ goes into the active state and generates an output signal, starting the process of signal propagation through the chain. In this case, three cases are possible, described in the introduction. In [2], conditions were formulated under which one or another of the three cases occurs (see Table 2 below).

Figure 1 [1] shows a timing diagram of the functioning of a certain chain. Bold lines indicate periods of element activity. The signal no longer passes through the third element: the duration of activity of $N_2$ is not enough for $N_3$ to turn on. Vertical lines correspond to the boundaries of time-steps. Events may coincide: for example, the switching on of $N_1$ coincides with the beginning of the growth of potential $N_2$.

Let us consider the structure of the functioning process of the $N_i$. The on-off cycle of $N_i$, which begins with the supply of an input signal, will be called complete if it consists of 5 phases (see the graph for $N_1$ in Fig. 1): 1) charging (potential growth from $U_0$ to $P$, 2) potential growth from $P$ to $U_{\max}$; 3) the potential remains at the point $U_{\max}$; 4) discharge (decreasing potential from $U_{\max}$ to $P$); 5) potential drop to $U_0$. Let us denote the durations of these phases by $q_{1i}, q_{2i}, q_{3i}, q_{4i}, q_{5i}$, where $i = 1, \ldots, n$ – element number. Phases 1 and 2 are said to be complete in a given cycle if they are followed by phases 2 and 3, respectively; phases 4 and 5 are complete if they are preceded by phases 3 and 4, respectively. Without loss of generality, we assume that the power $d_0$ of the external signal is equal to $d$. In any case, starting from the output of the first element, the power signal $d$ will propagate through the circuit. Therefore, if $d_0 \neq d$, the results obtained are valid for a circuit where $N_1$ is an external source and the circuit starts from element $N_2$. Further, $Q_0$ is the duration of the external signal; $Q_i$ is the duration of activity of $N_i$ and its output signal, $t_{ji}$ is the moment of the beginning of phase $j$ of element $N_i$, $t_{zi}$ is the moment of $U_i$ falling to $U_0$. For an external signal, $t_{00} = 0$ is the moment of its beginning, $tz_0$ is the moment of its end. Some events coincide: for example, $t_{z0} = t_{41}$.

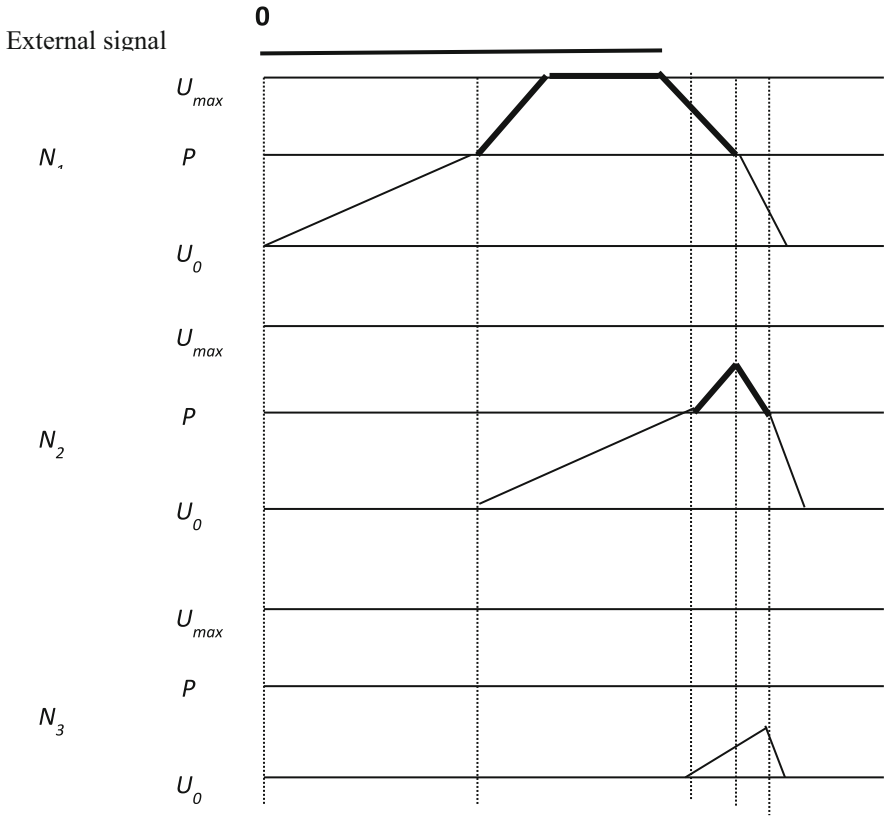


**Fig. 1.** Timing diagram of signal propagation through a chain of 3 elements.

The signal is called long if $Q_i \geq q_1 + q_2$, short if $q_1 < Q_i < q_1 + q_2$, insufficient if $Q_i \leq q_1$. With a long signal, the element reaches $U_{\max}$ and thus phase 3; with a short signal, the element is activated, but does not have time to reach phase 3; if the signal is insufficient, the element potential does not reach the threshold, the element is not activated and does not generate a signal.

**Table 2.** Signal propagation along the circuit at various ratios $q_1$ and $q_4$.

| Signal | Type 1: $q1 = q4$ | Type 2: $q1 < q4$ | Type 3: $q1 > q4$ |
|---|---|---|---|
| Long | Passes with preservation of duration | Passes with increasing duration | Shortens; does not pass with a chain length $n < z1$ |
| Short | Shortens; does not pass with a chain length $n < z3$ | There is a point of equilibrium:<br>1. The equilibrium signal passes with the preservation of duration;<br>2. a signal shorter than the equilibrium one does not pass with a chain length $n < z2$;<br>3. a signal longer than the equilibrium one passes with increasing duration | |
| Insufficient | Does not pass through the first element | | |

The main results of signal propagation through the chain are contained in Table 2 [2]. The equilibrium point mentioned in it is such a value $\varepsilon^* \leq q_2$, that an external signal of duration $\varepsilon^* \leq q_2$, (equilibrium) passes through the chain without changing the duration.

## 3 Signal Propagation in the Ring. Duration Preservation Case

A homogeneous ring of reactive elements $N_1$,…, $N_n$ is a network obtained from a homogeneous chain by connecting the output of the last element to the input of the first element. Therefore, when analyzing signal propagation along the ring, the properties of the chain and, accordingly, the definitions and results of the previous section will be used.

In this section we will look at the basic case:

Case 1: the signal is long and $q_1 = q_4$, i.e. the duration of $Q_0$ in the first cycle is preserved.

For this case, we prove the following statement.

**Lemma.** Let $q_1 = q_4$. Then, if any element of the ring is active during the segment [$t$, $t'$], the duration of which exceeds $nq_1$, i.e.

$$t' > t + nq_1, \tag{1}$$

then all elements of the ring are active at any moment $t'' > t'$.

Let some element $N_i$, $1 \le i \le n$, be active on the interval [$t$, $t'$], and $t' - t > nq_1$. Then element $N_i + 1$ is active on the interval $[t + q_1, t' + q_1]$, element $N_{i+2}$ is active on the interval $[t + 2q_1, t' + 2q_1]$,…, element $N_n$ is active on the interval $t + (n - i)q_1$, $t' + (n - i)q_1]$,…, element $N_{i-1}$ is active on the interval $[t + nq_1, t' + nq_1]$. From (1) it follows that 1) a signal of duration $t' - t$ comes from $N_{i-1}$ to the input $N_i$, when $N_{i-1}$ is still active, and, therefore, will be active for the duration $t' - t$; 2) on the interval [$t + nq_1$, $t'$] all elements of the ring are active. Repeating this reasoning for moment $t'$ and subsequent moments separated from each other at a distance $t' - t$, we obtain that all elements of the ring will be active at any moment $t'' > t'$.

For case 1, 4 options are possible, differing in the duration $Q_0$ of the input signal.

$$1.1 \qquad nq_1 \le Q_0. \tag{2}$$

This means that either the number of ring elements is small, or the duration of the external signal is quite long.

Since the condition of the lemma is already satisfied for the external signal, thanks to the preservation of the duration, it will also be satisfied for $N_1$. It follows that all elements of the ring will be active indefinitely, starting from moment $nq_1$.

$$1.2 \qquad Q_0 < nq_1 \le Q_0 + q_1. \tag{3}$$

In this case, the external signal ends before the moment $nq_1$ of activation of $N_n$, but the moment $nq_1$ occurs before the moment $Q_0 + q_4 = Q_0 + q_1$, when the activity of $N_1$ should have ended. Therefore, the forefront of the signal from $N_n$ will catch $N_1$ in phase 4, when it is still active, and, consequently, its activity will last at least until the moment $nq_1 + Q_0 + q_1 = (n + 1)q_1 + Q_0$, and at this moment $N_1$ will be in phase 3. Thus, $N_1$ will be active on the interval $[q_1, n + 1)q_1 + Q_0]$,, i.e. the conditions of the lemma for $N_1$ are satisfied, and all elements of the ring will be active indefinitely, starting from moment $nq_1$.

$$1.3 \qquad nq_1 = Q_0 + q_1 + q_{15}, \tag{4}$$

where $q_{15}$ is the duration of shortened phase 5 of element $N_1$. In this case, the forefront of the signal from $N_n$ will catch $N_1$ in phase 5, when it is already turned off, but has not yet reached $U_0$ (see Fig. 2). Phase 1 for $N_1$, starting the second cycle, will also be less than full; let's denote its duration by $q_{11}$. The second time $N_1$ is activated at the moment $Q_0 + q_1 + q_{15} + q_{11}$.

$N_2$ activity in the first cycle begins at time $2q_1$. If the inequality $2q_1 + Q_0 > q_1 + Q_0 + q_{15} + q_{11}$ is true, which is equivalent

$$q_1 > q_{15} + q_{11}, \tag{5}$$

then the pause between two activities $N_1$ is less than $q_1$, and accordingly $q_4$. Therefore, the re-activation of $N_1$ will begin when the activity of $N_2$ in the first cycle has not yet ended, i.e. $N_1$ will be active on the interval $[q_1 + Q_0 + q_{15} + q_{11}, Q_0 + q_1 + q_{15} + q_{11} + Q_0]$, which after transformations looks like this:

$$\left[q_1 + Q_0 + q_{15} + q_{11}, Q_0 + nq_1 + q_{11}\right]. \tag{6}$$

Then $N_2$ will be continuously active on the interval $[2q_1, Q_0 + (n + 1)q_1 + q_{11}]$, the duration of which is

$$Q_0 + (n + 1)q_1 + q_{11} - 2q_1 = Q_0 + (n - 1)q_1 + q_{11}, \tag{7}$$

which, taking into account (4), is obviously greater than $nq_1$. Thus, the conditions of the lemma are satisfied for $N_2$, and therefore, starting from the moment $q_1 + Q_0 + q_{15} + q_{11}$ (the beginning of the interval (6)), all elements of the ring will be active indefinitely.

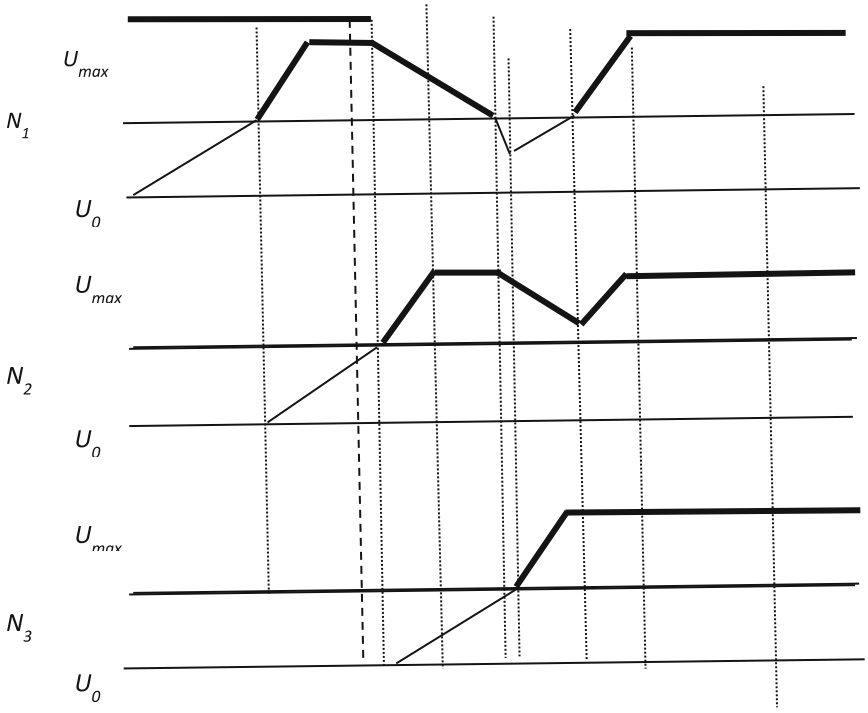


**Fig. 2.** Case 1.3a

If instead of (5) it is true

$$q_1 < q_{15} + q_{11}, \tag{8}$$

then the behavior of the ring depends on the specific relationships between the number $n$ of elements in the ring, the duration of the external signal $Q_0$ and the parameters of

the ring elements. To obtain these relations, we denote the value of the potential $U_1$ at the moment $q_{15}$ by $x_1$ and express $q_1$, $q_{15}$, $q_{11}$ in terms of $x_1$ and the parameters of the ring elements. We get

$$1 = \frac{P}{wd - |v_{en}^0|}, \tag{9}$$

$$q15 = \frac{P - x_1}{|v_{en}^0|}, x1 = P - q15|v_{\text{en}}^0|, \tag{10}$$

$$q11 = \frac{P - x_1}{wd - |v_{en}^0|}. \tag{11}$$

Representing equality (4) in the form $(n - 1)q_1 = Q_0 + q_{15}$ and substituting the right-hand sides (9) and (10) into it, we obtain

$$\frac{P(n-1)}{wd - |v_{en}^0|} = Q0 + \frac{P - x_1}{|v_{en}^0|}. \tag{12}$$

Inequality (8) after similar substitutions and transformations takes the form

$$P < (P - x1)\frac{wd}{|v_{en}^0|}. \tag{13}$$

Besides,

$$0 < x_1 < P. \tag{14}$$

Relations (4), (12) – (14) and the general conditions of case 1 (the signal is long and $q_1 = q_4$) determine the possible values of n and $Q_0$ for case 1.3 and the behavior of the ring for different sets of these values. Let us illustrate with an example one of the possible options.

**Example.** Let the parameters of the ring elements be given in Table 1, $n = 4$. Then $wd = 1.3$; $wd - |v_{\text{en}}^0| = 0.5$. From (4) we obtain $3{\cdot}0.8 = Q_0 + q_{15}$ and $q_{15} = 2.4 - Q_0$. Using this expression for $q_{15}$ in (10), we obtain $x_1 = 0.8\ Q_0 - 1.52$. Substituting this expression into (14) gives a pair of inequalities $0 < 0.8\ Q_0 - 1.52 < 0.4$. As a result, we obtain the range of values $Q_0$.

$$1.9 < Q_0 < 2.4, \tag{15}$$

for which case 1.3 occurs for given parameter values.

Let us now consider the behavior of the ring with these parameters and $Q_0 = 2$. Then $q_{15} = 0{,}4$, $x_1 = 0{,}08$, $q_{11} = 0{,}64$ and inequality (8) is satisfied. The second activity $N_1$ will occur at the moment $t_{c12} = Q_0 + q_1 + q_{15} + q_{11} = 2 + 0.8 + 0.4 + 0.64 = 3.84$ and will last at least until the moment $3.84 + 2 = 5.84$.

The first cycle of $N_2$ activity consists of segments $2q_1$, $Q_0$, $q_{25}$ and ends at $t_{c12}$. We get the equation

$$t_{c12} = 2q_1 + Q_0 + q_{25},$$

whence $q_{25} = 3.84 - 1.6 - 2 = 0.24$, $x_2 = 0.4 - 0.24 \cdot 0.8 = 0.208$, $q_{21} = (0.4 - 0.208)/0.5 = 0.384$. Thus, the second activity of $N_2$ will occur at the moment $t_{c22} = t_{c12} + q_{21} = 4.324$ and will last at least until the moment 6.324.

$N_3$ activity begins at time $3q_1$, and its duration is at least $Q_0$. But $3q_1 + Q_0 = 2.4 + 2 = 4.4 > t_{c22}$. Therefore, at the moment $t_{c22}$, when $N_3$ is still active, a new signal from $N_2$ will arrive at its input, and, therefore, the activity of $N_3$ will last at least on the interval $[3q_1, t_{c22} + Q_0]$, the length of which significantly exceeds $4q_1$. Thus, for $N_3$ the conditions of the lemma are satisfied, and, starting from the moment $t_{c22} + Q_0]$, all elements of the ring will be active indefinitely.

$$1.4. \quad nq_1 = Q_0 + q_1 + q_5 + q_x. \tag{16}$$

In this case, the forefront of the signal from $N_n$ will arrive at input $N_1$ when $U_1(nq_1) = U_0$. This situation exactly repeats the situation of the first cycle, with the difference that the role of the external signal for $N_1$ is played by a signal from $N_n$ with the same duration $Q_0$, and $q_x$ is the segment between the moment when the potential $N_1$ reaches $U_0$ and the moment $nq_1$. Therefore, the structure of the second cycle for $N_1$ will coincide with the structure of the first cycle, which is a sequence of segments $[q_1, Q_0, q_5, q_x]$ and will be repeated indefinitely.

Thus, a ring of asynchronous threshold elements turns into a system of two-phase oscillators, where the duration of the period is equal to $nq_1$, the duration of the unit phase (activity phase) is equal to $Q_0$, and the duration of the zero phase is equal to $q_5 + q_x + q_1 = nq_1 - Q_0$, and for $N_1$ the unit phase in the first cycle it starts at time $q_1$, and for each subsequent element it is shifted by $q_1$. An illustration of this case is shown in Fig. 3.

Case 1.4 is known in biology as reverberation [4].

## 4 Signal Propagation in the Ring. Other Cases

In case 1, two types of behavior of the ring are possible: either an oscillatory process is established in the ring (option 1.4), or ultimately the entire ring is excited and remains so indefinitely. The transition to constant excitation can begin from any element of the ring and occur both in the first cycle and in subsequent cycles.

The behavior of the ring for other cases is determined by similar cases for the chain indicated in Table 2. If the parameters of the elements and the duration of the external signal are such that when passing through the circuit of these elements the signal will be shortened, then in the ring it will also be shortened, and ultimately the ring will become completely passive. Depending on the number of elements in the ring and the duration of the external signal, this can happen either in the first cycle or in subsequent ones. If the signal in the circuit passes with increasing duration, then a ring of these elements will ultimately become, as in cases 1.1–1.3 excited for an infinitely long time.

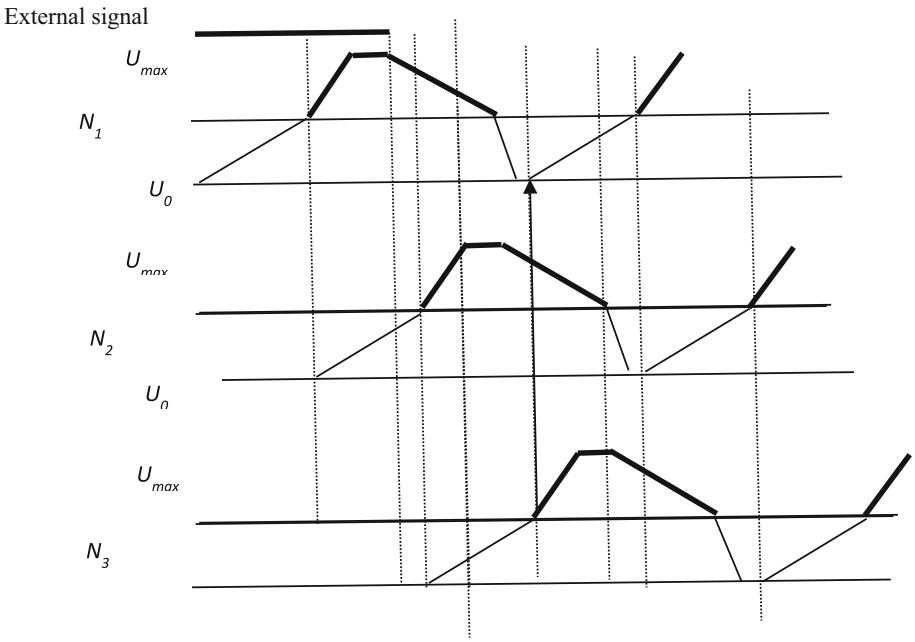


**Fig. 3.** Case 1.4 for a ring of 3 elements. The vertical arrow shows the beginning of the second cycle

## 5 Conclusion

The results obtained can be used in neurobiology both in the analysis of reverberation processes [4] and linear propagation of signals in nervous systems [5, 6]. It is interesting to note that the three possible stable states of the ring (constantly excited, constantly passive and oscillatory) correspond to three modes of electrical activity of neurons - Tonic, reactive and oscillatory (phasic) [7–10].

## References

1. Kuznetsov, O.P.: On the condition for the passage of signal through a chain of asynchronous threshold elements. Autom. Remote Control **83**(6), 919–934 (2022)
2. Kuznetsov, O.P.: Signal spreading through a chain of asynchronous threshold elements/lecture notes in networks and systems. In: Proceedings of the Fifth International Scientific Conference "Intelligent Information Technologies for Industry" (IITI'21), vol. 330, pp. 24–34 (2022)
3. Brzozowski, J.A.: Topics in asynchronous circuit theory. Recent Adv. Formal Lang. Appl. **25**, 11–42 (2006)
4. Ribeiro, S., Gervasoni, D., Soares, E., Yi, Z., Lin, Sh.-Ch., Pantoja, J., Lavine, M., Nicolelis, M.: Long-lasting novelty-induced neuronal reverberation during slow-wave sleep in multiple forebrain areas. PLoS Biol. **2**(1), E24 (2004)
5. Reyes, A.D.: Synchrony-dependent propagation of firing rates through layered networks of noisy neurons. Nat. Neurosci. **6**(6), 593–599 (2003)

6. Feinerman, O., Segal, M., Moses, E.: Signal propagation along unidimensional neuronal networks. J. Neurophysiolog. **94**(5), 3406–3416 (2005)
7. Liu, C., Goel, P., Kaeser, P.S.: Spatial and temporal scales of dopamine transmission. Nat. Rev. Neurosci. **22**(6), 345–358 (2021)
8. Roberts, P.D.: Classification of temporal patterns in dynamic biological networks. Neural Comput. **10**(7), 1831–1846 (1998)
9. Wiencke, K., Horstmann, A., Mathar, D., Villringer, A., Neumann, J.: Dopamine release, diffusion and uptake: a computational model for synaptic and volume transmission. PLoS Comput. Biol. **16**(11), e1008410 (2020)
10. Bazenkov, N.I., Boldyshev, B.A., Dyakonova, V.E., Kuznetsov, O.P.: Simulating small neural circuits with a discrete computational model. Biol. Cybern. **114**(3), 349–362 (2020)

# Advanced Metrics for the Detection Problem on Perspective Transformed Images

Andrew Ponomarev[1](✉), Anton Agafonov[1], Alexander Smirnov[1], Nikolay Shilov[1], Andrey Sukhanov[2], and Andrey Shulzhenko[2]

[1] SPC RAS, 14th Line, 39, 199178 St. Petersburg, Russian Federation
{ponomarev,smir,nick}@iias.spb.su, agafonov.a@spcras.ru
[2] Rostov Branch of JSC NIIAS, Lenina, 44/13, 344038 Rostov-on-Don, Russian Federation
{a.suhanov,a.shulzhenko}@vniias.ru

**Abstract.** Machine Learning-based object detection and tracking are powerful techniques employed in variety of applications. In some cases, the cameras' point-of-view is rather wide and detected objects are obscured by the perspective (it is often the case in surveillance and technical vision use cases). This paper describes a simple yet effective technique to deal with this problem. The core of the technique is object detection on perspective transformed (warped) images. Such transformation allows to simplify the spatial structure of the image and, therefore, its analysis. In some cases, after the proposed transform a detection problem can be recast as unidimensional. The paper proposes several specialized metrics for measuring the quality of unidimensional detection problem, as well as encompasses several ways to leverage the simplified structure of the image during detection model training. The proposed methods are illustrated by a practical application of positioning wagons on a classification bowl of the sorting freight railway station.

**Keywords:** Computer Vision · Object Detection · Object Tracking · Image Processing · Problem-Specific Metrics · Railway Objects Detection · Hump Yard Intelligence

## 1 Introduction

Object detection and tracking using machine learning are widely used across various fields. In some situations, cameras have a wide field of view, causing detected objects to be partially obscured and distorted due to perspective; for example, it is a common issue in surveillance, monitoring and technical vision scenarios. Inverse perspective transformation facilitates the simplification of an image's spatial structure, thereby streamlining its analysis. In certain applications, following this transformation, the detection task can be converted into a unidimensional problem. Although widely used metrics for detection tasks in most cases accurately reflect the typical objectives of using detection models, they may be inefficient in the case of unidimensional settings. In addition, there are scenarios where, although the images possess a specific structure that constrains where the objects of interest can be located, the application itself might be more susceptible


S. Kovalev et al. (Eds.): IITI 2024, LNNS 1209, pp. 420–430, 2024.
https://doi.org/10.1007/978-3-031-77688-5_40

to certain types of errors while being more forgiving of others. One of the applications where the need arises to use problem-specific metrics (and a motivating application for this paper) is the detection of railway objects.

A key freight railway station of each country consists of hump yard and classification bowl (Fig. 1) [1].

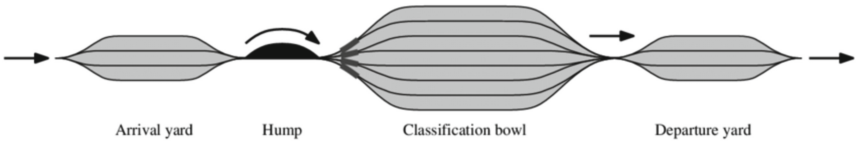


**Fig. 1.** Railway freight station with hump yard

Hump yard provides breaking up of inbound trains staying at arrival yard into the cuts of several cars, which are humped then into classification bowl and making up into new outbound trains following to departure yard. Classification bowl consists of significant number of sorting tracks (more than 40 tracks for a big station) with the total length of 40 km. To correctly automate the hump yard management, it is required to automate the control over position of every rolling stock (car wagon or locomotive) on every track.

Almost all railway sensors allow to control the position on only one railway track and must be placed into the rails. Because of this it is rather difficult to track the wagons in classification bowl using the sensors placed directly on rails. In 2021, we've implemented the computer vision complex for classification bowl control (entitled KZSP) [2, 3]. Its profit is control over rolling stocks placed on multiple tracks. It detects the key objects (objects of interest), which are railway rolling stocks, on the preliminary transformed (warped) image (Fig. 2) obtained from camera. For the obtained image, warping is utilized to eliminate the perspective errors and make the objects rectangular (which is typical for object detection problems) not parallelogram. Resulting coordinates of objects are mapped into the scheme of classification bowl (Fig. 3), which is a profit of KZSP recently implemented by authors.

This paper refers to the problem of metrics choice for machine learning (ML) algorithms applying for the warped image. We propose the unidimensional metrics, which allow to correctly evaluate ML model, when the dimensions of images are not equivalent (i.e. objects can be placed along the certain lines of images). We also propose modifications to several popular loss functions in order to improve model training in these situations. Authors believe that the result is prominent not only for the certain example of railway rolling stock tracking problem, but also for other areas, where the vertical and horizontal axes of an image differently affect on the detection result.

Section 2 describes the proposed metrics and its advantages with the conventional ones (e.g., IoU, mAP@). Section 3 proposes Loss Function optimization. The experimental results with the real data are presented in Sect. 4. The conclusion and future work are shown in Sect. 5.

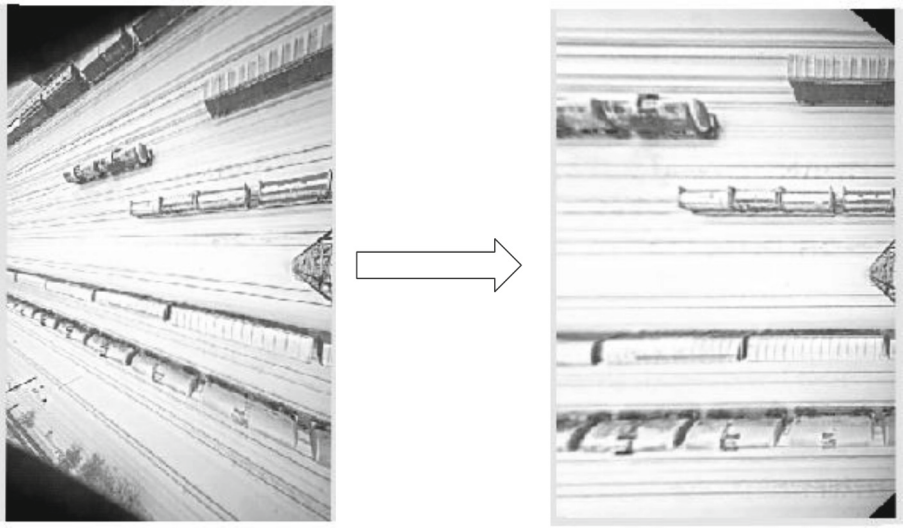

**Fig. 2.** Frame obtained from camera and warped one

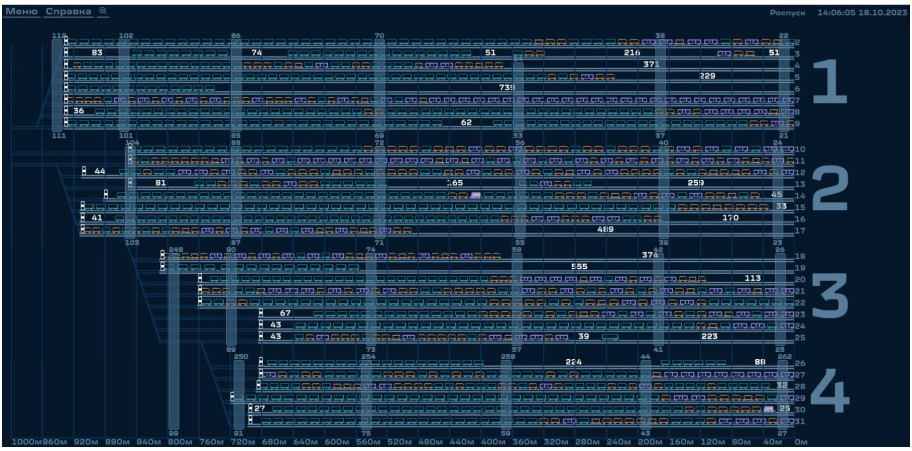


**Fig. 3.** Results of image detection algorithm mapped into classification bowl scheme (user interface of KZSP)

## 2 Unidimensional Metrics for the Detection Problem

Widely used metrics for the detection problem (e.g., IoU, mAP@) [4, 5] perfectly capture typical goals of employing the detection models – when the object of interest may occur in any part of an image, the end user wants that this object was correctly located (IoU mostly corresponds to this goal) and was correctly recognized (mAP@ measures mostly that). However, in some practical cases the images, on the one hand, may have certain structure (limiting possible locations of the objects of interest), on the other hand, the

application might be more sensitive to one errors and less sensitive to other. This situation generally calls for adjusted metrics, more precisely aligned with the application goals.

A prominent example of such situation is a railroad scene of classification bowl after warping. Such image contains several vertical regions, corresponding to the railroad tracks, and rolling stock moves only inside the corresponding vertical region and along its vertical axis. This gives certain structure to the images. Besides, the rolling stock positioning problem is mostly focused on determining the position inside the respective track, therefore, the error of the bounding polygon along the vertical axis becomes the most interesting, and the accuracy along the horizontal axis should only be sufficient to assign the bounding box to the correct track.

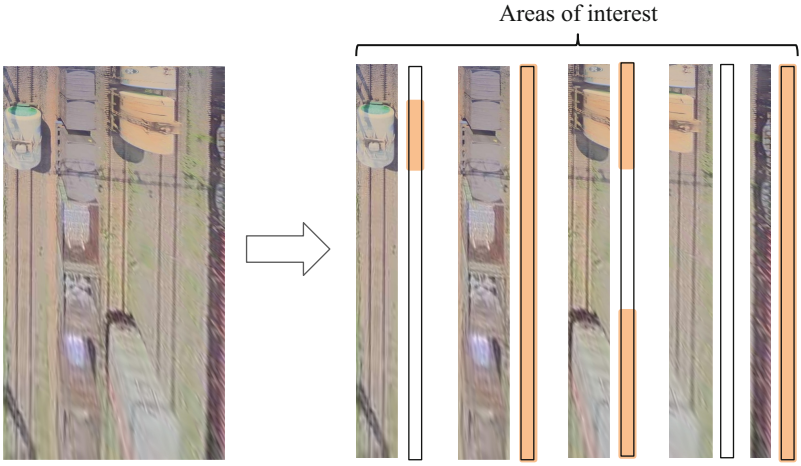


**Fig. 4.** Example of decomposition of an image into several independent vertical areas of interest (railroad tracks) on which objects of interest can be located.

This allows to recast the problem (at least, for the purpose of measuring success) as a pseudo-unidimensional one, where each track can be perceived as a separate area of interest, defining the (unidimensional) line along which objects of interest may be located (and move). The goal is to detect the presence and estimate the position of the objects of interest along that line (see Fig. 4).

In particular, there are two aspects of the problem that have to be adequately addressed by the metrics:

1. Object of interest identification quality, i.e., how identified objects of interest correspond to the real ones. In this paper, we assume that there is only one type of object of interest (this assumption is driven by the application of KZSP), however, this approach can easily be generalized to the multi-class case.
2. Positioning error for the objects of interest. As it was already noted, positioning error is important only in one dimension (along the area of interest, or the railroad track, if speaking in the application terms).

The first aspect can be captured by widely used metrics in information retrieval i.e. Recall, Precision, and F1. However, to estimate these metrics one has to define what are the true and false positives (as well as negatives). When the model output is binary, it is straightforward, however, in the considered case of a pseudo-unidimensional detection, the model output as well as ground truth are represented as segments. In this case, positives can be formalized similarly to the widely used metrics in detection, based on segment intersection. If the predicted segment significantly intersects one of the ground truth segments, then it is considered a true positive, if not, it is considered a false positive, all the ground truth segments not intersected with any of the predicted segments are considered false negatives. To quantify the intersection significance one can adapt the popular IoU metric to a one-dimensional case.

Let $x$, $y$ be two segments, and $l(.)$ and $r(.)$ be left and right bounds of these segments (segment start and end respectively), then:

$$\cap_{1D}(x, y) = (\max(l(x), l(y)), \min(r(x), r(y)),$$

$$\cup_{1D}(x, y) = (\min(l(x), l(y)), \max(r(x), r(y))),$$

$$IoU_{1D}(x, y) = \frac{\cap_{1D}(x, y)}{\cup_{1D}(x, y)}.$$

Please, note, that in the particular case used for the illustration, segments are vertically oriented, so we could also refer to their bounds as top and bottom rather than left and right. We decided to use left and right as horizontal orientation seems to be more natural for a unidimensional object. To obviate this confusion, one could also refer to the bounds as minimal and maximal value along the dimension respectively.

Segment matching (to identify positives and negatives) is done using Algorithm 1. Note, that the set returned by the Algorithm 1 is valid only in context of a certain threshold $\theta$ – a greater value of this threshold corresponds to a more restrictive definition of true positive (and it is expected that the number of true positives is non-increasing with the $\theta$). Therefore, it is reasonable to refer to all these values in the context of a certain $\theta$; we will denote the number of true positives for the threshold value $\theta$ as $TP@\theta$.

**Algorithm 1. Segment matching**

**Input**: $Y$ – the set of true segments for the area of interest,
$\hat{Y}$ – the set of predicted segments for the area of interest,
$\theta$ – threshold for $IoU_{1D}$ ($\theta \in [0.5; 1.0]$).

```
TP := ∅
for p ∈ Ŷ:
  for q ∈ Y:
    if IoU_1D(p, q) ≥ θ:
      TP := TP ∪ {(q, p)}
      Ŷ := Ŷ \ {p}
      Y := Y \ {q}
return TP
```

Model detection metrics are defined in the following way:

$$Recall_{1D}@\theta = \frac{\sum_i \left| TP@\theta\left(Y_i, \widehat{Y}_i\right)\right|}{\sum_i |Y_i|},$$

$$Precision_{1D}@\theta = \frac{\sum_i \left| TP@\theta\left(Y_i, \widehat{Y}_i\right)\right|}{\sum_i |\widehat{Y}_i|}.$$

here summation is done along all the areas of interest.

Positioning quality is measured only for true positives and is defined based on the boundary error for each correctly recognized segment:

$$PE@\theta = \sum_i \sum_{y,\hat{y} \in TP@\theta\left(Y_i, \widehat{Y}_i\right)} \left|l(y) - l\left(\hat{y}\right)\right| + \left|r(y) - r\left(\hat{y}\right)\right|.$$

The proposed metrics are illustrated in Fig. 5. In the figure only one area of interest is considered, there are two true segments (objects) and two predicted. However, the first predicted segment doesn't significantly intersect with any of the true segments, while the second one does. This gives both *Recall*@0.5 and *Precision*@0.5 of 0.5. *PE*@0.5 is calculated based on the only matching pair.

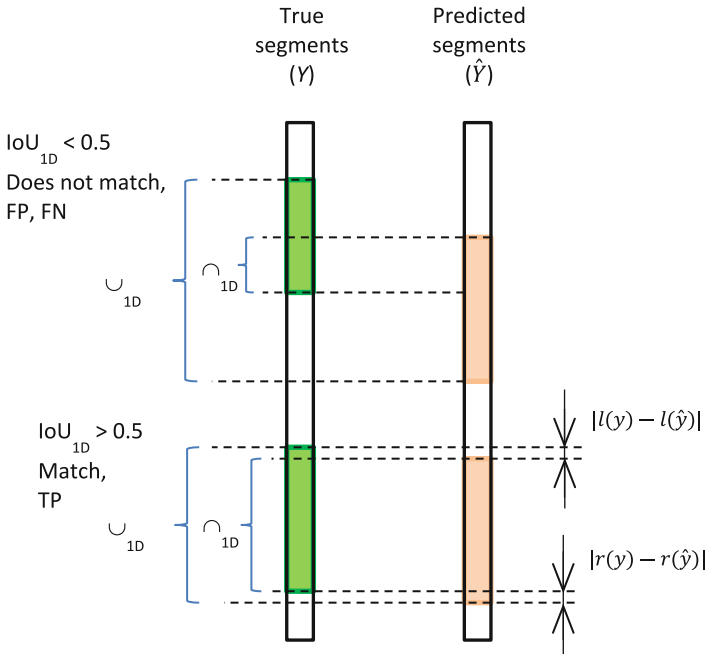


**Fig. 5.** Illustration for the metrics calculation.

## 3 Loss Function Adaptations for Unidimensional Detection Problem

While the proposed metrics are well-aligned to the goals of object detection and are useful for evaluating models, they cannot be directly used during optimization process (i.e., model training). In order to reduce the gap between problem-specific metrics proposed in the previous section and the optimization objective we also propose adjustments to typical loss functions widely used for detection. The rationale is that we can force the model to account for the specifics of the situation during the training process, thus, improving the problem-specific metrics. In particular, we consider loss functions used by various generations of YOLO models. We decided to focus on YOLO (rather than other detection architectures), because inference time is important in the motivating application (wagon tracking) and YOLO architecture provides an appealing tradeoff between inference time and detection quality.

Object detection using YOLO models and its various modifications has become widespread in a number of applications [6, 7]. So, in [8], the problem of detecting ships is considered and a method for improving YOLOv8 is proposed, based on the integration of LW-swin transformer [9] into it, which strengthens the representation capability of the detection network. In [10], the problem of detecting cows is considered and a modification of YOLOv7 is proposed to address the problem of low detection accuracy caused by non-uniform cow distribution and large target scale changes. In [11], the problem of animal detection is considered, a YOLO-based network is proposed, into which the authors integrate DenseNet blocks and two proposed residual blocks for effective extraction of spatial features. In [12], an improved object detection model based on the YOLOv5 model is proposed to improve the accuracy of detecting key components of power transmission lines. Several papers address the problem of underwater detection [13, 14] and suggest ways to improve YOLO for video object detection. In particular, a loss function is proposed in [13], including regression and jitter losses.

The proposed adjustments to the loss function are based on the same observation as the proposed metrics – for unidimensional detection problem positioning error along one dimension is crucial, but along the other dimension it is irrelevant. However, when doing unidimensional detection via postprocessing after the conventional 2D segmentation, absolutely ignoring the other dimension will cause severe errors (the recognized boxes are not “forced” to overlap with the training ones – only to be located on the same vertical “level”). Therefore, errors along the both dimensions must contribute to the loss, however, we can ensure that error on one dimension is more important than the error along the other.

### 3.1 MSE-Based Loss

Object detection loss is typically a complex function penalizing both misclassifications and bounding box positioning errors. More precisely, it is typically a sum of several components. In MSE-based object detection loss functions positioning errors are dealt with by MSE components, penalizing bounding box center and geometry (width and height) mismatch. For example, the loss function of the original YOLO model [15] includes the following components:

$$\mathcal{L}_{MSE} = \lambda_{coord} \sum_i \sum_j \mathbb{I}_{ij}^{obj} \left[ (x_i - \hat{x}_i)^2 + (y_i - \hat{y}_i)^2 \right] + \lambda_{coord} \sum_i \sum_j \mathbb{I}_{ij}^{obj} \left[ \left( \sqrt{w_i} - \sqrt{\hat{w}_i} \right)^2 + \left( \sqrt{h_i} - \sqrt{\hat{h}_i} \right)^2 \right].$$

Here, $i$ iterates over image cells and $j$ – over candidate bounding boxes in each cell, multiplication by an indicator $\mathbb{I}_{ij}^{obj}$ means that the loss penalizes bounding box coordinate error if that predictor is "responsible" for the ground truth box (i.e. has the highest IOU of any predictor in that grid cell).

A straightforward way of embedding the idea that one dimension is more important than the other one in such loss function is by adding a weighting factor $\lambda \in (0; 1)$ for one of the dimensions:

$$\mathcal{L}^*_{MSE} = \lambda_{coord} \sum_i \sum_j \mathbb{I}_{ij}^{obj} \left[ (1-\lambda)(x_i - \hat{x}_i)^2 + \lambda (y_i - \hat{y}_i)^2 \right] + \lambda_{coord} \sum_i \sum_j \mathbb{I}_{ij}^{obj} \left[ (1-\lambda) \left( \sqrt{w_i} - \sqrt{\hat{w}_i} \right)^2 + \lambda \left( \sqrt{h_i} - \sqrt{\hat{h}_i} \right)^2 \right].$$

With $\lambda = 0.5$ $\mathcal{L}^*_{MSE}$ gives the same importance to the both dimensions, however, one might still want to adjust $\lambda_{coord}$, because the total weight of the positioning error becomes two times less than in the original version.

Note, though, that this loss is mostly used by early object detection models, e.g. original YOLO model [15] and currently is mostly superseded by IoU-based losses.

### 3.2 IoU-Based Losses

Modern object detection models mostly use the IoU-based losses: GIoU [16], CIoU [17], EIoU [18], etc. All these losses include the calculation of the IoU between the ground truth box and the prediction; they differ by additional terms accounting for certain unwanted situations. E.g. CIoU (used in YOLOv8 [19]) is defined by the following expression:

$$\mathcal{L}_{CIoU} = 1 - IoU + \frac{d^2}{C^2} + \alpha v.$$

In this case, relative importance of one dimension can be established by an additional term:

$$\mathcal{L}^*_{*IoU} = \mathcal{L}_{*IoU} + \lambda \left[ (y - \hat{y})^2 + \left( h - \hat{h} \right)^2 \right].$$

Here, $\mathcal{L}_{*IoU}$ is the original loss, $y$ and $\hat{y}$ are $y$-coordinates of the centers of the ground truth bounding box and the predicted bounding box, $h$ and $\hat{h}$ are the heights of the ground truth bounding box and the predicted ones, and $\lambda \geq 0$ is the weight of the additional term.

## 4 Experimental Evaluation

In this section, we compare two approaches to object detection on transformed images obtained from KZSP cameras. The first approach is using standard 2D object detection followed by post-processing, the second approach is cutting transformed images into areas of interest followed by unidimensional detection.

To compare these approaches, we use a dataset collected from a sorting hump, consisting of 6111 images of 720 $\times$ 1280. On each image there are several tracks (typically 4 or 5), and on each track there may be zero or more carriages.

The dataset was split into train and test sets, consisting of 5020 and 1091 images respectively. The split was done in such a way, that all images from one camera (representing one point of view) were assigned either to train or to test subsets.

The first approach (YOLOv8+ in the Table 1) is pre-trained (on COCO dataset) YOLOv8 (small) trained with $\mathcal{L}^*_{EIoU}$. We used the following hyperparameters: $\lambda = 2$; 300 epochs; patience is 50; batch size is 65; image size fed into the model is 640. An SGD optimizer with a learning rate of 0.01 was used. YOLOv8 was the last version of this architecture at the time of writing. Note, that the architecture itself remains intact, we only modified the loss function.

Model predictions were split into areas of interest and unidimensional metrics were calculated for each area.

The second approach (UD in the Table 1) is the unidimensional detection network of a custom architecture. This network receives only one area of interest as input and outputs segments detected in this area.

**Table 1.** Detection Quality Comparison

| Metric ($@IoU_{1D} = 0.5$) | YOLOv8+ | UD |
|---|---|---|
| $Precision_{1D}$ | **0.9905** | 0.9079 |
| $Recall_{1D}$ | **0.9932** | 0.9743 |
| $PE_{1D}$ | **0.0071** | 0.0205 |

It can be seen from the Table 1, that unidimensional approach to learning turned out to be significantly worse than the YOLOv8 trained with the proposed $\mathcal{L}^*_{EIoU}$. It can be explained by several factors. First, cutting into the areas of interest reduces the context available to the model, which makes it harder to analyze an image. Second, the UD model was not pretrained on a large dataset as it leverages custom architecture and uses very unusual input shape. Example of wagon detection using YOLOv8+ is shown in Fig. 6.


**Fig. 6.** Example of wagon detection using YOLOv8+

## 5 Conclusion

The paper discusses a specific case of the object detection problem, when after certain image transformation (e.g., inverse perspective transformation), detection problem can be decomposed into several unidimensional detection problems in non-overlapping rectangular (vertically or horizontally aligned) areas of interest. A motivating example of such situation is wagon tracking using cameras placed in classification bowl of the railway freight station.

We have proposed a family of specialized metrics, taking into account the image structure. The proposed metrics are well-aligned with the detection goals and are more interpretable w.r.t. the problem than widely used universal detection metrics. We have also proposed corrections for some popular loss functions used in object detection to account for uneven importance of dimensions in the unidimensional detection.

## References

1. Bohlin M. et al.: Hump yard track allocation with temporary car storage. 4th International Seminar on Railway Operations Modelling and Analysis. (2011)
2. Olgeizer, I.A., et al.: Computer vision as a way of intellectualization of mountain automation systems. Problems of mechanical engineering and automation **1**, 46–53 (2022)
3. Sukhanov A. V. Railway rolling stock tracking based on computer vision algorithms. The International Symposium on Computer Science, Digital Economy and Intelligent Systems. Springer International Publishing, pp. 56–63. (2019)
4. Zhou D. et al.: IoU loss for 2D/3D object detection. International conference on 3D vision (3DV). IEEE. pp. 85–94. (2019)
5. Padilla R., Netto S. L., Da Silva E. A. B. A survey on performance metrics for object-detection algorithms. International conference on systems, signals and image processing (IWSSIP). IEEE. pp. 237–242. (2020)

6. Terven, J., Córdova-Esparza, D.M., Romero-González, J.A.: A Comprehensive Review of YOLO Architectures in Computer Vision: From YOLOv1 to YOLOv8 and YOLO-NAS. Mach. Learn. Knowl. Extr. **5**, 1680–1716 (2023). https://doi.org/10.3390/make5040083
7. Vijayakumar, A., Vairavasundaram, S.: YOLO-based Object Detection Models: A Review and its Applications. Multimed. Tools Appl. (2024). https://doi.org/10.1007/s11042-024-18872-y
8. Yasir, M., Shanwei, L., Mingming, X., Jianhua, W., Hui, S., Nazir, S., Zhang, X., Tugsan Isiacik Colak, A.: YOLOv8-BYTE: Ship tracking algorithm using short-time sequence SAR images for disaster response leveraging GeoAI. Int. J. Appl. Earth Obs. Geoinf. 128, (2024). https://doi.org/10.1016/j.jag.2024.103771
9. Liu, Z., Lin, Y., Cao, Y., Hu, H., Wei, Y., Zhang, Z., Lin, S., Guo, B.: Swin Transformer: Hierarchical Vision Transformer using Shifted Windows. In: 2021 IEEE/CVF International Conference on Computer Vision (ICCV). pp. 9992–10002. IEEE (2021). https://doi.org/10.1109/ICCV48922.2021.00986
10. Zheng, Z., Li, J., Qin, L.: YOLO-BYTE: An efficient multi-object tracking algorithm for automatic monitoring of dairy cows. Comput. Electron. Agric. 209, (2023). https://doi.org/10.1016/j.compag.2023.107857
11. Roy, A.M., Bhaduri, J., Kumar, T., Raj, K.: WilDect-YOLO: An efficient and robust computer vision-based accurate object localization model for automated endangered wildlife detection. Ecol. Inform. 75, (2023). https://doi.org/10.1016/j.ecoinf.2022.101919
12. Chen, C., Yuan, G., Zhou, H., Ma, Y.: Improved YOLOv5s model for key components detection of power transmission lines. Math. Biosci. Eng. **20**, 7738–7760 (2023). https://doi.org/10.3934/mbe.2023334
13. Pan, H., Lan, J., Wang, H., Li, Y., Zhang, M., Ma, M., Zhang, D., Zhao, X.: UWV-Yolox: A Deep Learning Model for Underwater Video Object Detection. Sensors. 23, (2023). https://doi.org/10.3390/s23104859
14. Malik, H., Naeem, A., Hassan, S., Ali, F., Naqvi, R.A., Yon, D.K.: Multi-classification deep neural networks for identification of fish species using camera captured images. PLoS One. 18, (2023). https://doi.org/10.1371/journal.pone.0284992
15. Redmon, J., Divvala, S., Girshick, R., Farhadi, A.: You Only Look Once: Unified, Real-Time Object Detection. (2015)
16. Rezatofighi, H., Tsoi, N., Gwak, J., Sadeghian, A., Reid, I., Savarese, S.: Generalized Intersection over Union: A Metric and A Loss for Bounding Box Regression. (2019)
17. Zheng, Z., Wang, P., Ren, D., Liu, W., Ye, R., Hu, Q., Zuo, W.: Enhancing Geometric Factors in Model Learning and Inference for Object Detection and Instance Segmentation. (2020)
18. Zhang, Y.-F., Ren, W., Zhang, Z., Jia, Z., Wang, L., Tan, T.: Focal and Efficient IOU Loss for Accurate Bounding Box Regression. Neurocomputing **506**, 146–157 (2021)
19. Ultralytics YOLO Official GitHub. https://github.com/ultralytics/ultralytics/

# Adversarial Adaptive Sampling for Physics-Informed Neural Network

Yao Li, Yuanxun Xu(✉), Shengzhu Shi(✉), and Boying Wu

School of Mathematics, Harbin Institute of Technology, 92 W. Dazhi St., Harbin 150006, Heilongjiang, China
1904477164@qq.com, mathssz@hit.edu.cn

**Abstract.** In recent years, physically-informed neural networks (PINNs) have emerged as a promising approach for solving partial differential equations (PDEs). However, vanilla PINNs encounter challenges when dealing with PDEs exhibiting multi-scale, chaotic, or turbulent behavior. In this study, we introduce an innovative method for improving PINNs by modifying the loss function to enable the model to accurately capture temporal causality during the training process. However, the observed effect did not yield the desired outcome in numerical experiments. Additionally, the quantity and spatial distribution of training data in the training process of PINNs will directly impact the efficacy of the model. Therefore, this study employs a projected gradient descent-based adversarial attack approach to dynamically select the training data, thereby bolstering the resilience of PINNs through fine-tuning the model with adversarial samples. We integrate pre-training with adaptive sampling using adversarial attacks. Pre-training aims to reduce the training time required for model training by breaking down a complex problem into several simpler ones. Effective pre-training in a shorter time frame can provide initial network parameter estimates and additional supervised learning datasets for training across the entire time domain.

**Keywords:** PINNs · causality · adversarial attack · pre-training

## 1 Introduction

Physically informed neural networks (PINNs) have emerged as a promising framework for integrating observational data and physical laws in science and engineering [1,2]. In contrast to purely data-driven neural network learning, PINNs incorporate physical information as a constraint in the loss function, thereby facilitating the development of more generalized models with reduced data requirements.

PINNs have demonstrated potential in solving partial differential equations (PDEs). However, they struggle with PDEs whose solutions are highly nonlinear, multi-scale, or exhibit chaotic behavior [3,4]. Over the past few years, numerous approaches have been proposed to enhance the vanilla PINNs, aiming to increase


S. Kovalev et al. (Eds.): IITI 2024, LNNS 1209, pp. 431–442, 2024.
https://doi.org/10.1007/978-3-031-77688-5_41

the accuracy and robustness of these models. These enhancements include, but are not limited to, optimization algorithms for adaptive training, algorithms for adaptive selection of training data batches, novel network architectures, domain decomposition methods, and innovative activation functions [5].

Despite these advancements, PINNs continue to face significant challenges in addressing many practically relevant problems in science and engineering. Understanding the limitations of PINNs in these contexts is crucial for further improvement. This paper aims to tackle these challenges by proposing an adaptive sampling method based on adversarial attack, combined with other training techniques, to enhance the accuracy of PINNs in solving time-evolution PDEs.

### 1.1 Related Works and Contributions

Although many achievements have been made using PINNs, vanilla PINNs face significant difficulties when solving complex problems. To improve performance, researchers have proposed various methods to enhance deep learning techniques, one of which is the adaptive sampling of training points. In 2019, a study first introduced a residual-based adaptive refinement (RAR) method to increase the efficiency of PINNs [6]. RAR enhances the distribution of training points by sampling more locations with large PDE residuals during training. Mao et al. [7] proposed dividing the entire domain into several subregions and introduced an adaptive sampling method (ASM) based on the residual average and solution gradient of each subregion.

Different from RAR and ASM, Nabian et al. [8] employed importance sampling to generate a set of training points based on a probability density function proportional to the residual of the PDEs. This importance sampling approach can be easily integrated into existing PINN frameworks and has proven to be computationally efficient for transient diffusion problems. Another method from the perspective of probability density is the Adaptive Sampling of Failure Information (FI-PINN) method, which enhances model performance by placing more collocation points in regions where the PDE residuals exceed a given tolerance [9,10]. A similar idea is employed in [11], where the training point set is updated by adding sampling points in areas with relatively large residuals to improve model accuracy. Building on the concept of residual minimization, the DAS-PINN method was proposed in [12]. This method uses the difference between the induced density model and the residual-induced distribution to generate new collocation points, further improving the accuracy of the approximate solution.

When the solutions of PDEs contain high-frequency or multi-scale features, PINNs may fail in training and produce incorrect predictions [13,14]. Mattey et al. [15] demonstrated that the accuracy of PINNs is adversely affected by high degrees of nonlinearity and high-order partial differential operators. Through extreme neural tangent kernel training of PINNs, Wang et al. [16] discovered that the convergence rates of different loss components varied significantly, preventing the total training error from being minimized effectively. Wight et al. [17] found that the performance of PINNs is closely related to the combination of loss terms, introducing a non-adaptive weighting method and a temporal adaptation

of the loss function. Li et al. .[18]proposed a dynamic weighting method called dwPINN, which dynamically adjusts the weight of loss terms that are difficult to train.

### 1.2 Organization

The rest of this paper is organized as follows. In Sect. 2, we provide a brief review of PINNs and introduce causal training for PINNs. In Sect. 3, we propose an adversarial training scheme to improve PINNs by incorporating pre-training methods. In Sect. 4, we conduct several numerical experiments to demonstrate the effectiveness of our method. Finally, in Sect. 5, we offer conclusions for the work.

## 2 PINNs

PINNs use deep neural networks as function approximators to directly solve nonlinear problems. They leverage automatic differentiation techniques [21] to differentiate the input coordinates and model parameters, thereby incorporating physical laws into the neural network. When establishing physical information neural network, we consider PDEs taking the form

$$u_t + \mathcal{N}[u;\lambda] = 0, t \in [0,T], x \in \Omega \tag{1}$$

subject to the initial and boundary conditions

$$u(0,x) = g(x), x \in \Omega \tag{2}$$

$$\mathcal{B}[u] = 0, t \in [0,T], x \in \partial\Omega \tag{3}$$

where $\mathcal{N}[\cdot]$ is a linear or nonlinear differential operator with parameter, $\mathcal{B}[\cdot]$ is a boundary operator corresponding to Dirichlet, Neumann, Robin, or periodic boundary conditions, and $u$is the solution of the above PDEs.PINNs can approximate the unknown solution $u(t,x)$ using a deep neural network$u_\theta(t,x)$, where $\theta$ represents all tunable parameters in the neural network. Subsequently, a physical information model can be trained by minimizing the following composite loss function.

$$\mathcal{L}(\theta) = \lambda_{ic}\mathcal{L}_{\text{ic}}(\theta) + \lambda_{bc}\mathcal{L}_{bc}(\theta) + \lambda_r\mathcal{L}_r(\theta) \tag{4}$$

where

$$\mathcal{L}_{\text{ic}}(\theta) = \frac{1}{N_{\text{ic}}}\sum_{i=1}^{N_{\text{ic}}}\left|u_\theta\left(x_{\text{ic}}^i, 0\right) - g\left(x_{\text{ic}}^i\right)\right|^2 \tag{5}$$

$$\mathcal{L}_{bc}(\theta) = \frac{1}{N_{bc}}\sum_{i=1}^{N_{\text{bc}}}\left|\mathcal{B}[u_\theta]\left(x_{bc}^i, t_{\text{bc}}^i\right)\right|^2 \tag{6}$$

$$\mathcal{L}_{\text{r}}(\theta) = \frac{1}{N_r}\sum_{i=1}^{N_{\text{r}}}\left|\frac{\partial u_\theta}{\partial t}\left(x_r^i, t_r^i\right) + \mathcal{N}[u_\theta]\left(x_r^i, t_r^i\right)\right|^2 \tag{7}$$

When utilizing data-driven methods to solve PDEs, the total number of training points is typically relatively small, usually ranging from hundreds to thousands. The L-BFGS algorithm can be chosen to optimize the loss function, which is a quasi-Newton optimization algorithm based on the full batch gradient [22]. Larger datasets can be handled using stochastic gradient descent and its corresponding variants. If the given PDE is well-solved and has a unique solution, then a vanilla PINNs can achieve high prediction accuracy with a network structure of sufficient width and depth, along with an adequate number of training points.

According to the work of Wang et al. [16], PINNs can violate physical causality. PDEs are usually time discretized by sequential algorithms, ensuring that the solution at time $t$ is successfully solved before the approximate solution at time $t + \Delta t$. But this dependence on time is not present in the loss function of most continuous-time PINNs. In fact, even before fitting the initial conditions, PINNs prefer to approximate the PDE solution first at a later time instead of in chronological order during gradient descent training, thus violating temporal causality.

To address the inherent drawback of PINNs in satisfying the physical causality of equations when solving PDEs, one can be achieved by defining a weighted residual loss as

$$\mathcal{L}_{\mathrm{r}}(\theta) = \frac{1}{N_t} \sum_{i=1}^{N_t} \omega_i \mathcal{L}_{\mathrm{r}}(t_i, \theta) \tag{8}$$

where the weight $\omega_i$ is defined as

$$\omega_i = \exp\left(-\varepsilon \sum_{k=1}^{i-1} \mathcal{L}_r(t_k, \theta)\right), i = 2, 3, ..., N_t \tag{9}$$

where $\varepsilon$ is the causality parameter, which is manually adjusted to govern the extent to which the weight $\omega_i$ influences the residual loss. It is important to note that there is an inverse relationship between the weight $\omega_i$ and the residual loss at preceding time steps. Consequently, $\mathcal{L}_{\mathrm{r}}(t_i, \theta)$ will not be minimized unless all previous residuals $\{\mathcal{L}_{\mathrm{r}}(t_k, \theta)\}_{k=1}^{i-1}$ decrease to some small value such that$\omega_i$ is large enough.

## 3 Adaptive Sampling with Adversarial Attacks

### 3.1 Adversarial Attacks

Adversarial attacks can be categorized into two main types: white-box and black-box attacks. Based on the attacker's objectives, adversarial attacks can further be classified into targeted and non-targeted attacks. Targeted attacks aim to force the model to misclassify the input into a predetermined class, and non-targeted attacks merely generate adversarial samples to deceive the neural network, preventing it from accurately completing the task. For a regression problem that

approximates a function $r(x) \in \mathbb{R}$ with $r(x;\theta) \in \mathbb{R}$, targeted adversarial attack is an optimization problem that

$$\max_{\zeta} \mathcal{L}\left(r\left(x+\zeta;\theta\right), r\left(x+\zeta\right)\right) \tag{10}$$

$$s.t. \|\zeta\|_{\infty} \leq \varepsilon$$

where $\mathcal{L}(\cdot,\cdot)$ is a distance function of $r(x+\zeta;\theta)$ and $r(x+\zeta)$, and $\varepsilon$ is the threshold of maximum allowable adversarial perturbation.

**PGD.** For the regression problem of (10), we extends the basic PGD attack as in algorithm 1. In the random initialization step, an uniformly distributed random variable $\mathcal{U}[-\varepsilon,\varepsilon]$ is added to the original sample $x$. Then the perturbed sample is clipped back to the problem domain $\Omega$. In the projected gradient descent process, as we are maximizing the residual, gradient ascent are applied. The model takes a step of $\eta$ to the direction of the loss gradient each time. The *clip* can restrict the range of the perturbation to not exceed the previously agreed range.

**Algorithm 1.** PGD

**Require:** he original sample $x$, the problem domain $\Omega$, the regression model $r(x;\theta)$, the target function $r(x)$, the loss $\mathcal{L}(\cdot)$, the maximum perturbation threshold $\varepsilon$, number of iteration steps $T$, and the step size of each iteration $\eta$.

$g_0 \leftarrow 0$
$x \leftarrow x + \mathcal{U}[-\varepsilon,\varepsilon]$
$x \leftarrow clip_{\Omega}(x)$
**for** $t = 1 : T$ **do**
    $g_x \leftarrow \eta * sign\left(\nabla_x r(x;\theta)\right)$
    $g_0 \leftarrow clip_{[-\varepsilon,\varepsilon]}\left(g_0 + g_x\right)$
**end for**
$x \leftarrow x + g_0$
$x \leftarrow clip_{\Omega}(x)$

### 3.2 Adversarial Attack-Based Sampling

The details of the adaptive sampling method based on adversarial attacks are outlined in Algorithm 2. At initialization, $N_0$ samples are generated using LHS. Then at the iteration$k$, adversarial samples are calculated for all samples $\left\{a_k^{(n)}\right\}_{n=1}^{N_{k-1}}$,..., $\left\{a_{k-m}^{(n)}\right\}_{n=1}^{N_{k-m-1}}$, $\left\{a_1^{(n)}\right\}_{n=1}^{N_0}$ generated in the previous $m$ iterations and the initial samples $\left\{s_{k-1}^{(n)}\right\}_{n=1}^{N_{k-1}}$,..., $\left\{s_{k-m-1}^{(n)}\right\}_{n=1}^{N_{k-m-1}}$, $\left\{s_0^{(n)}\right\}_{n=1}^{N_0}$. These calculated adversarial samples serve as candidate samples. New samples

are selected from the $N_k$ highest residual candidate samples, where $N_k$ is the number of samples in the $k$-th iteration. Revisiting the samples from the first $m$ iterations can expedite the convergence of samples to regions of high residual error. And revisiting the initial sample can prevent the iteration from becoming trapped in a local region. The model is subsequently retrained on the new samples before the commencement of the next adversarial training iteration.

**Algorithm 2.** Adversarial Attack-based Sampling

**Require:** The model $u(x;\theta)$, the residual $r(x;\theta)$ of model, the number of training iterations $K$, the number of sampling points in each iteration $N_k$, $k = 0, \ldots 0, K$, the problem domain $\Omega$, the maximum perturbation threshold $\varepsilon$, the number of iteration steps $T$, the step size of each iteration $\eta$, and the number of revisiting iterations $m$.

Sample $\left\{s_0^{(n)}\right\}_{n=1}^{N_0}$ through LHS
$u(x;\theta) \leftarrow$ train on $\left\{s_0^{(n)}\right\}_{n=1}^{N_0}$
**for** $k = 1 : K$ **do**
  **for** $i = (k-1-m) : (k-1)$ **do**
    $\left\{a_{i+1}^{(n)}\right\}_{n=1}^{N_i} \leftarrow \left\{\mathrm{PINN-PGD}\left(s_i^{(n)}, |r(x;\theta)|, \varepsilon, \eta, T, \Omega\right)\right\}_{n=1}^{N_i}$
  **end for**
  $\left\{a_1^{(n)}\right\}_{n=1}^{N_i} \leftarrow \left\{\mathrm{PINN-PGD}\left(s_0^{(n)}, |r(x;\theta)|, \varepsilon, \eta, T, \Omega\right)\right\}_{n=1}^{N_0}$
  $\left\{s_k^{(n)}\right\}_{n=1}^{N_k} \leftarrow \{\arg\max_x r(x;\theta)\}_{N_k}, \forall x \in \left(\bigcup_{i=k-m}^{k}\left\{a_i^{(n)}\right\} \bigcup \{a_1^n\}\right)$
  $u(x;\theta) \leftarrow$ train on $\left(\bigcup_{i=0}^{k}\left\{s_i^{(n)}\right\}\right)$
**end for**

### 3.3 Pre-training Strategy for PINNs

Following the original work of Guo et al. [23], we improve PINNs using the pre-training strategy. The pre-training strategy is composed of the pre-training step and the formal training step. In pre-training process, Eq. 1is trained in the time interval $[0, T_p]$ by using the vanilla PINNs method as the pretraining step. During formal training, the additional supervised learning points from pre-training enhances the performance of PINNs. The pre-training step can also provide an additional supervised learning component, which is crucial for enhancing the performance of subsequent formal training.

## 4 Numerical Experiments

### 4.1 Kuramoto-Sivashinsky Equation

The Kuramoto-Sivashinsky equation exhibits a wealth of spatially and temporally nontrivial dynamical behavior including chaos, and has served as a model

example in efforts to understand and predict the complex dynamical behavior associated with a variety of physical systems. The equation takes the form

$$u_t + \alpha u u_x + \beta u_{xx} + \gamma u_{xxxx} = 0 \tag{11}$$

subject to periodic boundary conditions and an initial condition

$$u(0, x) = u_0(x) \tag{12}$$

We start with a relatively simple scenario by setting $\alpha = 5$, $\beta = 0.5$, $\gamma = 0.005$, and a spatial domain $[-1, 1]$. The initial condition is given by $u_0 = -\sin(\pi x)$. The goal of the model is to learn the solution of the equation up to time $T = 1$.

Figure 1(a) demonstrates that when unprocessed PINNs are utilized for time fitting within the range of 0<t<1, the fit is suboptimal. Figure 1(b) depict the model's fit using a modified loss function for this equation. However, this fit does not match the theoretical result and falls short even compared to the performance of unprocessed PINNs. The primary reason is that the hyperparameter $\varepsilon$ in the weight $\omega_i$ formula requires manual adjustment. The choice of hyperparameters, tailored to the specific equation, significantly influences the minimization of loss. Based on the weight $\omega$ configuration, $\omega_i$ can only be sufficiently large if all previous residual losses decrease to a specified level. However, due to inherent characteristics of the equation, the reduction in residual loss $\{\mathcal{L}_r(t_k, \theta)\}_{k=1}^{i-1}$ at a given time is sluggish, limiting the optimization of overall weight $\omega$. Consequently, the efficacy of causal PINNs may not surpass that of vanilla PINNs.

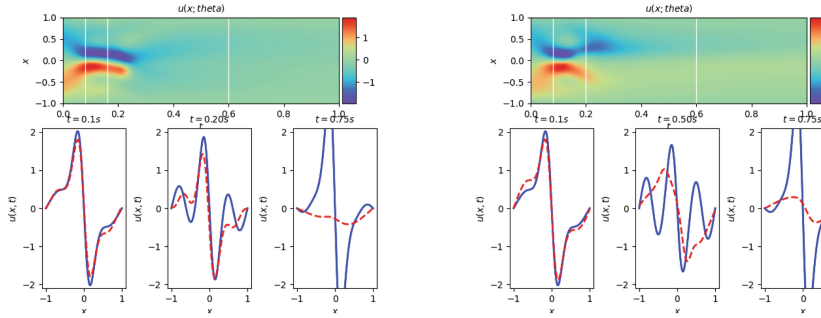


(a) Effect of the vanilla PINNs (b) Effect of causal PINNs

**Fig. 1.** Fitting effect of PINNs on Kuramoto-Sivashinsky equations.

This approach to preserving physical causality in the network merely forces the model to progressively minimize the loss function over time, without optimizing for the reduction of the equation's residual loss. The issue that vanilla PINNs fail to sufficiently minimize the residual loss when dealing with equations exhibiting highly nonlinear or high-frequency solutions remains unresolved. This results in difficulties when calculating the weight $\omega$. Specifically, when the residual loss

is processed in a time-ordered manner, it may encounter challenges during the minimization of loss $\mathcal{L}_{\mathrm{r}}(t_i, \theta)$ at certain times, explaining why the experimental outcome does not match the theoretical expectation.

### 4.2 Convection Equation with Large Convection Coefficient

In this case, we consider using the adaptive sampling method and pre-training method to solve a spatially 1D convection equation:

$$\begin{gathered} \frac{\partial u}{\partial t} + \beta \frac{\partial u}{\partial t} = 0, (x, t) \in (0, 2\pi) \times (0, 1] \\ u(x, 0) = \sin(x) \end{gathered} \tag{13}$$

$$u(0, t) = u(2\pi, t), t \in (0, 1]$$

The exact solution is $u(x, t) = \sin(x - \beta t)$, the vanilla PINN method fails to learn the solution in the cases of relatively large convection coefficients $\beta \geq 10$.

In this example, convection coefficient $\beta = 50$, the PINNs model is a fully connected neural network with eight hidden layers with 40 neurons each. The number of boundary points is set to 800. The model was first trained on 3000 Latin hypercube sample points for 150,000 epoch using the Adam optimizer with learning rate $l_r = 0.0001$.

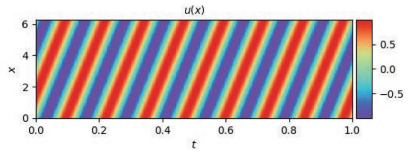


(a) Exact solution of the equation

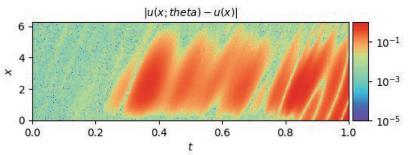


(b) Absolute error of vanilla PINNs

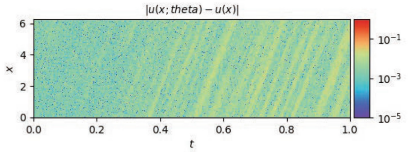


(c) Absolute error of adversarial PINNs

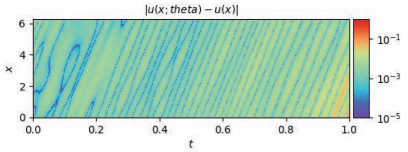


(d) Absolute error of pre-training PINNs

**Fig. 2.** The exact solution and absolute error.

Figure 2(a) illustrates the accurate solution for the one-dimensional convection equation for $\beta = 50$ at $t = 0.1$. Figure 3(a) displays the performance of the vanilla PINNs in fitting the data. The fit appears to be satisfactory at points

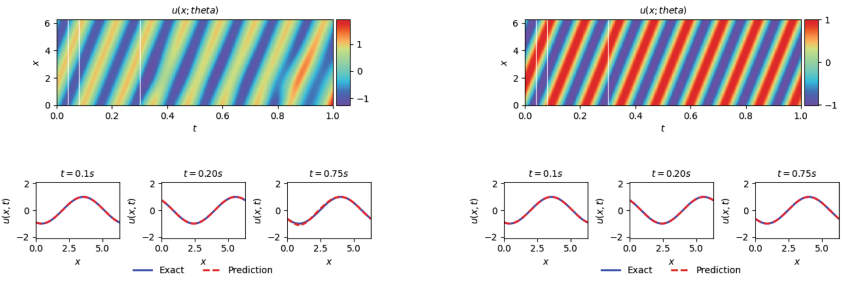


(a) Effect of the vanilla PINNs (b) Effect of the modified PINNs

**Fig. 3.** Fitting effect of PINNs on one-dimensional convection equations.

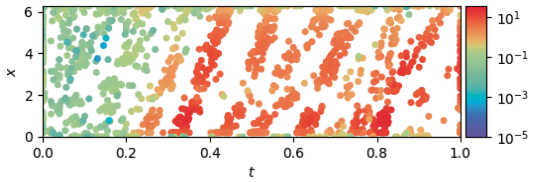

**Fig. 4.** Adaptive sampling points.

$t = 0.1$ and $t = 0.2$, but there is a significant discrepancy between the approximated solution at point $t = 0.75$ and the actual solution. The heat map of variable $u(x;\theta)$ indicates that the fit deteriorates as the value of $u(x)$ increases.

Based on this approach, the adversarial attack-based method is employed to selectively determine the residual points as the training point set. Figure 4 illustrates the adaptive generation of residual points using the adversarial attack-based method. By examining the absolute error plot in Fig. 2(b), which depicts the use of vanilla PINNs models for problem-solving, it becomes evident that the adversarial attack concentrates on areas with substantial residual error and failure zones near the boundary points. Additionally, a comparison of the model's fitting effect in Fig. 3(a) with the distribution of adaptive sampling reveals that the model prioritizes areas with suboptimal fitting effects. Figure 4 further demonstrates that adversarial examples enhance already well-trained intervals. Figure 2(c) respectively display the absolute error and fitting effect of adaptive sampling points utilizing adversarial attacks. A comparison with vanilla PINNs reveals that areas with significant residual error have been more effectively addressed, and the fitting effect of u has also been enhanced. Figure 3(b) and Fig. 2(d) depict the fitting effect following the integration of the pre-training method, revealing that the modified model maintains satisfactory accuracy, even when $\beta = 50$.

### 4.3 Basic 1D Wave Equation

The governing PDE is

$$u_{tt} - 4u_{xx} = 0 \tag{14}$$

The domain is $\Omega \times T = [0, 1] \times [0, 1]$. The boundary conditions are

$$u(0, t) = u(1, t) = 0 \tag{15}$$

The initial condition:

$$u(x, 0) = \sin(\pi x) + \frac{1}{2}\sin(4\pi x) \tag{16}$$

$$u_t(x, 0) = 0 \tag{17}$$

The analytical solution of this problem is

$$u(x, t) = \sin(\pi x)\cos(2\pi t) + \frac{1}{2}\sin(4\pi x)\cos(8\pi t) \tag{18}$$

Vanilla PINNs are inadequate for solving the one-dimensional wave equation. This chapter introduces a combination of adaptive sampling and pre-training methods, based on adversarial attack, to address this issue. The experimental setup involved a fully connected neural network with eight layers, each containing 40 neurons. Three pre-training intervals, $(0, 0.2]$, $(0, 0.6]$, and $(0, 0.8]$, were chosen. During the first training interval, Latin hypercube sampling was employed to select 3000 training points, with each training round consisting of 200,000 iterations. Subsequently, the adaptive sampling method, grounded in adversarial attack principles, was utilized to enhance the training on $(0, 0.2]$. Once the training efficacy was satisfactory, the same adaptive sampling technique was employed to determine the training points for the subsequent interval, continuing this process until all intervals had been trained.

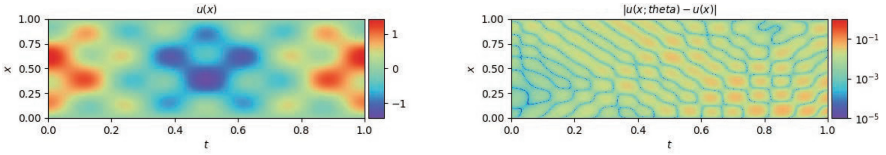


(a) Effect of the vanilla PINNs (b) Effect of the modified PINNs

**Fig. 5.** The exact solution and absolute error.

In Fig. 5(a), a heat map depicting the analytical solution of the one-dimensional wave equation is presented. Figure 6(a) illustrates the sampling points chosen by the adaptive sampling technique, which is predicated on adversarial attack. By examining the absolute error plot of the fitting effect in Fig. 5(b), one can discern that the training points are primarily located in regions with significant errors. This allows the model to focus on areas where the training effect is suboptimal and enhance the training in these regions. Subsequently,

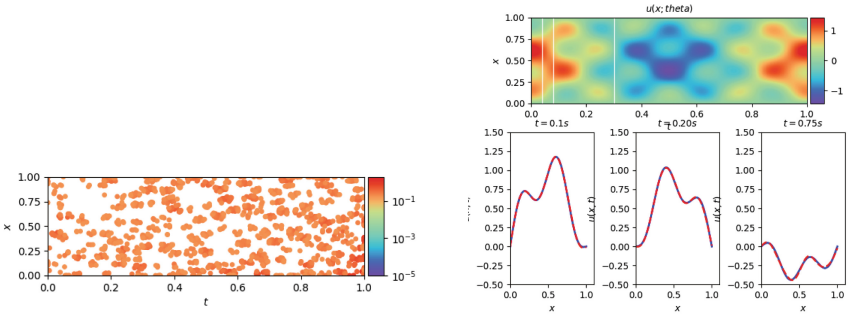


(a) Adaptive sampling points. (b) Effect of the modified PINNs

**Fig. 6.** The modified PINNs.

Fig. 5(b) presents the improved fitting effect of the PINNs model, which has been enhanced through a pre-training strategy combined with the adversarial attack adaptive sampling method applied to the one-dimensional wave equation. A comparison with the analytical solution images in Fig. 5(a) reveals that an excellent fitting effect has been attained.

## 5 Conclusion

In this study, we investigate the challenges faced by vanilla PINNs when processing inter-evolution equations from a causality standpoint. We introduce the architecture of a Causal Information Neural Network. During numerical experiments, setting the causal parameter $\varepsilon$ manually proved challenging, resulting in suboptimal performance. Recognizing the significance of training point distribution on PINNs' efficacy, we propose an adaptive sampling technique grounded in adversarial attacks. Experiments involving one-dimensional convection equations with substantial convection coefficients demonstrate that this adversarial attack-based sampling approach enhances PINNs' performance. Furthermore, we present a pre-training strategy and integrate it with our adaptive sampling method, yielding superior fitting outcomes in convection equation and fluctuation experiments.

## References

1. Raissi, M., Perdikaris, P., George, E.K.: Physics-informed neural networks: a deep learning framework for solving forward and inverse problems involving nonlinear partial differential equations. J. Comput. Phys. **378**, 686–707 (2019)
2. Raissi, M., Yazdani, A., George, E.K.: Hidden fluid mechanics: learning velocity and pressure fields from flow visualizations. Science **367**(6481), 1026–1030 (2022)
3. Wang, S.F., Wang, H.W., Perdikaris, P.: On the eigenvector bias of fourier feature networks: From regression to solving multi-scale PDEs with physics-informed neural networks. Comput. Methods Appl. Mech. Eng. **384**, 113938 (2021)

4. Karniadakis, E.G., Kevrekidis, G.I., Lu, L., Perdikaris, P., Wang, S.F.: Physics-informed machine learning. Nat. Rev. Phys. 1–19 (2021)
5. Wang, S., Teng, Y.J., Perdikaris, P.: Understanding and mitigating gradient flow pathologies in physics-informed neural networks[J]. SIAM J. Sci. Comput. **43**(5), A3055–A3081 (2021)
6. Lu, L., Meng, X., Mao, Z.: DeepXDE: a deep learning library for solving differential equations. SIAM Rev. **63**(1), 208–228 (2021)
7. Mao, Z., Meng, X.: Physics-informed neural networks with residual/gradient-based adaptive sampling methods for solving partial differential equations with sharp solutions[J]. Appl. Math. Mech. **44**(7), 1069–1084 (2023)
8. Nabian, M.A., Gladstone, R.J., Meidani, H.: Efficient training of physics-informed neural networks via importance sampling. Comput.-Aided Civ. Infrastruct. Eng. **36**(8), 962–977 (2021)
9. Zhu, M., Tan, Q., Kartha, Y., Lu, L.: A comprehensive study of non-adaptive and residual-based adaptive sampling for physics-informed neural networks. Comput. Methods Appl. Mech. Eng. **403**, 115671 (2023)
10. Psaros, A., Kawaguchi, K., Karniadakis, G.: Meta-learning PINN loss functions. J. Comput. Phys. **458**, 111121 (2022)
11. Zeng, S., Zhang, Z., Zou, Q.: Adaptive deep neural networks methods for high-dimensional partial differential equations. J. Comput. Phys. **463**, 111232 (2022)
12. Tang, K., Wan, X., Yang, C.: DAS-PINNs: a deep adaptive sampling method for solving high-dimensional partial differential equations. J. Comput. Phys. **476**, 111868 (2023)
13. Raissi, M.: Deep hidden physics models: deep learning of nonlinear partial differential equations. J. Mach. Learn. Res. **19**(1), 932–955 (2018)
14. Fuks, O., Tchelepi, H.A.: Limitations of physics informed machine learning for nonlinear two-phase transport in porous media. J. Mach. Learn. Model. Comput. **1**(1), 19–37 (2020)
15. Mattey, R., Ghosh, S.: A novel sequential method to train physics informed neural networks for Allen Cahn and Cahn Hilliard equations, Comput. Comput. Methods Appl. Mech. Eng. **390**, 114474 (2022)
16. Wang, S., Yu, X., Perdikaris, P.: When and why PINNs fail to train: a neural tangent kernel perspective. Comput. Phys. Commun. **449**, 110768 (2022)
17. Wight, C.L., Zhao, J.: Solving Allen-Cahn and Cahn-Hilliard equations using the adaptive physics informed neural networks. Commun. Comput. Phys. **29**(3), 930–954 (2021)
18. Li, S., Feng, X.: Dynamic weight strategy of physics-informed neural networks for the 2D Navier-Stokes equations. Entropy **24**(9) (2022)
19. Wang, S., Sankaran, S., Perdikaris, P., Respecting causality for training physics informed neural networks. Comput. Meth. Appl. Mech. Eng. 116813 (2024)
20. Gao, Z., Yan, L., Zhou, T.: Failure-informed adaptive sampling for PINNs. SIAM J. Sci. Comput. **45**(4), A1971–A1994 (2023)
21. Liu, D.C., Nocedal, J.: On the limited memory BFGS method for large scale optimization. Math. Program. 503–528 (1989)
22. Baydin, A.G., Pearlmutter, B.A., Radul, A.: Automatic differentiation in machine learning: a survey. J. Mach. Learn. Res. (2015)
23. Guo, J.W., Yao, Y.Z., Wang, H., Gu, T.X.: Pre-training strategy for solving evolution equations based on physics-informed neural networks. J. Comput. Phys. 112258 (2023)

# Leveraging Single and Multi-task Reinforcement Learning Algorithms for Autonomous Mobile Aloha Robot

Aditya Narendra[1(✉)], Dmitry Makarov[1,2(✉)], and Aleksander I. Panov[1,2,3(✉)]

[1] Moscow Institute of Physics and Technology, Moscow, Russia
narendra.a@phystech.edu
[2] Federal Research Center Computer Science and Control RAS, Moscow 117312, Russia
makarov@isa.ru
[3] Artificial Intelligence Research Institute, Moscow 105064, Russia
panov.ai@mipt.ru

**Abstract.** Traditional Reinforcement Learning (RL) methods often require careful algorithm design, hyper-parameter tuning, and experimentation to perform optimally across multiple tasks. Multi-task models, however, offer increased efficiency, better generalization, and improved resource utilization, which are crucial for robots performing diverse autonomous tasks. On the other hand, single-task models often demonstrate better results and more robust task-specific policies. In this paper, we demonstrate the versatility of these models through experiments on the Mobile Aloha robot, which has both manipulation and navigation capabilities. The main idea behind our work is to demonstrate the use of various types of RL algorithms (single and multi-task) for multi-control robots (in our case, Mobile Aloha) which has not been explored much in the past. We conclude the paper with comparative results of experiments with state-of-the-art RL algorithms across different types of tasks including navigation, manipulation, and a combination of both.

**Keywords:** Multi-Task Learning · Reinforcement Learning · Autonomous Robots · Model-Based Control

## 1 Introduction

The Mobile Aloha robot, a new and promising platform, offers advanced capabilities for complex multi-task control, making it a significant focus in the field of robotics. It has both manipulation and navigation capabilities and has demonstrated remarkable performance in challenging, real-world tasks. However, these impressive results have predominantly been achieved through behavior-cloning methods using Action Chunking with Transformers (ACT) [4] rather than conventional RL approaches. Moreover, the study on the use of multi-task RL algorithms for multi-control robots such as Mobile Aloha [4] is limited and has not been explored much in the past.


S. Kovalev et al. (Eds.): IITI 2024, LNNS 1209, pp. 443–453, 2024.
https://doi.org/10.1007/978-3-031-77688-5_42

In this paper, we explore the usage of state-of-the-art RL methods to enhance the versatility and efficiency of the Mobile Aloha robot. While modern RL algorithms are pivotal in modeling the behavior of autonomous robots for single tasks (like manipulation or navigation), their effectiveness often degrades when extended to multi-task domains due to the complexities involved in designing reward functions, task-specific hyper-parameter tuning, and experimental validation [14].

For our analysis, we compare a range of baseline models for single-task RL, such as Soft Actor-Critic (SAC) [6] and Proximal Policy Optimization (PPO) [16], against multi-task RL algorithms like Temporal Difference Model Predictive Control 2 (TDMPC2) [9] and DreamerV3 [7]. In addition, we also consider two more Temporal Difference (TD) based RL algorithms, namely, Fuzzy Q-Learning (FQL) [1] and Dynamical Fuzzy Q-Learning (DFQL) [3] which are baseline RL algorithms based on Temporal Difference (TD) learning and are a more advanced implementation of Q-Learning [12]. Through a series of experiments conducted on the Mobile Aloha robot, the results show that TDMPC2 stands out by managing multiple tasks without the need for extensive, task-specific hyper-parameter tuning, unlike traditional Model-Based RL (MBRL) systems. This simplification significantly reduces the overhead associated with task and domain switching.

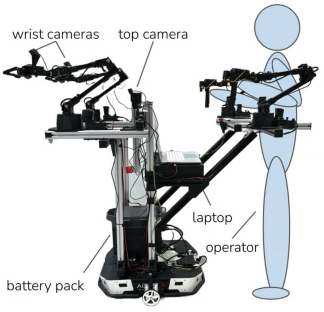


**Fig. 1.** Mobile-Aloha Robot with teleoperation. It has 2 DOF (Degrees of Freedom) for base (wheels) and 14 DOF for manipulators (7 for each). It also contains a LIDAR sensor and two cameras mounted on both manipulators. Reference[4]

## 2 Related Works

There are multiple prior works which have tried to implement robust to hyper-parameters RL algorithms which maintain their resilience across a variety of architectures and variations in tasks and data, such as Double Q-learning [11], Randomized Ensembled Double Q-Learning (RED-Q) [2], Stabilized Q-Value Estimation under Augmentation (SVEA) [8]. MoDem-V2, as introduced by [15], provides an example of the application of Model-Based Reinforcement Learning

(MBRL) in real-world settings and highlights the importance of safety and efficiency by incorporating exploration centering, agency transfer, and actor-critic architecture which allow direct real-world usage without extensive task-specific tuning.

Further work on these concepts has been explored by [13] at Google Robotics, which focuses on using a large-scale multi-task learning system that aims to reduce the cost of learning across multiple skills by enabling a shared learning structure across diverse tasks. Yet the problems of data inefficiency, extrapolation errors, scalability, and real-world application remain a challenge. At the same time, methods like Action Chunking with Transformers (ACT) [17] have been successfully implemented for multi-control robots like Mobile-Aloha before, but they normally require extensive training data mainly through tele-operation. Hence, the task of effectively using RL algorithms for the same is a novel one.

For the sake of comparison, we use the state-of-the-art baselines including Soft Actor-Critic (SAC) [6], which is a model-free RL algorithm known for its sample efficiency and is an off-policy algorithm similar to TDMPC2. We also use Proximal Policy Optimization (PPO) [16], which is an on-policy algorithm and can provide a neat contrast as compared to off-policy TDMPC2. The third baseline we are using is DreamerV3 [7], which similar to TDMPC2 is a multi-task model and can be used for direct comparison across various tasks using Mobile Aloha. We also consider Fuzzy Q-Learning (FQL) [1] and Dynamical Fuzzy Q-Learning (DFQL) [3] as Temporal Difference learning-based baseline algorithms.

## 3 Preliminaries

We formulate the robotic tasks of Navigation, Manipulation, and Mobile Manipulation within a unified Markov Decision Process (MDP) framework. This framework is used to model decision-making scenarios where outcomes are partly random and partly under the control of a decision maker. Each task is modeled as follows:

- **State Space** ($S$): Represents all possible configurations and statuses of the robot and its environment. This includes the robot's spatial coordinates, orientation, velocities, state of manipulative appendages (e.g., gripper open or closed), and positions of relevant objects (e.g., obstacles, cubes).
- **Action Space** ($A$): Consists of all actions the robot can perform, including navigation (e.g., linear and angular velocity), and manipulative actions (e.g., grasp, lift).
- **Transition Dynamics** ($P$): Defines the probabilities $P(s'|s, a)$ that taking action $a$ in state $s$ will lead to state $s'$.
- **Reward Function** ($R$): A function $R(s, a, s')$ providing a scalar feedback signal after transitioning from state $s$ to state $s'$ due to action $a$.
- **Terminal Conditions**: Each task has conditions under which it is considered complete. This includes reaching a target location, successful manipulation of objects to designated states, and timestep constraints.

The MDP is represented by the tuple $(S, A, P, R, \gamma)$, where $\gamma$ is the discount factor. The goal in each task is to find a policy $\pi : S \rightarrow A$ that maximizes the expected cumulative reward:

$$\max_{\pi} \mathbb{E}\left[\sum_{t=0}^{\infty} \gamma^t R(s_t, a_t, s_{t+1})\right],$$

where $s_t$ is the state at time $t$, $a_t = \pi(s_t)$ is the action taken according to policy $\pi$, and $s_{t+1}$ is the state resulting from action $a_t$.

### 3.1 Mobile-Aloha Control Algorithm

Mobile Aloha is a low-cost mobile manipulation system developed for bi-manual and whole-body tele-operation as shown in Fig. 1. It is designed to perform complex, long-horizon tasks by leveraging imitation learning from human demonstrations. The system includes onboard power and computation, and it supports autonomous execution as well as tele-operation, for the base controls, we use the unicycle model. The controller takes in desired linear and angular velocities $[u, \omega]$ as input and outputs the desired angular velocity of each wheel $[\dot{\theta}_L, \dot{\theta}_R]$. To demonstrate the control of the robot's base wheels, we will introduce the following notation and a corresponding algorithm. **Notations:** Let $v$ and $\omega$ denote the linear and angular velocities of the vehicle, respectively. The wheel radius is $r$, and $L$ is the wheelbase. The maximum linear and angular velocities are $v_{max}$ and $\omega_{max}$. The angular velocities of the left and right wheels are $\dot{\theta}_L$ and $\dot{\theta}_R$, with $\dot{\theta}_{max}$ as the maximum wheel angular velocity.

*Algorithm*

1. **Input Command**:

$$\text{command} = \begin{bmatrix} v \\ \omega \end{bmatrix} \tag{1}$$

2. **Limit Vehicle Speed**:

$$v = \begin{cases} -v_{\max} & \text{if } v < -v_{\max}, \\ v_{\max} & \text{if } v > v_{\max}, \\ v & \text{otherwise} \end{cases}, \quad \omega = \begin{cases} -\omega_{\max} & \text{if } \omega < -\omega_{\max}, \\ \omega_{\max} & \text{if } \omega > \omega_{\max}, \\ \omega & \text{otherwise} \end{cases} \tag{2}$$

3. **Calculate Wheel Speeds**:

$$\dot{\theta}_L = \frac{2v - \omega L}{2r}, \quad \dot{\theta}_R = \frac{2v + \omega L}{2r} \tag{3}$$

4. **Limit Wheel Speeds**:

$$\dot{\theta}_L = \begin{cases} -\dot{\theta}_{\max} & \text{if } \dot{\theta}_L < -\dot{\theta}_{\max} \\ \dot{\theta}_{\max} & \text{if } \dot{\theta}_L > \dot{\theta}_{\max} \\ \dot{\theta}_L & \text{otherwise} \end{cases}, \quad \dot{\theta}_R = \begin{cases} -\dot{\theta}_{\max} & \text{if } \dot{\theta}_R < -\dot{\theta}_{\max} \\ \dot{\theta}_{\max} & \text{if } \dot{\theta}_R > \dot{\theta}_{\max} \\ \dot{\theta}_R & \text{otherwise} \end{cases} \tag{4}$$

5. **Return Control Effort (action)** :

$$\text{Effort} = \begin{bmatrix} \dot{\theta}_L \\ \dot{\theta}_R \end{bmatrix} \tag{5}$$

For manipulator we use `OperationalSpaceController` from: https://github.com/abr/abr_control, taking in target end-effector pose (position and orientation) as input and outputs the joint effort (torque) required by each joints.

$$\text{Effort}_i = \begin{cases} \text{min\_effort}_i & \text{if } u_i < \text{min\_effort}_i \\ u_i & \text{if min\_effort}_i \leq u_i \leq \text{max\_effort}_i \\ \text{max\_effort}_i & \text{if } u_i > \text{max\_effort}_i, \end{cases} \tag{6}$$

where $u_i$ is the torque.

### 3.2 Simulation Environment

To evaluate the performance of the RL algorithms, we conducted our experiments in a simulated environment using Mujoco and OpenAI Gym. The simulation utilizes the Unified Robotics Description Format (URDF) model of Mobile Aloha provided by AgileX Robotics available on their GitHub repository: https://github.com/agilexrobotics/mobile_aloha_sim.
*Note: For the sake of simplicity, we have used single arm manipulations and state-based observations.*

## 4 Experiments

### 4.1 Problem Formulation

**Table 1.** Experiments

| Task | Observation dimension | Action dimension |
|---|---|---|
| Navigation | 16 | 2 |
| Manipulation | 17 | 7 |
| Pick-and-Place | 26 | 9 |

The algorithms are evaluated on the basis of three tasks (as described in Table 1) using the Mobile Aloha robot. The experiments were designed to test the agent's ability to perform both individual tasks and combined tasks. We compared the performance of single-task state-of-the-art algorithms like SAC and PPO with multi-task RL algorithms like TDMPC2 and DreamerV3 along with comparisons with other TD-based RL algorithms like FQL and DFQL. The following experiments were conducted:

### 4.2 Experiment 1: Navigation

The robot must reach a designated target position within the environment. The environment contains obstacles that the robot must avoid while navigating to the target position as seen in Fig. 2. The target position is specified by coordinates within the simulation space. The reward function is defined as follows:

$$r_t = -d_t + R_{\text{goal}} \cdot \mathbb{I}(\text{Reached Target}) - R_{\text{coll}} \cdot \mathbb{I}(\text{Collision}) \tag{7}$$

where $d_t$ is the distance between robot and target, $\mathbb{I}$ is the Indicator Function. $R_{\text{goal}}$ is a constant reward, give when the robot reaches the goal position and $R_{\text{coll}}$ is the negative reward (subtracted) in case of collision of robot with an obstacle.

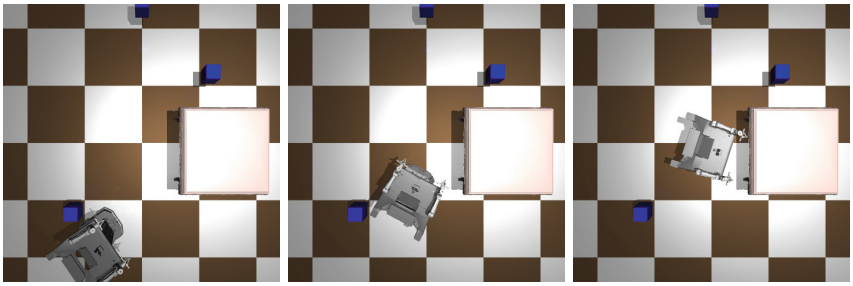

**Fig. 2.** Navigation Task: The robot maneuvers around the obstacles (blue cube) to reach the target position (table)

### 4.3 Experiment 2: Manipulation

The robot must pick up a target cube and lift it to a specified height. The environment, as seen in Fig. 3, includes a target cube placed at a random position within the robot's reach. The reward function is defined as follows:

$$\begin{aligned} r_t = -d_{\text{cube}} &+ R_{\text{pickup}} \cdot \mathbb{I}(\text{Picked Up Cube}) \\ &+ R_{\text{height}} \cdot \mathbb{I}(\text{Lifted Cube to Certain Height}), \end{aligned} \tag{8}$$

where $-d_{\text{cube}}$ is the distance of the cube from the target position, $R_{\text{pickup}}$ is the reward for picking up the cube,$R_{\text{height}}$ is the reward for lifting the cube to a certain height and $\mathbb{I}$.

### 4.4 Experiment 3: Navigation and Manipulation

The robot must navigate to the target cube, pick it up and place it at a designated target position. The environment, Fig. 4, contains a target cube and a

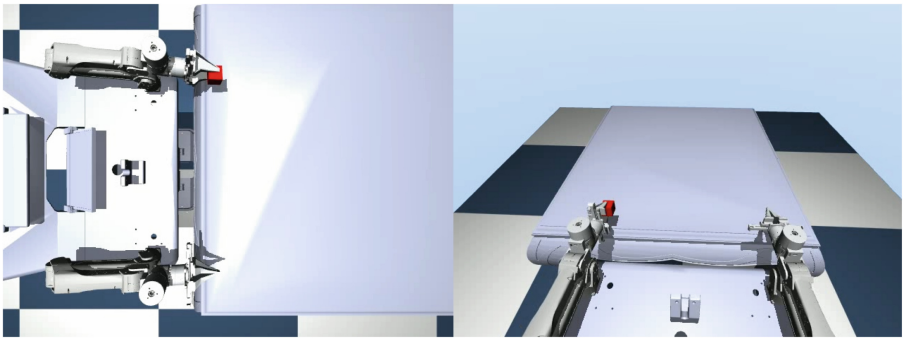

**Fig. 3.** Mobile Aloha Performing Static Pick-Up Manipulation Task with footage from top-mounted camera (right)

target position. The robot must first navigate to the cube, pick it up and then navigate to the target position to place the cube. The reward function is defined as follows:

$$r_t = \begin{cases} -r_{cube} + R_{pickup} \cdot \mathbb{I}(\text{Picked Up Cube}) \\ \quad -R_{coll} \cdot \mathbb{I}(\text{Collision}), \text{ if cube not picked up} \\ -r_{target} + R_{place} \cdot \mathbb{I}(\text{Placed Cube}) \\ \quad -R_{coll} \cdot \mathbb{I}(\text{Collision}), \text{ if cube picked up} \end{cases} \tag{9}$$

Here, all the variables correspond to those used in the reward functions for the Manipulation and Navigation tasks.

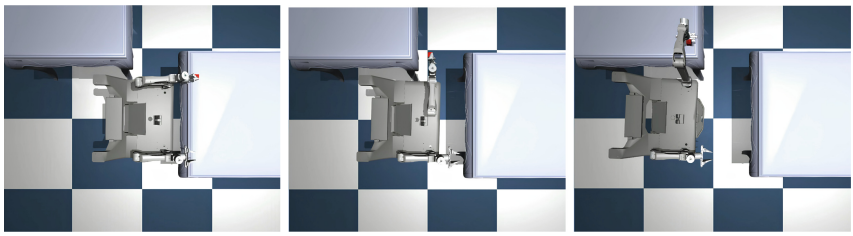

**Fig. 4.** Manipulation+Navigation Task. Mobile Aloha picks up the cube (left), navigates to the target table (middle) and places it on the target table (right)

## 5 Results

In our experiments, we compared the performance of multi-task TDMPC2 and DreamerV3 with single-task PPO and SAC, along with a comparison of

**Table 2.** Hyperparameters for Different Algorithms

| TDMPC2 | | DreamerV3 | | SAC | |
|---|---|---|---|---|---|
| Hyperparameter | Value | Hyperparameter | Value | Hyperparameter | Value |
| Encoder dim | 256 | Hidden size | 384 | MLP Hidden size | 1024 |
| MLP dim | 384 | Recurrent units | 3072 | Seed steps | 1000 |
| Latent State dim | 128 | Batch length | 64 | MLP activation | RELU |
| Encoder layers | 2 | Return lambda | 0.95 | Momentum coeff. | 0.99 |
| Q-functions | 2 | Batch size | 16 | Batch size | 2 |
| PPO | | FQL | | DFQL | |
| Hyperparameter | Value | Hyperparameter | Value | Hyperparameter | Value |
| Hidden layers | 2 | Initial Q-value | 0 | Initial Q-value | 0 |
| Epochs | 10 | Learning rate | 0.1 | Learning rate | 0.1 |
| Clip range | 0.2 | Discount factor | 0.95 | Discount factor | 0.95 |
| GAE parameters | 0.95 | Exploration rate | 0.99 | Exploration rate | 0.99 |
| Batch size | 4096 | Batch size | 128 | Rule addition threshold | 0.2 |

TDMPC2 with FQL and DFQL. Hyperparameters are defined as parameters that govern the training of the RL algorithm (e.g. learning rate, discount factor, etc.). We used the default hyperparameters recommended by the TDMPC2 authors [9] with 1 million parameters for each task.

For the DreamerV3, we utilized the "S" model size configuration and hyperparameters recommend in their paper [7]. For SAC, we followed the TDMPC paper [10] in their decision to benchmark against the SAC implementation from https://github.com/denisyarats/pytorch_sac. For PPO, we employed RayTune with RLlib to optimize the hyperparameters. The implementation of FQL and DFQL is based on the reference [5] and the python based code from https://github.com/seyedsaeidmasoumzadeh/Fuzzy-Q-Learning. The models were trained for 500k timesteps and then evaluated over 1M timesteps.

*Note: Some of the main hyperparameters of the selected RL algorithms and their values are mentioned in the Table 2. A complete list of hyperparameters can be found in the papers specified above.*

For simple Navigation task with low action dimension, all algorithms have more or less optimal, as shown in Fig. 5. Overall, TDMPC2 demonstrates more consistent performance and outperforms the baselines, particularly in challenging tasks. This trend is evident in the TDMPC2 [9] paper, where TDMPC2 outperformed SAC, DreamerV3, and vanilla TDMPC on high-complexity, difficult tasks such as Dog Run, Humanoid Walk (DMControl), and Pick YCB (ManiSkill2). At the same time, both FQL and DFQL exhibited subpar performance and failed to converge on any tasks.

To demonstrate the effectiveness of multi-task approach, we compare the results of single-task TDMPC2 agent with multi-task TDMPC2 agent. The mod-

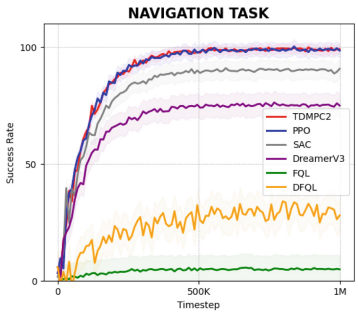


(a) Navigation Control Results

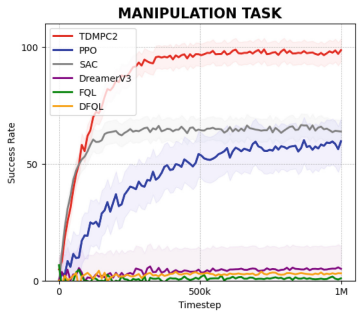


(b) Manipulation Task Results

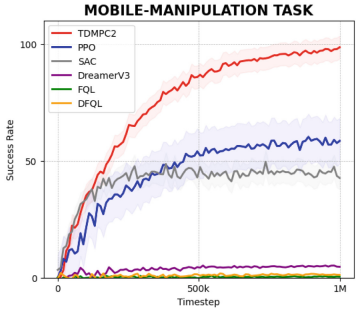


(c) Mobile Navigation Task Results

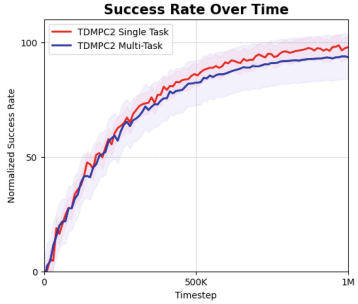


(d) Single vs Multi-task Learning Results

**Fig. 5.** Experiment Results

els were trained on a dataset 2M transitions obtained from the replay buffers of the three single-task agent as recommended in the original TDMPC2 paper[9]. From Fig. 5d. We can observe that initially the performance of both single and multi-task agents is more-or-less the same but single-task agent performs slightly better than the multi-task agent which might be attributed to the increasing complexity of the tasks.

## 6 Conclusion and Limitations

### 6.1 Analysis and Discussion

While TDMPC2 showed promising performance across multiple tasks without the need for task-specific tuning, the other algorithms also demonstrated distinct strengths and weaknesses. PPO and SAC, although they required more specific hyperparameter adjustments facilitated by tools like RayTune and RLlib, still managed to perform optimally in tasks with lower action dimensions. DreamerV3, utilizing its "S" model size, displayed sub-optimal performance, particularly in complex scenarios. On the other hand both FQL and DFQL showed sub-

par performance which might be attributed to the fact that navigation, manipulation, and mobile-manipulation tasks involve complex space and action state hence FQL and DFQL, being simpler in their approach, often lack the sophistication required to handle high-dimensional, continuous state and action spaces effectively.

However, each algorithm also exhibited specific limitations. For example, TDMPC2, while robust in handling diverse tasks with a single hyperparameter set, was noted for potential numerical instabilities in high-dimensional tasks. PPO and SAC, although generally effective, often required extensive tuning to reach optimal performance, particularly in complex tasks.

### 6.2 Conclusion

The comparative analysis across TDMPC2, PPO, SAC, and DreamerV3, as well as FQL and DFQL, reveals that no single algorithm universally excels in all aspects of multi-task learning for autonomous robots. Each algorithm has its own strengths and trade-offs, suggesting a potential benefit in hybrid approaches or further algorithmic development to mitigate their respective limitations. TDMPC2, despite outperforming other baselines in a simulated environment, has yet to be tested or implemented in real-world applications or on actual robots.

Future research should focus on enhancing the scalability, stability, and efficiency of these algorithms to better adapt to diverse and dynamical real-world applications. Additionally, addressing the specific challenges of transitioning from simulation to physical robots will be crucial for advancing the practical deployment of these technologies in autonomous systems. Overall, our findings underscore the importance of continued exploration and improvement of multiple RL algorithms to fully leverage their potential in complex, multi-task environments.

**Acknowledgments.** The results of Sect. 4 were obtained with the support of Sberbank (No 70-2021-00138) which is part of the program and plan of research center in the field of AI provided by the Analytical Center for the Government of the Russian Federation (ACRF) in accordance with the agreement on the provision of subsidies (identifier of the agreement 000000D730324P540002) and the agreement with the Moscow Institute of Physics and Technology dated November 1, 2021 No. 70-2021-00138.

## References

1. Berenji, H.: Fuzzy q-learning: a new approach for fuzzy dynamic programming. In: Proceedings of 1994 IEEE 3rd International Fuzzy Systems Conference, vol. 1, pp. 486–491 (1994). https://doi.org/10.1109/FUZZY.1994.343737
2. Chen, X., Wang, C., Zhou, Z., Ross, K.: Randomized ensembled double q-learning: learning fast without a model (2021)
3. Er, M.J., Deng, C.: Online tuning of fuzzy inference systems using dynamic fuzzy q-learning. IEEE Trans. Syst. Man Cybern. Part B (Cybernetics) **34**(3), 1478–1489 (2004). https://doi.org/10.1109/TSMCB.2004.825938

4. Fu, Z., Zhao, T.Z., Finn, C.: Mobile aloha: learning bimanual mobile manipulation with low-cost whole-body teleoperation. arXiv preprint arXiv:2401.02117 (2024)
5. Glorennec, P.: Fuzzy q-learning and dynamical fuzzy q-learning. In: Proceedings of 1994 IEEE 3rd International Fuzzy Systems Conference, vol. 1, pp. 474–479 (1994). https://doi.org/10.1109/FUZZY.1994.343739
6. Haarnoja, T., Zhou, A., Abbeel, P., Levine, S.: Soft actor-critic: off-policy maximum entropy deep reinforcement learning with a stochastic actor (2018)
7. Hafner, D., Pasukonis, J., Ba, J., Lillicrap, T.: Mastering diverse domains through world models (2024)
8. Hansen, N., Su, H., Wang, X.: Stabilizing deep q-learning with convnets and vision transformers under data augmentation. In: Conference on Neural Information Processing Systems (2021)
9. Hansen, N., Su, H., Wang, X.: Td-mpc2: scalable and effective model-based reinforcement learning with time-delayed model-predictive control. arXiv preprint arXiv:2310.16828 (2023)
10. Hansen, N., Wang, X., Su, H.: Temporal difference learning for model predictive control. In: International Conference on Machine Learning (ICML) (2022)
11. van Hasselt, H., Guez, A., Silver, D.: Deep reinforcement learning with double q-learning (2015)
12. Jang, B., Kim, M., Harerimana, G., Kim, J.W.: Q-learning algorithms: a comprehensive classification and applications. IEEE Access **7**, 133653–133667 (2019). https://doi.org/10.1109/ACCESS.2019.2941229
13. Kalashnikov, D., et al.: Mt-opt: continuous multi-task robotic reinforcement learning at scale (2021)
14. Kober, J., Bagnell, J., Peters, J.: Reinforcement learning in robotics: a survey. Int. J. Rob. Res. **32**, 1238–1274 (2013). https://doi.org/10.1177/0278364913495721
15. Lancaster, P., Hansen, N., Rajeswaran, A., Kumar, V.: Modem-v2: visuo-motor world models for real-world robot manipulation (2024)
16. Schulman, J., Wolski, F., Dhariwal, P., Radford, A., Klimov, O.: Proximal policy optimization algorithms. arXiv preprint arXiv:1707.06347 (2017)
17. Zhao, T.Z., Kumar, V., Levine, S., Finn, C.: Learning fine-grained bimanual manipulation with low-cost hardware (2023)

# Joint Assessment of Automotive Systems Safety and Security Using Bayesian Networks

Oleg Kirovskii(✉) and Anton Korolev

MIREA – Russian Technological University, Vernadskogo Avenue 78, 119454 Moscow, Russia
Oleg.Kirovskii@gmail.com

**Abstract.** Modern developments in automotive systems allow them to perform new complex functions, leading to a situation where standardized functional safety and security lifecycles are sometimes not able to meet their goals both in terms of risk reduction and agility.

To address the issue, the authors suggest using a model to jointly represent the safety and security of an automotive system. The model is based on a Bayesian Network (BN). The activities performed in the safety and security lifecycles impact both the structure and conditional probabilities of the BN. The network allows assessment of safety and security properties by calculating the likelihood for the relevant claims both during the development and after it. We demonstrate the implementation of our approach with the example of an advanced driver assistance system (ADAS).

**Keywords:** Automotive · Functional Safety · Cybersecurity · ISO 26262 · ISO 21434 · Bayesian networks · Safety Analysis · Safety Assessment

## 1 Introduction

Modern developments in automotive systems allow them to perform new functions besides the control of brakes and engines. ADAS gradually take over the role of the driver, while V2X communications make the road a safer place. This increase in terms of functionality necessarily challenges the required stack of engineering methods. This research puts focus on probabilistic modelling with priority on SW.

### 1.1 Challenges in SW Development for Modern Automotive Systems

The engineering team must solve three problems: its principal problem of system design, the process problem, and the certification problem.

1. **The principal problem** is the management of complexity itself, including the proper choice of architecture, coding, and testing. The current paper does not consider this problem explicitly.


S. Kovalev et al. (Eds.): IITI 2024, LNNS 1209, pp. 454–465, 2024.
https://doi.org/10.1007/978-3-031-77688-5_43

2. **The process problem** is related to two factors. The first factor is the uncertainty faced by engineers during SW development. The second factor is the need for agility. Direct application of safety standards is cumbersome and may not always justified by the gains in system quality[1]. The literature related to this problem is quite extensive (e.g. [1]).
3. **The certification problem** manifests after the development is finished. Currently, most automotive certifications just check if the system and SW were developed according to a process. Certification based on semi-formal proof (i.e. *safety case*) is promoted by researchers (cf. [2–4]).

### 1.2 Problem Statement and Structure of This Paper

The previous section shows that there are many sources of uncertainty in automotive system development. The proper tool to work with uncertainty is probabilistic calculations. Two of the problems listed in Sect. 1.1, namely the process problem (2) and certification (3) can be formulated into one research question: *How to handle uncertainties during and after the development phase to create provably safe and secure SW-defined automotive system?*

This paper's answer to this question is: *The uncertainties are best handled using a probabilistic model (PM).* The solution shall conform to the following properties:

1. There shall be a method to derive the PM from existing development artifact(s), and this method shall require as small amount of effort as possible.
2. There shall be a method to analyze the PM for actionable results, at least the following:
   a. Decisions guiding the design process.
   b. Decisions on acceptability of the developed system in terms of its safety and security
   c. Decisions on acceptability of the safety case for assessment of safety and security
3. The PM shall integrate as many system properties as possible.
4. The PM shall be universal in terms of sources of information it can integrate.

## 2 Safety and Security Assurance and Probabilistic Models

### 2.1 Safety, Security, Assurance, Protection

Achieving quality attributes (e.g. safety, security etc.) can be a key factor for system's success on the market [5]. There are more than 100 quality attributes known [6]. In this paper, we focus our attention on just two: safety and security.

[1] One of the authors once took part in a "dry run" of ISO 26262-based processes in a well-established Russian IT company. First, a SW unit (memory allocation manager) was implemented according to established company process by a small development team. Then, the same functionality was implemented by another (but equally able) team according to ISO 26262-based processes. The second team required ca. 120% more effort to complete the work. Both SW units later underwent fuzzing testing (fuzzing testing is not part of ISO 26262). There was no significant difference in testing results. This exercise very much undermined the company leaders' belief in ISO 26262 as a tool to improve SW safety.

Safety is a system property related to the absence of unreasonable risk, while risk is understood as possible harm to people having some probability [7]. Cybersecurity is a condition in which assets are sufficiently protected against threats [8]. Both refer to some negative event (harm to people or assets) that shall be prevented to some degree (reasonable risk, sufficient protection). Also, neither of two is directly measurable. The only way to prove safety or security is to argue for them, so that the argument can be accepted or refuted.

In this Chapter we will focus on safety arguments and safety cases. Everything that is true about safety arguments is also true for security. In Sects. 3 and 4, where the difference between safety and security becomes important, we introduce another word to encompass both safety and security: *protection.*

## 2.2 Process-Based and Evidence-Based Approaches to Safety Case

Safety case is the argument that safety is achieved for items or elements and satisfied by evidence compiled from work products of activities during development [7]. In the framework of ISO 26262, the safety case is seen as an account of development, and its goal is to show that all prescribed steps have been implemented. However, ISO 26262 is a *process assurance-based* safety standard.

Alternatively, there are *product evidence-based* safety standards, e.g. UK Defense Standard 00-56 [9]. This standard does not prescribe any process for system development. According to this standard, the development team prepares an argument to logically prove that their work meets both the measurable requirements (functional and non-functional) and the quality attributes such as safety and security. This approach is advantageous regarding *the process problem* (see Sect. 1.1).

For the rest of this paper, we adopt the definition based on [9]: *a safety case is a structured argument, supported by a body of evidence, that provides a compelling, comprehensible and valid case that a system is safe for a given application in a given context*.

**Table 1.** Lexicon of the Goal-Structured Notation (excerpt).

| Letter code | Graphical representation | Name | Definition [10] | Modelled by (cf. [11]) |
|---|---|---|---|---|
| G |  | Goal | Claim forming part of the argument. | Claim |
| C |  | Context | Contextual artifact: statement or reference to the source of information | Axiom |
| J |  | Justification | Statement of rationale | Axiom |
| St |  | Strategy | Inference between a goal and its supporting goals or solutions | Inference rule |
| Sn |  | Solution | Reference to an evidence item | Evidence |
| NA | 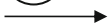 | SupportedBy | "Supported by" relation between elements. | Not modelled directly, encodes PM structure |
| NA |  | InContextOf | Relation between a goal and a context element. | Not modelled directly, encodes PM structure |

### 2.3 Semi-formal Representations of Safety Cases

Several attempts have been made to formalize the representation of safety cases, the most popular are Structured Assurance Case Metamodel (SACM) [12] by Object Modelling Group (OMG) and Goal-Structured Notation (GSN) [10] by Safety-Critical Systems Club (SCSC).

In this paper we will focus on GSN. The relevant part of the lexicon (i.e. signs that can be used) is shown in Table 1. A safety case rendered in GSN is presented on Fig. 1.

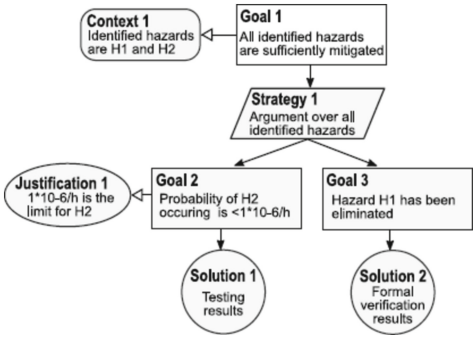


**Fig. 1.** A safety case fragment in GSN format (from [11])

### 2.4 Probabilistic Modelling of Safety Cases

In this section, we demonstrate a probabilistic model of a structured argument and show how to use it for modeling a safety case in GSN. The description here follows the method presented in [11].

The model is a tuple consisting of sets of statements $M\ \langle Q, A, E, R\rangle$, where $Q$ is the set combining all claims, $A$ is the set of axioms, $E$ is the set of evidence, and $R$ is the set of inference rules. A *claim* is a statement which we need to prove in the argument, e.g. *The system is safe*. Claims can depend on other claims, evidence, and axioms. An *axiom* is a statement which is always true within the range of the validity of the model, *e.g. Only hazards related to malfunctions of system components are analyzed*. Any violation of an axiom invalidates the model. *Evidence* is a statement which can be true or false depending on the observation, e.g. *A hazard analysis was carried out*. We can check if the mentioned work product was prepared or not.

*Inference rule* is a pair $r = (\{\phi_1, \phi_2, \ldots, \phi_n\}, \varphi)$, where $\{\phi_1, \phi_2, \ldots, \phi_n\}$ are called *premises* and $\varphi$ is a formula called conclusion. A formula puts a restriction on which premises it can accommodate and informs how its result depends on the value of the premises.

All the elements listed above are sources of uncertainty. Let us consider one claim $q$ that uses one inference rule $r$ having n premises $p_1, p_2, \ldots, p_n$, in the contexts of axioms $\boldsymbol{A}$ and evidence $\boldsymbol{E}$:

$$P(q|A,E) = P(q,r,p_1,\ldots,p_n|A,E) + P(q,r,p_1,\ldots,\overline{p_n}|A,E) + \cdots + P(q,r,\overline{p_1},\ldots,\overline{p_n}|A,E) \tag{1}$$

All members of the sum in (1) are non-negative. To obtain a pessimistic assessment, we drop all members of the sum but the first:

$$P(q|A,E) \geq P(q,r,p_1,\ldots,p_n|A,E) \tag{2}$$

Considering premises to be independent from each other, we get:

$$P(q|A,E) \geq P(q,r,p_1,\ldots,p_n|A)P(r|A)\prod\nolimits_i P(p_i|A,E) \tag{3}$$

## 3 Probabilistic Modelling of a Protection Case

### 3.1 Forming a Protection Case by Combining Safety and Security

Our aim is to present a unified approach to non-measurable quality attributes. As a first step, we introduced the attribute *protection* (see Sect. 2.1), which combines functional safety (FS) and cybersecurity (CS). Both attributes have their own structured arguments represented by the models $M_{FS}$ and $M_{CS}$ respectively. To combine the arguments, we need to calculate the union over their models.

For axioms ($A$), evidence ($E$) and inference rules ($R$) the union has the same meaning as in set theory. However, it is different for claims ($Q$), as claims within different cases may be contradictory. To solve this issue, we upgrade the model presented in [11] with two more sets: the set of system properties $S$ and set of allocations $L$. Allocation $l$ is a relation between a claim and a system property that it is related to:

$$l \in L : q \in Q \xrightarrow{l} S^* \in S \tag{4}$$

One claim can be allocated to at least one system property, i.e. $S^*$ is a non-empty set. Now we can formally define rules to define the set $Q^*$ as union over claims $q_1$ and $q_2$:

$$q_1 + q_2 | q_1 \xrightarrow{l_1} S_1^*, q_2 \xrightarrow{l_2} S_2^* = \begin{cases} S_1^* \neq S_2^* \Rightarrow Q^* = q_1 \cup q_2 \\ S_1^* = S_2^* = S^*, q_1 = q_2 = q \Rightarrow Q^* = q \\ S_1^* = S_2^* = S^*, q_1 \neq q_2 \Rightarrow Q^* = Q\prime \end{cases} \tag{5}$$

In plain words, if there are two non-equal claims related to the same set of system properties, one needs to introduce a new non-empty set of claims $Q^*$ that supports the new case. In the equation above $Q^{'}$ is a new set of claims that put possible contradictions in line with each other. $Q^{'}$ shall be obtained analytically.

Now we update $L$ with new non-empty set of allocations $L^*$:

$$l_1 + l_2 | q_1 : q_1 \xrightarrow{l_1} S_1, q_2 : q_2 \xrightarrow{l_2} S_2 = \begin{cases} S_1 \neq S_2 \Rightarrow L^* = \{l_1; l_2\} \\ S_1 = S_2 = S^* : \forall q^* \in Q^* \Rightarrow l^* : q^* \xrightarrow{l^*} S; L^* = l^* \end{cases} \tag{6}$$

In plain words, all claims retain their allocations, and the newly created claims from $Q^{'}$ inherit allocations from their parents.

### 3.2 Determination of the BN Structure

Now we need to transform the case model into the PM in the form Bayesian network (BN). As the definition of the model was updated, we need to update (2):

$$P(q|A, E) \geq P(q, r, p_1, \ldots, p_n|A, E, L, S) \tag{7}$$

Let us denote the right side of the inequality as $P_M$ and analyze it:

$$P_M = P(q, r, p_1, \ldots, p_n|A, E, L, S) = P(q, r, p_1, \ldots, p_n|A)P(r|A)\prod_i P(p_i|A, E, L, S)P(L)P(S) \tag{8}$$

First, we consider probabilities dependent on allocations. We assume for any part $x$ of the model $P_M(x|L) = P_M(x)$. This is not to say that claim allocations are always correct, but the belief in allocation is not separable from our belief in a claim.

Second, we consider dependencies on system properties. Claims do not depend on real system properties, just on the evidence they expect (see Sect. 2.4). Therefore, we may state that $P(p_i|A, E, S) = P(p_i|A, E)P(S)$. The value $P(S)$ denotes the belief that the system property $s_i \epsilon S$ requested by the argument is achieved.

Below is the final form of (8). The BN is based on this equation.

$$P_M = P(q, r, p_1, \ldots, p_n|A, E) = P(q, r, p_1, \ldots, p_n|A)P(r|A)\prod_i P(p_i|A, E)\prod_j P(s_j) \tag{9}$$

### 3.3 Determination of Conditional Probabilities

Each node of the BN contains the conditional probabilities table (CPT). CPTs are used to calculate the probabilities of the outcomes related to the node depending on the probabilities known for other nodes. Conditional probabilities (CPs) can be obtained based on rules, assigned based on assessment, or learnt.

**Rule-based assignment of probabilities** usually results in the assignment of the values of 0 or 1 or defining a full group of events (a group for which all CPs sum up to 1). For this work, we use rules described in [11].

**Assessment-based assignment of probabilities** brings less precise results but a wider scope, which makes this method inevitable. A range of tools has been proposed: majority voting, consent method for decision making [13] Kendall's Coefficient of Concordance (KCC) [14], but definitely the most popular method is the "Estimate – Talk – Estimate" (ETE) method, also known as Delphi method, that relies on structured approach to questioning a panel of experts [15].

### 3.4 Continuous Assessment of Protection Quality Attribute

The BN formed from the protection case represents a *hypothesis* connecting the system properties with the quality attribute "protection". After the hypothesis is formed, it can be tested either during verification and validation or after the development.

There are methods to learn both the structure and CPTs for BNs [16]. Here the structure of the BN represents the structure of arguments because the goal is to see how well reality corresponds to the model-based prediction. The measure for this is likelihood, i.e. the probability that the observed values are obtained conditioned on the parameters of the BN and the model structure [16]:

$$L = P(S|\theta, M) \tag{10}$$

The likelihood can be used to estimate the parameters of the BN (Maximal Likelihood Estimator, MLE) or to control how well the observations correspond to the model prediction. A likelihood limit can be set, and models with likelihood beyond thus limit can be dropped.

## 4 Use of BN Model in Engineering and Assessment Practice

### 4.1 ADAS System and the Protection Case

**ADAS External Lights System** is used to illustrate the concepts presented above. The block diagram of the system is shown below.

The ELS is the single point of control for the headlights of the car. Lights power control is a system part that activates or deactivates the physical switches controlling the flow of energy into the lamps.

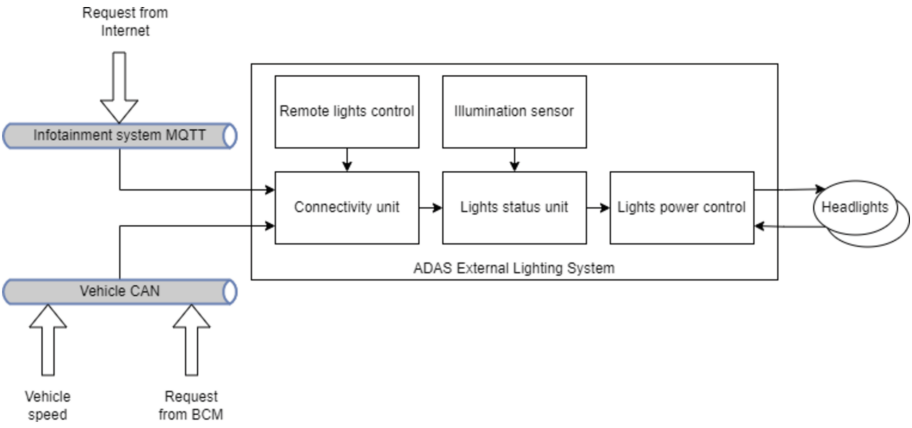


**Fig. 2.** ELS Block Diagram

We ignore the hardware and the middleware of the system, focusing just on the application SW as shown on Fig. 2. Remote lights control (RLC) is a small radio device placed within the car key. It allows the driver to turn on the headlights of the car remotely. Illumination sensor (IS) is placed under the windshield. Connectivity unit (CU) ensures connectivity with other systems. The infotainment system transmits the signals from a cloud interface which can be used to turn vehicle lights ON or OFF using a smartphone

app. Light Status unit (LSU) receives the signals from the illumination sensor and the CU and decides if the lights must be switched ON or OFF. The Light power control (LPC) implements the LSU decisions.

**Table 2.** Combining two GSN cases into one (excerpt)

| Set | Safety | Security | Protection | Comment |
|---|---|---|---|---|
| $Q$ | **G_FS_02**. All unit-level requirements are elicited | **G_CS_02**. All relevant threats and attack vectors are identified | **G_P_02**. All relevant threats and attack vectors are identified **G_P_04**. All unit-level requirements are elicited | The claims are related to different system properties (security and safety): $Q^* = q_1 \cup q_2$ |
| | **G_FS_03.** All requirements are satisfied | **G_CS_03**. Mitigation of all relevant vulnerabilities is implemented | **G_P_03**. Mitigation of all relevant vulnerabilities is implemented **G_P_05**. All requirements are satisfied | Although **G_FS_03** and **G_P_05** have the same wording, they are different claims because the requirements in question and the ways to prove them are different $Q^* = Q^{'}$ |
| $L$ | $l_{FS}$: **G_FS_02 → Sn_FS_01** | $l_{CS}$: **G_CS_02 → Sn_CS_01** | $l_P$: **G_P_04 → Sn_P_01** | The requirements for protection shall take threats into account |

**The protection case for ELS** is combined from FS and CS cases as shown in Sect. 3.1. Both cases share the top claim: "When the speed of the car is about 5 km/h, the lights can be deactivated by the driver only", because turning off lights in the dark at high speed may cause harm. The cases are created based on generic safety and security processes (not aligned with the standards).

Now we need to demonstrate the procedure for forming a protection case by combining the GSN cases for safety and security. Sets $Q$ and $L$, however, shall be unified according to the rules outlined in Eqs. 5 and 6 respectively. Table 2 makes examples of such unifications.

**BN for the protection case** is based on model described in Sect. 3.2. For simplicity, we will only consider the part of the case related to CU and ignore all others. The BN is shown in Fig. 3. The nodes of the BN are denoted according to the elements of the GSN protection case, e.g. **G_P_06** means our belief in the goal, i.e. the statement "*Unit implementation is correct*", and **S_P_04** denotes our belief in the strategy, i.e. the fact that "*Validation according to applicable guidelines*" is a good way to prove that goal. Probabilistic variables linked to the end nodes of the BN denote our belief in quality of

the relevant products, e.g. the value of **Sn_P_13** shows how good the validation plan is, with "1" meaning that it is very good, and "0" meaning that it completely misses the point, and the value of **C_P_07** is related to our belief in the quality of the "*Company SW validation guideline*" in the same way.

**Table 3.** CPT corresponding to **G_P_06**

| S_P_04 | G_P_07 | G_P_08 | G_P_09 | G_P_06 | ¬G_P_06 |
|---|---|---|---|---|---|
| 1 | 1 | 1 | 1 | PG_P_06 | 1 – PG_P_06 |
| 1 | 1 | 1 | 0 | 0 | 1 |
| 1 | 1 | 0 | 1 | 0 | 1 |
| … | … | … | … | … | … |
| 0 | 0 | 0 | 0 | 0 | 1 |

Table 3 shall have $2^4 = 16$ rows. However, to satisfy inequality (2), we should set the probability that the goal is achieved to zero for all lines where at least one of the subgoals is not achieved. A wrong choice of strategy nullifies our belief in the goal as well. Therefore, we only need to estimate one parameter: the probability that the goal is satisfied when all impacting values are positive ($P_{G\_P\_06}$ in Table 3). This CP does not have to be equal to 1, but rather depends on the expert assessment or field evidence.

### 4.2 Protection Assessment Within Safety Lifecycle

We used a tool called UnBBayes[2] to model and analyze Bayesian networks. The BN shown on Fig. 3 was modelled using the tool.

**Checking the soundness of the model** is our primary concern. The model is sound if it behaves in the way the modelled process (safety engineering process) in our case would behave given the same inputs.

All the model all "input" variables (i.e. variables that don't have any incoming links, just outgoing ones) are instantiated with two states: "Yes" and "No". "Yes" means that we believe in the statement behind the variable (see Sect. 4.2) and "No" means that we do not believe in it. The need to instantiate two states instead of one comes from the peculiarities of the tool. All other variables are instantiated with CPTs like the Table 3 above.

After that, we set probability of the state "Yes" for all axioms (that is, context variables, denoted by letter "C" in Fig. 3) to 1. This corresponds to the notion that we are quite sure of the quality of the process framework used to develop the system. Logically, we had to set the probability of "No" to 0 (UnBBayes would check that the full group probability is one, otherwise the calculation does not start, and an error message is shown). For all other variables (solutions, denoted by "Sn" in Fig. 3) we set the probability of "Yes" to 0 to demonstrate that initially we have no work products ready.

[2] https://unbbayes.sourceforge.net/.

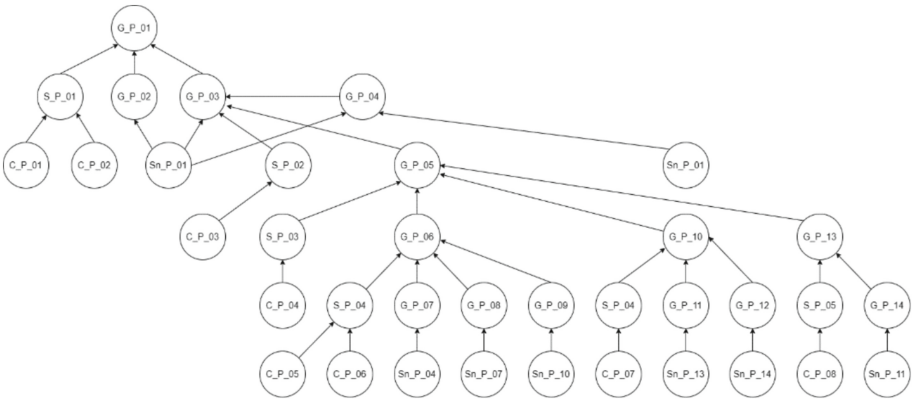


**Fig. 3.** BN corresponding to the ELS protection case

To model the progression of the safety process, we switched our belief in different solutions (work products) one after the other. The order and the result are shown in Table 4.

**Checking the soundness of the model** is our primary concern. The model is sound if it behaves in the way the modelled process (safety engineering process) in our case would behave given the same inputs. Table 4 shows that the BN is sound.

**The impact of different engineering domains** on the lifecycle is another problem that is worth discussing. Can good SW engineering "mask" poor analysis? By analysis we found out that all engineering domains are equally important. This is explained by the form of the CPTs.

**Table 4.** BN soundness check

| Process step | "Activated" Sn nodes | G1 Top claim | G2. All threats known | G3. Mitigation implemented | G4. All requirement elicited | G5. All requirement satisfied |
|---|---|---|---|---|---|---|
| Start | – | 0 | 0 | 0 | 0 | 0 |
| Analysis finished | 00, 01 | 0 | 1 | 0 | 1 | 0 |
| Coding finished | 00, 01, 04, 07 | 0 | 1 | 0 | 1 | 0 |
| Verification planned | 00, 01, 04, 07, 10 | 0 | 1 | 0 | 1 | 0 |
| Verification finished | 00, 01, 04, 07, 10, 13 | 0 | 1 | 1 | 1 | 0 |

(*continued*)

**Table 4.** (*continued*)

| Process step | "Activated" Sn nodes | G1 Top claim | G2. All threats known | G3. Mitigation implemented | G4. All requirement elicited | G5. All requirement satisfied |
|---|---|---|---|---|---|---|
| Validation planned | 00, 01, 04, 07, 10, 13, | 0 | 1 | 1 | 1 | 0 |
| Validation finished | 00, 01, 04, 07, 10, 13, 14 | 0 | 1 | 1 | 1 | 0 |
| Penetration testing finished | 00, 01, 04, 07, 10, 13, 14, 11 | 1 | 1 | 1 | 1 | 1 |

## 5 Outcomes and Further Work

The paper states a problem of handling uncertainties in modern automotive development (Sect. 1.2) and gives an overview on probabilistic modelling of assurance cases (Sect. 2).

The paper presents a formalized approach to combining assurance cases expressed in goal-structured notation (GSN). To do this, an extended formal model of GSN safety case is given (Sect. 3.1). The paper presents a method for obtaining probabilistic models in form of Bayesian networks (BNs) from the assurance cases (Sects. 3.2–3.4). Finally, the paper validates the probabilistic approach (Sect. 4.2) and shows some of the benefits of the proposed representation of an assurance case (Sect. 4.2).

At the meantime, the following research tasks are under investigation. First, the BN structure needs to be improved. Current model assumes that a work product can be assessed with one value, which is clearly a simplification. Besides that, the approach presented here is process-agnostic. It is equally applicable to V-model, agile or any combination thereof. Introduction of the process model can be used to improve the precision of the assessment.

## References

1. Alexander, R., Kelly, T., Kurd, Z., McDermind, J.: Safety Cases for Advanced Control Software: Safety Case Patterns. Department of Computer Science, University of York, York (2007)
2. Bass, L., Clements, P., Kazman, R.: Software Architecture in Practice. Addison-Wesley Professional (2012)
3. Brown, B.B.: Delphi Process: A Methodology Used for the Elicitation of Opinions of Experts. Rand Corp, Santa-Monica (1968)
4. Fields, A.P.: Kendall's Coefficient of Concordance. In: Encyclopedia of Statistcs in Behavioral Science, pp. 1010–1011. Wiley, Chichester (2005)
5. ISO 21434. Road vehicles. Cybersecurity (2021)
6. ISO 26262 Road Vehicles. Functional Safety (2018)
7. Koski, T., Noble, J.M.: Bayesian networks. In: An Introduction. Wiley, Chichester (2009)
8. Leveson, N.: The Use of Safety Cases in Certification and Regulation. MIT (2011)

9. Haeberle, M., et al.: Softwarization of automotive E/E architectures: a software-defined networking approach. In: IEEE Vehicular Networking Conference (VNC), New York, pp. 1–8 (2020)
10. Myklebust, T., Stalhane, T.: The Agile Safety Case. Springer, Trondheim (2018)
11. Nesic, D., Nyberg, M., Gallina, B.: A probabilistic model of belief in safety cases. Safety Sci. **138** (2021)
12. Object Modelling Group. About the Structured Assurance Case Metamodel Speicifcation Version 2.3 (2023). https://www.omg.org/spec/SACM. Accessed 02 May 2024
13. Rau, T.: Consent decision making. 06 21 (2023). https://www.sociocracyforall.org/consent-decision-making/. Accessed 05 June 2024
14. Richards, M., Ford, N.: Fundamentals of Software Architecture: An Engineering Apporach. O'Reilly (2020)
15. Safety-Critical Systems Club. Goal Structured Notation (2021). https://scsc.uk/gsn. Accessed 2 May 2024
16. UK DEFSTAN 00-56 Safety Management Requirements for Defence Systems (2007)
17. Yu, H., Lin, C., Kim, B.: Automotive software certification: current status and challenges. SAE Int. J. Passeng. Cars - Electron. Electr. Syst. **9**(1), 74–80 (2016)

# Algebraic Bayesian Networks: Refinement of the Approximate Generation of the Knowledge Pattern Canonical Representation

Artyom Vyatkin(✉) and Maxim Abramov

St. Petersburg Federal Research Center of the Russian Academy of Sciences, St. Petersburg, Russia
{aav,mva}@dscs.pro

**Abstract.** Among probabilistic graphical models we can distinguish a class of algebraic Bayesian networks defined over structurally smaller objects — mathematical models of knowledge patterns (KPs). The KPs themselves store closely related information about the subject domain, which is formalised, in particular, as a set of quanta with scalar or interval estimates of the probability of truth. When computational and time resources are scarce, it can be useful to search for a canonical representation of the KP — moving from objects with interval estimates to the most representative objects with scalar estimates. Previously, an algorithm for finding an approximate canonical representation of a KP was proposed, using a Monte Carlo method and looking for the average between a large number of KPs with scalar estimates. This paper considers a refinement of this algorithm by replacing the gamma distribution, which was used to generate the scalar estimates, with an exponential distribution. As a result, it was experimentally shown that the canonical representations of KPs obtained in this case are generated 8 times more accurately.

**Keywords:** machine learning · probabilistic graphical models · algebraic Bayesian networks · knowledge pattern · Monte Carlo method · canonical representation · uniform sampling from a simplex

## 1 Introduction

Among machine learning models, we can distinguish a class of probabilistic graphical models [1–3] that allow us to work with probability estimates. The range of practical applications of probabilistic graphical models covers a wide area, including their use in computer vision [4], assessment of environmental impact on human health [5], industrial systems risk assessment [6,7], another industrial systems diagnostics [8,9], video generation [10], study of chemical reactions [11], medicine [12–14], genetics [15]. Besides, the class of probabilistic graphical models includes the class of algebraic Bayesian networks (ABN) [16].


S. Kovalev et al. (Eds.): IITI 2024, LNNS 1209, pp. 466–474, 2024.
https://doi.org/10.1007/978-3-031-77688-5_44

ABNs are used to describe knowledge about a subject domain, which can be represented as statements with truth probability estimates.

One of the empirical assumptions on which the theory of ABN relies is the decomposability of knowledge, and hence of the statements to which they refer, into separate, smaller parts — knowledge patterns (KPs), where the logical and probabilistic relationship between statements is described as completely as possible. KPs can be mathematically rigorously formalised using various representations: a set of quanta or an ideal of conjuncts, where each element of the set or ideal is matched with a scalar or interval estimate of the probability of truth. The advantage of interval estimates over scalar estimates is a wider coverage of the incompleteness of the information available in the network. However, the operation of algorithms that consider networks with interval estimates is computationally more complex and time consuming.

Accordingly, if there is a lack of time or a shortage of computational resources and power, then working with ABN or a particular KP having scalar estimates may be preferable to processing models with interval estimates. Thus, there may be a need to switch from objects (ABN or KP) with interval estimates to objects with scalar ones. For such a transition, in order to provide the result closest to the result of processing objects with interval estimations, it is necessary to search for such an object with scalar estimations, which would maximally preserve the information contained in interval estimations. The latter is precisely what formulates the search for a canonical representation, an ABN or a separate KP.

In an earlier paper [17], an approximate construction of the canonical representation of the KP was described, where the Monte Carlo method was used. Such a method involves finding the average between randomly generated KPs with scalar estimates. However, as will be shown later in the current paper, the generated KPs are not uniformly distributed, which gives a bias in the final estimates of the canonical KP representation. Thus, the aim of this paper is to improve the algorithm described in [17], which allows us to refine the construction of the canonical representation of the KP by uniform generation of KPs with scalar estimates, as well as to experimentally confirm this refinement.

The theoretical significance of the paper consists in a more detailed description of the representation of KP as a convex polytope, which accompanies further research on relations between ABN objects using interval and scalar estimates. Practical significance of the work consists in refinement of the algorithm of approximate generation of canonical representation of KP, leading to more accurate results of processing of KP, using the construction of canonical representation.

## 2 Problem Statement

In this section, the basic concepts and their properties used later in the paper, as well as the algorithm for generating the canonical representation, will be described in a concise but mathematically more rigorous format. The description of the theoretical framework builds on earlier work on the theory of ABN [16,18].

As partially mentioned above, algebraic Bayesian networks (ABN) are viewed as global structures defined over a set (base) of mathematical models of knowledge patterns formalising knowledge patterns viewed as sets of statements. Hereinafter, for brevity, a mathematical model of a knowledge pattern will also be denoted as a KP. Before giving a more rigorous definition of a KP, let us say that a KP is considered over some *alphabet* — a set of *atoms* (*atomic propositions*) to which the corresponding statements are mapped. For example, an alphabet can be $\{x_0, x_1\}$. We will call the conjunction of all elements of the alphabet or their negations a *quantum*, and a *conjunct* — the conjunction of a subset of elements of the alphabet, including the empty one. Thus, given an alphabet, we can define a KP as the set of all possible quanta or the ideal of conjuncts (the set of all possible conjunctions) constructed over the given alphabet, where each element of the set or ideal has a *scalar* or *interval* estimates of the probability of truth. So, for example, for the alphabet $\{x_0, x_1\}$ the set of quanta will be the set $\{\bar{x}_1\bar{x}_0, \bar{x}_1x_0, x_1\bar{x}_0, x_1x_0\}$, and the ideal — $\{\varepsilon, x_0, x_1, x_1x_0\}$, where $\varepsilon$ — is an empty conjunct. The probability of the propositional formula is based on the probability proposed by Nilsson in 1986 [19]. It is also worth noting that probability estimates are assigned holistically in the sense that all elements of the KP are assigned either scalar or interval probability estimates.

The use of one or another mathematical representation of the KP is conditioned by the requirements of a particular problem, and there are mutually unambiguous matrix transitions between the representations. Thus, the probability estimates of the truth of the elements of the KP are subject to some linear constraints depending on the chosen representation. In this paper we will consider the representation using the set of quanta, which follows from the convenience of imposing restrictions on the estimates. Let us consider the case of scalar estimates of quanta $\{q_1, ..., q_n\}$:

$$\begin{cases} \sum\limits_{i=1}^{n} p(q_i) = 1, \\ p(q_i) \geq 0, \ \forall i \in \{1, ..., n\}, \end{cases} \tag{1}$$

where the estimate of the probability of truth of quantum $q_i$ is denoted as $p(q_i)$.

Let us turn to interval estimates. They are defined, for example, as $p(q_i) = [0.1, 0.3]$. Such estimates simultaneously consider all possible scalar estimates enclosed in an interval. Assigning interval estimates to all quanta in the set, on the other hand, specifies a set of distributions of scalar estimates, each of which obeys the constraints (1).

Thus, a KP with interval estimates, represented as a set of quanta, can be viewed as a convex polytope in $n$-dimensional space, where $n$ — the number of estimates and $n = 2^k$, $k$ — the cardinality of the alphabet over which the KP is constructed. By KP we will hereafter also mean this convex polytope. Any point inside this convex polytope is matched by the assignment of scalar estimates, so given the constraints (1), the convex polytope will lie in the $(n-1)$-dimensional standard simplex [20]. The final constraints forming the polytope are given by

interval estimates. An example of what such a polytope lying in a 2-dimensional simplex might look like is shown in Fig. 1. The light polyhedron in this figure represents the 2-dimensional simplex, the dark one — the KP itself.

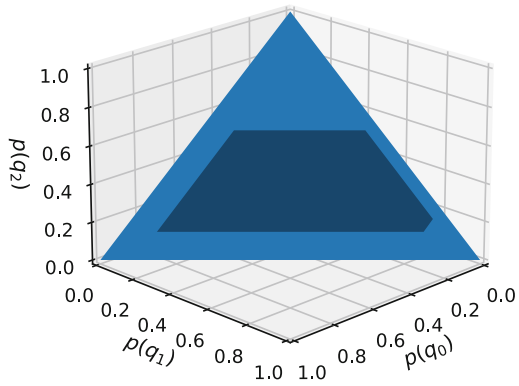


**Fig. 1.** An example of what a KP with interval estimates lying in a 2-dimensional simplex might look like.

It should be noted at once that in reality there could not be such a KP depicted in Fig. 1, since the number of quanta and their estimates should be equal to $2^k$ for some $k$. However, the constraints specifying the dark polytope and the constraints specifying the polytopes matched by KP with interval estimates have a similar structure and this visualisation is easy to perceive, so we will use it.

Speaking about the main algorithms that can be used with ABN or individual KPs, we can single out the algorithms of *apriori*, *aposteriori* inference [21], as well as the algorithm of *consistency maintenance*. The first algorithm allows us to determine the truth probability estimates of any propositional formula composed of atoms, the second — to model the incorporation of new information into ABN or KP by determining new truth probability estimates, and the third algorithm is aimed at detecting inconsistencies in the assigned estimates, as well as at reconciling them. In the case of interval estimates, these algorithms require solving linear programming problems, while in the case of scalar estimates — perform simpler matrix operations. It has been shown that the operation of the algorithms in the case of scalar estimates is orders of magnitude faster [22].

Therefore, if time or computational resources are scarce, a situation may arise in which objects with scalar estimates are preferred, and thus a switch from interval estimates to scalar estimates may be necessary. Finding scalar estimates that represent interval estimates as completely as possible is the problem of finding the *canonical representation*, which is defined as the centre of mass of the convex polytope given by the KP. Relative to Fig. 1, the canonical representation would be the centre of mass of the dark polytope.

Finally, let us consider an algorithm for approximate construction of the canonical representation of KP [17], which we will further improve. The algorithm is based on the Monte Carlo method. Let us briefly describe this algorithm:

1. First, some (100–1000) number of points lying in the KP is generated. Algorithm for generating one point:
   (a) A point is created where each coordinate is independently generated according to the law of *gamma*-distribution, the density of which is as follows
   $$f_X(x) = \begin{cases} x^{k-1}\frac{e^{-x/\theta}}{\theta^k \Gamma(k)}, & x \geq 0, \\ 0, & x < 0, \end{cases}$$
   where $X$ — random variable, $\Gamma(k)$ — Euler's gamma function, $k$ and $\theta$ — distribution parameters. In the [17] algorithm, $k$ and $\theta$ were equal to 2.
   (b) The coordinates of the resulting point are normalised by dividing by the sum of the coordinates.
   (c) If the obtained point is not in the KP, new coordinates are generated (return to step 1.a).
2. A linear combination of the generated points is constructed, resulting in a point whose coordinate value is the average of the corresponding coordinates of the generated points. The constructed point — is the canonical representation of the KP.

## 3 Refinement of the Generation of the KP Canonical Representation

The improvement of the approximate generation algorithm will rely on replacing the distribution, which is used to generate the coordinates of new points. Let us consider a drawback of the current algorithm: the original algorithm used the *gamma*-distribution, but its application does not allow uniform generation of points within the simplex, and hence within the KP.

In earlier work related to the study of probability distributions and not based on ABN theory, it was shown that to generate points uniformly within a simplex of any dimension, it is necessary to use the exponential distribution [23], where the rate parameter can be any (the value of 1 was chosen for the experiment). After using the exponential distribution, we need to continue with step 1.b and normalise the coordinates.

Let us compare the use of the old and new distribution on a 2-dimensional simplex example, the corresponding examples are shown in Fig. 2 and Fig. 3. In each case, 20000 points were generated and their coordinates were obtained using the corresponding distribution followed by normalisation. It can be seen that, indeed, using the exponential distribution gives a uniform distribution on the simplex. When using the gamma distribution, the approximate value of the canonical representation of the KP will be shifted towards the centre of mass of the entire simplex.

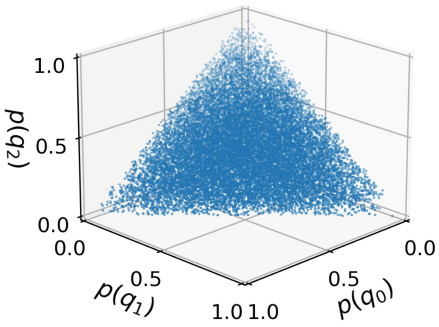


**Fig. 2.** Generation of points with gamma distribution.

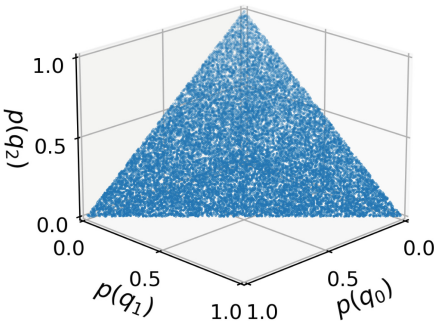


**Fig. 3.** Generation of points with exponential distribution.

## 4 Description of the Computational Experiment

In this section, we experimentally validate the refinement of the generation of an approximate canonical representation of the KP [17], in whose algorithm the gamma distribution was replaced by an exponential distribution.

All algorithms were implemented in the Python programming language. To evaluate the accuracy of constructing the obtained approximate canonical representations of KP, we used the algorithm for constructing the exact canonical representation of KP [24], which calculates the exact value of the center of mass. This algorithm can be applied to KPs constructed over an alphabet whose size does not exceed 3. Thus, the comparison was performed over the KPs constructed over alphabets of size between 1 and 3 atoms.

100 KPs were generated for each of the alphabet sizes, for a total of 300 KPs. To generate one approximate canonical representation, 100 point-scalar KPs were generated; the KPs with interval estimates themselves were generated using the algorithm described in [25].

To analyse the performance of the two versions of the algorithm, the running times of the algorithms were compared, as well as the accuracy of constructing the canonical representations. The accuracy was calculated using the RMSE metric using the following formula:

$$\mathrm{RMSE} = \sqrt{\frac{\sum\limits_{i=1}^{n} (p_a(q_i) - p_e(q_i))^2}{n}},$$

where $p_a(q_i)$ and $p_e(q_i)$ — $i$-th coordinates of the resulting canonical representations using the approximate and exact algorithms, respectively.

The experimental results are shown in Fig. 4 and Fig. 5. For convenience, the running time of the algorithms is shown as the logarithm of time (sec.).

Thus, it can be seen that the algorithm using the exponential distribution is more accurate in generating an approximate canonical representation — on

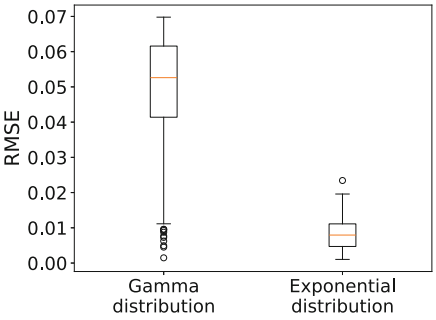


**Fig. 4.** Accuracy of two versions of the approximate algorithm.

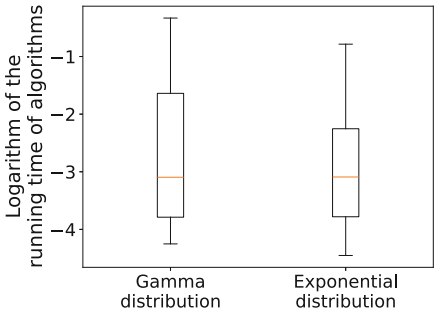


**Fig. 5.** Running time of two versions of the approximate algorithm.

average, the value of the RMSE metric is 8 times smaller. The running times of the algorithms are, expectedly, practically no different.

It is worth noting a drawback of the algorithm mentioned in [17], which was revealed during the computational experiment. The interval KP for which a canonical representation is sought may have "narrow" estimates. By this we mean that one or more intervals may have a relatively small length (e.g., $[0.1, 0.101]$). Due to this small length, the coordinates of the generated points may relatively rarely fall within the specified "narrow" interval, which increases the running time of the algorithm. Thus, in further research, this drawback can be addressed and the algorithm itself can be improved accordingly.

## 5 Conclusion

This paper describes a method of refinement of the algorithm for approximate generation of the canonical representation of the KP using the Monte Carlo method and considered in [17]. The refinement is performed by replacing the gamma distribution by the exponential distribution, which is used to generate scalar probability estimates. As a result of this replacement, the generated KPs with scalar estimates become uniformly distributed within the KPs with interval estimates. Thus, the approximate estimates of the probability of truth at the resulting canonical representation of the KP (centre of mass of the KP with interval estimates) become more accurate: an 8-fold refinement was shown in the course of the experiment.

Future work may investigate the effect of canonical representation generation errors on the accuracy of algorithms considered in ABN theory. In addition, the proposed method allows us to expand the practical use of ABN, including the study of social engineering attacks [26,27].

## References


1. Glasser, I., Pancotti, N., Cirac, J.I.: From probabilistic graphical models to generalized tensor networks for supervised learning. IEEE Access **8**, 68169–68182 (2020)
2. Vu, M., Thai, M.T.: PGM-explainer: probabilistic graphical model explanations for graph neural networks. Adv. Neural. Inf. Process. Syst. **33**, 12225–12235 (2020)
3. Yoon, K., et al.: Inference in probabilistic graphical models by graph neural networks. In: 2019 53rd Asilomar Conference on Signals, Systems, and Computers, pp. 868–875. IEEE (2019)
4. Ji, Q.: Probabilistic Graphical Models for Computer Vision. Academic Press (2019)
5. Pérez, S., German-Labaume, C., Mathiot, S., Goix, S., Chamaret, P.: Using Bayesian networks for environmental health risk assessment. Environ. Res. **204**, 112059 (2022)
6. Steijn, W.M.P., Van Kampen, J.N., Van der Beek, D., Groeneweg, J., Van Gelder, P.H.A.J.M.: An integration of human factors into quantitative risk analysis using Bayesian Belief Networks towards developing a 'QRA+'. Saf. Sci. **122**, 104514 (2020)
7. Devaraj, L., Ruddle, A.R., Duffy, A.P.: Electromagnetic risk analysis for EMI impact on functional safety with probabilistic graphical models and fuzzy logic. IEEE Lett. Electromagn. Compat. Pract. Appl. **2**(4), 96–100 (2020)
8. Li, T., Zhao, Y., Yan, K., Zhou, K., Zhang, C., Zhang, X.: Probabilistic graphical models in energy systems: a review. In: Building Simulation, pp. 1–30 (2021)
9. Yuan, Y., Dehghanpour, K., Wang, Z., Bu, F.: Multisource data fusion outage location in distribution systems via probabilistic graphical models. IEEE Trans. Smart Grid **13**(2), 1357–1371 (2021)
10. De Souza, C.R., Gaidon, A., Cabon, Y., Murray, N., López, A.M.: Generating human action videos by coupling 3d game engines and probabilistic graphical models. Int. J. Comput. Vision **128**(5), 1505–1536 (2020)
11. Cohen, M., Goculdas, T., Vlachos, D.G.: Active learning of chemical reaction networks via probabilistic graphical models and Boolean reaction circuits. React. Chem. Eng. **8**(4), 824–837 (2023)
12. Ni, Y., Baladandayuthapani, V., Vannucci, M., Stingo, F.C.: Bayesian graphical models for modern biological applications. Stat. Methods Appl. **31**(2), 197–225 (2022)
13. Cai, M.B., Shvartsman, M., Wu, A., Zhang, H., Zhu, X.: Incorporating structured assumptions with probabilistic graphical models in fMRI data analysis. Neuropsychologia **144**, 107500 (2020)
14. Nguyen, T.M., Poh, K.L., Chong, S.L., Loh, S.W., Heng, Y.C.K., Lee, J.H.: The use of probabilistic graphical models in pediatric sepsis: a feasibility and scoping review. Transl. Pediatr. **12**(11), 2074 (2023)
15. He, Z., Zhou, J.: Inference attacks on genomic data based on probabilistic graphical models. Big Data Min. Anal. **3**(3), 225–233 (2020)
16. Tulupyev, A.L., Sirotkin, A.V., Nikolenko, S.I.: Bayesian Belief Networks. SPbSU Press, Saint-Petersburg, Russia (2009). in Russian
17. Kharitonov, N.A., Tulupyev, A.L.: Algebraic bayesian networks: the generation of the knowledge pattern canonical representation. In: Proceedings of 2021 24th International Conference on Soft Computing and Measurements, SCM 2021, pp. 144–146 (2021)
18. Tulupyev, A.L., Nikolenko, S.I., Sirotkin, A.V.: Bayesian Belief Networks: Probabilisticlogic Approach. Nauka, Saint-Petersburg, Russia (2006). in Russian

19. Nilsson, N.J.: Probabilistic Logic. Artificial Intelligence. Elsevier Science Publishers BV, Amsterdam (1986)
20. Kostrikin, A.I., Manin, J.I.: Linear Algebra and Geometry. 2nd ed. Nauka, Moscow (1986). in Russian
21. Vyatkin, A.A., Abramov, M.V., Kharitonov, N.A., Tulupyev, A.L.: Application of tertiary structure of algebraic bayesian network in the problem of a posteriori inference. Bull. S. Ural State Univ. Ser. Comput. Math. Softw. Eng. **12**(1), 61–88 (2023). in Russian https://doi.org/10.14529/cmse230104
22. Kharitonov, N., Vyatkin, A., Tulupyev, A.: Algebraic bayesian networks: the generation of the network canonical representation. In: Proceedings of the Seventh International Scientific Conference "Intelligent Information Technologies for Industry" (IITI'23), Lecture Notes in Networks and Systems, vol. 777, pp. 13–22 (2023). https://doi.org/10.1007/978-3-031-43792-2_2
23. Devroye, L.: Non-Uniform Random Variate Generation. Springer-Verlag, New York (1986)
24. Vyatkin, V.A., Abramov, M.V.: Algebraic bayesian networks: the exact generation of the knowledge pattern canonical representation. In: Proceedings of 2024 27th International Conference on Soft Computing and Measurements, SCM 2024 (2024). in press
25. Vyatkin, A.A., Tulupyev, A.L.: Statistical comparison of the running times of global posteriori inference algorithms in algebraic bayesian networks. In: Proceedings of 2023 XXVI International Conference on Soft Computing and Measurements, SCM 2023, pp. 24–28 (2023). https://doi.org/10.1109/SCM58628.2023.10159044
26. Korepanova, A.A., Oliseenko, V.D., Abramov, M.V.: Applicability of similarity coefficients in social circle matching. In: Proceedings of 2020 XXIII International Conference on Soft Computing and Measurements, SCM 2020, pp. 41–43. (2020)
27. Khlobystova, A.O., Abramov, M.V.: Adaptation of the model of multi-pass social engineering attacks taking into account information influence. In: Proceedings of 2021 XXIV International Conference on Soft Computing and Measurements, SCM 2021, pp. 65–68 (2021). in Russian

# Author Index





S. Kovalev et al. (Eds.): IITI 2024, LNNS 1209, pp. 475–477, 2024.
https://doi.org/10.1007/978-3-031-77688-5